Vol. 187, September 30, 1986
Complete in one issue

ISSN 0003-2670

60

ANALYTICA CHIMICA ACTA

International journal devoted to all branches of analytical chemistry

EDITORS

A. M. G. MACDONALD (Birmingham, Great Britain)
HARRY L. PARDUE (West Lafayette, IN, U.S.A.)
ALAN TOWNSHEND (Hull, Great Britain)
J. T. CLERC (Bern, Switzerland)

Editorial Advisers

F. C. Adams, Antwerp
H. Bergamin F°, Piracicaba
G. den Boef, Amsterdam
A. M. Bond, Waurn Ponds
D. Dyrssen, Göteborg
S. R. Heller, Beltsville, MD
G. M. Hieftje, Bloomington, IN
J. Hoste, Ghent
G. Johansson, Lund
D. C. Johnson, Ames, IA
P. C. Jurs, University Park, PA
J. Kragten, Amsterdam
D. E. Leyden, Fort Collins, CO
F. E. Lytle, West Lafayette, IN
D. L. Massart, Brussels
A. Mizuike, Nagoya
M. E. Munk, Tempe, AZ
M. Otto, Freiberg
E. Pungor, Budapest
J. P. Riley, Liverpool
J. Robin, Villeurbanne
J. Růžička, Copenhagen
D. E. Ryan, Halifax, N.S.
S. Sasaki, Toyohashi
J. Savory, Charlottesville, VA
W. I. Stephen, Birmingham
M. Thompson, Toronto
W. E. van der Linden, Enschede
A. Walsh, Melbourne
P. W. West, Baton Rouge, LA
T. S. West, Aberdeen
J. B. Willis, Melbourne
E. Ziegler, Mülheim
Yu. A. Zolotov, Moscow

ELSEVIER

ANALYTICA CHIMICA ACTA

International journal devoted to all branches of analytical chemistry
Revue internationale consacrée à tous les domaines de la chimie analytique
Internationale Zeitschrift für alle Gebiete der analytischen Chemie

PUBLICATION SCHEDULE FOR 1986

	J	F	M	A	M	J	J	A	S	O	N	D
Analytica Chimica Acta	179	180	181	182	183	184	185	186	187	188 189	190	191

Scope. *Analytica Chimica Acta* publishes original papers, short communications, and reviews dealing with ever aspect of modern chemical analysis both fundamental and applied.

Submission of Papers. Manuscripts (three copies) should be submitted as designated below for rapid and efficier handling:

Papers from the Americas to: Professor Harry L. Pardue, Department of Chemistry, Purdue University, West Lafayette IN 47907, U.S.A.

Papers from all other countries to: Dr. A. M. G. Macdonald, Department of Chemistry, The University, P.O. Box 36 Birmingham B15 2TT, England. Papers dealing particularly with computer techniques to: Professor J. T. Cler Universität Bern, Pharmazeutisches Institut, Baltzerstrasse 5, CH-3012 Bern, Switzerland.

Submission of an article is understood to imply that the article is original and unpublished and is not being considere for publication elsewhere. Upon acceptance of an article by the journal, authors will be asked to transfer the copyrigh of the article to the publisher. This transfer will ensure the widest possible dissemination of information.

Information for Authors. Papers in English, French and German are published. There are no page charge Manuscripts should conform in layout and style to the papers published in this Volume. Authors should consu Vol. 170 for detailed information. Reprints of this information are available from the Editors or from: Elsevier Editori Services Ltd., Mayfield House, 256 Banbury Road, Oxford OX2 7DH (Great Britain).

Reprints. Fifty reprints will be supplied free of charge. Additional reprints (minimum 100) can be ordered. An orde form containing price quotations will be sent to the authors together with the proofs of their article.

Advertisements. Advertisement rates are available from the publisher.

Subscriptions. Subscriptions should be sent to: Elsevier Science Publishers B.V., Journals Department, P.O. Bo 211, 1000 AE Amsterdam, The Netherlands. Tel: 5803 911, Telex: 18582.

Publication. *Analytica Chimica Acta* appears in 13 volumes in 1986. The subscription for 1986 (Vols. 179–191) i Dfl. 2730.00 plus Dfl. 312.00 (p.p.h.) (total approx. US $1192.94). All earlier volumes (Vols. 1–178) except Vols. 2 and 28 are available at Dfl. 231.00 (US $90.59), plus Dfl. 15.00 (US $5.88) p.p.h., per volume.

Our p.p.h. (postage, packing and handling) charge includes surface delivery of all issues, except to subscribers in th U.S.A., Canada, Japan, Australia, New Zealand, P.R. China, India, Israel, South Africa, Malaysia, Thailand, Singapore South Korea, Taiwan, Pakistan, Hong Kong, Brazil, Argentina and Mexico, who receive all issues by air deliver (S.A.L. — Surface Air Lifted) at no extra cost. For the rest of the world, airmail and S.A.L. charges are available upo request.

Claims for issues not received should be made within three months of publication of the issues. If not they cannot b honoured free of charge.

For further information, or a free sample copy of this or any other Elsevier Science Publishers journal, readers in th U.S.A. and Canada can contact the following address: Elsevier Science Publishing Co. Inc., Journal Informatio Center, 52 Vanderbilt Avenue, New York, NY 10017, U.S.A., Tel: (212) 916-1250.

© 1986, ELSEVIER SCIENCE PUBLISHERS B.V.

0003-2670/86/$03.5

All rights reserved. No part of this publication may be reproduced, stored in a retrieval system or transmitted in any form or by any means, electroni mechanical, photocopying, recording or otherwise, without the prior written permission of the publisher, Elsevier Science Publishers B.V., P.O. Box 33 1000 AH Amsterdam, The Netherlands. Upon acceptance of an article by the journal, the author(s) will be asked to transfer copyright of the article to th publisher. The transfer will ensure the widest possible dissemination of information.

Submission of an article for publication entails the author(s) irrevocable and exclusive authorization of the publisher to collect any sums or considerations f copying or reproduction payable by third parties (as mentioned in article 17 paragraph 2 of the Dutch Copyright Act of 1912 and in the Royal Decree of Jur 20, 1974 (S. 351) pursuant to article 16b of the Dutch Copyright Act of 1912) and/or to act in or out of Court in connection therewith.

Special regulations for readers in the U.S.A. — This journal has been registered with the Copyright Clearance Center, Inc. Consent is given for copying articles for personal or internal use, or for the personal use of specific clients. This consent is given on the condition that the copier pays through the Cent the per-copy fee for copying beyond that permitted by Sections 107 or 108 of the U.S. Copyright Law. The per-copy fee is stated in the code-line at th bottom of the first page of each article. The appropriate fee, together with a copy of the first page of the article, should be forwarded to the Copyrigl Clearance Center, Inc., 27 Congress Street, Salem, MA 01970, U.S.A. If no code-line appears, broad consent to copy has not been given and permission copy must be obtained directly from the author(s). All articles published prior to 1980 may be copied for a per-copy fee of US $ 2.25, also payable throug the Center. This consent does not extend to other kinds of copying, such as for general distribution, resale, advertising and promotion purposes, or f creating new collective works. Special written permission must be obtained from the publisher for such copying.

Printed in The Netherlands

ANALYTICA CHIMICA ACTA
VOL. 187 (1986)

ANALYTICA CHIMICA ACTA

International journal devoted to all branches of analytical chemistry

EDITORS

A. M. G. MACDONALD (Birmingham, Great Britain)
HARRY L. PARDUE (West Lafayette, IN, U.S.A.)
ALAN TOWNSHEND (Hull, Great Britain)
J. T. CLERC (Bern, Switzerland)

Editorial Advisers

F. C. Adams, Antwerp
H. Bergamin F°, Piracicaba
G. den Boef, Amsterdam
A. M. Bond, Waurn Ponds
D. Dyrssen, Göteborg
S. R. Heller, Beltsville, MD
G. M. Hieftje, Bloomington, IN
J. Hoste, Ghent
G. Johansson, Lund
D. C. Johnson, Ames, IA
P. C. Jurs, University Park, PA
J. Kragten, Amsterdam
D. E. Leyden, Fort Collins, CO
F. E. Lytle, West Lafayette, IN
D. L. Massart, Brussels
A. Mizuike, Nagoya
M. E. Munk, Tempe, AZ
M. Otto, Freiberg
E. Pungor, Budapest
J. P. Riley, Liverpool
J. Robin, Villeurbanne
J. Růžička, Copenhagen
D. E. Ryan, Halifax, N.S.
S. Sasaki, Toyohashi
J. Savory, Charlottesville, VA
W. I. Stephen, Birmingham
M. Thompson, Toronto
W. E. van der Linden, Enschede
A. Walsh, Melbourne
P. W. West, Baton Rouge, LA
T. S. West, Aberdeen
J. B. Willis, Melbourne
E. Ziegler, Mülheim
Yu. A. Zolotov, Moscow

ELSEVIER Amsterdam–Oxford–New York–Tokyo

Anal. Chim. Acta, Vol. 187 (1986)

© 1986, ELSEVIER SCIENCE PUBLISHERS B.V.

0003-2670/86/$03.50

All rights reserved. No part of this publication may be reproduced, stored in a retrieval system or transmitted in any form or by any means, electronic, mechanical, photocopying, recording or otherwise, without the prior written permission of the publisher, Elsevier Science Publishers B.V., P.O. Box 330, 1000 AH Amsterdam, The Netherlands.

Upon acceptance of an article by the journal, the author(s) will be asked to transfer copyright of the article to the publisher. The transfer will ensure the widest possible dissemination of information.

Submission of an article for publication entails the author(s) irrevocable and exclusive authorization of the publisher to collect any sums or considerations for copying or reproduction payable by third parties (as mentioned in article 17 paragraph 2 of the Dutch Copyright Act of 1912 and in the Royal Decree of June 20, 1974 (S. 351) pursuant to article 16b of the Dutch Copyright Act of 1912) and/or to act in or out of Court in connection therewith.

Special regulations for readers in the U.S.A. – This journal has been registered with the Copyright Clearance Center, Inc. Consent is given for copying of articles for personal or internal use, or for the personal use of specific clients. This consent is given on the condition that the copier pay through the Center the per-copy fee for copying beyond that permitted by Sections 107 or 108 of the U.S. Copyright Law. The per-copy fee is stated in the code-line at the bottom of the first page of each article. The appropriate fee, together with a copy of the first page of the article, should be forwarded to the Copyright Clearance Center, Inc., 27 Congress Street, Salem, MA 01970, U.S.A. If no code-line appears, broad consent to copy has not been given and permission to copy must be obtained directly from the author(s). All articles published prior to 1980 may be copied for a per-copy fee of US $2.25, also payable through the Center. This consent does not extend to other kinds of copying, such as for general distribution, resale, advertising and promotion purposes, or for creating new collective works. Special written permission must be obtained from the publisher for such copying.

PRINTED IN THE NETHERLANDS

Analytica Chimica Acta, 187 (1986) 1—16
Elsevier Science Publishers B.V., Amsterdam — Printed in The Netherlands

FLUORIDE ION-SELECTIVE ELECTRODE IN FLOW INJECTION ANALYSIS
Part 2. Interference Studies

WOLFGANG FRENZEL* and PETER BRÄTTER

Hahn-Meitner-Institut für Kernforschung, Glienicker Str. 100, D-1000 Berlin 39 (Federal Republic of Germany)

(Received 18th March 1986)

SUMMARY

The influence of the sample composition on the response characteristics of the fluoride ion-selective electrode in flow injection analysis is described. Sample parameters such as ionic strength, viscosity and pH affect the response time of the electrode and cause transient signals when limiting values are exceeded. The respective limiting values depend on the total ionic-strength adjustment buffer (TISAB) used and these interferences can be minimized by proper choice of the TISAB. The complex formation of fluoride by several elements in the presence of TISAB containing CDTA is discussed. Aluminium and magnesium were found to interfere when present at levels above 1 and 100 mg l^{-1}, respectively. The signal decrease in the presence of iron, calcium and silicon can be attributed to ionic strength effects rather than complexation. Provided that the ionic strength is taken into account and corrected for, no influence occurs even in the presence of 0.5, 2 and 5% of iron, calcium and silicon, respectively.

The unique properties of the lanthanum fluoride crystal as an ion-selective membrane for potentiometric measurements are well documented [1—5]. However, it is of great importance to consider both solution and electrode interferences and sources of error which are caused by liquid-junction potentials, erratic performance of the reference electrode or other reasons [6]. The electrode potential generated against a reference electrode reflects the activity of the fluoride ions present in the sample. The activity, however, is influenced by factors such as ionic strength, pH value and the presence of fluoride-complexing ions. In order to measure concentrations instead of activities, these factors must be rigorously controlled. For the fluoride electrode, this is usually achieved by means of a total ionic strength adjustment buffer (TISAB) [7—10]. Although different formulae have been given for particular TISAB solutions, the following features are common to all: (i) a high salt concentration to provide a background of constant ionic strength between sample and standard solutions; (ii) adjustment to pH 5.0—5.2 to prevent the formation of hydrogen complexes and the interference of hydroxyl ions; and (iii) a masking agent for elements such as aluminium, iron, magnesium and others is added to release complexed fluoride.

0003-2670/86/$03.50 © 1986 Elsevier Science Publishers B.V.

In contrast to batch measurements and flow-through systems which are based on steady-state potential readings, flow-injection potentiometry relies on reproducible and controllable response-time characteristics of the ion-sensitive electrode (ISE). This is because the electrode potential is usually measured when equilibrium has not been attained [11—13]. The experimental factors affecting the response time were evaluated in Part 1 of this series [14]. In continuation, the influence of the sample composition on the response characteristics was investigated for flow-injection potentiometry. In this study of interferences, special emphasis was given to problems related to the application of the fluoride-selective electrode in the analysis of water, beverages and biological samples. Such applications will be described separately.

EXPERIMENTAL

Apparatus

The flow-injection system used was described in detail in Part 1 [14]. In the present work, all measurements were made with the wall-jet electrode configuration. The distance between the inlet nozzle and the sensing membrane was adjusted to 0.5 mm. Gravity flow at a rate of 1.0 ml min^{-1} was used throughout.

To investigate the response of the fluoride-selective electrode to sudden changes of the carrier composition, e.g., fluoride concentration, pH, ionic strength, viscosity and interfering elements, an additional valve was inserted upstream between the injection valve and the carrier reservoir (see Fig. 1). Thus a change from one solution to another can be achieved quickly by switching this valve without use of the injection valve. The distance between

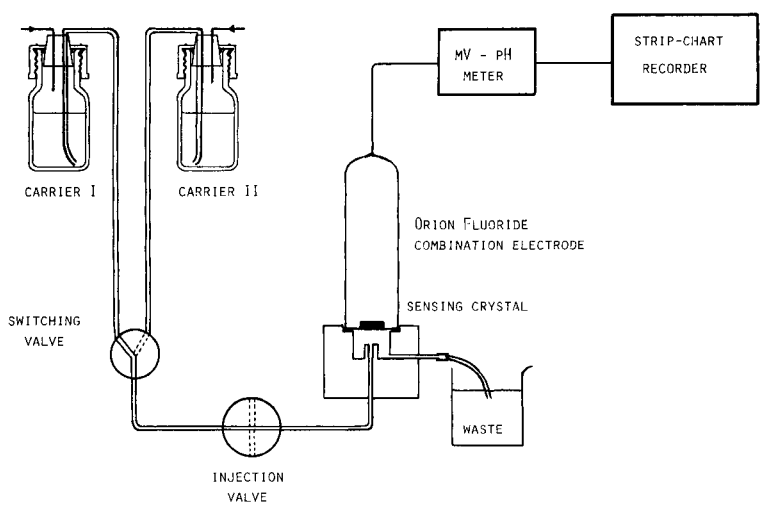

Fig. 1. The complete system for ion-selective electrode flow-through measurements.

the switching valve and the flow-through cell was kept short (8—10 cm) to minimize mixing at the front zone of the solution under study.

Reagents and solution

Stock solutions (Merck Titrisol) containing 1 g l^{-1} fluoride, 10 g l^{-1} aluminium, silicon or iron, and 100 g l^{-1} calcium or magnesium, were used to prepare appropriate standards. Concentrated solutions of sodium nitrate (5.0 mol l^{-1}), potassium chloride (4.0 mol l^{-1}), sodium chloride (3 mol l^{-1}) and potassium nitrate (3 mol l^{-1}) were made from high-purity reagents (Merck Suprapur). The concentrated mineral acids were also of high purity. Glycerine (87%) and sodium hydroxide were of analytical-reagent grade.

All solutions were prepared with deionized/twice-distilled water. Commercially available TISAB-III solution (Orion Research) was used as recommended (1:10 dilution). A TISAB of higher ionic strength was prepared by adding sodium nitrate to the TISAB-III concentrate to obtain a final concentration of 6 mol l^{-1} (242 g of $NaNO_3$ per 475 ml of TISAB-III stock).

All solutions used as carriers were degassed thoroughly by means of water suction and stored in polyethylene bottles.

RESULTS AND DISCUSSION

Response-time measurements

Response-time measurements of ISE's have been examined by various authors in order to understand the rate-determining processes in the establishment of the potential after an activation step, and to obtain information about factors that influence the electrode response [15—20]. The former are beyond the scope of this series. The latter were partially studied in Part 1, but the factors were restricted to those which can be set and held constant during a series of measurements (system parameters). Response-time changes which are associated with properties of the sample (sample parameters) are, however, of utmost importance in flow-injection potentiometry because they influence the accuracy and reliability of the method.

In order to obtain data for use as reference values in later studies of the effects of interfering substances, varied ionic strength, viscosity and pH, the response time of the fluoride electorde was first studied under ideal conditions. In this connection, it must be emphasized that each electrode may exhibit individual response characteristics and therefore the response-time values for different electrodes cannot be expected to be very consistent. And even with the same electrode, variations in the response characteristics can be caused by ageing and changes in the surface properties [14, 17, 21]. Favourable conditions for such investigations are obviously obtained when the composition of the carrier is constant and only the activity of fluoride is altered. Therefore, a carrier solution containing 50 μg l^{-1} fluoride in TISAB-III (1:10) was continuously passed through the cell until a stable potential reading (± 0.05 mV) was obtained. Then the upstream valve was switched to

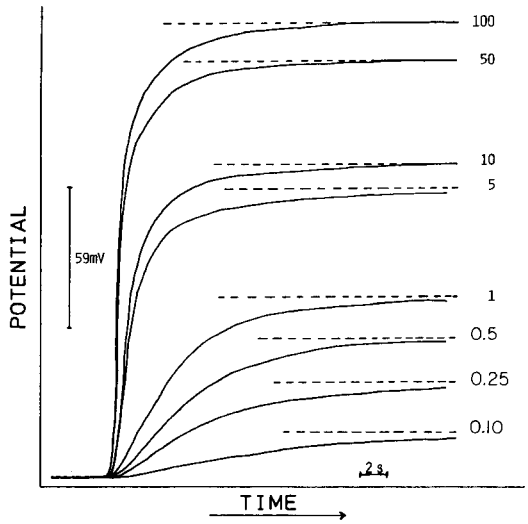

Fig. 2. Typical potential/time curves for various activity steps. Background fluoride concentration 50 μg l^{-1}. Final potentials reached after switching to the respective fluoride concentration are marked by broken lines. The numbers on the curves refer to mg l^{-1}.

allow solutions with higher or lower fluoride levels to pass the electrode while the potential/time response was recorded. Figure 2 shows the results for several concentration jumps. For comparison, the same starting point on the chart was set in all cases. The potential differences for various activity steps and the time necessary to reach 50%, 90% and 95% of the equilibrium potential are given in Table 1. The criterion of equilibrium potential is defined as one which does not change by more than 0.05 mV over a period of 30 s.

TABLE 1

Response times (to 50, 90 and 95% of equilibrium potential) and potential differences of the fluoride-selective electrode for activity steps from 50 μg l^{-1} F^- to various fluoride activities

Final fluoride activity (mg l^{-1})	Potential difference (mV)	Response time (s)		
		50%	90%	95%
100	189.3	0.98	3.76	5.92
50	174.3	1.00	3.80	5.98
10	131.4	1.35	4.65	7.41
5	121.4	1.50	5.85	10.55
1	75.0	4.05	12.00	20.25
0.5	57.9	4.95	14.61	22.40
0.25	39.0	5.55	17.25	26.75
0.10	18.7	7.95	22.65	34.50
0.01	7.9	33.6	>5 min	>5 min
0.001	34.0	94.3	>5 min	>5 min

In agreement with theoretical predictions [16], and earlier experimental results [17, 21], the response time of the fluoride-selective electrode decreases with the height of the activity step. Further, when the activity is changed from lower to higher values, the response time is shorter than in the reverse situation. The dependence of the response time on the concentration jump explains the deviation from Nernstian behaviour in flow-injection potentiometry at fluoride levels where the steady-state readings still show linearity [13].

Sample viscosity

The hydrodynamic conditions in flow systems depend significantly on the viscosity of the flowing solution. Because of the higher hydrodynamic resistance after injection of viscous fluids, the flow rate decreases and the dispersion pattern alters [22]. Additionally, in potentiometric measurements, the thickness of the boundary layer at the sensing membrane increases, which obviously affects the response time.

The influence of sample viscosity on the electrode response was studied by adding glycerine in small portions to TISAB-III solutions containing 0.5—5.0 mg l^{-1} fluoride. In Fig. 3A, the signals obtained with increasing glycerine contents are shown for the 0.5 mg l^{-1} fluoride standard. No influence is observed up to 6% glycerine. The kinematic viscosity of this solution is ca. 1.2 cp [23], which is rarely reached in real samples. Higher amounts cause

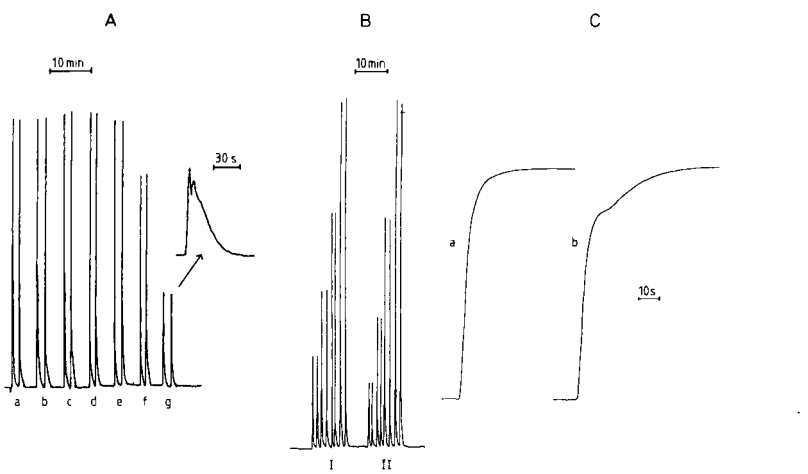

Fig. 3. (A) Influence of sample viscosity on peak height and shape in flow-injection potentiometry. Duplicate injections are made of a 0.5 mg l^{-1} fluoride standard with increasing glycerine content: (a) 0; (b) 1%; (c) 2%; (d) 4%; (e) 6%; (f) 10%; (g) 20%. The last peak is also shown at higher recorder speed. (B) Electrode response to increasing fluoride activities in the absence (I) and presence (II) of 10% glycerine; double injections are shown for 0.5, 1.0, 2.0 and 5.0 mg l^{-1} fluoride. (C) Response/time curves after switching from 50 μg l^{-1} to 500 μg l^{-1} fluoride in the absence (a) and presence (b) of 10% glycerine.

a significant decrease and distortion of the peak shape. At higher fluoride levels, even increased viscosities are acceptable without loss in peak height (see Fig. 3B). Comparison of the potential/time curves after switching to samples containing 0.5 mg l^{-1} fluoride in the absence and presence of 10% glycerine is shown in Fig. 3C with response times at half-height of 3.6 and 3.9 s, respectively. A shoulder is visible in the latter, which is probably due to back-mixing in the flow cell. The final potentials reached are identical.

Effects of ionic strength

As is well known, if concentrations are to be measured rather than activities, ionic-strength buffers are needed to swamp out differences in ionic strength between samples and between samples and standards [6—10, 24, 25]. To investigate the effect of ionic strength on the electrode response, various solutions were made by adding defined volumes of concentrated salt solutions to the TISAB-containing fluoride standards. Different salts were used to examine whether or not this is an influencing factor. The ionic strength was calculated from the usual equation $I = 1/2\, c_i z_i^2$. For the TISAB-III concentrate, it is 9.8 mol l^{-1}, which corresponds to 0.98 mol l^{-1} after the specified dilution. The results given in Table 2 show decreased fluoride activity in the presence of sodium chloride and sodium nitrate at ionic strength above 0.05 mol l^{-1}. When potassium salts are used, the influence is much less pronounced, which can be explained by a lower association between potassium and fluoride ions [26]. The influence of calcium ion is similar to that of sodium ion. Therefore, it may be supposed that ionic strength effects

TABLE 2

Influence of the ionic strength on the potential difference of the fluoride-selective electrode in the presence of different salts

Activity step 50 to 500 $\mu g\ l^{-1}$ fluoride. Carrier and standards are buffered with TISAB-III solution which gives an ionic strength of 0.98 mol l^{-1}

Salt added	Salt conc. (mol l^{-1})	Corresponding ionic strength (mol l^{-1})	Potential difference (mV)	Salt added	Salt conc. (mol l^{-1})	Corresponding ionic strength (mol l^{-1})	Potential difference (mV)
None	—	0.98	−36.8	KNO_3	0.20	1.18	−36.5
					0.50	1.48	−35.9
NaCl	0.05	1.03	−36.8		1.00	1.98	−34.7
	0.10	1.08	−35.5				
	0.20	1.18	−34.7	$CaCl_2$	0.067	1.18	−34.3
	0.50	1.48	−32.0		0.17	1.48	−30.6
	1.00	1.98	−29.0		0.33	1.98	−26.8
$NaNO_3$	0.20	1.18	−34.8	$MgCl_2$	0.067	1.18	−14.7
	0.50	1.48	−31.9		0.17	1.48	+1.2
	1.00	1.98	−29.1		0.33	1.98	+13.8
KCl	0.20	1.18	−36.8				
	0.50	1.48	−36.3				
	1.00	1.98	−35.1				

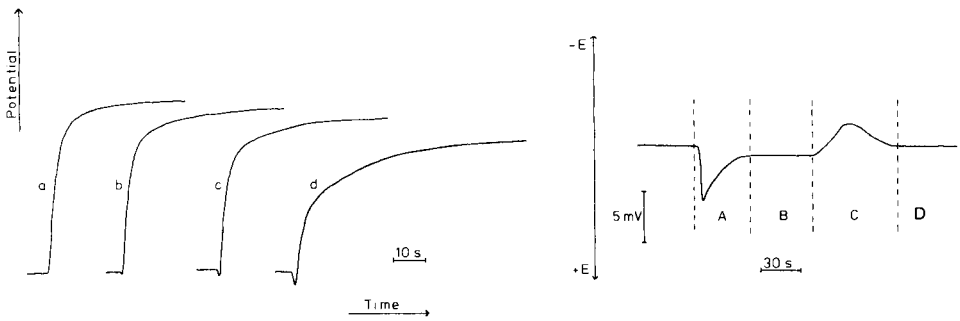

Fig. 4. Response/time curves at increasing ionic strength with sodium chloride added to TISAB-III-containing solutions: (a) 0; (b) 0.2; (c) 0.5; (d) 1.0 mol l^{-1} NaCl. See text for detail.

Fig. 5. Transient electrode phenomena caused by changes of ionic strength in the carrier. For explanation, see text.

were not considered when calcium interference was observed [27, 28]. Interferences of calcium and magnesium are discussed in detail below.

The response-time characteristics of the fluoride-selective electrode at high ionic strength were also examined. Figure 4 shows the recorder traces obtained after switching from a TISAB carrier containing 100 μg l^{-1} fluoride to solutions of increasing ionic strength containing 500 μg l^{-1} fluoride.

The main features of the above observations are the decrease in fluoride activity, the increase in the response time, and the short transient in the positive potential direction at the beginning of the signal. The response times were measured at 50% of the steady-state potential and were found to be 3.0, 3.4, 3.9 and 5.9 s in the presence of 0.0, 0.2, 0.5 and 1.0 mol l^{-1} sodium chloride, respectively. Additional measurements were made by switching between solutions of constant fluoride concentration (100 μg l^{-1} F^-) but varied ionic strength; a typical response curve is shown in Fig. 5. A positive transient occurs (section A) when the solution of higher ionic strength enters the cell; the following steady-state potential (section B) corresponds to the fluoride activity in this solution. Switching back to the original carrier produces a negative transient (section C) and then a return to the initial potential (section D). Both the change in response time with sample composition and the occurrence of transients are of particular interest in flow-injection potentiometry because they may interfere with the non-steady-state readings. In Fig. 6, this is clearly demonstrated for the injection of samples of increasing ionic strength containing 500 μg l^{-1} fluoride into a 100 μg l^{-1} fluoride carrier. The decrease in peak height depends on both the concentration (Fig. 6A) and kind (Fig. 6B) of salt added. Close comparison of the entire peaks without and with increased ionic strength shows a positive transient shortly before the electrode responds to the change in fluoride activity and a shoulder on the falling part of the peak which increases its half-width in the latter case.

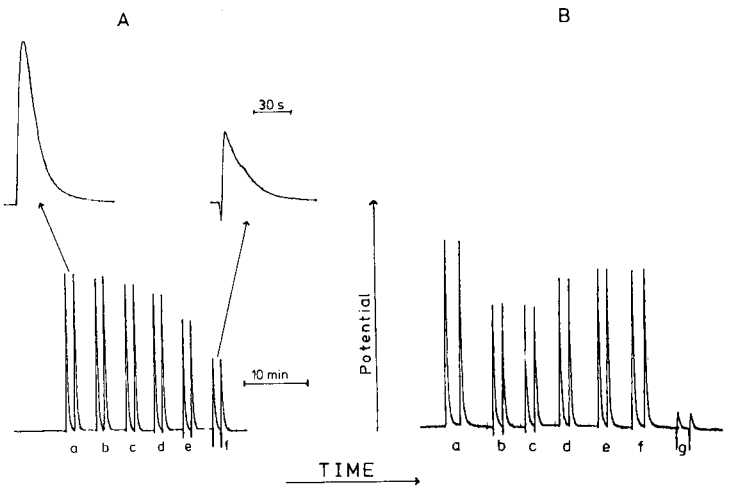

Fig. 6. (A) Influence of increasing ionic strength on the peak height and shape in flow-injection measurements shown by addition of sodium chloride to TISAB-III-containing samples (500 μg l^{-1} F^-): (a) 0; (b) 0.05; (c) 0.1; (d) 0.2; (e) 0.5; (f) 1.0 mol l^{-1} NaCl (peaks corresponding to (a) and (f) are also shown at high recorder speed). (B) Influence of various salts on the peak height when the ionic strength was maintained at 0.5 mol l^{-1}: (a) no addition; (b) NaCl; (c) $NaNO_3$, (d) KNO_3; (e) KCl; (f) $CaCl_2$; (g) $MgCl_2$.

Both can be interpreted as an overlapping response to fluoride ions with a secondary effect of the interferent.

Fluoride measurements at concentration below the fluoride levels present in the carrier confirmed the postulation of an overlapping response as the peak height increases at higher ionic strength. However, the peak shape also deviates from that obtained in the absence of interferents. Thus, the interference is to some extent self-evident, which is an advantageous feature of the flow-injection method.

So far, no satisfactory explanation has been found for the transient signals obtained. The possibility of changes in liquid-junction potential was investigated but was excluded by tests in which the cell arrangement had no liquid junction; these tests will be reported later. Similar findings have been reported for glass [25], liquid membrane [29, 30] and solid-state electrodes [31] in studies on electrode response in the presence of interfering compounds. Divergent theoretical explanations based on different mechanisms have been given by Cammann [32], Tóth et al. [31] and Morf [33], of which the first seems to be the most comprehensive. However, in the case of the lanthanum fluoride crystal, other reasons than interfering ions must be assumed to be responsible for the transient phenomena because only hydroxyl ions are known to interfere [3, 7]. Further studies are planned and the results will be published when available.

For the application of the fluoride electrode to real samples, the effect of changing ionic strength could be a serious limitation, but it is easily solved

by using a buffer of higher ionic strength. The modified buffer used here contains additional sodium nitrate to give a resulting ionic strength of 1.58 mol l^{-1} after the 1:10 dilution. This prevents any effect of $\leqslant$0.2 mol l^{-1} ionic strength actually in the samples. Further modifications can, of course be made as required for special applications. In general, it is desirable that the matrix composition of the samples and standards be as similar as possible.

Effects of pH

The pH-dependent response of the fluoride electrode has been extensively studied [2, 3, 9, 34]. Theoretical explanations have been given for the decrease in fluoride activity at low pH; these are based on stability constant calculations for hydrogenfluoride complexes [2, 35]. The increase in the alkaline region has also been investigated [4, 34, 36, 37]. There is, however, some disagreement as to whether this is caused by the formation of a lanthanum hydroxide film at the sensing membrane which may liberate fluoride ions [3, 34] or by hydroxide replacing fluoride in the LaF_3 crystal lattice [1].

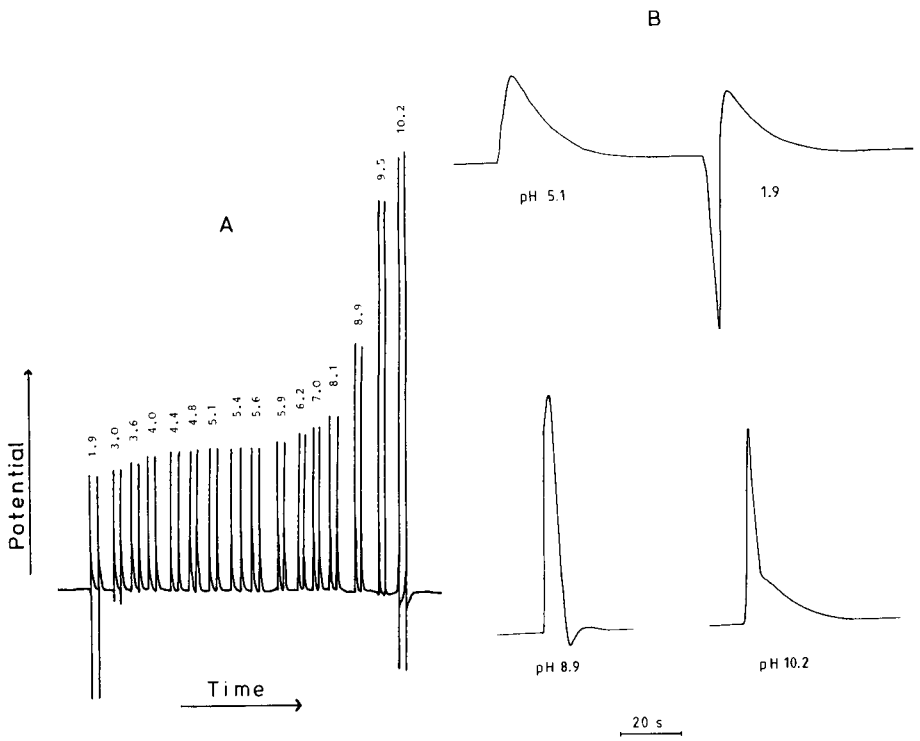

Fig. 7. (A) The influence of sample pH in the 1.9–10.2 range (as indicated on the peaks) on the signal in flow-injection measurements with the fluoride-selective electrode for 500 μg l^{-1} fluoride samples and 100 μg l^{-1} background fluoride. (B) Peak shapes obtained at different pH values on an expanded time scale.

Here, the electrode response was investigated in the pH range 2—10 by adding nitric acid or sodium hydroxide to the TISAB-containing sample solutions. From Fig. 7A, it is clear that pH does not affect matters in the range 4.4—5.6 whereas there are increasing errors outside this range. This viable pH window is significantly narrower than those reported for equilibrium measurements [9, 37]. The actual pH of the buffered sample should therefore be strictly controlled. As for variations in ionic strength (Fig. 5), transients appear in Fig. 7. In Fig. 7B four peaks are shown on an expanded time scale to illustrate the distortion of the normal signal when the pH is changed. Calculation of the ionic strength with varied pH showed that the changes in ionic strength are reasonably low and cannot be responsible for the electrode behaviour. The time constants of the transients are also different. Nevertheless, similar reasons are assumed for the transient phenomena in both cases.

Complexation of fluoride

Among the elements which are considered to form complexes with fluoride (see, e.g., [3, 7, 9]), aluminium, iron, magnesium, calcium and silicon are of particular interest for applications to environmental samples. A simple means of overcoming the problem of complexed fluoride is the addition of a suitable masking agent for the metal. *Trans*-1,2-cyclohexylenedinitrilotetraacetic acid (CDTA) which is present in TISAB-III solution has proved to be effective [7, 38, 39], although some authors prefer citric acid [8, 40, 41], or other substances [42—44]. The success of these procedures depends not only on the kind of complexing agent, but also on the absolute amount of interfering element and on the concentration ratio between these elements and fluoride. Therefore, fluoride standards in the 0.5—5 mg l^{-1} range were prepared and various concentrations of interfering ions were added. The influence on the peak height in the flow-injection method and the change in response time were examined for all the above elements.

Calcium. The complex formation between calcium and fluoride is known to affect the fluoride determination [1, 3, 7, 28]. In Fig. 8A, the influence of increasing calcium nitrate concentrations on the peak height is shown. Above 250 mg l^{-1} calcium, the signal decreases and a positive transient occurs at slightly higher concentrations. Suppression of the fluoride signal persists even at higher fluoride concentrations (Fig. 8B). Response times were measured and compared to results obtained in the absence of calcium. Significant deviations raise doubts as to whether the decrease can be attributed to complexation or to increasing ionic strength. The ionic strength of a solution containing 1 g l^{-1} calcium (as nitrate) was calculated to be about 0.07 mol l^{-1}, at which value interference was also observed in the presence of sodium salts (see above).

The results of experiments with the modified TISAB buffer which swamps out even higher differences in ionic strength between samples and standards are shown in Fig. 9. The interference is depressed which suggests that in the

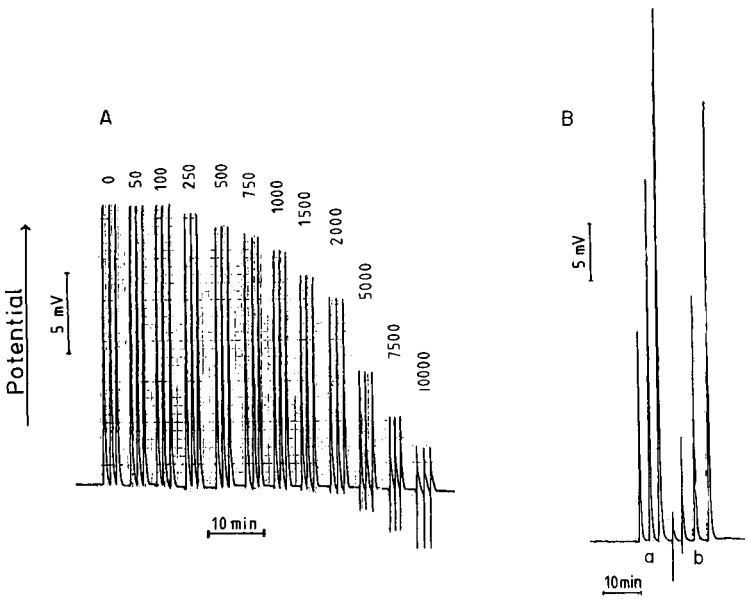

Fig. 8. (A) Influence of increasing calcium concentrations in the 50–10 000 mg l^{-1} range on the electrode response to samples containing 500 μg l^{-1} F^- in TISAB-III (1:10 dilution) with a carrier fluoride concentration of 100 μg l^{-1}. (B) Influence of calcium on the peak height at various fluoride concentrations: (a) peaks corresponding to the injection of 0.5, 1 and 2 mg l^{-1} fluoride; (b) peaks to the injection of 0.5, 1, 2 and 5 mg l^{-1} fluoride in the presence of 1% Ca^{2+}.

case of calcium, the effect of ionic strength is more serious than the possible complexation of fluoride. Support for this view is given by Tušl [45] who determined fluoride in pure calcium phosphate without interference after proper adjustment of ionic strength.

Magnesium. Magnesium forms weak complexes with fluoride [35] and therefore interferes in the fluoride determination with the selective electrode [1, 9, 40, 46]. In studies of the flow-injection method, decreased signals appear at magnesium concentrations above 100 mg l^{-1} (Fig. 10), which agrees with reported values [41]. Lower signals were also obtained at higher fluoride concentrations when magnesium ions were present (Fig. 10, peaks a and b). The response-time measurement was not affected by the presence of magnesium ions, which excludes any effects of ionic strength of the kind found for calcium. The interference persisted when the modified TISAB-III was used (Fig. 9, peaks d).

Silicon. Hexafluorosilicate appears to interfere only at low pH [9, 10]. Hydrolysis is essentially complete in TISAB solutions at pH 5. A slight decrease in peak height was observed at silicon (as sodium silicate) concentrations above 100 mg l^{-1}, which is rather surprising because the ionic strength of this solution is reasonably high. It seems likely that polymeric silicic acids are formed which hardly contribute to the ionic strength of the solution.

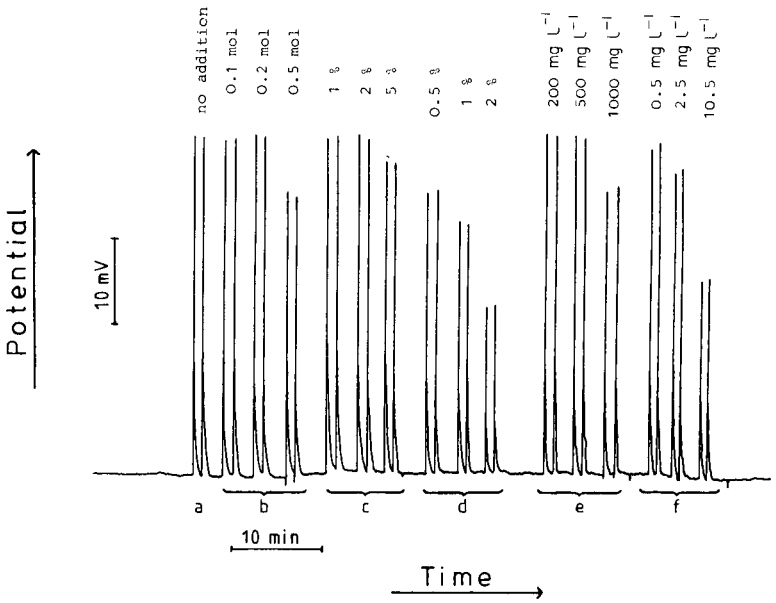

Fig. 9. Interference study with the modified TISAB-III at higher ionic strength. Decreased interference is observed for sodium (b), calcium (c) and iron (e), when compared to results given in Figs. 6, 8 and 11, respectively. The influence of Mg (d) and Al (f) persists (cf. Figs. 10 and 12). For comparison, the signal in absence of interference is also shown (a). Fluoride concentrations in samples and carrier as for Fig. 8.

Iron. Detailed studies are available concerning the complex formation between iron and fluoride at low pH [29, 47]. Investigations in connection with the interference of iron in potentiometry at the pH of the TISAB have produced divergent results. Bock and Strecker [9] observed no influence whereas Kauranen [41] obtained decreased fluoride activities above 100 mg l^{-1} iron(III), which was also found in the present work (Fig. 11). However, considering the ionic strength of the 500 mg l^{-1} iron solution (0.02 mol l^{-1}) and the appearance of transients, it may be suggested that the signal decrease is caused by ionic strength effects rather than complexation of fluoride. Measurements in which the modified TISAB was used confirmed that complexation is not serious (Fig. 9) because the interference is largely eliminated. This is indeed not surprising because hydrolysis of iron is expected in the presence of acetate.

Aluminium. The formation of fluoroaluminate complexes has been extensively studied [29, 47] and the problems associated with ion-selective electrode measurements have been evaluated [9, 10, 38]. Several modifications of the TISAB composition proposed to suppress the interference were found to be more or less successful [41, 43, 48]. Figure 12 shows the influence of aluminium on the fluoride activity in TISAB-III-containing solutions. Decreased signals are obtained above 1 mg l^{-1} aluminium(III) and this

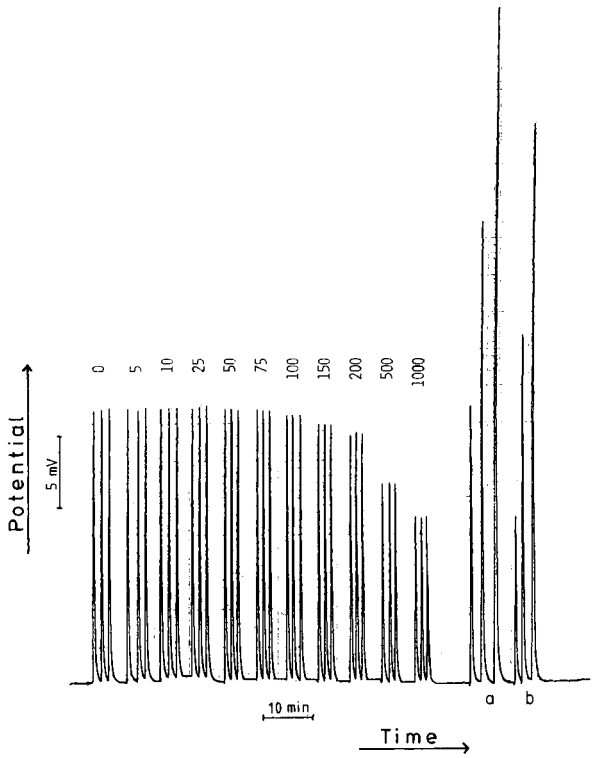

Fig. 10. Recording obtained for 500 $\mu g\ l^{-1}$ fluoride samples with increasing Mg^{2+} concentrations (5—1000 mg l^{-1}). Peaks (a) are the signals for samples containing 0.5, 1 and 2 mg l^{-1} fluoride; peaks (b) are for the same fluoride concentrations in presence of 1000 mg l^{-1} Mg^{2+}.

is largely independent of the fluoride concentrations investigated (Fig. 12B). As expected, the interference cannot be eliminated by using the modified TISAB-III (Fig. 9) because the concentration of CDTA was not altered. Preliminary results obtained with higher CDTA contents and other complexing reagents as tiron (4,5-dihydroxy-1,3-benzenedisulfonic acid) and Tris-buffer [tris(hydroxymethyl)aminomethane] indicate effective reduction of the interference even at levels above 100 mg l^{-1} aluminium(III).

Conclusions

The results reported above demonstrate the significance of considering the sample composition in preventing interferences in flow-injection potentiometry. Because the potential in the flow-injection method is taken at a fixed point on the response-time curve rather than at a steady state, any change in the response characteristics of the electrode causes errors. Therefore, special attention must be paid to variations in the response characteristics with respect to the sample composition. The transient phenomena observed when

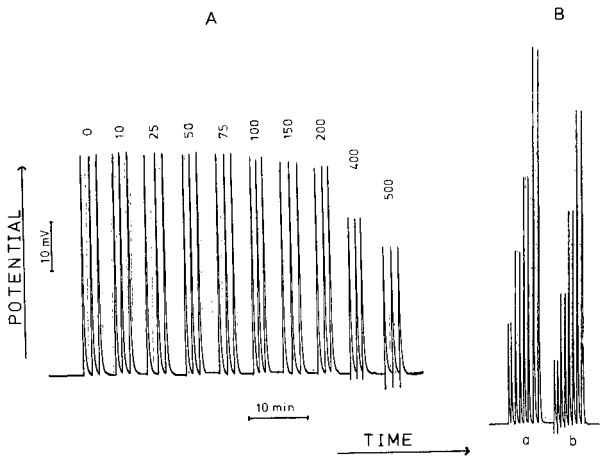

Fig. 11. (A) Influence of increasing iron concentration in the 10–500 mg l^{-1} range for samples containing 500 μg l^{-1} fluoride. (B) Influence of 500 mg l^{-1} Fe^{3+} at various fluoride concentrations: (a) peaks for samples containing 0.5, 1, 2 and 5 mg l^{-1} fluoride; (b) as for (a) with iron added.

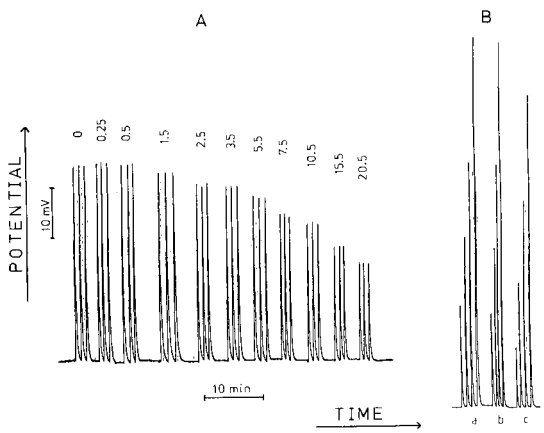

Fig. 12. (A) Influence of increasing aluminium concentration in the 0.25–20 mg l^{-1} range for samples containing 500 μg l^{-1} fluoride. (B) Influence of aluminium on signals at various fluoride concentrations: (a) 0.5, 1, 2 and 5 mg l^{-1} fluoride; (b) as (a) with 5.5 mg l^{-1} aluminium added; (c) as (a) with 20.5 mg l^{-1} aluminium added.

the injected samples were not adequately adjusted with respect to ionic strength and pH, are of general interest in the application of ion-selective electrodes in flow injection analysis.

The concept of matrix matching of standards and samples by means of TISAB is helpful but limited in application. The commercially available TISAB-III (Orion Research) is adequate for adjusting the pH but seems ill-suited to swamp out ionic-strength differences as far as applications to en-

acknowledged.

REFERENCES

1 M. S. Frant and J. W. Ross, Science, 154 (1966) 1553.
2 K. Srinivasan and G. A. Rechnitz, Anal. Chem., 40 (1968) 509.
3 J. M. Butler, in R. A. Durst (Ed.), Ion-Selective Electrodes, NBS Spec. Publ. No. 314, 1969, p. 148.
4 J. Buffle, N. Parthasaranthy and W. Haerdi, Anal. Chim. Acta, 68 (1974) 253.
5 R. Combes, P. Letellier and N. Baffier, Actual. Chim., 6 (1979) 27.
6 R. A. Durst, in H. Freiser (Ed.), Ion-Selective Electrodes in Analytical Chemistry, Vol. 1, 1978, p. 311.
7 M. S. Frant and J. W. Ross, Anal. Chem., 40 (1968) 1169.
8 J. Tušl, Anal. Chem., 41 (1969) 352.
9 R. Bock and S. Strecker, Fresenius Z. Anal. Chem., 235 (1968) 322.
10 B. Vickery and M. L. Vickery, Analyst, 101 (1976) 445.
11 J. Růžička and E. H. Hansen, Anal. Chim. Acta, 78 (1975) 145.
12 E. Pungor, Z. Fehér, G. Nagy, K. Toth, G. Horvai and M. Gratzl, Anal. Chim. Acta, 109 (1979) 1.
13 M. Trojanowicz and W. Matuszewski, Anal. Chim. Acta, 138 (1982) 71.
14 W. Frenzel and P. Brätter, Anal. Chim. Acta, 185 (1986) 127.
15 G. A. Rechnitz and H. F. Hameka, Fresenius Z. Anal. Chem., 214 (1965) 252.
16 W. E. Morf, E. Lindner and W. Simon, Anal. Chem., 47 (1975) 1596.
17 J. Mertens, P. Van den Winkel and D. L. Massart, Anal. Chem., 48 (1976) 272.
18 K. Cammann and G. A. Rechnitz, Anal. Chem., 48 (1976) 856.
19 E. Lindner, K. Tóth and E. Pungor, Anal. Chem., 48 (1976) 1071.
20 R. P. Buck, in H. Freiser (Ed.), Ion-Selective Electrodes in Analytical Chemistry, Vol. 1, 1978, p. 124.
21 W. J. van Oort and E. J. M. van Eerd, Anal. Chim. Acta, 155 (1983) 21.
22 D. Betteridge and J. Růžička, Talanta, 23 (1976) 409.
23 Handbook of Chemistry and Physics, CRC press, 66th edn., Palm Beach, 1985—86, D230.
24 P. L. Bailey, Analysis with Ion-Selective Electrodes, Heyden, London, 1976.
25 K. Cammann, Das Arbeiten mit Ionenselektiven Elektroden, Verlag Chemie, Weinheim, 1977, pp. 25, 199.
26 J. Bragg, Anal. Chem., 48 (1976) 1811.
27 L. Singer and W. D. Armstrong, Anal. Chem., 40 (1968) 613.
28 D. C. Cowell, Med. Lab. Sci., 35 (1978) 265.
29 G. A. Rechnitz, in R. A. Durst (Ed.), Ion-Selective Electrodes, NBS Spec. Publ. No. 314, 1969, p. 313.
30 W. E. Morf, in E. Pungor and I. Buzás (Eds.), 3. Proceedings of the Symposium on Ion-Selective Electrodes, Matrafüred, Hungary, Anal. Chem. Symp. Ser. 8, Elsevier, Amsterdam, (1980) 267.
31 K. Tóth, E. Lindner and E. Pungor, in E. Pungor and I. Buzás (Eds.), 3. Proceedings of the Symposium on Ion-Selective Electrodes, Matrafüred, Hungary, Anal. Chem. Symp. Ser. 8, Elsevier, Amsterdam, (1980) 135.

32 K. Cammann, in E. Pungor and E. Buzas (Eds.), Ion-Selective-Electrodes, Akademia Kiado, Budapest, 1977, p. 297.
33 W. E. Morf, Anal. Lett., 10 (1977) 87.
34 J. Vesely and K. Štulík, Anal. Chim. Acta, 73 (1974) 157.
35 L. G. Sillén and A. E. Martell, The Chemical Society, London, Spec. Publ. No. 17, 1964, pp. 43, 365, and Spec. Publ. No. 25, 1971, p. 247.
36 R. A. Durst, Am. Sci., 59 (1971) 353.
37 T. S. Light, in R. A. Durst (Ed.), Ion-selective Electrodes, NBS Spec. Publ. No. 314, 1969, p. 366.
38 J. E. Harwood, Water Res., 3 (1969) 273.
39 J. Tušl, Anal. Chem., 44 (1972) 1693.
40 P. E. Ke, L. W. Regier and H. E. Power, Anal. Chem., 41 (1969) 108.
41 P. Kauranen, Anal. Lett., 10 (1977) 451.
42 B. C. Jones, J. E. Heveran and B. Z. Senkowski, J. Pharm. Sci., 58 (1969) 607.
43 S. Tanikawa, H. Kirihara, N. Shiraiski, G. Nakayama and K. Kodama, Anal. Lett., 8 (1975) 879.
44 N. T. Crosby, J. Appl. Chem., 19 (1969) 100.
45 J. Tušl, J. Assoc. Off. Agric. Chem., 53 (1970) 267.
46 G. Reusmann and J. Westphalen, Staub-Reinhalt. Luft, 29 (1969) 413.
47 K. Srinivasan and G. A. Rechnitz, Anal. Chem., 40 (1968) 181, 1955.
48 H. Ballczo and M. Sager, Fresenius Z. Anal. Chem., 298 (1979) 382.

Analytica Chimica Acta, 187 (1986) 17—29
Elsevier Science Publishers B.V., Amsterdam — Printed in The Netherlands

TIME-DEPENDENT SELECTIVITY OF GLASS MEMBRANE ELECTRODES

MARK A. ARNOLD*, STAN A. ZISMAN and STEPHEN M. HISE
Department of Chemistry, University of Iowa, Iowa City, Iowa 52242 (U.S.A.)
(Received 15th April 1986)

SUMMARY

Time-dependent selectivities of both sodium- and hydrogen-selective glass membrane electrodes are investigated. Results indicate that these electrodes display little selectivity shortly after an increase or decrease in the activity of another cation at the electrode surface. Selectivity appears to increase as the potential approaches a steady-state value. A physical model is considered which accounts for the time-dependent selectivity with the generation of a chemical potential difference across the interface between the bulk solution and the hydrated glass layer.

Although the steady-state selectivity of glass membrane electrodes is well established [1—3], little attention has been given to the time-dependent selectivity properties of this class of membrane electrodes. Several reports indicate that glass-membrane electrodes exhibit a time-dependent response to cationic species which do not interfere in the steady-state mode. Friedman et al. [4] and Eisenman et al. [5] were the first to report a transient potentiometric response to activity increases in potassium ion at the surface of sodium-selective glass membrane electrodes. Rechnitz and Kugler [6] have reported similar transient responses with a sodium-selective glass electrode caused by changes in potassium and ammonium ion activity, and for a monovalent cation-selective glass electrode caused by changes in strontium and calcium ion activity. Karlberg [7] was the first to report a time-dependent response for pH-selective glass membrane electrodes. Karlberg showed significant transient potential excursions caused by increases in sodium ion activity in 2-propanol solutions with several commercial glass pH electrodes. Kennedy [8] described small potential transients in response to activity increases and decreases of certain divalent cations, using a pH glass electrode. Akimoto and Hozumi [9] reported transitory responses from both sodium- and pH-selective glass electrodes.

It is difficult to compare the results from the above-mentioned studies because the experimental conditions that were used in each case differ considerably. This paper describes results from an initial investigation into the time-dependent selectivity of glass membrane electrodes. An attempt was made to estimate the significance of this time-dependent selectivity under

0003-2670/86/$03.50 © 1986 Elsevier Science Publishers B.V.

common operating conditions for glass membrane electrodes. The results show significant transitory responses from sodium- and hydrogen-selective glass membrane electrodes caused by rapid increases and decreases in the activity of numerous cations at the electrode surface. The magnitudes of these transient signals range from 2 to 60 mV with durations of the order of minutes. Finally, the results are discussed in terms of a physical model which is proposed to explain the time-dependent selectivity of membrane electrodes.

EXPERIMENTAL

Apparatus and reagents

Electrode potentials were measured with a Corning model 12 pH/mV potentiometer in conjunction with a Sargent-Welch XKR strip-chart recorder. Miniature glass electrodes with tip diameters of 1.2 mm were used throughout (Microelectrodes, Inc., Londonberry, NH). Sodium-selective glass membrane electrodes (Model MI-420) were composed of Corning NA-0152 glass and pH-selective electrodes (Model MI-405) were based on Corning 0150 glass. A single junction, silver/silver chloride reference electrode (Orion Research, Cambridge, MA) was used in all experiments. A Fisher model 80 temperature bath was used with glass-jacketed cells to maintain solution temperatures at 25°C.

All solutions were prepared with distilled/deionized water which was treated with a Milli-Q three-chamber purification unit immediately before use. All salts were of analytical-grade purity and were appropriately dried before use.

Procedures

Figure 1 shows a schematic representation of the experimental arrangement used. A Technicon AutoAnalyzer II proportioning pump was used to pump the solution of interest over the electrode surface. A three-way valve, composed of teflon (Ace, model 1102), was used to achieve rapid change from one solution to another and solutions were pumped through small-bore, thick-walled teflon tubing (0.5 mm i.d.; 1.8 mm o.d.). In some experi-

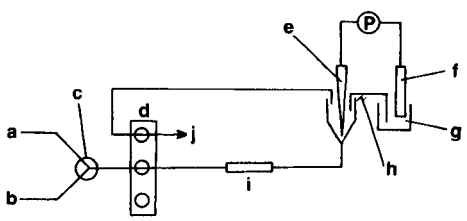

Fig. 1. Schematic diagram of experimental arrangement: (a) background solution; (b) test solution; (c) valve; (d) pump; (e) glass electrode; (f) reference electrode; (g) 3 M KCl; (h) salt bridge; (i) microporous teflon tubing; (j) waste.

ments, the valve was removed and the small-bore teflon tubing was simply moved from one solution to another. The distance from the sample container to the electrode was kept as short as possible (approximately 30 cm) to minimize solution dispersion [10]. A short length of microporous teflon tubing (Gore & Associates, Elkton, MD) was positioned between the pump and the electrode to release any trapped air bubbles before they reached the electrode [11]. Solution flow rates were measured periodically by measuring the volume of water displaced during a specified time interval. Unless otherwise noted, flow rates were 1.4 ml min^{-1} throughout.

Glass electrodes were positioned inside a disposable, polyethylene pipet tip and the solution was allowed to flow into the tip from the bottom and over the electrode surface (see Fig. 1). Solution reaching the top of the pipet tip was removed by a second line from the proportioning pump. The electrochemical cell included the glass electrode in the flowing solution and a reference electrode which was placed in 3 M potassium chloride. A thin salt bridge, composed of 3 M potassium chloride in an agar matrix, was positioned between these solutions to complete the cell. The coaxial shielding around the cable of the glass electrode was grounded to reduce noise levels.

In a typical experiment, a background solution was pumped over the electrode surface until a steady-state potential was attained. At an appropriate time, the solution being pumped over the electrode surface was changed to the test solution, which was identical to the background solution except for the addition of an ion of interest at a specified concentration. After a new steady-state potential had been obtained with this test solution, the system was changed back to the original background solution. Electrode potentials were continuously monitored and recorded on the strip-chart recorder. Potential values were obtained either by following the meter directly or by extrapolating from the recorder output. In the latter case, the recorder was calibrated with a known voltage prior to the experiment.

RESULTS AND DISCUSSION

Transient response of sodium-selective glass membrane electrode

The first experiment was designed to observe the effect of increases and decreases of potassium and ammonium ion concentrations on the potentiometric response of the sodium-selective glass membrane electrode. The electrode was initially equilibrated with 54 mM potassium chloride and the potentiometric response was monitored as the potassium-ion activity was rapidly decreased to 10 mM. After this initial response, the potential was monitored as the potassium ion activity was returned to 54 mM. Figure 2 shows the type of potentiometric response obtained. When the potassium-ion activity was stepped from 54 to 10 mM, a negative deviation in the potential was observed and a positive deviation was measured when the potassium-ion activity was increased from 10 to 54 mM. The maximum potential excursion for the activity decrease was -24.2 ± 0.3 mV and that

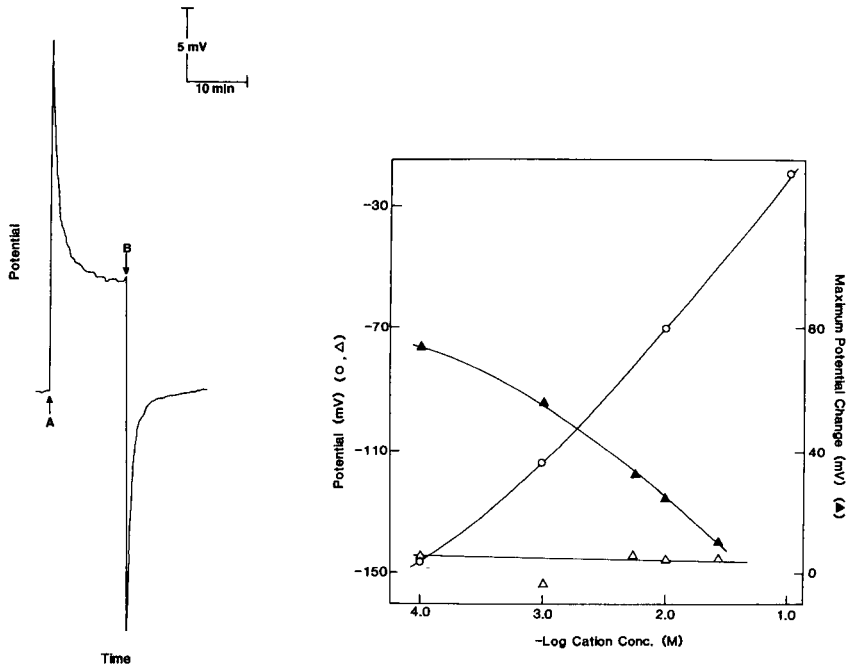

Fig. 2. Potential/time trace for the sodium-selective electrode: (A) 10 mM KCl; (B) 54 mM KCl.

Fig. 3. Steady-state responses and maximum potential excursions for the sodium glass electrode: (○) sodium (steady-state); (△) potassium (steady-state); (▲) potassium (transient).

for the activity increase was 24.6 ± 0.6 mV. Approximately 6 s was required to reach the maximum transient potential, and the time required to re-establish a steady-state potential was about 10 min. In comparison, the response time of the meter-recorder combination for a similar magnitude of potential change is only 3 s as measured with a common square-wave generator with a potential rise-time of less than 0.2 s.

Similar results were obtained when ammonium-ion activity was rapidly changed at the electrode surface. For changes in ammonium-ion activity from 54 to 10 mM, an average transitory maximum of − 18.4 ± 0.5 mV was measured and for activity increases from 10 to 54 mM, a maximum potential excursion of 17.9 ± 0.3 mV was observed. After each change in ammonium-ion activity, the potential maximum was achieved in 5—6 s, and 4—8 min were required to establish a steady-state potential.

Under the conditions of the above-mentioned experiment, the membrane potentials are governed by solution pH and potassium- or ammonium-ion activities. Based on established selectivity coefficients for this glass matrix, $K^{Pot}(H^+/K^+)$ = 0.0001; $K^{Pot}(H^+/NH_4^+)$ = 0.00003 [12], only slight potentiometric responses are expected from the above-mentioned activity steps. As

shown in Fig. 2, however, considerable potentiometric responses were observed under these conditions. These transient responses can be interpreted as time-dependent selectivities for the electrode system. Immediately after the change in cation activity, the electrode displays little or no selectivity and a large potential change is observed. As the response continues, the selectivity of the electrode appears to increase as the response decays toward a steady-state potential. A maximum selectivity is eventually obtained and a new steady-state position is established. The maximum selectivity is described by the well known steady-state selectivity coefficient and the final steady-state potential is that predicted by the extended Nernst equation including this steady-state selectivity coefficient.

It is interesting to note the dynamic response of the sodium-selective glass electrode to changes in sodium-ion activity. Steps from 0.01 to 0.1 M generate an initial potential change that rapidly peaks and then slowly decays to a final steady-state value. A total response time of 3 min was required to achieve a steady-state potential and the difference between the final steady-state potential and the peak potential (the overshoot potential) was less than 1 mV. For a change in sodium-ion activity from 0.001 to 0.01 M, larger potential overshoots (2.5 mV) and longer equilibration times (10 min) were observed. Much like the transient responses to interfering cations, the overall dynamic response to changes in sodium-ion activity appears to involve two processes, a quick initial potential change followed by a slower approach to steady state.

The steady-state electrode response to sodium and potassium ions and the maximum potential excursion of the transient response for various changes in potassium-ion activity are compared in Fig. 3. The transitory responses in this experiment were obtained by equilibrating the electrode in 54 mM potassium chloride and rapidly stepping the potassium activity down to the indicated value. The steady-state potential response for potassium shown in Fig. 3 is the steady-state potential obtained at the end of the transitory response at the corresponding potassium-ion activity. Comparison of the transient and steady-state responses to potassium ions shows that, although the electrode displays considerable selectivity for sodium over potassium ions under steady-state conditions, the transitory response displays little selectivity. Figure 3 also shows that, as the cation activity deviates further from the initial equilibration condition, the magnitude of the potential excursion increases.

In order to see if a constant sodium-ion activity affected the transitory response for changes in potassium-ion activity, a sodium-selective glass electrode was equilibrated in 5 mM sodium chloride and the electrode response was monitored as the potassium-ion activity was changed from zero to 100 mM at the glass surface with no change in the sodium-ion activity. A large transitory response was observed with a potential excursion maximum of $+46.3 \pm 0.7$ mV. A second potential excursion of -34.5 ± 0.4 mV was recorded when the potassium-ion activity was returned to zero. The effect of potassium-ion activity on the maximum potential excursion with a

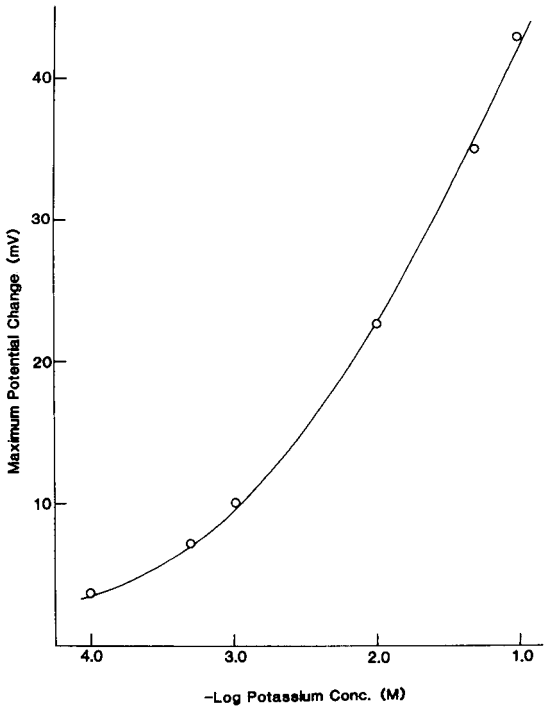

Fig. 4. Maximum potential excursions for potassium with a constant background of sodium-ion activity at a sodium-selective electrode.

constant background sodium-ion activity is shown in Fig. 4. A non-linear response was obtained.

In each of the above-mentioned experiments, the ionic strength of the transient generating solution was different than that of the initial equilibration solution. To see if the transient response was caused by this ionic strength difference, a change in potassium-ion activity was generated at the surface of the glass electrode while the ionic strength was varied only slightly; the initial equilibration solution was composed of 0.1 M Tris-HCl and 0.1 mM sodium acetate at pH 7.5 and the transient-generating solution was the same except that 1 mM potassium chloride was added. The ionic strength of the equilibration buffer was 0.100 M and that for the transient-producing solution was 0.101 M. A strong transitory signal was observed under these conditions which was similar to transient signals without the ionic strength control.

To ensure that the transient phenomenon is truly an effect associated with the glass membrane and not some type of ionic phenomenon that occurs at the salt bridge, the transient response of the glass electrode was monitored with a solid-state silver/silver chloride electrode in place of the glass-membrane electrode. In this case, the equilibration solution was composed of 0.1 M Tris-HCl with 5 mM sodium nitrate and the activity-step solution

was the same as the equilibration solution but with 0.1 M potassium nitrate added. Nitrate salts were required in this experiment to avoid changes in chloride-ion activity which would cause potential changes at the silver/silver chloride electrode. When the sodium-selective glass electrode was used, transient responses were obtained which were identical to those measured for the chloride salts. No response was found, however, when the glass electrode was replaced with the chloride electrode. The silver/silver chloride electrode used was constructed to match closely the dimensions of the glass electrode in order to maintain similar hydrodynamic conditions in the vicinity of the electrode surface.

Table 1 summarizes the transient responses that were obtained for various cations. These transient signals were generated by using an initial equilibration buffer composed of 0.1 M Tris-HCl/1 mM sodium chloride at pH 7.5 and changing to a 10 mM solution of the cation of interest in the same buffered 1 mM sodium chloride. In all cases, the chloride salt of the cation was used. Values correspond to the maximum potential excursion for the initial transient response caused by the rapid introduction of the cation at the electrode surface and for the reverse transient response caused by the rapid removal of the cation from the electrode surface. The reported duration of the transient signals corresponds to the time required for half of the transient decay.

As can be seen, all cations tested gave a transient response which suggests that the effect is general for cations. The response to lithium ions was small under these conditions. In fact, measurement of a reverse transient response was impossible. The time-dependent response to lithium is complicated by the fact that the glass membrane selectivity is such that a significant steady-state response to the change in lithium-ion activity is observed under these conditions. Initial transients were measured as the extent of overshoot

TABLE 1

Transient response to various cations[a]

Cation	Maximum potential excursion (mV)		Duration of transient signal (min)[b]	
	Introduction	Removal	Introduction	Removal
K^+	50.7 ± 0.4	35.4 ± 3.8	1.8 ± 0.5	1.4 ± 0.4
Li^+	2.4 ± 0.2	—	2.0 ± 0.5	—
NH_4^+	34.6 ± 0.8	26.7 ± 2.1	1.1 ± 0.3	1.1 ± 0.1
Mg^{2+}	5.9 ± 0.2	4.7 ± 0.2	1.0 ± 0.7	1.3 ± 0.6
Ca^{2+}	13.4 ± 0.5	9.4 ± 0.8	0.8 ± 0.1	1.3 ± 0.1
Ba^{2+}	20.5 ± 0.9	12.7 ± 1.0	1.1 ± 0.3	1.5 ± 0.2

[a]Each value represents an average of at least three determinations. Measurements were made with a 0.1 M Tris-HCl/1.0 mM sodium chloride, pH 7.5 buffer as the background solution and with cation-activity steps from zero to 10.0 mM. [b]Corresponds to transient width at 1/2 the maximum potential excursion.

above the final steady-state potential. No overshoot was observed during the removal of lithium ions from the electrode surface.

Transient response of pH-selective glass membrane electrodes

In this study concerning the time-dependent selectivity of glass pH electrodes, experiments were first done to verify the results of Kennedy [8], who used unbuffered solutions. It was thought that his small potential changes might be due to actual pH changes, but our results confirmed those originally reported by Kennedy. Small potential transients (0.9—16.9 mV) which decayed fairly slowly to equilibrium values were measured when micromolar concentrations of transition metals were rapidly introduced at the electrode surface; and reverse transients were found when these cations were removed from the electrode surface. Because unbuffered solutions were used, pH adjustments were difficult which made these experiments time-consuming and difficult to perform.

To improve the pH stability, a 0.1 M Tris-HCl (pH 7.5) buffer with 0.10 mM sodium acetate was used as the equilibration solution. Figure 5 shows the potential/time response of the glass pH electrode when the potassium-ion activity was repeatedly changed from zero (position A) to 0.25 mM (position B). Approximately 2 min were required for the potential changes to decay completely to a steady-state value. Average peak potential changes were 19.7 ± 0.5 mV for activity increases and −14.2 ± 0.6 mV for activity decreases which correspond to apparent pH changes of 0.33 and 0.24, respectively. The maximum potential excursion depended on the activity of the potassium ion, as shown in Fig. 6. A potassium-ion activity of only 0.4 mM generated a 30-mV potential excursion which corresponds to an apparent pH change of 0.5.

Comparison of the transient responses for potassium-ion activity steps using pH- and sodium-selective glass electrodes reveals similar maximum potential excursions. The decay process, however, is much faster with the pH electrode.

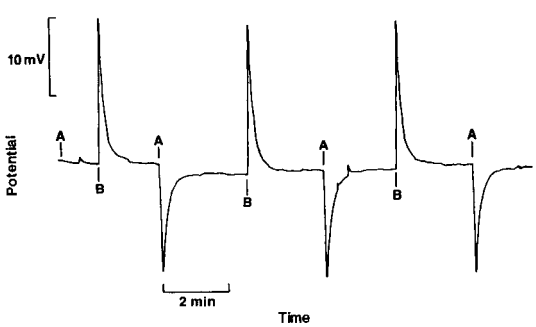

Fig. 5. Transient response of glass pH electrode: (A) 0.1 M Tris-HCl/0.1 mM sodium chloride, pH 7.5; (B) 0.1 M Tris-HCl/0.1 mM sodium chloride/0.25 mM potassium chloride, pH 7.5.

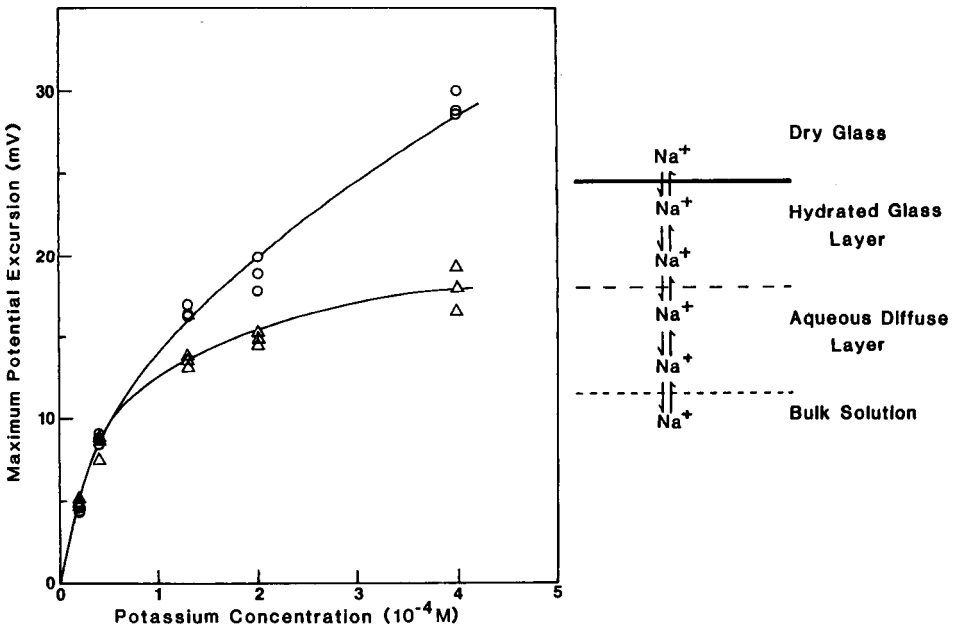

Fig. 6. Effect of potassium-ion concentration on the maximum potential excursion of the pH electrode: (○) introduction; (△) removal of potassium.

Fig. 7. Various dynamic equilibria at the surface of a glass membrane electrode.

Physical model for time-dependent selectivity

Several attempts have been made to explain the time-dependent selectivity of glass membrane electrodes. Rechnitz [13] suggested that differences in the time dependency of equilibria that involve ion exchange at the membrane surface and ion mobility within the hydrated glass layer are principally responsible for the observed transient behavior. Morf [14] proposed a mathematical model to describe the transient response of glass membrane electrodes. This latter model treats the glass membrane as a heterogeneous layer with two distinct selectivities. Qualitatively, Morf's model matches the explanation proposed by Rechnitz [13] if the hydrated layer displays little or no selectivity against the transient-producing cation while the bulk, dry glass layer possesses a high degree of selectivity for the primary ion.

Gratzl et al. [15] provided a convincing model to explain similar transitory responses of solid-state membrane electrodes. Their model involves initial adsorption of the interfering ion on the solid-state membrane which is followed by desorption of the primary ion in order to maintain electroneutrality on the membrane. Subsequently, the desorbed ions diffuse away from the electrode surface through the stagnant diffusion layer. The initial desorption of the primary ion creates a high activity of the primary ion immediately at the electrode surface which generates the initial transient response. The

transient decay is governed by the rate of primary ion diffusion through the diffusion layer. Application of this particular model to the transient response of glass electrodes seems inappropriate. Slow transient decay rates for glass electrodes suggest that ion transport in the glass hydrated region is important as opposed to transport in the aqueous diffusion region. Hence, slow transport of the transient-generating cation through the hydrated glass layer would be expected to result in transients with slow initial potential rises as well as slow potential decays.

Karlberg [7] and Isard [16] suggested that a concentration gradient across the hydrated region of the glass membrane initiates the potential excursion with the subsequent potential decay caused by the adjustment of this ionic gradient with time. For the specific case of the sodium-selective glass electrode, the electrode/solution interface can be considered to be composed of layers involving the bulk solution, the stagnant aqueous diffusion layer, the hydrated glass layer, and the bulk dry glass. Under steady-state conditions, several dynamic equilibria are established between ions in the bulk solution and these various layers, as is shown in Fig. 7. In the present treatment, the processes which occur in the diffuse layer will be assumed to be fast with respect to other processes at the electrode surface. Furthermore, only the interaction between sodium and potassium ions at the electrode surface will be considered, although it must be recognized that hydrogen ions participate in the same dynamic equilibria as described for sodium ions.

Initially, the electrode is in equilibrium with solution cations and a steady-state potential is maintained. With the instantaneous arrival of potassium ions at the electrode surface, a potassium-ion concentration gradient is generated across the aqueous solution/hydrated glass layer interface. This difference in chemical potential is within the overall electrochemical cell, and hence, is a measurable potential that corresponds to the initial potential excursion of the transient response. Subsequently, mass transport of potassium ions into the hydrated glass layer occurs to eliminate this chemical potential difference. As mass transport continues, the chemical potential across the hydrated layer decreases which corresponds to the decrease in the transitory response. Eventually, the chemical potential caused by this concentration gradient will be zero when potassium ions are evenly distributed in the hydrated region.

Considering the lack of uptake of anions into the various layers of the glass matrix [17], an equivalent number of sodium ions must leave the hydrated layer as potassium ions enter in order to maintain electroneutrality in this region. Accordingly, the sodium-ion activities at the hydrated/dry glass interface must adjust to this modification of sodium-ion activity in the hydrated layer such that the ion-exchange equilibrium at this interface is maintained. Therefore, as the potassium-ion activity in the hydrated layer increases, sodium-ion activities in both the dry and hydrated layers will decrease. The ratio of these sodium-ion activities and the corresponding boundary potential should remain constant according to the ion-exchange

equilibrium. Hence, the same steady-state potential is attained after the new equilibrium is established. This treatment assumes absolute selectivity for sodium over potassium ions under steady-state conditions, which corresponds to no interaction between the dry glass layer and potassium ions in the hydrated region.

A similar transitory potential response is expected when a difference in chemical potential is established across the hydrated layer/solution interface as potassium ions are rapidly removed from the surrounding aqueous solution. In comparison to the concentration gradient caused by an increase in potassium-ion activity, this latter gradient is in the opposite direction. Mass transport of potassium ions out of the hydrated region occurs to eliminate the gradient and sodium ions enter the hydrated layer to maintain electroneutrality. Accordingly, the sodium-ion activities at the hydrated/dry glass interface must adjust to maintain the ion-exchange equilibrium and the corresponding boundary potential.

Several of the above experimental observations support this model. First, the transient signal is observed for both increasing and decreasing cation-activity steps which suggests that the ion environment of the glass membrane is significantly modified during the transient response. Such a modification is expected from the model owing to the build-up or removal of cations in the hydrated glass layer. As the model predicts, positive and negative potential excursions are observed for cation-activity increases and decreases, respectively.

In addition, the proposed model is supported by the experimental observations of Vitiello et al. [18], Czaban [19] and Karlberg [7] which showed that the transient response of both sodium- and hydrogen-selective glass membrane electrodes could be eliminated by removing the hydrated layer and that the transient response returned as the hydrated layer slowly grew. Short-lived transients were expected for thin hydrated layers because less time was required to equilibrate this small region. The present results show faster decay for potassium-ion transients with the hydrogen electrode than with the sodium electrode; this is expected because the thickness of the hydrated layer for pH-selective glasses is known to be thinner than that for sodium-selective glasses [20].

The present results indicate that diffusion of the transient-producing cation is not the rate-limiting process. If such diffusion were the major mechanism of mass transport, a direct dependence between ionic size and transient decay rate would be expected based on slower diffusion coefficients for larger cations. Such a dependency was not observed for the cations that were tested (see Table 1). Little variation in transient relaxation rates with respect to cation size was observed for both increases and decreases in activity.

The proposed model is simply a starting point in understanding this phenomenon. The effects of diffusion potentials and currents in the hydrated glass layer during the transient process are not considered here. There is no

reason to impose a zero-current restriction on the transient response because of the nonequilibrium status of the system [17, 21]. A zero-current condition will only be valid if the sodium- and potassium-ion fluxes are exactly matched. Otherwise, a finite current will be established with the net flow of ionic species. Also, this model does not consider the complex structure which has been proposed for the pH-selective glass membrane [20—22].

The results presented clearly demonstrate the significance of the time-dependent selectivities of both sodium- and hydrogen-selective glass membrane electrodes. The time-dependent selectivities are observed under typical operating conditions, such as reasonable flow rates and moderate interferent concentrations. Investigation of such phenomenon will be continued in order to establish the effect of this time-dependent selectivity on the accuracy of glass-membrane electrodes as detectors in automated analysis arrangements. In many automated systems, the electrode potential is obtained in a transient mode because the sample passes by the electrode before a steady-state potential can be established. The results presented here suggest that under such conditions the lack of selectivity will result in considerable interference and inaccuracies.

S. A. Zisman was visiting from the Department of Physical Science, Cameron University, Lawton, OK, as a 1984 Summer Undergraduate Research Fellow. S. M. Hise was visiting from Central High School, Davenport, IA, as a participant in the 1985 Summer Research Training Program. Acknowledgement is made to the donors of The Petroleum Research Fund, administered by the American Chemical Society, for partial support of this research. This work was also partially supported by a Northwest Area Foundation Grant of Research Corporation.

REFERENCES

1 A. K. Covington, Ion-Selective Electrode Methodology, Vol. I, CRC Press, Boca Raton, FL, 1979, Chap. 5.
2 P. L. Bailey, Analysis with Ion-Selective Electrodes, Heyden Press, Philadelphia, PA, 1980, Chap. 4.
3 J. Koryta, Ion-Selective Electrodes, Cambridge University Press, Cambridge, 1975, Chap. 4.
4 S. M. Friedman, J. D. Jamieson, J. A. M. Hinke and C. L. Friedman, Science, 130 (1959) 1250.
5 G. Eisenman, R. Bates, G. Mattock and S. M. Friedman, The Glass Electrode, Interscience Publishers, New York, 1966.
6 G. A. Rechnitz and G. C. Kugler, Anal. Chem., 39 (1967) 1682.
7 B. Karlberg, J. Electroanal. Chem. Interfacial Electrochem., 42 (1973) 115.
8 C. D. Kennedy, Analyst, 108 (1983) 1003.
9 N. Akimoto and K. Hozumi, Bunseki Kagaku, 25 (1976) 554.
10 J. T. Vanderslice, G. R. Beecher and A. G. Rosenfeld, Anal. Chem., 56 (1984) 292.
11 G. B. Martin, H. K. Cho and M. E. Meyerhoff, Anal. Chem., 56 (1984) 2612.
12 G. Eisenman, Glass Electrodes for Hydrogen and Other Cations: Principles and Practice, M. Dekker, New York, 1967.

13 G. A. Rechnitz, in R. A. Durst (Ed.), Ion-Selective Electrodes, NBS Special Publ. 314, 1969.
14 W. E. Morf, Anal. Lett., 10 (1977) 87.
15 M. Gratzl, E. Lindner and E. Pungor, Anal. Chem., 57 (1985) 1506.
16 J. O. Isard, Phys. Chem. Glasses, 17 (1976) 1.
17 R. P. Buck, J. Electroanal. Chem. Interfacial Electrochem., 18 (1968) 363.
18 J. D. Vitiello, S. D. Kearney, J. D. Czaban and A. D. Cormier, AACC National Meeting Abstract, Clin. Chem., 26 (1980) 1021, Abstract Number 328.
19 J. D. Czaban, Instrumentation Laboratory, Inc., personal communication, 1985.
20 A. Wikby, Talanta, 22 (1975) 663.
21 G. Johansson, B. Karlberg and A. Wikby, Talanta, 22 (1975) 953.
22 F. G. K. Baucke, J. Non-Cryst. Solids, 14 (1974) 13; 19 (1975) 75.

Analytica Chimica Acta, 187 (1986) 31—37
Elsevier Science Publishers B.V., Amsterdam — Printed in The Netherlands

IMMOBILIZATION OF CREATININE DEIMINASE ON A SUBSTITUTED POLY(METHYLGLUTAMATE) MEMBRANE AND ITS USE IN A CREATININE SENSOR

IZUMI KUBO

Fuji Electric Corporate Research and Development Ltd., 2-2-1 Nagasaka, Yokosuka 240-01 (Japan)

ISAO KARUBE*

Research Laboratory of Resources Utilization, Tokyo Institute of Technology, 4259 Nagatsuta, Midoriku, Yokohama 227 (Japan)

(Received 18th February 1986)

SUMMARY

A substituted poly(γ-methyl-L-glutamate) membrane is used for chemical immobilization of creatinine deiminase. The permeability of the membrane is controlled by the conditions used for membrane preparation. The creatinine sensor based on the immobilized enzyme membrane with immobilized nitrifying bacteria and an oxygen electrode exhibited greater sensitivity than the sensor previously reported which had a 1,8-diamino-4-aminomethyloctane membrane. The sensor gave a linear response to creatinine over the range 1—10 mg dl^{-1}; responses remained stable for two weeks.

Creatinine is a very important diagnostic index of kidney function, and biosensors for creatinine determination which depend on potentiometric detection have been reported [1, 2]. A hybrid creatinine sensor based on an amperometric detection method has also been described [3]. Creatinine deiminase in this sensor was immobilized on a triamine membrane containing 1,8-diamino-4-aminomethyloctane. It had good selectivity for creatinine and was not affected by other substances commonly found in biological fluids. The activity of the immobilized creatinine deiminase, however, was too low for clinical application. The concentration of creatinine in normal human blood is 0.5—1.0 mg dl^{-1}, which is below the detection limit of this sensor.

A polymer based on partially transesterified poly(γ-methyl-L-glutamate) (PMG) for use as an enzyme carrier has been reported [4]. The modified polymer possesses functional groups that can react with enzyme amino groups in organic solvents [5]. The enzyme/polymer conjugate can be fabricated into laminar porous sheets that retain high activity. Urease was immobilized on this polymer and exhibited enhanced activity and stability [5]. This paper describes the immobilization of creatinine deiminase onto the polymer. The creatinine deiminase membrane obtained is utilized in a hybrid creatinine sensor.

0003-2670/86/$03.50 © 1986 Elsevier Science Publishers B.V.

Creatinine deiminase catalyzes the reaction [1]:

Creatinine → *N*-methylhydantoin + NH_3

In the hybrid creatinine sensor, the ammonia released is oxidized to nitrite and nitrate by nitrifying bacteria, and the resulting consumption of oxygen is monitored by an oxygen electrode. The principles behind the hybrid creatinine sensor were discussed in detail previously [3]. Adoption of the PMG membrane improved the detection limit of the creatinine sensor.

EXPERIMENTAL

Materials

Creatinine deiminase (E.C. 3.5.4.21, 2.3 U mg^{-1}) was kindly donated by Kyowa Hakko Kogyo Co.; PMG (A-2000) was purchased from Ajinomoto Co. All other reagents were commercially available and solvents were purified by distillation. The nitrifying bacteria were as reported previously [3].

Derivatization of PMG. The PMG was transesterified to form poly(γ-trichloroethylglutamate) (PTG) [2] as described previously [4]. The PTG obtained was found by elemental analysis to have a content of transesterified groups (n) of 72% and a residual methylester (m) content of 28%. After modification, i.r. C—Cl absorption peaks appeared at 710 cm^{-1} and 795 cm^{-1} and the polymer showed greater solubility in organic solvents than the original PMG.

Preparation of immobilized creatinine deiminase membrane. Creatinine deiminase (10 mg) and 100 mg of PTG were dissolved in 1 ml of either dimethylformamide (DMF) or dimethylsulfoxide (DMSO) solvent. The polymer and enzyme solution were mixed well and cast onto a glass plate, then immediately immersed in 100 ml of 0.01 M phosphate buffer, pH 7.0, at a temperature above 10°C, for 1 h.

Apparatus for creatinine sensor

The hybrid creatinine sensor consisted of an oxygen electrode, immobilized nitrifying bacteria, an immobilized creatinine deiminase membrane and a dialysis membrane, as described previously [3]. The sensor was placed in a flow cell (0.2-ml volume) filled with oxygen-saturated buffer solution (0.01 M borate/HCl, pH 8.5) and maintained at 30°C with a thermostated water circulator. The flow rate of the buffer solution was 1 ml min^{-1}. When the sensor was placed in the buffer solution, an initial current was observed resulting from the endogenous respiration of the immobilized bacteria (Fig. 1). When 100 μl of creatinine sample solution was injected through the injection port into the cell, the current output decreased immediately and reached a steady state within 1 min (Fig. 1). The difference between the initial and steady-state currents was used as a measure of creatinine concentration.

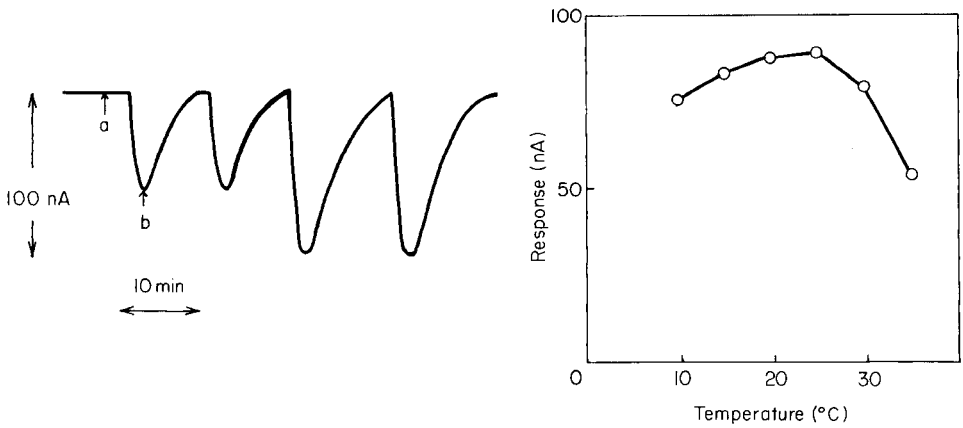

Fig. 1. Typical responses of the hybrid creatinine sensor: (a) initial current; (b) maximum response after injection of creatinine. Conditions: pH 8.5 (0.01 M borate/HCl), 30° C, flow rate 1 ml min^{-1}.

Fig. 2. Effect of casting temperature on the response of the creatinine sensor. Operating conditions as in Fig. 1.

RESULTS AND DISCUSSION

Effect of solvent on immobilization

During the immobilization procedure, PTG and creatinine deiminase were dissolved in an organic solvent. It was expected that inactivation or denaturation of the enzyme by organic solvents would occur; DMF and DMSO were chosen for use because of their water solubility and high boiling point. Creatinine deiminase dissolved in DMF lost its activity after the solvent was removed and the residue dissolved in water. However the enzyme dissolved in DMSO gave a 90% activity yield (specific activity 2.1 μmol min^{-1}) compared to the free enzyme. When the membrane was prepared from enzyme and polymer dissolved in DMF, no activity was detected in the membrane, but the membrane prepared with DMSO had creatinine deiminase activity. In the previous study, urease was also inactivated by DMF [5] but glucose oxidase and alcohol oxidase retain their activity in DMF. Urease and creatinine deiminase both catalyze reactions that produce ammonia and it is therefore suggested that traces of amine present in DMF may inactivate urease or creatinine deiminase.

Immobilized creatinine deiminase membrane

Several factors must be considered in the construction of an immobilized enzyme membrane. Obviously, the activity of the immobilized enzyme, be it the specific activity or the activity yield, is greatly dependent on the immobilization methods used, the boiling point and dielectric constant of the chosen solvent and the temperature during immobilization. However, drastic

variations in the observed response of the sensor can be produced by the structure of the membrane and its permeability to the substrates and products of the enzyme reaction. The membrane used in this study is porous to water, possessing a highly porous micro-structure, the composition of which is determined by the conditions used during casting of the membrane and the initial concentration of the polymer mixture. The effect of the polymer mixture concentration on the observed activity of the sensor, and any resultant changes in the membrane micro-structure, were therefore examined. Polymer mixture containing PTG and enzyme (10 mg ml^{-1}), was cast onto a glass plate and immersed in buffer solution at 20° C. A creatinine sensor was constructed from this membrane and used to assay creatinine solution (5 mg dl^{-1}) at pH 8.5. The slope of the calibration graph for ammonia was 0.96 μA l mol^{-1} under the same conditions. The activity yield and specific activity of the enzyme membrane was calculated on the basis of this calibration graph.

As shown in Table 1, an increase in the concentration of PTG caused a drop in response until, at 15% polymer, no response was observed. The greatest response was observed at 5% PTG. Membrane thickness varied with polymer concentration, as shown in Table 1, therefore it was assumed that the membrane formed from 2.5% polymer is too thin to permit the immobilization of sufficient enzyme. For membranes formed from a high concentration of polymer, the thickness of the membrane limits the diffusion of substrates and products of the enzyme reaction. It was found that the amount of enzyme immobilized on the membrane was sufficient because the observed response of the sensor was not increased by raising the concentration of enzyme during the membrane casting procedure. All other experiments were done with 5% PTG membranes; in this membrane the activity yield was 20%.

The effect of temperature during membrane preparation was also examined. The response increased with increasing temperature up to 25° C but decreased above this temperature (Fig. 2). The pore size of membranes prepared at higher temperatures appeared to be larger. Figure 3 shows electron micrographs of membranes prepared at different temperatures. It was thought that

TABLE 1

Effect of PTG concentration on the electrode response[a]

PTG concentration (%)	Response (nA)	Membrane thickness (μm)	Specific activity (μmol min^{-1})	Activity yield (%)
2.5	64	3.5	0.35	15
5.0	86	8.0	0.46	20
10	52	11	0.28	12
15	0	15	0.00	0

[a]1 ml of the cited enzyme solution was used in all preparations.

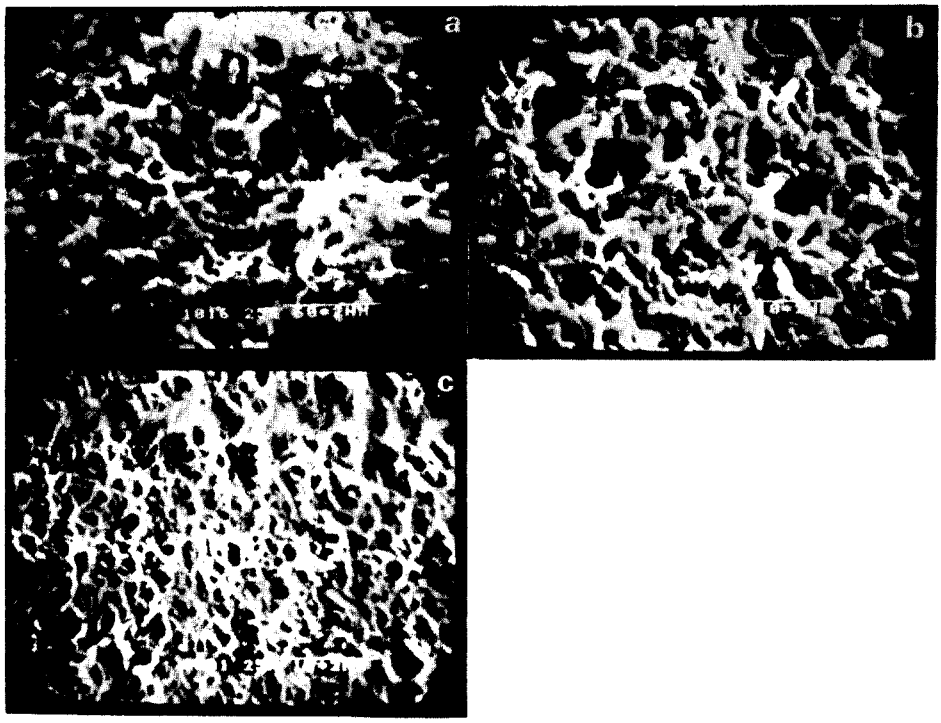

Fig. 3. Electron micrographs of membranes cast at: (a) 30° C (× 5000); (b) 20° C (× 10 000); (c) 10° C (× 10 000).

at high temperature, rapid elution of DMSO into the buffer occurred, giving rise to a fast agglutination reaction and large pore size. Diffusion of substrates and products across the membrane should increase with a large pore size, producing a faster response by the sensor. Denaturation of the enzyme took place at temperatures above 30° C and so all other experiments were done with membranes prepared at 20° C.

Response of hybrid creatinine sensor

The response time of the sensor to creatinine addition was ca. 60 s and was independent of creatinine concentration. The recovery time, however, depended on the creatinine concentration and was in the 7—10 min range. A linear relationship was observed between the change in current output and creatinine concentration in the range 1—10 mg dl^{-1}, as shown in Fig. 4, above which the signal was less sensitive. The detection limit (2σ) was 0.5 mg dl^{-1}, but the response was only 70% of the expected value. This is the effect of slight alteration of flow rate on sample injection. Therefore the linear range might be extended to 0.5 mg dl^{-1} by improvement of the apparatus.

Substances commonly found in biological fluids were investigated for their interference on the creatinine sensor. Citrate (50 mg dl^{-1}), oxalate

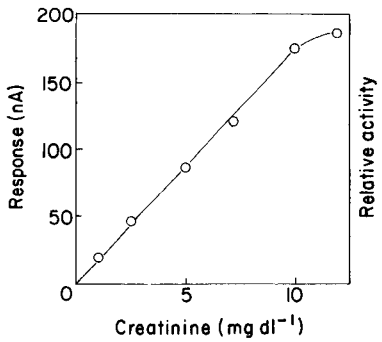

Fig. 4. Calibration graph for creatinine. Conditions as for Fig. 1.

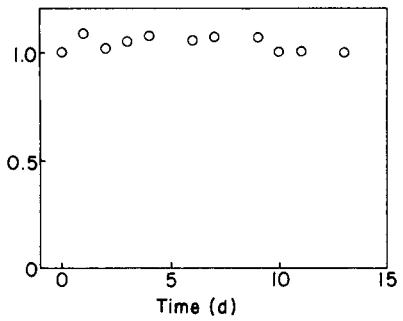

Fig. 5. Stability of the creatinine sensor over 15 days (2.5 mg dl^{-1} creatinine).

TABLE 2

Comparison of characteristics of hybrid creatinine electrodes based on triamine [3] and PTG membranes

Membrane	Response time (min)	Recovery time (min)	Linear range (mg dl^{-1})	Stability[a] (%)	RSD[b] (%)
Triamine	3	15—20	5—100	98	6.7
PTG	1	7—10	1—10	100	8.0

[a]Activity after 2 weeks. [b]For mid-range concentrations (n = 10).

(10 mg dl^{-1}), aspartate (2.5 mg dl^{-1}), uric acid (3 mg dl^{-1}), creatine (2 mg dl^{-1}) and urea (25 mg dl^{-1}) did not produce a detectable response from the sensor.

The sensor was used to assay creatinine an average of 10 times per day. Response repeatability is shown in Fig. 5, where 1.0 relative activity refers to the current output on the first day. The sensor response remained stable for two weeks, only a slight (4%) variation being observed. The sensor was stored at room temperature in buffer solution when not in use.

In a previous study, creatinine deiminase was covalently immobilized onto a triamine membrane; the detection limit of the sensor was only 5 mg dl^{-1}, ten times greater than in this work. Comparison of the two electrodes is made in Table 2. The reaction between the enzyme and triamine membrane took place on the surface of the membrane, and the pore size of the membrane was uncontrolled. In this work, the immobilization reaction proceeded in an organic solution of the enzyme and the polymer, so that the enzyme was more accessible to the functional groups on the polymer. Therefore more enzyme was immobilized on the PTG than on the triamine membrane.

Pore size and thickness of the membrane, which greatly affect permeability to the substrates and products of the enzyme reaction and consequently the observed response of the sensor, were optimized and under better control, so that the activity of the immobilized creatinine deiminase was much higher than has previously been reported.

We thank Mr. J. M. Dicks for his help in writing this report and for useful discussions.

REFERENCES

1 M. Mascini and G. Palleschi, Anal. Chim. Acta, 155 (1983) 213.
2 B. Danielsson, F. Winquist, K. Mosbach and I. Lundstrom, Proc. Int. Meet. Chem. Sensors, Japan, Sept. 19—22, 1983, Kodansha, Tokyo, p. 507.
3 I. Kubo, I. Karube and S. Suzuki, Anal. Chim. Acta, 151 (1983) 371.
4 I. Kubo, I. Karube, S. Suzuki, Y. Nambu, T. Endo and M. Okawara, J. Biotechnol., in press.
5 I. Kubo and I. Karube, Anal. Lett., in press.

Analytica Chimica Acta, 187 (1986) 39—45
Elsevier Science Publishers B.V., Amsterdam — Printed in The Netherlands

LACCASE/GLUCOSE OXIDASE ELECTRODE FOR DETERMINATION OF GLUCOSE

U. WOLLENBERGER, F. SCHELLER* and D. PFEIFFER

Central Institute of Molecular Biology, Academy of Sciences of the GDR, 1115 Berlin-Buch (German Democratic Republic)

V. A. BOGDANOVSKAYA and M. R. TARASEVICH

A. N. Frumkin Institute of Electrochemistry, Academy of Sciences of the USSR, Moscow (U.S.S.R.)

G. HANKE

District Policlinic Schwerin, 27 Schwerin (German Democratic Republic)

(Received 24th February 1986)

SUMMARY

The electrode involves a layer of co-immobilized glucose oxidase and laccase in a gelatin membrane placed over a modified oxygen electrode. Hexacyanoferrate(III) is added to the samples to oxidize reductive interferents such as ascorbic acid, and the hexacyanoferrate(II) formed is re-oxidized by a laccase-catalyzed reaction. Ascorbic acid is completely eliminated up to a concentration of 20 mM in the sample.

A well established principle of blood glucose measurement with enzyme electrodes is the combination of an immobilized glucose oxidase membrane and a hydrogen peroxide electrode [1, 2]. However, amperometric detection of hydrogen peroxide suffers from interferences from other oxidizable substances present in biological samples, e.g., ascorbic acid, glutathione, cysteine, uric acid and bilirubin. In order to eliminate these substances, hydrogen peroxide-permselective membranes have been used [3, 4]. In addition, electrochemical interferences have been compensated by simultaneous use of a non-enzymatic membrane electrode [5]. In spectrophotometric assays of blood glucose and cholesterol, samples have been pretreated with soluble bilirubin oxidase, ascorbate oxidase and laccase to remove their respective substrates [6]. However, this method is expensive because of the high consumption of enzymes. Recently, multilayer enzyme electrodes for eliminating interfering substances have been described for sucrose measurements in glucose-containing solutions [7, 8].

This paper describes interference-free glucose measurements with a bi-enzyme electrode bearing a layer of co-immobilized glucose oxidase and laccase. The value of this method is exemplified for glucose determinations in glucose/ascorbic acid mixtures.

EXPERIMENTAL

Chemicals

Catalase-free glucose oxidase (GOD) from *Penicillium notatum* (E.C. 1.1.3.4., 46 U mg^{-1}) was purchased from VEB Arzneimittelwerk Dresden. Laccase from *Polyporus versicolor* (diphenol: oxygen oxidoreductase; E.C. 1.10.3.2.; 180 000 U ml^{-1}) was obtained from the Institute of Biochemistry, Academy of Sciences, Armenian SSR. Other reagents used were of analytical grade. The background solution was a Sörensen phosphate buffer of pH 5.0, with or without 5.0 mM potassium hexacyanoferrate(III).

Membrane preparation

Glucose oxidase was immobilized alone or co-immobilized with laccase by entrapment in gelatin [9]. Acid photogelatin (50 ng; VEB Gelatinewerk Calbe) was suspended in 0.5 ml of double-distilled water and allowed to swell for 60 min at room temperature; 0.5 ml of 0.05 M phosphate buffer, pH 6.5, was added, and the solution was thoroughly mixed and heated in a water bath at 40°C for another 60 min. Glucose oxidase (2800 U) alone, or with 5600 U of laccase, was added and the mixture was gently stirred and cast on a flat polyvinyl chloride support. The liquid was spread over an area of 50 cm^2 with a glass rod. The enzyme layer was allowed to dry at room temperature for 6 h, and then removed from the support. The layer had a thickness of 20—30 μm.

The bienzyme membrane contained 56 U cm^{-2} glucose oxidase and 112 U cm^{-2} laccase. The single-enzyme membrane contained 56 U cm^{-2} glucose oxidase.

Apparatus and procedure

For preparation of the sensor, the mono- or bi-enzyme layer was fixed on the dialysis membrane (Nephrophan, 17 μm thick; VEB CK Bitterfeld, GDR) of the modified oxygen electrode, which comprised a platinum indicator electrode of 0.5 mm diameter (VEB Metra Radebeul, GDR) covered by a dialysis membrane held by an O-ring. For glucose determination by hydrogen peroxide detection, the platinum electrode was polarized at +600 mV vs. Ag/AgCl (0.1 M KCl). In the laccase reaction, all reactant are electrochemically measurable if the appropriate potential is applied. Thus, hexacyanoferrate(III) reduction can be monitored, at +150 mV, hexacyanoferrate(II) oxidation at +600 mV and oxygen reduction at −600 mV.

Each electrode was inserted into a measuring cell containing 2 ml of stirred Sörensen phosphate buffer, pH 5.0, at room temperature. Current/time curves obtained with the new electrode were measured with the GWP 673 polarographic system (ZWG Berlin, GDR) and a chart recorder. Sample volumes added to the buffer were $\leqslant$100 μl. The bi-enzyme membrane was also used in the enzyme electrode-based glucose analyzer GKM 02 (ZWG Berlin, GDR), in which case the maximum of the first derivative of the current/time curve was displayed.

RESULTS AND DISCUSSION

The principle of glucose measurement with the laccase/glucose oxidase electrode is shown in Fig. 1. It is based on the amperometric detection at +600 mV of hydrogen peroxide produced in the enzymatic conversion of glucose by the immobilized glucose oxidase:

$$\text{glucose} + O_2 \rightarrow \text{gluconolactone} + H_2O_2$$

$$H_2O_2 \rightarrow O_2 + 2H^+ + 2e^-$$

At +600 mV various substances besides hydrogen peroxide, e.g., ascorbic acid, are oxidized. These interfering substances are converted by reaction with hexacyanoferrate(III) in the measuring cell to their respective oxidation products, which do not affect the hydrogen peroxide oxidation at the electrode. However, the hexacyanoferrate(II) formed is also oxidized at +600 mV. In the bi-enzyme membrane, laccase catalyzes the re-oxidation of hexacyanoferrate(II) by dissolved oxygen. In this way, consumption of oxygen is the only result of the removal of the electrochemically interfering reducing substances.

Glucose oxidase electrode

The relations between the response of the glucose oxidase electrode and the concentrations of glucose and ascorbic acid are shown in Fig. 2. The electrode has a linear concentration dependence in the range 0—50 mM glucose in the sample. The signal for anodic oxidation of ascorbic acid is about 30% higher than the peroxide oxidation current for the same glucose concentration. The presence of ascorbic acid in the sample therefore causes a positive error in the measured glucose concentrations. The physiological concentration of ascorbic acid in blood is only ca. 60 μM, so its effect on

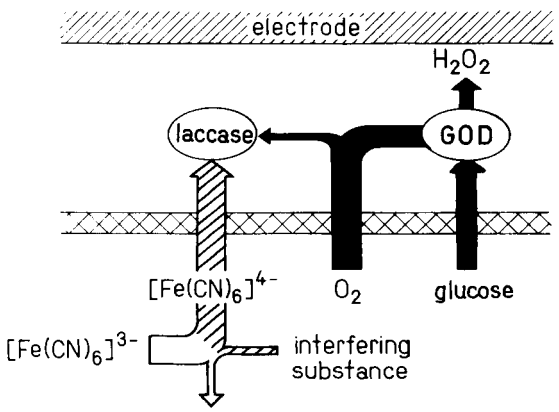

Fig. 1. Principle of glucose determination with elimination of electrochemically interfering substances.

glucose determination in blood can be neglected, but this may not be so for glucose measurements in urine, soft drinks and juices. In order to eliminate this and similar interferences, the glucose oxidase/laccase membrane was produced and tested.

Glucose oxidase/laccase electrode

Provided that the appropriate potential is applied in the investigation of the laccase-catalyzed reaction, the substrates hexacyanoferrate(II) and oxygen, and the product, hexacyanoferrate(III), can be detected with the electrode. Initially, the effectiveness of the immobilized laccase was tested by measuring the extent of oxidation of hexacyanoferrate(II) in the enzyme layer by detecting the residual hexacyanoferrate(II) reaching the electrode surface (Fig. 3, curve b). When first used, at +600 mV vs. Ag/AgCl, the electrode had an oxidation current that was almost zero up to a final hexacyanoferrate(II) concentration of 4.3 mM, indicating complete oxidation of hexacyanoferrate(II) in the laccase layer. Higher concentrations were only partially oxidized in the laccase layer, as is reflected by the linearly increasing oxidation current (Fig. 3, curve b). The reduction current at +150 mV gives evidence of hexacyanoferrate(III) formation by laccase (Fig. 3, curve a). It increases linearly with hexacyanoferrate(II) concentration up to 2 mM, with a slope 3 times that of hexacyanoferrate(II) oxidation at +600 mV.

These differences might be explained by the coupling of electrochemical and enzymatic reactions in this sensor. In amperometric electrodes, the concentration gradient of the electroactive substance at the membrane/electrode

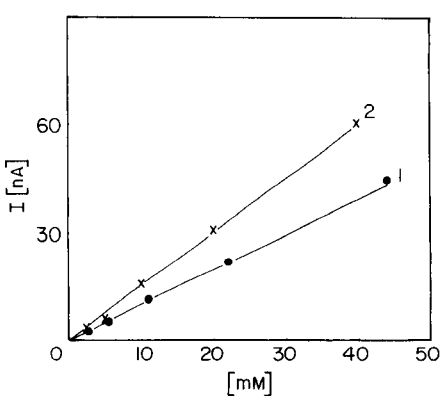

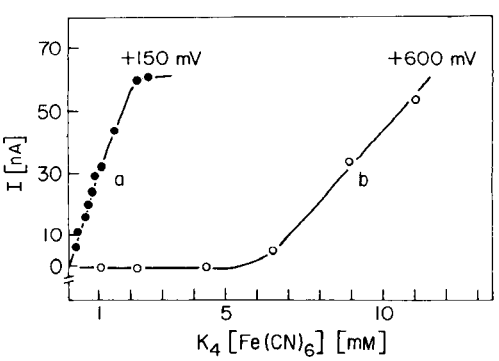

Fig. 2. Concentration dependences of the glucose oxidase electrode: (1) glucose; (2) ascorbic acid. Conditions: +600 mV vs. Ag/AgCl (0.1 M KCl).

Fig. 3. Relationship between the response of the glucose oxidase/laccase electrode (on the first day after preparation) and the final potassium hexacyanoferrate(II) concentration. Ion detected: (a) hexacyanoferrate(III) at +150 mV (cathodic current), (b) hexacyanoferrate(II) at +600 mV (anodic current).

interface determines the electrode current. When hexacyanoferrate(II) is monitored (+600 mV), there is a uniform concentration gradient from the bulk solution to the electrode. In the membrane, the concentration drops from the value at the membrane/solution interface to zero at the membrane/electrode interface, in the diffusion-limited process, for <4.3 mM hexacyanoferrate(II). In the product-sensitive mode, the hexacyanoferrate(III) concentration rises from zero at the membrane/solution interface through a maximum and returns to zero at the electrode surface, so that diffusion occurs in two opposite directions [10]. Furthermore, electrochemical regeneration of hexacyanoferrate(II) by reduction of hexacyanoferrate(III) at the electrode produces additional substrate formation for laccase and thus a cycling amplification [11].

The stability of the immobilized laccase in the bi-enzyme electrode was investigated by determining the maximum amount of hexacyanoferrate(II) which is completely eliminated by laccase. Whereas this diffusion-controlled region extends to 4.3 mM on the first day of use, the limit decreases to 1.5 mM, 0.7 mM and 0.5 mM after 8, 10 and 14 days, respectively (Fig. 4). Taking into account a decrease of 65% in laccase activity over 8 days, the capacity of the laccase membrane is adequate for all practically important interfering substances if the sample is diluted 40—100 fold.

Ascorbic acid, one of the potentially interfering substances in glucose measurements based on electrochemical hydrogen peroxide detection, was chosen to check the effectiveness of laccase/hexacyanoferrate(III) for removing interferences. For this purpose, the dependence of the current on the ascorbic acid concentration, both with and without 5 mM hexacyanoferrate(III), was recorded. Figure 5 shows that in the absence of hexacyanoferrate(III), at final ascorbic acid concentrations below 0.025 mM, there is

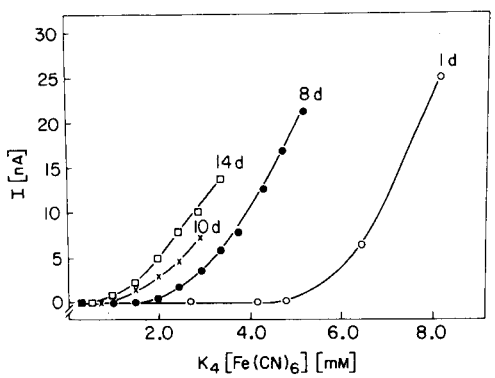

Fig. 4. Dependence of the relationship between oxidation current and final measured hexacyanoferrate(II) concentration on the time (days) after electrode preparation: (○) 1 d; (●) 8 d; (X) 10 d; (□) 14 d.

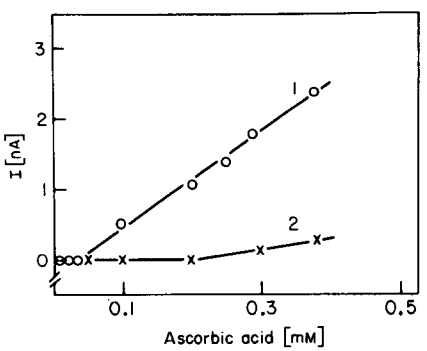

Fig. 5. Dependence of the bi-enzyme electrode current on ascorbic acid concentration: (1) without hexacyanoferrate(III); (2) with 5 mM hexacyanoferrate(III).

no current increase because laccase directly catalyzes the oxidation of ascorbic acid. This was proved by using a laccase/glucose oxidase electrode polarized at —600 mV. After addition of ascorbic acid to the measuring cell, oxygen consumption was observed. In the presence of 5 mM hexacyanoferrate(III), no current was observed for up to 0.2 mM ascorbic acid, giving evidence for complete oxidation of ascorbic acid by hexacyanoferrate(III) and complete re-oxidation of the hexacyanoferrate(II) formed by the immobilized laccase. Considering the sample dilution, 8—20 mM ascorbic acid in the sample (20—50 μl) can be completely eliminated. Other reported electrodes, with a hydrogen peroxide permselective membrane [3] and a negatively charged membrane [4], rejected 5.68 mM and 0.0852 mM ascorbic acid, respectively.

Figure 6 shows the response curves obtained by successive addition of glucose, ascorbic acid and hexacyanoferrate(III) to the measuring cell in which the bi-enzyme electrode was inserted. The introduction of 50 μl of 11 mM glucose produces an anodic current increase of 16.4 nA within 30 s because of the hydrogen peroxide formed in the glucose oxidase catalyzed reaction. When the current/time curve has reached a steady state, addition of 50 μl of 100 mM ascorbic acid causes a further current increase (29 nA) resulting from the electrochemical oxidation of ascorbic acid at the same potential as that of hydrogen peroxide. This current increase is only 15% of the response of a laccase-free electrode for ascorbic acid (Fig. 2) because

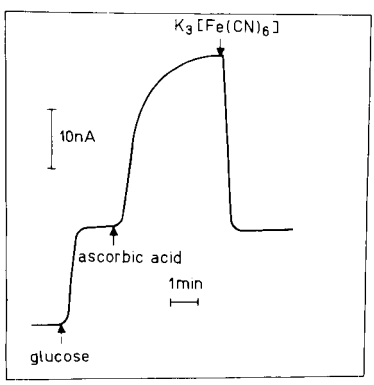

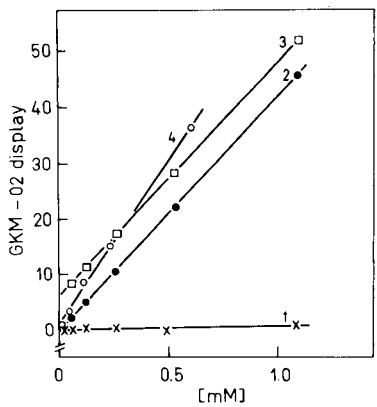

Fig. 6. Response of the laccase/glucose oxidase electrode to successive additions of 50 μl of 11 mM glucose, 100 mM ascorbic acid and 100 mM potassium hexacyanoferrate(III) to 2 ml of pH 5.0 Sörensen phosphate buffer at +600 mV vs. Ag/AgCl (0.1 M KCl).

Fig. 7. Dependence of the maximum of the first derivative of the current/time curve displayed by the GKM 02 unit on the final concentration of: (1) hexacyanoferrate(II); (2) glucose or glucose with ascorbic acid (2.5 mM or 5 mM) and hexacyanoferrate(III) (5 mM); (3) glucose in the presence of 5 mM ascorbic acid; (4) ascorbic acid at +600 mV vs. Ag/AgCl (0.1 M KCl). The GKM 02 display indicates mM glucose in the sample.

laccase catalyzes the oxidation of some of the ascorbic acid in the membrane of the bi-enzyme sensor. The addition of 50 μl of 100 mM hexacyanoferrate(III) results in a rapid current decrease to the level reached with glucose in the absence of ascorbic acid, illustrating the complete elimination of the effect of ascorbic acid.

Measurement of glucose in samples containing ascorbic acid

The calibration graph obtained for glucose using the enzyme electrode-based analyzer with the laccase/glucose oxidase electrode, was linear up to 50 mM. The ratio between the sensitivity to glucose as measured by hydrogen peroxide oxidation and the direct oxidation of ascorbic acid is 1:1.24 (Fig. 7). Ascorbic acid (5 mM) in glucose samples simulates an increased value of glucose concentration of 6.2 mM (Fig. 7). However, in the presence of 5 mM hexacyanoferrate(III), ascorbic acid does not increase the glucose signal. The concentration dependence shown for glucose in Fig. 7 is also the same for mixtures of glucose with ascorbic acid (5 mM or 2.5 mM) in the presence of 5 mM hexacyanoferrate(III). Therefore an interference-free glucose measurement is possible.

The concentration range studied exceeds the maximum ascorbic acid/glucose ratio in blood and urine even in the case of therapeutic vitamin C treatment. Some initial results for the determination of glucose in urine obtained with the proposed anti-interference sensor compare well with the Polamat (reference method for glucose measurement in urine [12]), which show the potential of the proposed measuring system. For normal urine samples, an average glucose concentration of 1.3 mM was found by the laccase/glucose oxidase electrode. This value is in accord with the normal physiological value whereas the laccase-free sensor indicated values an average of 4.5 mM too high.

This principle of elimination of interferences may be extended to other enzyme electrodes where hydrogen peroxide is detected anodically, e.g., to lactate or cholesterol sensors with their respective oxidases.

REFERENCES

1 G. G. Guilbault and G. J. Lubrano, Anal. Chim. Acta, 64 (1973) 439.
2 F. Scheller and D. Pfeiffer, Z. Chem., 2 (1978) 50.
3 T. Tsuchida and K. Yoda, Enzyme Microb. Technol., 3 (1981) 326.
4 E. Lobel and J. Rishpon, Anal. Chem., 53 (1981) 5.
5 D. R. Thevenot, R. Sternberg and P. Coulet, Diabetes Care, 5 (1982) 203.
6 Jpn. Pat. DE 3239236, 1982.
7 F. Scheller and R. Renneberg, Anal. Chim. Acta, 152 (1983) 265.
8 R. Renneberg, F. Scheller, K. Riedel, E. Litschko and M. Richter, Anal. Lett., 16 (1983) 877.
9 F. Scheller, D. Pfeiffer and M. Jänchen, GDR Pat. G01 N/127843, 1979.
10 D. A. Gough and J. K. Leypoldt, in L. B. Wingard, Jr., E. Katchalski-Katzir and L. Goldstein (Eds.), Applied Biochemistry and Bioengineering, Vol. 3, Academic Press, London, 1981, pp. 175.
11 T. Wasa, K. Akimoto, T. Yao and S. Murao, J. Chem. Soc. Jpn., 9 (1984) 1398.
12 DAB 7 (D. L.), Deutsches Arzneibuch, Diagnostische Laboratoriumsmethoden, Akademie-Verlag, Berlin, 1968.

Analytica Chimica Acta, 187 (1986) 47—54
Elsevier Science Publishers B.V., Amsterdam — Printed in The Netherlands

A RELIABLE L-LACTATE ELECTRODE WITH A NEW MEMBRANE FOR ENZYME IMMOBILIZATION FOR AMPEROMETRIC ASSAY OF LACTATE

GILBERT BARDELETTI, FLORENCE SECHAUD and PIERRE R. COULET*

Laboratoire de Génie Enzymatique, Atelier de Biotechnologie (CNRS, Université Lyon I), ESCIL, Université Claude Bernard, 43 Boulevard du 11 Novembre 1918, 69622 Villeurbanne Cedex (France)

(Received 27th March 1986)

SUMMARY

Lactate oxidase from *Pediococcus* species can be rapidly and simply immobilized on a commercially available pre-activated membrane fixed to an amperometric probe detecting hydrogen peroxide, to provide a very sensitive practical L-lactate sensor. At 25°C, in a phosphate buffer pH 7.1, the detection limit is 1.25×10^{-7} M, calibration is linear between 2.5×10^{-7} and 2.5×10^{-4} M, the response time is <2 min, and the probe can be used for hundreds of assays over several weeks. With a microprocessor-based instrument including the same type of electrode, sample injections can be made at 90-s intervals, the response being displayed after only 30 s. High selectivity is achieved because the differential measurement system continuously subtracts currents at the chosen potential arising from the presence of electroactive species. Samples (20 μl) from sera and dairy products were successfully tested without pretreatment; a relative standard deviation between 1 and 3% was routinely obtained. Correlation of the data with data obtained by the conventional spectrophotometric method was excellent.

There is a strong demand for lactate determinations in clinical laboratories because of the association of lactate with several severe diseases, as well as in the food industry, for dairy products and for the control of additives. Several methods have been described. The oldest involve chemical reactions based on detection of acetaldehyde by spectrophotometry or gas chromatography following lactate oxidation [1—4]. An enzymatic method with soluble lactate dehydrogenase (LDH, E.C. 1.1.1.27) associated with NADH detection at 340 nm is also used [5]. More recently, different enzyme electrodes prepared with either soluble or immobilized enzymes have been described. For this purpose, ferricytochrome-C oxidoreductase, (E.C. 1.1.2.3, cytochrome b_2) or lactate dehydrogenase [6—13] have been used. Attempts to improve the performance of this type of sensor have also been made using mono-enzyme systems like lactate-2-mono-oxygenase (E.C. 1.13.12.4) leading to acetate production [14—16] or lactate oxidase (LOD) [17—20] which catalyzes the following reaction:

$$\text{L-lactate} + O_2 \xrightarrow{\text{LOD}} \text{pyruvate} + H_2O_2$$

0003-2670/86/$03.50 © 1986 Elsevier Science Publishers B.V.

Bi-enzyme systems such as LOD/LDH [21, 22] and cytochrome b_2/LDH [23] have also been proposed.

Most of the systems described, although they appear conceptually attractive, are generally slow and laborious to set up and exhibit performances still far from what is required in clinical and food analysis. Very often, pretreatment of the sample is compulsory in order to obtain accurate results. Also, even when electrochemical sensors are available and easy to set up, the preparation of the associated enzymatic systems appears generally time-consuming and dependent on local availability of material and thus can be difficult to prepare outside the laboratory where they were originally conceived.

In recent years, mono- and bi-enzyme electrodes have been developed [24—28] based on collagen membranes bearing immobilized enzymes covalently linked by an acyl/azide procedure [29]. This has made it possible to design a glucose electrode and an enzymatic probe-based apparatus for glucose determination, which are now commercially available (Solea-Tacussel, Villeurbanne).

Recently, the utilization of polyamide membranes, normally used for immunodiagnostic purposes, has been proposed as a support for immobilization of enzymes in biosensors [30]. The aim of the work reported here was to develop a reliable L-lactate sensor, mainly with regard to detection limit, linearity, stability and response time, by using such membranes which are very easy to handle and allow fast and simple enzyme immobilization.

EXPERIMENTAL

Chemicals

Lactate oxidase (E.C. number not available, from *Pediococcus* species, lyophilized powder, 10—30 U mg^{-1}), L-lactic acid, lithium L-lactate and flavine adenine dinucleotide (FAD) disodium salt, were from Sigma Chemical Co. Comparisons were made with the conventional spectrophotometric method for L-lactate determination in foodstuffs (Boehringer, Mannheim). Other regular reagents of the highest available grade were supplied by Prolabo, Paris.

Membrane and enzyme immobilization

Biodyne immuno-affinity membranes (120 μm thick, 0.2-μm or 3-μm pore diameter; Pall, Glen Cove, NY 11542) were used. These membranes are provided in a pre-activated form for antigen and antibody immobilization. The supplier's instructions were adapted for lactate oxidase immobilization. The procedure remains simple. Coupling was achieved at 4° C by simple immersion of 8-mm diameter disks cut from the pre-activated membrane in 1 ml of a stirred lactate oxidase solution of the required concentration and pH (see Results) for 2 h. The disks were then washed twice for 20 min in 1 M potassium chloride at room temperature and stored at 4°C in 0.1 M phosphate buffer, pH 7 which was 0.1 M in potassium chloride, 10 mM in magnesium chloride and 10 μM in FAD.

Instrumentation and procedure

Different electrochemical devices (Solea-Tacussel, Villeurbanne) were used. The amperometric enzyme probe, type "Gluc 1", is normally designed for glucose determination when a suitable immobilized enzyme membrane is used. It was plugged into a polarograph type PRGE. The potential of the platinum anode of the probe was fixed at +650 mV vs. a Ag/AgCl reference electrode for hydrogen peroxide detection. The anodic current was output to a Sefram-Servotrace recorder. The enzyme disk was tightly pressed against the platinum tip with a screw cap. The diameter of the platinum tip in contact with the disk was 3 mm. The electrode was immersed in a thermostatted vessel containing 20 ml of the phosphate buffer into which lactate samples (20—100 μl) were injected.

A microprocessor-based instrument (Glucoprocesseur) was also used. High selectivity from the dynamic response can be obtained with the differential measurement system which allows the continuous subtraction of the interfering current from other electroactive species at the chosen potential. This subtraction is done by means of a compensating electrode of the same type as the bioactive electrode but covered with a non-enzymatic membrane. The substrate-containing sample is injected into the thermostatted measurement cell (3 ml) with a glass capillary micropipette (10, 20 or 50 μl; S.M.I., Emeryville, CA). Thermostatting (precalibrated at 30°C or 37°C), filling and emptying the cell are automatic. The apparatus was connected to an Epson printer.

In the work reported here, both systems were adapted to L-lactate determination by using the new synthetic membranes with immobilized lactate oxidase replacing the normal glucose oxidase collagen membranes.

RESULTS

Coupling conditions

Two types of buffer were tested, 0.1 M phosphate buffer, pH 7.1 and 0.1 M glycine sodium hydroxide buffer, pH 9, both 0.1 M in potassium chloride, 10 mM in magnesium chloride and 10 μM in FAD. The coupling solution contained 1.5 mg ml^{-1} lactate oxidase. These membranes after immobilization were mounted on the "Gluc 1" probe and tested for their response to lactate. The initial sensitivity, found for two sets of four membranes, corresponding to each buffer, was in the range 0.95—1.1 mA M^{-1}.

In order to measure the effect of the original enzyme concentration on the activity of the disk, five pre-activated disks were immersed in coupling solutions with enzyme concentrations from 0.25 to 4 mg ml^{-1} in the glycine buffer. Figure 1 shows that the probe sensitivity increased with enzyme concentration up to ca. 1.5 mg ml^{-1}. This concentration was selected for further experiments, to conserve enzyme.

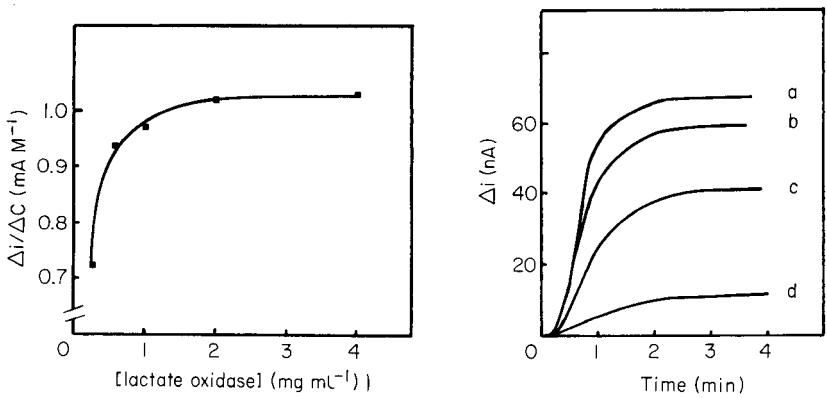

Fig. 1. Dependence of sensor sensitivity on lactate oxidase concentration in the coupling solution (0.1 M glycine/NaOH buffer pH 9/0.1 M KCl/10 mM $MgCl_2$/10 μM FAD). Measurements were made with the "Gluc 1" probe for 2.5×10^{-6}—2.5×10^{-5} M final concentration of L-lactate in the 0.1 M phosphate buffer/0.1 M KCl/10 mM $MgCl_2$/10 μM FAD solution at pH 7.1 (25°C).

Fig. 2. Responses curves for a 50 μM L-lactate final concentration obtained with the "Gluc 1" probe at different pH: (a) 7.1; (b) 6.8; (c) 6.4; (d) 5.9. 0.1 M phosphate buffer as in Fig. 1 (25°C).

Sensor performances obtained with the "Gluc 1" probe

When the enzymatic probe was immersed in phosphate buffer at various pH values, injection of a L-lactate solution (50 μM final concentration) gave rise to a current increase which reaches a steady state within 2—4 min depending on the pH. It can be seen in Fig. 2 that the time required to reach the plateau was slightly less when the pH was close to 7. Sensitivity was greatest at pH 7.1. In order to ascertain if the response dependence on pH was due only to the enzyme, L-lactate sensitivity was normalized to the sensitivity for hydrogen peroxide quantified with the same probe. The results are shown in Fig. 3; pH 7.0—7.5 appears to be the optimum for the L-lactate sensor. The sensitivity is strongly dependent on pH in acidic solutions (Fig. 2). Between pH 7 and 8, this dependence is far less pronounced and the probe can conveniently be used in this range. At pH 9 in the glycine buffer, the probe exhibited only 30% of its greatest sensitivity and it was not possible to obtain a steady-state response within 4 min.

In order to assess the temperature dependence of the probe, assays were done at several temperatures between 16°C and 36°C (Fig. 4) for 2.5×10^{-6}—2.5×10^{-5} M lactate. The sensitivity ($\Delta i/\Delta C$) varied between 0.65 and 1.05 mA M^{-1}, the greatest value being obtained at ca. 30°C. When these values were normalized to hydrogen peroxide sensitivity, a shift of the optimum temperature towards lower values was observed.

Assays done at 36°C were followed by control measurements at 25°C with the same enzymatic disk. The sensitivity was 25% lower at 25°C than the

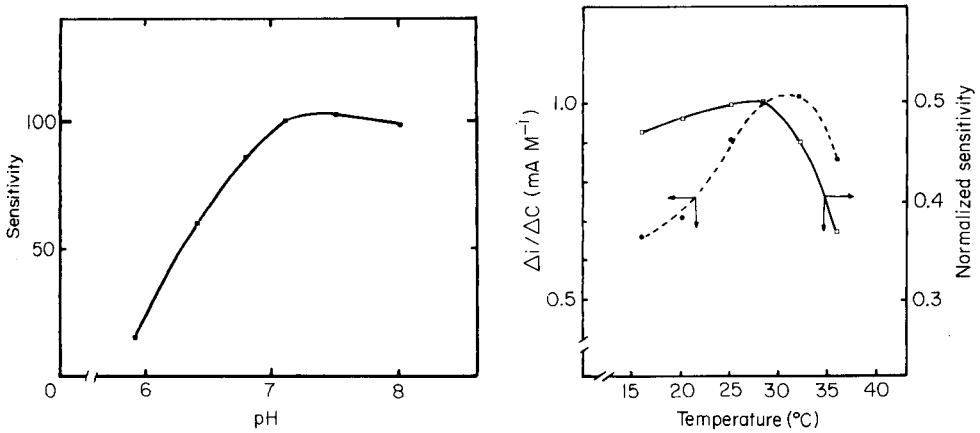

Fig. 3. Influence of pH on L-lactate sensor sensitivity after correction for changes in H_2O_2 sensitivity. The "Gluc 1" probe was used; 0.1 M phosphate buffer and lactate concentration range as in Fig. 1; pH 7.1 was selected as 100%.

Fig. 4. Variation of sensor sensitivity with temperature. Sensitivities: (□) normalized; (•) not normalized. The "Gluc 1" probe was used with 0.1 M phosphate buffer pH 7.1 and L-lactate concentration range as in Fig. 1.

original sensitivity obtained at that temperature. The time during which the probe had been kept at 36°C was ca. 30 min. For temperatures lower than 28°C, the initial sensitivity was recovered. Thus a temperature close to 25°C was selected for lactate determination with the "Gluc 1" probe.

The dependence of the time taken to reach a steady-state response on L-lactate concentration was studied for 5×10^{-6}—1.25×10^{-4} M lactate. This time never exceeded 2 min for the higher concentrations and was close to 1 min for the lower ones.

The detection limit, which depends on the noise level of the system, can be defined as the lowest concentration yielding a significant deviation from the background current. For 1.25×10^{-7} M L-lactate, the signal/noise ratio (ratio of the variation of current produced by L-lactate to the maximum amplitude of variation of the baseline current) was 3. Thus the detection limit was 1.25×10^{-7} M lactate.

Accurate lactate measurements and calibration linearity were obtained between 2.5×10^{-7} M and 2.5×10^{-4} M. At higher concentrations, the response levelled off. For the practical range routinely used (1×10^{-6} M—1×10^{-4} M), the calibration graph was linear with a slope of 1.15 mA M^{-1}. The relative standard deviation for 10 replicate assays of 2.5×10^{-6} M L-lactate final concentration was 1.8%.

In a typical experiment, sensor sensitivity was tested over definite times for alternate periods of storage (4°C) and operation (25°C). Figure 5 shows that there was no change in sensitivity for 3 weeks, and the probe retained 70% of its initial sensitivity after 36 days. It must be emphasized that even

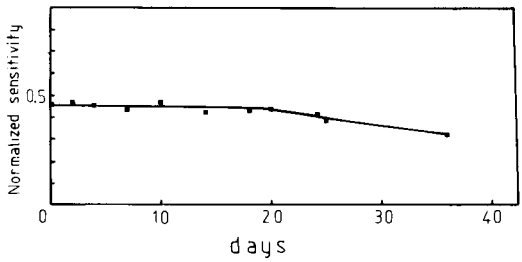

Fig. 5. Stability of the normalized sensitivity for L-lactate over 5 weeks ("Gluc 1" probe, 0.1 M phosphate buffer pH 7.1, operating temperature 25°C; storage temperature 4°C).

when the sensitivity decreases, the detection limit and linearity are maintained so that measurements can still be made easily and accurately.

L-Lactate determination with the "Glucoprocesseur"

The same disks were used with the enzyme electrode microprocessor-based instrument (Glucoprocesseur). The lower value of the precalibrated temperatures, 30°C, was used for all the experiments, and the phosphate buffer was used. The wider working concentration range used was 6.6×10^{-7}—6.6×10^{-5} M final concentration in the measurement cell, i.e., 1×10^{-4}—1×10^{-2} M L-lactate in the sample. For higher concentrations, the sample must be diluted. The response was printed 30 s after each sample injection, which can be made at 90-s intervals.

Samples from different origins (Table 1) were assayed. Three sera were tested without pretreatment; the lactate level fell into the working range of the apparatus so that there was no need for dilution. Several samples from the dairy industry were also assayed. Whey from cream cheese and plain yoghourt were injected directly after dilution with water (1:100). Solutions (20 g l^{-1}) were prepared from sweet and acid-type dry wheys. A dilution

TABLE 1

Concentration of L-lactate in serum and whey measured with the "Glucoprocesseur" equipped with a lactate electrode

	Sample serum			Whey solution				
	a	b	c	Cream cheese	Plain yoghourt		Reconstituted powder[a]	
					a	b	Sweet	Acid
L-Lactate[b] (mM)	5.20	8.05	2.56	99.0	83.7	80.6	1.23	24.40
S.d.	0.08	0.11	0.07	1.40	0.94	1.60	0.01	0.80
R.s.d. (%)	1.5	1.3	2.7	1.4	1.1	2.1	1.2	3.2

[a]20 g l^{-1}; see text. [b]Mean of 6 replicates, with standard deviation and relative standard deviation; a—c indicate different samples.

(1:20) was necessary only for the acid type. As shown in Table 1, the relative standard deviation ranged from 1.1 to 3.2%.

DISCUSSION

The great interest in the analytical use of immobilized enzymes is attested by the large number of references, mainly dealing with enzyme electrodes, as reviewed recently by Guilbault [31]. This abundance contrasts strongly with the very small number of enzyme sensors commercially available, thus showing the gap which still persists between the performance of the probes described and the requirements which must be fulfilled for routine industrial use.

In order to improve the design of enzyme membrane electrodes, the influence of several parameters, especially the membrane resistance, on the transfer of electroactive products (H_2O_2) through the membrane has recently been discussed [32]. The membranes routinely used in the work reported here (0.2-μm pore diameter) were found to be porous enough for the purpose required, and 3-μm pore diameter membranes did not give better results. The membrane also allowed simple and rapid enzyme immobilization. A ready-to-use probe could be made routinely in 3 h (or 1 h if a few μl of enzyme was simply placed on the pre-activated disk).

Where proper comparisons can be made, the present results compare very favourably with data reported by other workers. To our knowledge, only two papers mention a lower detection limit (i.e., 0.8×10^{-7} M [21] and 5×10^{-9} M [22]). In these cases, a bi-enzyme system (LOD/LDH consuming NADH) was used and the response times were ca. 4 and 9 min, respectively; the type of system proposed seems to be elegant and promising, but the preparation of the enzyme support involved different sophisticated steps and took several days, and pretreatment of the samples was necessary. The lifetime of the present sensor, defined as the time during which accurate results can be obtained within the full calibration range, is longer than the lifetimes obtained (when reported at all) by other workers.

When the "Glucoprocesseur" was used, subtraction of effects of interferences was automatic, allowing lactate measurements to be made in complex mixtures (e.g., sera and food products) with relative standard deviations between 1 and 3%.

The concentrations of L-lactate in different kinds of dairy products (cream cheese, plain yoghourt, and sweet and acid reconstituted whey from powder) and also in red wine, white wine and sauerkraut broth were determined by both the amperometric procedure and the conventional spectrophotometric method. The regression equation obtained for the data was $y = 0.981x + 0.015$ (y = electrode result, x = spectrophotometric result, both given as mM) with a correlation coefficient of 0.997 (n = 12).

Thanks are due to CNRS-PIRSEM-AFME (AIP decision no. 3112) for financial support and to M. G. Doussau, Pall Industries, France, for membrane samples.

REFERENCES

1 S. B. Barker and W. H. Summerson, J. Biol. Chem., 138 (1941) 535.
2 N. W. Hoffman, J. J. Barboriak and H. F. Hardman, Anal. Biochem., 9 (1964) 175.
3 J. Savory and A. Kaplan, Clin. Chem., 12 (1966) 559.
4 M. E. Teaford and A. Kaplan, Clin. Chim. Acta, 15 (1967) 133.
5 I. Gutman and A. W. Waklefeld, in H. U. Bergmeyer (Ed.), Methods of Enzymatic Analysis, Verlag Chemie, Weinham, 2nd edn., 1974, p. 264.
6 D. L. Williams, A. R. Doig and A. Korosi, Anal. Chem., 42 (1970) 118.
7 H. Durliat, M. Comtat, J. Mahenc and A. Baudras, J. Electroanal. Chem., 66 (1975) 73.
8 W. J. Blaedel and R. A. Jenkins, Anal. Chem., 48 (1976) 1240.
9 F. S. Cheng and G. D. Christian, Clin. Chim. Acta, 91 (1979) 295.
10 T. Shinbo, M. Sugiura and N. Kamo, Anal. Chem., 51 (1979) 100.
11 T. Yao and S. Musha, Anal. Chim. Acta, 110 (1979) 203.
12 A. K. Chen and C. C. Liu, Process Biochem., 14(1) (1979) 12.
13 J. J. Kulys and G. J. S. Svirmickas, Anal. Chim. Acta, 117 (1980) 115.
14 M. Mascini, P. Palleschi and D. Moscone, Anal. Chem. Symp. Ser., 17 (1983) 603.
15 M. Mascini, D. Moscone and P. Palleschi, Anal. Chim. Acta, 157 (1984) 45.
16 E. B. Makovos and C. C. Liu, Biotechnol. Bioeng., 27 (1985) 167.
17 I. Karube, T. Matsunaga, N. Teraoka and S. Suzuki, Anal. Chim. Acta, 119 (1980) 271.
18 F. Mizutani, K. Sasaki and Y. Shimura, Anal. Chem., 55 (1983) 35.
19 L. C. Clark, L. K. Noyes, T. A. Grooms and C. A. Gleason, Clin. Biochem., 17 (1984) 288.
20 J. J. Cannon, L. F. Chen, M. C. Flickinger and G. T. Tsao, Biotechnol. Bioeng., 26 (1984) 167.
21 F. Mizutani, Y. Shimura and K. Tsuda, Chem. Lett., 2 (1984) 199.
22 F. Mizutani, T. Yamanaka, Y. Tanabe and K. Tsuda, Anal. Chim. Acta, 177 (1985) 153.
23 F. Schubert, D. Kirtein, K. L. Schöder and F. W. Scheller, Anal. Chim. Acta, 169 (1985) 391.
24 D. R. Thevenot, R. Sternberg, P. R. Coulet, J. Laurent and D. C. Gautheron, Anal. Chem., 51 (1979) 96.
25 P. R. Coulet and C. Bertrand, Anal. Lett., 12 (1979) 581.
26 C. Bertrand, P. R. Coulet and D. C. Gautheron, Anal. Chim. Acta, 126 (1981) 23.
27 G. G. Guilbault and P. R. Coulet, Anal. Chim. Acta, 152 (1983) 223.
28 G. Bardeletti and P. R. Coulet, Anal. Chem., 56 (1984) 591.
29 P. R. Coulet, J. H. Julliard and D. C. Gautheron, Biotechnol. Bioeng., 16 (1974) 1055.
30 C. H. Assolant-Vinet and P. R. Coulet, Anal. Lett., 19 (1986) 875.
31 G. G. Guilbault, Analytical Uses of Immobilized Enzymes, M. Dekker, New York, 1984.
32 G. Bardeletti, B. Maïsterrena and P. R. Coulet, Enzyme Microb. Technol., 8 (1986) 365.

Analytica Chimica Acta, 187 (1986) 55—65
Elsevier Science Publishers B.V., Amsterdam — Printed in The Netherlands

PERFORMANCE OF REFERENCE ELECTRODES WITH FREE-DIFFUSION JUNCTIONS
The Effect of Ionic Strength and Bore Size on Junctions with Simple Cylindrical Geometry

W. DAVISON* and T. R. HARBINSON

The Freshwater Biological Association, The Ferry House, Far Sawrey, Ambleside, Cumbria LA22 0LP (Great Britain)

(Received 29th April 1986)

SUMMARY

The performance of free-diffusion liquid junctions formed in a capillary between saturated potassium chloride solution and a range of solutions with ionic strengths varying from 10^{-5} to 0.5 mol kg^{-1} is described. Precision, response time and noise associated with convection were adversely affected at ionic strengths less than 10^{-3} mol kg^{-1}. Increasing the bore of the capillary from 0.5 mm to 3 mm also had a detrimental effect. Capillaries with 0.5-mm bore performed optimally with errors <0.2 mV for solutions with ionic strength $>10^{-4}$ mol kg^{-1}, but deteriorating to 1 mV for 10^{-5} mol kg^{-1} solutions. Equivalent errors if free-diffusion junctions were used in pH measurements would be 0.003 and 0.017 pH, indicating that, given well-controlled experimental conditions, it is possible to achieve precise measurements in very dilute solutions.

Any potentiometric measurement with an ion-selective electrode requires a reference electrode capable of maintaining a constant potential in calibration and test solutions. The calomel or silver/silver chloride electrodes which are commonly used provide reproducible potentials and cause few problems. However, where the filling solution of concentrated potassium chloride contacts the solution being measured, a liquid junction potential develops, and is incorporated in the overall potential difference of the cell. If the junction potentials are the same in the calibration and test solutions, they cancel out, but if there is a difference, known as a residual liquid junction potential [1], it introduces an error in the potentiometric determination.

The liquid junction potential depends on ionic strength, and deviations are particularly pronounced when the measured solution has a higher ionic strength than the standard solutions, which for pH measurements are usually at an ionic strength of ca. 0.1 mol kg^{-1}. As a result, special pH scales have been developed for certain well-defined solutions with high ionic strength such as sea water [2] and blood [3]. When pH is measured in solutions of low ionic strength (<0.1 mol kg^{-1}), the residual liquid junction potential is assumed to be zero [4]. However, recent work has shown that the design of the junction can critically affect such measurements [5—8]. It seems that a

0003/2670/86/$03.50 © 1986 Elsevier Science Publishers B.V.

considerable and unpredictable residual liquid junction potential may result from forming the junction in a constraining element, such as the ceramic frits which are commonly used commercially.

The British Standard pH scale is based on the premise that the residual liquid junction potential will be zero if the junction is formed at a sharp boundary in a cylinder, and the solutions are allowed to diffuse freely into one another [9]. Such junctions have also been used to verify the internal consistency of the NBS scale [9]. Use of such a free-diffusion junction stems from the work of Guggenheim [10], who showed that junctions formed in this fashion were most reproducible but did not make any measurements in solutions of low ionic strength. Although recent attempts to measure accurately the pH in such solutions, particularly freshwater, have used free-diffusion junctions with some success [7, 8], there has been no systematic evaluation of their performance characteristics.

During development of these junctions, it was found that their geometry could critically affect their performance. Therefore, a series of studies was initiated to test various designs of free-diffusion junctions over a wide range of ionic strengths, from values appropriate to rainwater (10^{-5} mol kg^{-1}) to those similar to sea water (0.7 mol kg^{-1}). Here, the basic data are presented for static junctions with cylindrical geometry. Future work will consider other geometries and flowing solutions.

Principles

It is theoretically impossible to measure single liquid junction potentials [9], so performance was tested by measuring the potential difference between two nearly identical junctions. Two reference electrodes, A and B, were connected via bridge solutions to their respective liquid junctions which were in contact with the test solution (Fig. 1). The measured e.m.f., E, was therefore composed of the individual potentials of the reference electrodes and junctions: $E = E_{RA} - E_{RB} + E_{JA} - E_{JB}$. By disconnecting the liquid junctions and opening a tap connecting the bridge solutions it was possible to bypass the liquid junctions and obtain the bias potential, i.e., the potential difference between the reference electrodes: $E_{\Delta R} = E_{RA} - E_{RB}$. The potential difference caused by the liquid junctions is then the difference between these two measured potentials: $E_{\Delta J} = E - E_{\Delta R}$.

EXPERIMENTAL

Apparatus

The measuring cell consisted of a rectangular glass tank (20 × 15 × 10 cm) which was fitted with a water jacket and maintained at 20 ± 0.1°C. The glass capillaries where the liquid junctions were formed, and a perspex block housing the reference electrodes (Radiometer K4112, calomel/saturated KCl), were contained within the tank (Fig. 2). PTFE tubing (1-mm bore) carried the salt bridge and provided connections to two micrometer syringes mounted

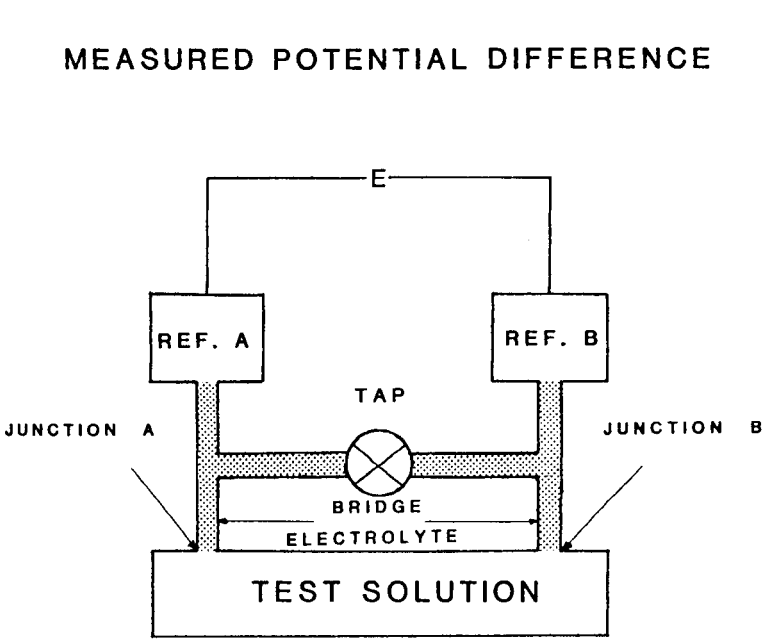

Fig. 1. Schematic diagram of the measuring system.

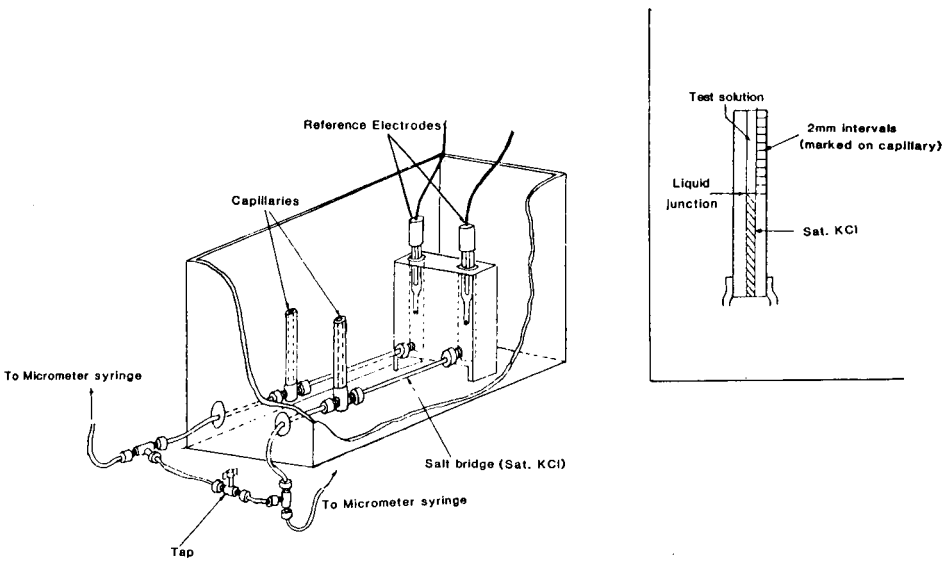

Fig. 2. Pictorial representation of the measuring vessel without the water jacket. The inset is an enlarged view of one of the capillaries where the junction was formed.

outside the cell. These syringes could accurately control the level of the liquid junction within the capillary. The shorting tap between the two bridge solutions was also located outside the cell. A magnetic stirrer unit was placed under the tank and used to control a 5-cm magnetic follower on the floor of the cell. The whole assembly was enclosed in a Faraday cage.

Potential differences were measured by using a high-impedance buffer amplifier based on a Burr-Brown OPAIII operational amplifier. The output was simultaneously displayed on a chart recorder, the scale of which could be expanded to 0.1 mV cm^{-1}, and on a 5-digit multimeter (Thurlby 1905a) which could discriminate 1 μV. The cell was emptied, filled and rinsed by using a peristaltic pump.

Analytical reagent-grade chemicals were used to prepare saturated potassium chloride bridge solutions and solutions containing sodium chloride. Hydrochloric acid was AVS grade (BDH).

Procedure

Two junctions were formed at the same time by a routine procedure which emulated a system previously used for practical pH measurements [5]. While the tank was empty, the potassium chloride solution was adjusted with the micrometer syringes to 1 cm below the top of the capillaries. After filling with solution, the resulting two trapped air bubbles were slowly expelled, leaving, at the end of each capillary, a junction between the two solutions. Each junction was then withdrawn to the required depth by means of the micrometer syringes. The junctions appeared very sharp when they were formed with dyes, but there was the possibility that, after withdrawal, traces of potassium chloride could be left on the capillary walls, making the junctions electrically ill-defined. Some junctions were therefore also formed by a different procedure. Air bubbles were introduced between the potassium chloride solution and the top of the 1-mm capillaries and, by slowly removing the bubbles with a syringe needle, solution was withdrawn into the tube to form a sharp junction. There was no difference in performance, even with 10^{-5} mol kg^{-1} solutions.

Bubbles were introduced into the capillaries to isolate the solution before the tap was opened to measure the bias potential.

Experiments

Four parameters were measured on each solution. The stable potential in quiescent solution, E, was used to calculate the difference in the liquid junction potentials, $E_{\Delta J}$, by subtracting the bias potential which was measured on each occasion. Potentials were taken to be steady when their rate of change was $\leqslant 0.01$ mV min^{-1} and, with this criterion, a differential response time, R, for quiescent solutions was estimated. Switching on the stirrer brought about a shift in potential, measured as E (stirred) $-$ E (quiescent) $= E_s$, and also introduced high-frequency perturbations, the amplitude of which gave E_n, known as the stirring noise. Substitution of a stirrer driven by compressed air

confirmed that none of these effects was associated with electrical interference. Introduction of a supporting aluminium template also confirmed that they were not due to vibration of the capillaries.

The most comprehensive data set was obtained for junctions formed with 0.5-mm bore capillaries. Five different solutions were used: 10^{-5} mol kg^{-1} HCl; 10^{-4} mol kg^{-1} HCl; 10^{-4} mol kg^{-1} HCl + 10^{-3} mol kg^{-1} NaCl; 10^{-4} mol kg^{-1} HCl + 10^{-2} mol kg^{-1} NaCl; and 10^{-4} mol kg^{-1} HCl + 0.5 mol kg^{-1} NaCl. During each day of experimental work, measurements were made on one of these solutions using junctions formed at 2, 5, 10, 15 and 20 mm depth down each capillary, two new junctions, with fresh solution in the cell, being formed for each depth. This procedure was repeated on four different days to obtain information about the reproducibility of all measurements. Thus, in all, a matrix of $5 \times 5 \times 4 = 100$ experiments was obtained.

To isolate the effect associated with the depth down the capillary at which the junction was formed, a further 5×4 data set was obtained for a solution of 10^{-4} mol kg^{-1} hydrochloric acid. One junction was maintained at a constant depth of 20 mm and the depth of the other was varied.

The experimental procedure was repeated for 10^{-4}, 10^{-2} and 0.5 mol kg^{-1} solutions with both capillaries having 0.15-, 1- or 3-mm bores. Junction depths within the two capillaries were varied simultaneously and only one set of measurements was obtained for each capillary bore and each different solution.

RESULTS

Bias potential

Reproducibility of the bias potential gives an estimate of the precision associated with experimental factors other than the liquid junctions. The variation of five consecutive measurements made in one day was usually within 0.01 mV, and measurements made on separate days were within 0.03 mV of one another. This estimate of experimental error was well within variations associated with the liquid junctions (see later).

Capillaries with 0.5-mm bore

Each of the four parameters, $E_{\Delta J}$, R, E_s and E_n, was subjected to analysis of variance [11] to separate variation associated with depth of the junction in the capillary, random errors arising within a day, and day-to-day random errors. Except for measurements made on the most dilute solution, 10^{-5} mol kg^{-1} hydrochloric acid, there was no systematic variation of any of the four parameters with depth of the junction in the capillaries. Errors associated with measurements made on a single day were similar to those arising from day-to-day variations. Therefore, a mean value and standard deviation of each parameter could be calculated for the five different solutions (Table 1).

Although R, E_s and E_n were independent of depth of the junctions within the capillaries for 10^{-5} mol kg^{-1} hydrochloric acid, the potential difference

TABLE 1

Mean values and standard deviations (in parentheses) of the potential difference associated with 0.5-mm junctions, $E_{\Delta J}$, the differential response time, R, the shift in potential from stirred to quiescent solution, E_s, and the stirring noise, E_n, for each ionic strength[a]

Ionic strength (mol kg^{-1})	Potential difference (mV)	Stirring shift (mV)	Stirring noise (mV)	Response time (min)
10^{-5}	+0.63(0.44)[b]	−0.17(0.14)	±0.04(0.02)	9.55(3.25)
10^{-4}	+0.12(0.05)	−0.20(0.09)	±0.04(0.01)	8.05(2.47)
10^{-4} [c]	+0.10(0.06)	−0.16(0.03)	±0.04(0.01)	8.11(1.46)
10^{-3}	+0.14(0.05)	+0.05(0.03)	±0.01(0.00)	5.11(1.90)
10^{-2}	+0.09(0.06)	+0.03(0.02)	±0.03(0.00)	2.71(0.78)
0.5	−0.08(0.01)	+0.06(0.00)	±0.01(0.00)	2.31(0.64)

[a]All standard deviations except the one marked are for 19 degrees of freedom. [b]Mean of potentials measured at 2- and 5-mm depths in the capillaries; the standard deviation has 7 degrees of freedom. [c]Results when one junction was kept at a constant depth.

associated with the junctions, $E_{\Delta J}$, increased systematically with depth (Fig. 3). No systematic effects of the depth of the junction were observed for 10^{-4} mol kg^{-1} hydrochloric acid when one junction was kept at a constant depth of 20 mm (Table 1).

Capillaries with other bores

The dependence of stirring shift, E_s, and stirring noise, E_n, on the depth at which the junction is formed and the bore of the capillary, is illustrated by the recorder traces (Fig. 4). All data for the 0.15-mm bore capillary refers to a junction depth of approximately 1 cm because fine control of the depth proved impractical with such a small bore. E_s and E_n both increased with depth for the 3- and 1-mm bore capillaries, whereas no significant trend was discernible for the 0.5-mm bore.

Response times (Fig. 5) increased as ionic strength decreased for all sizes of capillaries. Junctions formed in capillaries with 0.15-, 0.5- and 1-mm bores achieved equilibrium in similar times, but increasing the bore to 3 mm appreciably slowed the response at all ionic strengths.

There was no discernible dependence of the equilibrium potential difference caused by the liquid junctions, $E_{\Delta J}$, on depth of the junction in capillaries with 1- and 3-mm bores. By treating the observed variation as random, estimates of the mean values and standard deviations could be calculated for each solution and bore (Table 2).

DISCUSSION

Variations in $E_{\Delta J}$, R, E_s and E_n clearly show that the reproducibility of liquid junctions depends on their geometry, and on the ionic strength of the

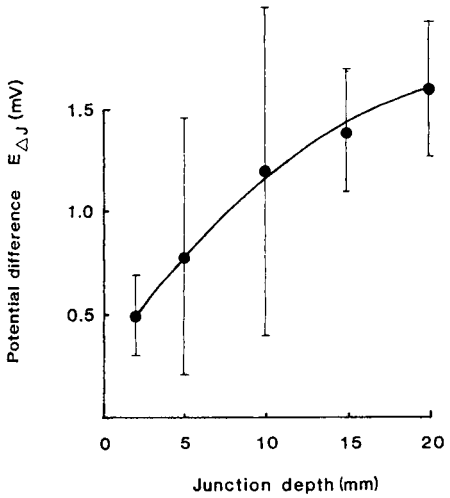

Fig. 3. Variation of the potential difference associated with the junction, $E_{\Delta J}$, with the depth at which each junction was formed in the capillaries, for 10^{-5} mol kg^{-1} HCl. The error bars give the standard deviation for each measurement (3 degrees of freedom).

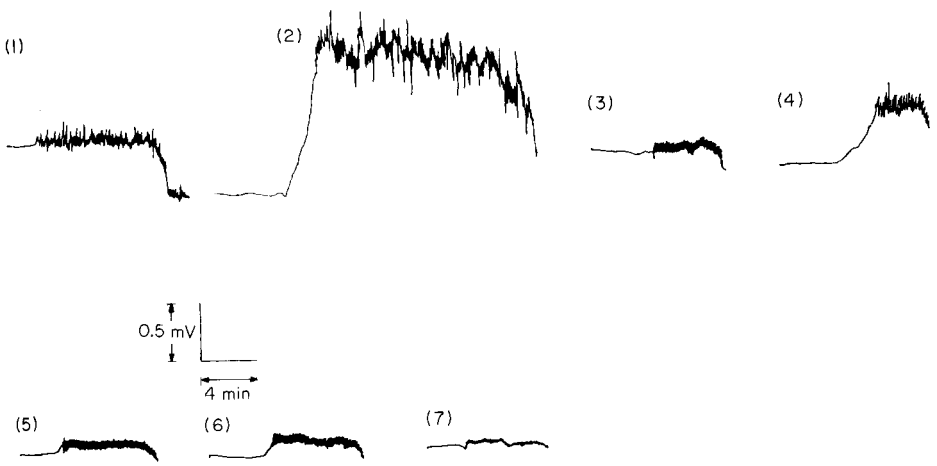

Fig. 4. Recorder traces showing how, for 10^{-4} mol kg^{-1} HCl, E_s and E_n depend on the bore of the capillary and depth at which the junction is formed. Capillary bore: (1, 2) 3 mm; (3, 4) 1 mm; (5, 6) 0.5 mm; (7) 0.15 mm. Junction depth: (1, 3, 5) 2 mm; (2, 4, 6) 20 mm; (7) ≈10 mm. Initial smooth sections correspond to quiescent conditions and serrated sections to stirred solutions.

solution. More detailed interpretation of the results requires an appreciation of how the measured parameters of this work relate to a potentiometric measurement, such as the determination of pH. In the subsequent discussion errors in mV will be accompanied by the equivalent pH error, for example 0.1 mV, 0.0017 pH.

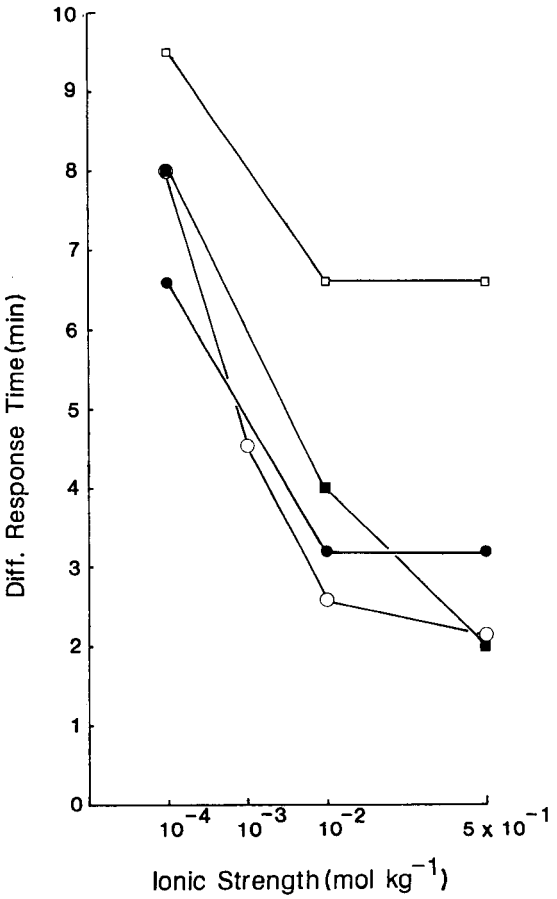

Fig.5. Variation of mean differential response time, R, with ionic strength for capillaries with different bores: (□) 3 mm; (●) 1 mm; (○) 0.5 mm; (■) 0.15 mm.

TABLE 2

Mean values and standard deviations (in parentheses) of the potential difference associated with the junctions, $E_{\Delta J}$, for solutions of three different ionic strengths and for capillaries of four different bores

Bore (mm)	Ionic strength (mol kg^{-1})		
	10^{-4}	10^{-2}	0.5
3[a]	+0.66(0.72)	−0.21(0.05)	−0.14(0.08)
1[a]	−0.18(0.16)	−0.13(0.07)	−0.02(0.06)
0.5[b]	+0.12(0.05)	+0.09(0.06)	−0.08(0.01)
0.15[c]	−0.15	−0.03	−0.02

[a]Standard deviations have 4 degrees of freedom. [b]Standard deviations have 19 degrees of freedom. [c]No replicates available.

Reproducibility

Random variations in $E_{\Delta J}$, given by the standard deviations in Tables 1 and 2, provide an estimate of the precision with which the same junctions can be repetitively formed. The most precise measurements (±0.02 mV, 0.0003 pH) were those made in 0.5 mol kg^{-1} solution with a 0.5-mm bore capillary. Both increasing the bore and decreasing the ionic strength adversely affected the precision, the worst combination of a 3-mm bore and a 10^{-4} mol kg^{-1} solution producing an error of ±0.72 mV (0.012 pH).

Because for most experiments the two junctions were formed in the same way with the same geometry, the potential $E_{\Delta J} = E_{JA} - E_{JB}$ should, within experimental error, be zero. In practice, the mean value of the absolute potential was sometimes appreciably larger than the standard deviation (Tables 1, 2). Largest values of $E_{\Delta J}$ again occurred at low ionic strengths and in measurements with larger bore capillaries. For the lowest ionic strength, 10^{-5} mol kg^{-1}, values of $E_{\Delta J}$ were as large as 1.5 mV, even with 0.5-mm bore capillaries (Fig. 3). Moreover, $E_{\Delta J}$ increased as the junction was formed at greater depth within the capillaries. Although no explanation is yet available, clearly there is an effect which biases the potential systematically.

The existence of finite values of $E_{\Delta J}$ indicates that there is a difference between the two ostensibly identical liquid junctions. The potential generated by this difference represents a further error which gives an indication of the difficulty of constructing liquid junctions of repeatable performance, as would be necessary for inter-laboratory studies. Total errors associated with the free-diffusion junction might pessimistically be assumed to be the sum of the value of $E_{\Delta J}$ and the standard deviation. On this basis, measurements made with a 0.5-mm bore capillary would have an error less than 0.2 mV (0.003 pH) for ionic strengths between 10^{-4} and 0.5 mol kg^{-1}. Increasing the bore to 1 mm would only marginally increase the error (0.3 mV, 0.005 pH). The worst errors are encountered at low ionic strength; in a 10^{-4} mol kg^{-1} solution with a 3-mm capillary, the error was 1.4 mV (0.024 pH) and in a 10^{-5} mol kg^{-1} solution with a 0.5-mm capillary it was 2 mV (0.034 pH).

These results agree with those of other workers. NBS buffers with ionic strengths of 10^{-2}—10^{-1} mol l^{-1}, were checked with a free-diffusion junction with 0.7-mm bore, and found to be consistent to 0.004 pH [9]. Covington et al. [7] tested a free-diffusion junction formed in a T of 1-mm capillaries, by measuring the second dissociation constant of phosphoric acid in 10^{-2} and 10^{-3} mol kg^{-1} solutions; discrepancies of 0.01—0.03 pH were noted. These are similar to the worst cases observed here, albeit for more dilute solutions.

Response times, stirring noise and shift

The criteria of 0.01 mV min^{-1} used to measure differential response times represents a change of 0.00017 pH per minute or 0.01 pH per hour. Although this is a more stringent test than would be required in any routine measurement of pH, it does reveal (Fig. 5) that equilibrium conditions are achieved more slowly in low ionic strength solutions and in wider bore capillaries.

Agitating the solution with a magnetic stirrer increased the noise of the signal, E_n, in all solutions (Table 1, Fig. 3). The magnitude of the noise depended on the bore of the capillary rather than on ionic strength. Errors from this term are very small, however, being <0.04 mV (0.0007 pH).

The shift in potential from quiescent to stirred solution, E_s, could be appreciable; it was larger than 1 mV (0.017 pH) for a 3-mm capillary in dilute solutions. For the 1- and 3-mm capillaries, the shift systematically increased as the junction was formed at greater depth in the capillary. This was surprising because deeper junctions should be more protected from convective effects. Although it is possible that the junction is less well defined when it is formed by withdrawing further down the capillary, there was no evidence that this was so from tests with alternative procedures to form the junctions. While the stirring shifts are not large, they cannot be disregarded because they are similar to the other errors in the system, as exemplified by $E_{\Delta J}$ and its standard deviation (Table 1).

Implications for practical potentiometric measurements

The results for this work were obtained under well-controlled laboratory conditions, and required painstaking attention to detail, particularly with respect to the careful formation of new junctions for each measurement. Although they represent the most optimistic results which could be obtained for any routine analytical procedure, they provide useful insight into measurements in a range of ionic strengths. The results confirm that free-diffusion junctions can provide results precise to 0.02 mV (0.0003 pH) in solutions with ionic strengths greater than 10^{-2} mol kg^{-1}. Geometric differences between junctions have little effect in these concentrated solutions, but at lower ionic strengths they can be important. In this work, the best results were obtained by forming the junctions in a capillary with a 0.5-mm bore. Capillaries with 1-mm bores behaved nearly as well but increasing the bore to 3 mm adversely affected precision and response times. Even the performance of junctions formed in 0.5-mm capillaries deteriorated at an ionic strength of 10^{-5} mol kg^{-1}, where precision was only good to 1 mV (0.017 pH).

Dilute solutions commonly encountered in practice are boiler-feed water, rainwater, soft freshwater, and hard calcareous freshwater with typical ionic strengths of 10^{-5}, 10^{-5}—10^{-4}, 10^{-4}—10^{-3} and 10^{-3}—10^{-2} mol kg^{-1}, respectively. Measurements based on free-diffusion junctions should be fairly straightforward in hard waters, but more difficult for soft water, where precision, response time and convective movements of the solution can all introduce appreciable errors.

This work, which attempted to establish an optimum bore for a free-diffusion junction with cylindrical geometry, did not include investigation of possible bias potentials associated with changing the bore size or transgressing from a simple cylindrical geometry. Work is continuing, with a 0.5-mm bore cylindrical junction as a reference, to investigate the effects of changing the geometry of both static and dynamic junctions. The ultimate aim is to develop

easily used free-diffusion junctions of known performance which are suitable for routine measurements.

We thank Professor Arthur Covington, University of Newcastle-upon-Tyne, for stimulating this work and for his constructive comments, and Jessica Maslen for preparing the manuscript. The Surface Water Acidification Programme of the Royal Society provided financial support.

REFERENCES

1 A. K. Covington, R. G. Bates and R. A. Durst, Pure Appl. Chem., 55 (1983) 1467.
2 M. Whitfield, R. A. Butler and A. K. Covington, Oceanology Acta, 8 (1985) 423.
3 A. H. J. Maas, H. F. Weisberg, W. G. Zijlstra, R. A. Durst and O. Siggaard-Andersen, Clin. Chem. Clin. Biochem., 21 (1983) 313.
4 R. G. Bates, Crit. Rev. Anal. Chem., 10 (1981) 247.
5 D. P. Brezinski, Analyst, 108 (1983) 425.
6 A. K. Covington, P. D. Whalley and W. Davison, Analyst, 108 (1983) 1528.
7 A. K. Covington, P. D. Whalley and W. Davison, Anal. Chim. Acta, 169 (1985) 221.
8 W. Davison and C. Woof, Anal. Chem., 57 (1985) 2567.
9 R. G. Bates, Determination of pH, Wiley, New York, 1964.
10 E. A. Guggenheim, J. Am. Chem. Soc., 52 (1930) 1315.
11 D. T. E. Hunt and A. L. Wilson, The Chemical Analysis of Water; General Principles and Techniques, 2nd edn., R. Soc. Chem., London, 1986.

Analytica Chimica Acta, 187 (1986) 67—77
Eslevier Science Publishers B.V., Amsterdam — Printed in The Netherlands

INSTRUMENTAL CONFIGURATIONS FOR THE DETERMINATION OF SUB-MICROMOLAR CONCENTRATIONS OF ELECTROACTIVE SPECIES WITH CARBON, GOLD AND PLATINUM MICRODISK ELECTRODES IN STATIC AND FLOW-THROUGH CELLS

J. W. BIXLER[a], A. M. BOND*, P. A. LAY[b], W. THORMANN[c] and P. VAN DEN BOSCH

Division of Chemical and Physical Sciences, Deakin University, Waurn Ponds, Victoria 3217 (Australia)

M. FLEISCHMANN

Chemistry Department, The University, Southampton SO9 5NH (Great Britain)

B. S. PONS

Department of Chemistry, Chemistry Building, University of Utah, Salt Lake City, Utah 84112 (U.S.A.)

(Received 25th April 1986)

SUMMARY

Microelectrodes should provide greater analytical sensitivity than electrodes of conventional size. However, the detection of micromolar or lower concentrations with microdisk electrodes requires measurement of femtoamp currents, which is outside the range of most commercially available instrumentation. The novel use of a picoammeter or femtoammeter as a current amplifier permits commercial instrumentation to be used with microdisk electrodes. Such instrumentation incorporating a picoammeter or femtoammeter is limited by the relatively slow rise time; this places restrictions on scan rates in all voltammetric techniques and on pulse widths in transient techniques such as differential pulse and square wave voltammetry. Because of the small currents, the ohmic (iR) drop is very small and polarization of the reference electrode is unimportant; thus a two-electrode format without a potentiostat can be used. Consequently, a microprocessor-based function generator and data storage system, in conjunction with a pico- or femto-ammeter, is satisfactory in providing inexpensive, versatile and very sensitive instrumentation for voltammetric detection with microdisk electrodes. Convenient methods for fabricating platinum, gold and carbon microdisk electrodes for use in stationary and flowing solution configurations are also presented.

The use of microelectrodes has been an important area of research in electrochemistry in the past decade. Microcylinder and microdisk electrodes, as

---

[a]On leave from Department of Chemistry, State University College at Brockport, Brockport, NY 14420, U.S.A.

[b]Present address: Department of Inorganic Chemistry, University of Sydney, N.S.W., 2006, Australia.

[c]Present address: Center for Separation Science, University of Arizona, Tucson, AZ 85721, U.S.A.

0003-2670/86/$03.50 © 1986 Elsevier Science Publishers B.V.

well as arrays of microelectrodes, have been designed, characterized and used in various electrochemical applications [1—14]. The advantages of microelectrodes over conventional-size electrodes have been extolled for several reasons: (i) (ohmic) iR drop distortions (particularly at high scan rates) are minimized [5, 8, 9]; (ii) redox processes can be examined at very positive and very negative potentials [10]; (iii) electrochemical measurements are possible in the absence of added supporting electrolyte [11]; (iv) electroformation of a single metal nucleus can be observed [12]; and (v) electrochemical detection becomes viable where microsensors are required [3, 4, 14, 15]. A disadvantage of microcylinder electrodes is that they cannot be polished reproducibly, which prevents their widespread use in analytical applications. Conversely, microdisk electrodes are well suited for reliable and stable electrochemical detection.

Theoretically, single microdisk electrodes have been shown to provide the potential for considerably greater analytical sensitivity than conventional-size electrodes [5], i.e., the ratio of faradaic to charging current is larger for microelectrodes than for conventional electrodes. The experimental exploitation of this enhancement is complicated by the difficulty of monitoring extremely small voltammetric currents (pico- to femto-amperes) at low concentrations of electroactive species, because it requires extremely sensitive instrumentation. To our knowledge, none of the commercially available electrochemical analyzers provides this feature. Consequently, there has been a great deal of interest in using arrays of microelectrodes [7, 15—17] (i.e., multiple microelectrodes connected in parallel) which yield much higher currents without altering the desirable characteristics of the single microelectrodes. This allows voltammetric techniques to be done with commercial instruments. Such an ensemble of microelectrodes may further increase the analytical sensitivity when overlap of adjacent diffusion layers is present, as theoretically predicted by digital simulation [18]. For instance, the sensitivity is predicted to be up to three orders of magnitude higher by use of pulsed wave-forms with microelectrode arrays instead of conventional size electrodes. While the array of electrodes can be used in many applications, their combined physical size excludes their use where extremely small sensors are needed, such as in on-line detection for capillary separative techniques. Furthermore, arrays of microelectrodes are more difficult to polish reproducibly than are single microdisk electrodes. This has necessitated further development of voltammetric instrumentation for single microelectrodes. In particular, investigations for the proper measurement of extremely small voltammetric currents are needed.

Noise levels are undesirably high when sub-nanoampere currents are measured under the potentiostatic control provided by commercial instruments. Wightman and co-workers modified three electrode potentiostats of conventional design for sub-pA current measurements with time constants of 10 ms [3, 15] and 100 ms [7] respectively, permitting the detection of 10^{-7} M analyte [3]. The very small currents at microelectrodes, however, eliminate

the need for a potentiostat so that electrochemical experiments may be done conveniently with a simple two-electrode system incorporating a wave-function generator and a picoammeter or femtoammeter [4, 11, 12, 19, 20]. In this paper, the advantages and disadvantages are assessed for various instrumental and electrode configurations based on single microdisk electrodes in micromolar analytes which yield sub-picoampere currents. The use of a picoammeter as a current preamplifier for commercially available instrumentation is reported. Methods for the simple construction of platinum, gold and carbon fibre disk electrodes with diameters of 1—60 μm are also discussed. Both stationary and flow-through cell configurations are considered.

EXPERIMENTAL

Instrumentation

All electrochemical experiments were done with a two- or three-electrode system enclosed in a solid aluminium Faraday cage. Various instrumental configurations were used. Conventional instruments used were an EG & G Princeton Applied Research (PAR) 174A polarographic analyzer, a Metrohm VA detector (model E611) with a Metrohm scanner (model E612) and a BAS-100 electrochemical analyzer (Bioanalytical Systems). Other instrumentation was constructed from the following function generators, current-measuring devices and recording units. Function generators used were a PAR-175 universal programmer, a Metrohm VA scanner (model E612) or a Motorola D2 kit [21]. In the two-electrode format, a Keithley 480 picoammeter or a Keithley 614 electrometer in the current mode was used to measure currents. The latter electrometer enables femtoamp currents to be measured. Plots of data were recorded on a Houston Instruments Omnigraphic 2000 Recorder for scan rates <500 mV s^{-1} or a Tektronix Model 5103 N dual-beam storage oscilloscope in conjunction with a Tektronix C-5 oscilloscope camera for scan rates >500 mV s^{-1}. Outputs from the BAS 100 were recorded with a Houston Instrument HIPLOT DMP-40 plotter. The D2 Kit was interfaced directly into a Sphere computer (Paris Electronics, Sydney) and subsequently to a DEC 20/50 computer if required [22], thereby enabling data storage, data evaluation and background correction to be made. Flow-through cell applications were tested with a BAS LC-6 pump, a Rheodyne 7125 injector and Metrohm EA-1096 wall-jet cell in a flow-injection mode.

The Keithley 480 picoammeter was also used as current amplifier to the BAS-100 analyzer or the Metrohm VA detector. An illustration of how a picoammeter was used as a preamplifier for enhanced sensitivity is illustrated as follows for the Metrohm detector. The working electrode was connected to the input of the Keithley 480 picoammeter, the high analog output was connected to the working electrode input of the Metrohm 611 potentiostat and the low output of the picoammeter was connected to the potentiostat shield. Because the full-scale output of the picoammeter is 1 V across

1000 ohms on all ranges, the low impedance input stage of the potentiostat "saw" an apparent cell current of 0—1 mA. For example, an actual cell current of 5 pA produced a full-scale current output signal from the potentiostat when the picoammeter was set on the 1-nA range and the potentiostat was set on the 5-μA range. This is in contrast to the 0.1% of full-scale current output that resulted for the same cell current when only the potentiostat was at its most sensitive (5-nA full scale) range. Similar considerations are valid for the same picoammeter as a preamplifier to the BAS-100 analyzer.

Electrodes and materials

A silver (0.1 M $AgNO_3$ in acetonitrile), a silver/silver chloride (aqueous 3 M NaCl) or a platinum wire was used as the reference electrode for data obtained in acetonitrile for the oxidation of ferrocene (Fc): $Fc \rightleftharpoons Fc^+ + e^-$. In the case of a three-electrode assembly, a platinum wire was used as the auxiliary electrode. Two-electrode configurations, with either the PAR 174A or BAS 100 instruments, rather than the standard three-electrode mode, were achieved by connecting both the auxiliary and reference leads to the reference electrode.

The range of platinum and gold microelectrodes used in this work was prepared at Southampton University as described earlier [11, 13]. These electrodes were mounted in all-glass assemblies. Alternative and simpler construction methods involved sealing metal wires or carbon fibres in glass, or epoxy contained in a glass tube, to produce the microelectrodes shown in Fig. 1. Platinum wire (99.9%; 10—50-μm diameter) or Wollaston wire (99.9% platinum coated with a silver layer; 1—5-μm diameter; Goodfellow Metals, Cambridge, England) was used. Carbon fibres (5-μm diameter; type magnatite) were obtained from Hercules Corporation (Magna, Utah). Construction methods for microelectrodes in both the stationary and flow-through cell configuration are described below. Microelectrodes were cleaned and polished before each experiment as outlined below [11, 19].

Acetonitrile (HPLC grade), ferrocene (analytical-reagent grade), and tetraethylammonium perchlorate (electrochemical grade; TEAP) were used as received. For experiments requiring dry acetonitrile, the solutions were dried in situ by adding neutral alumina (Brockman Activity 1, predried at 200° C) to the cell [11, 23].

Fabrication of microelectrodes for a stationary cell configuration

Epoxy-sealed microelectrodes. A 2-ml volumetric pipette (Fortuna W.G. Co.; soda glass) was cut through the center of the bulb. The narrow ends were fused and drawn out in such a way that the thickness of the glass (ca. 0.7 mm) was retained and the outer diameter was ca. 2 mm at the thinnest point. Cutting at the thinnest point provided two glass holders for microelectrodes (Fig. 1A). A small hole was blown 1.5 cm from the bottom tip and acted as the inlet for introduction of the sealing resin. The platinum electrode wire (ca. 15 mm long) was soldered to a copper wire and inserted

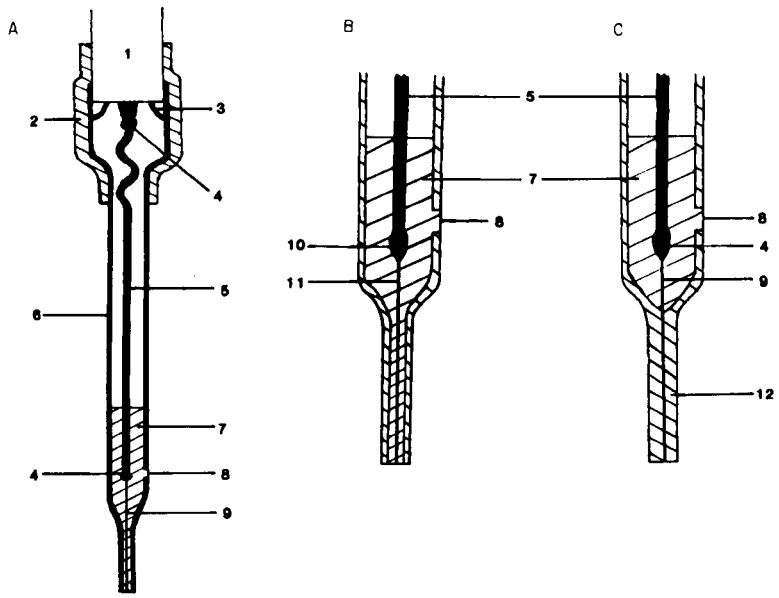

Fig. 1. Construction principles of microdisk electrodes: (A) epoxy-sealed metal wire microelectrode; (B) enlargement of epoxy-sealed carbon fibre electrode; (C) enlargement of glass-sealed metal wire electrode. Parts: (1) coaxial cable; (2) heat-shrink sleeve; (3) earth; (4) solder; (5) copper wire; (6) glass support; (7) epoxy resin; (8) hole for injection of epoxy resin; (9) metal wire; (10) electrical connection with silver epoxy; (11) carbon fibre; (12) glass-sealed tip.

into the tube so that it just protruded. The sealing resin was injected carefully into the tube from a plastic syringe until the resin just appeared at the tip of the electrode. Araldite (Super-Strength Araldite, Ciba-Geigy) or Torr-Seal (Varian Associates) was used as the resin. The thickness of the epoxy seal should be <0.5 mm, otherwise reproducible polishing was difficult. A coaxial cable was connected to the copper wire and was sealed into the top of the electrode by using heat-shrink sleeving (teflon).

After a curing period of at least 24 h, the tip was ground flush by using a rotating diamond disk. It was then polished by hand on wet and dry emery paper, starting with B500 and working down in steps to P1200. Finally, it was polished with alumina (1 μm) water slurries on a polishing cloth. The alumina polishing was used before each experiment.

The 5-μm diameter electrodes from Wollaston wire were constructed by a modified method. After the wire had been soldered to the copper support, it was passed through the tip of the glass holder so that 10 mm of the wire protruded. A gentle flow of air was passed down through the tube to prevent corrosive vapors dissolving the tin solder, and the silver coating was removed from the bottom 5 mm of wire as described elsewhere [19]. As an alternative

to protecting the solder joint by a flow of air, it can be covered with Torr-Seal during the etching stage. The wire was then sealed into the tube as described above. The construction of the epoxy-sealed platinum microelectrodes is illustrated in Fig. 1A.

Carbon-fibre microelectrodes were prepared in a similar manner as the platinum microelectrodes except that the fibre and copper support were connected by using silver epoxy resin (RS Components, cat. no. 555673). This connection is illustrated in Fig. 1B. The carbon-fibre electrodes were polished with the alumina treatment described above.

Glass-sealed microelectrodes. Glass-sealed microdisk electrodes were prepared with the same glass support as the epoxy-sealed microelectrodes (Fig. 1C). The platinum electrode was allowed to protrude from the tip of the tube by a few millimetres. After the hole in the side of the glass gube had been temporarily sealed, the top of the tubing was connected to a water suction pump. The wire was then sealed into the remainder of the thin tip by very gentle heating with a narrow-bore oxy-acetylene torch. When the sealing procedure was complete, Araldite was injected into the remainder of the electrode in order to act as a solid support for the wire. This construction procedure was more difficult than the epoxy-seal method for the smaller (Wollaston wire) microelectrodes.

Fabrication of microelectrodes for a flow-through cell configuration

Two micro-disk electrodes were prepared so as to fit the working electrode port of a Metrohm EA-1096 wall-jet type flow-through detector cell. The cell design required that the disk be located at the centre of the flat end face of a 7-mm o.d. insulating rod. One microsensor was made by fusing glass around a 50-μm diameter platinum wire. The second was prepared by sealing a 5-μm diameter Magnamite carbon fibre into a glass capillary tube with Torr-Seal. Further details are provided elsewhere [24].

RESULTS AND DISCUSSION

Instrumental configurations

The electrochemistry of the Fc/Fc^+ couple in acetonitrile at platinum, gold and carbon microdisk electrodes with diameter from 1—60 μm was examined using a number of instrumental configurations and experimental conditions. It was found that the best instrumental configuration depended on the type of electrochemical measurement that was being made. Each system was examined in terms of sensitivity, voltage range, scan-rate range and versatility.

The three-electrode format is usually considered as mandatory for most voltammetric experiments, but was found not to be universally optimal when microelectrodes were used. Generally, the currents produced by electroactive species in submillimolar concentrations were so small that they could not be detected by most commercially available instruments. Several

options were available to achieve a two-electrode format with an ability to measure pico or femto-ampere currents. First, a conventional electrochemical system was used (BAS-100, Metrohm VA detector), except that the current was preamplified by a picoammeter and the reference and counter electrode connections were both attached to the reference electrode of the two-electrode configuration. Alternatively, electrochemistry was conveniently done with a picoammeter or a femtoammeter with a function generator in a two-electrode system. Examples of the detection of micromolar concentrations of electroactive species in stationary and flow-through cell configurations are shown in Figs. 2 and 3, respectively. In these and all subsequent figures, the raw data are presented without background correction on the stated instrumentation. The cyclic voltammetric data depicted in Fig. 2 were obtained with the picoammeter as preamplifier to the BAS-100 electrochemical analyzer using a 2.0-μm diameter platinum microdisk electrode. This experiment was done without any deliberately added supporting electrolyte and with an analyte concentration of 6.6 μM. The result indicated a

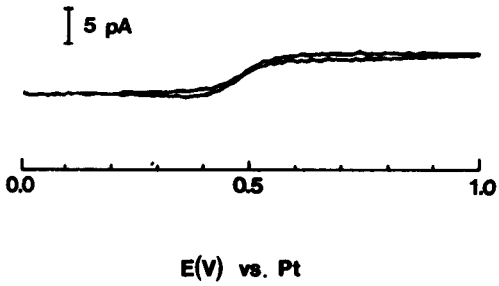

Fig. 2. Cyclic voltammogram at a 2.0-μm diameter platinum microdisk electrode for oxidation of 6.6 μM ferrocene in acetonitrile without any deliberately added supporting electrolyte. The scan rate was 5 mV s^{-1}. A two-electrode configuration was used with the Keithley 480 picoammeter as preamplifier to the BAS-100 electrochemical analyzer.

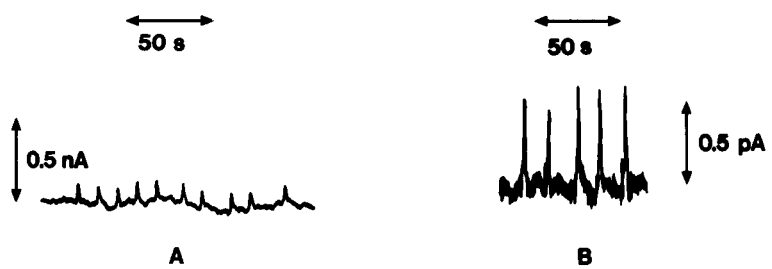

Fig. 3. Flow-injection peaks for ferrocene in acetonitrile with microdisk electrodes in a Metrohm EA1096 wall-jet cell in the three-electrode mode (sample size 20 μl, flow rate 1.4 ml min^{-1}): (A) 50-μm platinum microdisk electrode, 4 μM ferrocene in 0.01 M TEAP, E = 1.1 V vs. Ag/AgCl (3 M aq. NaCl), Metrohm 611 detector only; (B) 5-μm carbon fibre microdisk, 0.1 μM ferrocene in 1 mM TEAP, E = 1.0 V vs. Ag/AgCl (3 M aq. NaCl), Metrohm 611 detector with the Keithley 480 picoammeter as preamplifier.

detection limit of about 2 pA under linear-sweep conditions without background subtraction when the picoammeter was used as preamplifier to the BAS-100. The detection limit was considerably lower if the picoammeter was used as a preamplifier to the Metrohm 611 instrument. This performance was not possible with any single commercial instrument.

Figure 3 illustrates the flow-injection signals obtained with microdisk electrodes in a wall-jet flow cell and highlights the new aspects which need to be considered in this area. Fig. 3A actually shows the limit of detection for ferrocene (4 μM) with the larger 50-μm diameter platinum electrode when the Metrohm 611 detector was used without preamplification. This detection limit was not achieved with the smaller carbon disk, because its diameter, and hence the current, was considerably smaller than for the platinum disk. However, Fig. 3B shows that excellent sensitivity was obtained with the smaller electrode when the picoammeter was used as preamplifier. A detailed presentation of the behavior of these and other microelectrodes in the wall-jet flow-through configuration will be given elsewhere [24].

Two-electrode operation with current preamplification from the picoammeter provided an improvement of about two orders of magnitude in the current detection limit compared to the performance of the commercial instruments. The most versatile and powerful instrumental combination, however, was a versatile function generator, such as one based on the D2 microprocessor kit [21, 22] or equivalent system [25], coupled to a pico- or femto-ammeter (Fig. 4). Such a configuration enabled all electrochemical techniques, including pulse and a.c. methods, to be utilized with extremely

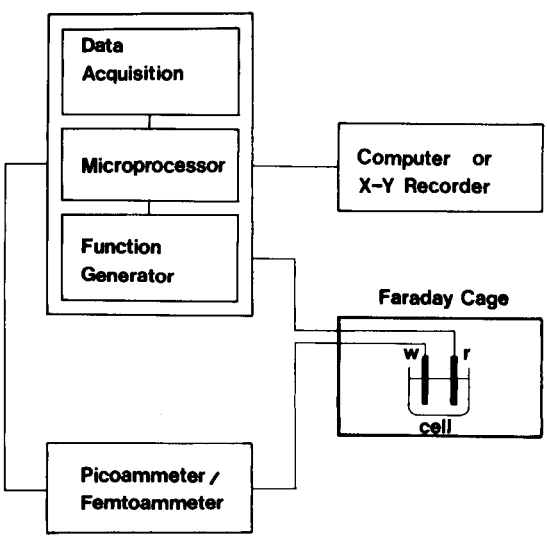

Fig. 4. Block diagram of versatile microprocessor-based instrumentation for the measurement of low currents associated with microdisk electrodes: w, working electrode; r, reference/auxiliary electrode.

high sensitivity, provided that the time constant of the current-measuring device was appropriate for the time scale of the experiment.

While the use of a pico- or femto-ammeter greatly improved the sensitivity of the method, the Keithley instruments used here have relatively slow response times. For example, the scan rates which can be applied in cyclic voltammetry were limited to <500 mV s^{-1} when the picoammeter was introduced into the circuit. The Keithley 614 electrometer only allows sweep rates <50 mV s^{-1} to be used. Similar considerations applied for differential pulse and related techniques. Figure 5 shows the differential-pulse and square-wave voltammograms for oxidation of 1 mM ferrocene in acetonitrile (0.1 M TEAP), when the Motorola D2 kit was used as the wave generator and for data acquisition together with the picoammeter in a two-electrode format. A long pulse width (>60 ms) and a slow sweep rate (<30 mV s^{-1}) were essential when the picoammeter was incorporated and large amplitudes were used. The limiting values with the Keithley 614 electrometer were about an order of magnitude larger for the pulse width and an order of magnitude smaller for the scan rate than those with the picoammeter. Similar restrictions were reported for the three-electrode potentiostats modified for low current measurements [3, 15]. It is very difficult to use a potentiostatically con-

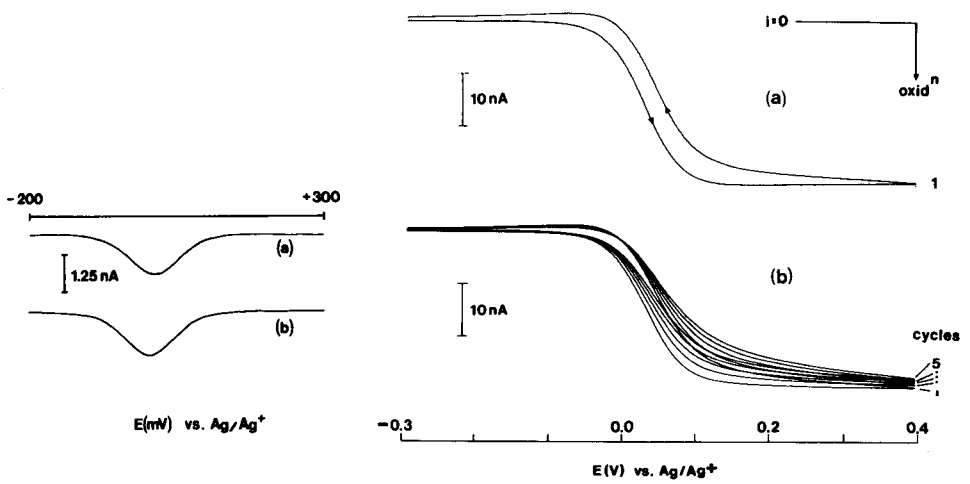

Fig. 5. Differential pulse (a) and square wave (b) voltammetric responses for oxidation of 1 mM ferrocene in acetonitrile (0.1 M TEAP) with the Motorola D2 kit wave generator/data acquisition system and the Keithley 480 picoammeter in the two-electrode format (Fig. 4) with a 60-μm diameter gold microdisk electrode. Pulse width, 100 ms; staircase ramp, 5 mV; amplitude, 50 mV. Scan rates: (a) 5.1 mV s^{-1}; (b) 25.0 mV s^{-1}. Peak positions: (a) 12 mV; (b) 7.5 mV. Peak currents: (a) 1.29 nA; (b) 1.41 nA. The width at half height in both cases is 102.5 mV.

Fig. 6. Cyclic voltammograms for oxidation of 1 mM ferrocene in acetonitrile (0.1 M TEAP) with a 50-μm diameter platinum microdisk embedded in epoxy resin (Torr-Seal): (a) the response of a properly polished electrode; (b) the degradation in successive scans. Scan rate, 5 mV s^{-1}.

trolled system with transient techniques when femtoampere currents have to be measured [26, 27].

The detection of trace amounts of analytes with microelectrodes yielded currents in the picoampere to femtoampere range. With the technology described above, measurements were restricted to slow scan rate, low frequency or long pulse-width methods. In summary, a two-electrode format with a versatile function generator coupled to a picoammeter or femtoammeter with fast response time would appear to provide the most useful instrumental arrangement for electrochemical detection with microelectrodes (Fig. 4). Under steady-state conditions, detection limits in the nanomolar range should be accessible even in non-aqueous solvents such as acetonitrile. Practical examples are being examined and will be described later.

Performance of microdisk electrodes

The goal in most electroanalytical applications is to measure the concentration of electroactive species by the monitored current and to identify the component via the half-wave potential. This requires that the electrodes retain constant properties throughout the experiment which can be experimentally assessed by repetitive cyclic voltammetry. Construction of microdisk electrodes involves the sealing of a metal wire or a carbon fibre with glass or with epoxy resin confined in a glass tube (see Fig. 1). The sealing with epoxy resin is simple, cheap and convenient. Electrodes having diameters down to 5.0 μm were successfully prepared in this manner in our laboratories and elsewhere [2—4]. In general, all glass electrodes were superior with respect to analytical performance. It was found that both the magnitudes and the shapes of the responses in successive cycles degraded quite substantially with epoxy-sealed electrodes, when the epoxy layers were about 0.5 mm thick (Fig. 6). Only minor changes of the limiting current and the half-wave potential were observed for glass-sealed microdisks. A carefully applied epoxy seal gave equivalent results, provided that the thickness of the insulating epoxy layer around the electrode was not much larger than the diameter of the microdisk.

Conclusions

For both dilute solutions of analytes and microdisk electrodes with diameters <10 μm, simple instrumentation consisting of a microprocessor-based function generator/data acquisition system and a pico- or femto-ammeter used in a two-electrode format, is to be preferred to the potentiostatic three-electrode configuration. Unfortunately, commercially available pico- and femto-ammeters are characterized by large time constants ($\geqslant$1 ms) which restricts their use to slow scan rates, large pulse widths and low frequencies. Microelectrodes, however, yield voltammetric currents in the picoampere to femtoampere range and have unique properties in the micro- to milli-second time domains. This calls for the design of new femtoampere (or even sub-femtoampere) current-measuring devices with time constants much less than 1 ms.

This work was partly sponsored by a grant provided by the Australian Research Grants Scheme. P.A.L. is grateful for the support of a Queen Elizabeth II Postdoctoral Fellowship and related grants.

REFERENCES

1 P. Bindra, A. P. Brown, M. Fleischmann and D. Pletcher, J. Electroanal. Chem., 58 (1975) 31.
2 M. A. Dayton, J. C. Brown, K. J. Stutts and R. M. Wightman, Anal. Chem., 52 (1980) 946.
3 A. G. Ewing, M. A. Dayton and R. M. Wightman, Anal. Chem., 53 (1981) 1842.
4 R. M. Wightman, Anal. Chem., 53 (1981) 1125A.
5 J. Heinze, Ber. Bunsenges. Phys. Chem., 85 (1981) 1096.
6 K. Aoki, K. Akimoto, K. Tokuda, H. Matsuda and J. Osteryoung, J. Electroanal. Chem., 171 (1984) 219.
7 W. L. Caudill, J. O. Howell and R. M. Wightman, Anal. Chem., 54 (1982) 2532.
8 J. O. Howell and R. M. Wightman, J. Phys. Chem., 88 (1984) 3915.
9 J. O. Howell and R. M. Wightman, Anal. Chem., 56 (1984) 524.
10 J. Cassidy, S. B. Khoo, S. Pons and M. Fleischmann, J. Phys. Chem., 89 (1985) 3933.
11 A. M. Bond, M. Fleischmann and J. Robinson, J. Electroanal. Chem., 168 (1984) 299.
12 B. Scharifker and G. Hills, J. Electroanal. Chem., 130 (1981) 81.
13 A. M. Bond, M. Fleischmann and J. Robinson, J. Electroanal. Chem., 172 (1984) 11.
14 L. A. Knecht, E. J. Guthrie and J. W. Jorgenson, Anal. Chem., 56 (1984) 479.
15 W. L. Caudill, A. G. Ewing, S. Jones and R. M. Wightman, Anal. Chem., 55 (1983) 1877.
16 N. Sleszynski, J. Osteryoung and M. Carter, Anal. Chem., 56 (1984) 130.
17 W. Thormann, P. van den Bosch and A. M. Bond, Anal. Chem., 57 (1985) 2764.
18 H. Reller, E. Kirowa-Eisner and E. Gileadi, J. Electroanal. Chem., 161 (1984) 247.
19 M. Fleischmann, F. Lasserre, J. Robinson and D. Swan, J. Electroanal. Chem., 177 (1984) 97.
20 T. E. Edmonds, Anal. Chim. Acta, 175 (1985) 1 (and references cited therein).
21 J. E. Anderson, R. N. Bagchi, A. M. Bond, H. B. Greenhill, T. L. E. Henderson and F. L. Walter, Am. Lab., February (1981) 21.
22 A. M. Bond, H. B. Greenhill, I. D. Heritage and J. B. Reust, Anal. Chim. Acta, 165 (1984) 209.
23 O. Hammerich and V. D. Parker, Electrochim. Acta, 18 (1973) 537.
24 A. M. Bond and J. W. Bixler, Anal. Chem., in press.
25 A. M. Bond and A. Norris, Anal. Chem., 52 (1980) 367.
26 M. A. Dayton, J. C. Brown, K. J. Stutts and R. M. Wightman, Anal. Chem., 52 (1980) 946.
27 A. G. Ewing, R. Withnell and R. M. Wightman, Rev. Sci. Instrum., 52 (1981) 454.

Analytica Chimica Acta, 187 (1986) 79—87
Elsevier Science Publishers B.V., Amsterdam — Printed in The Netherlands

BEVELLED CARBON-FIBER ULTRAMICROELECTRODES

RICHARD S. KELLY and R. MARK WIGHTMAN*
Department of Chemistry, Indiana University, Bloomington, Indiana 47405 (U.S.A.)
(Received 13th March 1986)

SUMMARY

A technique for polishing the surface of carbon-fiber ultramicroelectrodes to a bevelled tip is described which simplifies electrode preparation. The bevelled surface has an active area that is more than twice that of a disk electrode fabricated from the same material. This results in larger faradaic currents. It is found that the chronoamperometric current at these electrodes is equal to that calculated for a disk of equivalent area to the elliptical area of the electrode. While the area is increased, the residual current is not, and thus quantitative applications of these electrodes as in vivo probes are facilitated. Furthermore, the bevelled tip results in an electrode that minimizes tissue damage during insertion into brain tissue.

Electroanalytical techniques are useful for the quantitation of several biogenic amines of neurochemical importance [1, 2]. Work in this laboratory has been involved with the development of ultramicroelectrodes for use as in vivo chemical probes [3, 4]. In this report, an improvement in the method of preparation of carbon fiber (10-μm radius) ultramicroelectrodes is described. It is demonstrated that by polishing the surface of the electrode to a bevelled tip, the electrode properties are improved over those previously described, while at the same time, electrode preparation is made easier. The result is an electrode which is practical for routine use.

The preparation of bevelled micropipets has been reported for use as electrodes for intracellular recording of potential [5, 6]. Smooth tissue penetration is facilitated with bevelled intracellular electrodes and they minimize tissue damage along the track made by the electrode. These are desirable characteristics for microvoltammetric electrodes as well. Thus, the previously described methodology has been modified for use with carbon fiber electrodes. As will be shown, this has resulted in an electrode which minimizes tissue damage inherent in in vivo measurements.

The difficulty in the preparation of reliable, reproducible microvoltammetric electrodes was found to be reduced with the use of the polishing technique described herein. Previously, it was necessary to cut the tips of the microelectrodes with a scalpel under a microscope as the final step prior to use [7]. This is difficult to do without a great deal of practice, and under the best of circumstances results in a rough surface which has a significantly higher capacitance than expected. This report describes the new method of

0003-2670/86/$03.50 © 1986 Elsevier Science Publishers B.V.

preparation, and the electrode response is characterized under a variety of conditions. The magnitude of the background current was measured with staircase voltammetry, and was found to be reduced relative to that for cut disk electrodes. The voltammetric response of polished microelectrodes for a number of compounds important for in vivo voltammetry has been obtained. The current amplitude was found to be in agreement with that predicted for disk electrodes when the increase in geometric area is considered.

EXPERIMENTAL

Reagents

All chemicals were reagent grade and were used as received from commercial sources. The buffer used in cyclic voltammetric measurements was composed of citrate and phosphate (9.2 mM, 181.6 mM, pH 7.4). Residual current measurements and in vitro chronoamperometry were done in 1.0 M potassium chloride adjusted to pH 4.4 with 0.10 M hydrochloric acid.

Electrode preparation

Microvoltammetric electrodes are prepared by aspirating carbon fibers of 5-μm radius (Thornell P-55, Union Carbide, New York) into glass capillaries of 1.0-mm outside diameter containing an inner filament. The capillaries are then pulled in a standard electrode puller (Model PE-2, Narishige Scientific Instruments, Tokyo) and cut with a scalpel so that the glass tip has an approximate diameter of 15 μm. The fiber is then sealed in the capillary with epoxy (Epon 828 with 14% metaphenylene diamine, Miller-Stephenson Chemical Co., Danbury, CT) and cured at 110°C overnight.

Polishing procedure. Microelectrodes to be polished are mounted in a tilt-base micromanipulator (Model 55133, Stoelting Co., Chicago) at an angle of approximately 45°. The base of the manipulator is attached to a heavy laboratory jack for stability during the polishing procedure. A thin layer of diamond polishing compound (Metadi II, 1-μm particle size, Buehler Ltd., Lake Bluff, IL) is spread over the reflective glass surface of a microelectrode beveller (Model 1300, World Precision Instruments, New Haven, CT) which has been modified to rotate at a rate of 180 rpm. This glass surface is optically flat to within 2.5 μm and is coated with 0.05-μm alumina powder embedded in urethane. Identical results are obtained by using a locally constructed polishing wheel with a rotation rate of 180 rpm and a simple uncoated glass plate as the support for 1-μm diamond polishing compound. The tip of the microelectrode is lowered using the coarse control of the micromanipulator until it is just above the surface of the diamond polish. The wheel is then started and, using the manipulator fine control (10-μm calibration), the microelectrode is lowered until the tip just touches the surface of the polish. After making a reading of the micromanipulator position, the electrode is lowered between 50 and 100 μm further and left in contact with

the rotating wheel for a period of 10 min. This final distance through which the electrode is moved depends on the roughness of the tip before polishing and the thickness of the layer of diamond polish. After polishing, the electrode is carefully retracted from the glass plate (with the wheel still turning) and dipped in toluene at a temperature just below the boiling point for 15—30 s to remove traces of the polishing compound which remain on the electrode tip.

Once polished, the tip of the microelectrode should be smooth and free from cracks. The length of the bevel can be changed as desired by controlling the angle of incidence to the polishing wheel or the amount of pressure with which the electrode is held against the wheel during polishing.

Apparatus

All potentials are reported vs. a sodium chloride-saturated calomel electrode (SSCE). In vitro measurements were done with a 25-ml glass bottle with a plastic top that was drilled with holes for the electrodes and the nitrogen used to purge the electrochemical cell.

Linear-sweep voltammetry of the catecholamines and related compounds were recorded at polished electrodes which had been electrochemically pretreated in pH 7.4 buffer. The treatment consisted of a triangular wave (70 Hz, 0.00 to +2.00 V) applied for 2—3 s until the observed reversibility for dopamine was the same for each electrode. In vivo chronoamperometric measurements were made at polished microelectrodes acutely implanted in the caudate nuclei of anesthetized rats, and have been detailed previously [8]. Chronoamperometry of potassium hexacyanoferrate(III) was done at untreated, polished microelectrodes using a potential step between +0.50 and −0.40 V, and step times of 1.0 s.

Voltammetry and chronoamperometry were done with the use of an IBM-PC (Boca Raton, FL) with a Labmaster interface card (Scientific Solutions, Solon, OH) which includes a programmable clock, digital-to-analog and analog-to-digital converter. The digital-to-analog converter controlled the potential. A locally-constructed, low-noise, 3-electrode potentiostat [9] was used. The output of the current-to-voltage converter was filtered with a two-pole filter with a roll-off frequency of 0.20 kHz for chronoamperometry. The signal was digitized and stored on floppy disks. In chronoamperometry, the current for the forward potential step was corrected for background contributions by subtracting the current during a potential pulse obtained in a solution of supporting electrolyte prior to the addition of hexacyanoferrate(III). The time dependence of the chronoamperometric current was evaluated by a linear regression against $t^{-1/2}$.

Residual currents for both cut and polished electrodes were measured by using a staircase waveform generated from the IBM-PC [9] at scan rates from 0.05 to 20 V s^{-1}. Scans were run between 0.00 and 0.80 V in a solution of 1.0 M KCl containing no electroactive species. Appropriate filtering was used to control the time constant of the 3-electrode potentiostat at each scan rate.

The current was sampled at the end of each potential step. The residual current, normalized for area, was measured at +0.40 V and divided by the scan rate (v) [10]. Geometric areas for polished electrodes were measured with scanning electron microscopy.

RESULTS AND DISCUSSION

Properties of polished electrodes

A scanning electron micrograph of the tip of a microelectrode which has been polished by the proposed procedure is shown in Fig. 1. The total average electrode width (including insulation) at the region of the bevel is approximately 20 μm. The sharp tip of the electrode can be seen in the micrograph, and contributes to the ease of tissue penetration when used as an in vivo probe (vide infra). The active area of the microelectrode, defined by the surface area of exposed carbon fiber, is elliptical rather than disk-shaped. This provides a major advantage because an increase in working surface area is obtained that is confined virtually to the same space as a cut microelectrode. The increased surface area results in increased voltammetric currents, which has been shown to be an important consideration when working at low concentrations for which currents are often in the range of 10–100 pA [9]. If spatial resolution is not a concern, the degree of the bevel can be extended to approach 200 μm by reducing the angle of incidence of the electrode to the wheel when polishing.

In the enlargement shown on the right side of Fig. 1, the integrity of the seal between the epoxy and the glass and carbon fiber is readily apparent. The grooves that appear on the surface are probably due to the particle size

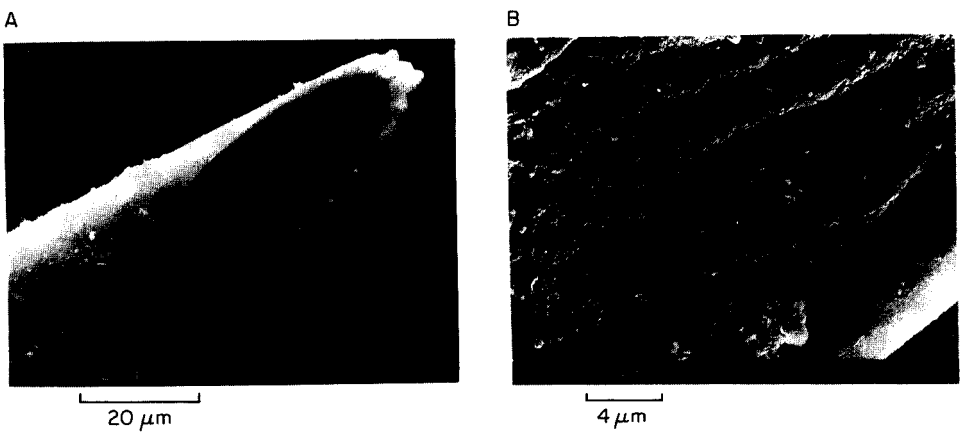

Fig. 1. Electron micrographs of ultramicroelectrodes bevelled using 1-μm diamond polish: (A) electrode of approximately 10-μm tip radius with the extent and angle of bevel shown; (B) enlargement showing detail of the seal between the carbon fiber (at center), epoxy, and the glass capillary.

of the polishing compound used in the procedure, and, to a lesser degree, the roughness of the polishing surface. Polishing on 0.25-μm diamond polish requires substantially longer polishing times and, therefore, is unsatisfactory for routine use. Carbon fiber electrodes can be polished with 1-μm and smaller alumina particles; however, this procedure gave voltammetric results that were less reversible than obtained with diamond polish and, in some cases, the electrode broke during polishing.

The reproducibility of electrodes polished with the reported procedure is illustrated in Fig. 2. The limiting current from voltammograms for the oxidation of 0.10 mM dopamine at four carbon fiber electrodes sequentially polished under the same conditions, was found to be 428 ± 15 pA (3.5%). The sigmoidal shape of the voltammograms is characteristic of ultramicroelectrodes [11] and arises because the electrolysis rate is approximately equal to the rate of diffusion of molecules to the electrode surface. The average value of the half-wave potential ($E_{1/2}$) for dopamine at these electrodes is 140 ± 2 mV.

The half-wave potentials and respective degrees of electrochemical reversibility of a number of easily oxidizable species observed at polished carbon fiber electrodes are given in Fig. 3. These compounds are all present in varying concentrations in the mammalian brain and their voltammetric characteristics are of interest for applications of voltammetry in vivo. The selectivity of an electrode for any of these species is dependent on the surface state of the carbon interface, which can be altered according to the type of pretreatment

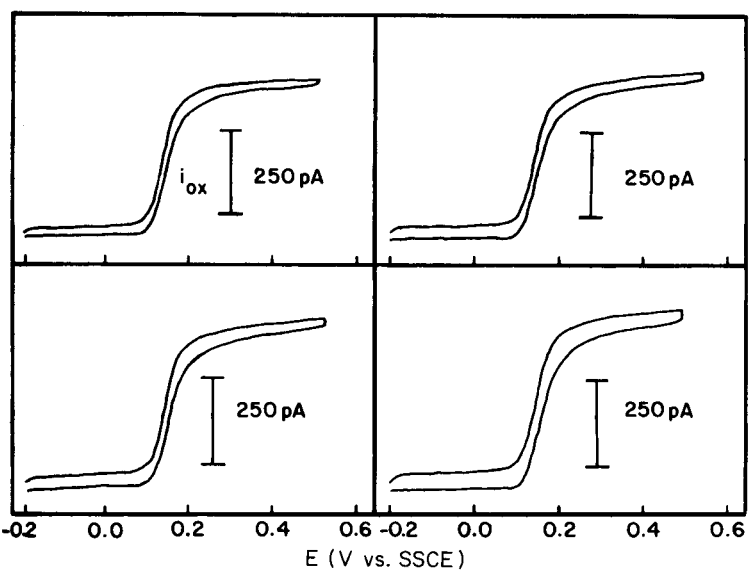

Fig. 2. Cyclic voltammograms of 0.10 mM dopamine recorded at four different ultramicroelectrodes which were polished sequentially by the procedure outlined in the text. Scan rate was 0.10 V s^{-1} in each case.

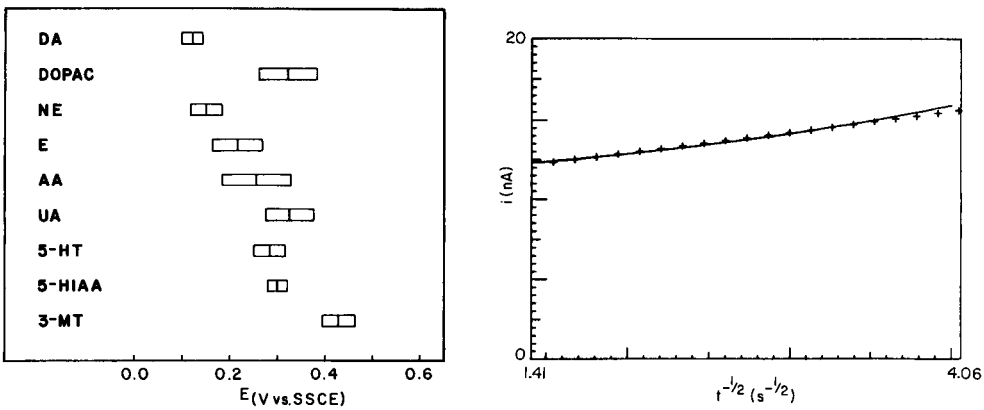

Fig. 3. Voltammetric properties of neurochemically important compounds at polished ultramicroelectrodes. The data are plotted according to the convention of Miner et al. [13] with one edge of the bar at $E_{1/4}$, the other edge at $E_{3/4}$, and the center line at $E_{1/2}$. The width of the bar is indicative of the electrochemical reversibility of the compound. Concentration of each was 0.10 mM in pH 7.4 citrate/phosphate buffer, and the scan rate was 0.10 V s^{-1}. The abbreviations used are: DA, dopamine; DOPAC, 3,4-dihydroxyphenylacetic acid; NE, norepinephrine; E, epinephrine; AA, ascorbic acid; UA, uric acid; 5-HT, 5-hydroxytryptamine; 5-HIAA, 5-hydroxyindoleacetic acid; 3-MT, 3-methoxytyramine.

Fig. 4. A representative plot of chronoamperometric current vs. $t^{-1/2}$ for the reduction of 4.0 mM hexacyanoferrate(III) in 1.0 M KCl at a polished ultramicroelectrode. E_{step} = −0.40 V, 0.5-s duration, background-corrected.

[12]. The observed electrochemistry for the species in Fig. 3 at polished microelectrodes is not significantly different from that reported for glassy carbon or for unmodified carbon fiber electrodes which were cut with a scalpel [3]. When the electrochemical pretreatment reported here is used, the potentials shown in Fig. 3 are quite reproducible from electrode to electrode after polishing. Similar "mild" electrochemical pretreatments were found to be efficacious at glassy carbon [14] and the cylindrical axis of carbon fibers [15]. More vigorous oxidation of the electrode surface results in adsorption of some catechols [15, 16].

Chronoamperometry

The current observed at ultramicroelectrodes has been shown to be a function of the size of the diffusion layer relative to the diameter of the electrode [7]. A rigorous expression for the observed current at a stationary finite disk electrode during a potential step experiment has been derived [17, 18]. This expression predicts a transition between the time-dependent (Cottrell) and steady-state regions in the current/time curves obtained in quiescent solutions. For large values of the ratio Dt/r^2 (D is the diffusion coefficient, r is the radius of the disk), Szabo has shown that the current (i) during chronoamperometry is given by

$$i = [8\,nFAD^{1/2}c/\pi^2(\pi t)^{1/2}] + 4rnFDC \quad (1)$$

where A is the electrode area, and the other terms have their usual electrochemical meaning. Values larger than 4 are predicted for the coefficient in the last term of the equation for microelectrodes in which the thickness of the glass insulating material around the carbon fiber is almost the same size as the fiber itself [19]. A linear least-squares fit of the current vs. $t^{-1/2}$ under conditions for which Eqn. 1 holds should give a straight line, the slope of which can be used to determine the electrochemically active area, and the intercept of which gives the steady-state term [20]. Chronoamperometry at the bevelled electrodes, which have an elliptic geometry, was examined to determine deviations from the behavior expected from Eqn. 1.

Chronoamperometry at bevelled electrodes was examined in 1.0 M KCl with potassium hexacyanoferrate(III), a system for which the diffusion coefficient is well known [21]. The results of the regression of the measured current vs. $t^{-1/2}$ for one of the polished microelectrodes is shown in Fig. 4 (data at times less than 60 ms were disregarded because Eqn. 1 is valid only for large values of Dt/r^2). Correlation coefficients between 0.966 and 0.973 were obtained for similar regressions of the results of six electrodes. The electrochemical area for each of the six electrodes was then calculated from the slopes. An average value for electrode area of $(1.98 \pm 0.50) \times 10^{-6}$ cm^2 was determined in this manner, which was found to be in excellent agreement with the geometric area of $(1.94 \pm 0.30) \times 10^{-6}$ cm^2 obtained from electron microscopy. The latter value for area was then used to calculate the radii of disks having an equivalent area to the ellipse. These radii were used, along with the intercepts, to determine an experimental value for the coefficient in the second term of Eqn. 1. A value of 4.14 ± 0.36 was obtained. This is an empirical observation and may not be valid for all values of Dt/r^2. However, these results indicate that Eqn. 1 can be used for quantitative applications of these electrodes where exact adherence to theory is not required.

Residual current measurements

The residual current as a function of scan rate was examined for both polished and cut microelectrodes. The quality of the seal between the carbon fiber and the glass insulating material directly affects the magnitude of the observed residual current. Imperfections in the seal result in an increased solution/electrode interface [10], and thus higher residual currents, especially at low scan rates. For both the cut and the polished microelectrodes, the residual current divided by scan rate remains essentially constant for scan rates between 0.05 and 20 V s^{-1}, suggesting that a relatively good seal exists with both types of electrodes (Fig. 5). The mean value (normalized for electrochemically determined area) of polished electrodes was $(28.2 \pm 4.7)A$ s cm^{-2} V^{-1} ($n = 4$ with 9 values of scan rate for each). Electrodes which were cut with a scalpel had a value of $(55.4 \pm 11.7)A$ s cm^{-2} V^{-1} ($n = 4$). This difference is significant at the 99.9% confidence level ($p < 0.001$, Students'

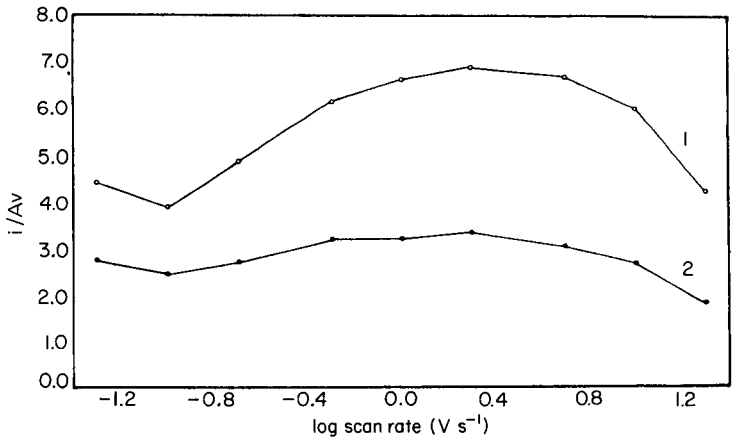

Fig. 5. Residual current divided by scan rate as a function of scan rate: (1) for cut electrodes; (2) for polished electrodes. Current measurements were made at +0.40 V vs. SCE in 1.0 M KCl for scan rates between 0.05 and 20 V s^{-1}, and normalized for electrochemical area.

two-sided *t*-test). The standard deviations obtained for the two measurements are in part an indication of the extent to which seal quality is maintained by the polishing procedure and the increased roughness of the cut electrodes observed with electron microscopy. As expected, the polished electrodes show a smaller deviation in the value of residual current from electrode to electrode, illustrative of the reproducibility inherent in the polishing technique.

In vivo comparison

Previous experiments in this [22] and other laboratories [23] have suggested that data from in vivo measurements with ultramicroelectrodes involve the transport of oxidizable species to the electrode surface through two distinct regions of diffusion. The first is a region of free diffusion close to the surface of the electrode, and is thought to correspond to a fluid pool surrounding the electrode tip. The second is a region of restricted diffusion, wherein the path followed by an oxidizable species is impeded by elements of neural tissue. The slope of i vs. $t^{-1/2}$ data for chronoamperometry, normalized by area, gives an indication of the relative pool size [22]. A recently formulated model for hemispherical electrodes allows the determination of the radius for the region of high diffusion coefficients from chronoamperometric data [8]. This model predicts, and it has been experimentally demonstrated at cut electrodes, that the chronoamperometric current for an irreversible electrochemical reaction exhibits greater time dependence in vivo than in vitro. The in vivo result arises because mass transport from the reduced volume fraction of brain extracellular fluid and the reduced diffusion coefficient in brain tissue impedes access of molecules to the electrode.

In this work, the chronoamperometric measurements were made for

polished microelectrodes, and the relative pool sizes calculated from the model were used to compare the tissue damage caused by each type of electrode. The polished electrodes gave an average pool radius of 10 ± 2.6 μm (n = 4), which is almost identical to that reported elsewhere for cut electrodes [8]. The similarity in apparent pool size exists even though the beveled electrode has a larger surface area, indicating proportionately less tissue damage. The small size of the standard deviation of the measurements with polished electrodes indicates that the damage done by electrode insertion is small, but reproducible. This increase in reproducibility should lead to more reliable data obtained in the application of polished electrodes to in vivo electrochemistry.

This research was supported by the National Institute of Health (PHS R01 NS-15841). The technical assistance of Bradley Johnson in obtaining the electron micrographs is gratefully acknowledged, as are experimental contributions from Paul Kovach and Robert Wilson.

REFERENCES

1 R. N. Adams and C. Marsden, in L. L. Iversen, S. D. Iversen and S. H. Snyder (Eds.), Handbook of Psychopharmacology, Vol. 15, Plenum, New York, 1982, p. 1.
2 J. A. Stamford, Brain Res. Rev., 10 (1985) 119.
3 P. M. Kovach, A. G. Ewing, R. L. Wilson and R. M. Wightman, J. Neurosci. Methods, 10 (1984) 215.
4 A. G. Ewing, J. C. Bigelow and R. M. Wightman, Science, 221 (1983) 169.
5 K. T. Brown and D. G. Flaming, J. Neurosci. Methods, 1 (1979) 25.
6 T. E. Ogden, M. C. Citron and R. Pierantoni, Science, 201 (1978) 469.
7 M. A. Dayton, J. C. Brown, K. J. Stutts and R. M. Wightman, Anal. Chem., 52 (1980) 946.
8 C. Amatore, R. S. Kelly, E. W. Kristensen, W. G. Kuhr and R. M. Wightman, J. Electroanal. Chem., in press.
9 J. O. Howell, W. G. Kuhr, R. E. Ensman and R. M. Wightman, J. Electroanal. Chem., 209 (1986) 77.
10 K. R. Wehmeyer and R. M. Wightman, J. Electroanal. Chem., 196 (1985) 417.
11 R. M. Wightman, Anal. Chem., 53 (1981) 1125A.
12 M. R. Deakin, P. M. Kovach, K. J. Stutts and R. M. Wightman, Anal. Chem., in press.
13 D. J. Miner, J. R. Rice, R. M. Riggin and P. T. Kissinger, Anal. Chem., 53 (1981) 2258.
14 J. C. Hoogvliet, C. M. B. Van den Beld, C. J. Van der Poel and W. P. Bennekom, J. Electroanal. Chem., 201 (1986) 11.
15 S. Sujaritvanichpong, K. Aoki, K. Tokuda and H. Matsuda, J. Electroanal. Chem., 198 (1986) 195.
16 P. M. Kovach, M. R. Deakin and R. M. Wightman, J. Phys. Chem., 90 (1986) 4612.
17 K. Aoki and J. Osteryoung, J. Electroanal. Chem., 122 (1981) 19.
18 D. Shoup and A. Szabo, J. Electroanal. Chem., 140 (1982) 237.
19 D. Shoup and A. Szabo, J. Electroanal. Chem., 160 (1984) 27.
20 A. S. Baranski, W. R. Fawcett and C. M. Gilbert, Anal. Chem., 57 (1985) 166.
21 M. Von Stackelburg, M. Pilgram and V. Toome, Z. Electrochem., 57 (1953) 342.
22 M. A. Dayton, A. G. Ewing and R. M. Wightman, J. Electroanal. Chem., 146 (1983) 189.
23 H.-Y. Cheng, J. Schenk, R. Huff and R. N. Adams, J. Electroanal. Chem., 100 (1979) 23.

Analytica Chimica Acta, 187 (1986) 89—97
Elsevier Science Publishers B.V., Amsterdam — Printed in The Netherlands

AMPEROMETRIC DETECTION OF THIOPURINES IN BLOOD PLASMA WITH A COBALT-PHTHALOCYANINE CHEMICALLY MODIFIED ELECTRODE AFTER LIQUID CHROMATOGRAPHY

MARY KIM HALBERT and RICHARD P. BALDWIN*

Department of Chemistry, University of Louisville, Louisville, Kentucky 40292 (U.S.A.)

(Received 6th March 1986)

SUMMARY

Cobalt phthalocyanine-containing carbon paste electrodes are used as electrocatalytic amperometric sensors for 6-mercaptopurine, 6-thioguanine, and several related thiopurines in blood plasma after separation by liquid chromatography. Required sample preparation is minimal, and total quantitation time is 8 min or less. Detection limits are 1.5—8 pmol, approximately an order of magnitude better than that obtained with ultraviolet or fluorescence detection.

6-Mercaptopurine (6-MP) and 6-thioguanine (6-TG) are widely used in the treatment of leukemia, and the determination of these compounds and their metabolites is essential for the characterization of their physiological activity and disposition. Existing liquid chromatographic procedures for these compounds, most of which utilize ultraviolet (u.v.) absorption [1–8] or fluorescence [9, 10] detection, possess one or more disadvantages that include inadequate sensitivity, poor selectivity, time-consuming sample preparation, low analyte recovery, and long chromatographic elution times. In addition, because the absorption maxima of the thiopurines occur at substantially different wavelengths, either wavelength-scanning detection or multiple injections of each sample must be used if optimum quantitation of several thiopurines is to be achieved.

An alternative approach, based on liquid chromatography with electrochemical detection (LCEC), has been reported by Imai et al. [11]. In that work, a 1-pmol detection limit was obtained by utilizing oxidation of 6-MP at +0.8 V vs. Ag/AgCl at an electrochemically treated glassy carbon electrode. Although this detection limit was somewhat superior to that generally attained by u.v. absorption, no thiopurines other than 6-MP were investigated; and, because of problems attributed to co-eluting interferences and electrode surface fouling, it was concluded that u.v. detection provided a preferable approach [11].

Recent work in this laboratory has demonstrated that, compared to conventional carbon electrodes, chemically modified electrodes containing surface-immobilized cobalt phthalocyanine (CoPc) can present distinct

0003-2670/86/$03.50 © 1986 Elsevier Science Publishers B.V.

advantages for LCEC determination of thiol compounds [12, 13]. Incorporated into a carbon paste matrix, CoPc acts as an electrocatalyst for the thiol oxidation and thereby enables the reaction to proceed at a lower potential than at the analogous unmodified surface. Accordingly, an LCEC procedure, with a CoPc electrode, was developed for cysteine and glutathione in plasma and whole blood [13]. Because these compounds were detected at the modified surface at +0.75 V vs. Ag/AgCl, which is several hundred millivolts lower than is required under the same conditions at bare carbon electrodes, greatly enhanced sensitivity and selectivity were obtained. Further, the CoPc-modified electrodes proved to be sufficiently rugged to be used with real samples; surface renewal, equilibration time (10 min), and reproducibility (<10% variation) all were sufficiently favorable that electrode instability problems, commonly encountered for electrochemical detection in complex matrices such as blood and usually ascribed to surface fouling by strongly adsorbing sample components, were significantly decreased.

In this work, the use of LCEC for the quantitation of various thiopurines in human blood plasma is examined in detail along with the application of CoPc chemically modified electrodes for this purpose. The resulting LCEC procedure represents an improvement over the existing methods in that it combines both excellent sensitivity (as low as 1.5 pmol injected for 6-MP) and minimal sample preparation and quantitation time (approximately 8 min per sample). The CoPc electrodes are useful in the detection of not only 6-MP but also other unsubstituted thiopurines including 6-TG and the riboside metabolites of both compounds.

EXPERIMENTAL

Chemicals and apparatus

Except for CoPc and 6-thiouric acid (6-TU), all chemicals used were obtained from Sigma Chemical Co. and were used as received without further purification. The CoPc was obtained from Eastman Kodak, and the 6-TU was prepared enzymatically by adding xanthine oxidase (obtained from Sigma) to a pH 7.4 solution of 6-MP according to the procedure of Van Baal et al. [8].

Unmodified and CoPc-modified carbon pastes were prepared as was described previously [12, 13]. The modified paste used in these experiments contained 2% CoPc by weight and was prepared by thoroughly mixing 0.10 g of CoPc with 4.9 g of graphite powder prior to the addition of Nujol oil.

The equipment used for cyclic voltammetry and liquid chromatography was as previously described [12, 13]. All potentials were measured against a Ag/AgCl reference electrode. For chromatographic experiments, a precolumn packed with 40-μm pellicular C-18 particles was placed before the injector to saturate the mobile phase and extend the life of the guard cartridge and primary column. The primary column was a 3-cm Perkin-Elmer

C-18 column containing 3-μm particles; a Brownlee Laboratory (Santa Clara, CA) C-18 guard cartridge was inserted between the injector and the primary column. The mobile phase consisted of 5% methanol/95% 0.05 M phosphate buffer (pH 7.0). The injection volume was 20 μl, and the flow rate was always 1.0 ml min^{-1}.

Sample preparation

Standard solutions of thiol compounds were prepared by a modification of the method of Van Baal et al. [8]. Each thiopurine was added to a 100-ml volumetric flask containing 10—15 ml of 0.025 M potassium dihydrogenphosphate. After 1—2 ml of 4.0 M potassium hydroxide was added and the solution was stirred to dissolve the thiopurine, the potassium hydroxide was neutralized with 4.0 M phosphoric acid. Dilutions to final volumes were made with 1 g l^{-1} disodium-EDTA to inhibit oxidation of the thiols by metal ions present.

Plasma was obtained from the Louisville Chapter of the American Red Cross, and EDTA was added to give a concentration of 1.5 g l^{-1} (equivalent to that which would be attained if commercially available EDTA tubes were used for blood collection). Samples were prepared by mixing 1 ml of plasma and 100 μl of the thiopurine standard solution in a 12 × 75-mm polyethylene sample tube. Plasma protein was precipitated by adding 200 μl of 60% trichloroacetic acid and then mixing the resulting suspension. After centrifugation at 4000 rpm for 10 min, 250 μl of the supernatant was diluted with 2.25 ml of EDTA solution.

RESULTS AND DISCUSSION

Cyclic voltammograms of 6-MP at plain carbon paste (CPE), glassy carbon (GCE), and 2% CoPc carbon paste electrodes are shown in Fig. 1. At the first two surfaces, broad, poorly defined oxidation waves were observed with peak potentials of +0.54 V at CPE and +0.48 V at GCE. No reduction signal was seen on the reverse scan. This agrees well with the voltammetric behavior reported previously for this compound at a specially pretreated glassy carbon [11]. In contrast, the cyclic voltammogram for 6-MP at the CoPc electrode exhibited an oxidation wave for the thiol group at +0.33 V. Peak current for this wave was roughly twice that of the waves seen for the same 6-MP concentration at the unmodified electrodes at +0.5 (GCE) and +0.6 V (CPE). For all electrodes, the observed currents were proportional to the 6-MP concentration and to the square root of the potential scan rate (up to 600 mV s^{-1}). Also, the oxidation waves shifted to more positive potentials with decreasing pH.

Directly analogous cyclic voltammetric results, summarized in Table 1, were obtained for a series of solutions containing other thiopurine compounds. These included 6-mercaptopurine riboside (6-MPR), 6-thioguanine (6-TG), 6-thioguanine riboside (6-TGR), 6-thiouric acid (6-TU), and 6-

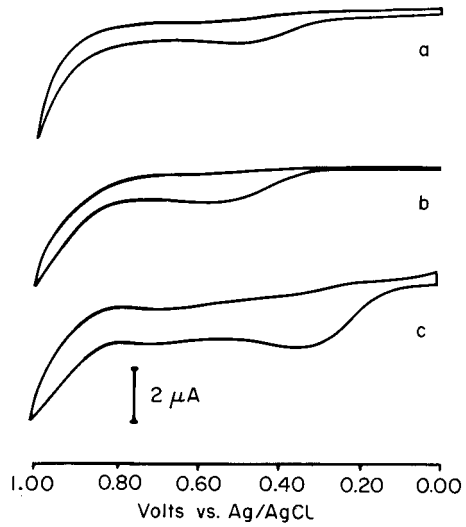

Fig. 1. Cyclic voltammograms of 0.10 mM 6-MP at (a) GCE, (b) unmodified CPE, and (c) 2% CoPc carbon paste electrode. Electrolyte, 0.10 M phosphate buffer, scan rate, 50 mV s^{-1}.

TABLE 1

Cyclic voltammetric data for thiopurines[a]

Compound	Peak potential (V) and peak current (μA) of first oxidation wave		
	CPE	GCE	CoPc CME
6-MP	+0.48 (0.9)	+0.54 (1.1)	+0.32 (2.5)
6-MPR	+0.47 (0.9)	+0.61 (1.0)	+0.33 (1.8)
6-TG	+0.60 (0.8)	+0.60 (0.9)	+0.33 (2.0)
6-TGR	+0.60 (0.8)	+0.60 (0.7)	+0.32 (1.3)
6-TX	+0.59 (1.4)	+0.59 (0.9)	+0.45 (1.5)
6-TU	+0.59 (1.8)	+0.60 (1.3)	+0.38 (2.4)
6-MTG	+0.94 (5.6)	+0.56(1.4)[b]	+0.73 (1.9)
6-MMP	+0.66 (0.2)	+0.63 (0.4)	+0.63 (0.5)

[a]Concentration of thiopurines was 0.10 mM; electrolyte was pH 7.0 phosphate buffer; scan rate was 50 mV s^{-1}. [b]Wave was peak-shaped and increased upon continued cycling; most likely, adsorption occurred.

thioxanthine (6-TX), which is not a metabolite of 6-MP or 6-TG but is frequently used as an internal standard in their determination. In all cases, oxidations observed at the unmodified carbon electrodes were irreversible and exhibited peak potentials between +0.5 V and +0.7 V vs. Ag/AgCl. However, cathodic shifts of 140 to 280 mV in peak potentials and two-fold increases in peak currents were observed at the CoPc electrode. Moreover, the

catalytic oxidation potentials were approximately the same, presumably because the oxidation mechanism is virtually the same in all cases. As was discussed in previous studies in which the CoPc electrode was utilized to enhance detection of thiols [12, 13], the thiol moiety is catalytically oxidized to the disulfide form by the surface-immobilized CoPc [14]. In the present case, the higher pH used permitted the catalytic oxidation to take place at a somewhat lower potential, presumably because of the greater degree of dissociation of the sulfhydryl species. Oxidation of the compounds in which the thiol group is methylated (e.g., 6-methylmercaptopurine (6-MMP) and 6-methylthioguanine (6-MTG)) was not altered by the presence of CoPc.

In view of these cyclic voltammetric results, LCEC, particularly when performed at electrodes modified with CoPc, appeared to offer considerable potential for thiopurine determination. As a first test of this possibility, chromatograms (shown in Fig. 2) were obtained for a standard solution containing 10 μM each 6-MP (retention time 2.5 min) and 6-MPR (4.0 min) at 2% CoPc, GCE, and CPE (all at +0.60 V). As expected from the cyclic

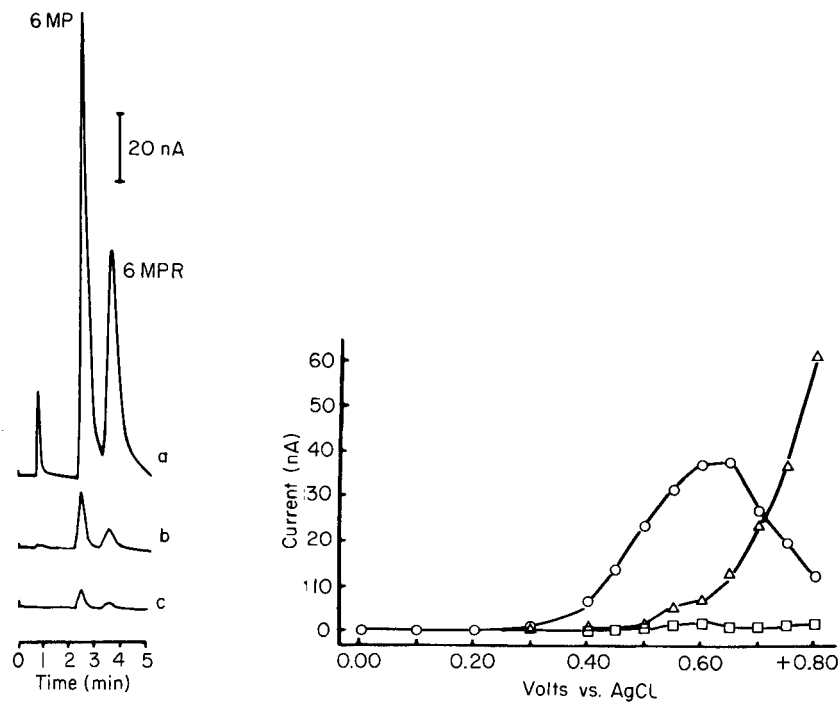

Fig. 2. Chromatograms of 10 μM standard solution of 6-MP and 6-MPR at (a) CoPc electrode, (b) GCE, and (c) CPE. Electrode potential, +0.60 V vs. Ag/AgCl; mobile phase, 5% methanol/95% 0.05 M phosphate buffer, pH 7.0; flow rate, 1 ml min^{-1}.

Fig. 3. Hydrodynamic voltammograms for LCEC of 6-MP: (○) at CoPc electrode; (□) at CPE; (△) at GCE. Same conditions as in Fig. 2.

voltammetric behavior, currents observed at this potential at the CoPc electrode were much larger than when the unmodified electrodes were used. Corresponding hydrodynamic voltammograms, summarizing LCEC current response over a range of detector potentials, are shown in Fig. 3 for 6-MP. As the application of higher potentials resulted in catalyst deactivation and a decrease in electrode response, the optimum detector potential for the 2% CoPc electrode was +0.60 V. This is approximately 150 mV lower than the potential at which the GCE gave an equivalent current and 450 mV lower than that for the CPE. Current response at the GCE reached a plateau only at about +1.2 V, while the response at the ordinary CPE did not reach a plateau at all in the potential range examined. The hydrodynamic voltammograms obtained for 6-MPR were identical in shape to those for 6-MP, but current levels were only about one-third as large. Similar chromatographic and hydrodynamic results were also obtained for 6-TG, 6-TGR, 6-TX, and 6-TU. The optimum detector potential was between +0.5 and +0.6 V for all compounds; the equivalent response at the conventional carbon electrodes required a detector potential 200 to 350 mV higher.

Additional factors important in determining the suitability of a modified electrode for use with biological samples are its stability and durability. This was a particular concern here because loss of response caused by adsorption and electrode fouling by constituents of biological matrices has been reported to be a severe problem for LCEC applications with the mercaptopurines [11]. In order to establish whether this would be a problem for the CoPc electrode, multiple injections of standard solutions of 6-MP and of plasma samples containing 6-MP were made with the detector potential at +0.60 V. In the former case, no change in the CoPc electrode response was observed even for 70 injections of a 100 μM standard solution over a 6-h period. Thus, the electrocatalytic activity of the CME appeared to be quite stable. However, as reported previously [13], repeated injection of plasma samples did result in a decrease in the magnitude of the peak currents seen for the mercaptopurines. Electrode response over 35 injections of doped plasma, prepared as described in the Experimental section, is shown for the CoPc-CPE, GCE and CoPc-CME in Fig. 4. Because the decrease of response was also observed at unmodified electrodes, it would appear that the deactivation was not related to the CoPc electrocatalysis per se. In fact, the rate of decrease at the CoPc electrode was actually less than at the other electrodes; while response at the GCE decreased by 91% over 35 injections and at the CPE by 75%, CoPc current declined by only 38%. Furthermore, because the response at the unmodified surfaces was initially much lower than that at the CoPc electrode, the former were quickly rendered unusable. However, after the first 20 or so injections, the CoPc electrode response largely stabilized and decreased only gradually upon continued use. After this initial break-in period, the same electrode surface could be used for several days and the stability was sufficient that calibration was necessary only once per day.

Chromatograms obtained for blank plasma and plasma to which 6-MP and

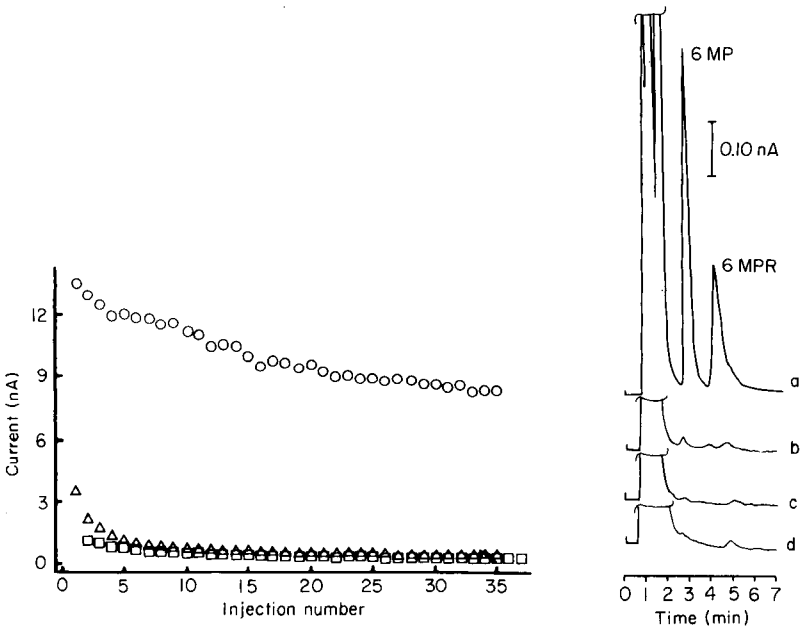

Fig. 4. Current response for repeated injections of plasma doped with 100 μM 6-MP: (○) at CoPc electrode; (△) at GCE; (□) at CPE. Same conditions as in Fig. 2.

Fig. 5. Chromatograms of plasma doped with 50 μM 6-MP and 6-MPR at (a) CoPc, (b) GCE, and (c) CPE. (d) Blank plasma at CoPc electrode. Same conditions as in Fig. 2.

6-MPR had been added are shown in Fig. 5. The response obtained at +0.60 V is shown for the conventional CPE and GCE as well as for the CoPc CME. Well-resolved peaks for the analytes appeared for the doped samples at the CoPc electrode, and no interferences were found in the blank plasma. Similar results were obtained for plasma doped with 6-TG and 6-TGR. Minimum detectable quantities were: for 6-MP, 0.8 pmol; for 6-MPR, 1.5 pmol; for 6-TG, 1.5 pmol; and for 6-TGR, 8 pmol. As expected, response for the analytes at the CoPc electrode was much greater than at the CPE and GCE at this potential. Consequently, detection limits at the latter electrodes were 50—200 times larger. Relative standard deviations (n = 4) were generally 5% or better for analytes present in concentrations of 5 μM or higher. Six plasma samples containing analytes in concentrations from 0.5 μM to 100 μM were injected to obtain calibration curves. Linear least-squares regression of current (i, nA) vs. mass (m, nmol), gave for 6-MP: i = 61.6 (±0.0013) nA nmol^{-1} × m − 0.081 (±0.082) nA; and for 6-MPR: i = 41.5 (±0.0028) nA nmol^{-1} × m + 0.130 (±0.028) nA, where m is the number of nanomoles injected. Standard errors of estimate were 0.075 nA and 0.046 nA, respectively. Linear least-squares regression gave for 6-TG : i = 40.8 (±0.0047) nA nmol^{-1} × m − 0.016 (±0.085) nA; and for 6-TGR : i = 28.0

(±0.0012) nA $nmol^{-1} \times m - 0.108$ (±0.090) nA. Standard errors of estimate were 0.028 nA for 6-TG and 0.127 nA for 6-TGR. Correlation coefficients were above 0.99 for all analytes.

Recoveries from plasma were above 96% for analyte concentrations of 100 μM or higher but decreased to 71% for 6-MP and 6-MPR at concentrations of 5 μM. Because oxidation of the thiol moiety has been commonly encountered with these kinds of samples [3, 4], the observed loss here may have been due to oxidation of a small amount of analyte during sample processing. When the EDTA usually added to the plasma to prevent this occurrence was intentionally omitted, recoveries of the thiopurines were much lower. Therefore, recommended assay procedures include the use of calibration standards prepared from plasma and the use of EDTA blood collection tubes for sample collection.

All mercapto compounds examined in this work and elsewhere [12, 13] exhibited similar electrocatalytic response at the CoPc CME. Therefore, several were examined to establish whether they might interfere with the 6-MP assay. Those specifically considered were cysteine, glutathione, 6-mercaptopurine riboside-5′-phosphate, 2-mercaptopurine, 6-TU, 6-TG, and dithiothreitol. Of these compounds, only the latter two possessed retention times close enough to that of 6-MP to present any difficulty. The 6-TG was not well resolved from 6-MP and, as seen above, did give an oxidation current at the modified electrode; but 6-TG would not normally be administered in tandem with 6-MP. However, dithiothreitol, which is frequently used to prevent thiol oxidation [3, 4], also eluted at 3.5 min and, if present in large excess, would obscure the analyte peaks. In addition, uric acid, guanine, adenine, xanthine, hypoxanthine, and methotrexate were also investigated for possible interferences. All of these compounds either gave no electrochemical response at the potential used or gave different retention times than the compounds of interest.

The LCEC method described here, based on a CoPc chemically modified electrode, compares favorably with alternative methods for determining 6-MP in plasma. Sensitivity for 6-MP, for example, was similar to that obtained by Imai et al. [11] for an electrochemically treated glassy carbon electrode; but the electrode fouling problems which plagued that assay have been reduced to a tolerable level. Detection limits obtainable with the CoPc electrode were at least one order of magnitude better than those reported previously for u.v. absorbance and fluorescence detection [1–10]. Further, because of the selective response of the modified electrode system, extensive sample treatment involving multiple extraction and evaporation steps [6, 7, 9, 10] and lengthy chromatographic times [4, 8] were not required. Last, unlike absorbance detection, in which use of several wavelengths may be necessary for optimum quantitation, all the unmethylated thiopurines were optimally detected at a single detector potential.

This work was supported by the College of Arts and Sciences of the University of Louisville.

REFERENCES

1 H. J. Breter, Anal. Biochem., 80 (1977) 9.
2 J. L. Day, L. Tterlikkis, R. Niemann, A. Mobley and C. Spikes, J. Pharm. Sci., 67 (1978) 1027.
3 T. L. Ding and L. Z. Benet, J. Chromatogr., 163 (1979) 281.
4 R. A. DeAbreu, J. M. Van Baal, T. J. Schouten and E. D. A. M. Schretlen, J. Chromatogr., 227 (1982) 526.
5 S. N. Lin, K. Jessup, M. Floyd, T. P. F. Wang, C. T. Van Buren, R. M. Caprioli and B. D. Kahan, Transplantation, 29 (1980) 290.
6 P. K. Narang, R. L. Yeager and D. C. Chatterji, J. Chromatogr., 230 (1982).
7 K. Tsutsumi, Y. Otsuki and T. Konoshita, J. Chromatogr., 231 (1982) 393.
8 J. M. Van Baal, M. B. Van Leeuwen, T. J. Schouten and R. A. DeAbreu, J. Chromatogr., 336 (1984) 422.
9 R. E. Jonkers, B. Oosterhuis, R. J. M. Ten Berge and C. J. Van Boxtel, J. Chromatogr., 233 (1982) 249.
10 N. K. Burton, G. W. Aherne and V. Marks, J. Chromatogr., 309 (1984) 409.
11 H. Imai, H. Yoshida, T. Masujima, I. Morita, K. Matsuura, A. Nakamaru, K. Katayama and H. Matsuo, Anal. Lett., 16 (1983) 1109.
12 M. K. Halbert and R. P. Baldwin, Anal. Chem., 57 (1985) 591.
13 M. K. Halbert and R. P. Baldwin, J. Chromatogr., 345 (1985) 43.
14 N. N. Kundo and N. P. Keier, Russ. J. Phys. Chem., 42 (1968) 707.

Analytica Chimica Acta, 187 (1986) 99—107
Elsevier Science Publishers B.V., Amsterdam — Printed in The Netherlands

CYCLIC VOLTAMMETRY OF NUCLEIC ACIDS AND DETERMINATION OF SUBMICROGRAM QUANTITIES OF DEOXYRIBONUCLEIC ACIDS BY ADSORPTIVE STRIPPING VOLTAMMETRY

EMIL PALEČEK,* PAVLA BOUBLÍKOVÁ and FRANTIŠEK JELEN
Institute of Biophysics, Czechoslovak Academy of Sciences, 612 65 Brno (Czechoslovakia)
(Received 20th August 1985)

SUMMARY

In cyclic voltammetry (at a mercury drop electrode) guanine residues in the polynucleotide chain give a characteristic anodic peak at potentials close to −0.3 V (vs. saturated calomel electrode). At low concentrations of polynucleotide, this peak can be enhanced substantially if the potential scan is preceded by adsorptive preconcentration of the polynucleotide at the hanging mercury drop electrode. With accumulation times shorter than 10 min at pH 6.8, the limit of detection of a single-stranded polynucleotide is <0.1 μg ml^{-1}. The peak of double-helical deoxyribonucleic acid (DNA) is considerably lower than that of single-stranded DNA under the same conditions, which can be exploited to determine low concentrations of single-stranded DNA in the presence of double-stranded DNA.

Modern voltammetric methods [1, 2] have proved useful in analyses for nucleic acids and their components [3, 4]. Differential pulse polarography (d.p.p.) has been used to quantify deoxyribonucleic acid (DNA) [4]. The method is based on the measurement of a cathodic peak caused by a reduction of adenine and cytosine residues in single-stranded polynucleotides. Under suitable conditions, DNA and ribonucleic acid (RNA) also give an anodic peak in cyclic voltammetry (c.v.) for which guanine residues are responsible [5, 6]. The concentration of single-strand nucleic acids required for d.p.p. [4] and c.v. [5] is usually in the low μg ml^{-1} range. In the work described here, the sensitivity is improved by adsorptive stripping voltammetry. Stripping voltammetry [7] provides many very sensitive procedures, cathodic stripping voltammetry (c.s.v.) being particularly useful for organic compounds. The technique can be used to determine purine and pyrimidine derivatives, as well as nucleic acid bases, with limits of detection around 10^{-8}—10^{-9} M [8—11]. Cathodic stripping voltammetry involves accumulation of the electroactive material on the electrode via a faradaic process. Adsorptive stripping voltammetry, in which there is no faradaic reaction during accumulation of the test substance on the electrode surface [12, 13], has recently become more frequently used and has been applied to the determination of osmium-modified DNA [14].

0003-2670/86/$03.50 © 1986 Elsevier Science Publishers B.V.

Here, adsorptive preconcentration is examined for the determination of chemically unmodified nucleic acids, particularly DNA. The behaviour of the peaks in cyclic voltammetry was investigated and it was found that the anodic peak allows DNA solutions to be quantified at substantially lower concentrations than the cathodic peak. The limit of detection of denatured DNA by means of the anodic peak is $<0.1\ \mu g\ ml^{-1}$.

EXPERIMENTAL

Poly(G) (polyguanylic acid) and poly(A, G, U) (polyadenylic-guanylic-uridylic acid) were supplied by Sigma, poly(C) (polycytidylic acid) by Serva and poly(A) (polyadenylic acid) by Calbiochem. Calf thymus DNA was isolated and characterized as described previously [15]; its molecular weight was ca. 20 kilo base pair (agarose gel electrophoresis). The DNA was denatured by heating its solution (100—200 $\mu g\ ml^{-1}$) in 0.015 M sodium chloride/0.0015 M sodium citrate, pH 7.0 (SSC/10) at 100°C for 6 min with subsequent rapid cooling in an ice bath. Sonication was done at a DNA concentration of 770 $\mu g\ ml^{-1}$ in SSC/10 at 0°C in an argon atmosphere (Model B-12 Sonifier; Branson Sonic Power Company).

For cyclic voltammetry a PAR 174 polarographic analyzer was used with a PAR 175 universal programmer and an X-Y recorder. The three-electrode system comprised a hanging mercury drop electrode (HMDE; Metrohm E-410), a platinum counter electrode, and a saturated calomel electrode. Unless otherwise stated, the HMDE had a surface area of 2.2 mm^2. Test solutions (1.2 ml) thermostatted at 25 ± 0.5°C were deoxygenated with a slow stream of argon and, during measurements, argon was passed over their surface.

The manner of polarization of the HMDE was as follows: the electrode was first held at a potential E_A for time t_A during which the polynucleotide accumulated on the electrode surface. After a quiescent period (15 s), a triangular voltage sweep was applied. Reduction of the guanine moiety occurred at a potential E_G near the apex of the triangular voltage sweep, for which the switching point was usually −1.85 V. Oxidation of the guanine reduction product occurred during scanning to positive potentials, the anodic peak appearing at about −0.3 V (Fig. 1). During the accumulation time, the solution was stirred at 150 rpm unless otherwise stated.

RESULTS

Single-strand polynucleotides were first measured under the conditions commonly used for linear-sweep voltammetry and cyclic voltammetry [1, 4, 16], i.e., at polynucleotide concentrations around 10^{-4} M (related to phosphorus content) with t_A = 140 s and without stirring. In conformity with previous results [4, 16], poly(A) and poly(C) (Fig. 1b, d) gave a cathodic peak at around −1.5 V. Poly(A, G, U) and thermally denatured DNA

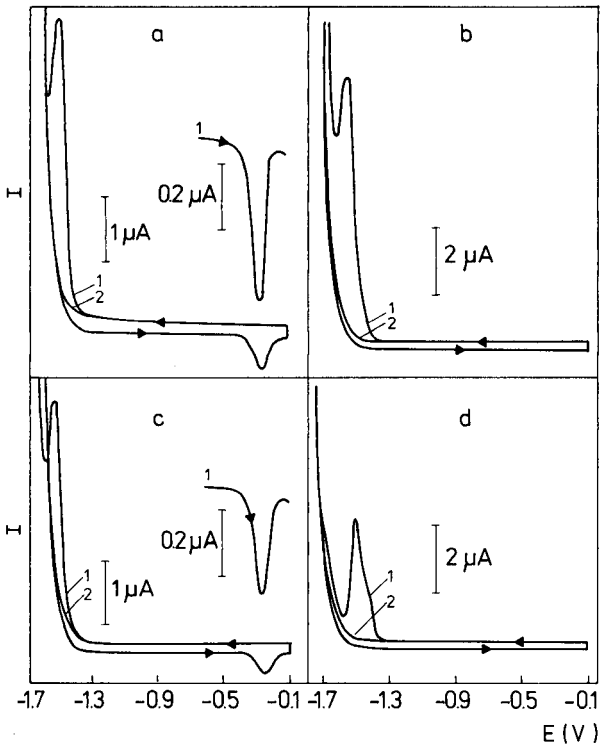

Fig. 1. Cyclic voltammograms of polyribopolynucleotides and denatured DNA: (a) poly(A, G, U); (b) poly(A); (c) denatured DNA; (d) poly(C). All polynucleotides were at a concentration of 2×10^{-4} M (related to monomer content); denatured DNA was at a concentration of 100 μg ml^{-1}. Conditions: 0.6 M ammonium formate/0.1 M sodium phosphate (pH 6.8) supporting electrolyte; scan rate 0.2 V s^{-1}; adsorption potential −0.1 V; switching potential −1.85 V; accumulation time 140 s, without stirring; 1 and 2 indicate the number of scans.

gave not only the cathodic peak but also an anodic peak at around −0.3 V (Fig. 1a, c), the latter being produced by a guanine reduction product [6]; guanine is reduced at highly negative potentials and its reduction peak in poly(A, G, U) is overlapped by the high background discharge. In the reverse scan, the reduction product (which remains near the electrode) is oxidized at around −0.3 V, giving a symmetrical anodic peak. The cathodic peak of poly(A), poly(C), poly(A, G, U) or denatured DNA (Fig. 1) does not appear on repeated voltage sweeps because reduction products of adenine and cytosine block the electrode surface [4, 16, 17], whereas the anodic peak can be observed on repeated scans (Fig. 1a, c) with only slight decrease in the peak heights on successive scans. A condition for the appearance of an anodic peak is polarization of the mercury electrode to sufficiently negative potentials. For example, with poly(G), under the conditions of Fig. 1, the anodic peak is seriously decreased when the switching potential is −1.65 V and disappears when the switching potential is −1.55 V.

Optimization of the conditions for adsorptive preconcentration

The anodic and cathodic peaks of poly(A, G, U) at concentrations of 4×10^{-5}, 2.5×10^{-5}, 5×10^{-6} and 5×10^{-7} M were examined at different accumulation times (t_A), with and without stirring. At the highest concentration of polynucleotide, changes in t_A and stirring had only a slight effect on peak heights, and at $t_A > 2$ min the peak height remained constant. At lower concentrations, both the anodic (Fig. 2a) and cathodic (Fig. 2b) peak heights depended on t_A, and stirring had a significant effect. At a concentration of 5×10^{-7} M, poly(A, G, U) gave an anodic peak only when the sample was stirred (Fig. 2a) and no cathodic peak appeared at all. The lowest concentration of thermally denatured DNA which gave a measurable cathodic peak (at t_A = 4 min) was around 4 μg ml^{-1}, whereas for the anodic peak it was < 0.2 μg ml^{-1}. The greater suitability of the anodic peak for quantifying polynucleotides at very low concentrations is mainly due to the symmetry of this peak (Fig. 1) and to the fact that its potential is sufficiently far from the

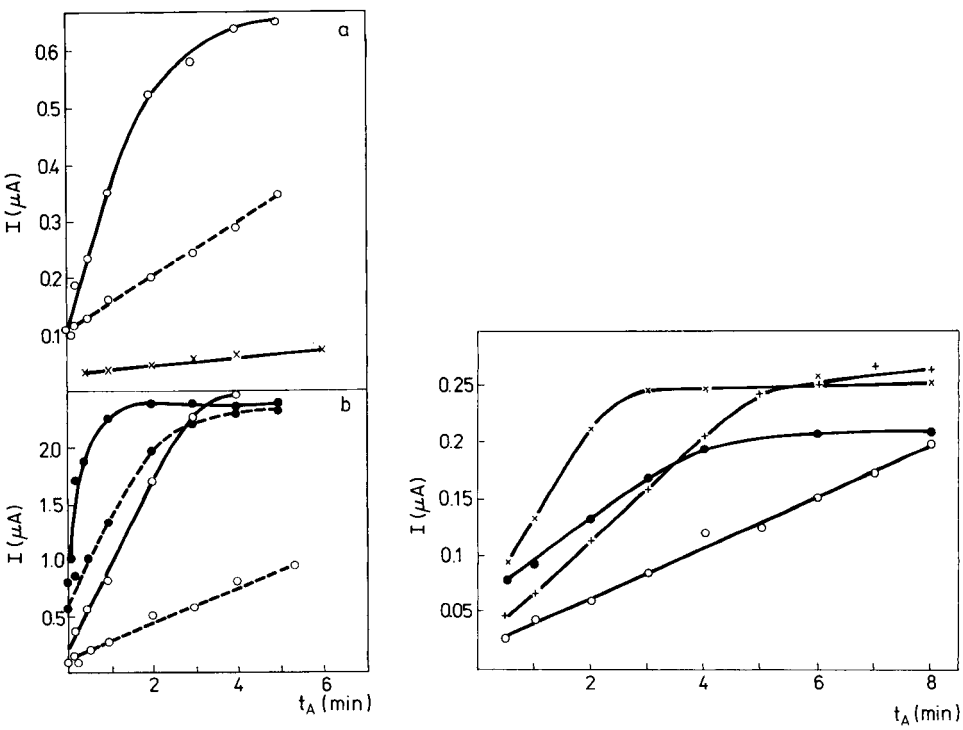

Fig. 2. Dependence of the height of the voltammetric peaks of poly(A, G, U) on t_A: (a) anodic peak; (b) cathodic peak. (○) 5×10^{-6} M; (×) 5×10^{-7} M; (●) 2.5×10^{-5} M. (—) With stirring; (- - -) without stirring. For other conditions, see Fig. 1.

Fig. 3. Dependence of the height of anodic peak of native and denatured DNA on t_A: (○) 2 μg ml^{-1} denatured DNA; (+) 4 μg ml^{-1} denatured DNA; (×) 8 μg ml^{-1} denatured DNA; (●) 40 μg ml^{-1} native DNA. Stirring rate 150 rpm; for other conditions, see Fig. 1.

background discharge. The asymmetric cathodic peak merges with the background discharge at low concentration. Accordingly, further attention was given to the anodic peak, which has not been fully investigated previously.

The anodic peak was measured for native and thermally denatured calf thymus DNA in dependence on stirring rate, t_A and accumulation potential E_A. In conformity with previous results [5, 6], native DNA gave a considerably lower peak than denatured DNA under the same conditions and so was further tested at a concentration more than 20 times greater than that of denatured DNA.

Stirring rate and accumulation time. Stirring was done either magnetically or with an electric stirrer. The latter was better for larger volumes of solution, while with volumes of 1—2 ml magnetic stirring was superior. With the magnetic stirrer, the peak height increased with stirring speeds of up to 150 rpm; at higher speeds, the heights of the native (46 μg ml^{-1}) and denatured (2 μg ml^{-1}) DNA peaks were independent of stirring speed (t_A = 2 min) provided that the HMDE remained stable. The optimum stirring speed depended, however, on the geometry of the vessel and the stirrer, the volume of sample analysed, etc. The dependence of peak height on t_A was examined for various DNA concentrations (Fig. 3). With 8 μg ml^{-1} denatured DNA, the peak height reached a limiting value at $t_A \approx 3$ min, whereas at 2 μg ml^{-1} a limiting value was not achieved even after 8 min. The peak of native DNA (40 μg ml^{-1}) reached its limiting value at $t_A \approx 4$ min.

The potential of adsorptive preconcentration. In the range 0.0 to —1.0 V, the peak heights of native and denatured DNA were almost independent of

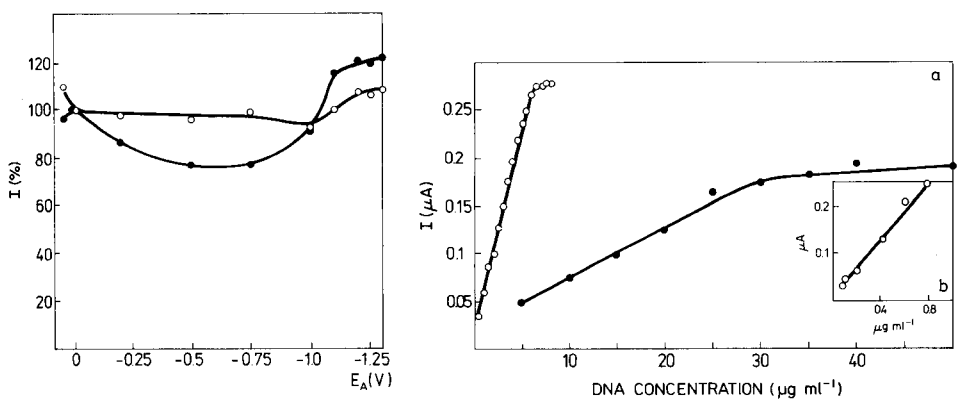

Fig. 4. Dependence of the height of the anodic peaks of native and denatured DNA on accumulation potential: (○) 2 μg ml^{-1} denatured DNA; (●) 20 μg ml^{-1} native DNA. Conditions: t_A = 4 min with stirring at 150 rpm; otherwise as for Fig. 1. Peak heights at 0 V are taken as 100%.

Fig. 5. Dependence of the height of the anodic peak on DNA concentration: (○) denatured DNA; (●) native DNA. (a) t_A = 4 min, stirring at 150 rpm, surface area 2.2 mm^2; (b) t_A = 8 min, stirring at 200 rpm, surface area 3.5 mm^2. Conditions: open-circuit accumulation, otherwise as for Fig. 1.

the accumulation potential, E_A (Fig. 4). For native DNA, the peak height increased in the region −1.1 to −1.3 V, in accordance with the assumed surface denaturation of DNA at such potentials [4, 16], which was found on the basis of measurements of the cathodic peak of DNA. The peak height of denatured DNA was less dependent on E_A in this potential range. Around an accumulation potential of −1.5 V, the peaks of native and denatured DNA decreased sharply in height (not shown). It is thus possible to select E_A in the range 0 to −0.8 V or to use open-circuit preconcentration for measurements of native and denatured DNA.

Other factors. Temperature changes in the region 20—30°C had only a very slight effect on the peak height of denatured DNA. The peak height for native and denatured DNA increased with scan rate in the range 50—500 mV s^{-1}, and the ratio of the peak height of denatured DNA to that of native DNA increased with increasing scan rate.

Dependence of peak height on concentration of native and denatured DNA

As shown in Fig. 5, the peak of denatured DNA grew linearly with concentration in the range 0.5—5 μg ml^{-1} and the peak of native DNA in the range 5—30 μg ml^{-1}. At higher concentrations, when the electrode surface was fully covered, the peak heights of the native (measured up to 80 μg ml^{-1}) and denatured (measured up to 8 μg ml^{-1}) DNAs were practically independent of concentration. The peak potential, E_p, did not change with DNA concentration. Denatured DNA showed a linear dependence of peak height on DNA concentration from a concentration as low as 0.08 μg ml^{-1} with t_A = 8 min (Fig. 5b). Denatured DNA (0.8 μg ml^{-1}) at t_A = 4 min was determined with a relative standard deviation of ±2.6% (n = 10).

The great difference in the peak heights of native and denatured DNA in the low concentration range (under the conditions of Fig. 5a, up to about 7 μg ml^{-1}) can be exploited for the determination of single-stranded DNA in the presence of double-stranded DNA. For example, the course of thermal denaturation of DNA (0.8 μg ml^{-1}) was observed with t_A = 8 min (at room temperature after rapid cooling of the sample); under such conditions, native

TABLE 1

Influence of some substances on the height of the DNA anodic peak

Substance	Tolerable concentration[a]	Substance	Tolerable concentration[a]
EDTA	5×10^{-4} M	$ZnSO_4$	1×10^{-6} M
$MgSO_4$	5×10^{-3} M	Thymine	1×10^{-4} M
Ethidium bromide	5×10^{-6} M	Histone[c]	0.15 μg ml^{-1}
SSC[b]	SSC/5		

[a]Highest concentration at which the peak of 2 μg ml^{-1} denatured DNA is unchanged (t_A = 4 min, stirring; otherwise as for Fig. 1). [b]0.15 M HCl/0.015 M sodium citrate, pH 7.0. [c]From calf thymus.

DNA did not give an anodic peak while, in the denaturation region, a well-developed peak characterizing the helix-coil transition appeared (not shown).

The effects of other substances which may occur in DNA samples on the height of the anodic peak were tested as shown in Table 1. At concentrations higher than those listed, these substances decreased the DNA peak height. Guanosine, which produces an anodic peak at concentrations around 10^{-6} M under the given conditions, can affect the DNA peak height if great care is not given to accumulation time and potential. The determination of DNA by differential pulse polarography [4] is very sensitive to the presence of ethidium bromide; the lesser sensitivity of the stripping peak to such interference may be of value.

DISCUSSION

The adsorptive preconcentration of DNA at a mercury electrode was first used about 20 years ago in conjunction with oscillographic polarography at controlled alternating current [2]. In later voltammetric work [2, 16], the cathodic peak was usually measured after 60—120 s. It is shown here that the sensitivity of determination of single-strand DNA can be increased by 2—3 orders of magnitude if the solution is stirred during accumulation on the electrode and the anodic peak of guanine is measured instead of the cathodic peak.

The mechanism of the electrode process responsible for the appearance of the anodic peak of guanine has not been studied in such detail as the electroreduction of adenine and cytosine [3, 4, 18]. Results recently obtained [19] suggest that at negative potentials guanine is reduced to dihydroguanine, which is re-oxidized back to guanine when the potential is scanned to more positive voltages, giving the anodic peak. In the case of adenine and cytosine, the double bonds which are the primary sites of reduction [4] form part of the system of hydrogen bonds in the Watson-Crick base pairs. In accordance with this, native DNA is not reducible at a neutral pH by d.c. polarography. In the case of guanine, none of the double bonds which could be the site of reduction is included in the system of hydrogen bonds in the Watson-Crick pairs. The difference in heights of the anodic peaks of single-strand and double-strand DNAs observed at full coverage of the electrode surface (Fig. 5) may be due to steric constraints which make some guanine residues in the double helix unavailable for reduction process, and/or to a difference in adsorbability of single- and double-stranded DNAs. The increase in the ratio of the peak heights for single-stranded and double-stranded DNAs observed with incomplete electrode coverage (Fig. 5) is probably due to the higher transport rate of single-stranded DNA to the electrode compared to the transport rate of double-stranded DNA.

The adsorption of nucleic acids at a mercury electrode has been studied in detail [3, 4, 16]. Single-stranded DNA is adsorbed at an electrode most strongly by hydrophobic bases. Double-stranded DNA is adsorbed in the

region of the potential of zero charge via the sugar-phosphate backbone (and sporadic bases if available) [4]. At low ionic strength, the double helical DNA is adsorbed electrostatically on a positively charged electrode surface by the inadequately screened negative charges of the phosphate groups. Around the potential of −1.2 V (the U region), double-helical DNA (at medium ionic strength) is denatured on the electrode surface. This surface denaturation is relatively slow [4, 20], and takes place in a narrow range of potentials. If the structure of double-helical DNA is not to be affected on the electrode, then E_A must be selected outside the U region and the scan rate must be high enough to minimize structural changes during scanning through the U region. In linear-sweep voltammetry, the lowest suitable scan rate for this purpose is about 1 V s^{-1} [4]. The scan rate of 200 mV s^{-1} used in this work was thus not fast enough, so that the signal of native DNA was slightly increased as a result of surface denaturation. However, this small increase did not affect the applicability of cyclic voltammetry for the determination of single-stranded and double-helical DNAs. (Higher scan rates would require the use of more sophisticated recording equipment.)

The background electrolyte used here was 0.6 M ammonium formate/0.05 M sodium phosphate (pH 6.8). Similar results can be obtained with other ammonium salts or with magnesium salts [6]. The optimal peak height was obtained in the pH range 5—7. The peak potential shifted by 60 mV/pH with falling pH. If a different electrolyte with a different pH is used, the optimal value of the switching potential must be established because it shifts to more positive potentials with falling pH.

The DNA is so strongly adsorbed at the electrode that the electrode can be removed from the solution with the adsorbed layer of DNA, rinsed and immersed in a solution of background electrolyte. The height of the anodic peak of DNA after such a transfer is virtually unaffected compared to the normal stripping peak. Preliminary results indicate that this phenomenon could be used to decrease considerably the sample volume required for DNA determination.

REFERENCES

1 A. M. Bond, Modern Polarographic Methods in Analytical Chemistry, M. Dekker, New York, 1980.
2 J. Kůta and E. Paleček, in G. Milazzo (Ed.), Topics in Bioelectrochemistry and Bioenergetics, Vol. 5, Wiley, Chichester, 1983, pp. 1—63.
3 G. Dryhurst, Electrochemistry of Biological Molecules, Academic Press, New York, 1977, p. 269.
4 E. Paleček, in G. Milazzo (Ed.), Topics in Bioelectrochemistry and Bioenergetics, Vol. 5, Wiley, Chichester, 1983, pp. 65—165.
5 L. Trnková, M. Studničková and E. Paleček, Bioelectrochem. Bioenerg., 7 (1980) 643.
6 E. Paleček, F. Jelen and L. Trnková, Gen. Physiol. Biophys., 5 (1986) 315.
7 F. Vydra, K. Štulik and E. Juláková, Stripping Voltammetry in Chemical Analysis, Wiley, Chichester, 1976.
8 E. Paleček and F. Jelen, Collect. Czech. Chem. Commun., 45 (1980) 3472.

9 E. Paleček, Anal. Biochem., 108 (1980) 129.
10 E. Paleček, F. Jelen, Mac Anh Hung and J. Lasovský, Bioelectrochem. Bioenerg., 8 (1981) 621.
11 E. Paleček, J. Osteryoung and R. A. Osteryoung, Anal. Chem., 54 (1982) 1329.
12 R. Kalvoda, Anal. Chim. Acta, 138 (1982) 11.
13 R. Kalvoda, Anal. Chim. Acta, 197 (1984) 197.
14 E. Paleček and Mac Anh Hung, Anal. Biochem., 132 (1983) 236.
15 E. Lukášová, F. Jelen and E. Paleček, Gen. Physiol. Biophys., 1 (1982) 53.
16 H. W. Nürnberg, in G. Milazzo and M. Blank (Eds.), Bioelectrochemistry, Vol. 1, Plenum, New York, 1983, pp. 183—225.
17 P. Valenta, H. W. Nürnberg and P. Klahre, Bioelectrochem. Bioenerg., 2 (1975) 204.
18 T. E. Cummings, M. A. Jensen and P. J. Elving, Bioelectrochem. Bioenerg., 4 (1977) 425.
19 L. Trnková, Thesis, Faculty of Science, J. E. Purkyně University, Brno, 1984.
20 F. Jelen and E. Paleček, Gen. Physiol. Biophys., 4 (1985) 219.

Analytica Chimica Acta, 187 (1986) 109—116
Elsevier Science Publishers B.V., Amsterdam — Printed in The Netherlands

DIFFERENTIAL-PULSE POLAROGRAPHIC DETERMINATION OF SELENIUM SPECIES IN CONTAMINATED WATERS

G. E. BATLEY

Analytical Chemistry Section, CSIRO Division of Energy Chemistry, Private Mail Bag 7, Sutherland, NSW 2232 (Australia)

(Received 4th March 1986)

SUMMARY

Selenium(IV), in the concentration range 2—100 $\mu g\ l^{-1}$ in contaminated waters, is determined by using the sensitive adsorption-controlled peak obtained by differential pulse polarography in dilute acid solution. Interfering heavy metals are removed on Chelex-100 resin. Selenium(VI) is not electroactive but can be determined after photolytic reduction in the absence of oxygen. Anion-exchange preconcentration is necessary if the total selenium is below the detection limit of 2 $\mu g\ l^{-1}$.

The polarographic behaviour of selenium has been the subject of considerable discussion for many years [1—3]. Recent increased awareness of the biological role of selenium has produced a revival of interest in methods for the determination of selenium and its speciation at trace concentrations [4]. Polarographic techniques can be used to advantage for speciation because only selenium(IV) is electroactive.

Classical d.c. polarography of selenium(IV) has shown as many as three reduction waves, depending on pH [3]. In acidic solution, it is generally accepted that reduction occurs in two stages, the first involving the formation of hydrogen selenide via the six-electron reaction

$$SeO_3^{2-} + 8H^+ + 6e^- \rightarrow H_2Se + 3H_2O \quad (1)$$

This reaction is compounded by the anodic wave for the reaction of hydrogen selenide with mercury to form mercury(II) selenide

$$H_2Se + Hg \rightarrow HgSe + 2H^+ + 2e^- \quad (2)$$

resulting in a net four-electron reduction,

$$SeO_3^{2-} + 6H^+ + 4e^- + Hg \rightarrow HgSe + 3H_2O \quad (3)$$

At a more negative potential, the second reduction step involves the dissolution of mercury(II) selenide in the reverse of reaction 2.

Because it is possible to accumulate HgSe at a stationary electrode, many recent studies [5—8] have applied cathodic stripping voltammetry (c.s.v.) to obtain lower limits of detection. Peak currents are highly dependent on

0003-2670/86/$03.50 © 1986 Elsevier Science Publishers B.V.

deposition potentials, which must be between the peak potentials for the two cathodic waves. Deldime and Hartman [6] found that −0.065 V vs. Ag/AgCl, gave the most reliable dependence of peak height on both electrolysis time and selenium(IV) concentration, whereas Adeloju et al. [8] found deposition at −0.35 V vs. Ag/AgCl, in the presence of added copper, to be optimum over the concentration range 0—100 $\mu g\ l^{-1}$. The detection limit of the latter method was 0.25 $\mu g\ l^{-1}$ for a 60-s deposition. Several workers [8, 9] have used anodic stripping of elemental selenium deposited at a gold electrode. The linear concentration range is narrower than that of the c.s.v. technique with similar detection limits.

The separation of organic and inorganic species of selenium is probably best achieved by ion chromatography, but to utilize the selectivity and sensitivity of electrochemical detection in the column effluent, a polarographic detector would be better than any system involving stationary electrodes. To this end, the reduction of selenium(IV) at a dropping mercury electrode has been more fully investigated.

EXPERIMENTAL

Instrumentation and reagents

Differential pulse polarography was done with a PAR model 174 polarographic analyzer, in conjunction with a PAR model 303 static mercury drop electrode and a Hewlett-Packard type 7004A X-Y recorder.

Sodium selenite and sodium selenate were AnalaR reagents (BDH Chemicals). All other chemicals were Merck GR grade.

Recommended procedure

Pass the sample (10 ml) at the natural pH through a pre-washed C_{18} Sep-Pak column (Millipore-Waters), followed by a 0.5 cm × 5 cm column of Chelex-100 resin (ammonium form). Transfer an aliquot of the sample (5 ml) to the polarographic cell and acidify to pH 2 with nitric acid. Determine selenite by differential pulse polarography (50 mV pulse width, 2 mV s^{-1} scan rate) and measure the peak at −0.6 V vs. Ag/AgCl obtained on a cathodic scan from −0.4 to −0.8 V vs. Ag/AgCl. Quantify by the method of standard additions.

Adjust a second aliquot of sample to pH 10.5 with a dilute sodium carbonate solution and, while degassing continually with nitrogen, subject it to u.v. radiation from a 550-W lamp for 3 h. After passing the sample through the Chelex-100 column (see above), measure the total selenium as selenite by differential pulse polarography. This method is also applicable to solid samples, which must first be digested with acids, and the pH adjusted accordingly, before treatment with u.v. radiation and then before passage through the Chelex-100 resin.

RESULTS AND DISCUSSION

The differential pulse polarography of selenium(IV) at a dropping mercury electrode gives two major reduction waves at pH values lower than 7. The first wave near 0 V vs. Ag/AgCl merges with at least two smaller peaks on its cathodic edge. The second wave near —0.6 V vs. Ag/AgCl is a sharp adsorption-controlled peak, which was further examined for its analytical possibilities.

This peak was strongly pH-dependent, reaching a maximum at pH values below 2, and minimum above pH 5 (Fig. 1). The pK_a value of the reducing species obtained from this plot was 3.6, which is in reasonable agreement with the published acidity constant of 3.9 for hydrogen selenide [10]. This is not unexpected on the basis of reaction 2 above.

The wave shape is unusual in being almost triangular and rising to a sharp peak (Fig. 2). It is much narrower than a normal diffusion-controlled wave, having a half-width ($b_{1/2}$) of 19.5 mV for a pulse amplitude of 50 mV and a scan rate of 2 mV s^{-1}, compared for example with 54.5 mV for the three-electron reduction of bismuth(III) under the same operational conditions. This shape originates from the adsorption contribution. Mercury(II) selenide presumably deposits on the surface of the growing drop, with rapid desorption occurring at the peak potential. This behaviour has been noted in studies of the oscillographic polarography of selenite in the presence of EDTA at pH 4 [11], when scan rates in excess of 250 mV s^{-1} were used, with the wave height diminishing with increasing scan rate.

The effects of scan rate and pulse width on the differential-pulse peak currents are shown in Fig. 3 and Table 1. For a 25-mV pulse width, the peak current exhibited a linear inverse dependence on scan rate. Increasing scan rates produced increased peak widths although peak areas were constant to within 2% over the range of scan rates studied. Increasing pulse width produced the expected increase in peak height, but the peak split at large pulse

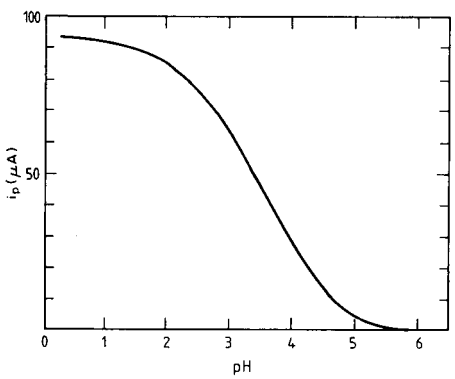

Fig. 1. Effect of pH on the peak current for 2 × 10^{-4} M Se(IV) in 0.5 M NaCl. Conditions: 25-mV pulse width, 2 mV s^{-1} scan, 0.5-s drop time.

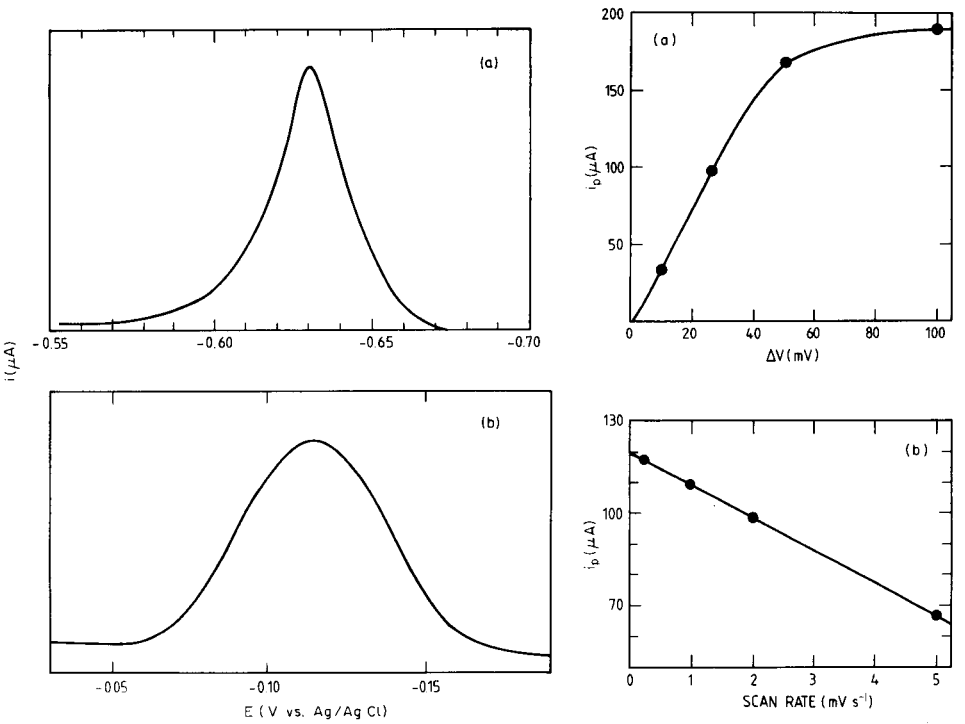

Fig. 2. Differential pulse polarograms: (a) 2×10^{-4} M Se(IV) in sea water + 0.1 M HNO_3; (b) 1×10^{-3} M Bi(III) in sea water + 1 M HCl. Conditions: 50-mV pulse width, 2 mV s^{-1} scan, 0.5-s drop time.

Fig. 3. Effect of pulse width and scan rate on peak current for 2×10^{-4} M Se(IV) in sea water, pH 2: (a) pulse width (2 mV s^{-1} scan); (b) scan rate (25-mV pulse width).

TABLE 1

Effect of pulse width and scan rate on peak height for 2×10^{-4} M selenite in sea water at pH 2

Effect of pulse width[a]				Effect of scan rate[b]			
Pulse width (mV)	i_p (μA)	$-E_p$[c] (V)	$b_{1/2}$ (mV)	Scan rate (mV s^{-1})	i_p (μA)	$-E_p$[c] (V)	$b_{1/2}$ (mV)
10	34	0.675	16.5	0.25	118	0.665	14.5
25	98	0.670	17.5	1.0	110	0.667	15.0
50	168	0.680	19.5	2.0	98	0.670	17.5
100	180	0.600	20.0	5.0	67	0.672	25.0
	27	0.650	27.0				

[a]2 mV s^{-1} scan rate, 0.5-s drop time. [b]25-mV pulse width, 0.5-s drop time. [c]Versus Ag/AgCl.

amplitudes to produce a second, more cathodic peak. This phenomenon was also observed at a hanging drop electrode under certain conditions. At 100-mV pulse width and slow scan rates (1 mV s^{-1}), the more cathodic peak becomes dominant whereas the reverse is true for a 5 mV s^{-1} scan. Split peaks of the type observed are not uncommon in stripping voltammetry, especially if the solubility of the depositing species in mercury is low (e.g., copper) and its concentration is high.

The concentration dependence of the differential pulse polarographic wave was linear in the range 2—100 mg Se(IV) l^{-1}. The limit of detection was 2 μg l^{-1} with a 50-mV pulse, a 2 mV s^{-1} scan rate and a medium size drop. For high concentrations, it is preferable to dilute the sample to avoid the formation of split peaks.

The peak potential of the selenium wave shifts cathodically with increasing pH. This dependence on pH is linear and the observed slope of 63 mV for the potential/pH plot is consistent with reaction 1.

Interferences

A major problem with the voltammetric determination of selenium has been the presence of other interfering ions. The concurrent deposition in the mercury drop of readily reduced metals such as copper significantly reduces the selenium peak height, presumably by changing the nature of the adsorbed intermetallic compound. There are several ways of overcoming this; either the interfering ions can be removed, or an excess is added to ensure a dominance of only one adsorbed species. The interfering ions can be effectively removed by anion-exchange. The batch procedure used by Adeloju et al. [8] to concentrate selenium could be used to advantage in the injector loop of an ion chromatograph, with subsequent separation of selenium species on an ion-exchange high-performance liquid chromatographic column.

When preconcentration is not required, passage of the sample through a column of Chelex-100 resin (ammonium form) is sufficient to remove interfering inorganic contaminants from water samples at their natural pH. No interferences were found from 5 mg l^{-1} humic acid, 10 mg l^{-1} fulvic acid, 19 mg l^{-1} alginic acid or 3 mg l^{-1} Triton X-100. Higher concentrations of surface-active organic materials depressed the selenium wave but were corrected for by using standard additions. Most of these interferences were removed by a prior clean-up with C_{18} Sep-Paks. This method was applied to the analysis of polluted waters, containing 570 μg l^{-1} zinc, 200 μg l^{-1} lead and 60 μg l^{-1} cadmium, to which selenium had been added. Recoveries of between 96 and 102% were obtained for 79 μg l^{-1} additions of both selenite and, after reduction, selenate. At concentrations of 20 μg l^{-1}, the standard deviation was 9% (n = 6).

Reduction of selenium (VI)

Because selenium(VI) is not electroactive, the polarographic method can be used to advantage in speciation studies, provided that selenium(VI) can be

converted selectively to some measurable form such as selenium(IV). The reduction of selenium(VI) by standard chemical reducing agents is kinetically slow and complicated by the fact that strong reducing agents, such as hydrazine, will reduce any selenium(IV) directly to the elemental form.

The commonly used reduction procedure is to boil the sample with 4 M hydrochloric acid for a fixed time, usually 5 min [12]. Experience with this technique showed that the operationally-defined conditions for complete reduction are so critically dependent on boiling time that deviation by more than a minute can result in 20% differences in recovery, whereas excessive boiling results in the reduction proceeding in part to elemental selenium [12]. Such conditions are hardly conducive to satisfactory trace determinations, so an alternative procedure was sought.

Measures and Burton [13] reported that u.v. photolysis of selenium(VI) resulted in reduction to selenium(IV). The reaction is pH-dependent, maximizing at pH 10. A constant proportionation of selenium between the tetravalent and hexavalent state was observed when a 1250-W lamp was used with hydrogen peroxide as catalyst. This proportionation was dependent on the lamp power. Such a procedure seemed rather arbitrary and further experimentation was undertaken to endeavour to understand the reaction. Studies were conducted on 0.5 M sodium chloride irradiated for 3 h in 100-ml tubes with a 550-W lamp [14]. The pH-dependence of the selenium(IV) yield is shown in Fig. 4. The use of a continuous stream of nitrogen to remove dissolved oxygen produced a dramatic enhancement in the efficiency of reduction (Table 2).

The reaction mechanism had been thought to parallel photolytic reduction of nitrate [15, 16], as this reduction exhibits a somewhat similar pH-dependence. Possible mechanisms involve the elimination of either an oxygen

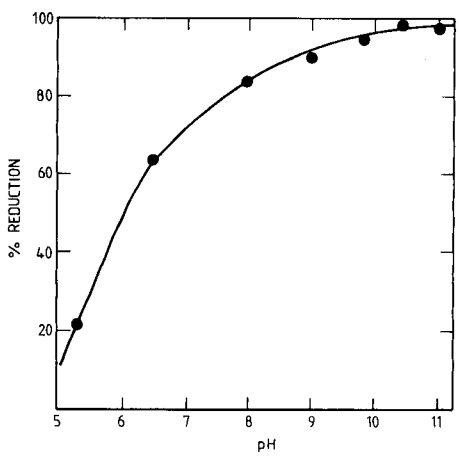

Fig. 4. Effect of pH on the reduction of 2×10^{-5} M Se(VI) in 0.5 M NaCl, degassed with nitrogen.

TABLE 2

Photolytic reduction of selenium(VI)

Sample	Solution conditions	pH	% Reduction
0.5 M NaCl	N_2 degassing	10.5	97.6
0.5 M NaCl	No degassing	10.5	78.9
0.5 M NaCl	Addition of 0.5 ml of 30% H_2O_2	10.5	73.9
0.5 M NaCl	Addition of 0.01 ml of ethanol	10.4	61.3
0.5 M NaCl	Addition of 10^{-3} M t-butanol	10.4	63.9
Sea water	N_2 degassing	10.4	94.8
Distilled water	N_2 degassing	10.5	89.2

atom, or a hydroxyl radical. The enhanced reduction of nitrate in the presence of hydroxyl radical scavengers implied the latter [16]. The reduction of selenium(VI) was found to be inhibited by t-butanol, ethanol and hydrogen peroxide (Table 2). Whether the reaction involves an intermediate of higher oxidation states (e.g., SeO_4^-) which has been observed in flash photolysis [17], is uncertain. The overall reaction, given the inhibiting effect of dissolved oxygen, is of the form:

$$2SeO_4^{2-} \rightarrow 2SeO_3^{2-} + O_2$$

with the primary reaction being $SeO_4^{2-} \rightarrow SeO_3^{2-} + O$.

When the 550-W lamp was used, the reduction was complete in under 2 h, although a 3-h period was adopted for use in the recommended procedure. A study of the photolytic reduction in the presence of nitrogen with a 40-W immersible pen-ray lamp (Ultraviolet Products) showed 88% reduction after only 11 min. The temperature of the solution in this instance did not exceed 30°C. This indicates the potential for inclusion of the reduction step in a flowing system and this will be the subject of a later publication.

Conclusion

Selenium above 2 $\mu g\ l^{-1}$ can be determined in contaminated waters by using the sensitive adsorption-controlled peak for selenium(IV) obtained in differential pulse polarography in dilute acid solution. Selenium(VI) can be determined after photolytic reduction using nitrogen to remove product oxygen. The procedure may be adaptable to on-line determination of selenium by ion chromatography after anion-exchange loop preconcentration of selenium.

The experimental assistance of Bruce Saunders is gratefully acknowledged.

REFERENCES

1 J. J. Lingane and L. W. Nedrack, J. Am. Chem. Soc., 71 (1979) 196.
2 E. F. Speranskaga, Zh. Anal. Khim., 17 (1962) 347.

3 G. D. Christian, E. C. Knoblock and W. C. Purdy, Anal. Chem., 35 (1963) 1128.
4 G. Tolg, in P. Bratter and P. Schramel (Eds.), Trace Element Analytical Chemistry in Medicine and Biology, Vol. 3, Walter de Gruyter, Berlin, 1984, p. 95.
5 V. F. Turopora, Y. N. Polyakov, L. N. Medvedeva and L. N. Shindina, Zh. Anal. Khim., 27 (1972) 2041.
6 P. Deldime and J. Hartman, Anal. Lett., 13 (1980) 105.
7 R. Ahmad, J. O. Hill and R. J. Magee, Analyst, 108 (1983) 835.
8 S. B. Adeloju, A. M. Bond, M. H. Briggs and H. C. Hughes, Anal. Chem., 55 (1983) 2076.
9 R. W. Andrews and D. C. Johnson, Anal. Chem., 48 (1976) 1056.
10 H. Hagisawa, Bull. Inst. Phys. Chem. Res. (Tokyo), 20 (1941) 384; Chem. Abs., 36 (1942) 1231.
11 L. S. K. Opanskaya and A. T. Russo, Zh. Anal. Khim., 27 (1975) 738.
12 G. A. Cutter, Anal. Chim. Acta, 98 (1978) 59.
13 C. I. Measures and J. D. Burton, Anal. Chim. Acta, 120 (1980) 177.
14 G. E. Batley and Y. J. Farrar, Anal. Chim. Acta, 99 (1978) 283.
15 M. Daniels, R. Meyers and E. Belardo, J. Phys. Chem., 72 (1968) 389.
16 U. Shuali, M. Ottolenghi, J. Rabani and Z. Yelin, J. Phys. Chem., 73 (1969) 3445.
17 M. S. Subhani and M. Khalia, Rev. Roum. Chim., 23 (1978) 1117.

Analytica Chimica Acta, 187 (1986) 117—127
Elsevier Science Publishers B.V., Amsterdam — Printed in The Netherlands

SECONDARY-ION MASS SPECTRA AND FAST-ATOM-BOMBARDMENT MASS SPECTRA OF LIQUID POLYMERS: ALKOXYLATED PYRAZOLES AND HYDRAZINES

STEVEN J. DOHERTY and KENNETH L. BUSCH*
Department of Chemistry, Indiana University, Bloomington, IN 47405 (U.S.A.)
(Received 22nd May 1986)

SUMMARY

The positive-ion secondary-ion mass (s.i.m.) spectra of polyalkoxylated hydrazines and pyrazoles contain series of ions that reflect the degree of polymerization of the parent compound, and also suggest the presence of several discrete polymeric series. The spectra of two examples of pyrazoles are interpreted in terms of a series of polymeric $(M + H)^+$ ions. Three alkoxylated hydrazines yield particle-bombardment spectra which contain polymeric ion series that extend to the mass limit of the analyzer. Positive-ion fast-atom-bombardment mass spectra are also recorded. These spectra also reflect the polymeric structures of the compounds studied, and are similar in almost every detail to the s.i.m. spectra, despite a difference in primary beam parameters and the use of a sector rather than a quadrupole mass analyzer. The liquid compounds are processed as neat samples on a direct-insertion probe for the production of both secondary-ion and fast-atom-bombardment mass spectra, and provide stable, long-lasting secondary-ion signals even under high fluxes of primary particles.

The study of polymers has recently been a strong area of application for mass spectrometry, which provides an assessment of the distribution of molecular weights [1—3]. The complexity of polymer chemistry, and the development of larger and nonvolatile materials, have stretched the capabilities of the ionization sources in common use, namely electron and chemical ionization, both of which require the volatilization of the sample molecules prior to the ionization. Particle-induced desorption-ionization techniques, including fast-atom-bombardment (f.a.b.) and secondary-ion mass spectrometry (s.i.m.s.), have been developed which allow the direct ionization of material from the liquid or solid form without the need for prior evaporation. Although these methods are particularly successful for ions in the condensed phase [4—6], sample molecules which participate in acid/base reactions also form ionized species which then appear as abundant signals in the mass spectrum.

The development of fast-atom-bombardment ionization has centered on the use of a liquid reservoir of sample within the source of the mass spectrometer. A solution of the sample in a vacuum-compatible solvent (usually glycerol) produces a fairly stable and persistent mass spectrum. A constant

0003-2670/86/$03.50 © 1986 Elsevier Science Publishers B.V.

diffusion of sample from within the bulk of the solution replenishes that material which is sputtered from the surface, and also removes material that may be damaged by the irradiation. A neat liquid sample bombarded by an energetic particle beam also provides a stable mass spectrum via the same regenerative mechanisms.

In this paper, the positive-ion s.i.m. spectra of a series of polyalkoxylated pyrazoles and hydrazines processed as neat liquid samples are discussed. These compounds are used as anti-corrosive additives in hydraulic fluids. They possess a very low vapor pressure at room temperature, and can be introduced into the mass spectrometer with no pressure increase in the system. Our original interest in these materials was their possible use as solvent matrices for other types of samples. The complexity of the spectra produced precludes such use, but suggests that the particle-bombardment methods of ionization are quite useful for their own characterization.

EXPERIMENTAL

Positive-ion secondary ion mass spectra were obtained on a custom-built s.i.m.s. instrument [7] based on an Extrel quadrupole mass analyzer. Neat samples were introduced on a stainless-steel platform attached to the direct-insertion probe. A total of 10—20 μl of sample was spread over a 1-cm^2 area. The primary beam consisted of 8-keV cesium ions emitted from a thermionic source. The primary-ion current density at the sample surface was approximately 10^{-4} A cm^{-2}. Spectra were recorded directly on an x-y recorder; neither spectral averaging nor background subtraction was used. The only loss of sample material from the probe is through the process of sputtering; spectra persist for several hours at least, and probably much longer than that. Variations in the relative abundances of the ions in the spectra are ±10%, between or within runs.

Positive-ion fast-atom-bombardment mass spectra were obtained on a Kratos MS80RFAQQ mass spectrometer of EBQ geometry, using the intermediate detector located after the magnetic sector but before the quadrupoles. A resolution of 1000 was used to record all spectra. Xenon gas was fed into an Iontech gun to produce a beam of neutral particles with 8 kV of kinetic energy (10^{12} atoms cm^{-2} s^{-1} particle density). The neat sample (20 μl) was loaded onto a copper platform which intercepts the primary beam at an angle of 45°. Electron-ionization and direct-exposure-ionization mass spectra were also recorded with the Kratos instrument. The direct-exposure probe consisted of a heated loop of platinum wire which extends into the electron beam emitted from the filament.

Samples were obtained from Olin Chemical Company, and are sold under the Oxypruf trademark. Oxypruf-E is identified as ethoxylated dimethylpyrazole, and Oxypruf-P as propoxylated dimethylpyrazole. Oxypruf-6 is labelled as [di-(2-hydroxypropyl)-di-(2-hydroxypropoxypropoxypropyl)]-hydrazine, Oxypruf-12 as [tetra-(hydroxypropoxypropoxypropyl)]hydrazine,

and Oxypruf-20 as [tetra(propoxypropoxypropoxypropoxyhydroxypropyl)]-hydrazine. These are technical-grade samples, and lot-to-lot consistency is not assumed. No other information about these mixtures is available.

RESULTS AND DISCUSSION

Although these polymeric liquids have a very low vapor pressure at room temperature, they can be distilled into the vacuum with a direct-insertion probe, and their electron-ionization mass spectra can be recorded. Figure 1 is the electron-ionization mass spectrum of Oxypruf-P. A series of polymeric ions is evident with a spacing of 58 daltons that corresponds to successive additions of the propoxy group in a polymeric structure (*m/z* 387, 445, 503, 561, 619, and so on). The descriptions of these compounds in the patent literature imply that the polymeric series should extend to species that would be expected to have masses of over a thousand daltons, but these could not be observed in the electron-ionization experiment. This prompted an investigation of the particle-bombardment mass spectra of these compounds. Further, because these compounds are handled as neat samples, a direct comparison of secondary-ion mass spectra (s.i.m.s.) with fast-atom-bombardment (f.a.b.) mass spectra could be done. Mechanistically, no differences in the mass spectra were expected, but this comparison has not often been rigorously completed as it has been in this series of spectra.

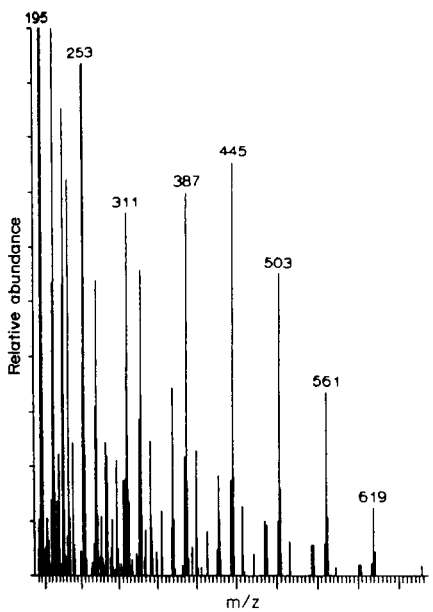

Fig. 1. Positive-ion electron-ionization mass spectrum of Oxypruf-P (propoxylated dimethylpyrazole).

Secondary-ion mass spectra

Alkoxylated pyrazoles. The positive-ion secondary-ion mass spectrum of Oxypruf-E is given in Fig. 2A. The general formula for this polymer is indicated below (I),

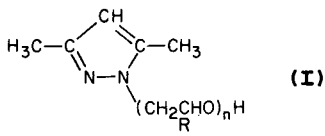

(I)

for which R = H for the ethoxy polymer and R = CH_3 for the propoxy polymer. The patent literature describes these compounds as polymers with n values varying between 2 and 20 [8]. Two series of ions are evident from the mass spectrum. The first consists of those ions at m/z 317, 361, 405, 449, 493, 537, 581, 625, 669, 713, 757, and 801, corresponding to $(M + H)^+$ ions of sequential n-mers in the series $(CH_3)_2(C_3HN_2)(CH_2CH_2O)_nH_2^+$, where n ranges from 5 for the ion at m/z 317 to 16 for the ion at m/z 801, and the spacing between the ions in the series is 44 daltons (the ethoxy group). Each of the ions identified in this series is accompanied by an ion 2 daltons less in mass, and of about one-half the abundance of its partner. This parallel series probably represents a dehydrogenation process occurring during sputtering, rather than a discrete polymeric series present in the original mixture. The members of the $(M + H)^+$ ion series fragment by loss of 18 daltons (water) to form the fragment ion series at m/z 299, 343, 387, and 431. As the number of ethoxy units in the polymeric molecule increases, the relative abundances of the members of the fragment ion series decrease. Further loss of a methyl group from the water loss ion, or concomitant loss of both methyl and water, provides the third series of ions apparent in the mass spectrum. The masses of these ions are not labelled in the figure, but appear at m/z 328, 372, 416, and 460.

Below m/z 300, the smoothly-varying pattern of ion abundances in the various ion series becomes more difficult to discern. For smaller n-mers, competition between the various fragmentation processes leads to ion products of near-equal abundances. Thus the relatively large ion at m/z 299 is loss of water from the pentamer at m/z 317. The tetramer at m/z 273 belongs in the original series of $(M + H)^+$ ions, but losses of hydrogen and water form fragment ions of higher relative abundances at m/z 271 and 255, respectively. Unlabelled ions at m/z 229, 227, and 211 correspond to the analogous ions and fragmentation processes. The $(M + H)^+$ ion of the dimeric form of the pyrazole is a very small ion at m/z 185; loss of hydrogen is observed, as well as a facile loss of water to form the abundant fragment ion at m/z 167.

Interpretation of the positive-ion s.i.m. spectrum of the propoxylated pyrazole polymer (Fig. 2B) is similarly accomplished. The substitution of propoxy for ethoxy increases the spacing between ions in the series of protonated molecular ions of the n-mers to 58 daltons. The major ions (m/z 387,

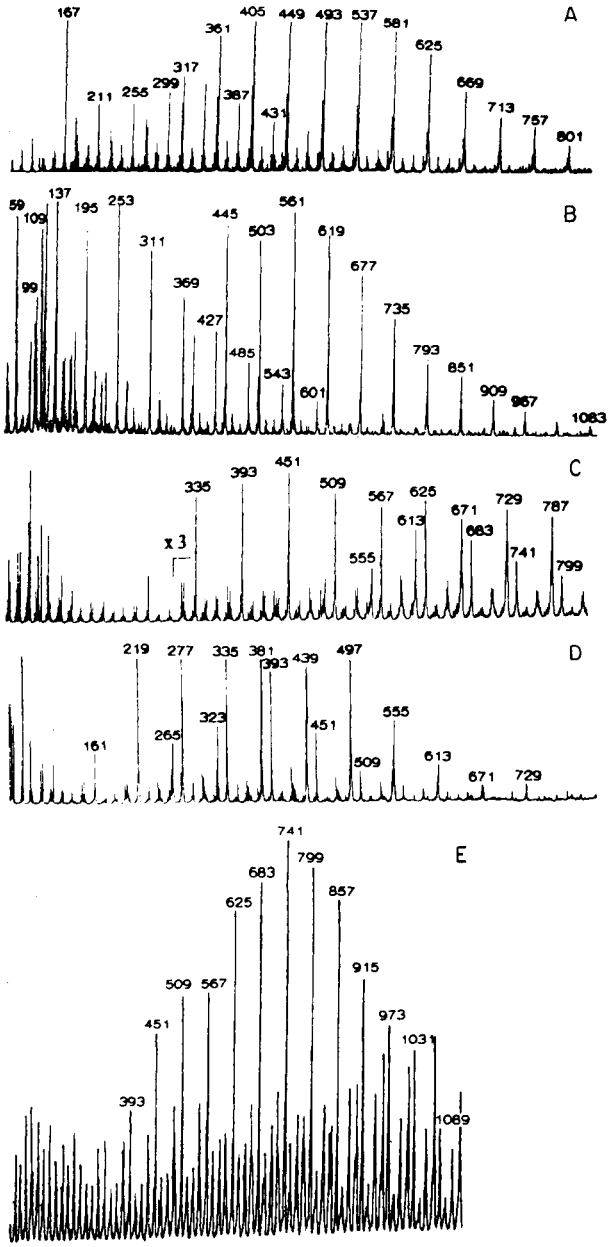

Fig. 2. Positive-ion s.i.m. spectra: (A) Oxypruf-E (ethoxylated dimethylpyrazole); (B) Oxypruf-P (propoxylated dimethylpyrazole); (C) Oxypruf-12 [tetra-(hydroxypropoxypropoxypropyl)hydrazine]; (D) Oxypruf-6 ([di-(2-hydroxypropyl)-di-(2-hydroxypropoxypropoxypropyl)]hydrazine); (E) Oxypruf-20 [tetra-(propoxypropoxypropoxypropoxyhydroxypropyl)hydrazine].

445, 503, 561, 619, 677, 735, 793, 851, 909, 967, 1025, and 1083) are members of the series given by the formula $(CH_3)_2(C_3HN_2)(CH_2CH_2CH_2O)_n$-$H_2^+$, where n ranges from 5 for the ion at m/z 387 to 17 in the ion at m/z 1083. Loss of 18 daltons (water) is again observed, and is more abundant for the lower members of the n-mer series. This fragmentation process accounts for the ion series at m/z 369, 427, 485, 543, 601, and 659. The loss of molecular hydrogen is not as prevalent for this compound as it was for the ethoxylated version, presumably because the alkene which would be formed in such a process is not necessarily in conjugation with the double bonds in the pyrazole ring. However, this loss still forms an abundant fragment ion for the lower members of the homologous series.

As with the ethoxylated polymer, the members of the various ion series below m/z 300 are not so readily discernible. The protonated molecular ions for the tetramer, trimer, and dimer are observed at m/z 329, 271, and 213, respectively, accompanied by the products of the dehydrogenation reaction at m/z 327, 269, and 211. Losses of water from these lower homologs form the ions at m/z 311, 253, and 195, all relatively abundant ions in the mass spectrum. The large ion at m/z 137 is loss of water from the protonated monomer, itself observed with a much lower relative abundance.

Alkoxylated hydrazines. Polyalkoxylated hydrazines are also used as corrosion inhibitors [8]. The general formula of these compounds as discerned from the patent literature is indicated by **II**.

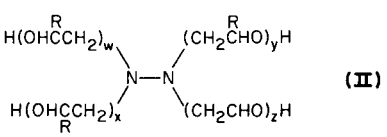

(II)

Here R is selected from hydrogen or one of the lower alkyl groups, or mixtures of the two, and the sum of w, x, y, and z can be 4—20.

The compounds in the present study might be expected to follow this general structural framework, with the particular pattern of substitution noted on the labels. It may be noted that each of the label descriptions can be formulated as a single structure rather than a polymeric mixture, while the spectra obtained resemble the n-mer distributions typified by the pyrazoles discussed in the previous section. The positive-ion s.i.m. spectrum of Oxypruf-6 is given in Fig. 2D. A major series of polymeric ions dominates the spectrum, with a spacing between ions of 58 daltons, corresponding to the propoxy group (m/z 265, 323, 381, 439, 497, 555, 613, 671, and 729). Accompanying each of the ions in this series are associated ions with masses 1 and 2 daltons less. For instance, the ion at m/z 497 is accompanied by an ion at m/z 496 of about 60% relative abundance, and an ion at m/z 495 of about 20% relative abundance. Each of the ions in the major series is also accompanied by a nominal loss of 19 daltons; this process is likely the loss of 18 daltons (water) from the associated ion one dalton lower in mass. For example, m/z 496 loses water to form m/z 478. Ions in the water-loss series appear at m/z 304, 362, 420, 478, and 536.

A second major series of ions at *m/z* 219, 277, 335, 393, 451, and 509, with fairly high relative abundances, is also osberved in this mass spectrum, peaking at mass values lower than the first dominant series, but with the same ion spacing of 58 daltons. Interestingly, these ions do not exhibit loss of 1 or 2 daltons as do the ions in the first series, and also seem to show a reduced propensity for loss of water, although some such losses can be tentatively identified in the spectrum. The mass difference between this series and the first series of ions described above is 46 daltons. The difference pairs *m/z* 219 with 265, *m/z* 277 with 323, etc. A fragmentation by loss of ethanol (46 daltons) may be the origin of this series. The reaction may occur during the original synthesis of the compound as the high abundance suggests that these ions are not necessarily the result of a fragmentation, but rather represent the molecular ions of another series of compounds present in the original mixture.

The mass spectrum also suggests that the composition of the material is not as well-defined as the labelling might suggest. A spectrally-convenient structure is that given by III,

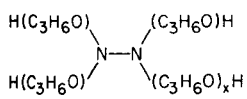

(III)

where $x = 4$ for the putative molecular ion (*m/z* 380, observed as the $(M + H)^+$ ion at *m/z* 381). The ions in the series observed in the mass spectrum are those formed by the increase of propoxy groups (*m/z* 439, 497, 555, 613, and 671). The second major series of ions (rationalized as loss of the elements of ethanol) can be similarly described (*m/z* 219, 277, 335, 393, 451, and 509).

Figure 2C is the positive-ion s.i.m. spectrum obtained for a second alkoxylated hydrazine, Oxypruf-12. The mass spectrum of this polymer is somewhat more complex than that of the first example discussed above. The 58-dalton (propoxy) spacing between members persists in two identifiable ion series. The first series includes *m/z* 335, 393, 451, 509, 567, 625, 683, 741, and 799, and the second series, for which the first member is evident at a higher mass, includes *m/z* 555, 613, 671, 729, and 787. The overlap in masses between these ion series and those observed in the previous example is evident, and reflects the similarity in the repeating unit. A mass difference of 46 daltons between the members of the two dominant ion series is evident, which may again represent a mechanism involving a loss of ethanol.

Finally, the positive ion s.i.m. spectrum of Oxypruf-20 is presented in Fig. 2E. The complexity of the spectrum generated by the numerous fragmentation processes and the overlapping ion series is clear. The repeating pattern continues to very high masses, and the mass scale has been condensed (with a sacrifice in apparent resolution) to illustrate this phenomenon. The dominant ion series becomes evident at the higher masses, with the expected ion spacing of 58 daltons. The masses of the most abundant ions in each of the several series correspond to those reported for Oxypruf-6 and -12, but

the most abundant series members appear at higher masses. The labelled series of ions extends from *m/z* 451 to *m/z* 1089. The ion series between these major ions are found at masses 18, 32, and 46 daltons less than the ions in the labelled series (losses of water, methanol, and ethanol, respectively), and these ions become more abundant at the higher masses.

Fast-atom-bombardment mass spectra

The fast-atom-bombardment mass spectra are remarkably similar to the secondary-ion mass spectra, especially considering the differences in details of the instruments with which they were recorded. The s.i.m. spectra were obtained with a cesium-ion gun and a quadrupole mass spectrometer with an upper mass limit of 1200 daltons. The f.a.b. mass spectra were obtained with xenon-atom bombardment and a double-focussing mass spectrometer with an upper mass limit of 2400 daltons.

Alkoxylated pyrazoles. The positive-ion f.a.b. mass spectrum of Oxypruf-E is given in Fig. 3A (compare to the s.i.m. spectrum given in Fig. 2A). The series of protonated molecular ions of the *n*-mer (n = 5 to 16) is observed at *m/z* 317, 361, 405, 449, 493, 537, 581, 625, 669, 713, 757, and 801. Again, the spacing between the ions of 44 daltons corresponds to additions of the ethoxy group in sequentially larger units of the polymer. As in the s.i.m. spectrum, each ion is accompanied by a fragment ion corresponding to the loss of molecular hydrogen. The series of ions corresponding to water loss is also observed, and, as in the s.i.m.s. results, the relative abundances of the ions in this series increases for the lower mass ions in the polymeric series. The combination of methyl and water loss is also observed for the lower mass ions in the series.

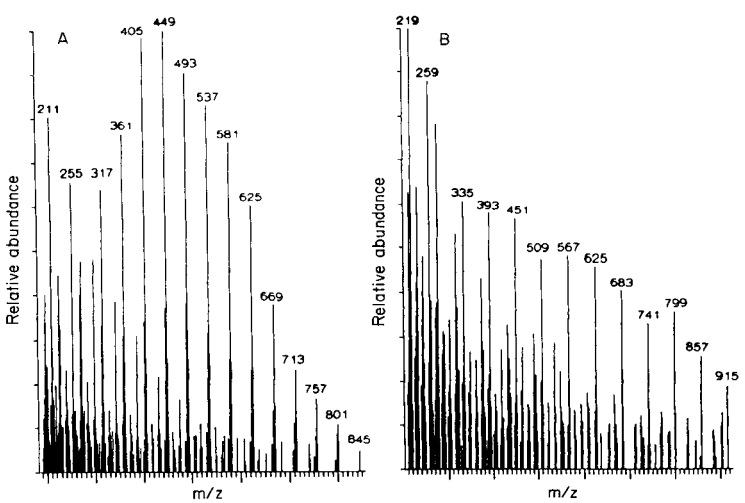

Fig. 3. Positive-ion f.a.b. mass spectra: (A) Oxypruf-E; (B) Oxypruf-20.

Propoxylated dimethylpyrazole also provides very similar secondary-ion and f.a.b. mass spectra. The distribution of ions parallels that established in the s.i.m. spectrum, with the exception being a reversal in the relative abundances of the ions at *m/z* 369 and 387. Again, the major ions in the mass spectrum are observed with a spacing of 58 daltons from *m/z* 387 to *m/z* 909, corresponding to the molecular ions of *n*-mers from 5 to 14. Loss of 18 daltons is observed, and occurs with greater facility for lower mass ions. Losses of hydrogen are also observed, as in the s.i.m. spectrum.

Alkoxylated hydrazines. The agreement between the secondary-ion and the f.a.b. mass spectra for the alkoxylated hydrazines is also quite close, with only a few minor differences in relative abundances. The spacing between ions in the major series is 58 daltons, corresponding to the propoxy group. One major series of ions includes *m/z* 265, 323, 381, 439, 497, 555, 613, and 671. The accompanying ions with masses 1 and 2 daltons less are observed, as are the fragment ions with masses 19 daltons less. The second major series of ions (also observed in the s.i.m. spectrum) occurs at *m/z* 161, 219, 277, 335, 393, 451, and 509, and the ions in this series are not accompanied by the partner ions for losses of hydrogen. As in the s.i.m. spectrum, these two dominant series of ions are separated by a spacing of 46 daltons, pairing *m/z* 219 with 265, *m/z* 277 with 323, and so on. The exact mass difference between the members of these ion pairs is consistent with the elements of C_2H_5OH (ethanol).

For Oxypruf-12, the secondary-ion and f.a.b. mass spectra are again very similar, and the predominant ion series overlap in mass with those observed for Oxypruf-6, as might be expected from the similarities in their structures. The first main series of ions (58 dalton spacing) extends from *m/z* 219 through *m/z* 277, 335, 393, 451, 509, 567, 625, 683, 741, and 799 to *m/z* 857. The second main series begins at higher masses and includes *m/z* 497, 555, 613, 671, 729, 787, 845, and 903. This second series of ions is accompanied by fragment ions from the loss of 1 and 2 hydrogens. Ions of the same masses undergo these same losses as demonstrated in the mass spectra of Oxypruf-6. The series of ions continues to higher observed masses in the spectrum of Oxypruf-12. The regularity of the spacing of the ions observed interspersed between the main series of ions permits the identification of several fragment ion series, including the loss of water from the ions in the second listed series.

Finally, the positive-ion f.a.b. mass spectrum of Oxypruf-20 is presented in Fig. 3B (compare to the s.i.m. spectrum in Fig. 2E). The structural relationship to Oxypruf-6 and -12 is reflected in the commonality of the ion series observed. One ion series predominates in this spectrum, extending from *m/z* 277 to *m/z* 915 with steadily decreasing ion relative abundances. The subordinate ion series (*m/z* 323, 381, . . .) and the losses of water from ions in the main series are also noted. More detailed interpretation is difficult because of the low relative abundances (less than 0.1%) of the ions in the mass spectrum.

CONCLUSIONS

These examples demonstrate the utility of particle-bombardment methods of ionization for the analysis of liquid polymers. The spectra are relatively easy to obtain and are long-lasting, allowing exact mass measurements and other experiments to be done when desired. For the alkoxylated pyrazoles, the distribution of ions among the expected members of the polymer *n*-mer series was clearly evident from the mass spectra produced. For the hydrazines, the spectra became much more complex, but the spectra still provided evidence for a regular polymeric structure. Despite gross differences in the instruments with which each was obtained, the secondary-ion and f.a.b. mass spectra are to all intents and purposes identical, underscoring the common sputtering mechanisms. An overview of the data suggests that the s.i.m. spectra may contain ions in the higher mass series with abundances higher than those recorded in the f.a.b. spectra. The difference is slight, and is attributed to the fact that the s.i.m.s. instrument incorporates a Bessel Box energy filter that is tuned for maximum signal for the ion of interest, typically the highest mass ion that was identified in a preliminary spectrum of the sample. The f.a.b. source on the sector instrument provides no such selection. It has been shown that the energy distributions of organic secondary ions can vary greatly [9], and the energy filter may have provided a discrimination against the lower mass ions in the s.i.m. spectra.

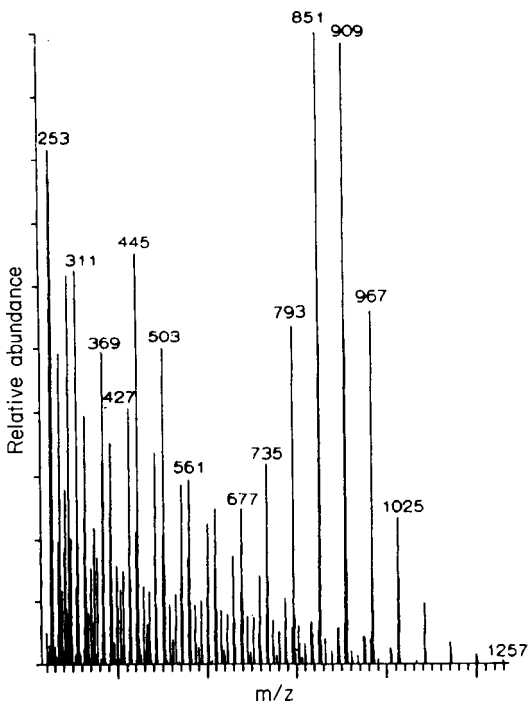

Fig. 4. Positive-ion direct-exposure electron-ionization mass spectrum of Oxypruf-P.

Because the particle-bombardment methods of ionization were successful in promoting the creation of high mass secondary ions from these polymers, it was of interest to examine the use of a direct-exposure probe as well, because this method has also demonstrated an ability to detect fairly non-volatile samples. Figure 4 is the positive-ion spectrum of Oxypruf-P obtained with the direct-exposure probe and electron ionization. By now, the pattern of ion series should be familiar. The masses of the ions are the same as those observed in the electron-ionization, the secondary-ion, and the fast-atom-bombardment mass spectra. The spectrum demonstrates that the series extends to still higher masses (up to *m/z* 1257) than observed in any of the previous spectra. The pattern of abundances is also shifted, so that the most abundant ions are observed at higher masses than in any of the other spectra. The heat applied to the direct-exposure probe, and interactions with the electron beam, may promote additional polymerization beyond that found in the original mixture. The relatively abundant ions observed at high masses in the secondary-ion, f.a.b., and direct-exposure electron-ionization mass spectra of these compounds suggest that they might serve as calibration compounds in these ionization modes, and this possibility is under further investigation.

The construction and evaluation of the s.i.m.s. instrument is supported by the Whitaker Foundation. The Kratos mass spectrometer was purchased with support from the National Science Foundation (CHE 81-11957). G. C. DiDonato is acknowledged for instrumental assistance.

REFERENCES

1 H. R. Schulten and R. P. Lattimer, Mass Spectrom. Rev., 3 (1984) 231.
2 H. L. C. Meuzelaar, W. Windig, A. M. Harper, S. M. Huff, W. H. McClennen and J. M. Richards, Science, 226 (1984) 268.
3 J. A. Gardella, Jr., S. W. Graham and D. M. Hercules, Adv. Chem. Ser., 203 (1983) 635.
4 R. J. Day, S. E. Unger and R. G. Cooks, Anal. Chem., 52 (1980) 557A.
5 K. L. Busch, S. E. Unger, A. Vincze, R. G. Cooks and T. Keough, J. Am. Chem. Soc., 104 (1982) 1507.
6 G. C. DiDonato and K. L. Busch, Biomed. Mass. Spectrom., 12 (1985) 354.
7 J. W. Fiola, G. C. DiDonato and K. L. Busch, Rev. Sci. Instrum., 57 (1986) 2294.
8 M. J. Collie (Ed.), Corrosion Inhibitors: Developments Since 1980. Chemical Technology Review Number 223, 1983.
9 L. Kelner and S. P. Markey, Int. J. Mass Spectrom. Ion Proc., 59 (1984) 157.

Analytica Chimica Acta, 187 (1986) 129—137
Elsevier Science Publishers B.V., Amsterdam — Printed in The Netherlands

CRYOGENIC-TEMPERATURE FLUORESCENCE SPECTRA OF POLYNUCLEAR AROMATIC HYDROCARBONS OF MOLECULAR WEIGHT 302

ANDERS L. COLMSJÖ*

Department of Analytical Chemistry, Arrhenius Laboratory, University of Stockholm, S-106 91 Stockholm (Sweden)

STEPHEN A. WISE

Organic Analytical Research Division, Center for Analytical Chemistry, National Bureau of Standards, Gaithersburg, MD 20899 (U.S.A.)

(Received 1st May 1986)

SUMMARY

Shpol'skii cryogenic temperature fluorescence spectra of 19 of the possible 33 polynuclear aromatic hydrocarbons with a molecular weight of 302 are reported. The group consists of the benzo- and naphtho-pyrenes and fluoranthenes and also the benzoperylenes. There is a large variation in the degree of selectivity and sensitivity achieved by the Shpol'skii technique within this group of compounds.

Polynuclear aromatic hydrocarbons (PAHs) are a group of compounds on which great interest has been focused for the last two decades. The reasons for this interest are numerous. The presence of PAHs in the environment is largely a result of human activities, mostly by the incomplete combustion of fossil fuels. Various individual PAHs are also known to be strong carcinogens, which has drawn attention to the importance of monitoring the levels of PAHs. A complete determination of the individual PAHs in a sample is often an enormous task, which could involve identification and quantification of hundreds of compounds within the concentration range of interest. For example, more than 900 PAHs from tobacco smoke were separated and identified by Snook et al. [1, 2] by using a combination of liquid chromatography, gas chromatography, u.v. spectrometry and mass spectrometry.

A major problem associated with such an analysis, which is often disregarded, is the positive identification of each isomer. Chromatographic methods give information on retention times; however, most chromatographic detectors used only hint at the structure of the compounds. Thus, mass spectra of PAHs usually yield only the molecular weight of a compound, making it difficult to differentiate between isomers. If only a few tens of compounds are to be determined and the origin of a sample is well documented, the experience and skill of the analyst generally leads to a solution

0003-2670/86/$03.50 © 1986 Elsevier Science Publishers B.V.

of this problem. Fluorescence spectroscopy combined with liquid chromatography makes it possible, to a certain extent, to achieve selective isomer-specific detection. This method can be further enhanced by utilizing the property of many PAHs to emit Shpol'skii fluorescence [3—5], yielding a sensitive and selective tool for the identification and quantification of many PAHs [6, 7].

The Shpol'skii effect is often exhibited if a PAH is dissolved in a certain *n*-alkane and the temperature is lowered to cryogenic levels, giving a quasi-line structured spectrum. Thus, broad-banded emission lines are concentrated into narrow wavelength regions, yielding the quasi-line spectrum, which in many cases is superimposed on a weak continuous spectrum. Cryogenic-temperature quasi-line fluorescence exhibits the paradox of both increased sensitivity and resolution when compared with room-temperature fluorescence. If this cryogenic fluorescence method is to be used for identification of an unknown compound, a previously-recorded spectrum from a standard compound must be available for comparison. The compilation of a data base containing Shpol'skii spectra of particular PAHs is thus a very important part of providing a useful basis for conducting further analysis with the aid of this spectroscopic technique [8].

So far, the most studied PAHs are found among the more volatile isomers, primarily because gas chromatography has been the main method of separation. Depending on the availability of reference compounds and also for historical reasons, the most studied PAHs have been those with molecular weights up to 300 (coronene), with a predominant interest typically focused on benzo[a]pyrene [9]. Nevertheless, various mutagenic and carcinogenic compounds are found in the group of PAHs with molecular weights exceeding 300 [10—12]. Compounds within this group are at present most efficiently separated by liquid chromatography, which leads to the possibility of identification by means of Shpol'skii spectroscopy. To facilitate their identification and to illustrate some ambiguities in the origin of some spectra, cryogenic-temperature fluorescence spectra of 19 PAHs with a molecular weight of 302, i.e., naphtho- and dibenzo- pyrenes and fluoranthenes as well as two benzoperylenes, are reported and discussed in this paper.

EXPERIMENTAL

The sample compartment and optical set-up have been described [6]. The recording unit consisted of an amplifier, a 12-bit A/D converter and an ABC-800 microcomputer, which provided signal treatment, spectral calculations and the storage of spectra on diskettes. Noise reduction, wavelength calibration and plotting were done by the computer. The compounds used were commercially available, obtained from other laboratories, or synthesized [10].

RESULTS

The 33 possible isomers of polynuclear aromatic hydrocarbons with a molecular weight of 302, which comprise the dibenzo- and naphtho- pyrenes and fluoranthenes as well as the benzoperylenes, are shown in Fig. 1. Table 1 lists the 19 isomers investigated here by low-temperature fluorescence. The transformation of an ordinary fluorescence spectrum into quasi-lines has been interpreted by means of the Debye-Waller factor, which is defined as the ratio between emitted photons in the quasi-line and emitted photons in the phonon wing [13]. For a spectrum consisting of a large number of not fully resolved lines, this factor is difficult to estimate. Thus, a less well-defined scale from continuous (c) to well resolved (+++) peaks (Table 1) was introduced in order to provide an estimate of the resolution of the spectra at 63 K.

In general, the compounds based on pyrene exhibit well resolved quasi-line spectra at 63 K, whereas compounds of the fluoranthene series exhibit the whole scale of possibilities from non-fluorescent compounds, continuous low-temperature fluorescence spectra, moderately resolved spectra to excellently resolved spectra.

In Fig. 2A—F, the cryogenic fluorescence spectra of the five possible dibenzopyrenes are presented. For standardizing purposes, the solvent used throughout this investigation was n-hexane and the temperature applied was 63 K. All of the dibenzopyrenes exhibit distinct spectra with fairly high resolution. The spectrum of dibenzo[a,l]pyrene (Fig. 2D) has previously been published incorrectly because of ambiguities in the synthesis of this compound. A correct route of synthesis and the verification of the structure were reported by Lavit-Lawy and Buu-Hoi [14]. Two out of the five possible naphthopyrenes were available for this study and their spectra are shown in Fig. 2F, G. The spectrum of naphtho[2,3-a]pyrene has a strong resemblance to a red-shifted spectrum of benzo[a]pyrene, whereas the spectrum of naphtho[2,3-e]pyrene exhibits a stronger O—O′ transition than that of the more symmetrical benzo[e]pyrene.

Among the benzofluoranthenes studied, dibenzo[a,f]fluoranthene (compound 12) was found not to fluoresce, whereas dibenzo[j,l]fluoranthene (compound 20) showed weak fluorescence. Further purification of the latter compound is necessary in order to exclude interferences from impurities. The spectrum is not reported here and the compound is denoted as weakly fluorescent or non-fluorescent. Dibenzo[a,e]fluoranthene, a compound that was found to contain dibenzo[a,l]pyrene in previous determinations, shows a continuous spectrum superimposed on a few resolved lines (Fig. 2H). The resolution of this spectrum can probably be substantially increased by further lowering of the temperature. Dibenzo[a,k]fluoranthene dissolved in n-hexane also exhibits a quasi-line spectrum superimposed on a continuous spectrum in the longer wavelength region (Fig. 2I). The continuous part of this spectrum extends beyond the scan limit (540 nm) reported in the figure.

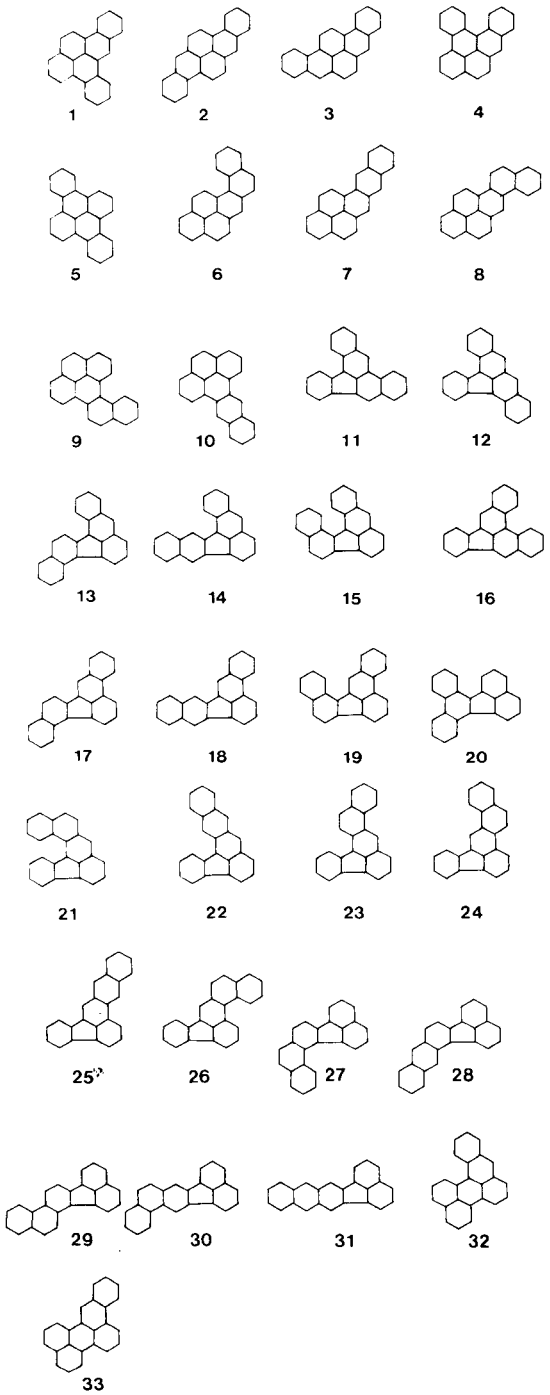

Fig. 1. Chemical structures of the compounds in Table 1.

TABLE 1

List of isomers examined with emission and excitation maxima and an indication of resolution of the spectra

Compound number[a]	Name[b]	Resolution[c]	Emission maximum (nm)	Excitation wavelength (nm)
1	DB[a,e]P	+++	394.8	305
2	DB[a,h]P	++	448.2	315
3	DB[a,i]P	+++	430.7	360
4	DB[a,l]P	++	419.6	381
5	DB[e,l]P	+++	382.7	318
7	N[2,3-a]P	++	459.8	332
10	N[2,3-e]P	+++	406.0	326
11	DB[a,e]F	+	462.1	401
12	DB[a,f]F	—	—	—
14	DB[a,k]F	+	474.1	405
16	DB[b,e]F	++	399.5	331
18	DB[b,k]F	+++	400.0	312
20	DB[j,l]F	w	—	—
25	N[2,3-b]F	+++	412.0	325
28	N[2,3-j]F	+	521.5	353
30	N[1,2-k]F	+++	410.3	326
31	N[2,3-k]F	+++	441.6	338
32	B[a]Pe	c	522.4	483
33	B[b]Pe	++	443.1	414

[a]From Fig. 1. [b]DB, dibenzo; P, pyrene; N, naphtho; F, fluoranthene; Pe, perylene. [c]c, continuous; w, weak intensity; +, ++, +++, increasing resolution.

The intense, well-resolved cryogenic fluorescence spectrum exhibited by dibenzo[b,k]fluoranthene is shown in Fig. 2K. The intensity of the spectrum makes this compound very well suited for detection at low concentrations. The detection limit for the system used was 5 pg of benzo[b,k]fluoranthene (signal/noise ratio of 4). The dibenzo[b,e]fluoranthene spectrum is fairly well resolved (Fig. 2J). A characteristic trend among the resolution of the spectra of dibenzofluoranthenes is that the resolution of the spectrum generally increases with increasing wavenumber of the O—O′ transition (decreasing wavelength) (Table 1). This feature is also true within many other groups of isomers.

Fluorescence was emitted by all the naphthofluoranthenes investigated. Of the spectra obtained, all but one can be regarded as quasi-linear at the temperature and with the solvent applied (Fig. 2L—N). Great care must be taken in distinguishing between the spectra of naphtho[2,3-b]fluoranthene and naphtho[1,2-k]fluoranthene, because the spectra and liquid chromatographic behaviour of these are rather similar. Finally, the cryogenic fluorescence spectra of the benzoperylenes are shown in Fig. 2O, P. A continuous unresolved spectrum of benzo[a]perylene can be observed in the region

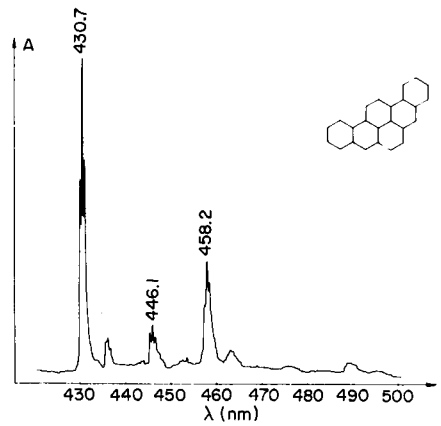
A
430.7
446.1
458.2
430 440 450 460 470 480 490 500
λ (nm)

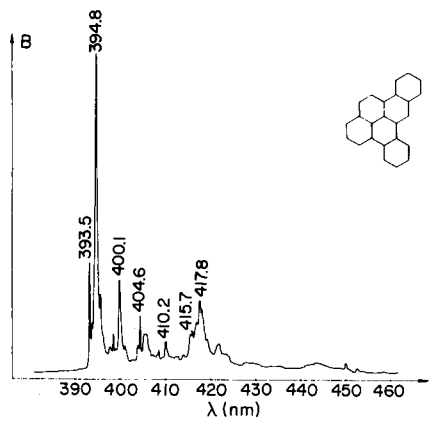
B
394.8
393.5
400.1
404.6
410.2
415.7
417.8
390 400 410 420 430 440 450 460
λ (nm)

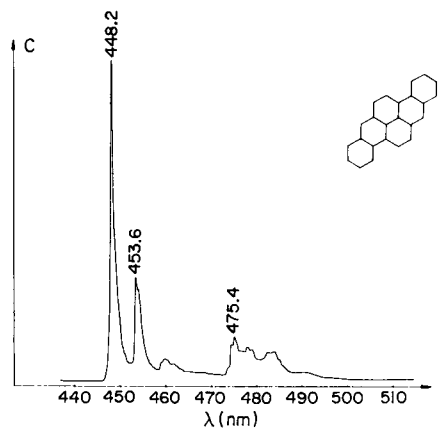
C
448.2
453.6
475.4
440 450 460 470 480 490 500 510
λ (nm)

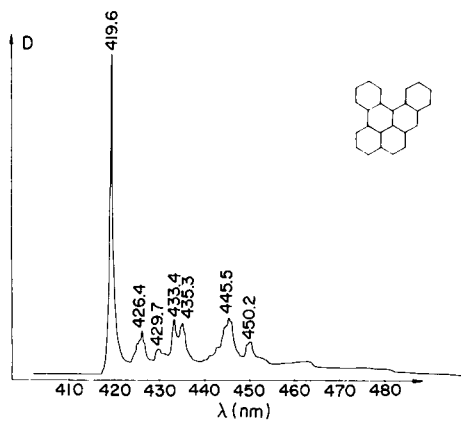
D
419.6
426.4
429.7
433.4
435.3
445.5
450.2
410 420 430 440 450 460 470 480
λ (nm)

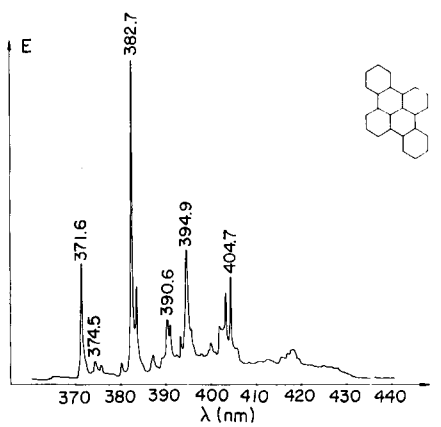
E
382.7
371.6
374.5
390.6
394.9
404.7
370 380 390 400 410 420 430 440
λ (nm)

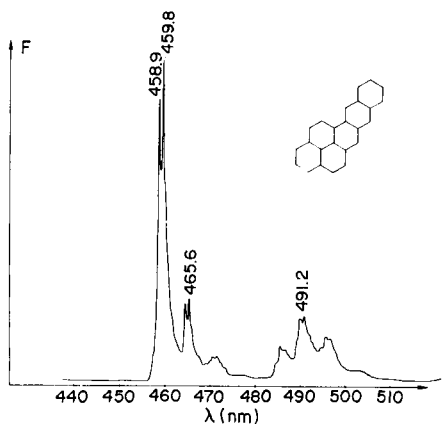
F
459.8
458.9
465.6
491.2
440 450 460 470 480 490 500 510
λ (nm)

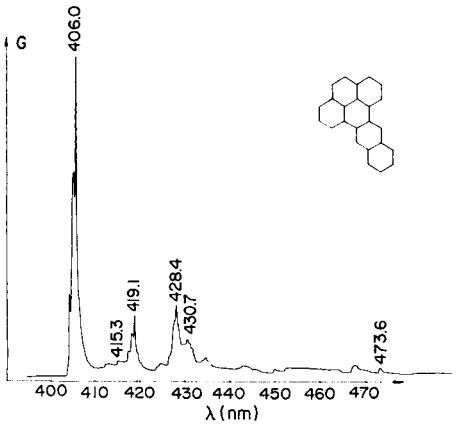
G
406.0
415.3
419.1
428.4
430.7
473.6
400 410 420 430 440 450 460 470
λ (nm)

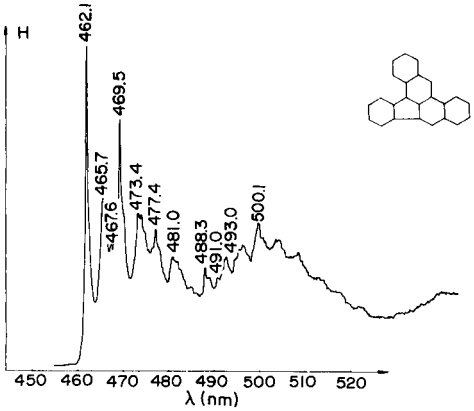
H
462.1
469.5
465.7
467.6
473.4
477.4
481.0
488.3
491.0
493.0
500.1
450 460 470 480 490 500 510 520
λ (nm)

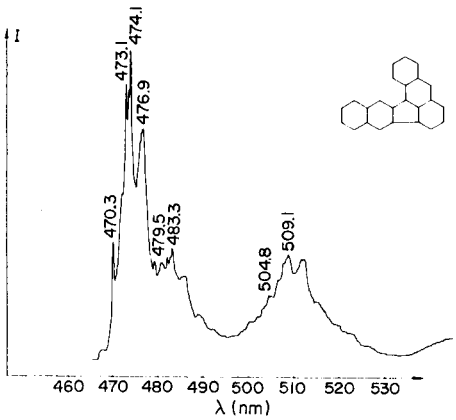
I
473.1
474.1
476.9
470.3
479.5
483.3
504.8
509.1
460 470 480 490 500 510 520 530
λ (nm)

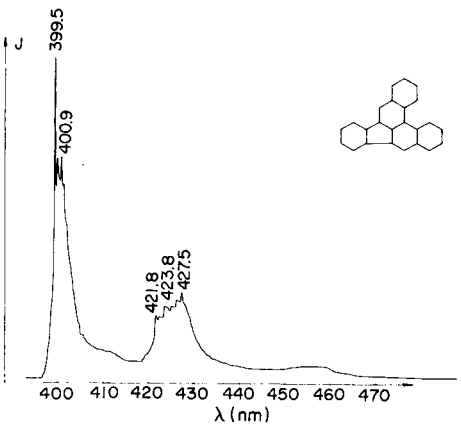
J
399.5
400.9
421.8
423.8
427.5
400 410 420 430 440 450 460 470
λ (nm)

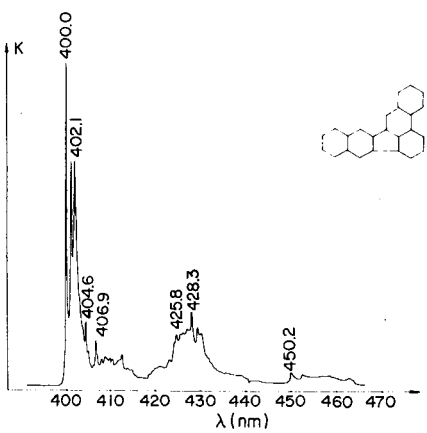
K
400.0
402.1
404.6
406.9
425.8
428.3
450.2
400 410 420 430 440 450 460 470
λ (nm)

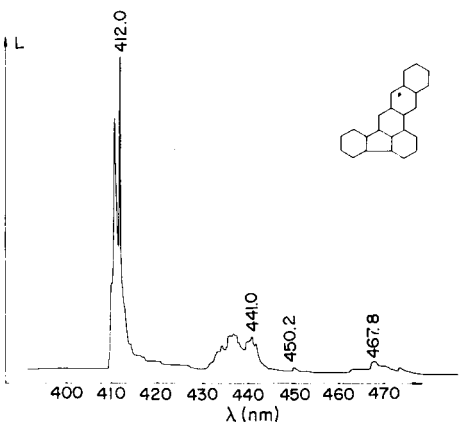
L
412.0
441.0
450.2
467.8
400 410 420 430 440 450 460 470
λ (nm)

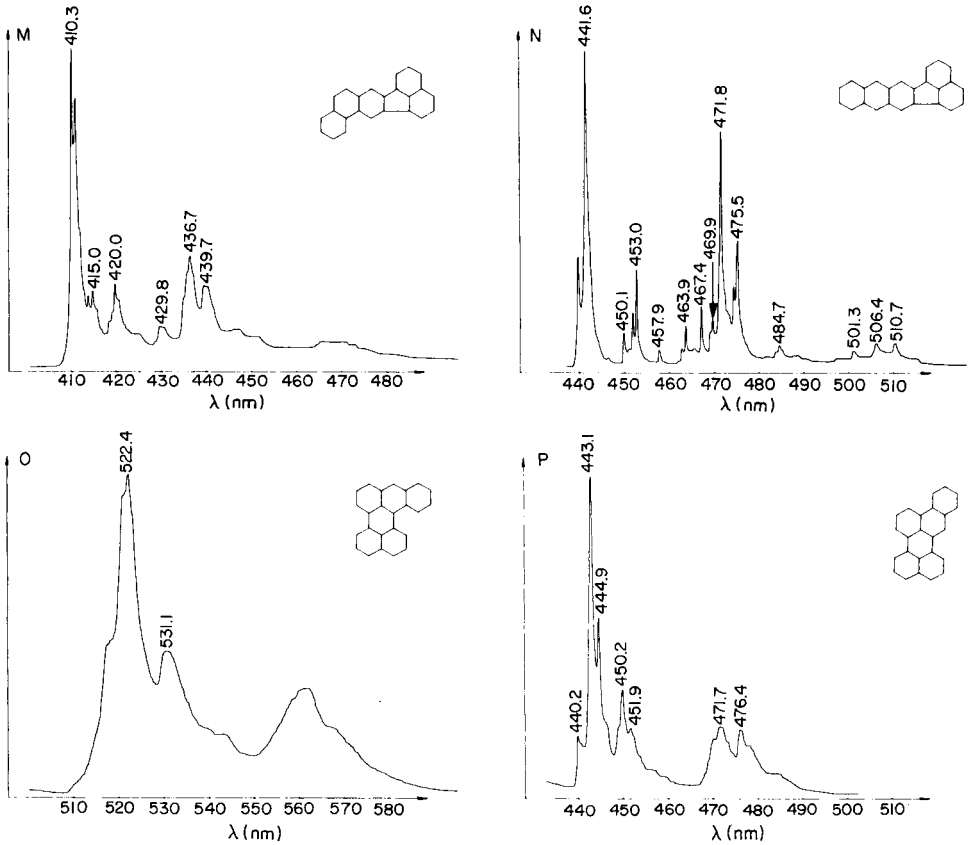

Fig. 2. Fluorescence spectra in n-hexane at 63 K. A, Dibenzo[a,e]pyrene; B, dibenzo[a,h]-pyrene; C, dibenzo[a,i]pyrene; D, dibenzo[a,l]pyrene; E, dibenzo[e,l]pyrene; F, naphtho-[2,3-a]pyrene; G, naphtho[2,3-e]pyrene; H, dibenzo[a,e]fluoranthene; I, dibenzo[a,k]-fluoranthene; J, dibenzo[b,e]fluoranthene; K, dibenzo[b,k]fluoranthene; L, naphtho-[2,3-b]fluoranthene; M, naphtho[1,2-k]fluoranthene; N, naphtho[2,3-k]fluoranthene; O, benzo[a]perylene; P, benzo[b]perylene.

510—600 nm, whereas the spectrum of benzo[b]perylene is better resolved and is situated at 440—500 nm.

A group of polynuclear aromatic compounds, therefore, has again been shown to exhibit quite different properties with respect to ability to emit quasi-linear fluorescence [15]. So far, the theoretical explanations for this are too inexact or insufficiently developed to allow the prediction of shape or resolution of the low-temperature fluorescence spectrum of a compound. The large variation within the group can, however, be utilized to achieve increased selectivity for certain compounds [16]. Thus, based on the appearance of a quasi-line spectrum, a number of compounds within the group can be positively identified, while the presence of others can be excluded.

The detection limits for those compounds emitting quasi-linear fluorescence vary over two orders of magnitude, emphasizing the necessity of

applying some kind of separation of the sample prior to the fluorescence spectrometry. Two compounds present in equal concentrations in a solution, for example, might exhibit a spectrum derived from only one of the compounds, even if the compounds separately exhibit well resolved cryogenic temperature fluorescence spectra.

When the cryogenic-temperature fluorescence method was applied to a complex real sample, a number of unknown spectra were found for PAHs with a molecular weight of 302. This stresses the necessity of synthesizing the remaining 14 isomers not considered in this paper in order to record their cryogenic-temperature fluorescence spectra.

The authors thank J. Fetzer, J. L. Monkman, J. Jacob, M. E. Snook and S. Terol for supplying reference compounds and Beryl Holm for reviewing the manuscript.

REFERENCES

1 M. E. Snook, R. F. Severson, H. C. Higman, R. F. Arrendale and O. T. Chortyk, Beitr. Tabakforsch., 8 (1976) 250; 9 (1978) 222.
2 M. E. Snook, R. F. Severson, H. C. Higman, R. F. Arrendale and O. T. Chortyk, in P. Jones and P. Leber (Eds.), Polynuclear Aromatic Hydrocarbons, Ann Arbor Science Publ., 1979, p. 231.
3 E. V. Shpol'skii, A. A. Illina and L. A. Klimova, Dokl. Akad. Nauk, SSSR, 87 (1952) 955.
4 E. J. Bowen and B. J. Brocklehurst, J. Chem. Soc., (1954) 3875; (1955) 4320.
5 B. Muel and G. Lacroix, Bull. Soc. Chim. Fr., (1960) 2139.
6 A. Colmsjö and U. Stenberg, Anal. Chem., 51 (1979) 145.
7 A. Colmsjö and U. Stenberg, in P. Jones and P. Leber (Eds.), Polynuclear Aromatic Hydrocarbons, Ann Arbor Science Publ., 1979, p. 121.
8 A. Colmsjö and C. Östman, in Atlas of Shpol'skii Spectra and Other Low Temperature Spectra of POM, University of Stockholm, Sweden, 1981.
9 J. W. Cook, C. L. Hewett and I. Hieger, J. Chem. Soc., (1933) 395.
10 E. Clar, in Polycyclic Hydrocarbons, Academic Press, London, 1964.
11 E. LaVoie, B. Bedenko, N. Hiroto, S. S. Hecht and D. Hoffman, in P. Jones and P. Leber (Eds.), Polynuclear Aromatic Hydrocarbons, Ann Arbor Science Publ., 1979, p. 705.
12 D. J. Sardella, E. Bogen and P. K. Godhal, in M. Cooke and A. Dennis (Eds.), Polynuclear Aromatic Hydrocarbons, Battelle Press, Columbus, OH, 1981, p. 529.
13 W. C. McColgin, A. P. Marchetti and J. H. Eberly, J. Am. Chem. Soc., 100 (1979) 5622.
14 D. Lavit-Lamy and N. P. Buu-Hoi, Chem. Commun., 4 (1966) 92.
15 A. Colmsjö, Y. Zebühr and C. Östman, Chem. Scr., 24 (1984) 95.
16 A. Colmsjö and C. Östman, Anal. Chem., 52 (1980) 2093.

Analytica Chimica Acta, 187 (1986) 139—145
Elsevier Science Publishers B.V., Amsterdam – Printed in The Netherlands

SIMULTANEOUS FLOW-INJECTION FLUORIMETRIC DETERMINATION OF AMMONIA AND HYDRAZINE WITH A NOVEL MODE OF FORMING pH GRADIENTS

A. RÍOS, M. D. LUQUE DE CASTRO and M. VALCÁRCEL*

Department of Analytical Chemistry, Faculty of Sciences, University of Córdoba, Córdoba (Spain)

(Received 10th December 1985)

SUMMARY

A flow injection configuration is suggested for the simultaneous determination of ammonia and hydrazine at the $\mu g\ ml^{-1}$ level by formation of zones of different pH. The analytes react with *o*-phthalaldehyde and mercaptoethanol to form fluorescent derivatives at different pH values. In addition to the normal flow method, a stopped-flow method is proposed to increase the ranges that can be quantified. The analysis of samples containing hydrazine and ammonia in ratios between 0.3 and 70.0 is described.

The simultaneous determination of two species based on the construction of pH gradients by flow injection analysis (f.i.a.) was first suggested by Betteridge and Fields [1] who later reported the exploitation of such gradients [2]. In spite of its interest, however, this mode has scarcely been used since then. Recently, a new configuration of establishing pH gradients was reported [3] which improves the results obtained by Betteridge and Fields and which involves the insertion of a second injection valve into the loop of the main valve. Solutions of reagents at two different pH values are utilized; one circulates along the single-channel system as the carrier, the other filling the loop of the second injection valve, while the loop of the main valve is filled with the sample. Simultaneous injection from the two valves yields a profile of four sample/reagent interfaces and produces a pH difference between the extreme interfaces and the central ones as large as is required by the chemical system. In addition, the configuration ensures the appropriate reagent concentration at the center of the segment, which is unachievable in the configuration of Betteridge and Fields and constitutes one of its most significant shortcomings. As, in general, the volume of the second valve is rather small, only three peaks appear on the recorder chart; the two outer peaks correspond to one of the analytes, the central peak to the other.

To resolve a mixture by this procedure, each analyte must react with the reagent(s) within a pH range in which the other species does not contribute to the signal. The reactions of ammonia and hydrazine with *o*-phthalaldehyde and mercaptoethanol yield fluorescent derivatives at different pH values, in

0003-2670/86/$03.50 © 1986 Elsevier Science Publishers B.V.

an acidic medium for hydrazine and in an alkaline one for ammonia [4]. The reaction product is an *N*-substituted 1-(2-hydroxyethyl)-thio-isoindole [5, 6], and has previously been used in the determination of traces of amino acids [7], peptides [8] and proteins [9]. In this paper, the suggested configuration is used for the simultaneous determination of ammonia and hydrazine in water samples.

EXPERIMENTAL

Reagents

One carrier solution, pH 3.0 contained 1.50 g of *o*-phthalaldehyde (OPA), 50 ml of methanol, 125 ml of NaH_2PO_4 (0.1 M)/sulfuric acid buffer at pH 3.0 and 0.5 ml of mercaptoethanol diluted with distilled water to 250 ml. The other carrier solution, pH 10.7, contained 0.050 g of OPA, 50 ml of methanol, 160 ml of NaH_2PO_4 (0.1 M)/sodium hydroxide buffer at pH 10.7 and 0.5 ml of mercaptoethanol diluted with distilled water to 250 ml. Solutions (1.000 g l^{-1}) of ammonia and hydrazine sulfate (Merck) were prepared in distilled water, from which the standard solutions were prepared, adjusting the pH to 3.3—3.5.

Apparatus

A Perkin-Elmer LS-1 LC fluorescence detector, furnished with a 4 μl flow cell and a microprocessor which allowed automatic change of sensitivity, was used with a Perkin-Elmer 56 recorder. A Tecator 5020 analyzer equipped with a microprocessor was used for stopped-flow measurements. Dual home-made injection valves with variable injection volumes were also used.

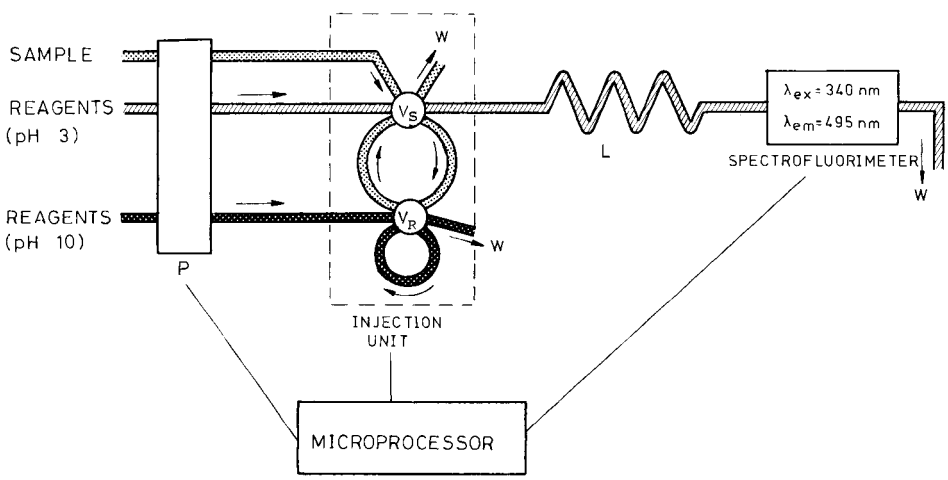

Fig. 1. Configuration used for resolution of hydrazine/ammonia mixtures (V_S = 1.61 ml; V_R = 57 μl, w = waste).

As shown in Fig. 1, the flow configuration consisted of a single channel for OPA/mercaptoethanol at pH 3.0 in which the sample injection valve, V_S, was inserted. Its loop accommodated a second valve, V_R, the loop of which was filled with an OPA/mercaptoethanol solution at pH 10.7. The simultaneous injection of both provided three reaction zones. The pH of the central zone was close to 3.0, whereas that of the outer zones was about 10. The reaction, which occurred in reactor L, yielded three fluorescence peaks, which were measured at λ_{ex} = 340 nm and λ_{em} = 495 nm. A microprocessor controlled the system for the stopped-flow measurements.

RESULTS AND DISCUSSION

Optimization

The most important shortcoming in the resolution of ammonia/hydrazine mixtures with the proposed configuration lies in the different rates of the two reactions involved. While, for example, ammonia reacts completely in 8 min, the same concentration of hydrazine requires 30 min [4]. For normal flow-injection procedures, where measurements are made 1—2 min after injection, these times are far too long to allow complete reaction. The resulting relative sensitivity, therefore, is opposite to the conventional non-flow spectrophotometric method, in which the reaction with hydrazine is the more sensitive. Therefore the optimization of the flow and chemical variables was aimed at favoring the reaction of hydrazine to the detriment of that of ammonia, in order to be able to determine similar concentrations of both analytes.

The pH of each carrier was important. The values of 3.0 and 10.7 were found to be most suitable. Samples were adjusted to pH 3.3—3.5.

The optimum concentration of *o*-phthalaldehyde was different for each analyte. The sensitivity for hydrazine increases with reagent concentration with no significant increase in the blank signal at its working pH, while the blank signal for ammonia dramatically increases with the OPA concentration at its optimum pH. Thus, the recommended reagent solution contains 0.60 g of OPA in 100 ml at pH 3.0 and 0.02 g of OPA in the same volume at pH 10.7. Both solutions include 10% of methanol to assist the dissolution of OPA. The recommended concentration of mercaptoethanol is 0.2% (v/v). Higher concentrations decreased the fluorescence of the products.

With respect to the flow-injection variables, the injection volumes, V_S and V_R (Fig. 1) are of prime importance for ensuring good resolution of the three peaks. The ratio V_S/V_R must be high enough to satisfy this requirement, but not so high as to cause a very low sampling frequency. However, it is not advantageous to have a large value for V_R to make the two central interfaces merge. The optimum values found were V_S = 1.61 ml and V_R = 57 μl. Because the sample is injected into a reagent carrier and the reagent is injected into a sample stream, the proposed configuration may be considered a normal flow-injection/reverse flow-injection hybrid. The optimum values for the other variables were: flow rate, 1.6 ml min^{-1}; reactor length (L), 250 cm; and inner diameter, 0.5 mm.

Determination of ammonia and hydrazine

A major problem involved in the resolution of a mixture of ammonia and hydrazine is that the signal corresponding to ammonia in the mixture (central peak) does not coincide with that given by ammonia when alone. A negative synergic effect, not found in the conventional method, appears in this flow procedure (Fig. 2), possibly because equilibrium is not attained in the flow procedure; also, because the OPA concentration in the alkaline medium is very low, hydrazine competes with ammonia for the reagent.

It is easy to solve this problem [10, 11]. As the hydrazine concentration in the mixture is directly obtained from the first or third peak and the magnitude of the synergic effect observed for ammonia depends on the hydrazine concentration, calibration graphs for ammonia in the presence of different concentrations of hydrazine can be plotted. The ammonia concentration is obtained as a function of that of hydrazine concentration.

Normal flow-injection method. This method is useful when the hydrazine concentration in the mixture exceeds that of ammonia. It entails the use of the maximum fluorescence intensity of the three peaks given on each simultaneous injection. The two outer peaks are directly related to the hydrazine

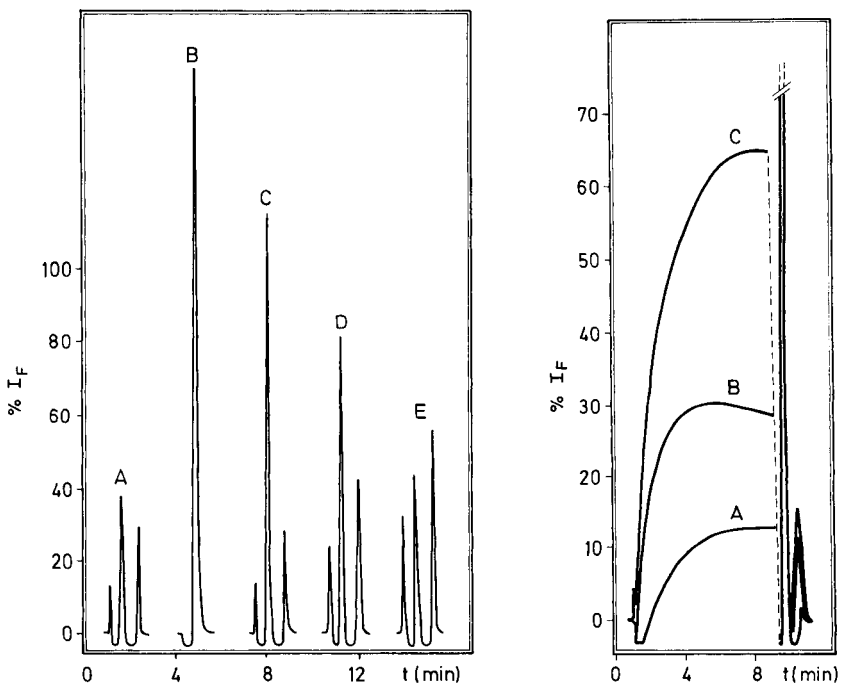

Fig. 2. Peaks obtained by the normal flow-injection method for different hydrazine + ammonia mixtures ($\mu g\ ml^{-1}$): (A) 10 + 0; (B) 0 + 1; (C) 10 + 1; (D) 20 +1; (E) 30 + 1.

Fig. 3. Fluorescence intensity/time responses obtained by the stopped-flow method for different hydrazine + ammonia mixtures ($\mu g\ ml^{-1}$): (A) 1 + 1; (B) 3 + 1; (C) 5 + 1.

concentration and the central one to that of ammonia. Thus, the equations for hydrazine are

$\%I_f$ (first peak) = 0.97 $[N_2H_4]$ + 5.4 (r = 0.9998, n = 7), for 7.0 ⩽ $[N_2H_4]$ ⩽ 35.0 μg ml^{-1}

$\%I_f$ (second peak) = 1.4 $[N_2H_4]$ + 14.4 (r = 0.9998, n = 7), for 4.0 ⩽ $[N_2H_4]$ ⩽ 30.0 μg ml^{-1}

where $\%I_f$ is the % fluorescence intensity. For ammonia, the equation is

$\%I_f = m\,[NH_3] + n$

where, m = −0.72 $[N_2H_4]$ + 30.4 (r = 0.9895, n = 7) and n = −0.63 $[N_2H_4]$ + 61.1 (r = 0.9978, n = 7)

which is obeyed for 15.0—40.0 μg ml^{-1} hydrazine and 0.5—7.0 μg ml^{-1} ammonia. When the first two peaks are used, the determination ranges are 0.5—7.0 μg ml^{-1} ammonia and 15.0—35.0 μg ml^{-1} hydrazine, i.e., hydrazine/ammonia ratios between 2.2 and 70.0. In the absence of hydrazine, the calibration equation for ammonia is $\%I_f$ = 121 $[NH_3]$ − 0.12, and the detection limit is 20 ng ml^{-1}.

The relative standard deviations (r.s.d.) for analysis of samples containing 3.0 μg ml^{-1} ammonia and 20.0 μg ml^{-1} hydrazine were 1.17% and 0.31% (n = 11), respectively. The sampling rate was 35 h^{-1}. Table 1 shows the results obtained by this method when applied to the resolution of some synthetic ammonia/hydrazine mixtures.

Stopped-flow method. This method was intended to increase the sensitivity of hydrazine determination, by stopping the first sample reagent zone in the detector. Ammonia was determined from the maximum fluorescence of the central peak, and hydrazine by stopping the flow 29 s after injection (travel time for the first peak 28 s). A typical kinetic curve is obtained

TABLE 1

Resolution of some synthetic ammonia/hydrazine mixtures by the normal flow-injection procedure

Taken (μg ml^{-1})		Found (μg ml^{-1})[a]		Error (%)	
Ammonia	Hydrazine	Ammonia	Hydrazine	Ammonia	Hydrazine
3.00	20.0	3.02	20.1	+0.7	+0.5
1.50	15.0	1.46	14.8	−2.7	−1.3
0.75	22.0	0.76	22.3	+1.3	+1.4
4.50	25.0	4.48	24.9	−0.4	−0.4
7.00	30.0	6.97	29.5	−0.4	−1.7
5.50	17.0	5.52	16.6	+0.4	−2.4
2.50	20.0	2.45	19.6	−2.0	−2.0

[a]Mean of three determinations.

(Fig. 3); the most significant parameters are related to the hydrazine concentration in the mixture by the following calibration equations (n = 7 in all instances).

Initial-rate method:

$\%I_f\,(s^{-1}) = 0.092\,[N_2H_4] + 0.076$ ($r = 0.9999$); for $0.8 \leqslant [N_2H_4] \leqslant 5.0\,\mu g\,ml^{-1}$

$\%I_f\,(s^{-1}) = 0.039\,[N_2H_4] + 0.34$ ($r = 0.9967$); for $5.0 \leqslant [N_2H_4] \leqslant 20.0\,\mu g\,ml^{-1}$

Fixed-time method:

$\%I_f = 6.8\,[N_2H_4] - 6.2$ ($r = 0.9992$); for $1.0 \leqslant [N_2H_4] \leqslant 7.0\,\mu g\,ml^{-1}$

$\%I_f = 2.8\,[N_2H_4] + 17.4$ ($r = 0.9999$); for $7.0 \leqslant [N_2H_4] \leqslant 25.0\,\mu g\,ml^{-1}$

Maximum fluorescence method:

$\%I_f = 8.3\,[N_2H_4] - 1.48$ ($r = 0.9978$); for $1.0 \leqslant [N_2H_4] \leqslant 7.0\,\mu g\,ml^{-1}$

$\%I_f = 4.0\,[N_2H_4] + 29.2$ ($r = 0.9986$); for $7.0 \leqslant [N_2H_4] \leqslant 20.0\,\mu g\,ml^{-1}$

The initial rate method involves measuring the initial rate of increase of the fluorescence signal. This method has the lowest limit of determination and good sensitivity; it is also the fastest, because the initial rate is calculated within 20 s after stopping the pump. Fixed-time measurements were made 80 s after stopping the flow. Measurements of maximum fluorescence show a slightly higher sensitivity than that afforded by the fixed-time method, but must be made within 6—9 min after stopping the flow. In each measurement procedure, two linear portions are obtained for calibration, the sensitivity of the first being 2—3 times that of the second.

To obtain the concentration of ammonia in the sample, calibration graphs in the presence of several concentrations of hydrazine were constructed. All had a common intercept and their slopes decreased with increasing hydrazine concentration. Similarly to the method described above, the following equation was obtained:

$\%I_f\,(NH_3) = -4.25\,[NH_3]\,[N_2H_4] + 32.2\,[NH_3] + 7.5$

which is applicable within the ranges $0.15 \leqslant [NH_3] \leqslant 3.0\,\mu g\,ml^{-1}$ and $0.8 \leqslant [N_2H_4] \leqslant 5.0\,\mu g\,ml^{-1}$ (initial-rate method); $1.0 \leqslant [N_2H_4] \leqslant 7.0\,\mu g\,ml^{-1}$ (fixed-time and maximum fluorescence methods) for $[N_2H_4]/[NH_3]$ ($\mu g\,ml^{-1}$) ratios of 0.3—46.

The r.s.d. (n = 11) for 2.0 $\mu g\,ml^{-1}$ ammonia and 1.0 $\mu g\,ml^{-1}$ hydrazine was 1.44% for ammonia, and 1.70% (initial-rate) and 1.15% (maximum intensity) for hydrazine. The sampling frequency for hydrazine by the initial-rate method was 25 h^{-1}. The results for some synthetic mixtures resolved by the stopped-flow method are given in Table 2.

Conclusions

The viability of the suggested configuration for resolving ammonia/hydrazine mixtures by formation of two reacting zones with different pH values has been demonstrated. The methodology is applicable to the resolu-

TABLE 2

Resolution of some synthetic ammonia/hydrazine mixtures by the stopped-flow procedure

Taken ($\mu g\ ml^{-1}$)		Found ($\mu g\ ml^{-1}$)[a]			Error (%)		
Ammonia	Hydrazine	Ammonia	Hydrazine [b]	Hydrazine [c]	Ammonia	Hydrazine [b]	Hydrazine [c]
1.00	1.00	1.03	0.96	0.97	+3.0	−4.0	−3.0
2.50	1.80	2.47	1.82	1.80	−1.2	+1.1	0.0
1.25	3.50	1.23	3.45	3.47	−1.6	−1.4	−0.9
3.00	1.50	2.98	1.53	1.53	−0.7	+2.0	+2.0
3.00	5.00	3.04	4.94	4.97	+1.3	−1.2	−0.6
2.00	1.00	1.96	0.99	0.98	−2.0	−1.0	−2.0

[a]Mean of three determinations. [b]Initial-rate method. [c]Method based on fluorescence intensity at equilibrium.

tion of mixtures in which the analytes react in pH regions where the other species does not contribute to the signal yielded by a given species. In addition, this particular way of establishing two reacting zones with different pH values allows one to modify the reagent concentration or even to add different reagents to the carrier solution injected into the secondary injection valve.

The proposed methods have the advantages over the conventional procedure of greater rapidity, with similar sensitivity, higher precision and the possibility of determining the two components less laboriously. Moreover, the single-channel configuration is straightforward, which gives it various advantages over zone sampling [12], which can be used to develop similar methods. These include greater simplicity of the experimental set-up because no critical control of time is necessary to obtain the zone sample, nor is a specific-zone sampling injection valve required; other benefits are less dilution of the sample plug, resulting in increased sensitivity, and greater reproducibility.

The CAICyT is thanked for financial support (Grant No. 2012-83). A. Ríos gratefully acknowledges financial support from the Junta de Andalucía.

REFERENCES

1 D. Betteridge and B. Fields, Anal. Chem., 50 (1978) 654.
2 D. Betteridge and B. Fields, Anal. Chim. Acta, 132 (1981) 139.
3 A. Ríos, M. D. Luque de Castro and M. Valcárcel, Anal. Chem., 58 (1986) 663.
4 N. D. Danielson and C. M. Conroy, Talanta, 29 (1982) 401.
5 S. S. Simons and D. F. Johnson, J. Am. Chem. Soc., 98 (1976) 7098.
6 S. S. Simons and D. F. Johnson, Anal. Biochem., 90 (1978) 705.
7 J. R. Benson and P. E. Hare, Proc. Natl. Acad. Sci. U.S.A., 72 (1975) 619.
8 E. Méndez and J. G. Gavilance, Anal. Biochem., 72 (1976) 473.
9 E. C. Butcher and O. H. Lowry, Anal. Biochem., 76 (1976) 502.
10 A. Ríos and M. Valcárcel, Talanta, 32 (1985) 851.
11 A. Ríos, M. Silva and M. Valcárcel, Fresenius Z. Anal. Chem., 320 (1985) 762.
12 A. O. Jacintho, E. A. G. Zagatto, B. F. Reis, L. C. R. Pessenda and R. J. Krug, Anal. Chim. Acta, 130 (1981) 361.

Analytica Chimica Acta, 187 (1986) 147—155
Elsevier Science Publishers B.V., Amsterdam — Printed in The Netherlands

SPECTROFLUORIMETRIC DETERMINATION OF BERYLLIUM BASED ON THE INCLUSION COMPLEX OF 1-AMINO-4-HYDROXYANTHRAQUINONE WITH β-CYCLODEXTRIN AS LIGAND

F. GARCIA SANCHEZ* and M. HERNANDEZ LOPEZ

Department of Analytical Chemistry, Faculty of Sciences, The University, 29071-Malaga (Spain)

A. HEREDIA

Department of General Chemistry, Faculty of Sciences, The University, 29071-Malaga (Spain)

(Received 23rd January 1986)

SUMMARY

The use of the inclusion complex of 1-amino-4-hydroxyanthraquinone (AHA) in the internal cavity of β-cyclodextrin is compared with AHA alone as a ligand for the spectrofluorimetric determination of beryllium. The organizing ability of the cyclodextrin medium and the protection of the ligand from the micro-environment confers increased sensitivity, selectivity and detection limit, and allows the determination of 10—70 ng ml^{-1} beryllium, compared to 60—500 ng ml^{-1} in the absence of the cyclodextrin.

Cyclodextrins have been used to enhance the fluorescence intensities of several organic compounds by a process of partial encapsulation or inclusion of the organic guest molecules which isolates them and shields their excited singlet species from quenching reactions; it also prevents non-radiative decay processes. Aqueous cyclodextrin solutions have been applied [1—6] as molecular "organizing" media for both fluorimetric [7] and phosphorimetric [8] analysis and for the determination of several organic analytes. However, the analytical potential of cyclodextrin homologues (α, β, γ) as host molecules and as organizing media to promote fluorescent coordination reactions between organic ligands and metal ions, has not been exploited.

This paper describes the fluorimetric determination of beryllium by means of the ligand 1-amino-4-hydroxyanthraquinone partially encapsulated in the cavity of a cyclodextrin molecule. Anthraquinones have long been used as analytical reagents and particularly as chromogenic and fluorogenic ligands for various metal ions. Their coordination reactions have characteristically moderate selectivity and large absorbance changes. The moderate selectivity is a consequence of the intramolecular hydrogen bond formed between quinone oxygen and the neighbouring phenol or amine hydrogen. The large absorbance change results from the three condensed benzene rings. The inherent aromaticity, planarity and rigidity of the molecule give it great

0003-2670/86/$03.50 © 1986 Elsevier Science Publishers B.V.

fluorimetric potential. However, the decreased spectral shifts associated with the coordination process, and the relatively high blank signal, decrease its analytical performance. Moreover, the slight solubility of these compounds in polar solvents limits their use in water, so that mixed solvents or a previous extraction step are necessary.

1-Amino-4-hydroxyanthraquinone (AHA) has already been used for the determination of beryllium [9]. It is less sensitive but more selective for beryllium than morin. In this paper, the use as ligand of an inclusion complex for determination of beryllium is compared with that of the unbound ligand. Significant improvement in sensitivity and selectivity is achieved with the inclusion complex. This is considered to be of importance because sub-microgram quantities of the highly toxic beryllium are of biological importance [10]. Although complex and expensive analytical techniques are available for trace beryllium determinations [11], less expensive procedures are desirable, especially in clinical analysis.

EXPERIMENTAL

Apparatus and reagents

Fluorescence was monitored with a Perkin-Elmer model MPF-43A grating spectrofluorimeter equipped with an Osram XBO 150-W xenon lamp, excitation and emission monochromators, 1 × 1-cm quartz cells, an R-777 photomultiplier and a Perkin-Elmer 023 recorder. A set of polymer fluorescence samples (Perkin-Elmer) was used for daily adjustment and to compensate for changes in source intensity. Fluorescence data are given without spectral correction.

1-Amino-4-hydroxyanthraquinone (AHA; Aldrich Chemical Co.) was recrystallized twice from ethanol. β-Cyclodextrin (BCD; Sigma Chemical Co.) was recrystallized once from boiling water. Solutions of the reagent (4×10^{-5} M) were prepared by evaporation of ethanol from 5 ml of 2×10^{-3} M AHA solution and dilution with aqueous 1×10^{-2} M cyclodextrin solution to 250 ml. The reagent solution was stable for 5 days. A 0.1 M beryllium stock solution was prepared from beryllium nitrate tetrahydrate in distilled/demineralized water, and standardized gravimetrically. A pH 10.20 buffer solution was prepared by mixing appropriate volumes of 1 M sodium hydrogencarbonate and 1 M sodium hydroxide. All chemicals were of analytical-reagent grade unless otherwise stated.

Procedures

General procedure. Volumes of beryllium solutions sufficient to ensure final concentrations of between 10 and 70 ng ml^{-1} were added to 5 ml of 4×10^{-5} M AHA and 0.5 ml of the buffer solution in a 10-ml volumetric flask. The mixture was diluted to volume with an aqueous 1×10^{-2} M cyclodextrin solution. Fluorescence intensities were measured at 615 nm, with excitation at 585 nm, against a reagent blank.

Determination of beryllium added to biological samples. Fresh bovine liver or kidney was cut into small portions, care being taken to exclude major blood vessels and connective tissue. The samples were dried at 120°C to constant weight. Samples of milled bovine vertebra was dehydrated at 120°C and incinerated at 750°C. Samples of urine (10 ml) were concentrated by boiling to ca. 2 ml. Liver, kidney and bone samples (0.3, 0.3 and 0.2 g, respectively) were digested with a mixture of 2.5 ml of concentrated hydrochloric acid and 5 ml of concentrated nitric acid in a Berghof pressure digestor at 150°C for 20 min. The urine samples were subjected to the same treatment. The volumes were made up to 50 ml with deionized water to give clear acidic solutions. To aliquots of these acidic solutions (1 ml for urine, liver and kidney, and 0.5 ml for bone), 0.1 ml of 10% disodium-EDTA solution was added to complex heavy metals. Drops of 5 M sodium hydroxide were added to give neutral or weakly alkaline solutions, which were subjected to the general procedure.

RESULTS AND DISCUSSION

Inclusion complex

1-Amino-4-hydroxyanthraquinone is essentially insoluble in water, but in 10^{-2} M BCD solution it is sufficiently soluble to prepare 10^{-4} M solutions. This may be a result of the reagent molecule being partially included in the cyclodextrin cavity or being closely associated with the outside of the cyclodextrin structure.

When organic molecules are included within a cyclodextrin cavity or encapsulated by the cyclodextrin molecule, water is expelled. This strong hydrophobic interaction produces stable inclusion complexes. The stability derives from the polar character of the guest molecule and from the functional groups which attach to it. Molecules which are partly included within the host cavity may have enhanced fluorescence and modified spectra. This type of interaction occurs with molecules which have a greater affinity for the hydrophobic interior of the BCD molecule than for the aqueous phase. Inclusion decreases the rotational freedom of the included molecule, because it is bonded to the interior of the BCD cavity in a particular orientation. This physical constraint also decreases the constant rate of non-radiative processes, and so enhances fluorescence. Amino- and hydroxy-anthraquinones in their ground states are known to be weakly hydrogen-bonded in polar solvents like alcohol or water [12]. The characteristic fluorescence of the quinones is quenched by ethanol and water.

The lowest excited states of the anthraquinones have an intramolecular charge-transfer (CT) character [13]. The negative charge is located principally on the carbonyl oxygen in their CT excited states. Consequently, one would expect a dominant hydrogen-bonding interaction between the carbonyl oxygen and the solvent in the excited state. This interaction could markedly influence the fluorescence behaviour. The radiationless

deactivation from S_1 (CT) of quinone in ethanol or water is mainly induced by way of the vibrational modes of the intermolecular hydrogen bonds with the solvent molecules [14]. Recent work [12] showed that there is no significant contribution to radiationless deactivation by the intramolecular hydrogen bonds of the amino or hydroxy groups. However, the intermolecular hydrogen bonds at the carbonyl groups of quinones accelerate the nonradiative deactivation process in those polar solvents with hydrogen-bonding capacity. In this context, the partial inclusion of AHA in the BCD cavity shields the carbonyl groups from the quenching action of the solvent. The spectral shifts and enhanced fluorescence in BCD with respect to aqueous media support this argument.

This hypothesis is further strengthened by the acidity constants for quinone included in BCD. The pK_a values calculated by extrapolation for water [15] and obtained for 1×10^{-2} M BCD solution are very close (10.6 and 10.3, respectively), which is a good indication that inclusion does not involve the functional hydroxyl and amino groups. The hydrophobic environment inside the cavity would depress the proton dissociation of the hydroxyl groups. The higher proton dissociation rate suggests that the hydroxyl groups are located near an aqueous layer and that their interactions with BCD are weaker than with water. This would be an important limiting factor for the potential complexing capacity of the ligand because total inclusion in the BCD cavity would partly restrict the coordination process with the metal ion.

This is not a particular case; it can apply to an included or partly included organic ligand if molecular size and α, β, γ-CD internal cavity sizes are considered. Moreover, it is quite possible that, in several cases, both the size and the particular structural configuration of the ligand favour the formation of 2:1 or 3:1 CD/quinone inclusion complexes, which would confer additional protection to the ligand from the environment [4].

Figure 1 shows the fluorescence spectra of AHA in aqueous solutions at pH 6.2 containing BCD at various concentrations. It can be seen that guest-host complexation produces fluorescence enhancement and an 8-nm spectral blue shift.

The complex formation constant (K) of AHA with BCD was obtained by the Benesi-Hildebrand method [16—18], and is expressed as

$$\Delta F^{-1} = (\alpha\ [\text{guest}]_0\ K\ [\text{BCD}])^{-1} + (\alpha\ [\text{guest}])^{-1}$$

where ΔF is the change in fluorescence intensity on addition of BCD, $[\text{guest}]_0$ is the initial concentration of guest molecules and α is a proportionality constant. This equation can be applied to a 1:1 complex of guest with host. The slope of the linear relationship between ΔF^{-1} and $[\text{BCD}]^{-1}$ gives K. The formation constant $K = ([\text{AHA}] - [\text{BCD}]/[\text{AHA}]\ [\text{BCD}])$ determined in this way is $361 \pm 14\ \text{M}^{-1}$, which implies that a strong inclusion complex is formed.

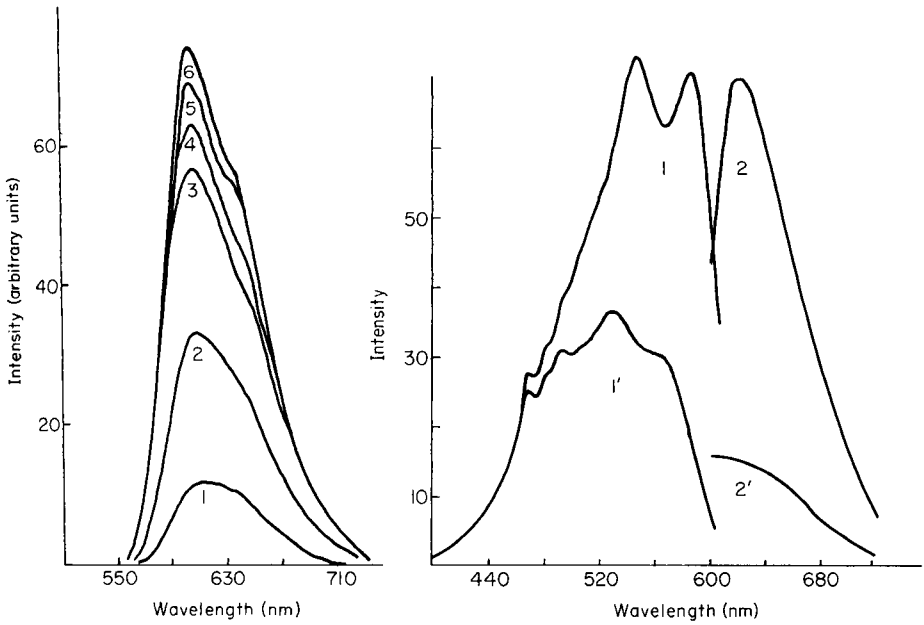

Fig. 1. Fluorescence intensity of aqueous AHA solutions (4×10^{-5} M) at the following BCD concentrations: (1) ○; (2) 1×10^{-3} M; (3) 2.5×10^{-3} M; (4) 5×10^{-3} M; (5) 7.5×10^{-3} M; (6) 1×10^{-2} M. (pH 6.5, excitation at 525 nm.)

Fig. 2. Fluorescence excitation and emission spectra: (1, 2) the AHA-beryllium chelate; (1', 2') the reagent blank. (1×10^{-2} M BCD, apparent pH 10.40, 2×10^{-5} M AHA, 5.5×10^{-6} M Be^{2+}.)

Influence of experimental variables

Figure 2 shows the fluorescence excitation and emission spectra of the AHA/BCD and the complex with beryllium at pH 10.40. Maxima are found at 585 and 615 nm for excitation and emission, respectively. There is an appreciable increase in intensity caused by chelation of beryllium. Figure 3 shows that the fluorescence intensity of the chelate is constant at pH 9.90—10.70. Figure 3 also shows the influence of pH on the fluorescence intensities of the reagent and the AHA/BCD chelate. Curve 2 has a shape typical of that for a compound in which the undissociated form is more intensely fluorescent than the dissociation product, the transition pH (pK_a value) being 10.3. As can be seen, there is little difference in intensity between the chelate and the reagent. The dramatic fall in reagent intensity above pH 11 is not reversible but is a consequence of the breakdown [19] of the cyclodextrin capsule, thus freeing the ligand, which precipitates in the aqueous solution. The irreversibility of the chelate response on increasing the pH in the range 10—12 gives additional support to this hypothesis. The pH can be adjusted to 10.40 by the addition of 0.5 ml of the buffer solution.

No fluorescence decrease was produced by an excess of reagent at least up

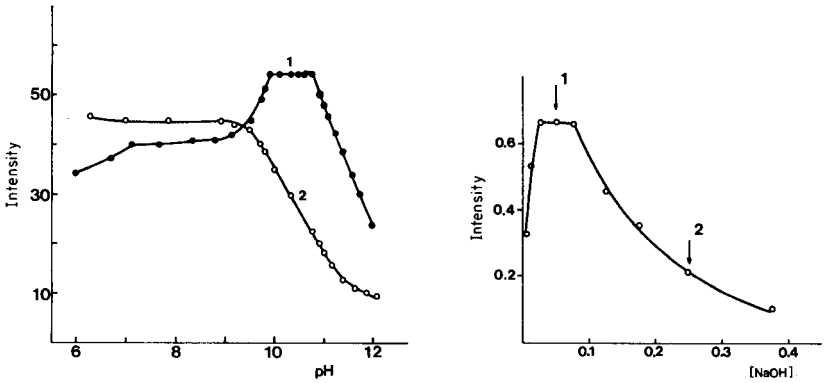

Fig. 3. Effect of pH on the fluorescence intensity: (1) the AHA-beryllium chelate; (2) the reagent. (1×10^{-2} M BCD, 1×10^{-5} M AHA, 3×10^{-6} M Be^{2+}.)

Fig. 4. Effect of sodium hydroxide concentration on the fluorescence intensity of the AHA-beryllium chelate in the absence of BCD. (3.3×10^{-4} M Be^{2+}, 4.1×10^{-4} M AHA.) Arrows: (1) optimized in this work; (2) from [9].

to 5×10^{-5} M. Accordingly, 5 ml of 4×10^{-5} M reagent solution was used in a final volume of 10 ml. No changes in fluorescence were observed when the sequence of addition was changed. The complex formed quickly and the fluorescence remained stable for at least 4 h. There was no temperature effect in the range 10—35°C.

The ratio of beryllium to AHA in the chelate, established by the mole ratio method, was 1:1.

Comparison with the conventional fluorimetric method

1-Amino-4-hydroxyanthraquinone has previously been used alone for the fluorimetric determination of beryllium [9]. However, the variables used then were not optimized for modern instrumentation, thus a detailed study of these variables was made to improve the conventional procedure. The best conditions found for the assay were $\lambda_{(ex)}$ = 580 nm, $\lambda_{(em)}$ = 610 nm, 0.05 M NaOH and 4×10^{-5} M AHA. The order of addition of the reagents was: beryllium, sodium hydroxide, reagent, deionized water. The sodium hydroxide was added before the reagent to keep it in solution. The optimum sodium hydroxide concentration used is rather less than that used previously (0.25 M). Figure 4 compares the fluorescence intensities at different sodium hydroxide concentrations. Again, a mole-ratio plot showed that a 1:1 AHA/beryllium complex is formed.

For the AHA/BCD system, the calibration graph was linear for 0—70 ng Be^{2+} ml^{-1}, whilst without BCD the graph was linear for 0–500 ng ml^{-1}. The sensitivity in the absence of BCD is only 8.5% that when BCD is present, and the intercept is 5 times greater. These and other analytical parameters for both procedures are listed in Table 1.

TABLE 1

Characteristics of the analytical methods[a]

Method	Relative sensitivity[b]	Detect. limit[c]	Determ. limit[d]	Linear range	Be taken	Be found[e]	Error[f] (%)
AHA/BCD	12.0	3	10	10–70	50	50.2 (2.1)	1.5
AHA	1.0	17	60	60–500	400	391.0 (2.8)	2.0

[a]Unless otherwise specified, the values listed refer to ng ml^{-1} beryllium. [b]From slope of calibration graph. [c]3 σ value. [d]10 σ value. [e]Mean of 10 determinations with relative standard deviation (%) in parentheses. [f]Relative error calculated from $100ts/\bar{x}\,n^{1/2}$, where t = Student's t value, s = standard deviation, $\bar{x}$ = mean amount found.

Interference study

The effects of various species on the determination of 20 ng Be^{2+} ml^{-1} by the AHA/BCD method were examined over a wide range of concentrations. The tolerance criterion was within two standard deviations of the analytical signal (10 measurements) from the mean value expected for beryllium alone. Tolerance values for the most troublesome species in the non-BCD method were also measured. The results obtained are shown in Table 2, from which it can be concluded that a significant improvement in selectivity is gained in the BCD method.

The effects of the principal interferences are positive (enhanced fluorescence) for Zr^{4+}, Sr^{2+}, Zn^{2+}, Al^{3+}, Mg^{2+}, Ca^{2+}, Pb^{2+}, Li^{+}, Cd^{2+} and Ga^{3+} and negative for Ni^{2+}, Ag^{+}, Co^{2+}, Cu^{2+}, Th^{4+}, Fe^{3+}, F^{-}, EDTA, CN^{-}, oxalate, tartrate and phosphate. This is expected because positive interference can be

TABLE 2

Tolerance for foreign ions

Species added		Tolerance ratio to Be (w/w)
AHA/BCD method	AHA method	
ClO_4^-, NO_3^-, SO_4^{2-}, Cl^-	—	$\geqslant 5 \times 10^5$
F^-, EDTA, CN^-, oxalate, tartrate, phosphate	—	5×10^4
	Tartrate	3×10^3
Al^{3+}, Cd^{2+}, Ga^{3+}	—	5×10^2
Th^{4+}, Zn^{2+}, Li^{+}, Fe^{3+}, Sr^{2+}	—	2.5×10^2
Mg^{2+}	—	1×10^2
Ca^{2+}, Pb^{2+}, Ag^{+}	—	50
Zr^{4+}	Li^{+}	25
Ni^{2+}	Ca^{2+}, Fe^{3+}, Zr^{4+}	10
Co^{2+}	Th^{4+}, Co^{2+}	5
Cu^{2+}	—	2
—	Cu^{2+}	1
—	Ni^{2+}	0.3

attributed to the fact that these elements form carbonate or hydroxide precipitates which scatter light if moderate concentrations are used. Probably, only the lithium interference can be assigned to the formation of a fluorescent chelate. Negative interferences are caused by species decreasing the concentration of the ligand or beryllium. The greater selectivity can be attributed to the protection conferred to the ligand by BCD.

Application to samples

The BCD procedure was applied to the determination of beryllium added to biological samples. Table 3 summarizes the results, from which it can be concluded that acceptable accuracy and precision can be obtained in the analysis of final solutions containing 15 or 25 ng Be ml^{-1}. Obviously, the natural level of beryllium in these samples is too low to detect. However, it would be suitable for monitoring subjects exposed to abnormal beryllium levels.

Conclusions

A new way of employing organic ligands in the fluorimetric determination of metal ions is described, which overcomes solubility and stability problems of the ligand and which eliminates the need for liquid—liquid extraction. The apparently good fit of the chelate within the BCD cavity provides improved quantum yields because of the increased order and stability in the protected micro-environment which, in turn, permits better detection limits. The method is economical, simple, rapid, reproducible and selective.

We thank the Comisión Asesora de Investigación Cientifica y Tecnica for supporting this study (Project No. 3007/83 C02-02).

TABLE 3

Determination of beryllium added to biological samples

Sample	Be conc. (ng ml^{-1})	
	Added	Found[a]
Liver	15.0	15.4 ± 0.6
	25.0	25.3 ± 0.4
Kidney	15.0	14.9 ± 0.6
	25.0	25.1 ± 0.3
Bone	15.0	15.2 ± 0.6
	25.0	25.1 ± 0.2
Urine	15.0	14.8 ± 0.3
	25.0	25.0 ± 0.3

[a]Mean ± SD of triplicate determinations.

REFERENCES

1 W. Saenger, Angew. Chem. Int. Ed. Engl., 19 (1980) 344.
2 H. Singh and W. L. Hinze, Analyst, 107 (1982) 1073.
3 T. Yorozu, M. Hoshino and M. Imamura, J. Phys. Chem., 86 (1982) 4426.
4 S. Hamai, Bull. Chem. Soc. Jpn., 55 (1982) 2721.
5 T. Yorozu, M. Hoshino, M. Imamura and H. Shizuka, J. Phys. Chem., 86 (1982) 4422.
6 F. Cramer, W. Saenger and H. Spatz, J. Am. Chem. Soc., 89 (1967) 14.
7 O. Jules, S. Scipinski and L. J. Cline Love, Anal. Chim. Acta, 169 (1985) 355.
8 L. J. Cline Love, M. L. Grayesky and J. Novoski, Anal. Chim. Acta, 170 (1985) 3.
9 C. E. White and C. S. Lowe, Anal. Chem., 13 (1941) 809.
10 T. Y. Toribara and R. E. Sherman, Anal. Chem., 25 (1953) 1594.
11 G. H. Morrison, Crit. Rev. Anal. Chem., 8(3) (1979) 287.
12 H. Inono, M. Hida, N. Nakashima and K. Yosihara, J. Phys. Chem., 86 (1982) 3184.
13 S. H. Etaiw, M. M. Sekkina, G. B. El-Hefnawey and S. S. Assar, Can. J. Chem., 60 (1982) 304.
14 M. Hida, Kogyo Kagaku Zasshi, 69 (1966) 874.
15 F. Garcia Sanchez, M. Hernandez, C. Cruces, A. Heredia and J. C. Marquez, unpublished work.
16 H. A. Benesi and J. H. Hildebrand, J. Am. Chem. Soc., 71 (1949) 2703.
17 H. Kondo, H. Nakatani and K. Hiromi, J. Biochem., 79 (1976) 393.
18 K. Kano, I. Takenoshita and T. Ogawa, J. Phys. Chem., 86 (1982) 1833.
19 G. S. Cox, N. J. Turro, N. C. Yang and M. J. Chen, J. Am. Chem. Soc., 106 (1984) 422.

Analytica Chimica Acta, 187 (1986) 157—162
Elsevier Science Publishers B.V., Amsterdam — Printed in The Netherlands

DIRECT DETERMINATION OF CADMIUM IN NATURAL WATERS BY ELECTROTHERMAL ATOMIC ABSORPTION SPECTROMETRY WITHOUT MATRIX MODIFICATION

KEN R. LUM* and MICHAEL CALLAGHAN

Environmental Contaminants Division, National Water Research Institute, P.O. Box 5050, Burlington, Ontario L7R 4A6 (Canada)

(Received 28th April 1986)

SUMMARY

A procedure for the determination of cadmium in fresh, coastal and estuarine waters by polarized Zeeman-effect graphite-furnace atomic absorption spectrometry is validated by using lake waters and seawater. The limit of detection for freshwaters is <2 ng l^{-1} cadmium. Undiluted seawater can be analyzed directly without the addition of matrix modifiers with the aid of a stabilized temperature platform. The instrument is calibrated with diluted NBS SRM 1643a (Trace Elements in Water). Analytical performance was tested extensively with fresh and brackish water samples and procedures were worked out to ensure that a high degree of accuracy is achieved consistently.

Cadmium and its compounds are subject to regulatory activity because of their adverse environmental and health effects. In aquatic systems, water quality objectives have been established on the basis of protection of sensitive biological species. Rapid, precise and accurate methods for the determination of cadmium in coastal (marine) and fresh waters are thus needed. In general, graphite-furnace atomic absorption spectrometry (a.a.s) is the method of choice because of its high sensitivity for cadmium. A detection limit of 13 ng l^{-1} cadmium has recently been reported for seawater [1]. Direct injection of freshwater usually poses no problems except for wastewaters [2], or iron-rich spring waters [3]. However, seawater analysis presents a difficult matrix requiring either chelation and extraction [4] or matrix modification [5] combined with use of a stabilized-temperature platform furnace (L'vov platform) to reduce background absorbance effects [1, 2, 6]. Here, a direct injection method is reported which relies on the background correction capability of the polarized Zeeman effect combined with a L'vov platform; no matrix modifier is needed and quantitation is achieved by using acidified standards.

EXPERIMENTAL

A Hitachi 180-80 Zeeman effect atomic absorption spectrometer was used with pyrolytically-coated graphite cuvettes and platforms (Ringsdorff-Werke,

0003-2670/86/$03.50 © 1986 Elsevier Science Publishers B.V.

Bonn-Bad Godesberg, F.R.G.). A Hamamatsu hollow-cathode cadmium lamp was operated at 7 mA.

For analysis, 20-μl aliquots were injected. The instrumental settings were as follows: wavelength, 228.8 nm; slit width, 1.3 nm; dry, 80—120°C for 30 s. For freshwaters, the optimum ashing temperature was 1100°C for 15 s, followed by atomization at 1800°C for 7 s. The clean-up step required heating the furnace at 2000°C for 3 s. The optimum atomization temperature for seawater was found to be 2100°C followed by clean-up at 2800°C. The peak-area mode was used for all determinations. Argon carrier gas was allowed to flow at 200 ml min^{-1} during the dry/ash cycles and was interrupted at atomization.

Analytical-grade chemicals (J. T. Baker Chemical Co.) were used throughout. Cadmium standards were prepared by serial dilution of a 1000 mg l^{-1} stock solution (Spex Industries). Line-distilled water was passed through a Barnstead mixed-bed ion-exchange cartridge before use.

RESULTS AND DISCUSSION

Optimization of temperature program

When the ashing and atomization programs recommended by previous workers were applied in the analysis of over 40 samples, unsatisfactory reproducibility and lack of sensitivity were encountered at cadmium concentrations less than 10 ng l^{-1}. Because of the differences in instrumentation, it was decided to optimize the ashing/atomization schedules for the Hitachi Zeeman system. The effect of various ashing programs was studied with a 150 ng l^{-1} cadmium standard as outlined in Table 1. The highest absorbance was observed at 400°C, in agreement with previous work [4], but reproducibility improved when the ashing temperature was increased. This observation

TABLE 1

Effects of ashing temperature and atomization temperature on the absorbance of a 150 ng l^{-1} cadmium standard in 0.16 mol l^{-1} nitric acid

Ashing temperature[a]	Absorbance (s.d.)	Atomization temperature[b]	Absorbance (s.d.)
400	0.086(0.016)	1500	0.027(0.003)
600	0.072(0.005)	1600	0.053(0.003)
800	0.061(0.002)	1700	0.061(0.002)
900	0.063(0.002)	1800	0.063(0.002)
1000	0.060(0.002)	1900	0.060(0.002)
1100	0.063(0.002)	2000	0.050(0.005)
1200	0.056(0.002)	2100	0.047(0.002)
1400	0.034(0.004)	2200	0.041(0.000)

[a]Atomization temperature of 1800°C for 7 s; clean-up at 2000°C for 3 s. [b]Ashing temperature of 1100°C for 15 s; clean-up at 2000°C for 3 s.

was confirmed by repeating the experiment twice with new graphite tubes (without platforms), to ensure that the poorer reproducibility at temperatures at which premature volatilization of analyte was avoided, was not an artifact caused by imperfections in a single tube. In 0.16 mol l^{-1} nitric acid, there was a loss of 27% of analyte when ashing was done at 1100°C relative to ashing at 400°C. Further justification for working at such a high ashing temperature became evident during extensive work on the analysis of fresh and brackish waters. At an ashing temperature of 300—400°C, the sensitivity was significantly impaired, presumably by the salt residue which accumulated on injection of samples, and which was clearly visible with brackish waters. However, sensitivity could be restored by ashing at 1100°C.

Similar experiments were done to establish the optimum atomization temperature with the ashing temperature set at 1100°C for 15 s. For dilute acid cadmium standards, the atomization temperature that yielded maximum absorbance was 1800°C (Table 1).

Changes in sensitivity as a function of tube batch and number of firings

Initial experiments indicated that tubes from the same batch gave significantly different analytical response. Accordingly, lake-water samples were analyzed by using five tubes selected from different boxes, with standardization by injection of a 1 $\mu g\ l^{-1}$ cadmium standard every five samples. Figure 1 shows that the initial readings ranged from 0.450 to 0.530 for the five tubes. In general, the sensitivity declined quite steeply after about 25 firings, but after 100 firings the response remained constant to at least 200 firings. Prior to any analytical measurements, each tube had to be conditioned by about 15 firings, in order to obtain reproducible absorbance values.

Limit of detection and accuracy of the determination of cadmium in freshwaters

The above procedure (without L'vov platforms) was applied to water samples from Lakes Erie and Ontario to establish the practical limit of

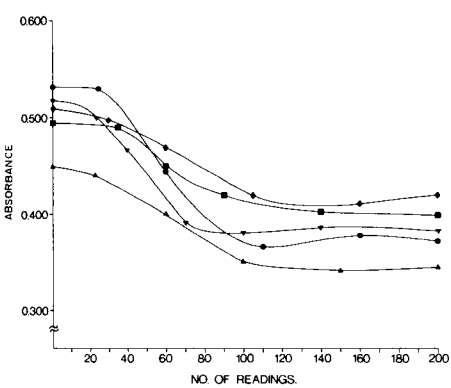

Fig. 1. Change in sensitivity of the determination of cadmium with number of firings. The curves relate to five graphite tubes selected at random from different boxes.

detection and average tube life. The average concentrations found were 10 ng l^{-1} for Lake Ontario and 29 ng l^{-1} for Lake Erie. Twenty-five samples (50 injections) which gave absorbance readings less than or equal to 0.003 were selected at random and their standard deviation was calculated to be 0.001. On average, a 1 μg l^{-1} standard gave an absorbance of 0.400 during the first 100—200 firings. Thus the limit of detection defined as twice the standard deviation of the absorbance of the 50 injections of samples is 5 ng l^{-1}. This limit could be lowered by using a tube during the most sensitive period of its lifetime and by injecting larger volumes. Good reproducibility was obtained with 100-μl injections of lakewater (r.s.d. 2.5%, n = 5) but the increase in absorbance was not proportional to the sample volume injected; for injections of 20, 50 and 100 μl, the absorbances were 0.065, 0.115 and 0.156, respectively. Thus, the practical limit of detection can easily be improved to <2 ng l^{-1}. The use of three times the standard deviation of the blank to derive a detection limit (see, e.g., [4]) was not applicable here; blanks were prepared by filling 125-ml acid-cleaned plastic bottles with deionized/distilled water followed by preservation with nitric acid on board ship as part of the field program, and only one out of twelve field blanks had a detectable concentration of cadmium (100-μl injections). Pruszkowska et al. [1] and Campbell and Ottaway [7] used twice the standard deviation on results for samples in their estimates of the detection limit.

The accuracy of the procedure for freshwaters was evaluated by using the National Bureau of Standards SRM-1643a (Trace Elements in Water) which was diluted to give a concentration of 100 ng l^{-1} and was run periodically during the analysis of freshwaters. The diluted reference material gave results that were within 3% of the calculated value compared to a 100 ng l^{-1} dilution of a 1 μg l^{-1} cadmium standard solution. During these measurements, it was observed that accuracy at concentrations close to the detection limit (<10 ng l^{-1}) could be achieved only in the first 100—120 firings; after that, sensitivity was degraded very significantly and in cases of doubt, samples were analyzed again with a new tube. In the case of samples with concentrations >10 ng l^{-1}, a tube could be used for >300 firings, in agreement with the observations summarized in Fig. 1.

Analysis of seawater

During the validation of the procedure for fresh-water samples, the accuracy of the method was tested several times with the National Research Council of Canada Nearshore Seawater Reference Material, CASS-1. In order to decrease the background absorbance caused by the salt-water matrix to a level correctable by the Zeeman effect (i.e., absorbance <1.5), it was necessary to work at lower ashing and atomization temperatures (600 and 1600°C, respectively). However, the marked decrease in reproducibility caused by the residue that accumulated in the tube, necessitated drastic measures. After injections of seawater, blank firings yielded absorbances that could not be brought to zero even by repeated boost-firings. Soaking tubes overnight in

1.6 mol l^{-1} nitric acid restored zero blank absorbances, but at the sacrifice of sensitivity; the tubes were then unsuitable for use in the analysis of samples containing 20—30 ng l^{-1} cadmium. An analogous procedure has recently been proposed [8] to remove this memory effect of the graphite tube; 100 μl of 1 mol l^{-1} nitric acid was injected and the tube was heated at 327°C for 40 s. It was found here that the determination of cadmium in CASS-1 seawater with a pyrolytically-coated graphite tube was possible, but data were accurate only for a very few (5) firings. However, losses of cadmium in the analysis of seawater because of the volatility of cadmium chloride were not observed. Recent work by Hulanicki et al. [8] indicated that as the amount of cadmium injected into the graphite furnace is decreased from 20 ng to 2 ng, the appearance temperature of cadmium atoms is 807°C and the maximum occurs at 1127°C, which is analogous to the results for cadmium nitrate, though the flow rate of sheathing gas used by Hulanicki et al. [8] was 7.5 times that used here. It has been reported [8], that when cadmium chloride is repeatedly atomized from the same tube, the absorbance peak becomes distorted and the maximum shifts to higher temperatures. In earlier work [1], the decrease in absorbance of cadmium was less in the presence of seawater than in 2% sodium chloride, and at 1000°C the decrease was 73%; the presence of the same amount of ammonium phosphate modifier in both seawater and sodium chloride samples in that study suggests that there are constituents in seawater which decrease the volatility of cadmium as its chloride and essentially perform a useful role as a matrix modifier. During the work reported here, the routine use of low argon flow rates and the injection of small amounts of cadmium (ca. 0.5 ng) did not lead to losses of analyte that outweighed the advantage of using a high ashing temperature, which was found to be essential for minimizing the build-up of salt residue and thus prolonging usable tube life for seawater analyses.

Use of the L'vov platform. The use of atomization from a platform as a means of minimizing interferences (especially vapour-phase interferences) has been shown considerably to improve the analysis of difficult matrices such as seawater [1, 6]. Previous workers have relied on matrix modification [1, 2, 5, 6] and dilution [6, 7] of samples in order to minimize spectral and non-spectral interferences. Neither of these procedures is desirable if one is interested in achieving the lowest detection limits consistent with minimum contribution to the blank from reagents. Thus, direct injection of seawater without dilution or matrix modifier was investigated to see if intractable background interference problems were encountered when a L'vov platform was used.

The optimum temperature program and performance characteristics of the platform were established for the CASS-1 Reference Material. The first five firings were a combination of boost and blank firings to obtain zero absorbance. Firings 6—12 were used to select the optimum atomization temperature between 2050° and 2150°C. Maximum sensitivity was achieved at 2100°C at which the background absorbance lay in the range 1.0—1.3. Injections of

CASS-1 were made in duplicate followed by a blank firing. If a memory effect was observed, 0.32 mol l^{-1} nitric acid was injected which cleaned up the platform but resulted in absorbances close to 0.000 for subsequent injections of CASS-1. The loss of sensitivity was rectified by increasing the atomization temperature to 2150°C. At firing 75, the sensitivity was again affected but this time the baseline absorbance could not be brought back to zero by injection of nitric acid. As outlined above, soaking the platform in 0.32 mol l^{-1} nitric acid overnight cured this problem but the loss of sensitivity was permanent. The average cadmium concentration found in CASS-1 during this experiment was 29 ng l^{-1} (s.d. = 7, n = 20) when the NBS SRM-1643a diluted to 100 ng l^{-1} was used for standardization. The performance of the method during this period is in good agreement with the reference value for CASS-1 (26 ± 5 ng l^{-1}). The relative standard deviation of the present measurements of the cadmium content in CASS-1 (24%) suggests that the above procedure is unsuitable for the analysis of nutrient-depleted open ocean waters but provides similar capability to that reported by Grobenski et al. [6] who analyzed the CASS-1 nearshore seawater for cadmium, with a precision of 22.6% for an unspecified number of replicates.

The procedure followed here is therefore applicable to nearshore and nutrient-rich seawaters and has the advantage of not requiring either dilution or addition of matrix modifier. Blank problems are therefore virtually eliminated and the ability to use the diluted NBS dilute acid (freshwater) standard reference material for calibration of the analysis should be of particular value in estuarine work where salinity varies over a wide range.

We are grateful to Professor J. P. Riley for his helpful comments. Financial support for M. C. was provided by the Canada Works Program.

REFERENCES

1 E. Pruszkowska, G. R. Carnick and W. Slavin, Anal. Chem., 55 (1983) 182.
2 U. Vollkopf, Z. Grobenski and B. Welz, At. Spectrosc., 4 (1983) 165.
3 A. Criaud and C. Fouillac, Anal. Chim. Acta, 167 (1985) 257.
4 P. J. Statham, Anal. Chim. Acta, 169 (1985) 149.
5 R. Guevremont, R. E. Sturgeon and S. S. Berman, Anal. Chim. Acta, 115 (1980) 163.
6 Z. Grobenski, R. Lehmann, B. Radziuk and U. Voellkopf, At. Spectrosc., 5 (1984) 87.
7 W. C. Campbell and J. M. Ottaway, Analyst, 102 (1977) 495.
8 A. Hulanicki, E. Bulska and K. Wrobel, Analyst, 110 (1985) 1141.

Analytica Chimica Acta, 187 (1986) 163—169
Elsevier Science Publishers B.V., Amsterdam — Printed in The Netherlands

DETERMINATION OF TIN IN ATMOSPHERIC PARTICULATE MATTER BY HYDRIDE GENERATION AND ATOMIC ABSORPTION SPECTROMETRY

K. DE DONCKER, R. DUMAREY, R. DAMS and J. HOSTE*

Institute for Nuclear Sciences, Rijksuniversiteit Gent, Proeftuinstraat 86, B-9000 Gent (Belgium)

(Received 22nd April 1986)

SUMMARY

A procedure is described for the determination of tin in atmospheric particulate matter collected on Whatman 41 cellulose filters. The samples are decomposed with sulfuric acid and nitric acid, followed by hydrofluoric acid to dissolve residual silicates. The analytical parameters for the hydride generation and the subsequent atomic absorption spectrometric measurements are optimized. Severe memory effects encountered with an automatic generator system are avoided when a manual apparatus is used. The precision of the entire method is within 10%. The detection limit is 0.20 ng m^{-3} tin if 500 m^3 of air is filtered. The concentrations found in residential and industrial areas varied between 1.8 and 47.5 ng m^{-3}.

Natural processes are not the only sources of tin in the environment. Anthropogenic activities such as combustion, smelting, refining and detinning operations mean that the atmospheric tin concentrations can vary considerably. Values from 0.17 ng m^{-3} for background areas to 300 ng m^{-3} for industrial zones have been reported [1, 2]. Therefore, the analytical methods used must be sensitive and selective over a wide concentration range. Among the techniques of atomic absorption spectrometry, the direct flame method is of low sensitivity and is subject to many interferences [3—5]. The latter is also one of the major disadvantages of electrothermal atomization in a graphite furnace [6]. However, since equipment for hydride generation/atomic absorption spectrometry became commercially available, this technique has been more widely applied for determinations of tin because of its sensitivity and selectivity [7—10]. In recent years, several modifications, mainly instrumental, have been proposed, e.g., direct measurement of the gaseous tin hydride or collection. The choice is not obvious. Chapman and Dale [11] claim that stannane is not stable enough to be handled at ambient temperature so that preconcentration is excluded. Others, however, describe both procedures as being successful [9, 12, 13].

In the present paper, a method is proposed for the determination of tin in atmospheric particulate matter collected on Whatman 41 filter paper, by continuous hydride generation/atomic absorption spectrometry. The analytical parameters as well as practical applications are described.

0003-2670/86/$03.50 © 1986 Elsevier Science Publishers B.V.

EXPERIMENTAL

Apparatus and reagents

A Perkin-Elmer model 3030 atomic absorption spectrometer equipped with a Cathodeon tin hollow-cathode lamp was used for all determinations. The output signal was shown on a video screen and printed on a Perkin-Elmer PR-100 printer.

The stannane was generated by the automatic MHS-1 or the manual MHS-10 attachment, both from Perkin-Elmer. The two devices differ in the way in which atomization is achieved; also, the MHS-1 has a quartz optical cell closed at both ends by quartz windows, whereas the MHS-10 uses an open quartz tube provided with graphite rings at the ends for cooling.

All reagents were of analytical grade or better: sulfuric acid (95—98%; J. T. Baker), nitric acid (70%; J. T. Baker), hydrochloric acid (37%; J. T. Baker) and hydrofluoric acid (50%; Carlo Erba). Solutions required were 2% (w/v) hydrazine sulfate (Merck) and sodium tetrahydroborate (Aldrich) stabilized with 1% (w/v) sodium hydroxide (Carlo Erba).

The tin stock solution (1000 mg l^{-1}) in 3 M hydrochloric acid was prepared from tin tetrachloride. Working standards (1 mg l^{-1} and 100 μg l^{-1}) were obtained by dilution with 2% (v/v) hydrochloric acid.

Memory effects

During the optimization study, memory signals were encountered when the automatic MHS-1 system was used. The height of a blank, measured immediately after the analysis of a standard solution, seemed to depend on the concentration of the latter and decreased systematically during consecutive blank measurements. This effect was also observed for standards. Figure 1 illustrates the peak shapes obtained for solutions containing 100 ng of tin(IV) measured immediately after a blank, a 50-ng tin standard and an 80-ng tin standard. The first recording shows only one peak, whereas the second and third show two separated peaks. Moreover, the height of the first peak depends on the concentration of tin in the solution analyzed in the preceding run.

A systematic study, to elucidate this effect, indicated that it probably arises from reversible sorption in the generator system. Weber [14] mentioned that the tin hydrides are very susceptible to adsorption. Experiments reported by Kuldvere [15], who used polypropylene reaction flasks in connection with the MHS-1, showed that polypropylene adsorbs tin(II) chloride within the time of the determination (2 min). As the manifold of the MHS-1 is made of polypropylene, partial sorption of the stannane seems very likely. Furthermore, the presence of hydrogen gas seems to be necessary to remove tin from the manifold. Increasing the purging time with argon cannot solve this problem. Because the manual MHS-10 apparatus has a simpler manifold and no polypropylene parts, several determinations were done with this system. Figure 2 compares the peak shapes of a blank and a standard, measured

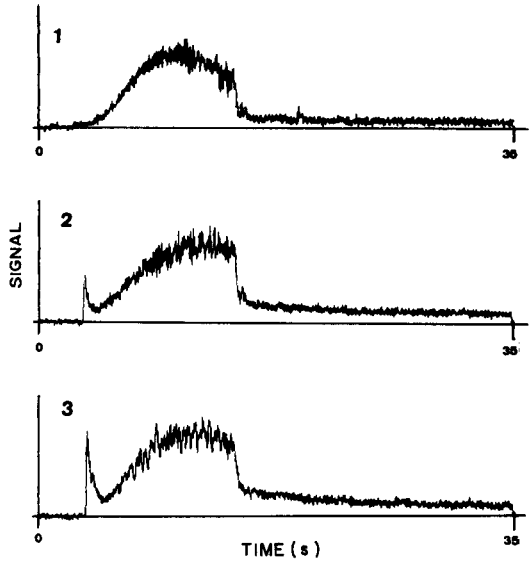

Fig. 1. Peak shape for a 100 ng Sn^{4+} solution measured immediately after a blank (1), a 50 ng Sn^{4+} standard (2) and an 80 ng Sn^{4+} standard (3).

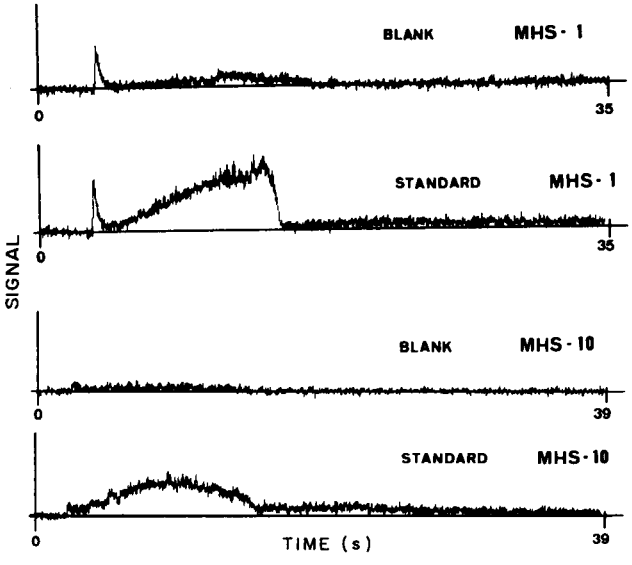

Fig. 2. Peak shapes for a blank and a standard, measured with the MHS-1 (automatic) and MHS-10 (manual) generators, immediately after a 50 ng Sn^{4+} solution.

immediately after solutions containing 50 ng of tin(IV) for both generators. As can be seen, memory effects completely disappear with the MHS-10 and therefore all further determinations were done with the manual system.

Optimization of the hydride generation

Chemical and instrumental parameters influencing the formation of stannane were investigated to optimize the procedure with the MHS-10 attachment. Signals were measured as peak area after an integration time of 35 s.

Effect of the sodium tetrahydroborate concentration. With the MHS-10, the reductant can only be added as a solution. The influence of increasing concentrations of sodium tetrahydroborate, stabilized with 1% (w/v) sodium hydroxide, was investigated. The optimal concentration was found to be 3% (w/v) for a 10-ml sample. The solution remains stable for at least four weeks when stored at 4°C. For higher concentrations, the excess of hydrogen diffuses into the ambient air, sometimes resulting in an explosion of the oxygen/hydrogen mixture.

Effect of different acids. Hydrochloric acid, sulfuric acid and nitric acid were tested for blank values, signal suppression and reproducibility. The influence of varying acid concentrations on the signal from 50 ng of tin(IV) is shown in Fig. 3. The sensitivity depends strongly on the concentration, but the maximum signal is quite similar for the three acids. Because sulfuric acid has a lower blank and hydrochloric acid accelerates the devitrification of the quartz cell [16], a 0.09 M sulfuric acid solution was selected for further work.

Cell temperature. Normally, the cell is placed in an air/acetylene flame but for convenience electrothermal heating was applied. Below 850°C, only partial atomization was achieved, whereas above 950°C the signal was slightly reduced. The latter is probably due to dilution effects caused by expansion of the argon/hydrogen carrier gas mixture [17] at the higher temperatures; this effect is emphasized in a closed atomization cell.

Sample volume. The minimum amount of solution that can be used depends mainly on the shape of the reaction vessel, which is about 5 ml for the MHS-10. Increasing the volume produces a sharp fall in sensitivity. Optimal signals were obtained with 5 ml. However, analyses of real samples showed

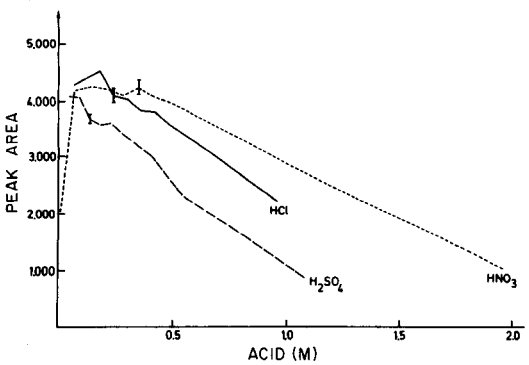

Fig. 3. Effect of acid concentration on the signal from 50 ng of tin(IV). Acid: (···) HNO_3; (—) HCl; (---) H_2SO_4. The bars indicate the mean standard deviation of all measurements with the particular acid.

that 10 ml is more suitable, owing to the severe matrix effect of sulfuric acid. The peak broadening for higher volumes indicates delayed aeration of the stannane from the sample.

Purging time. Prior to the addition of the reductant, the generator and sample are purged with an inert gas (1100 ml min^{-1} argon) to expel air. The purging time has a significant influence on the output signal. The optimal value found (20 s) agrees approximately with the value recommended by the manufacturer. The cause of the suppression when purging is prolonged is not obvious. Melcher and Welz [18] suggested that the signal is correlated with the amount of air in the sample, which in turn depends on the purging time. This confirms the opinion of other authors [19, 20] who noticed that the addition of small amounts of oxygen (1%) to the carrier gas enhanced the sensitivity.

Sample decomposition

The procedure for the acid digestion of particulate matter collected on cellulose filters previously described for antimony determinations [21] was slightly modified in the present work. Owing to the high tin blank of the hydrogen peroxide, this reagent was replaced by nitric acid. Quantitative recoveries were obtained when about 8 ml of sulfuric acid and 4 ml of nitric acid were used. Hydrofluoric acid was added to dissolve any silicates present. After the digestion, the solution was filtered if necessary and diluted appropriately.

Tin was quantified in the final sample solutions by using the optimized parameters given in Table 1.

RESULTS AND DISCUSSION

Analytical characteristics

Standard addition was applied because of the severe matrix effect of sulfuric acid. For this purpose, known amounts (5, 15 and 25 ng) of tin were added to portions of the digested sample solution. The calibration was linear up to an absolute amount of 120 ng of tin(IV) (10 ml of sample).

The precision of the technique was evaluated by a replicate analysis of fractions of the same filter. The relative standard deviations varied between

TABLE 1

Operating parameters for the determination of tin

Liquid volume	10 ml of 0.09 M H_2SO_4/ 2 ml of sample	Hollow-cathode lamp	12 mA
Reductant	3% (w/v) $NaBH_4$	Wavelength	224.6 nm
Argon flow	ca. 550 ml min^{-1}	Spectral bandpass	0.2 nm
Purging time	20 s	Background correction	Off
Atomization temperature	950°C		

1% and 10%. These data include uncertainties arising from the digestion and spectrophotometric procedure as well as those from the inhomogeneity of the filter.

No environmental reference materials certified for tin are available, so that direct evaluation of the accuracy was impossible. Therefore, the method was tested by analyzing filters loaded with particulates and spiked with a known amount of tin before the digestion. The average recovery was 98.0 ± 8.5% (n = 4).

The detection limit was defined as the tin concentration corresponding to three times the standard deviation of the blank. The theoretical value for the system amounts to 3 ng of tin(IV). However, for real samples, the practical detection limit is more meaningful; this amounts to 4 ng. This value includes the blank values of the Whatman filter paper and of the different reagents used for the digestion. A detection limit of 4 ng per 2-ml aliquot of sample injected into the reaction flask corresponds to 100 ng in 50 ml of sample solution and to 0.20 ng m^{-3} when 500 m^3 of air is filtered.

Field sampling results and analysis of an urban particulate standard

The optimized procedure was applied for the determination of tin in atmospheric particulate matter collected in two areas with varying degrees of pollution. Several samples were collected in the proximity of two non-ferrous plants (A), the first producing antimony alloys and oxides, and the second producing solder, copper sulfate, nickel sulfate, etc. The other samples were taken at this institute, situated slightly south of the city of Ghent and at a distance of about 50 m from a highway (B).

The sampling was based on the LIB method [22]. The particulate matter was collected by using a carbon vane rotary pump (Becker VT-25) which has a sampling rate of approximately 20 m^3 h^{-1} when Whatman 41 cellulose filters are used. The air volumes were measured with a Contigea SG integrating gas meter. Sampling was continued for 21 h to about 48 h, depending on the tin concentration expected; these times correspond to air volumes of 450 m^3 and 1000 m^3, respectively.

The results for the two sampling sites are given in Table 2. The highest value of 47.5 ng m^{-3} for the industrial area can be explained by the contribution of the second non-ferrous plant mentioned above, from which tin is a major emission product. However, the value of 26.2 ng m^{-3} cannot be attributed to the same source when the wind direction during the sampling is considered. The existence of other emission sources such as the combustion of coal or domestic waste seems likely but to locate them would require a more extended study based on a large network of sampling sites. In the residential area (B), the average concentration of tin was 4.3 ± 2.4 ng m^{-3}.

Finally, tin was determined in NBS Urban Particulates (SRM 1648). About 40 mg of the material was digested, by the same procedure as described for the atmospheric aerosols. A mean value of 119.9 ± 6.2 μg g^{-1} was obtained for four separate samples. Neither an indicative value on the certificate, nor results from other laboratories are available for comparison.

TABLE 2

Tin concentrations in atmospheric particulate matter

Industrial area (A)		Residential area (B)	
Sampling period	Sn found (ng m^{-3})	Sampling period	Sn found (ng m^{-3})
03/06/80	4.3 ± 0.1	09/06—13/06/83	2.4 ± 0.2
10/06/80	26.2 ± 1.9	04/07—06/07/83	6.6 ± 0.5
08/07/80	47.5 ± 1.3	26/08—29/08/83	2.1 ± 0.2
21/05/80	7.5 ± 0.8	12/09—15/09/83	5.9 ± 0.5
		15/09—19/09/83	1.8 ± 0.1
		01/10—04/10/83	7.0 ± 0.4

This work was supported by the Interuniversitair Instituut voor Kernwetenschappen, to whom we are sincerely grateful.

REFERENCES

1 K. A. Rahn, The Chemical Composition of Atmospheric Aerosols. Technical Report, University of Rhode Island, U.S.A., 1976.
2 M. Piscator, in L. Friberg, G. F. Nordberg and V. B. Vouk (Eds.), Handbook on the Toxicology of Metals, Elsevier/North Holland, Amsterdam, 1979, p. 613.
3 P. N. Vijan and C. Y. Chan, Anal. Chem., 48 (1976) 1788.
4 P. O. Juliano and W. W. Harrison, Anal. Chem., 42 (1970) 84.
5 J. R. Levine, S. G. Moore and S. L. Levine, Anal. Chem., 42 (1970) 412.
6 E. Lundberg, B. Bergmark and W. Frech, Anal. Chim. Acta, 142 (1982) 129.
7 V. F. Hodge, S. L. Seidel and E. D. Goldberg, Anal. Chem., 51 (1979) 251.
8 R. S. Braman and M. A. Tompkins, Anal. Chem., 51 (1979) 12.
9 M. O. Andreae and J. T. Byrd, Anal. Chim. Acta, 156 (1984) 147.
10 P. K. Hon, O. W. Lau, W. C. Cheung and M. C. Wong, Anal. Chim. Acta, 115 (1980) 355.
11 J. F. Chapman and L. S. Dale, Anal. Chim. Acta, 111 (1979) 137.
12 E. L. Fricke, W. D. Robbins and J. A. Caruso, J. Assoc. Off. Anal. Chem., 61 (1978) 1118.
13 K. C. Thompson and D. R. Thomerson, Analyst, 99 (1974) 595.
14 G. Weber, Fresenius Z. Anal. Chem., 321 (1985) 217.
15 A. Kuldvere, Analyst, 107 (1982) 179.
16 M. Verlinden, Anal. Chim. Acta, 140 (1982) 229.
17 D. D. Siemer and P. Koteel, Anal. Chem., 49 (1977) 1096.
18 B. Welz and M. Melcher, Analyst, 108 (1983) 213.
19 P. D. Goulden and P. Brooksbank, Anal. Chem., 46 (1974) 1431.
20 M. O. Andreae, Anal. Chem., 49 (1977) 820.
21 K. De Doncker, R. Dumarey, R. Dams and J. Hoste, Anal. Chim. Acta, 153 (1983) 33.
22 Verein Deutscher Ingenieure, VDI 2463-Blatt 4, VDI Verlag GmbH, Dusseldorf, 1976.

Analytica Chimica Acta, 187 (1986) 171—179
Elsevier Science Publishers B.V., Amsterdam — Printed in The Netherlands

LEAST MEDIAN OF SQUARES: A ROBUST METHOD FOR OUTLIER AND MODEL ERROR DETECTION IN REGRESSION AND CALIBRATION

DESIRE L. MASSART* and LEONARD KAUFMAN

Pharmaceutical Institute, Vrije Universiteit Brussel, Laarbeeklaan 103, 1090 Brussels (Belgium)

PETER J. ROUSSEEUW and ANNICK LEROY

Department of Statistics, Vrije Universiteit Brussel, Pleinlaan 2, 1050 Brussels (Belgium)

(Received 13th January 1986)

SUMMARY

The least median of squares method is a robust regression method, which means that it is not sensitive to outliers or other violations of the assumptions of the usual normal model. This contrasts with the conventional regression method, which minimizes the sum of squares. It is demonstrated that the proposed method can be used to detect or correct for outliers or model errors in calibration applications and in comparing two procedures.

Linear regression is used very often by analytical and clinical chemists to obtain calibration lines, to compare two analytical procedures or to relate analytical results to some outside variable. This technique, together with the *t*-test for comparing means of series of observations, is certainly the most used statistical method for analytical purposes. It is usually done by the least-squares technique, and has become so conventional that other possibilities are rarely considered. Weighting factors may sometimes be introduced but basically the criterion (i.e., to minimize the sum of squares of the residuals) remains the same. There are, however, also robust methods; Phillips and Eyring [1] have shown that these methods can be applied in chemical analysis and that these methods possess several advantages over the more conventional least-squares technique. There are, however, many different robust techniques and they have different degrees of robustness. The aim of this paper is to propose the use of a recent technique with a very high degree of robustness and to study the possibilities of its application.

THEORY

The least-squares technique (LS) consists of minimizing the sum of squares of the residuals. For linear univariate regression, these are given by $r_i = y_i - ax_i - b$, where r_i is the residual of measurement y, and a and b are regression coefficients.

0003-2670/86/$03.50 © 1986 Elsevier Science Publishers B.V.

A problem with regression techniques is the effect of outliers. Outliers may occur for three main reasons, namely, recording errors (or copying errors, misplaced decimal points, etc.), inclusion of a case with special characteristics (i.e., not a part of the population being investigated), and modelling errors caused by choosing the wrong model [e.g., use of a linear first-order (straight line) regression instead of a second-order model]. In this case, the errors usually appear at one end of the x-scale, where they are most influential.

A very extreme situation is given in Fig. 1. When the least-squares method is applied to the data shown, point A pulls the least-squares line downwards.

Breakdown point

Hampel [2] defined the breakdown point as the smallest percentage of contaminated data (outliers) that can cause the estimator to take on arbitrarily large aberrant values. The breakdown point of the LS estimator is 0%. This means that even a single outlying point can result in an entirely wrong regression line. Several suggestions have been made to remedy this situation. This has led to "robust" regression methods. A method with the theoretically highest breakdown point possible, namely 50%, has been proposed by Rousseeuw [3], who replaced the least sum of squares by the least median of squares (LMS). The LMS estimator is given by

$$\text{minimize } \text{med}_i(y_i - ax_i - b)^2$$

instead of

$$\text{minimize } \text{sum}_i(y_i - ax_i - b)^2.$$

The LMS estimator provides protection from outlying x data as well as against outlying y data, making it very appropriate for situations with errors in both variables.

Phillips and Eyring [1] applied a robust method based on the iteratively

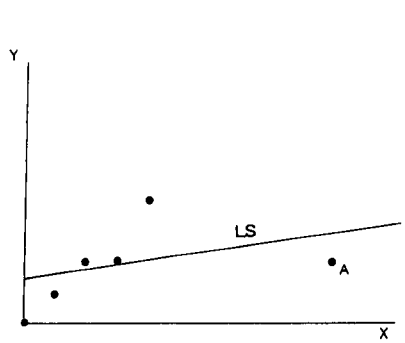

Fig. 1. Effect of outlier on a least-squares line.

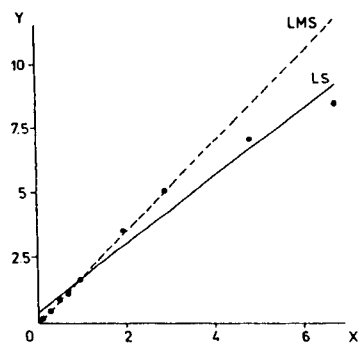

Fig. 2. Detection of deviation from the linear model on a calibration line (data from [10]).

reweighted least-squares (IRLS) procedure described by Beaton and Tukey [4]. Good results were obtained on some chemical data sets. It is not clear where the breakdown of this particular IRLS method occurs. In general, IRLS methods have breakdown points between 0% and $1/(p + 1) \times 100\%$, where p is the number of coefficients in the regression equation. This implies that they soon deteriorate in multivariate situations, unlike the LMS method.

Algorithm

The algorithm has been published [3]. Briefly, the slope of the line for which the median of the residuals takes on the minimal value is evaluated by scanning over all angles and with a certain mesh size. After the line that gives the best results has been selected, this procedure is repeated with smaller angle increments around that optimum.

In order to describe an algorithm for the LMS line, the special case of n observations $z_1, z_2, \ldots, z_n$ of the same quantity is first considered. In this case, the LMS estimate is the number b given by

$$\text{minimize } \text{med}_i(z_i - b)^2.$$

The optimal b can be found explicitly. The observations are first ordered as $z_{(1)} \leqslant z_{(2)} \leqslant \ldots \leqslant z_{(n)}$. Then the smallest of the differences is sought from $z_{(h)} - z_{(1)}, z_{(h+1)} - z_{(2)}, \ldots, z_{(n)} - z_{(n-h+1)}$, where h is the largest integer $\leqslant (n/2) + 1$. If $z_{(k)} - z_{(j)}$ is the smallest difference, then $b = (1/2)z_{(j)} + (1/2)z_{(k)}$. For simple linear regression, the LMS coefficients, a and b, are given by

$$\text{minimize } \text{med}_i((y_i - ax_i) - b)^2.$$

For each value of a, the above algorithm can be applied to the $z_i = y_i - ax_i$ to evaluate the corresponding b. Therefore, it is necessary only to minimize the continuous function

$$f(a) = \min_b \text{med}_i[(y_i - ax_i) - b]^2$$

of the single variable a, which is achieved by scanning over a.

This yields the line for which the median of the squared residuals is minimal. Full details are given by Rousseeuw [3].

In the case of multiple regression, the LMS coefficients are given by

$$\text{minimize } \text{med}_i(y_i - \theta_1 x_{i1} - \ldots - \theta_{p-1} x_{ip-1} - \theta_p)^2.$$

Again the constant θ_p is computed explicitly as soon as $\theta_1, \ldots, \theta_{p-1}$ are known. To evaluate the latter, it is necessary to work with trial estimates as described in ref. 5.

EXPERIMENTAL

All literature data were taken from papers in Clinica Chimica Acta; this journal was not selected for any fundamental reason except that it is essentially analytical in nature. The data were obtained by measuring the coordi-

nates of the measurement points in centimetres. This may lead to slight discrepancies with the original figures. The units of the figures in the present paper are centimetres measured on the original plots. In the figures shown, it is sometimes concluded that the LS estimation leads to disputable regression lines. It is not implied that this invalidates other conclusions reached by the authors in the papers cited. The inductively-coupled plasma data were provided by Kornblum [6].

The LMS and LS computations were performed by a FORTRAN program [7], the portability of which was checked by submitting it to PFORT [8]. It should run on any FORTRAN-IV or FORTRAN-77 compiler. An Apple-2 version in APPLESOFT BASIC and an IBM/PC version in FORTRAN were also prepared. The times needed to run the program are given in Table 1. These times may appear rather long for the Apple version, but use of a BASIC compiler should increase considerably the speed of the program if this is considered important. The least-squares second-order polynomials and F-tests were computed with BMDP [9].

RESULTS AND DISCUSSION

Phillips and Eyring [1] demonstrated the effect of using IRLS on a calibration run for which the data are given in Table 2. Here LMS was applied to the same data and the results obtained by LS, IRLS and LMS are compared in Table 2. It can be seen that the same effect but slightly different results are obtained with LMS and IRLS. In both cases, the outlier is eliminated.

Figures 2—10 (with the exception of Fig. 8) give the results obtained with LS and LMS on some data sets from the literature. Figure 2 is a typical example of a calibration line where measurements are made outside the linear range. Solis and Codoceo [10] realized this and used only the seven lowest points; it is clear that if they had not, use of LMS would automatically have discounted the two highest points. As will be shown, however, there are less easily detectable situations of the same kind. Moreover, regression is very often done without plotting and then this situation would have passed undetected. It should be stressed here that LMS is used in these examples as an exploratory tool (i.e., to discover what information the data contain) rather than as a confirmatory technique (to prove or disprove a preconceived hypothesis).

TABLE 1

Time needed to run LMS on microcomputers

No. of points	5	10	15	20	25	27	30
Basic interpreter/ Apple II[a]	5	9.5	17	24	32	44	60
Fortran IBM-PC[b]	14	16	20	30	48	51	55

[a]Time in minutes. [b]Time in seconds.

TABLE 2

Comparison of LS, IRLS and LMS with hypothetical data

Concentration	Signal	Residual[a]		
		LS	IRLS[b]	LMS
1	1.1	0.32	—0.01	0.00
2	2.0	—0.04	—0.03	0.00
3	3.1	—0.20	0.15	0.20
4	3.8	—0.76	—0.07	0.00
5	6.5	0.68	1.71	1.80
a[c]	—	1.26	0.92	0.90
b[c]	—	—0.48	0.19	0.20

[a]Residual = observed signal — predicted signal. [b]The data and the residuals for IRLS were taken from Phillips and Eyring [1]. [c]Coefficients of signal = a (concentration) + b.

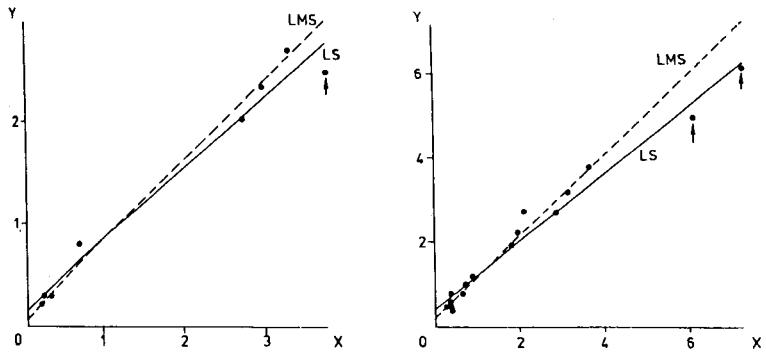

Fig. 3. Influence of outlier (arrowed) on the regression line in the comparison of two methods by LS, and detection of the outlier by LMS (data from [11]).

Fig. 4. Non-linear relationship between the results of two methods as detected by LMS (data from [12]).

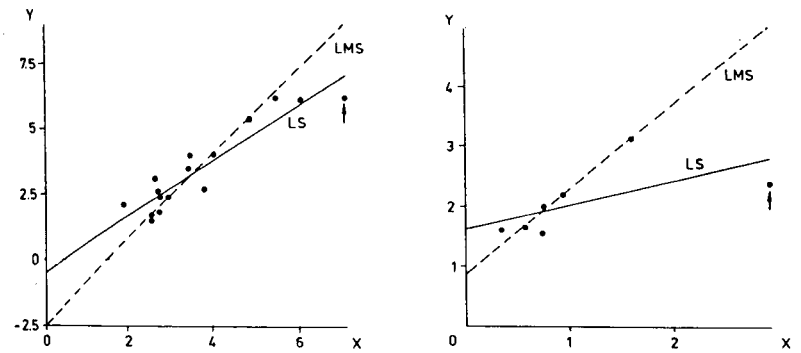

Fig. 5. Influence of outlier (arrowed) on the regression line in the comparison of two methods by LS, and detection of the outlier by LMS (data from [13]).

Fig. 6. Influence of outlier (arrowed) on the regression line in the comparison of two methods by LS, and detection of the outlier by LMS (data from [14]).

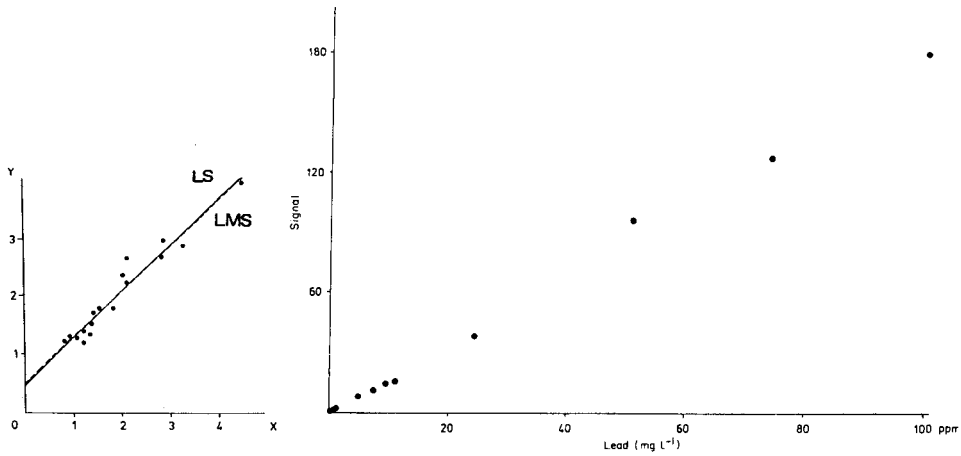

Fig. 7. When no outliers or model errors occur, LMS and LS coincide (data from [15]).

Fig. 8. Scatterplot of the data in Table 3. This plot does not reveal the model error at low concentration by visual inspection; the discrepancy between LMS and LS does show the error.

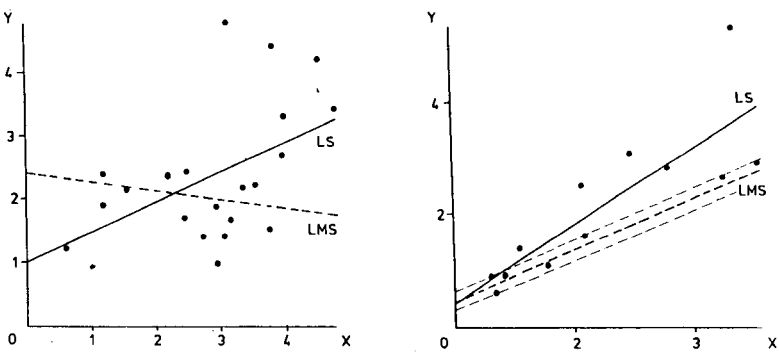

Fig. 9. The discrepancy between LMS and LS on these very diffuse data shows the regression to be meaningless (data from [16]).

Fig. 10. LMS indicates the existence of a linear cluster in the data (data from [17]) because seven points lie within a narrower range around the LMS line.

The following figures give examples where the discrepancy at the end of the scale is less easily detectable, at least if the LMS lines are removed from the figure. In each case, the original authors did not perceive the problem. Figure 3 describes the relationship between an enzymatic end-point method and a rapid kinetic method for lactate determination [11]. The LS line is affected by the measurement indicated by an arrow. To the LMS algorithm, this point is an outlier. Figure 4 [12] is also very typical; it describes two methods for determining breath H levels. The two arrowed measurement points at the end of the scale influence the slope of the LS line to a high

degree whereas the LMS rejects them as outliers. It seems probable that the relationship between the two methods is not linear over the complete measurement range. A still more pronounced effect is found in Fig. 5 [13]. This describes the relationship between the measurements obtained in the comparison of two methods for the determination of phospholipids. The LS line is forced downwards by the arrowed point. The LMS line detects about ten points which fall nearly on the line and takes only those points into account. An extreme (but not unique) example is shown in Fig. 6 [14], which describes the relationship between phosphatase activity and the reticulocyte count in sickle cell disease. The arrowed measurement point has an enormous influence on the LS line, whereas the LMS line shows clearly that the LS regression line as given in the original article is not justified.

These examples indicate one possible use of LMS. When both the LMS and LS methods are applied to the same data and when the two lines do not coincide, then the LS line is likely to be affected by outliers at the end of the scale, i.e., model errors are probable. This can then be assessed visually by inspection of the plot. Indeed, several runs on data in which there was no model error showed that LMS and LS gave very similar results. This was true even when the spread around the regression line was not negligible, as in the case of Fig. 7 [15].

A further example concerns the calibration of lead measurements by plasma emission spectrometry (Fig. 8). The data are given in Table 3. The LMS method detects a model error caused by curvature of the calibration line at the low end of the scale. Because most points were measured at this end and the value of residuals around the line is smaller at low concentrations, the lower points determine the direction of the LMS line. In contrast, the LS line minimizes the higher residuals in the higher concentration range. Neither LMS nor LS permits correct calibration over the whole range. Comparison of the results, however, immediately pinpoints the problem which would not have been possible by visual inspection.

Of course, the use of differences between LMS and LS to detect model errors does not have the character of a statistical test, but there are not many good alternatives. To detect model errors with classical parametric tech-

TABLE 3

Calibration line obtained for lead ions by inductively-coupled plasma emission spectrometry [6]

Conc. ($mg\ l^{-1}$)	Intensity	Conc. ($mg\ l^{-1}$)	Intensity	Conc. ($mg\ l^{-1}$)	Intensity
0.248	0.4738	4.921	7.7360	24.207	38.6705
0.492	0.6997	7.419	11.0610	50.820	96.9765
0.732	1.0432	9.992	15.2173	74.230	127.6312
0.983	1.1836	11.276	15.7363	99.992	180.3638
1.238	1.7150				

niques, three methods can be applied: (1) tests for lack of fit by analysis of variance, but these require replication of the measurements which is always uneconomic and often impossible; (2) analysis of the residuals, but this requires sufficient measurement points to be statistically meaningful and residuals from a least-squares fit may be unduly affected by deviating points, thereby obscuring them; and (3) comparison with higher-order models. In this third method, the fit obtained by LS with the first-order polynomial $y = b + ax$ is compared with the fit obtained by LS with the second-order polynomial $y = b + a_1x + a_2x^2$. An F-test is applied to decide whether or not the fit obtained with the second-order equation is significantly better. If it is better, then it can be concluded that the linear first-order model is not correct, i.e., the model error is detected. In the present study, this was found to be the case for the example shown in Fig. 2 and also for Figs. 4 and 6, but not for Figs. 3, 5 and 8. In the latter cases, therefore, only the LMS method detects that there may be an undue influence from measurement points at the end of the scale.

The detection of model errors seems the most important application of LMS, but LMS can also be used for other purposes. Application of linear regression to very diffuse data sets leads to meaningless regression lines. Application of both LS and LMS is a good way to show this. Again, when the LS line and the LMS line lead to divergent conclusions, the validity of the LS line should be questioned. Figure 9 is an example of this. The data come from Duvivier et al. [16], who described the relationship of estrogen receptor content in cytosol of breast tumor and arterial 17-α-hydroxyprogesterone levels. The authors concluded that there was a relationship, but the opposite (decreasing) direction of the LMS line does induce doubt about the validity of the relationship. Because LMS is not a statistical test, it does not really allow the proposed relationship to be invalidated but it does indicate the necessity of obtaining more measurements.

Finally, LMS can find some features of the data besides outliers. In Fig. 10 [17], the LMS uses only seven of the twelve points and operates very close to the breakdown point. This happens because these seven points form a linear cluster. Whether this makes sense for this particular set of data (which is concerned with the comparison of two methods for the determination of enteropeptidase activity) is impossible to verify but it suggests a possible use of LMS in clustering. Most clustering methods detect only round or ellipsoid clusters. In chemistry, as was pointed out by Wold [18], clusters are very often linear and there is no good clustering method for detecting this kind of cluster. In fact, Buydens [19], using a more complete version of LMS permitting multiple regression [5] to investigate QSAR relationships between gas chromatographic retention and some physicochemical parameters, was able to isolate different linear clusters in this way.

In conclusion, LMS seems to have some desirable properties warranting further investigation of its practical usefulness. It should be stressed that LMS does not reject 50% of the data. Rather, it finds a regression corre-

sponding to the majority of the points, which can then be used to identify the actual outliers (which may be only one or two). This diagnosis of outliers is one of the most difficult aspects of regression, especially in the multivariate situation where the data can no longer be plotted and outliers often go unnoticed. After elimination of the outliers detected by LMS, conventional or weighted least-squares can be computed (as is done by Leroy and Rousseeuw [5]). Finally, it may be noted that the LMS is not only useful for dealing with outliers, but also performs well when the y_i data are not normally distributed around their theoretical value (as in the usual linear model).

REFERENCES

1 G. R. Phillips and E. M. Eyring, Anal. Chem., 55 (1983) 1134.
2 F. R. Hampel, Ann. Math. Stat., 42 (1971) 1887.
3 P. J. Rousseeuw, J. Am. Stat. Assoc., 79 (1984) 871.
4 A. E. Beaton and J. W. Tukey, Technometrics, 24 (1974) 95.
5 P. J. Rousseeuw and A. Leroy, Robust Regression and Outlier Detection, Wiley-Interscience, New York, 1986, in press.
6 G. Kornblum, personal communication.
7 A. Leroy and P. J. Rousseeuw, Revue Belge de Statistique, d'Informatique et de Recherche Operationelle, 24 (2) (1984) 28.
8 B. G. Ryder, The PFORT Verifier, Software Practice and Experience, 4 (4) (1974) 359.
9 W. J. Dixon and M. B. Brown (Eds.), BMDP-79 Biomedical Computer Programs P-series, University of California Press, Los Angeles, CA, 1979.
10 C. Solis and R. Codoceo, Clin. Chim. Acta, 122 (1982) 433.
11 C. Cuthbert and K. G. M. M. Alberti, Clin. Chim. Acta, 90 (1978) 183.
12 T. A. Robb and G. P. Davidson, Clin. Chim. Acta, 111 (1981) 281.
13 M. Sugiwara, T. Oikawa and K. Hirano, Clin. Chim. Acta, 89 (1978) 447.
14 J. Delaunay, S. Fischer, J. P. Piau, M. Tortolero and G. Schapira, Clin. Chim. Acta, 93 (1979) 15.
15 M. Knob and I. Seidl, Clin. Chim. Acta, 106 (1980) 287.
16 J. Duvivier, C. Colin, J. Hustin, A. Albert, J. Lavigne, G. Dive and F. Montfort, Clin. Chim. Acta, 112 (1981) 21.
17 I. Antonowicz, F. J. Hesford, J. R. Green, P. Grogg and B. Hadorn, Clin. Chim. Acta, 101 (1980) 69.
18 S. Wold, J. Chromatogr. Sci., 13 (1975) 525.
19 L. Buydens, personal communication.

Analytica Chimica Acta, 187 (1986) 181—194
Elsevier Science Publishers B.V., Amsterdam — Printed in The Netherlands

IDENTIFICATION OF HYDROLYSIS PRODUCTS OF ALUMINIUM IN NATURAL WATERS

Part 1. *n*-Dimensional Calibration of Al/F Kinetic Pathways

JORGE ARES

Institut für Bodenkunde und Waldernährung, Universitat Göttingen, Büsgenweg 2, 3400 Göttingen (Federal Republic of Germany)

(Received 18th January 1985)

SUMMARY

The kinetics of complexation of aluminium(III) with fluoride in dilute solutions is studied by means of a fluoride-selective electrode. A statistical treatment is presented to model some measurable characteristics of the reaction path in terms of the underlying mass-balance constraints involved in the complexation reaction. Two basic types of kinetic pathways were identified and related to the distribution of hydrolyzed aluminium species in the solution, and to the prevalence of various coordination mechanisms. The results indicate that fluoride reacts simultaneously with different hydrolyzed aluminium species at different rates at the experimental concentrations used. A combination of stepwise regression techniques and least-squares correlation is used to derive a matrix of relative reaction-rate coefficients characterizing fitting surfaces of the complexation paths. These can be used to describe the distribution of reactive aluminium species in unknown solutions.

The kinetics of formation of complexes of aluminium with fluoride was studied in detail by Srinivasan and Rechnitz [1] by means of the fluoride-selective electrode in the range 7.9×10^{-6}—1.0×10^{-4} M fluoride with 0.0304—0.1316 M hydrogen ion and 5.0×10^{-2}—6.3×10^{-2} M aluminium(III) in aqueous solutions. At such concentrations, aluminium is expected to be present almost exclusively as $Al(H_2O)_6^{3+}$ [2], and formation of the AlF^{2+} complex can be expected to predominate over complexes with higher coordination number. Also, the electrode response in this range is Nernstian and computations of fluoride activity are greatly simplified.

In many applications concerning natural waters and soil solutions, aluminium is present in a range considerably lower than that mentioned above, typically 1.0—8.0×10^{-4} M. Also, in these systems, the hydrogen ion concentration is 1.0×10^{-5}—1.7×10^{-3} M. The extension of the studies of Al/F complexation kinetics to these conditions requires additional evaluation of the possible reaction of fluoride with hydrolysed forms of aluminium [1]. Also, Al/F complexes with lower coordination in this range of aluminium are formed at fluoride activities of 1.0×10^{-4}—3.0×10^{-7} M, the latter being at the lowest limit of operation of the fluoride-selective electrode [3], where

the electrode response is not Nernstian and so requires special calibration techniques. However, at these levels, the reaction times for complexation are in the range 2—30 min, which is instrumentally convenient and allows a detailed examination of the complexation path.

MASS-BALANCE CONDITIONS OF COMPLEXATION KINETICS

The aqueous system containing aluminium ions, hydrolysis products and other ligands (L) is described by the vector: $[L^-, Al(H_2O)_6^{3+}, Al(OH)_n^{(3-n)+}, Al_m(OH)_n^{(3m-n)+}]$, where the terms correspond to the activities of ligand, Al aqua-ion, and general monomeric and polymeric hydrolysis products, respectively. The ligand L is assumed to be able to form complexes with various coordination numbers by interaction with all forms of aluminium through different mechanisms, to produce $Al_m F_n^{(3m-n)+}$ forms, with reaction velocity V_R (mol s^{-1}). The following generalized reactions are expected to govern V_R:

$$n'L + Al(H_2O)_6^{3+} \rightleftharpoons Al(H_2O)_6\ L_n^{(3-n')+} \quad (1)$$

$$n'L + Al(OH)_n^{(3-n)+} \rightleftharpoons Al(OH)_{n-n'}L_n^{(3-n)+} + n'OH^- \quad (2)$$

$$n'L^- + Al_m(OH)_n^{(3m-n)+} \rightleftharpoons Al_m(OH)_{n-n'}L_n^{(3-n)+} + n'\,OH^- \quad (3)$$

Also, because of competition with reactions 1—3, the following hydrolysis and polymerization reactions are involved:

$$Al(H_2O)_6^{3+} + nH_2O \rightleftharpoons Al(H_2O)_6\ (OH)_n^{(3-n)+} + nH^+ \quad (4)$$

$$Al(OH)_n^{(3-n)+} \rightleftharpoons Al(OH)_{n-1}^{(3-n+1)+} + OH^- \quad (5)$$

$$mAl(H_2O)_6^{3+} + nH_2O \rightleftharpoons Al_m(OH)_n^{(3m-n)+} + 6H_2O \quad (6)$$

Reaction (1) may or may not require the release of water from the inner coordination sphere; also, it could occur through replacement of a hydroxide after deprotonation of the aqua-ion. Reactions 5 are generally rapid and reversible, while reactions 6 are usually slow [4]. Also, the aqua-ion species form mononuclear hydrolysis products by deprotonation of successive water molecules from the coordination sphere, in a relatively fast reaction. In contrast, polynuclear forms react more slowly to reach equilibria. The picture of possible reaction mechanisms is further complicated by considering that the coordination mechanisms of the main complexation reactions (1—3) can change during the course of the reaction because of the depletion of faster-reacting forms, and modifications in the mole ratio L^-/Al.

The reaction rate of Al/F complex formation can be described in terms of

$$V_R = a_1\ L^-\ Al(H_2O)_6^{3+} + a_2\ L^-\ Al(OH)_n^{(3-n)+} + \ldots + a_n\ L^-\ Al_m(OH)_n^{(3m-n)+} \quad (7)$$

where the number of a_i cannot be defined exactly because of the generalized notation used here for Al forms. A set of a_i' estimators can be obtained by least-squares regression of the kinetic paths, such that

$$V_R = a'_1\, L^- Al(H_2O)_6^{3+} + a'_2\, L^- Al(OH)_n^{(3-n)+} + \ldots + a'_n\, L^- Al_m(OH)_n^{(3m-n)+} + e \quad (8)$$

where e is a vector of normal distributed errors, with $\bar{e} = 0$. However, because of the simultaneous occurrence of reactions 4–6 and possible competition between forms with slow and fast reactions, the a'_i values cannot be expected to estimate actual reaction-rate coefficients, as described earlier [1]. Particularly, $a'_i \geqslant 0$ does not necessarily hold.

Irrespective of the actual reaction mechanism involved, equations of mass balance can be formulated which must hold during the complexation process. The reacting system can be expressed in terms of a system of first-order differential equations (the notation used in the following equations is $\dot{y} = dy/dt$):

$$\dot{L}^- = f_1 L^- - f_2 AlL_n^{(3-n)+} \quad (9)$$

$$Al\dot{(H_2O)}_6^{3+} = f_4 AlL_n^{(3-n)+} + f_{13} Al_m(OH)_n^{(3m-n)+} + f_{10} Al(OH)_n^{(3-n)+} - f_{14} Al(H_2O)_6^{3+} - f_9 Al(H_2O)_6^{3+} - f_3 Al(H_2O)_6^{3+} \quad (10)$$

$$Al\dot{(OH)}_n^{(3-n)+} = f_9 Al(H_2O)_6^{3+} + f_{11} Al_m(OH)_n^{(3-n)+} + f_8 AlL_n^{(3-n)+} - f_{12} Al(OH)_n^{(3-n)+} - f_{10} Al(OH)_n^{(3-n)+} - f_7 Al(OH)_n^{(3-n)+} \quad (11)$$

$$\dot{Al}_m(OH)_n^{(3m-n)+} = f_{14} Al(H_2O)_6^{3+} + f_{11} Al(OH)_n^{(3-n)+} + f_6 AlL_n^{(3-n)+} - f_5 Al_m(OH)_n^{(3m-n)+} - f_{13} Al_m(OH)_n^{(3m-n)+} - f_{11} Al_m(OH)_n^{(3m-n)+} \quad (12)$$

$$\dot{AlL}_n^{(3-n)+} = f_3 Al(H_2O)_6^{3+} + f_5 Al_m(OH)_n^{(3m-n)+} + f_7 Al(OH)_n^{(3-n)+} - f_4 AlL_n^{(3-n)+} - f_6 AlL_n^{(3-n)+} - f_8 AlL_n^{(3-n)+} \quad (13)$$

With the boundary condition,

$$\dot{L}^- = -\sum_n \dot{AlL}_n^{(3-n)+} \quad (14)$$

where the f_i indicate mass flow-rate coefficients and are affected by stoichiometric ratios.

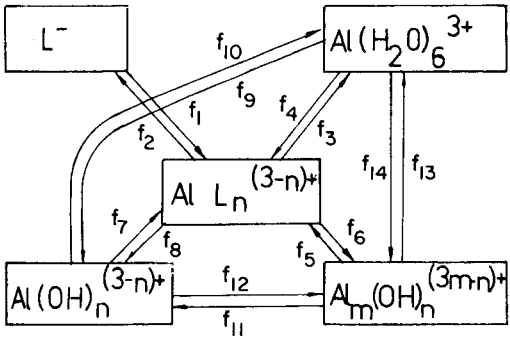

Fig. 1. Diagram of donor-controlled mass-balance model related to the set of Eqns. 10–14 describing the possible reaction paths in the formation of the $AlL_n^{(3-n)+}$ complex.

Figure 1 shows a schematic donor-controlled model related to the system of Eqns. 10—14; the state variables (blocks) are expressed in activity units, and the f_i in activity/time units representing the mass flow rates of the complexation, hydrolysis and polymerization reactions. This formulation of the complexation system sheds some insight into the competitive nature of the interaction between the hydrolysis, polymerization and complexing reactions. Equation 13, which is a mass balance expression for the reaction velocity V_R, can be rearranged to

$$\dot{AlL}_n^{(3-n)+} = f_3(L^-)^{-1} - f_4 r_c [Al(H_2O)_6^{3+}]^{-1}\ Al(H_2O)_6^{3+}L^- +$$
$$\{f_5(L^-)^{-1} - f_6 r_c [Al_m(OH)_n^{(3m-n)+}]^{-1}\}\ Al_m(OH)_n^{(3m-n)+}L^- +$$
$$\{f_7(L^-)^{-1} - f_8 r_c [Al(OH)_n^{(3-n)+}]^{-1}\}\ Al(OH)_n^{(3-n)+}L^- \qquad (15)$$

where $r_c = AlL_n^{(3-n)+}/L^-$, which is the instantaneous ratio of the concentrations of complexed and free ligand L. The terms involving reactant species at the right-hand side depend on the reactant concentration, stoichiometry of the reaction and the degree to which the complexing reaction has progressed. Equation 15 is conceptually equivalent to Eqn. 7, where the set a_i is replaced by the terms of Eqn. 15: $[f_i(L^-)^{-1} - f_j r_c(Al)_p^{-1}]$, where Al_p is one of the p hydrolysis product terms in the initial vector.

EXPERIMENTAL

A set of aqueous 1.85×10^{-4} M aluminium chloride solutions was prepared from a 1 g dm^{-3} TITRISOL standard. The pH of different aliquots was adjusted to 2.75, 3.25, 3.50, 4.00, 4.50 and 4.75, a range where $Al(OH)_3$ is not expected to precipitate. Each aliquot was titrated in discrete steps with standard 5.265×10^{-4} M sodium fluoride (Orion 940907 Standard; 10 mg F^- l^{-1}). Changes in fluoride activity and pH were measured throughout the titration (fluoride-selective electrode Orion 96-09 and Orion 90-92 reference electrode, attached to an Orion Ion-meter 417 and a Metrohm E500 microvoltmeter linked to a two-channel chart recorder Kipp-Zonen BD41). The solution was maintained at 25 ± 0.1°C. Any pH changes were corrected after each titration step.

Under these experimental conditions, the half response time of the fluoride electrode after each addition of fluoride was in the range 2—12 s, which is well below the range of half reaction times for $AlF_n^{(3-n)+}$ complex formation (60—600 s).

The expected ion activities of all anions and cations and each of the 21 possible complexes were computed, for each pH condition and each titration step, by means of the thermodynamic equilibrium program GEOCHEM [5]. The numerical problem solved by the model is the calculation of a set of ion activities satisfying a given set of mole balance equations (one equation for each metal and each ligand) in the system being investigated, subject to input values of thermodynamic equilibrium constants stored in the computer

program. During the computation, the ionic strength is calculated from the current values of the concentrations of all species and conditional equilibrium constants are computed in the usual way from the values of equilibrium constants, with the help of single ion activity coefficients. For the case here described, vectors of equilibrium composition were obtained which described the molar ionic activities of all ions, including ligands, at each pH and titration step. Also, for each of these steps, an observed value of reaction rate and pH change was available for kinetic analysis.

The fluoride-selective electrodes were polished every 24 h, during the period of experimentation, with wet polishing strips (Orion 94-82-01) in order to avoid passivation of the membrane by the formation of films on it, as suggested by Buffle et al. [6]; in this way, minimal, reproducible response times were achieved in the range 1.0×10^{-8}—1.0×10^{-4} M free fluoride.

Twelve standards of fluoride activity in this range were prepared by addition of standard sodium fluoride solution to standard aluminium chloride solutions, according to computations performed by GEOCHEM. The non-Nernstian response observed was fitted by a polynomial regression procedure, which was used to interpolate for unknowns.

RESULTS AND DISCUSSION

Equilibrium changes during the titration procedure

Figure 2(a—c) describes the changes of free fluorides, aluminium ion and the total Al/OH forms concentrations, once equilibrium was attained after each titration step at all pH conditions inspected. Figure 2(a) shows that at high total fluoride concentration, the fluoride activity at various pH reflects increasing hydroxylation. Complete complexation of aluminium is attained at the maximum total fluoride utilized (Fig. 2b). Figure 2(c) shows that the experimental conditions resulted in a wide range of relative concentrations of complexing ions, complexes and hydrolysis products which allowed an adequate statistical treatment of the complexing system.

Surface-fitting to reaction paths

The reaction path as monitored through the fluoride shows a strong dependence on pH (Fig. 3a and b). At low pH values, the fluoride activity remains higher during the complexing reaction with respect to the final equilibrium value (this will be called Type I kinetics); when almost all the aluminium has been complexed, this type reverts to the normal one observed when fluoride is added to pure water, a unimodal path (Type II) where the increases in fluoride concentration approach the increases in total fluoride. Type II kinetics, where fluoride concentration is maximal at the final equilibrium point, is also observed at low fluoride concentration and high pH. An excess of citrate reverts Type I to Type II at low pH. Table 1 describes the ranges of fluoride and aluminium ion concentrations at which these computations are valid. Other data shown in this Table will be discussed later. As indicated

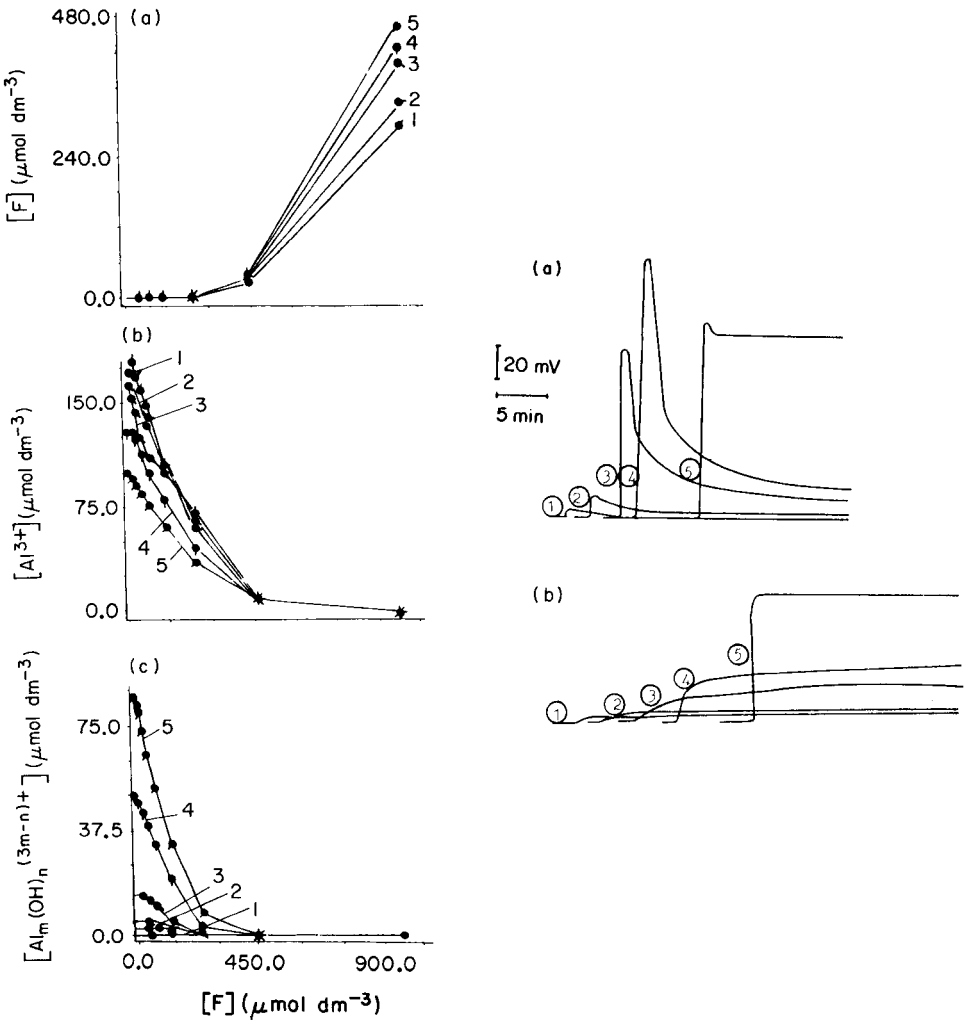

Fig. 2. Equilibrium changes at each titration step calculated by GEOCHEM as a function of the total fluoride concentration in the batch titration system: (a) fluoride activity; (b) aluminium(III) activity; (c) total Al/OH complex concentration. pH: (1) 3.25 (and 2.75); (2) 3.50; (3) 4.00; (4) 4.50; (5) 4.75.

Fig. 3. Types of Al/F complexation paths at selected titration steps covering the range of $AlCl_3$ titrations: (a) at pH 3.25; (b) at pH 4.75. Numbers 1—5 indicate discrete titration steps, where the total pF varied as follows: (1) 5.89 to 5.63; (2) 5.3 to 5.06; (3) 4.59 to 4.32; (4) 4.10 to 3.89; (5) 3.35 to 3.01.

above, the following reactions could be expected to lead to Al/F complex formations in aqueous solutions:

$$Al^{3+} + HF \rightleftharpoons AlF^{2+} + H^{+} \quad (16)$$

$$Al(OH)_3 + F^- \rightleftharpoons AlOH_2F + OH^- \quad (17)$$

$$AlOH^{2+} + HF \rightleftharpoons AlF^{2+} + H_2O \quad (18)$$

Equilibrium computation with GEOCHEM, however, indicated that in the presence of aluminium ions, the species HF is not formed. However, Eqn. 16 could still be an important mechanism in the complexation process. Study of the pH changes during the reaction path, however, gives further indications that Eqn. 1 is probably the most frequent reaction; increases in pH are observed only after NaF additions and are proportional to the relative amount of Al/OH forms (Fig. 4). Changes in pH are also proportional to total fluoride at low total fluoride levels, with a maximum dependent on pH, above which pH changes diminish as a consequence of the disappearance of Al/OH from the system (at low ΔpH values).

Figure 5 shows typical examples of paired fluoride activity and pH paths during the complexation reaction for various ranges of total fluoride and pH values where Al/OH forms are abundant. It can be observed that the change in pH occurs very quickly at the beginning of the reaction, and subsequent changes in fluoride are not accompanied by further pH changes; also, pH overshoots its final equilibrium value. These indicate that at low pH, reactions of the type

$$Al(H_2O)_6^{3+} + F^- \rightleftharpoons Al(H_2O)_6F^{2+} \quad (19)$$

are probably the prevailing mechanism, while at higher pH the reaction mechanism is probably better described by an F—OH replacement of the type shown in Eqn. 17. These possibilities can be practically explored or rejected if models of the type indicated in Eqn. 8 with formal meaning in Eqn. 15 fail to account for the observed data throughout the whole experimental range, or if reduced models containing a subset of reactants are efficient enough to describe the observed reaction rates. In order to explore these possibilities, several kinetic parameters were defined on the basis of the observed fluoride paths during the reaction, as shown in Fig. 6. From Fig. 6, $V_h = 0.5\Delta F^-/t_h$ can be defined as the half reaction rate of the complexation reaction.

Figure 7 shows the dependence of t_h throughout the range of experimental conditions. It can be observed that high values of t_h prevail at low pH. The reaction path can be related to the known initial free concentrations of hydrolyzed aluminium species. If $\mathbf{Al} = Al_{ij}$ is defined as a real positive matrix, where Al_{ij} are the activities of potentially reactive i Al species which from equilibrium considerations are assumed to exist in the solution at times j during the reaction, and if $\Sigma_{i=j}^{n} Al_{ij}$ is the total reactive aluminium, then, analogously to Eqn. 8,

$$V_R = a'_{1j}\, Al_{1k}\, F_j^- + a'_{2j}\, Al_{2j}\, F_j^- + \ldots + a'_{ij}\, Al_{ij}\, F_j^- \quad (20)$$

The set a'_{ij} of apparent reaction rates depends on the ratio F^-/Al. As fluoride is gradually added to a solution containing aluminium, the complex AlF^{2+}

TABLE 1

Characteristics and ranges of computation of n-dimensional calibration surfaces of the Al/F complexation paths, as inspected by potentiometric titrations. Variables 1—16 in μmol dm^{-3}, 17—22 in μmol^2 dm^{-6} and 23 in μmol s^{-1}

A. Ranges and distribution properties of kinetic variables for high R = F/Al ratio ($7.52 \times 10^{-4} < R < 3.06 \times 10^{-3}$).

Variable	Name	Mean	Standard deviation	Minimum	Maximum
1	H^+	360.8	665.2	17.8	1778.3
2	F (total, before spiking)	81.6	28.7	20.4	104.7
3	F (total, after spiking)	91.4	30.3	25.7	114.8
4	F^- (before spiking, as computed with GEOCHEM)	0.1	0.1	0.1	0.4
5	$Al(OH)^{2+}$	16.2	15.1	0.42	43.6
6	$Al(OH)_2^+$	5.1	6.8	0.0	17.7
7	$Al_2(OH)_2^{4+}$	0.1	0.1	0.0	0.4
8	$Al_3(OH)_4^{5+}$	0.0	0.0	0.0	0.0
9	Al^{3+}	81.9	15.7	51.2	104.7
10	$F^-(t = 0)$	0.1	0.1	0.1	0.5
11	$F^-(t = 25$ s)	0.4	0.3	0.1	1.0
12	$F^-(t = 50$ s)	0.3	0.2	0.1	0.7
13	$F^-(t = 150$ s)	0.2	0.1	0.1	0.6
14	$F^-(t = 300$ s)	0.2	0.1	0.1	0.6
15	$F^-(t = 600$ s)	0.2	0.1	0.1	0.6
16	F^-(final eq. time)	0.2	0.2	0.1	0.5
17	$F_t \cdot Al^3$	823.7	274.3	481.6	1300.5
18	$F_t \cdot Al(OH)^{2+}$	141.6	112.6	4.3	351.4
19	$F_t \cdot Al(OH)_2^+$	42.1	52.3	0.0	143.1
20	$F_t \cdot Al_2(OH)_2^{4+}$	0.9	1.1	0.0	2.7
21	$F_t \cdot Al_3(OH)_4^{5+}$	0.1	0.2	0.0	0.4
22	$F_t \cdot H^+$	4026.9	7594.4	96.1	220087.3
23	V_i = 25 s (see Eqn. 29)	0.4	0.1	0.2	0.5

Regression of 5-dimensional surface fitting (a_{ij} *in* dm^{-6} μmol^{-1} t^{-1}, *cf. Eqn. 21).*

Multiple R 0.998 Std. error of est. 0.035

Multiple R-Square 0.996

Analysis of variance

	Sum of squares	*D.f.*	*Mean square*	*F ratio*
Regression	1.844	6	0.307	254.88
Residual	0.007	6	0.001	

Variable number	a''_{ij} *coefficients*	*Std. error*
17	0.34	0.42×10^{-4}
18	0.11×10^{-2}	0.43×10^{-3}
19	0.001	0.001
20	−0.14	0.04
21	0.04	0.14
22	0.33×10^{-5}	0.25×10^{-5}

TABLE 1 (continued)

B. Ranges and distribution properties of kinetic variables for low R = F/Al ratio ($0.00 < R < 3.7 \times 10^{-4}$).

Variable	Name	Mean	Standard deviation	Minimum	Maximum
1	H^+	658.9	708.8	17.8	1778.2
2	F (total, before spiking)	8.2	8.9	1.1	25.7
3	F (total, after spiking)	10.8	11.1	2.1	31.6
4	F^- (before spiking, as computed with GEOCHEM)	0.0	0.0	0.0	0.0
5	$AlOH_1^{2+}$	12.2	16.0	0.7	47.9
6	$AlOH_2^+$	3.0	6.6	0.0	19.5
7	$Al_2OH_2^{4+}$	0.1	0.2	0.0	0.6
8	$Al_3OH_4^{5+}$	0.0	0.0	0.0	0.1
9	Al^{3+}	159.7	26.3	97.7	181.9
10	F_t^- (t = 0)	0.0	0.0	0.0	0.0
11	F_t^- (t = 25 s)	0.1	0.2	0.0	0.4
12	F_t^- (t = 50 s)	0.1	0.2	0.0	0.4
13	F_t^- (t = 150 s)	0.1	0.1	0.0	0.3
14	F_t^- (t = 300 s)	0.1	0.1	0.0	0.2
15	F_t^- (t = 600 s)	0.0	0.0	0.0	0.1
16	F_t = (final eq. time)	0.0	0.0	0.0	0.0
17	$F_t \cdot Al^3$	426.3	363.1	100.25	955.7
18	$F_t \cdot AlOH_1^{2+}$	18.1	18.2	0.9	53.6
19	$F_t \cdot AlOH_2^+$	3.4	7.0	0.0	21.8
20	$F_t \cdot Al_2OH_2^{4+}$	0.1	0.2	0.0	0.7
21	$F_t \cdot Al_3OH_4^{5+}$	0.0	0.0	0.0	0.1
22	$F_t \cdot H^+$	2159.6	3278.9	18.2	10553.5
23	V_i = 25 s (see Eqn. 29)	0.1	0.1	0.0	0.2

Regression analysis of 5-dimensional surface fitting (a''_{ij} *in* dm^{-6} μmol^{-1} t^{-1}, *cf. Eqn. 21*).

Multiple R 0.989 Std. error of est. 0.060

Multiple R-square 0.976

Analysis of variance

	Sum of squares	*D.f.*	*Mean square*	*F ratio*
Regression	2.141	5	0.428	117.44
Residual	0.047	13	0.003	

Variable number	a''_{ij} *coefficients*	*Std. error*
17	0.37×10^{-3}	0.47×10^{-4}
18	-0.33×10^{-4}	0.54×10^{-3}
19	0.53×10^{-3}	0.16×10^{-2}
20[a]	–	–
21	−0.02	0.20
22	0.21×10^{-5}	0.33×10^{-5}

[a]Excluded because of low significance.

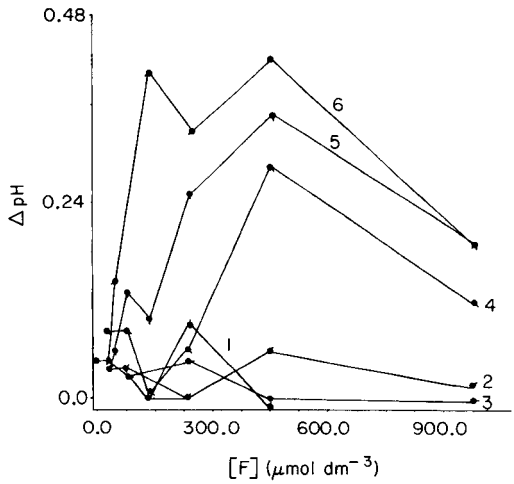

Fig. 4. pH changes produced after addition of fluoride to $AlCl_3$ solutions to produce the total concentrations plotted. Initial pH: (1) 2.75; (2) 3.25; (3) 3.50; (4) 4.00; (5) 4.50; (6) 4.75.

predominates compared to the other components of the possible series with coordination numbers up to AlF_6^{3-}; as the addition of fluoride is continued, free AlF^{2+} drops while free AlF_2 becomes more abundant, and so on with higher coordination numbers.

The stability of these successively predominant complexes decreases with increasing coordination number [7]. Accordingly, depending on the existing F^-/Al ratio in the solution, successive equal additions of F determine increasing changes in F^-. This effect was used here to obtain information about the dependence of the a'_{ij} on the ratios F^-/Al at various total fluoride levels.

Equation 20 was fitted by a regression procedure, where fluoride was affected by coordination numbers 0.5, 1, 2 and 3. Table 2 shows the values of the apparent reaction-rate coefficients for various ranges of fluoride with a constant aluminium concentration, and the goodness of fit achieved. The results indicate that the most stable mechanism (constancy of the regression coefficient) in a wide range of F^-/Al is that with coordination number 1, which predominates in the range $0.0 < F^-/Al < 5 \times 10^{-4}$. Equation 20 can also be expressed as

$$\lim_{t_i \to 0} \Delta F^-/\Delta t_j = \sum_{j=1}^{n} a'_{ij}\, Al_{ij}\, F_j^-$$

To a first approximation, Δt_i can be operationally chosen to be the t_j intervals in Fig. 6 (j = 1—5):

$$\bar{V}_i = \sum_{j=1}^{n} a''_{ij}\, Al_{i0}\, F_j^- + e \qquad (21)$$

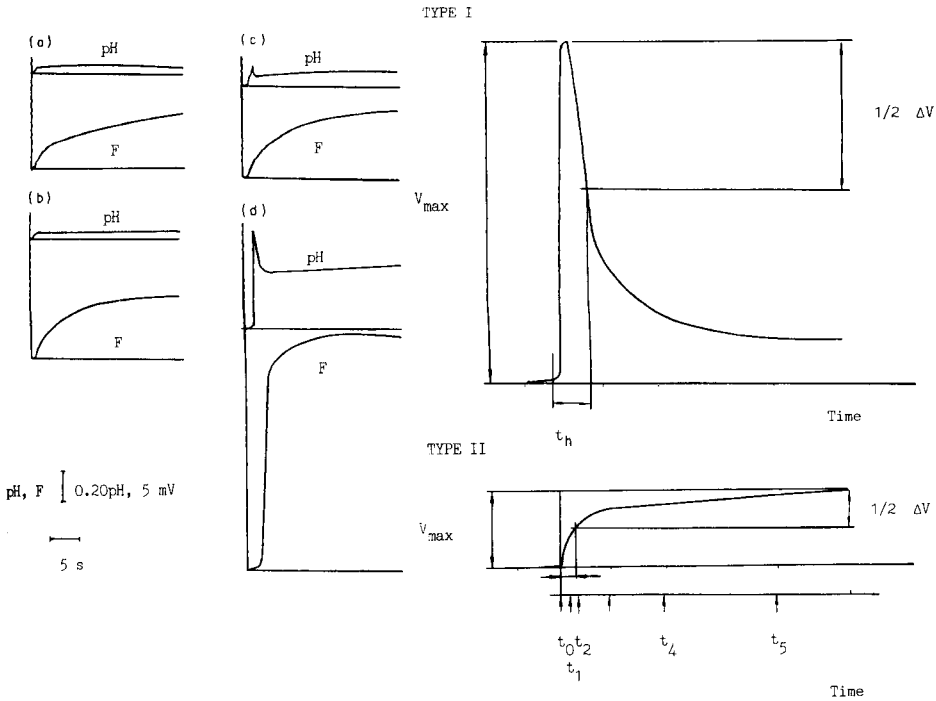

Fig. 5. Paths of fluoride and pH electrode output during the complexation of aluminium at different pH and spiking steps (cf. Fig. 3): (a) pH 4.00, step 4; (b) pH 4.00, step 5; (c) pH 4.75, step 4; (d) pH 4.75, step 5.

Fig. 6. Definition of kinetics parameters of the Al/F reaction on the basis of electrode output potential, kinetic paths type I and type II. V_{max}, maximum electrode potential during the reaction; 1/2 ΔV, half ion activity change; t_h, half reaction time; t_j, discrete time intervals used to describe the reaction path; t_0, initial reaction time; t_1, 25 s; t_2, 50 s; t_3, 150 s; t_4, 300 s; t_5, 600 s.

because, given the excess of aluminium, the initial concentrations, Al_{i0}, of the different Al_i can be assumed constant. $\bar{V}_i$ is a vector of apparent reaction rates and a''_{ij} is a matrix of estimators of the a'_i (Eqn. 7) with the functional dependence shown in Eqn. 15. The estimation of the matrix a''_{ij} was achieved on the basis of the titration data at times $t_j = t_0, \ldots t_5$, as indicated in Fig. 6, to obtain least-squares estimates through a multiple regression procedure with the assumption of the hydrolysis equilibria accounted for in GEOCHEM. The selection of the Al_i species was dictated by a similar previous analysis, where only those forms of hydrolyzed aluminium were further retained, which significantly contributed to the total sum of squares of $\bar{V}_i$, as indicated by a stepwise multiple regression [8]. The species selected through this procedure were $Al(H_2O)_6^{3+}$, $AlOH^{2+}$, $Al(OH)_2^+$ $Al_2(OH)_2^{4+}$ and $Al_3(OH)_4^{5+}$. The uncharged species $Al(OH)_3^0$ and the anion $Al(OH)_4^-$ were excluded by the regression procedure, a result which can be expected considering the probable

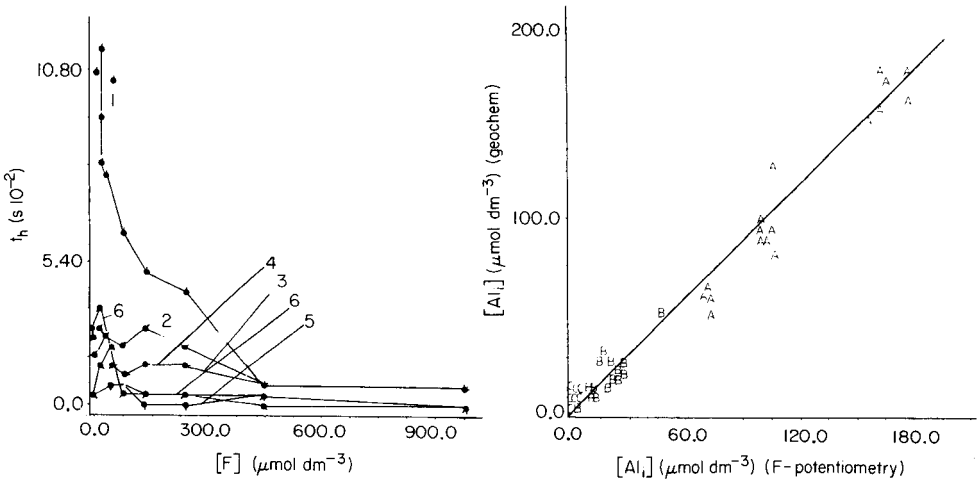

Fig. 7. Observed half reaction times as defined in Fig. 6 at different pH and total F values. Curves numbered as in Fig. 4.

Fig. 8. Estimates of Al species in a dilute aqueous solution as computed by GEOCHEM (ordinates) and calculated from regression based on fluoride potentiometry. (A) Al^{3+}; (B) $AlOH^{2+}$; (C) $Al(OH)_2^+$.

low stability of outer-sphere complexes of these species with fluoride. Also, equilibrium constants for these species [$pK_{Al(OH)_4^-} = 22.1$, $pK_{Al(OH)_3^0} = 15.0$] indicate that they contribute very little to the total aluminium pool in solution.

The remaining n species were used as independent variables in n-dimensional least-squares fitting by the usual multiple regression. Table 1 summarizes the properties of selected fitting surfaces which encompass the best and worst fittings achieved. In these listings, variables 4—9 describe the expected concentrations before or after addition of fluoride, as computed by GEOCHEM. These values are themselves a hypothesis, depending on the values selected for the equilibrium constants presently inserted in GEODAT [5]. Variables 10—16 describe the path of fluoride activity as recorded potentiometrically. Values of these variables were obtained by comparing the electrode response with a standard calibration function. Variables 17—22 correspond to the concentration products described in Eqn. 21, to which a term $F_t \cdot H^+$ (variable 22) was added to account for possible kinetic interaction between fluoride and hydrogen ion. The two surfaces shown were selected from a total of 90 equations which were computed to over-determine the equation system (Eqn. 21), as will be explained in the succeeding paper.

Inspection of the mean values of variables 5—9 indicates that Al^{3+}, $AlOH^{2+}$ and $Al(OH)_2^+$ constitute the most important hydrolysis products within the range of variable 1 utilized in these experiments. Most fitting surfaces, however, always select the infrequent species $Al_2(OH)_2^{4+}$ and $Al_3(OH)_4^{5+}$, although

TABLE 2

Dependence of the half-rates of reaction in the AlF system on various kinetic terms for various ranges of concentration of the reactants (Al concentration constant at 3.74×10^{-4} M. Kinetic equations of the form: $V_h = a\,(Al \times F^{-(n)})$, $n = 0.5, 1, 2, 3$)

Range of F^- (mol dm^{-3})	D.f.	Apparent reaction order[a]					
		0.5			1.0		
		R	*a*	*SE*	*R*	*a*	*SE*
$4.0 \times 10^{-9}/1.2 \times 10^{-8}$	7	0.765	0.003	0.001	0.751	0.13×10^{-2}	0.50×10^{-3}
$6 \times 10^{-9}/1.6 \times 10^{-8}$	11	0.754	0.004	0.001	0.766	0.14×10^{-2}	0.37×10^{-3}
$9 \times 10^{-9}/3 \times 10^{-8}$	12	0.763	0.006	0.001	0.780	0.15×10^{-2}	0.36×10^{-3}
$1 \times 10^{-8}/6 \times 10^{-8}$	18	0.799	0.006	0.001	0.794	0.12×10^{-2}	0.23×10^{-3}
$3 \times 10^{-8}/9.6 \times 10^{-8}$	9	0.869	0.008	0.001	0.891	0.14×10^{-2}	0.26×10^{-3}
$6 \times 10^{-8}/1.9 \times 10^{-7}$	7	0.734	0.018	0.007	0.738	0.26×10^{-2}	0.98×10^{-3}
$9 \times 10^{-8}/3 \times 10^{-7}$	6	0.478	0.041	0.025	0.530	0.005	0.002
$1 \times 10^{-7}/1 \times 10^{-6}$	10	0.564	0.064	0.031	0.614	0.007	0.003
			2			3	
$4 \times 10^{-9}/1.2 \times 10^{-8}$	7	0.724	0.20×10^{-3}	0.81×10^{-4}	0.702	0.31×10^{-4}	0.13×10^{-4}
$6 \times 10^{-9}/1.6 \times 10^{-8}$	11	0.764	0.15×10^{-3}	0.41×10^{-4}	0.743	0.15×10^{-4}	0.44×10^{-5}
$9 \times 10^{-9}/3 \times 10^{-8}$	12	0.765	0.77×10^{-4}	0.19×10^{-5}	0.738	0.36×10^{-5}	0.10×10^{-5}
$1 \times 10^{-8}/6 \times 10^{-8}$	18	0.724	0.42×10^{-4}	0.98×10^{-5}	0.651	0.12×10^{-5}	0.35×10^{-6}
$3 \times 10^{-8}/9.6 \times 10^{-8}$	9	0.905	0.35×10^{-4}	0.58×10^{-5}	0.882	0.74×10^{-6}	0.14×10^{-6}
$6 \times 10^{-8}/1.9 \times 10^{-7}$	7	0.741	0.51×10^{-4}	0.91×10^{-4}	0.739	0.97×10^{-6}	0.36×10^{-6}
$9 \times 10^{-8}/3 \times 10^{-7}$	6	0.584	0.67×10^{-4}	0.31×10^{-4}	0.580	0.67×10^{-6}	0.31×10^{-6}
$1 \times 10^{-7}/1 \times 10^{-6}$	10	0.647	0.84×10^{-4}	0.33×10^{-4}	0.640	0.80×10^{-6}	0.31×10^{-6}

[a] *R*, multiple correlation coefficient; *a*, regression coefficient; *SE*, standard error of *a*.

the error associated with their regression coefficients is high. The quality of the fitting surfaces like the examples shown in Table 2 can be better ascertained by comparison of the estimates of the components of the initial vector as computed by GEOCHEM, and the same values obtained by averaging the a''_{ij} estimates obtained by regression as shown in Table 1; details will be given in the next paper. Figure 8 shows the scatter diagram of both series of estimates. The agreement is quite good, with almost equal mean values and distribution properties. Outliers (2 out of 42) do not exceed the threshold t = 12 μmol dm^{-3}, which is about 7% of the total amount of aluminium present.

REFERENCES

1 K. Srinivasan and G. A. Rechnitz, Anal. Chem., 40,12 (1968) 1818.
2 V. Nair and J. Prenzel, Z. Pflanzenernaehr. Bodenkd., 141 (1978) 741.
3 O. Talibundeen and M. B. Page, Soil Analysis: Instrumental Techniques and Related Procedures, M. Dekker, New York, 1983.
4 C. F. Baes and R. Mesmer, The Hydrolysis of Cations, Wiley, New York, 1976.
5 G. Sposito and S. V. Mattigod, GEOCHEM: a computer program for the calculation of chemical equilibria in soil solutions and other natural water systems, Dept. Soil Environ. Sci., CA, Riverside, 1980.
6 J. Buffle, N. Parthasarathy and W. Haerdi, Anal. Chim. Acta, 68 (1974) 253.
7 W. L. Lindsay, Chemical Equilibria in Soils, Wiley, New York, 1975.
8 BMDP, Statistical Software, Dept. Biomath. Univ. Calif. Los Angeles, University of California Press, 1981.

Analytica Chimica Acta, 187 (1986) 195—211
Elsevier Science Publishers B.V., Amsterdam — Printed in The Netherlands

IDENTIFICATION OF HYDROLYSIS PRODUCTS OF ALUMINIUM IN NATURAL WATERS

Part 2. ALSPEC, a Computerized Procedure for Quantifying Equilibria with Inorganic and Organic Ligands

JORGE ARES

Institut für Bodenkunde und Waldernährung, Universität Göttingen, Büsgenweg 2, 3400 Göttingen (Federal Republic of Germany)

(Received 18th January 1985)

SUMMARY

Calibration surfaces describing the kinetics of Al/F complex formation are used to develop a linear programming procedure with which the distribution of aluminium species in various solutions is investigated. Samples tested include prepared solutions containing different levels and ratios of hydroxide, fluoride, sulfate, citrate and a fulvic acid, and solutions from soil water extracts and lysimeter water. The results show that the calibration surfaces are robust for describing all the cases tested. Results obtained with fulvic acid solutions agree with reported data on aluminium/fulvic acid complexes. The results obtained with soil solutions are internally consistent and in line with the expected behaviour of humic materials. A software package is described for combining potentiometry with a fluoride-selective electrode with linear programming routines in order to solve problems of aluminium speciation in solutions containing ligands which have unknown thermodynamic characteristics and may be colloidal polyelectrolytes.

In acidic natural waters and soil solutions, aluminium can have a toxic effect on living organisms, and this effect depends on the relative abundance of different ionic aluminium species present [1—3]. In these systems, aluminium can be variously bound to sulfate, fluoride, hydroxide and to naturally occurring anions of complex structure. Although the properties of naturally occurring inorganic aluminium complexes are relatively well understood, those of the organic complexes remain the subject of a considerable amount of theoretical and experimental research and speculation. An experimental technique which would allow direct estimation of the activity of different aluminium species in equilibrium with complex organic ligands, would favour the development of proper theoretical treatments of these equilibria.

In the preceding paper [4], it was shown that potentiometry with a fluoride-selective electrode can be used to develop an n-dimensional calibration system which allows the determination of aluminium species in dilute aqueous solutions of aluminium chloride. The procedure relies on the fact that fluoride reacts at different speeds with the Al^{3+} aqua-ion and with its hydrolysis products, if the quantity of fluoride added to the system is low enough not to modify significantly the distribution of aluminium species.

The matrices of a''_{ij} (apparent reaction-rate coefficients) contain the necessary information to perform calculations of aluminium speciation from the potentiometric data. The Al-species vector can be estimated directly by inversion of the a''_{ij} matrix; however, because the a''_{ij} values are stochastic estimates of the true a_{ij}, the solution obtained in this way can be affected by considerable errors. An over-determination of the kinetic equation system is necessary to achieve acceptable precision and stability of the solution; this is here achieved through a linear programming solution.

Also, if the technique is to be useful for inspection of binding in systems containing ligands other than hydroxide and fluoride, it must be verified that the reaction mechanisms in the presence of these ligands are not modified to an extent that would produce very different regression solutions of the system. This question is addressed through the inspection of solutions containing known amounts of the naturally occurring ligands, citrate, sulfate and a soil fulvic acid. Also, soil water extracts and water samples from a lysimeter are examined for consistent behaviour under various pH conditions.

In this paper, an integrated procedure which couples the potentiometric procedure with adequate existent software is presented to help solve the problem of aluminium speciation in acidic natural waters. The results obtained with these solutions give further insight into the nature of naturally occurring organic complexes of aluminium.

EXPERIMENTAL

Preparation of solutions and natural water samples

Solutions containing 1.0×10^{-1}, 1.26×10^{-3} and 1.26×10^{-4} mol dm^{-3} of citric acid (reagent grade) were prepared from a 1 M standard solution. These concentrations were selected in order to obtain an approximate 50% of total aluminium complexation from 1.85×10^{-4} mol dm^{-3} Al in solutions at pH 2.75, 3.5 and 4.5, respectively. The necessary computations were done with the GEOCHEM program with the values for the thermodynamic equilibrium constants of the expected complexes described in Table 1. Values for the aluminium citrate complexes are those given by Kwong and Huang [5].

Sulfuric acid (TITRISOL standard) was added to a similar set of solutions without citrate to produce 40—60% complexation of aluminium.

A sample of soil fulvic acid, prepared as described by Schnitzer and Desjardings [11], was obtained from Dr. Schnitzer's laboratory; this material has been extensively studied with respect to chemical properties and complexing capacity. The sample was dried at 50°C to constant weight and solutions at pH 2.75, 3.00, 3.50, 4.00 and 4.50 were prepared by adding 30 mg of fulvic acid to 120 ml of twice-distilled water. According to available estimates of the molecular weight of this material, this would produce a ca. 3.15×10^{-4} M solution; this compares closely with values utilized in complexation studies with aluminium [12], and with the usual total carbon

TABLE 1

Complexes and equilibrium constants (pK) considered in GEOCHEM in relation to the Al/F system compared with values from other sources

Complex	pK values				
	GEOCHEM [6]	[7]	[8]	[9]	[10]
$Al(OH)_3(s)$	10.4				
$Al(OH)^{2+}$	5.0	5.0	4.9	4.9	
$Al(OH)_2^+$	10.1	9.3	9.3	10.1	
$Al(OH)_3^0$	15.0	14.9	15.0		
$Al_2(OH)_2^{4+}$	7.7	7.6	7.7		
$Al_3(OH)_4^{5+}$	13.9		13.9		
$Al(OH)_4^-$	22.1	23.3	23.0	22.1	
$Al_{13}(OH)_{32}$			98.7		
AlF^{2+}	−7.0	−6.9			−7.0
AlF_2^+	−12.6	−12.6			−12.7
AlF_3^0	−16.7	−16.6			−19.7
AlF_4^-	−19.1	−19.0			−20.9
AlF_5^{2-}	−20.6				−20.9
AlF_6^{3-}	−20.5				−20.8
$AlSO_4^+$	−3.2	−3.2			
$Al(SO_4)_2^-$	−1.8				
$Alcit^0$	−7.3				
$Alcit_2^{3-}$	−13.9				

content in soil solutions at equilibrium. The fulvic acid dissolved almost completely under the above-mentioned conditions; samples were vigorously stirred during potentiometric measurements to maintain a homogeneous suspension if some material did precipitate. Accordingly, the experiments with fulvic acid reported below should be interpreted as obtained from equilibria in heterogeneous systems, where molar fractions can differ from theoretical estimates. This is considered an advantage of the proposed procedure rather than a limitation, because natural waters are often suspensions of complex colloidal materials, and the observed equilibria involve not only the usual chemical binding but also adsorption phenomena, Donnan-type equilibria, etc. [13].

Samples of soil water extracts from a depth of 0—10 cm from fertilized (lime) and unfertilized plots at a *Picea abies* stand in Solling Plateau were obtained as described by Fassbender and Ahrens [14]. The fertilizer produced a considerable increase in the Ca/Al ratio in the soil exchange complex. The procedure used to obtain the water extracts is believed to give an estimate of the usual composition of a soil solution under conditions of unsaturated flow. Table 2 shows a typical average composition for this type of soil extract and Table 3 shows the expected distribution of ionic species as computed with GEOCHEM, when no organic ligands are included in the computations. Aliquots of the water extracts were passed through a column

TABLE 2

Expected chemical speciation in samples of soil water extracts at Solling plateau (*Picea abies* stands), according to measurements of total concentrations as described earlier [14], and equilibrium computations done with GEOCHEM
(Ionic strength = 1.87×10^{-3} M, fixed pH = 3.370, Computed $[H^+] = 0.506 \times 10^{-3}$ M)

Substance	Free conc.[a]	Total conc.[a]	Remainder[a]
Na	6.15×10^{-5}	6.16×10^{-5}	3.65×10^{-13}
K	1.23×10^{-4}	1.23×10^{-4}	9.87×10^{-13}
Ca	9.50×10^{-5}	9.77×10^{-5}	6.79×10^{-13}
Mg	8.52×10^{-5}	8.71×10^{-5}	6.67×10^{-13}
Fe	8.51×10^{-8}	3.31×10^{-4}	0
Mn	2.68×10^{-5}	2.75×10^{-5}	1.70×10^{-13}
Al	1.42×10^{-4}	1.73×10^{-4}	3.96×10^{-12}
Cl^-	7.56×10^{-5}	7.58×10^{-5}	8.40×10^{-13}
NH_3	8.71×10^{-11}	3.63×10^{-5}	2.27×10^{-12}
NO_3^-	1.12×10^{-4}	1.12×10^{-4}	3.80×10^{-14}
PO_4^{3-}	4.68×10^{-19}	5.75×10^{-6}	-1.93×10^{-12}
SO_4^{2-}	2.07×10^{-4}	2.45×10^{-4}	-2.78×10^{-12}
F^-	3.05×10^{-9}	3.16×10^{-6}	-7.98×10^{-13}
Solids[a]			
$FePO_4$	3.738×10^{-6}		
$Fe(OH)_3$	3.252×10^{-4}		

[a] All given as mol l^{-1} of solution.

TABLE 3

Primary distribution of metal ions and ligands

Substance	Distribution (% of total concentration)								
	Free ion	Complexed with							
		SO_4^{2-}	OH^-	PO_4^{3-}	F^-	Al^{3+}	H^+	Fe^{3+}	Ca^{2+}
Na	99.8	0.2	—	—	—	—	—	—	—
K	99.9	0.1	—	—	—	—	—	—	—
Ca	97.3	2.7	—	—	—	—	—	—	—
Mg	97.8	2.1	—	—	—	—	—	—	—
Fe	—	—	98.2[a] 0.5	1.1[a]	—	—	—	—	—
Mn	97.3	2.7	—	—	—	—	—	—	—
Al	82.0	14.5	1.6	—	1.8	—	—	—	—
Cl^-	99.7	—	—	—	—	0.2	—	—	—
NH_3	—	—	—	—	—	—	100	—	—
NO_3^-	99.9	—	—	—	—	—	—	—	—
PO_4^{3-}	—	—	—	—	—	—	31.8	65.0[a] 3.1	—
SO_4^{2-}	84.5	—	—	—	—	—	—	—	1.1
F^-	—	—	—	—	—	99.9	—	—	—

[a] In solid form.

of the cation-exchanger Amberlite IR-120 (20—50 mesh, Na^+ form); the pH of the samples changed in all cases during contact with the resin.

Percolation fractions of water from a lysimeter were obtained with porous-porcelain capsule lysimeters installed at Solling Forest in *Picea abies* and *Fagus silvatica* stands in the humus layer. About 10 l of solution was filtered repeatedly through a 0.45-μm membrane filter (Pellicon PCAC, cellulose acetate) with a nominal threshold at m.w. 1000. The material remaining on the filter was placed in a desiccator over P_2O_5 silica gel until constant weight was attained and was used to prepare solutions containing 30 mg in 120 ml of twice-distilled water, the pH of which was adjusted to 2.75, 3.00, 3.5, 4.00 or 4.5 by addition of hydrochloric acid or sodium hydroxide; the suspensions were maintained dispersed by magnetic stirring.

Total aluminium was quantified by atomic absorption spectrometry (a.a.s.) with a Perkin-Elmer 3000 instrument, used as specified by the maker.

Potentiometric measurements

The unknown solution or water sample (50 ml) was placed in a plastic 250-ml vessel at 25 ± 0.1°C. After immersion of the fluoride-selective and pH electrodes [4], standard 5.265×10^{-4} M sodium fluoride (10 mg l^{-1} fluoride) was added to give a minimum fluoride concentration of 10^{-6} M fluoride. This complexes about 2% of the aluminium in a solution containing 3.7×10^{-5} M aluminium (1 mg l^{-1}). The attainment of equilibrium was regarded as a potential change of >0.5 mV/20 min. The sodium fluoride solution was added (0.1—0.5 ml, depending on the total Al in the sample) from an Eppendorf pipette. The fluoride activity was followed with a chart recorder at a speed of 12 mm min^{-1} until the new equilibrium reading was attained.

Equation system for the fluoride potentiometric paths

The computation of the aluminium vector which solves the equation systems described in Part 1 [4] was achieved by use of the NAG E02GBF subroutine (Numerical Algorithms Group, Mayfield House, Oxford, 1983). The F_j^- vector is replaced by the values taken from the fluoride potentiometric data after spiking the unknown sample, and the vector of independent terms is replaced by the observed reaction rates in the relevant interval. The software system calculates a l_1 norm solution to an over-determined system of linear equations, subject to linear inequality constraints. Given a matrix A of a''_{ij} coefficients with m rows (number of fitting surfaces) and n columns (number of aluminium species in the solution), the routine calculates the solution to the over-determined equation system $\mathbf{A'x} = \mathbf{b}$, where $\mathbf{x}$ is the solution vector of aluminium species concentrations and $[H^+]$ (last term); $\mathbf{A'}$ is A multiplied line by line by the vector of F_j^- successive concentrations and b is the vector of observed reaction rates. The measured pH is used to eliminate H^+ from the solution by adding the corresponding term to the independent vector $\mathbf{b}$. Because the a''_{ij} are stochastic estimates of the a'_{ij}, over-determination is needed to attain accuracy and stability of the solution. Over-

determination was achieved by computing m different multiple regression models, suppressing in turn some of the aluminium species from the set of independent variables. This forces into the regression equations some variables which may not be selected eventually by the regression program because of their linear dependence on other independent variables. The NAG E02GBF calculates a vector $\mathbf{x}(n)$ which minimizes

$$r(1) = \sum_{i=1}^{n} ri, \text{ where } r_i = \mathbf{b}_i - \sum_{j=1}^{n} a''_{ij}\,\mathbf{x}_i \; (i = 1,2 \ldots n)$$

A unique solution vector can be calculated by constraining the vector of aluminium species. In aqueous solutions, maximum amounts of aluminium hydrolysis products can be defined on the basis of pH; these maxima were estimated with GEOCHEM in the range pH 2.75–5.00 at 0.25 intervals, for total aluminium concentrations of 38, 93, 186, 380, 758, 1530 and 3020 μmol dm^{-3}. The pC values of theoretical maxima are entered in ALSPEC (see below) in the form of a constraint matrix and the program performs a linear double interpolation between tabulated values to find theoretical maxima for the conditions of the unknown sample. Minima are set at 0.01 of the maximum values. The constrained solution is calculated through an iterative approach via an exact penalty function [15].

Structure of ALSPEC program

The necessary interface between the fluoride potentiometric data and the NAG subroutine is provided by ALSPEC, a Fortran program which receives as input three a''_{ij} calibration-fitting $m \times n$ matrices corresponding to the ranges $F^-/[Al]$: $0.0 \leqslant R < 8.5 \times 10^{-5}$, $8.5 \times 10^{-5} \leqslant R < 7.8 \times 10^{-4}$, and $7.8 \times 10^{-4} \leqslant R < 3.0 \times 10^{-3}$, respectively. Also input are a matrix (ALCONS) of theoretical constraints on the concentrations of hydrolyzed species of aluminium in the ranges $2.75 \leqslant \text{pH} \leqslant 5$ and $5 \leqslant \text{pAl} \leqslant 2.73$, and a vector containing j potential values from the fluoride potentiometric recording. In addition, the total aluminium concentration in the sample, pH and the coefficients of a polynomial electrode potential/pF function must be given by the user. An appropriate standard solution of fluoride (e.g., pF = 7.9) must be measured and the potential included as input; this corrects for possible shifts in electrode response between samples. ALSPEC performs the necessary conversion to fluoride activity, and computes the standard reaction rates for the relevant interval.

Table 4 describes the processing sequence of the program. Table 5 describes the sequence used during the computerized potentiometric procedure applied to the solutions described above. Table 6 summarizes the characteristics of the aqueous solutions and water samples examined. A copy of the ALSPEC computer program is available on request from the author.

TABLE 4

Operation sequence of the ALSPEC computer program

(1) Data input: electrode calibration function; equations of 40 fitting surfaces; sample kinetic measurements, pH, pAl_{total}; theoretical upper and lower limits of Al_i species (pH × pAl constraint matrix)
(2) Transformation of kinetic data and computation of forward reaction rates
(3) 2-Dimensional interpolation of sample pH and pAl_{total} to compute constraints of Al_i
(4) Linear programming solution of sample data according to given calibration surfaces
(5) Output: Al_i in absolute concentrations and as fractions of Al_{total} and theoretical maxima at given pH.

TABLE 5

Logical sequence in the development of ALSPEC relevant to data in Table 6

(1) Batch titrations of 1.85×10^{-3} M $AlCl_3$ at pH 2.75—5.00
(2) Equilibrium computations of titration steps with GEOCHEM
(3) Development of *n*-dimensional calibration surfaces
(4) Validation test I[a] on batch titrations
(5) Validation test II on equilibrium computation
(6) Linear programming solution of calibration surfaces
(6a) Equilibrium computation of systems containing sulfate and citrate (GEOCHEM): Validation test III
(6b) Preparation of solutions containing standard fulvic acid: Validation test IV
(6c) Resin extraction of soil water equilibrium solution: Validation test V

[a]Meaning of null hypothesis during the development of ALSPEC for validation tests I—V:
I. Kinetic equations inadequate to describe Al:F complexation; observed parameters of the kinetic paths inadequate.
II. Experimental errors too important or not reproducible; lack of consistency between actual experimental conditions and GEOCHEM simulations (numerical errors, lack of consistency between experiment and modelled situation); solution problems of the linear programming algorithm.
III. Effects caused by the presence of other ligands too important to be disregarded.
IV. Effects caused by polyelectrolytes too important to be disregarded (surface potentials).
V. Unknown higher-order effects caused by mixtures of organic and inorganic ligands too important to be disregarded.

RESULTS AND DISCUSSION

Structure of the ALSPEC program output

The program output in its present version supplies information about the initial sample conditions, intermediate calculations and the computed distribution of aluminium species expressed in different ways. Figure 1 shows a typical output for a soil solution. Constraint values for each aluminium species are obtained from the double interpolation routine as well as the interpolation rows in ALCONS. The calibration range used, depending on the computed F^-/Al ratio, is given, and the solution vector of Al_j species in three forms completes the output.

TABLE 6

Sample solutions inspected with ALSPEC

Type	Source	Concentration ranges, i. strength, pH, pretreatment, etc.	Predominant ligands	%Al complexation in the solution ($Al_{tot} - Al^{3+}$)/Al_{tot})
1	Artificial ($AlCl_3$ as metal source)	[Al] = 1.86×10^{-4}, 1.86×10^{-3}; pH 2.75—5.00; I.S. = 1×10^{-3}; 1×10^{-2}	OH^-	0—50
2		As Type 1	OH^-, F^-	0—50—90
3		As Type 1 + [SO_4^{2-}] = 3.16×10^{-3}—1.77×10^{-3} (cf. Table 7)	OH^-, SO_4^{2-}, F^-	0—50—90
4		As Type 1 + [cit] = 1×10^{-1}—1.25×10^{-4} (cf. Table 8)	OH^-, cit, F^-	0—50—90
5	Naturally occurring ligands	As Type 1 + [fulv] = 3.15×10^{-4}, Al/fulv = 0.07/1 to 0.55/1	OH^-, fulv, F^-	0—40
6	Soil equilibrium solutions	*P. abies* stand, fertilized, unfertilized, with or without ion-exchange treatment	OH^-, F^-, SO_4^{2-}, orglig.[a]	0—50
7	Extracted organic ligands (ultrafiltration)	Filtration residue used to prepare solutions. *Picea* and *Fagus* stands, lysimeter water, Dec. 1983.	OH^-, F^-, SO_4^{2-} orglig.[a]	0—50

[a]Orglig relates to the apparent complexing effect of a predominantly organic matrix composed of high-molecular-weight weak polyelectrolytes.

```
F1 DEPTH 0-10 PRE RESIN TREATMENT
ORIGINAL pH:   3.20          TREATMENT pH:   3.20          TOTAL AL (μMOL L⁻¹)   1819.7008
VECTOR OF F CONCENTRATIONS AT SUCCESSIVE TIMES:
          .02290862          .03162269          .02691528          .02511880          .02290862
VECTOR OF INTERVAL REACTION RATES
          .21481273          .10723208          .03675556          .01851072          .00877503
ALTOT:    2.74
INTRP1:   8
INTRP2:   13
CONSTRAINT TERMS:
          1778.2793          23.1206            .2432              .2064              .007   /   17.7828
             .2312              .0024              .0021              .0000
LOW RATIO MATRIX SELECTED
OUTPUT FROM MONITOR SUBROUTINE:
NUMBER OF ITERATIONS:   8
LATEST ESTIMATOR OF AL SPECIES VECTOR:  Al3, AlOH1, AlOH2, Al2OH2, Al3OH3  (μMOL L⁻¹)
1690.1222853247       23.1206459217       .2432203884       .2063795346       .0007036119
AL SPECIES VECTOR-pC VALUES:
   2.7720819          4.6360000          6.6140000          6.6853334          9.1526668
AL SPECIES VECTOR AS A FRACTION OF TOTAL AL:
    .9287913           .0127057           .0001337           .0001134           .0000004
AL SPECIES VECTOR AS A FRACTION OF THEORETICAL MAXIMUM AT SAMPLE pH:
    .9504257          1.0000000          1.0000000          1.0000000          1.0000000
```

Fig. 1. Typical output of ALSPEC corresponding to a soil solution sample of Type 6 (Table 6).

Aluminium speciation

Systems of Types 1 and 2 (Table 6). These systems were used to develop *n*-dimensional fitting surfaces and were used here for validation purposes, to check for numerical problems, lack of solution stability, etc., before any applications to unknown solutions. The properties of the fitting surfaces and speciation of aluminium in these systems were described in Part 1 [4]. Figure 2(a) shows a scatter diagram of the distribution of aluminium species estimated by ALSPEC and computed with GEOCHEM, expressed as a fraction

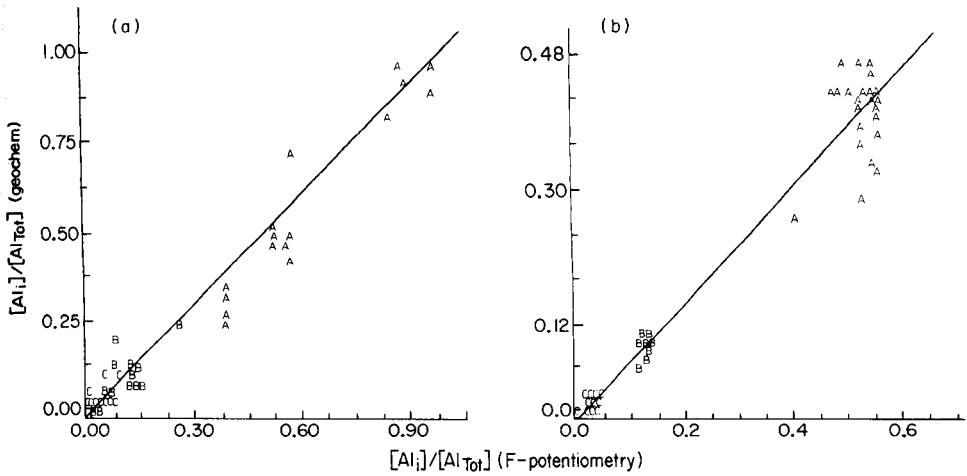

Fig. 2. Scatter diagram of distribution of Al species in different solutions as computed with GEOCHEM and estimated by the potentiometric method (ALSPEC). Solutions: (a) Types 1 and 2; (b) Type 3 (Table 6). (A) Al^{3+}; (B) $AlOH^{2+}$; (C) $Al(OH)_2^+$.

of the total Al present; there is good agreement between the calculated and measured values over the range of concentration studied ($Al_{Tot} = 1.86 \times 10^{-4}$—$1.86 \times 10^{-3}$ M). Maximum outliers do not exceed 0.05 $[Al]_{Tot}$ or 0.1 $[Al]_{i\,predicted}$ (each of the predicted Al_i fractions). Factors influencing these errors are inaccuracies in the measurement of the fluoride concentrations at different points of the reaction, and numerical errors in the solution of the calibration function system. In this case, as in similar graphs, the polynuclear species $Al_2(OH)_2^+$ and $Al_3(OH)_4^+$ are not represented because they constitute a very small fraction of the aluminium pool ($\leqslant 0.01$).

Systems of Type 3 (Table 6). Table 7 shows the expected composition of the solutions based on the equilibrium pK values given in Table 1. Figure 2(b) shows the scatter diagram for aluminium species values measured with ALSPEC and calculated with GEOCHEM. Predictions with ALSPEC slightly over-estimate the Al_i fractions; this is corrected when the pK ($AlSO_4^+$) value used is replaced by 3.1. Suppression of points at pH 4.5 also improved the fit. Because the pK value used for $Al(SO_4)_2^-$ during the computations with GEOCHEM is probably also affected by errors of this magnitude, the discrepancies observed are not considered to be significant for this type of analysis. The scatter around the regression line in Fig. 2(b), as in similar cases presented, does not depend on possible inaccuracies in the pK values but only on ALSPEC inaccuracies. The observed correlation is good. The quality of the fit suggests that the basic Al/F complexing mechanisms are not significantly altered by the weak Al/SO_4 complexes.

Systems of Type 4 (Table 6). The expected distribution of Al^{3+} and Al/OH forms in the presence of enough citrate to complex about 50% of the total aluminium present was computed with GEOCHEM, and measured with

TABLE 7

Composition of solutions of Type 3 (Table 6) and the theoretical concentrations of complexes computed with GEOCHEM

Total concentrations (pC, mol dm^{-3})

	pH 2.75	*pH 4.5*
Al	3.73	3.73
Na	5.05	5.05
F^-	5.05	5.05
Cl^-	3.63	3.63
SO_4^{2-}	2.50	2.75

Concentration of principal complexes (Integer digit columns after each complex concentration refer to metal, ligand and H/OH stoichiometry, respectively.)

pH 2.75																
Al	F	5.06	1	1	0	7.31	1	2	0	16.24	1	4	0	22.15	1	5	0
Al	Cl	6.71	1	1	0	10.01	1	2	0	18.93	1	4	0				
Al	SO_4	4.00	1	1	0	8.04	1	2	0								
Al	OH	6.55	1	0	−1	8.98	1	0	−2	10.45	2	0	−2	15.23	3	0	−4
Na	F	11.97	1	1	0												
Na	Cl	8.32	1	1	0												
Na	SO_4	6.17	1	1	0	8.07	1	1	1								
Na	OH	13.97	1	0	−1												
H	F	7.51	0	1	1												
H	Cl	14.83	0	1	1												
H	SO_4	3.48	0	1	1	16.56	0	1	2								
pH 4.5																	
Al	F	5.06	1	1	0	7.30	1	2	0	16.29	1	4	0	22.25	1	5	0
Al	Cl	6.67	1	1	0	9.93	1	2	0	18.82	1	4	0				
Al	SO_4	4.11	1	1	0	8.31	1	2	0								
Al	OH	4.75	1	0	−1	5.43	1	0	−2	6.96	2	0	−2	8.26	3	0	−4
Na	F	12.23	1	1	0												
Na	Cl	8.55	1	1	0												
Na	SO_4	6.59	1	1	0	8.23	1	1	1								
Na	OH	12.47	1	0	−1												
H	F	9.29	0	1	1												
H	Cl	16.56	0	1	1												
H	SO_4	5.42	0	1	1	20.23	0	1	2								

Primary distribution of metals and ligands

		(% of total element concentration)	
		pH 2.75	*pH 4.50*
Al	As free ion	41.7	40.7
	Bound with F^-	4.7	4.7
	Cl^-	0.1	0.1
	SO_4^{2-}	53.3	42.0
	OH^-	0.2	12.4
Na	As free ion	97.8	98.5
	Bound with SO_4^{2-}	2.2	1.4
F	As free ion	0.2	0.2
	Bound with Al^{3+}	99.4	99.8
	H^+	0.3	—
Cl	As free ion	99.7	99.8
	Bound with Na	0.2	0.1
SO_4	As free ion	84.3	94.0
	Bound with Al	3.1	4.4
	Na	2.2	1.4
	H	10.4	0.2

TABLE 8

Composition of solutions of Type 4 (Table 6) and the theoretical concentrations of complexes computed with GEOCHEM

Total concentrations (pC, mol dm^{-3})

	pH 2.75	*pH 4.50*
Al	3.73	3.73
Na	5.33	5.05
F^-	5.53	5.53
Cl^-	3.63	3.63
Citrate	1.00	3.90

Concentration of complexes (Integer digit columns after each complex concentration refer to metal, ligand and H/OH stoichiometry, respectively.)

pH 2.75																
Al	F	5.33	1	1	0	7.96	1	2	0	12.05	17.80	1	4	0	24.19	1 5 0
Al	Cl	6.52	1	1	0	9.75	1	2	0	13.83	18.63	1	4	0		
Al	Cit	4.23	1	1	0	4.58	1	2	0							
Al	OH	6.37	1	0	−1	8.77	1	0	−2	10.93	10.26	2	0	−2	14.97	3 0 −4
Na	F	12.63	1	1	0											
Na	Cl	6.52	1	1	0											
Na	Cit	8.47	1	1	0											
Na	OH	14.20	1	0	−1											
H	F	7.95	0	1	1											
H	Cl	14.80	0	1	1											
H	Cit	3.45	0	1	1	1.49	0	1	2	1.17						
pH 4.50																
Al	F	5.33	1	1	0	7.86	1	2	0	11.86	17.51	1	4	0	23.83	1 5 0
Al	Cl	6.61	1	1	0	9.81	1	2	0	13.88	18.68	1	4	0		
Al	Cit	4.24	1	1	0	4.60	1	2	0							
Al	OH	4.71	1	0	−1	5.35	1	0	−2	5.76	6.98	2	0	−2	8.31	3 0 −4
Na	F	12.54	1	1	0											
Na	Cl	6.51	1	1	0											
Na	Cit	8.45	1	1	0											
Na	OH	12.45	1	0	−1											
H	F	9.61	0	1	1											
H	Cl	16.54	0	1	1											
H	Cit	5.18	0	1	1	4.95	0	1	2	6.38						

Primary distribution of metals and ligands

		(% *of total element concentration*) *pH 2.75*	*pH 4.50*
Al	As free ion	50.9	39.2
	Bound with F^-	2.5	2.5
	Cl^-	0.2	0.1
	Cit	46.2	44.2
	OH^-	0.2	14.0
Na	As free ion	100.0	100.0
F	As free ion	0.2	0.2
	Bound with Al^{3+}	99.6	99.8
	H^+	0.6	
Cl	As free ion	99.7	99.8
	Bound with Al^{3+}	0.1	0.1
	Na^+	0.1	0.1
Cit	Bound with Al^{3+}	0.1	85.3
	H^+	99.9	14.6

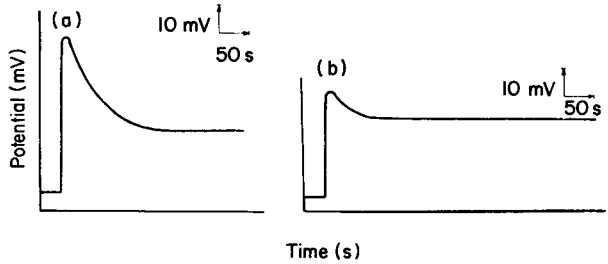

Fig. 3. Fluoride potentiometric outputs corresponding to solutions of Type 4 (Table 6) after addition of sodium fluoride: (a) at pH 2.75; (b) at pH 4.50. Total aluminium content, 186.21 μmol l^{-1}. For (a), the main features of the ALSPEC output are as follows. Vector of F^- concentrations at successive times: 0.019 0.030 0.107 0.063 0.040. Vector of interval reaction rates: 0.260 0.131 0.044 0.022 0.010. Al species as fraction of total Al: 0.528 0.000 0.000 0.000 0.000. For (b): Vector of F^- concentrations at successive times: 0.181 0.263 0.389 0.338 0.323. Vector of interval reaction rates: 0.170 0.083 0.027 0.014 0.006. Al species as fraction of total Al: 0.310 0.121 0.043 0.000 0.000.

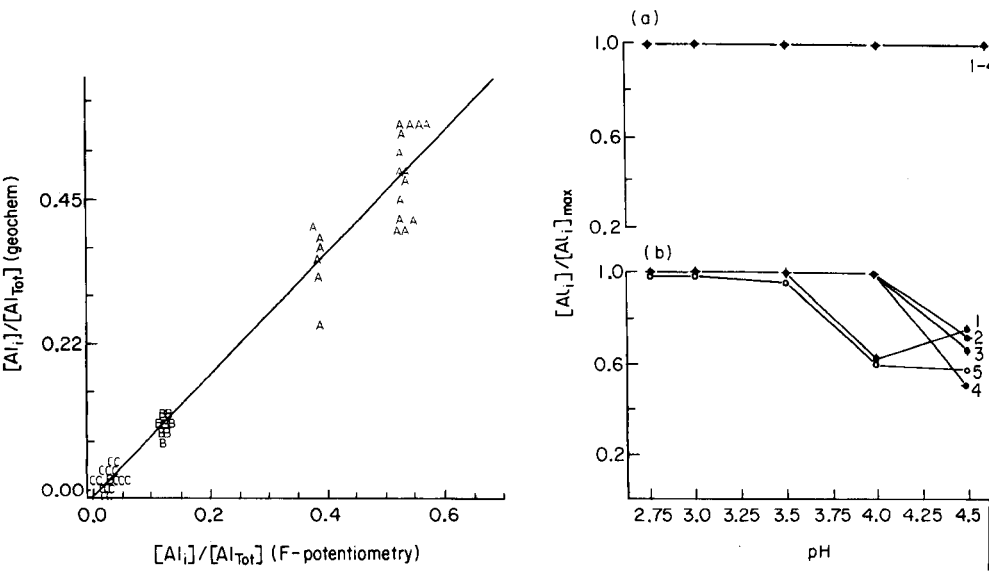

Fig. 4. Scatter diagram of distribution of Al species in solutions of Type 4 (Table 6) as computed with GEOCHEM and estimated by the potentiometric method. A—C as in Fig. 2.

Fig. 5. Free ionic fractions of several hydrolyzed aluminium species as a fraction of the theoretical maxima, in the presence of dilute solutions of Schnitzer's fulvic acid, in the pH range 2.75—4.75. $[Al]_{tot}$: (a) 22.4 μmol l^{-1}; (b) 173.8 μmol l^{-1}. Curves: (1) Al^{3+}; (2) $AlOH^{2+}$; (3) $Al(OH)_2^+$; (4) $Al_2(OH)_2^{4+}$; (5) sum of all Al complexes.

ALSPEC. Table 8 shows the compositions of two sample solutions at pH 2.75 and 4.50, and Fig. 3 the corresponding potentiometric output; part of the ALSPEC output is given in the legend. The correlation of the observed and

calculated values (Fig. 4) is good and the scatter around the regression line is similar to that observed in previous cases. This suggests that the presence of the stable aluminium/citrate complexes does not interfere with the usual Al/F kinetics in pure solutions. Although the existence of citrate in natural waters is unlikely, carboxylic binding sites are certainly important and citric acid should mimic some naturally occurring ligands. The pattern of Al/citrate complexation here assumed is simple [16] but the results obtained agree well with earlier data [5].

Systems of Type 5 (Table 6). The fulvic acid obtained shares properties of both weak organic acids and polyelectrolytes (see, e.g., [17]). Equilibria involving this material could be considered in terms of a series of weak acids with different acidity constants and metal complexes with varying stability constants. However, the uncertainties about the distribution of mole fractions and the dependence of these approximate constants on pH and ionic strength would render this exercise of little value. A direct comparison of the stability of aluminium/fulvic acid complexes is possible with the data of Schnitzer and Skinner [18], who estimated the amount of aluminium extracted by different known ligands, including hydroxide, in water, in the presence of 50 mg of aluminium/fulvic acid complexes at pH 5. Under these conditions, all complexing agents extracted more aluminium from complexes with lower Al/fulvic acid ratios than from complexes with higher ratios. With ratios similar to those used here, water extracted about 60% of the total aluminium at pH 5.0.

Figure 5 shows the results of equilibrating Schnitzer's fulvic acid (FA) with solutions containing a total Al concentration of 22.4 μmol dm^{-3} (Al/FA ratio = 0.07, assuming a molecular weight of 951 for fulvic acid [19]) or 173.78 μmol dm^{-3} (Al/FA = 0.55). As expected [18], more aluminium was extracted by hydroxide bonding in the former solution. In the latter solution, water extracted about 58% of the total aluminium at pH 4.5, in good agreement with the 60% mentioned above.

The trends observed in Fig. 5 are consistent with the properties of fulvic materials as weak acids. Gamble [17] concluded from electrometric titrations that fulvic acid behaves like low-molecular-weight weak polyelectrolytes. The mass-action coefficients K_1 and K_2 given [17], which correspond roughly to apparent dissociation constants, indicate that at pH 2—3 the dissociation of acid groups in these molecules is considerably lower than that observed at pH 4–5. In humic substances extracted from Smith Lake, Wilson and Kinney [20] reported that the dissociation of carboxylic groups is less than $\alpha = 0.17$ below pH 4.00, and that of phenolic groups attained this value at pH 9.5. According to Schnitzer and Khan [21], the formation of a metal complex usually involves the displacement of hydrogen ions from the ligand. Thus at low pH, protons would compete with metal ions for binding sites in these complex polyelectrolytes, and so binding of aluminium to fulvic acid would be effectively reduced. This situation also occurs with citric acid, where 0.1, 0.01 and 0.001 M concentrations result in approximately the same amount of complexation at pH 2.75, 3.5 and 4.5, respectively.

Systems of Type 6 (Table 6). Figure 6 shows the potentiometric outputs for soil equilibrium extracts from unfertilized plots, before and after contact with the ion-exchanger. As reflected in the large F_j^- increase, the exchange resin extracted a considerable amount of aluminium from the soil solutions. Values of total aluminium (determined by a.a.s.) give a better estimate of the amount of aluminium extracted (Fig. 7a). The treatment with the cation-exchanger produces other changes in the system; some organic carbon is retained in the exchanger, and the pH increases by about one because of the Al/Na exchange. In the extracts from the fertilized plots, the amount of aluminium in the extract is lower because of replacement of aluminium by calcium in the soil exchange matrix. In both extracts, the total amount of aluminium is reduced to about 20% of its original value after contact with the

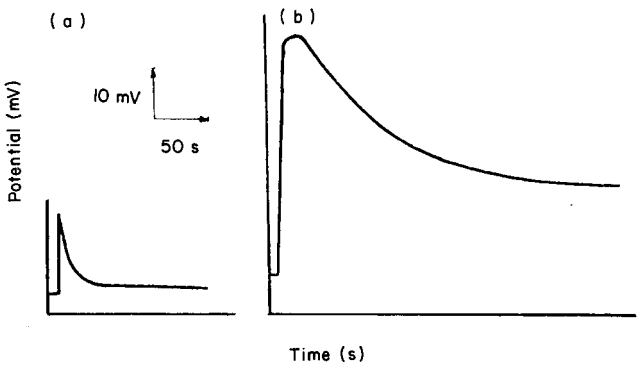

Fig. 6. Fluoride potentiometric outputs corresponding to soil water extracts before (a) and after (b) treatment with the ion-exchanger, after addition of sodium fluoride. (a) pH 3.20, total Al content, 1819.7 μmol l^{-1}; (b) pH 4.70, total Al content, 295.12 μmol l^{-1}. The ALSPEC output is analogous to that given in the legend to Fig. 3.

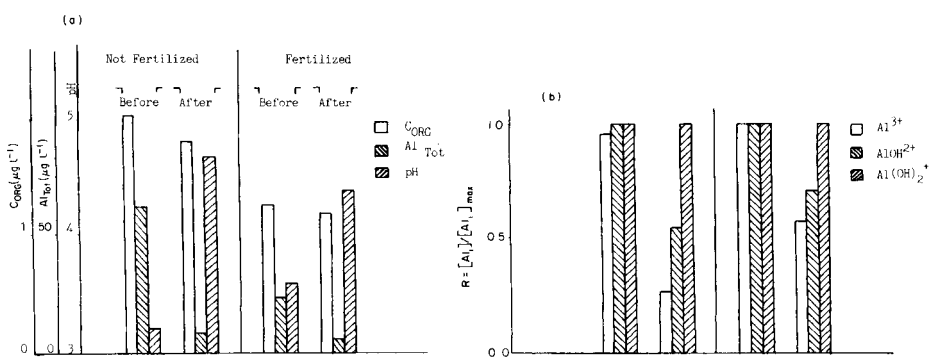

Fig. 7. Results for soil water extracts including treatment with the ion-exchanger. C_{org} is organic carbon, measured with a Beckman 015-B Carbon Analyzer. Before and after refer to the treatment with the ion-exchanger. The order of treatment in (b) is the same as that given in (a).

ion-exchanger. The free fraction of positively-charged hydrolyzed aluminium species would react more readily with the resin than organically-complexed aluminium, resulting in a depletion of free ionic species.

Figure 7(b) shows the results obtained with ALSPEC for these samples; before the resin treatment, about 96% of the total aluminium was in the free form. After resin extracts, however, only about 25% of the theoretical maximum of Al^{3+} is free, along with about 50% of $AlOH^{2+}$. If the organic ligands in these extracts behaved in a similar way to that observed in the case of Schnitzer's fulvic acid, then it would be expected that an increase in pH of the magnitude observed would favour complexation by the organic matrix during contact with the resin. The relative order $Al^{3+} \leqslant AlOH^{2+} \leqslant Al(OH)_2^+$ is in agreement with the expectation that the retention by the resin is proportional to the charge on the ion.

Systems of Type 7 (Table 6). Figure 8 shows the results obtained with ALSPEC in describing speciation of aluminium in solutions prepared with materials recovered by ultrafiltration of lysimeter water. In these solutions, most inorganic anions are absent because of the filtration procedure, and the percentage complexation observed is probably entirely due to organic ligands. The qualitative behaviour of these extracts as inspected with ALSPEC is comparable to that of Schnitzer's fulvic acid and the above soil water extracts,

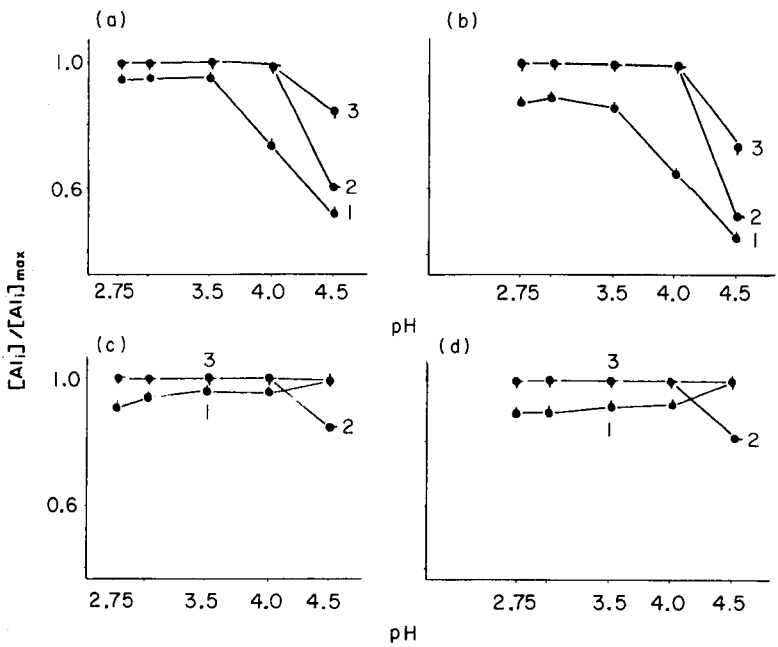

Fig. 8. Complexation of aluminium as a function of pH in solutions of Type 7 expressed as a fraction of the theoretical maximum at the given pH. (a) *Picea* stand with total Al content of 93.3 μmol l^{-1}; (b) *Fagus* stand with total Al content of 107.7 μmol l^{-1}; (c) *Picea* stand with total Al content of 1862.5 μmol l^{-1}; (d) *Fagus* stand with total Al content of 1870 μmol l^{-1}. Curves: (1) Al^{3+}; (2) $AlOH^{2+}$; (3) $Al(OH)_2^+$.

where significant complexation occurs at pH > 3.5. Type 7 solutions, however, show an overall greater complexing capacity for aluminium than Schnitzer's fulvic acid, probably reflecting the fact that the extraction procedure used here is less drastic than that used in conventional fulvic acid extractions, and would better preserve the structural properties of the organic colloidal matrix.

Conclusions

The *n*-dimensional calibration of the Al/F complexing pathway as inspected by potentiometric measurements of fluoride [4] furnishes a good fit with the theoretical speciation of aluminium in solutions where pH and aluminium concentration vary within the usual limits for acidic natural waters. Given the high stability of Al/F complexes, even in the presence of many other metal ions and ligands, the calibration coefficients can be used to speciate aluminium in samples of acidic natural waters. Possible interferences resulting from the presence of ligands which are not considered in the calibration procedure but are common in natural waters, are explored by a study of the effects of sulfate (as an example of a naturally occurring weak ligand) and citric acid (a strongly-complexing organic ligand). The results obtained with these mixtures, and with Schnitzer's fulvic acid, indicate that there are no significant departures from the calibration surfaces developed in the absence of these ligands, i.e., the Al/F complexation occurs essentially through mechanisms involving the aquated and hydrolyzed forms of aluminium.

The numerical problem of computing an aluminium species vector from the information stored from the potentiometric fluoride measurements can be solved in terms of a linear programming procedure under suitable constraints; these are given by the maxima expected to occur in aqueous solutions, depending on the given pH and total concentration of aluminium with due consideration of the complexing ability of hydroxide ions for aluminium ions. The combination of potentiometric measurement of fluoride with existing software allows the speciation of aluminium in acidic waters by a procedure which does not alter the structure of the organic colloidal matrix. The ALSPEC procedure may be useful in examining the naturally occurring patterns of aluminium species in the presence of highly complicated organic ligands.

The author thanks Dr. M. Spiteller for many valuable discussions and for supplying the sample of Dr. Schnitzer's fulvic acid and lysimeter water filtrates. Norman Loftfield did the ion-exchange experiments. The ALSPEC software was developed at the GWDB Computer Center with frequent support from their consulting service.

The results here shown were obtained while the author was an Alexander von Humboldt fellow at the University of Göttingen.

REFERENCES

1 E. Brenes and R. W. Pearson, Soil Sci., 116 (1973) 295.
2 M. A. Pavan and F. T. Bingham, Soil Sci. Soc. Am. Journal, 46 (1982) 983.
3 J. P. Baker and C. L. Schofield, Water, Air, Soil Pollut., (1982) 18.
4 J. Ares, Anal. Chim. Acta, 187 (1986) 181.
5 K. F. Kwong and P. M. Huang. Soil Sci., 128, 6 (1970) 337.
6 G. Sposito and S. V. Mattigod, GEOCHEM, Dept. Soil Environ. Sci., Riverside, CA, 1981.
7 W. L. Lindsay, Chemical Equilibria in Soils, Wiley, New York, 1979.
8 C. F. Baes and R. Mesmer, The Hydrolysis of Cations, Wiley, New York, 1976.
9 H. M. May, A. A. Hemke and M. L. Jackson, Chem. Geogr., 24 (1979) 259.
10 J. D. Hem, Georgr. Surv. Water, Suppl. Paper 1827-B, Washington, 1968.
11 M. Schnitzer and J. G. Desjardings, Soil Sci. Soc. Am. Proc., 26 (1962) 362.
12 M. Schnitzer and E. H. Hansen, Soil Scl., 109, 6 (1970) 333.
13 J. A. Marinsky and S. Gupta, Colloid Interface Chem., 89 (1982) 412.
14 H. W. Fassbender and E. Ahrens, Gott. Bodenk. Ber., 47 (1977) 1.
15 R. H. Bartels, A. R. Conn and J. W. Sinclair, SIAM J. Numer. Anal., 25 (1978) 224.
16 W. Knoche and A. M. Lopez Quintela, Thermochim. Acta, 62 (1983) 295.
17 D. S. Gamble, Can. J. Chem., 48 (1970) 2662.
18 M. Schnitzer and M. Skinner, Soil Sci., 98, 3 (1963) 197.
19 E. H. Hansen and M. Schnitzer, Anal. Chim. Acta, 46 (1969) 241.
20 D. E. Wilson and P. Kinney, Limnol. Oceanogr., 22, 2 (1977) 281.
21 M. Schnitzer and S. U. Khan, Humic Substances in the Environment, M. Dekker, New York, 1974, Chap. 6.

Analytica Chimica Acta, 187 (1986) 213—222
Elsevier Science Publishers B.V., Amsterdam — Printed in The Netherlands

MINICOMPUTER-BASED INSTRUMENTATION FOR ELECTROANALYTICAL TECHNIQUES

S. STEFANI

Dipartimento di Matematica dell'Università di Siena, Via del Capitano 15, 53100 Siena (Italy)

R. SEEBER*

Dipartimento di Chimica dell'Università di Siena, Pian dei Mantellini 44, 53100 Siena (Italy)

(Received 10th February 1986)

SUMMARY

The system comprises a PDP 11/23 PLUS (16-bit) computer and a home-made electrochemical interface which includes digital/analog and analog/digital conversion circuits, a potentiostat, and programmable timers allowing fast data transfer. The software developed includes operating system routines and user-level programs for cyclic voltammetry and chronoamperometry. The whole system provides the user with a computer-aided execution of experiments, including potential waveform synthesis and collection and evaluation of responses.

The development of modern electroanalytical techniques has been strongly linked with the evolution of automated instrumentation. First efforts in this direction [1—3] involved physical control of the experiment and data collection by numerical selectors, patchboard connectors, digital voltmeters, paper punches, etc. An alternative approach was based on programmable digital computers [4, 5] and has become more and more popular with the development of the digital electronic technology. Two main trends can be identified in this context; in the first, programmable digital hardware is used at board level (i.e., microcomputer boards and related modules) whereas in the second, standard minicomputers are used with operating system and utility software. The first type includes a broad spectrum of hardware systems ranging from inexpensive microprocessors [6—11] to a full modular assembly of several microcomputer boards [12—15], and data-acquisition systems supported by a personal computer [16, 17]. The second type reflects the general tendency to use minicomputers in electrochemistry [18—30]. The acknowledged advantages of using computerized electrochemical equipment has led to commercial instrumentation [31].

The importance of computers in the control of electrochemical instrumentation, as well as in the interpretation of experimental data, has been emphasized [32, 33]. In this context, direct interfacing of a potentiostat with a

0003-2670/86/$03.50 © 1986 Elsevier Science Publishers B.V.

minicomputer which is also capable of performing sophisticated digital signal processing is attractive. Although the production of a flexible system implies a notable effort in hardware and software development, once this has been done, electroanalytical measurements with quite sophisticated techniques are easily performed. The system described here is based on a PDP 11/23 PLUS (Digital Equipment Corporation) computer. This choice was made because this minicomputer family is widely available and is well documented.

SYSTEM DESCRIPTION

Computer hardware

The computer configuration, equipped with the RSX-11M operating system, is based on a LSI-11 CPU with memory management unit (KDF11-BA), completed by a MSV11-PL (512 kbyte) memory, a FPF11 floating-point processor, two RL02 disk drives served by a RLV12 disk controller, and a DLV11-J 4-channel (RS232C) asynchronous serial line unit module. Three video terminals (VT100 compatible), a LA-120 printer, and a digital plotter (Calcomp M84) are also part of the system. This constitutes quite a standard configuration for a PDP-11/23 PLUS system. The presence of the floating point processor is useful for performing non-trivial computations.

The external electrochemical interface is connected to the CPU via a DRV11-J parallel interface, located in a slot as near as possible to the CPU board.

Electrochemical interface

The electrochemical interface is produced as a standard 19-in. rack unit, where the relative power supplier and the potentiostatic module are also located. The role of the interface made here is to link the digital domain of the computer system with the analog input and output of a potentiostat connected to an electrochemical cell. The interface also provides timing to control the data transfer and generates interrupt requests to the computer. In addition, it allows the computer to know the status of any potentiostat control knobs set by the operator.

Figure 1 shows a block diagram of the interface, illustrating its internal organization. The internal bus adapter (IBA) interfaces the DRV11-J parallel ports to the instrument data buses and to the lines controlling the transfer of data. Two ports of DRV11-J provide the 16-bit paths, which correspond to the output and input internal bus, respectively. This configuration allows input and output data to be transferred simultaneously. In addition, this adapter module controls the generation of the interrupt pulse, which arrives at the computer through the DRV11-J. Finally, some additional control lines, from the computer to the electrochemical interface, are connected to a third port of the DRV11-J.

The board devoted to digital-to-analog conversion (DAC, pipeline registers PR) is based on a 18-bit DAC-1146 (Analog Devices), which supplies the

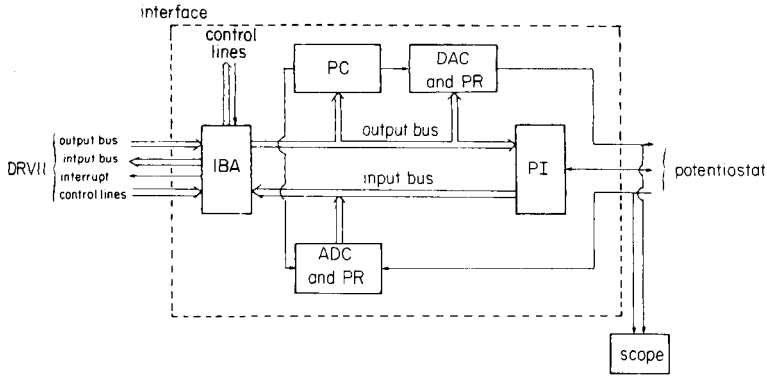

Fig. 1. Block diagram of the electrochemical interface.

potentiostat with a voltage in the range −10 to +10 V. This component is accurate enough to guarantee monotonicity at a 16-bit level, without the need for any special adjustment; in this way, the 16-bit digital value can be translated into an analog signal without any loss of accuracy. Furthermore, in order to operate with electrochemical techniques requiring continuously varying potentials, and therefore a great number of small potential increments, it can be useful to have a deglitching circuit to remove the short transient arising whenever the DAC bits change. A dual rank of 16-bit registers completes the DAC board; the first is used as a buffer for the data coming from the computer, and the second holds the data present in the input of the DAC.

The board performing analog-to-digital conversion (ADC, pipeline registers) uses a 12-bit A/D HS12B (Datel) converter. This module includes a sample-and-hold circuit and converts the analog input, spanning the −5 to +5 V range, in a time of 8 μs. In addition to the necessary "glue circuits", the same board carries one 16-bit register freezing the current range value and the ADC output, so that the computer can read the input data at an arbitrary instant of the instrument cycle. A further bit of this latch reports on any overload status of the potentiostatic circuit.

The programmable clock card (PC) consists of a 1-MHz reference oscillator and of two programmable timers, both constituted by a 16-bit programmable counter with associated preset register. These timers govern the period of the instrument cycle and the delay between a DAC output and the subsequent ADC sampling. Of course, the delay will be shorter than the instrument cycle period.

A home-made potentiostatic circuit is included in the same interface box. It is constructed in the conventional three-electrode configuration, with iR drop compensation. The input of the potentiostat is connected to the D/A converter, so that the working potential is directly governed by the DAC output, without the need of any additional preset. Manual control knobs of the potentiostat are located on the front panel of the electrochemical

interface box. The current range can be set through two switches. The first selects the feedback resistance of the current follower, within a set of five values in 1:10 ratios; the second selects a further gain equal to 1, 2, or 5. The position of these switches can be read by the computer via the potentiostat panel interface P (PI). A four-position switch and a multi-turn potentiometer allow coarse and fine adjustment of the iR drop compensation. Through a further knob it is possible to insert first-order low-pass filters between the D/A and A/D converters and the potentiostat. The time constant of the filters is either 20 or 200 μs. A 4½-digit panel meter is placed on the front of the box; a switch allows the most significant analog test-points of the equipment to be monitored. Three LEDS and three on/off switches are configured as write and read registers, respectively, being accessible by the computer. For example, the position of one switch can be controlled by the software in order to allow the experiment to start.

The interface can operate in two different modes, the presetting mode (p-mode) and the run mode (r-mode), selected by the software, in a way not visible to the user, for performing the different transfer operations. A similar organization is suggested by the need to achieve high speed in the data transfer from and to the computer during an experiment; this also allows the use of quite complicated waveforms and the collection of rapid transients. In the r-mode, the interface acts as master of the computer: its timers control data transfer and requests for interrupt services, with the sole constraint that the instrument cycle (i.e., the time interval between consecutive interrupt requests) cannot be less than the time required by the software driver, under RSX-11M operating system, to perform the service.

Figure 2 is a schematic diagram of the pipeline organization assumed by the interface which operates in the r-mode. It can be observed that, at any time, three consecutive data values are present within the interface. Their flow is controlled by the instrument cycle, τ, and by the output delay, δ. In response to an interrupt request generated by a given clock pulse, the

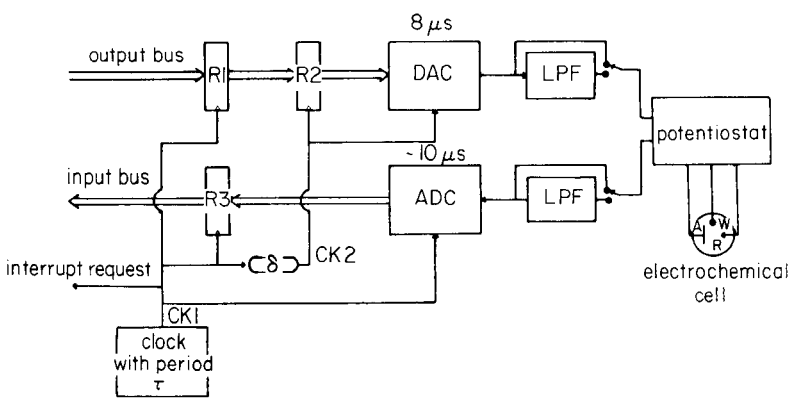

Fig. 2. Diagram of the basic organization of the data flow in the electrochemical interface.

computer presents a datum in the input to the R1 register. The subsequent clock pulse transfers this value to the same register and after a time δ ($\delta < \tau$) the datum advances into the R2 register. After a fixed conversion delay of 8 μs, the corresponding analog value reaches the potentiostat. The electrochemical cell response is sampled in correspondence with the subsequent clock pulse and, after about 10 μs required by the analog-to-digital conversion, the datum is present in the input to the R3 register. A third clock pulse transfers the datum into the same latch, making it available to the computer. It follows that the computer may transfer the data to and from the parallel interface at any instant in a τ period, without any additional constraint.

The time diagram in Fig. 3 summarizes the operation of the data pipeline described above. In particular, the time interval between the change in the output value on the DAC (i.e., on the potentiostat) and the subsequent sampling is given by $\delta' = \tau - (\delta + 8\ \mu s)$. Thus, varying the δ value in the interval 0—τ makes it possible to change the DAC output at any instant within the instrument cycle period. Therefore, if the response is reproducible, it is possible to synthesize a current/time curve with a sampling frequency as high as 1 MHz. This can be achieved by merging a suitable number of interleaved data sequences obtained by repeating the experiment with δ values scaled by 1 μs.

By operating in *p*-mode, it is possible to preset the values of τ and δ. It is also possible to write a single output datum on the D/A converter, to start

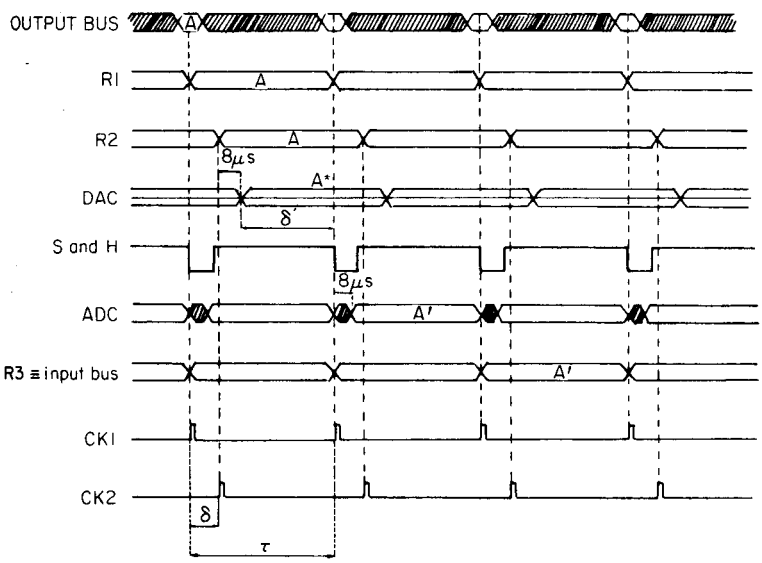

Fig. 3. Time diagram of the *r*-mode operation. The lines relative to R1, R2, DAC, ADC, and R3 refer to the corresponding outputs. S & H is the sample-and-hold control (the low level is the hold state). A is an output digital datum, A* the equivalent analog datum, and A' the corresponding input digital datum. In correspondence to the dashed regions, data are not defined.

the A/D conversion and to read the resulting value. Finally, one can read and write the instrument panel status. In summary, the software used by the experimenter operates in the *p*-mode to preset the interface timing, to obtain the actual current range, and to receive the start command; the program switches to the *r*-mode to run the electrochemical experiment.

Low-level software

Two types of software are required to interact with the electrochemical experiment. The organization of the software is outlined in Fig. 4. The low-level software, written in MACRO-11 assembly language, is a set of modules which supervise the input-output operations occurring through the DRV11-J parallel interface and implements a family of I/O primitives. The second type corresponds to the application level, and uses the above-mentioned primitive operations to perform the proper electrochemical experiment. The most notable part of the low-level software is the so-called "I/O driver", which is incorporated in the RSX-11M operating system. A suitable I/O driver was not available from the computer supplier, thus a driver tailored to the required applications was written. The driver is invoked by the executive, a part of the operating system, on request by the user's program. It provides a series of prescribed "entry points" to control the different steps of the I/O operations. The first entry point sets the configuration of the DRV11-J, the second initiates the different I/O operations, and the third constitutes the actual interrupt handler.

The I/O operations are of two different kinds. The first consists of reading or writing a single word in the appropriate register of the electrochemical interface (*p*-mode operation), and the second performs the timed I/O transfer of a whole data array (*r*-mode operation): subsequent points are sent to the potentiostat through the D/A converter, and these values are replaced by the output data of the A/D converter. Every point is transferred by the interrupt

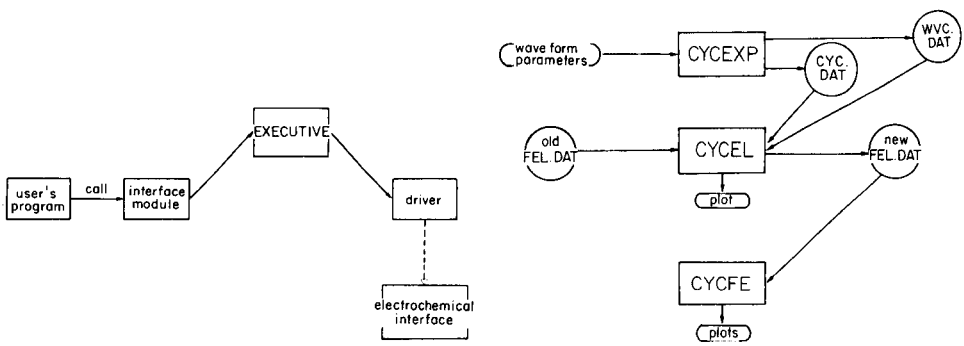

Fig. 4. Software handling of the instrument I/O.

Fig. 5. Connections between tasks and data files of the package of programs for running and evaluating cyclic voltammetric experiments.

handler, in response to an interrupt request generated by the programmable clock (see Fig. 2).

The low-level software is completed by a short module which is linked to the user's programs and translates the I/O operations invoked by the user through conventional subroutine calls into standard I/O requests, which make the executive activate the driver. This "software interface module" comprises three different subroutines, for writing a value in *p*-mode, reading a value in *p*-mode, and transferring data in *r*-mode.

Application software

As already stated, the system was constructed with the goal of providing great flexibility in running electrochemical experiments. In principle, it is also possible to perform experiments with unconventional potential waveforms. However, the first software packages developed are for cyclic voltammetry and chronoamperometry.

One package consists of three FORTRAN-77 programs devoted to cyclic voltammetry. The first program allows the user to run the experiment as follows: it generates one or more triangular waveforms, sends the array of potentials to the electrochemical cell and collects the current values; it writes these values, adjusted to the appropriate scale, on a disk file and writes a second file reporting the characteristics of the potential waveform. The second program reads these temporary disk files, extracts the significant parameters of the response and writes these on a further file dedicated to collecting a series of data referred to responses obtained at different potential scan rates. This program can also optionally apply a convoluting low-pass filter to the cell current data, smoothing the response if much noise is present. A 21-point filter with a cut angular frequency of $\pi/8$, designed by a Kaiser window for an overshoot of 20 dB, was used [34]. If a cut at a lower frequency is desired, the filtered response is down-sampled and then submitted to the same filter. This program also produces a plot of the current/potential curve. After a series of experiments has been completed, the third program derives the trends of the most typical parameters of the series of responses as a function of the corresponding potential scan rate and plots the relative diagrams on request. Figure 5 summarizes the relationships between the three programs and the files that they generate and use.

The second package consists of two programs for chronoamperometry. The first executes the chronoamperometric test, i.e., generates the potential step, collects the current (I) and time (t) data, and writes them on a disk file. The second program reads this temporary file, optionally applies a low-pass filter, calculates the $I\,t^{1/2}$ products, and optionally plots the I/t curve and/or the curve of $I\,t^{1/2}$ vs. t.

PERFORMANCE TESTS AND DISCUSSION

Figure 6 shows a cyclic voltammogram recorded with a platinum working electrode in an acetonitrile solution of bis(cyclopentadienyl)iron(II) with

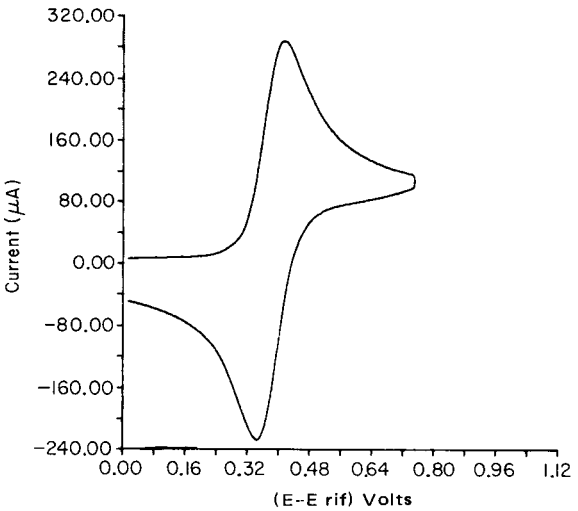

Fig. 6. Typical cyclic voltammetric curve (see text). The corresponding output information was as follows: potential scan rate, 3000 mV s^{-1}; forward peak current, 287.1 μA; peak current to square root of potential scan rate, 5.242; backward/forward peak height ratio, 1.059; forward peak potential, 0.414 V; backward peak potential, 0.345 V; forward peak width, 62 mV; peak potential difference, 69 mV.

0.1 M tetraethylammonium perchlorate as supporting electrolyte, using a three-electrode cell with suitable geometry. The response was obtained with analog iR-drop compensation, by using the 20-μs integrator in input to the ADC and by filtering the sampled response once with the low-pass finite-impulse-response filter. Similar satisfactory results were obtained at different potential scan rates, and in chronoamperometric tests.

Some details which have appeared to be of particular importance during the design and use of the instrument should be discussed. As regards generation of the waveform, the straightforward approach used here, based on a single D/A converter, requires some particular specifications to this component. When the waveform comprises small potential steps as in linear-sweep or cyclic voltammetry, the impedance characteristics of the electrochemical cell make it important to use a DAC with a small differential linearity and to keep spurious transients arising when the DAC output changes to a minimum; for this purpose, the deglitching circuit proved to be useful. Moreover, the insertion of a low-pass filter in the output of the DAC, as a "reconstruction filter" meeting the Nyquist criterion, allows the generation of continuously varying potential waveforms.

The potentiostatic unit built into the instrument, which was designed to meet conventional specifications, proved to be adequate in most cases, even where a faster potentiostat was necessary in order to exploit fully the characteristics of the interface. However, very fast time demands, e.g. in pulse techniques, will also often require particularly high current dynamics, and if reliable data are to be collected on the whole signal dynamics from a single

experiment involving potential pulses, a linear 12-bit A/D converter may be unsatisfactory. Obvious improvements consist of preceding the ADC with an autoranging amplifier [35], or with a suitable logarithmic amplifier. Further, in order to exploit the whole frequency bandwidth in techniques involving continuously varying potential, the characteristics of the output and input analog low-pass filters must be improved to cut more sharply near the Nyquist frequency.

When the computer interrupt is used under control of the RSX-11M operating system, the data-transfer frequency cannot be significantly higher than 5 kHz. Although this frequency is high enough for most applications, it can be increased almost tenfold if the CPU can be dedicated exclusively to data transfer during the running of the experiment. This would allow the range of available frequencies to be extended, so that techniques involving both a potential scan and superimposed perturbations which vary rapidly, e.g., digital a.c. polarography and faradaic admittance measurements based on pseudo random a.c. wave forms [36—39], staircase [40—42] and square-wave voltammetry [43—45], could be handled without any additional hardware. The use of the minicomputer makes it possible to elaborate the responses through sophisticated algorithms and to exploit quite rapidly the results obtained in order to plan subsequent experiments.

REFERENCES

1 E. R. Brown, D. E. Smith and D. D. DeFord, Anal. Chem., 38 (1966) 1130.
2 G. Lauer and R. A. Osteryoung, Anal. Chem., 38 (1966) 1137.
3 G. L. Booman, Anal. Chem., 38 (1966) 1141.
4 G. Lauer, R. Abel and F. C. Anson, Anal. Chem., 39 (1967) 765.
5 S. P. Perone, J. E. Harrar, F. B. Stephens and R. E. Anderson, Anal. Chem., 40 (1968) 899.
6 P. Barrett, L. J. Davidowski and T. R. Copeland, Anal. Chim. Acta, 122 (1980) 67.
7 A. M. Bond and A. Norris, Anal. Chem., 52 (1980) 367.
8 H.-Y. Cheng, W. White and R. N. Adams, Anal. Chem., 52 (1980) 2445.
9 J. E. Anderson and A. M. Bond, Anal. Chem., 53 (1981) 1394.
10 D. W. Paul, T. H. Ridgway and W. R. Heineman, Anal. Chim. Acta, 146 (1983) 125.
11 A. M. Bond, H. B. Greenhill, I. D. Heritage and J. B. Reust, Anal. Chim. Acta, 165 (1984) 209.
12 F. E. Woodard, W. S. Woodward and C. N. Reilley, Anal. Chem., 53 (1981) 1251A.
13 P. Baecklund and R. Danielsson, Anal. Chim. Acta, 154 (1983) 61.
14 H. Gunasingham, Anal. Chim. Acta, 169 (1985) 309.
15 D. Ph. Zollinger, M. Bos, A. M. W. Van Veen-Blaauw and W. E. Van Der Linden, Anal. Chim. Acta, 167 (1985) 89.
16 J. F. Price, S. L. Cooke, Jr., and R. P. Baldwin, Anal. Chem., 54 (1982) 1011.
17 S. C. Gates, Byte, May 1984, 366.
18 G. Lauer and R. A. Osteryoung, Anal. Chem., 40 (1968) 30A.
19 S. P. Perone, D. O. Jones and W. F. Gutknecht, Anal. Chem., 41 (1969) 1154.
20 H. E. Keller and R. A. Osteryoung, Anal. Chem., 43 (1971) 342.
21 S. C. Creason, R. J. Loyd and D. E. Smith, Anal. Chem., 44 (1972) 1159.
22 P. E. Whitson, H. W. VandenBorn and D. H. Evans, Anal. Chem., 45 (1973) 1298.
23 L. Kryger, D. Jagner and H. J. Skov, Anal. Chim. Acta, 78 (1975) 241.
24 Q. V. Thomas, L. Kryger and S. P. Perone, Anal. Chem., 48 (1976) 761.

25 K. F. Drake, R. P. Van Duyne and A. M. Bond, J. Electroanal. Chem., 89 (1978) 231.
26 H. J. Skov and L. Kryger, Anal. Chim. Acta, 122 (1980) 179.
27 D. Britz, Anal. Chim. Acta, 143 (1982) 95.
28 C. Y. Li, T. H. Barrett, Jr., D. Lunney and A. Salt, Anal. Chim. Acta, 134 (1982) 167.
29 J. Krawczyk, M. Lapkowski and J. W. Strojek, Anal. Chim. Acta, 152 (1983) 45.
30 M. Carlà, G. Aloisi, G. Papeschi and S. Bordi, J. Electrochem. Soc., 130 (1983) 1859.
31 P. He, J. P. Avery and L. R. Faulkner, Anal. Chem., 54 (1982) 1313A.
32 J. Osteryoung, Science, 218 (1982) 261.
33 P. He and L. R. Faulkner, J. Chem. Inf. Comput. Sci., 25 (1985) 275.
34 R. W. Hamming, Digital Filters, Prentice-Hall, Englewood Cliffs, NJ, 1977.
35 A. D. Salt and D. Lunney, Anal. Chem., 52 (1980) 2237.
36 J. E. Anderson and A. M. Bond, Anal. Chem., 53 (1981) 1394.
37 J. E. Anderson and A. M. Bond, Anal. Chem., 54 (1982) 1575.
38 S. C. Creason, J. W. Hayes and D. E. Smith, J. Electroanal. Chem., 47 (1973) 9.
39 R. J. Schwall, A. M. Bond, R. J. Loyd, J. G. Larsen and D. E. Smith, Anal. Chem., 49 (1977) 1797.
40 L. H. L. Miaw, P. A. Boudreau, M. A. Pichler and S. P. Perone, Anal. Chem., 50 (1978) 1988, and references therein.
41 S. Stefani and R. Seeber, Anal. Chem., 54 (1982) 2524.
42 R. Seeber and S. Stefani, Ann. Chim. (Rome), 75 (1985) 47.
43 L. Ramaley and M. S. Krause, Jr., Anal. Chem., 41 (1969) 1362.
44 J. H. Cristie, J. A. Turner and R. A. Osteryoung, Anal. Chem., 49 (1977) 1899.
45 S. Stefani and R. Seeber, Ann. Chim. (Rome), 73 (1983) 611.

Analytica Chimica Acta, 187 (1986) 223—231
Elsevier Science Publishers B.V., Amsterdam — Printed in The Netherlands

DETERMINATION OF BASIC AZAARENES AND POLYNUCLEAR AROMATIC HYDROCARBONS IN AIRBORNE PARTICULATE MATTER BY GAS CHROMATOGRAPHY

TORBEN NIELSEN* and PERAXEL CLAUSEN

Chemistry Department, Risø National Laboratory, DK-4000 Roskilde (Denmark)

FINN PALMGREN JENSEN

Danish Air Pollution Laboratory, National Agency of Environmental Protection, DK-4000 Roskilde (Denmark)

(Received 11 February 1986)

SUMMARY

Polynuclear aromatic hydrocarbons (PAH) and their nitrogen analogs, basic azaarenes, are extracted from samples of airborne particulate matter by toluene with ultrasonic treatment. The basic azaarenes are extracted from the toluene phase with phosphoric acid, re-extracted from the phosphoric acid phase (adjusted to pH 14 with potassium hydroxide) with dichloromethane, and determined by capillary gas chromatography (g.c.) with a nitrogen-sensitive detector. The PAH in the toluene phase are isolated by means of semi-preparative high-performance liquid chromatography and liquid-liquid extraction and determined by g.c. with a flame-ionization detector. Eleven basic azaarenes were identified; their concentrations were one to two orders of magnitude lower than those of PAH. Results from the determination of the concentrations of basic azaarenes and PAH in the atmosphere in a busy street and in a suburban residential area of Copenhagen are presented and discussed.

Polynuclear aromatic hydrocarbons (PAH) are formed in combustion processes [1] and are ubiquitous in environmental samples [2—6]. Their nitrogen analogs, the basic azaarenes, which have a C—H in the aromatic ring system replaced by a nitrogen atom have been investigated to a lesser extent, but azaarenes have been demonstrated to be present in stack gases from coal combustion sources [7], industrial source effluents [7], automobile exhaust gases [8], airborne particulate matter [9—15], water samples [16], and marine sediments [17, 18] which indicates that they are formed by combustion processes as PAH are. The presence of basic azaarenes in polluted air contributes to the carcinogenic and mutagenic effects of airborne polynuclear oganic matter [19]. It was postulated in older investigations [7—9] that the emission of azaarenes compared to that of PAH is source-dependent, implying that the azaarenes/PAH ratio perhaps could be a useful indicator for some atmospheric pollution sources. It is, therefore, desirable to have available simple and sensitive analytical techniques to determine the complex

0003-2670/86/$03.50 © 1986 Elsevier Science Publishers B.V.

mixture of azaarenes in environmental samples and to unravel thoroughly their presence in different sources and in the atmosphere. Azaarenes have been identified and quantified by the following techniques: high-performance liquid chromatography (h.p.l.c.), thin-layer and liquid-solid chromatography with u.v. absorbance and fluorescence detection [7—9, 12, 14]. None of these techniques is appropriate, however, for an extensive and detailed investigation of the complicated fraction of azaarenes in environmental samples.

Capillary gas chromatography (g.c.) is the most promising method for analysis of complex mixtures of azaarenes, and has been utilized with flame-ionization and mass-spectrometric detection for determining azaarenes in samples of sediments [17], cannabis smoke [20], coal tar [20] and wastewater [21]. Gas chromatography with a nitrogen-sensitive detector has been used for the analysis of samples of sediments [18], street dust [18] and synthetic fuels [22]. The work-up procedures required several liquid chromatographic steps.

This paper describes a relatively simple, selective and sensitive method for determining basic azaarenes. The method was utilized for small samples (300—500 m^3) of airborne particulate matter. The basic azaarenes are isolated by liquid-liquid extraction and quantified by capillary g.c. with nitrogen-sensitive detection. In addition to the azaarenes, the PAH are isolated by a combination of h.p.l.c. and liquid-liquid extraction and determined by g.c. with flame-ionization detection. The major implications of the results are discussed briefly.

EXPERIMENTAL

Sample collection and analysis for inorganic matter

Samples of suspended particulate matter were collected on membrane filters (cellulose nitrate) with a pore size of 1.2 μm by a medium-volume air sampler. Approximately 60 m^3 of air was sucked through a filter area of ca. 12 cm^2 during 24 h. The amount of particulate matter was determined gravimetrically. Portions of the filter were analyzed by proton-induced x-ray emission (p.i.x.e.) [23], to determine the concentrations of elements with atomic number greater than 13. Simultaneously, the concentration of sulphur dioxide was determined by the standard OECD method [24].

Procedures

Extraction. Approximately 4 μg each of *p*-terphenyl and β,β'-binaphthyl and 0.4 μg of 10-azabenzo(a)pyrene were added as internal standards to samples of airborne particulate matter corresponding to a typical volume of about 400 m^3 of air (14 half-filters). The samples were extracted from the filters ultrasonically by three 30-min treatments with 25 ml of toluene (Merck, Uvasol) each time. The toluene extracts were combined and concentrated to 5—10 ml in a rotary evaporator and to 2.0 ml by gentle evaporation with purified N_2.

Isolation of basic azaarenes. The isolation of basic azaarenes is outlined in

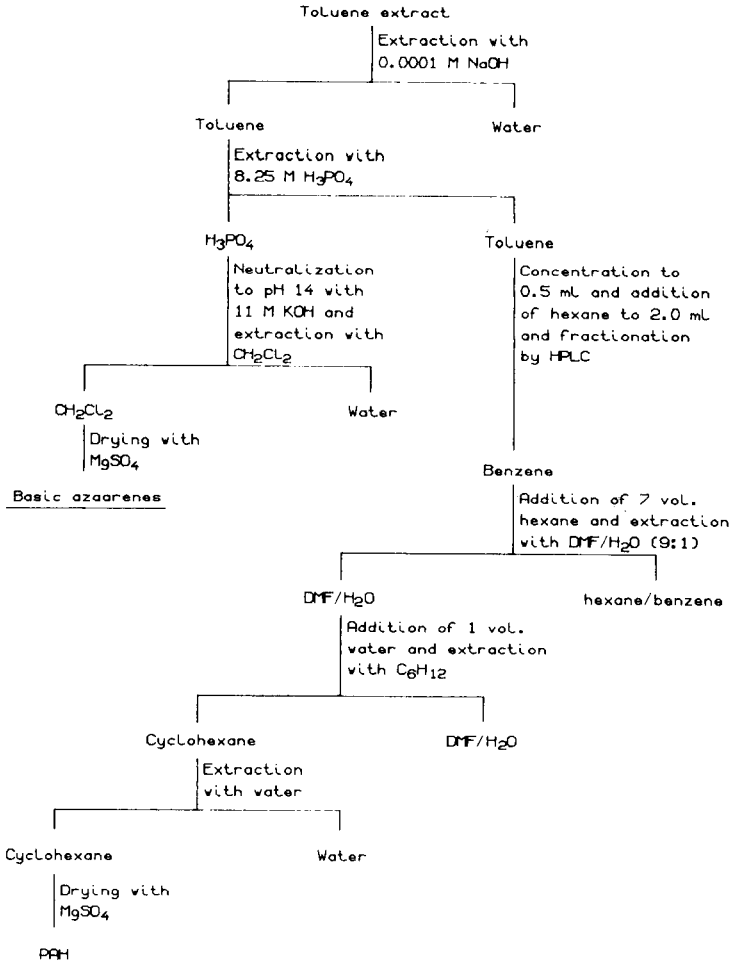

Fig. 1. Outline of the fractionation procedure for the isolation of basic azaarenes and PAH. For details, see text.

Fig. 1. Inorganic compounds (nitrate, nitrite, and sulphate) were extracted with 2.0 ml of 10^{-4} M sodium hydroxide (Merck, p.a.) by shaking for 30 min in order to avoid nitration or sulphonation of reactive PAH in the next step [25, 26]. The basic azaarenes in the toluene phase were then extracted with two 2.0-ml portions of 8.25 M phosphoric acid (Merck, p.a.) by shaking for 30 min each time. After this, the toluene phase still contained the PAH. The phosphoric acid phases were combined and adjusted to a pH of ca. 14 with about 9 ml of 11 M potassium hydroxide (Merck, p.a.) in an ice bath. The azaarenes were extracted from the alkaline aqueous phase with three 2.0-ml portions of dichloromethane (Merck, Lichrosolv) by shaking for 30 min each time. The combined dichloromethane extracts were dried with magnesium sulphate (Fisher, certified) and concentrated to 0.1 ml. Then 100 μl of

toluene was added and the mixture was concentrated to 0.10 ml in order to remove most of the dichloromethane. The samples were stored at −18° C until the amounts of basic azaarenes were determined by g.c. (see below).

Isolation of PAH. The isolation of PAH is also outlined in Fig. 1. The toluene phase containing the PAH including other organic compounds was concentrated to 0.5 ml by evaporation with N_2 and diluted to 2.0 ml with *n*-hexane (Merck, zur Rückstandsanalyse). The *n*-hexane/toluene solution was fractionated by means of h.p.l.c. on silica gel columns (Nucleosil Si-50-5; 12 cm × 4.6 mm/25 cm × 8.0 mm) with 3:1 *n*-hexane/benzene (Merck, Lichrosolv) eluent. The flow rate was 3.0 ml min^{-1}. The PAH fraction (3–7 rings) was collected. The h.p.l.c. fractionation procedure has been described in more detail elsewhere [27]. The PAH fraction from the cellulose nitrate filter samples, however, contained large amounts of unknown compounds which affected the gas chromatography of PAH with the flame ionization detector. The PAH fraction was, therefore, cleaned up by a modification of the extraction procedure of Bjørseth [28]. The collected PAH fraction was concentrated to 0.25 ml and 1.75 ml of *n*-hexane was added. The *n*-hexane/benzene solution was extracted with three 2.0-ml portions of 1:9 water/dimethylformamide (Fluka, p.a.) by shaking for 10 min each time. Then 6.0 ml of water was added to the combined dimethylformamide/water phases, and the solution was extracted with three 2.0-ml portions of cyclohexane (Merck, zur Rückstandsanalyse) by shaking for 10 min each time. The combined cyclohexane phases were washed with 0.5 ml of water by shaking for 10 min, dried with magnesium sulphate, and concentrated to 0.5 ml.

The PAH samples were also stored at −18° C until the amounts of PAH were quantified by g.c. with a flame ionization detector.

Gas chromatography of basic azaarenes and PAH. The gas chromatograph (Carlo Erba 2900) was equipped with on-column injection and flame ionization and nitrogen-sensitive detectors, and was connected to a Kipp-Zonen BD-9 recorder. The fused silica column used for the separation of PAH and basic azaarenes (Ultra-1; 25 m × 0.32 mm i.d.; Hewlett-Packard) was programmed for 71—300° C at 7° C min^{-1}. Figure 2 shows a chromatogram of a sample of basic azaarenes from airborne particulate matter.

RESULTS AND DISCUSSION

Extraction of basic azaarenes in airborne particulate matter

Ultrasonic extraction of basic azaarenes from airborne particulate matter with toluene, dichloromethane and acetone as solvents were tested as follows: 40.0 ml of the solvent and a solution containing ca. 4 mg of each of the nine basic azaarenes [quinoline, 6-methyl- and 2,6-dimethylquinoline, 4-azafluorene, 7,8-benzoquinoline, acridine, 5,7-dimethylbenz(a)acridine, 10-azabenzo(a)pyrene, and dibenz(a,h)acridine] were added to identical filter samples of airborne particulate matter corresponding to about 1000 m^3 of air. The filter samples were extracted ultrasonically for 30 min, and the

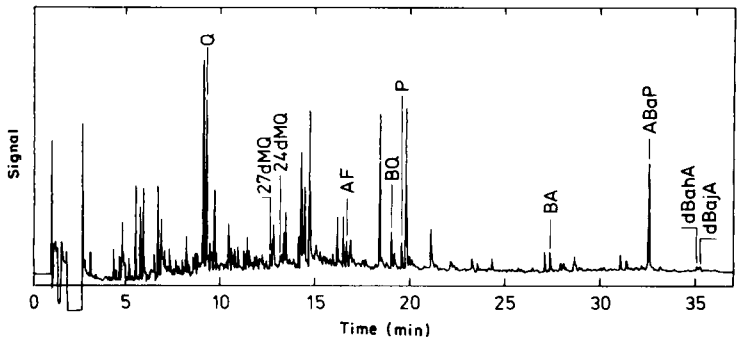

Fig. 2. Gas chromatogram with nitrogen-sensitive detection of the basic azaarenes in a sample of airborne particulate matter. Identity of the peaks: (Q) quinoline; (27dMQ) 2,6- and 2,7-dimethylquinoline; (24dMQ) 2,4-dimethylquinoline; (AF) 4-azafluorene; (BQ) 7,8-benzoquinoline; (P) phenanthridine and 5,6-benzoquinoline; (BA) 3,4-benzacridine; (ABaP) 10-azabenzo(a)pyrene (internal standard); (dBahA) dibenz(a,h)acridine; (dBajA) dibenz(a,j)acridine.

extracts were filtered and analyzed directly without further treatment. The recoveries (mean ± 2 σ) of the nine basic azaarenes (duplicate experiments) were 90 ± 5, 80 ± 13, and 57 ± 12% using, respectively, toluene, dichloromethane, and acetone as solvents. Thus, toluene is the most suitable solvent for extraction of basic azaarenes.

Isolation of basic azaarenes

The extraction of twelve basic azaarenes [quinoline, 6-methyl-, 2,6-dimethyl- and 2,4-dimethylquinoline, 4-azafluorene, 7,8-benzoquinoline, acridine, phenanthridine, 3,4-benzacridine, 5,6-dimethylbenz(a)acridine, 10-azabenzo(a)pyrene and dibenz(a,h)acridine] from toluene was quantitative (>99%) for each one after two extractions with equal volumes of 8.25 M phosphoric acid.

The efficiency of the extraction with dichloromethane from the alkaline aqueous phase was examined as follows (five experiments): 2.0 ml of a toluene solution of the twelve above azaarenes was extracted twice with 8.25 M phosphoric acid. The phosphoric acid extracts were combined and made alkaline and then extracted with four 2.0-ml portions of dichloromethane. Carbazole was added as internal standard to each of the dichloromethane extracts and the content of basic azaarenes was determined after drying with magnesium sulphate. The recoveries (mean ± 2 σ) of the basic azaarenes in the four extracts with dichloromethane were 57 ± 5, 16 ± 2, 10 ± 2, and 6 ± 2%, respectively. The mean recoveries for the basic azaarenes by three extractions with dichloromethane were in the range 75—95%, lowest for the 6-methyl- and dimethyl-quinolines and highest for 4-azafluorene and dibenz(a,h)acridine. Thus, the developed liquid-liquid extraction method for isolating the basic azaarenes gives satisfactory yields for the different azaarenes.

Determination of basic azaarenes in air samples

Figure 2 shows a gas chromatogram of the fraction consisting of basic azaarenes isolated from an air sample corresponding to 450 m^3 of air. Eleven basic azaarenes were identified by comparing their retention times with those of standard compounds. The chromatogram shows that the combination of the liquid-liquid extraction method for isolating the basic azaarenes and g.c. with a nitrogen-sensitive detector for their measurement is very satisfactory, especially when the small amount of sample is considered. 2,4-Dimethylquinoline seems to be a new compound on the list of basic azaarenes identified in environmental samples. The other compounds identified [quinoline, 2,6-dimethylquinoline, 4-azafluorene, 7,8-benzoquinoline, phenanthridine/5,6-benzoquinoline, benz(c)acridine, dibenz(a,h)acridine, and dibenz(a,j)acridine] have been described earlier [9—15] as present in samples of airborne particulate matter. The results thus confirm earlier findings with other techniques.

Wakeham [18] identified 4-azafluorene, 7,8-benzoquinoline, phenanthridine/5,6-benzoquinoline, 3,4-benzacridine, 1,2,3,4/1,2,5,6-dibenzacridine and 1,2,7,8-dibenzacridine in street dust from heavily used roads. The profiles of the azaarenes in the street dust [18] and in airborne particulate matter from a busy street in Copenhagen were quite similar. In street dust [18], the relative amounts of the compounds mentioned were 0.3:2:2:3:2:0.4, respectively, and in airborne particulate matter they were 0.3:4:2:2:1:0.9, respectively. The relative amounts found in air samples from a residential area in the suburbs of Copenhagen during winter were 0.3:3:0.8:1:2.5:2.5, respectively. The profile of azaarenes is different in these samples, where house heating is a major contribution. This appears to suggest that each type or at least some types of sources emit different profiles of azaarenes. Furthermore, it confirms the necessity of applying an efficient separation technique, e.g., capillary g.c., in the determination of azaarenes rather than limiting the analysis to a few components.

As mentioned earlier, the volumes of sample were small in this investigation. Therefore, it was not possible in this investigation to obtain information about the unidentified peaks in Fig. 2 by g.c. with mass spectrometric detection. But it is clearly necessary to acquire more knowledge on the composition of azaarenes in air samples, considering that the compounds show great variations in mutagenic and carcinogenic properties.

Table 1 shows the levels of azaarenes and PAH in the atmosphere in a busy road in Copenhagen and in a residential area in the suburbs in winter. The concentrations of some inorganic pollutants are included in Table 1 in order to give an appropriate characterization of the air pollution at the two sites. A main source of basic azaarenes and PAH is heating of buildings in the residential area, and the extent of heating affects the levels of both PAH and azaarenes. Thus, a significant negative correlation was observed between the expression (see below) (BeP—(Cor:1.3), abbreviated as X) and the ambient temperature: $X = -0.23\ T\ (^\circ C) + 0.53$ (with $r = -0.69$ and $p \approx 0.1$). The

TABLE 1

The average amounts of basic azaarenes, polynuclear aromatic hydrocarbons and inorganic pollutants in the air in a suburban residential area and in a busy street in Copenhagen in February in the years 1976—1982

Compound	Concentration[a]	
	Residential area	Busy street
Quinoline	0.11	0.4
2,7- + 2,6-Dimethylquinoline	0.05	0.03
2,4-Dimethylquinoline	0.04	0.06
4-Azafluorene	0.02	0.025
7,8-Benzoquinoline	0.2	0.3
Phenanthridine + 5,6-benzoquinoline	0.06	0.14
3,4-Benzacridine	0.09	0.17
Dibenz(a,h)acridine	0.2	0.08
Dibenz(a,j)acridine	0.2	0.07
Phenanthrene	7	9
Fluoranthene	1.2	2.2
Pyrene	0.9	1.8
Chrysene + triphenylene	1.8	2.3
Benzo(b,j and k) fluoranthene	3	3
Benzo(e)pyrene	1.2	1.8
Dibenz(a,j)anthracene	0.3	0.4
Indeno(1,2,3-cd)pyrene	1.4	1.9
Dibenz(a,c + a,h)anthracene	0.2	0.4
Benzo(ghi)perylene	1.7	3.2
Coronene	0.8	1.8
Particles	43	44 $\mu g\ m^{-3}$
Soot	17	25 $\mu g\ m^{-3}$
Potassium	0.16	0.16 $\mu g\ m^{-3}$
Vanadium	0.017	0.019 $\mu g\ m^{-3}$
Nickel	0.0062	0.0068 $\mu g\ m^{-3}$
Lead	0.27	0.48 $\mu g\ m^{-3}$
Sulphate	1.9	3.4 $\mu g\ S\ m^{-3}$
Sulphur dioxide	30	40 ppb
Nitrogen oxides	n.d.[b]	170 ppb

[a]Concentrations are given as ng m^{-3} unless stated otherwise. [b]Not determined.

concentrations of most of the azaarenes and PAH are about 70% higher in the busy street than in the residential area, while those of the dibenzacridines are 2.7 times higher in the residential area than in the street. This suggests that heating of buildings is a major source of dibenzacridines, and that the emission rate of dibenzacridines is much higher in combustion gases from home furnaces and stoves than that in car exhausts. This was supported by the significant positive correlation observed between the dibenz(a,h + a,j)-acridine and the expression (BeP)—(Cor:1.3) ($r = 0.68; p < 0.1$) (Spearmann ranking correlation analysis). The expression (BeP)—(Cor:1.3) is a relative

measure for that part of the PAH originating from house-heating [31], as the emission rate of benzo(e)pyrene (BeP) is much higher than that of coronene (Cor) with a ratio Cor/BeP $\leqslant$ 0.1 from different sources, e.g., burning of coal [29, 30], brown coal [5], peat [31] and oil [32], while in car exhaust gases the ratio Cor/BeP is about 1.3 [29]. The levels of azaarenes are one to two orders of magnitude lower than those of PAH. The ratios reported by others [9, 11–13, 15] are in agreement with this.

Conclusions

The procedure developed is satisfactory for the determination of basic azaarenes and polynuclear aromatic hydrocarbons in samples of airborne particulate matter. The use of liquid-liquid extraction for purifying the basic azaarene fraction gave chromatograms of high quality even when the amounts of the samples were modest. Eleven basic azaarenes were identified by g.c. with nitrogen-sensitive detection. Different profiles of azaarenes were observed in areas where house heating or traffic was the major source. The dibenzacridines appeared to originate mainly from heating of buildings.

This investigation was supported financially by the Danish Ministry of Energy. The skillful technical assistance of Bente Christensen is gratefully acknowledged. The samples of airborne particulate matter were collected by the Environmental Office of the City of Copenhagen.

REFERENCES

1 A. Franceschi, S. Zanelli and G. M. Cornetti, Combust. Sci. Technol., 14 (1976) 57.
2 J. B. Andelman and M. J. Suess, Bull. W. H. O., 43 (1970) 479.
3 P. S. Pedersen, J. Ingwersen, T. Nielsen and E. Larsen, Environ. Sci. Technol., 14 (1980) 71.
4 S. G. Wakeham, C. Schaffner and W. Giger, Geochim. Cosmochim. Acta, 44 (1980) 403.
5 G. Grimmer, J. Jacob, K.-W. Naujack and G. Dettbarn, Anal. Chem., 55 (1983) 892.
6 T. Nielsen, B. Seitz and T. Ramdahl, Atmos. Environ., 18 (1984) 2159.
7 E. Sawicki, J. E. Meeker and M. J. Morgan, Int. J. Air Water Pollut., 9 (1965) 291.
8 E. Sawicki, J. E. Meeker and M. Morgan, Arch. Environ. Health, 11 (1965) 773.
9 E. Sawicki, S. P. McPherson, T. W. Stanley, J. Meeker and W. C. Elbert, Int. J. Air Water Pollut., 9 (1965) 515.
10 D. Brocco, A. Cimmino and M. Possanzini, J. Chromatogr., 84 (1973) 371.
11 W. Cautreels and K. van Cauwenberghe, Atmos. Environ., 10 (1976) 447.
12 T. P. Wang and A. Brockhaus, Microchim. Acta, II (1976) 55.
13 W. Cautreels and K. van Cauwenberghe, Sci. Total Environ., 8 (1977) 79.
14 M. W. Dong, D. C. Locke and D. Hoffmann, Environ. Sci. Technol., 11 (1977) 612.
15 L. van Vaeck and K. van Cauwenberghe, Atmos. Environ., 12 (1978) 2229.
16 R. Shinohara, A. Kido, Y. Okamoto and R. Takeshita, J. Chromatogr., 256 (1983) 81.
17 M. Blumer, T. Dorsey and J. Sass, Science, 195 (1977) 283.
18 S. G. Wakeham, Environ. Sci. Technol., 13 (1979) 1118.
19 International Agency for Research on Cancer (IARC), IARC Monographs on the Evaluation of the Carcinogenic Risk of Chemical to Humans. Polynuclear Aromatic Compounds, Part 1, Chemical, Environmental and Experimental Data, Vol. 32, International Research on Cancer, Lyon, 1983.

20 F. Merli, M. Novotny and M. L. Lee, J. Chromatogr., 199 (1980) 371.
21 J. Adams and C.-S. Glam, Environ. Sci. Technol., 18 (1984) 391.
22 D. W. Later, M. L. Lee, K. D. Bartle, R. C. Kong and D. L. Vassilaros, Anal. Chem., 53 (1981) 1612.
23 F. Folkmann, J. Phys. E, 8 (1975) 429.
24 OECD, Methods of Measuring Air Pollution, OECD, Paris, 1965.
25 T. Nielsen, T. Ramdahl and A. Bjørseth, Environ. Health Perspect., 47 (1983) 103.
26 T. Nielsen, Environ. Sci. Technol., 18 (1984) 157.
27 T. Nielsen, Anal. Chem., 55 (1983) 286.
28 A. Bjørseth, Anal. Chim. Acta, 94 (1977) 21.
29 G. Grimmer, K.-W. Naujack and D. Schneider, in A. Bjørseth and A. J. Dennis (Eds.), Polynuclear Atomatic Hydrocarbons: Chemistry and Biological Effect, Battelle Press, Columbus, OH, 1980, pp. 107—126.
30 L. J. Brasser, in Proc. of the NATO Adv. Study Institute on Mobile Source Emissions incl. Polycyclic Organic Species, Ser. C: Mathematical and Physical Sciences, Vol. 112, Liege, Belgium, 1983, pp. 14—28.
31 T. Nielsen, Characterization of Polycyclic Organic Materials in Stack Gases from Coal-fired Power Plants in the Atmosphere and Investigation of their Transformation in the Atmosphere, Risø-M-2420, Risø National Laboratory, Roskilde, 1984 (in Danish).
32 G. Grimmer, Analysis, Data Reporting and Profile Concept, in Polycyclic Aromatic Compounds in the Air, Background Papers, OECD, Paris, 1983.

Analytica Chimica Acta, 187 (1986) 233—240
Elsevier Science Publishers B.V., Amsterdam — Printed in The Netherlands

THREE-DIMENSIONAL DERIVATIVE SPECTROCHROMATOGRAMS IN HIGH-PERFORMANCE LIQUID CHROMATOGRAPHY AND THEIR IMPLICATIONS FOR PEAK HOMOGENEITY VALIDATION

A. A. FASANMADE[a] and A. F. FELL*

School of Pharmaceutical Chemistry, University of Bradford, Bradford, West Yorkshire BD7 1DP (Great Britain)

H. P. SCOTT[b]

Department of Pharmacy, Heriot-Watt University, 79 Grassmarket, Edinburgh EH1 2HJ (Great Britain)

(Received 21st April 1986)

SUMMARY

The full ultraviolet spectra generated by a photodiode-array detector are transformed to the *n*th derivative ($d^nA/d\lambda^n$). The bipolar, three-dimensional data matrix ($d^nA/d\lambda^n$, λ, t) is presented with computer-aided graphics as an extension of the spectrochromatogram concept to aid peak validation. Existing display algorithms are modified to yield several presentations which reveal the full topography of the elution profile. These include rotation in three-dimensional space and inspection of the positive and negative data planes. A novel contour-plot representation is proposed to enable the derivative spectrochromatographic data to be presented in a two-dimensional format. Two planes of data (i.e., positive and negative amplitudes of ($d^nA/d\lambda^n$) in the (λ, t) plane) can be displayed as required for derivative data presentation. The technique is used to assess the homogeneity of overlapping peaks of ethynyloestradiol and norethisterone.

The use of chromatographic peak profiles in the quantitation of analytes requires adequate peak resolution. In chromatograms where analytes and contaminant peaks overlap, quantitative analysis becomes difficult or impossible, especially where the degree of overlap is so great that detection is not feasible by visual examination. Where band overlap occurs, least-squares fitting with weighting factors has been used to delineate the peaks [1—3]. The absorbance ratio at two detection wavelengths in high-performance liquid chromatography (h.p.l.c.) has also been used to detect the presence of overlapping peaks [4, 5]. The availability of rapid-scanning spectrophotometers for u.v.-visible detection in h.p.l.c. has introduced a number of new

---

[a]Present address: Faculty of Pharmacy, College of Medicine, University of Ibadan, Ibadan, Nigeria.

[b]Present address: Beecham Pharmaceuticals, Clarendon Road, Worthing, West Sussex, Great Britain.

0003-2670/86/$03.50 © 1986 Elsevier Science Publishers B.V.

possibilities for detecting peak non-homogeneity. These techniques include direct comparison of spectra obtained at various points in the chromatographic peak profile, spectral suppression [5], principal component analysis [3, 6, 7] and computer-generated graphics of the absorbance, wavelength and time (A, λ, t) data [7—13], either as a three-dimensional "spectrochromatogram" or as the equivalent two-dimensional contour plot of absorbance contours in the (λ, t) plane [13]. Other workers have used the derivative transformation of the chromatographic profile for peak homogeneity assessment in gas chromatography [14, 15] and in h.p.l.c. [13, 16—18]. The enhancement of resolution of overlapping spectra conferred by derivative transformation in the wavelength domain ($d^nA/d\lambda^n$) has had numerous applications in analytical spectroscopy [16, 18—20], but has been little used in h.p.l.c. [16, 21].

In the work described here, the derivative transformation in the wavelength domain of solutes separated by h.p.l.c. was examined in relation to the orthogonal elution time domain, with particular reference to the possibility of enhancing the resolution of overlapping solutes. The novel, bipolar, three-dimensional derivative spectrochromatogram so generated ($d^nA/d\lambda^n$, λ, t), and the equivalent contour representations of the data were examined as a new technique for assessing chromatographic peak purity.

EXPERIMENTAL

The modular liquid chromatograph assembled in the laboratory comprised a constant-flow pump with integral damping (Gilson Model 302), a Rheodyne injection valve equipped with a 20-μl loop, and a 100 × 5 mm i.d. stainless steel column which was slurry-packed in the laboratory with microparticulate ODS-Hypersil (5 μm) by the upward displacement technique recommended by the manufacturer. The mobile phase comprised acetonitrile/water (3:97, v/v). The flow rate was 2 ml min^{-1}. Samples of norethisterone and ethynyloestradiol (Sigma) were dissolved in the eluent and introduced by the full-loop injection technique.

A Hewlett-Packard 8450A optical multichannel detector system was used with an 8-μl quartz flow-cell (Hellma, Model 178-3 QS). The spectrophotometer was connected via the RS 232C port (9600 baud) to a model HP-85 microcomputer, equipped with 32-kbyte total RAM storage. The microcomputer was connected via the HP interface bus (IEEE-488) port to a graphic plotter (Model HP-7225B) and a dual 8-in. floppy disk mass storage unit (HP-9895A).

After the injection of a sample, spectral capture was initiated by the program at a predetermined time after injection. The (A, λ, t) data matrix was recorded at 1-s intervals throughout the elution band of each analyte. These spectrochromatographic data were stored on floppy disks under descriptive file names and recalled individually after the run for processing. In some cases, it was necessary to smooth individual spectra prior to further

data processing. Transformed spectra were processed in such a way as to reduce digital noise error caused by computer round-off of figures during storage [5]. Differentiation was performed using the Savitzky-Golay algorithm [22].

RESULTS AND DISCUSSION

Ethynyloestradiol (ET) and norethisterone (NO) peaks were not resolved under the chromatographic conditions used, although it would be possible to optimize the column and mobile phase in order to separate these analytes.

Figure 1 is the three-dimensional representation of a chromatogram showing the (A, λ, t) data matrix of the closely overlapping peaks of ET and NO. This represents the plot of full spectra of eluate at 1-s intervals during elution. As it was possible to rotate this plot in the wavelength/time plane, individual parts of the data could be examined to assess any asymmetry in the elution profile indicating peak contamination. In essence, this relies on there being a significant difference in the spectral profile for each overlapping component. However, in many instances, the potential contaminants have u.v. spectra that differ little from that of the compound of interest, thus making it difficult to discriminate the u.v. profiles of overlapping peaks in three-dimensional plots. If, however, the fine structure were made accessible in the u.v. spectrum, it should be easier to discriminate between such overlapping spectra. Such an increase in accessible information can be obtained by derivative transformation of the spectral data [16, 18—20, 23].

The transformation of a u.v.-visible spectrum to its first, second or higher order derivative ($dA/d\lambda$, $d^2A/d\lambda^2$, ... $d^nA/d\lambda^n$) yields bipolar functions and increases the number of characteristic bands from x in the zero order to $x(n + 1)$ in the nth order of differentiation [18, 19]. This technique enables the intrinsic fine structure of the peaks to become more accessible and accentuates any differences in the spectra of closely related compounds (Fig. 2). Thus it is possible to conceive of a family of derivative spectra of each of a

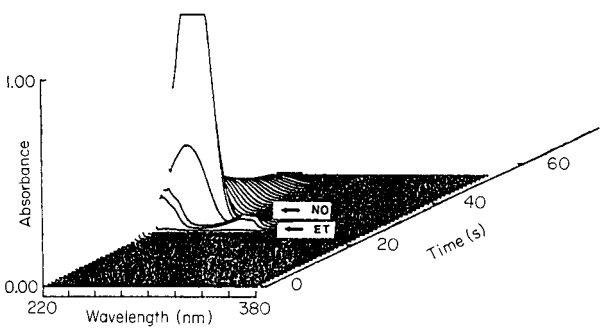

Fig. 1. Spectrochromatogram of (A, λ, t) data matrix of the elution profile of ethynyloestradiol (ET, 1.2 μg) and norethisterone (NO, 3.0 μg).

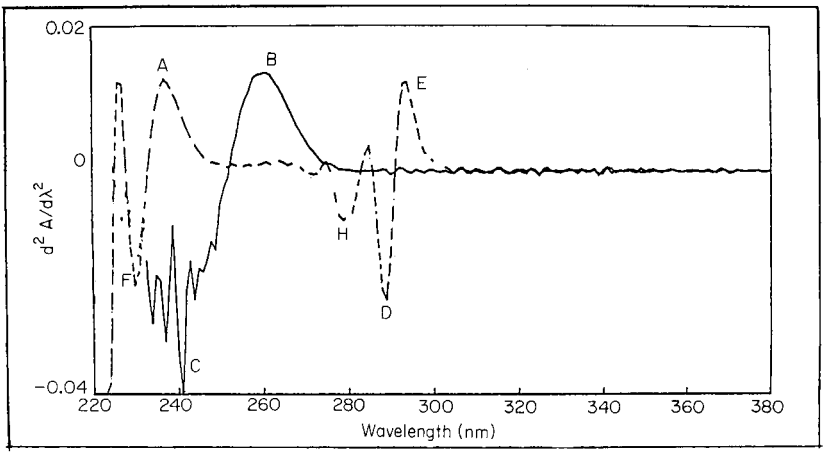

Fig. 2. Overlaid second-derivative spectra: (– – –) ethynyloestradiol; (——) norethisterone captured during chromatographic elution. A—H refer to features identified in subsequent figures.

sequential series of spectra captured at discrete elution times during chromatography, yielding a derivative spectrochromatogram in three-dimensional space described by the matrix ($d^nA/d\lambda^n$, λ, t). Of course, the process of differentiation leads to a progressive increase in noise level as the derivative order increases [20, 23].

Graphical presentation of derivative spectrochromatograms

A key difference between the derivative and the conventional spectrochromatogram is the presence of an additional plane of data arising from the bipolar nature of the derivative function. This poses some problems of representation; however, a shift in the zero baseline readily accomodates negative values to give a reasonable view of the data. Figure 3A shows a representation of the second-derivative spectrochromatogram for a mixture of ET and NO. Reflection of the data along the time axis enables the trailing edge of the chromatogram to be viewed (Fig. 3B). These graphical modifications indicate the potential of this mode of presentation, although much of the information, especially in the negative plane, is masked by the leading spectra and the "hidden-line removal" algorithm used [5].

This problem can be partly resolved by removing the leading, less informative spectra to reveal the hitherto unobservable negative peaks of low amplitude. The sectioning of the data does, however, distort the overall view of the spectrochromatogram, giving it the appearance of stacked derivative spectra at various concentrations of the analyte mixture. A facile solution to this problem is to present two three-dimensional plots for each set of data. In this technique, the positive data plane is plotted as for the conventional spectrochromatogram (Fig. 4A), while the negative data plane is inverted before being plotted as a conventional 3-dimensional spectrochromatogram (Fig. 4B).

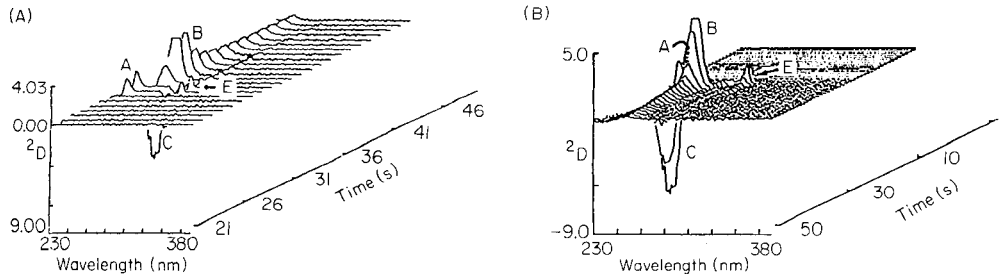

Fig. 3. Graphical presentation of a second-derivative spectrochromatogram. (A) Plot of wavelength-domain, second-derivative spectrochromatogram ($d^2A/d\lambda^2$, λ, t) of ET (1.2 μg) co-eluting with NO (3 μg). ^{2}D represents the second-order derivative amplitude (arbitrary scale). (B) Reflection of (A) along the time axis, so that the trailing slopes of the chromatogram can be viewed. Peak codes as in Fig. 2. Wavelength range, 230—380 nm.

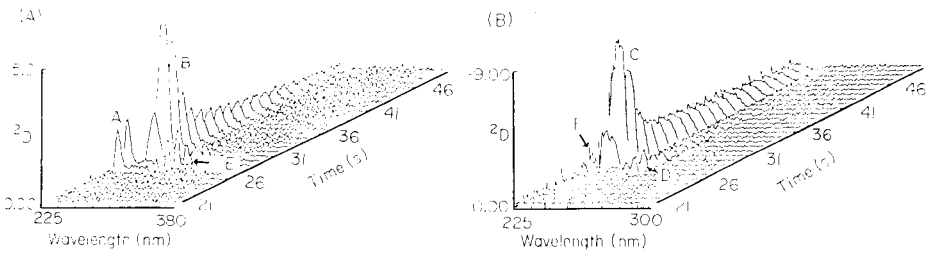

Fig. 4 (A) Positive projection; (B) negative projection (inverted) of the derivative spectrochromatograms shown in Fig. 3(A). Peak codes as in Fig. 2. Peaks D and F are only observed in (B).

The presentation of the regular spectrochromatogram as a two-dimensional contour plot, where isoabsorptive contours are plotted in the (λ, t) plane, has been proposed recently [13]. A similar approach can be applied to the ($d^nA/d\lambda^n$, λ, t) data matrix. As discussed above, the presence of negative values of the derivative function introduces severe difficulties of presentation. This problem can be resolved by using a different line format (e.g., a dotted line) and/or coloured contours to represent the negative peak amplitudes. Thus a bipolar contour plot combining both the positive and negative amplitude data in the (λ, t) plane can readily be presented as a two-dimensional plot (Fig. 5). This technique of graphically presenting essentially two planes of data opens up a number of interesting possibilities for advanced detection in h.p.l.c.

Interpretation of graphical plots

Interpretation of these three- and two-dimensional plots may not initially appear easy. However, with some experience, points of interest can readily be located in the topography of the plots. The general advantages of using a three-dimensional representation of the spectrochromatogram also hold in

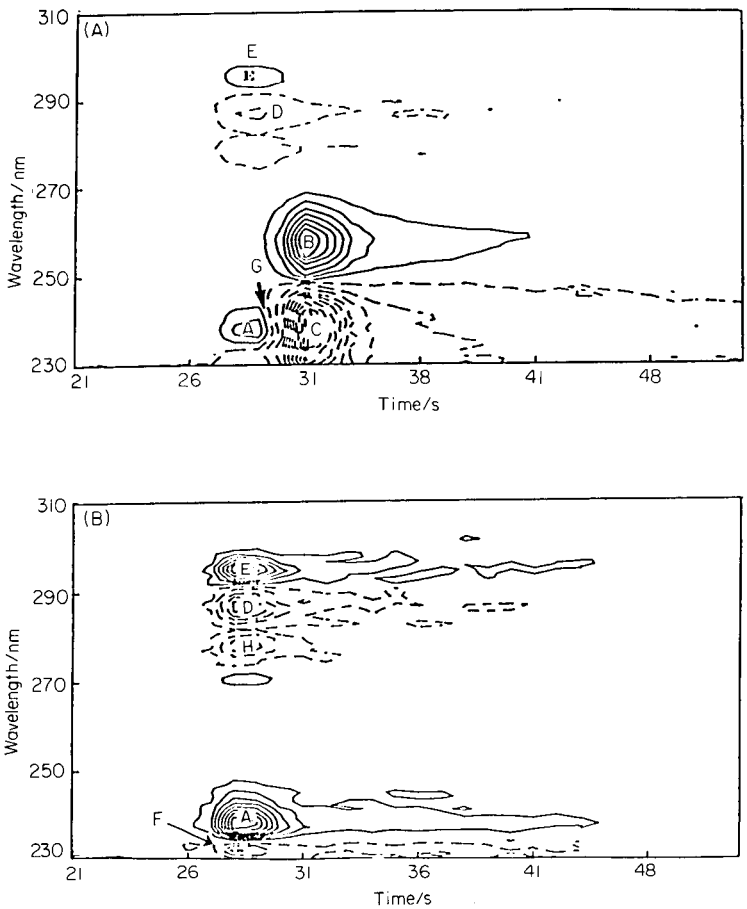

Fig. 5. (A) Contour representation of the ($d^2A/d\lambda^2$, λ, t) data matrix of the co-eluting steroids, ET and NO; solid contours indicate positive amplitudes; broken contours represent negative amplitudes; G indicates a "rift" between the sharp negative peak C of NO and the sharp positive peak A of ET (fewer contours are plotted than in Fig. 5B, for clarity). (B) Contour plot for ET alone; peak H is more distinctively shown in this plot; peak F was essentially merged with peak C of NO in Fig. 5A but is clearly shown here.

the derivative mode; for instance, the asymmetrical peak shapes of chromatograms with overlapping peaks can be detected by viewing the range of peak heights from various angles above the zero baseline. This applies even more in the derivative mode where, in addition to the positive projections, the troughs of negative data below the baseline of the topogram are represented. This capability is shown in Fig. 3B where peak A (for ET) is observed behind a large peak of NO (peak B), and peak C is actually the negative centroid peak derived from NO. Although the centroid peak for ET is obscured in this representation, it can be seen in Fig. 4B as peak D.

In the derivative spectrochromatogram, the possibility of detecting the non-homogeneous nature of an impure peak in a chromatogram is improved

because of the greater number of characteristic features in the data generated in derivative spectra. This point is illustrated by the spectra of ET and NO in Fig. 2, which explain certain features in Fig. 3A. In Fig. 3A, peak A is associated with ET, and peak B arises from the co-eluting component NO, because at ca. 260 nm the two leading spectra captured for peak A have zero or negative values in the second derivative, whereas the next series of derivative spectra captured for peak B at this wavelength have positive values. Because it is not possible for one analyte to have both positive and negative derivative amplitudes at the same wavelength, the presence of overlapping peaks is confirmed.

The corresponding bipolar contour plot (Fig. 5) can be more readily interpreted because all the information can be seen at a glance, without the need for viewing at different angles. When a negative derivative amplitude runs into a positive one at the same wavelength (e.g., at 240 nm) this can be seen as a sharp rift (position G in Fig. 5A). In the conventional zero-order contour plot, such features do not occur because the two overlapping peaks combine to give a positive range of values.

The situation exemplified in Fig. 3A at ca. 260 nm is also clearly evident in the contour plot. For instance, contour lines of peaks A, D and E that are associated with ET are observable at wavelengths characteristic of ET. These are seen just before the appearance of the extensive positive contours of peak B associated with NO. Thus any changes in the pattern of contours within a specified wavelength range and at a particular time interval, when compared with other time intervals in a chromatographic elution profile, are indicative of a contaminated peak. To confirm this conclusion, the contour plot in the derivative mode of the pure analyte of interest can be inspected (Fig. 5B), so that the distinctive features in a particular region of the chromatogram can be compared.

Conclusions

The increased number of characteristic features afforded by second-derivative spectra, in particular, and the graphical capability of the contour and three-dimensional presentations offer a significant new technique for peak homogeneity assessment in h.p.l.c. The extension of this technique to generate the equivalent three-dimensional and contour plots for signals transformed to the second derivative in the time domain at a series of discrete wavelengths is also useful. It will also be of interest to investigate the possibility of improved quantitative measurements where the chromatograms of co-eluting components are resolved in the wavelength domain by using data from the second-derivative spectrum. Applications in both these directions are currently being investigated in this laboratory.

Financial support from Ibadan University (for A. A. F.) and from the Home Office Forensic Science Service (for H. P. S.) is gratefully acknowledged.

REFERENCES

1 S. M. Roberts, D. H. Wilkinson and L. R. Walker, Anal. Chem., 42 (1970) 886.
2 E. Grushka, M. N. Myers and J. C. Giddings, Anal. Chem., 42 (1970) 21.
3 W. Lindberg, J. Ohman and S. Wold, Anal. Chem., 58 (1986) 299.
4 A. Bylina, D. Sybilska, Z. R. Grabowski and J. Koszowski, J. Chromatogr., 83 (1973) 257.
5 A. F. Fell, H. P. Scott, R. Gill and A. C. Moffat, J. Chromatogr., 273 (1983) 3.
6 B. Vandeginste, R. Essers, T. Bosman, J. Reijnen and G. Kateman, Anal. Chem., 57 (1985) 971.
7 D. W. Osten and B. R. Kowalski, Anal. Chem., 56 (1984) 991.
8 R. M. Wightman, R. L. Scott, C. N. Reilley, R. W. Murray and J. M. Burnett, Anal. Chem., 46 (1974) 1492.
9 L. N. Klatt, J. Chromatogr. Sci., 17 (1979) 225.
10 M. P. Fogarty, D. C. Shelley and I. M. Warner, J. High Res. Chromatogr. Chromatogr. Commun., 4 (1981) 561.
11 D. C. Shelley, M. P. Fogarty and I. M. Warner, J. High Res. Chromatogr. Chromatogr. Commun., 4 (1981) 616.
12 A. F. Fell, B. J. Clark and H. P. Scott, J. Pharm. Biomed. Anal., 1 (1983) 557.
13 B. J. Clark, A. F. Fell, H. P. Scott and D. Westerlund, J. Chromatogr., 286 (1984) 261.
14 T. Kambara, K. Saitoh and K. Ohzeki, Anal. Chem., 39 (1967) 409.
15 A. B. Berman, Yu. A. Frank and M. I. Yanovskii, Zavod. Lab., 34 (1968) 272.
16 A. A. Fasanmade, Ph.D. Thesis, Heriot-Watt University, Edinburgh, 1985.
17 D. T. Zelt, J. A. Owen and G. S. Marks, J. Chromatogr., 189 (1980) 209.
18 A. F. Fell, Anal. Proc., 17 (1980) 512.
19 W. L. Butler and D. W. Hopkins, Photochem. Photobiol., 12 (1970) 451.
20 A. A. Fasanmade and A. F. Fell, Analyst, 110 (1985) 1117.
21 A. F. Fell, H. P. Scott, R. Gill and A. C. Moffat, Chromatographia, 16 (1982) 69.
22 A. Savitzky and M. J. E. Golay, Anal. Chem., 36 (1964) 1627.
23 T. C. O'Haver and T. Begley, Anal. Chem., 53 (1981) 1876.

Analytica Chimica Acta, 187 (1986) 241—253
Elsevier Science Publishers B.V., Amsterdam — Printed in The Netherlands

A SOFTWARE-DRIVEN, SINGLE-PUMP LIQUID CHROMATOGRAPHIC SYSTEM FOR COLUMN-SWITCHING APPLICATIONS

M. D. WIEGAND[a], P. M. WIEGAND[a] and S. R. CROUCH*
Department of Chemistry, Michigan State University, East Lansing, MI 48824 (U.S.A.)
(Received 31st March 1986)

SUMMARY

A general-purpose, software-driven high-performance liquid chromatographic (HPLC) instrument is described for multidimensional chromatographic experiments. The system consists of a laboratory microcomputer, a commercial solvent delivery system, a flexible, computer-controlled valving system and a conventional, mixed-wavelength, ultraviolet (u.v.) detector. Reconfiguration of the instrument for a variety of multidimensional experiments involves only a change in software and the column/valve connections. Several single-valve and two-valve configurations, including those for back-flushing, auto-injection, heartcutting, sample cleanup and selectivity programming are illustrated along with chromatograms obtained on various complex mixtures.

Multidimensional high-performance liquid chromatography (HPLC), also known as column-switching HPLC, has become very popular since the advent of the first high-pressure, low dead-volume valve, thirteen years ago [1]. Multidimensional techniques provide the chromatographer with greater separating ability for a broader range of samples than is possible with single-column HPLC. Specific advantages include improved resolution, the removal of matrix interferences, and reduced time. The literature contains reports of many different multidimensional valving configurations and applications. These include sample clean-up [2], mode-coupling [3—5], back-flushing [6—9], heartcutting [10—12], recycling [13], trace enrichment [14, 15], and boxcar chromatography [16]. The reports cited have demonstrated the great power of multidimensional HPLC separations. However, the instrumentation described in those reports is often designed specifically for a particular application or separation mode, and is not readily reconfigured for other uses. Also, many of the multidimensional HPLC systems described require more than one pump. This can be expensive and difficult to synchronize with other system components. Only a few of the multidimensional instruments reported are easily adapted to accomplish the wide variety of multidimensional experiments that are possible.

---

[a]Present address: Union Carbide Corp., Charleston, WV, U.S.A.

0003-2670/86/$03.50 © 1986 Elsevier Science Publishers B.V.

This report describes a computer-controlled multidimensional HPLC system that provides the versatility and adaptability needed for a variety of column-switching experiments. The system consists of a laboratory microcomputer, a commercial solvent-delivery system, a flexible valving arrangement, and a mixed-wavelength u.v. detector. The microcomputer orders and synchronizes all the tasks necessary to accomplish several multidimensional experiments. Reconfiguration of the system for a variety of studies is possible simply by changing the software and the column/valve connections. Furthermore, the system described is capable of sophisticated decision making during multidimensional separations. For example, the timing of a column-switching event can be based on elapsed time or detector output. In our laboratories, the multidimensional HPLC instrument has been used to develop methods for the characterization of petroleum-derived crude oils and refined fuels. Examples from that work are presented to illustrate many of the system capabilities.

EXPERIMENTAL

Instrumentation

Figure 1 shows a block diagram of the multidimensional HPLC system. The heart of the system is a microcomputer, which was designed in-house [17], based on the Intel 8085 microprocessor. The microcomputer operates in a hierarchical configuration with a laboratory minicomputer (Digital Equipment Corporation LSI 11/23). Software is downloaded from the

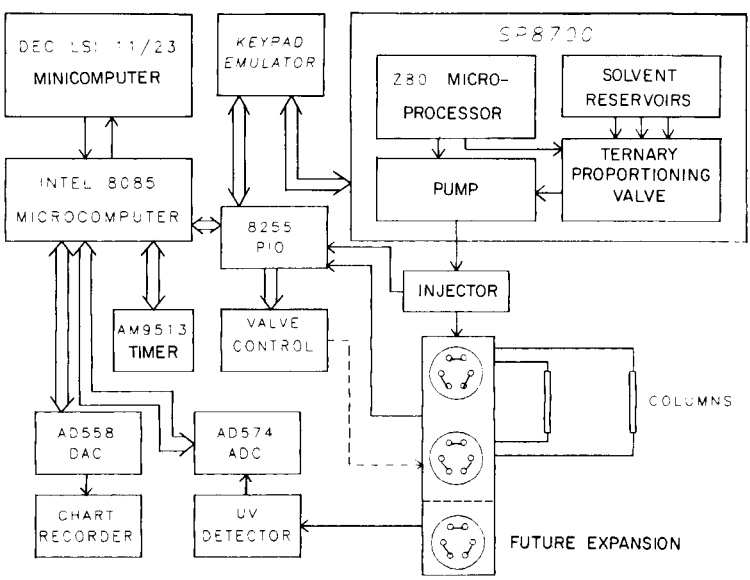

Fig. 1. Block diagram of the multidimensional HPLC instrument.

minicomputer, and acquired data are uploaded for post-run manipulation and plotting. In addition to the usual support circuitry, the microcomputer contains four peripheral boards: a parallel input/output module, a digital-to-analog (DAC) conversion module, an analog-to-digital conversion module (ADC), and a timing module. Timing functions use a real-time clock based on an LSI system timing controller chip (Advanced Micro Devices, AM 9513) [18] which contains five independent, programmable 16-bit counters.

Digitization of the detector signal is accomplished with a 12-bit ADC and a sample-and-hold amplifier (Analog Devices, AD574 and AD583 respectively). Real-time output is obtained by scaling and offsetting the digitized signal; an 8-bit DAC (Analog Devices AD558) is used to display the data on a strip-chart recorder. Finally, sensing and control of the valves and the solvent-delivery system is accomplished with two 8-bit parallel input/output (PIO) ports of a programmable peripheral interface chip (Intel 8255).

All solvent delivery is accomplished by a single Spectra-Physics SP8700 solvent delivery system. This system is a microprocessor-based module with a dual-piston reciprocating pump and a ternary proportioning valve at its inlet. The system employs two pressure/flow feedback loops. As a result, the system responds rapidly to back-pressure changes which occur as a result of column switching and maintains a constant flow rate.

The microcomputer controls the solvent delivery system through a keypad emulation circuit which has been described previously [19]. This circuit allows the microcomputer to simulate a keystroke on the solvent delivery system keypad by writing a bit pattern unique for that key to the PIO port. In this manner, the solvent delivery module can be programmed from the microcomputer in a fashion identical to manual entry of parameters.

Figure 2 shows the circuit used for valve control. Two air-actuated 6-port, 2-position switching valves (Rheodyne, Cotati, CA) and one manual

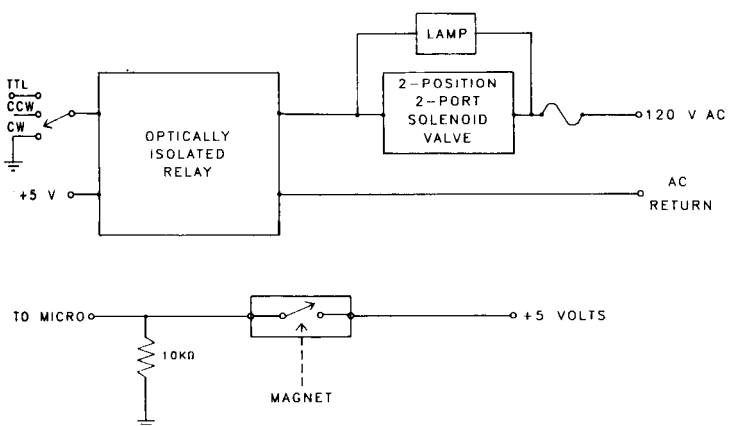

Fig. 2. Valve-control and position-sensing circuit for the multidimensional HPLC instrument.

injector valve (Rheodyne) are implemented. The system can accommodate up to four automated valves and sensors.

Port C on the PIO chip is split into four output bits and four input bits. Each output bit can be used to control a valve, and the corresponding input bit is used to sense the valve position. To turn a valve, the TTL signal from the PIO chip activates an optically isolated relay (Teledyne 611-3, Hawthorne, CA), which is used to control power to a 120-V, continuous-duty, solenoid valve (Scovill, Wake Forest, NC). This 4-port, 2-position valve directs air pressure to one side of an actuator and allows the other side of the actuator to vent. The position of the valve is governed by the state of a magnetically-operated reed switch mounted on the valve housing. A magnet is mounted on the valve shaft which moves into proximity of the reed switch when the valve is in the clockwise position and closes the switch. The resulting change of state at one bit of the input port enables the microcomputer to check if a valve rotation was successful.

The detector is a dual-wavelength u.v. detector with a 20-μl flow cell (Chromatronix 220, Berkeley, CA). Conversion of a ±4-mA full-scale output signal to a ±10-V input signal to the ADC is accomplished with a 2.5-kΩ load resistor.

Apparatus and chemicals

All chromatographic columns used were commercially available; they included a Perkin-Elmer high-speed (14 cm × 0.25 in. × 4.6 mm) 5-μm silica column, an Alltech Spherisorb (25 cm × 0.25 in. × 4.6 mm) 5-μm amino normal bonded-phase column, an Alltech Spherisorb (25 cm × 0.25 in. × 4.6 mm) 5 μm ODS bonded reverse-phase column, and an Analytical Sciences Incorporated 500-A Ultragel column. All solvents were LC/UV grade (Burdick and Jackson, Muskegon, MI). Ethanol-free chloroform preserved with amylene was used. The fuel studied was Residual Fuel No. 3, supplied by NASA, Lewis Research Center, Cleveland, Ohio.

Software

The operating system for the multidimensional HPLC instrument was based on the FORTH language (polyFORTH version, Forth, Hermosa Beach, CA). FORTH is a threaded language, developed for instrument control, in which a basic dictionary of commands is used to form more complex commands with which to run the experiment [20]. A FORTH operating system provides the user with a readable command set which requires a minimum of computer expertise to use. At the same time, the user has access to the complete power of a computer language. In addition, the FORTH operating system possesses an interactive compiler which enables the user to append new commands or programs at will. The polyFORTH version of FORTH also has multiprogramming capability. This enables several background tasks to operate concurrently with the foreground, or terminal task. A terminal task is normally a user program containing system control commands and parameters

for the background tasks. Examples of background tasks include data acquisition, data storage, peak recognition and counting, and chart recorder output.

Table 1 displays the system control commands for the multidimensional HPLC instrument. These fall into four basic categories. PRESS and ENTER are used for parameter entry to the solvent delivery system. The commands, CW and CCW, are used to turn valves clockwise and counterclockwise respectively. INJECT and SYNC are used to start the real-time clock upon injection and optionally synchronize it with the clock of the solvent delivery system. The clock can also be started without injection by the CLOCK command.

The last category of commands in Table 1 is used for event sequencing. Events such as valve switching, solvent change, or flow change can be based on time, HPLC status, or detector output. Time-based delay commands include EVENT, which waits until the specified time after injection, and WAIT, which is an absolute delay. Commands based on chromatographic or system status include FLOW?, which waits for the flow-ready condition, and CAM, which delays until the next cam cycle on the solvent delivery system; CAM is useful for synchronization and flow-programming applications.

Detector-based sequencing is more powerful and reliable than time-based sequencing, because it does not depend on reproducible retention times from one run to the next. Several commands are available for detector-based sequencing. The background task, which detects peaks, maintains a variable containing the current peak count (i.e., number of peaks detected so far), which can then be used in conditional execution. The command +%FS or

TABLE 1

System control commands

Valve control	
n CCW, *n* CW	Turn valve *n* and check validity (*n* = 1 to 4)
SP8700 communication	
k PRESS	Presses one key with code *k*
*k*1, *k*2, *kn* ENTER	Presses series of keys, then ENTER
n ENTER#	Converts number to key codes, then presses the keys and ENTER
Synchronization	
CLOCK	Starts micro clock counting from zero
INJECT	Starts micro clock upon injection
SYNC	Starts micro clock and SP8700 clock synchronously upon injection
Event sequencing	
m, *s* EVENT	Delays *m* minutes and *s* seconds after inject
h WAIT	Delays *h* hundredths of seconds
#PEAKS	Variable which contains the peak count since inject
n +%FS, *n* −%FS	Delays until signal rises/falls to *n*% full scale
n %FSCHG	Delays until signal changes by *n*% full scale

—%FS will delay until the signal is greater or less than the specified percent of the full-scale recorder deflection. This command is very useful for heart-cutting. The %FSCHG command delays until the signal changes by the specified percentage of full scale, regardless of the direction of the change. The commands + A/D, — A/D, and A/DCHG are similar to the FS commands, but take values which are in ADC units as arguments. Most applications use combinations of these commands, linked in either a logical AND mode or a logical OR mode. For example, an intelligent heartcut can be made by waiting for two peaks to elute at least six minutes after injection, and then switching a valve when a 10% change in the baseline signal occurs, which is the rising edge of the next peak.

RESULTS AND DISCUSSION

Several useful valve configurations for multidimensional HPLC experiments are illustrated in Fig. 3. Results of band-broadening studies and experiments involving one- and two-valve configurations are presented below.

Band-broadening studies

To investigate the amount of extra band-broadening introduced by the additional valve(s) and tubing, chromatograms were examined for a worst case situation. A single analyte was injected onto an analytical column; two type-B valves and their associated tubing were inserted between the end of the column and the u.v. detector. The peak shape was compared to that obtained with the effluent sent directly from the column to the detector. An 18% increase in the peak width at half-height, a 19% decrease in theoretical plates, and a 6% increase in the peak-asymmetry factor resulted from the valves and tubing. Further study showed that the most of this band-broadening could be attributed to the tubing used to connect the 25-cm columns to the valves. The band-broadening introduced by the valves themselves was negligible as has been observed previously [21]. Workers should thus be aware of this extra broadening and take care to minimize the amount of tubing used in multidimensional experiments.

Single-valve experiments

Simple back-flushing experiments were done by injecting a mixture of anthracene, nitrobenzene and ethylbenzoate onto a silica column configured in the type-A mode (see Fig. 3). The resulting chromatograms obtained with an isocratic hexane mobile phase are presented in Fig. 4. Comparison of the chromatograms illustrates the utility of back-flushing to solve the general elution problem. Back-flushing can shorten separation times and improve peak shape for late eluters, as can be seen by comparing chromatograms A and B. Because all back-flushed components co-elute, the chromatographer can decide when all components have eluted. This is particularly useful in the analysis of complex unknowns such as fuels. The co-elution of back-flushed

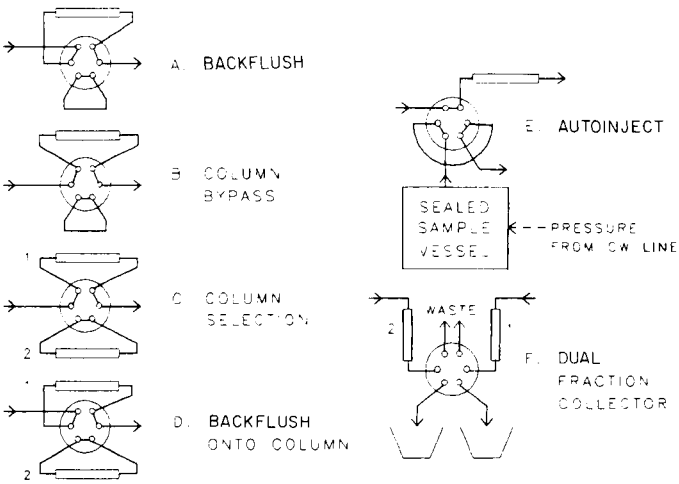

Fig. 3. Possible valving configurations for a 6-port, 2-position valve.

components also allows the chromatographer to quantify components which would separate upon forward elution. This was done in chromatogram C. Chromatogram D illustrates how separation times can be further shortened by using the keypad emulator to execute a flow program synchronous with the back-flush.

A programmable auto-injector can be created by using a single Type-E valve as shown in Fig. 3. This is very simple to construct and relatively inexpensive in comparison to most commercial auto-injectors. The auto-injector was used with a commercial fraction collector to collect repetitive chromatographic fractions in order to obtain large enough volumes for subsequent study. The auto-injector can also be used with a second valve configured as a Type-F valve, to collect just one fraction or peak out of a chromatogram.

Heartcut experiments can be done with a single valve configured as Type B in Fig. 3. In such a configuration, the primary analytical column (not shown) is always in-line prior to the valve. To take the heartcut, the second column is switched in and out of line. A chromatogram obtained in this fashion is shown in Fig. 5. The disadvantages of a one-valve heartcut are a consequence of the primary column always being in-line. This precludes the development of the heartcut on column 2 with a mobile phase incompatible with the stationary phase of column 1. If column 2 is developed with a compatible, but different, mobile phase, the overall time is lengthened because column 1 must be re-equilibrated before another experiment is possible. Sequential heartcuts are possible with a one-valve system only when the primary column is attached to the valve. In this case the second column is always in-line. The disadvantage of this arrangement is that the effluent from column 1 always passes through column 2. There are also severe mobile-phase restrictions in this configuration.

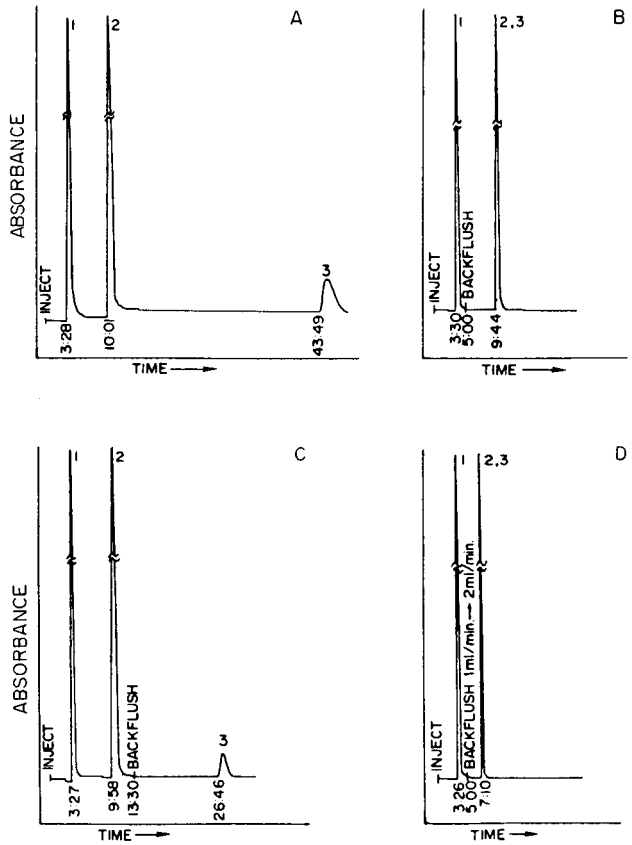

Fig. 4. Simple back-flushing chromatograms of a three-component mixture: (A) without back-flushing; (B) back-flushing after first component; (C) back-flushing of last component; (D) back-flushing with flow programming from 1 ml min^{-1} to 2 ml min^{-1}.

Two-valve experiments

A two-valve multidimensional system is much more powerful and versatile than a one-valve system. The introduction of a second Type-B valve into a heartcut setup eliminates the problems associated with the single-valve arrangement. This is illustrated by a specialized version of a two-valve heartcut configuration, shown in Fig. 6. This configuration was used to produce a size-polarity matrix to characterize a residual fuel sample. The experiment takes heartcuts from an Ultragel size-exclusion column. The components of the heartcuts are separated by an ODS column. The size-exclusion column is developed with tetrahydrofuran (THF) and the ODS column is developed with either a water/acetonitrile, or a water/THF gradient. Because the Ultrastyragel packing material is incompatible with water, care must be taken to ensure that none of the aqueous solvent is left in the tubing before the size-exclusion column is switched back in-line. The tubing can be flushed as necessary by switching both columns off-line.

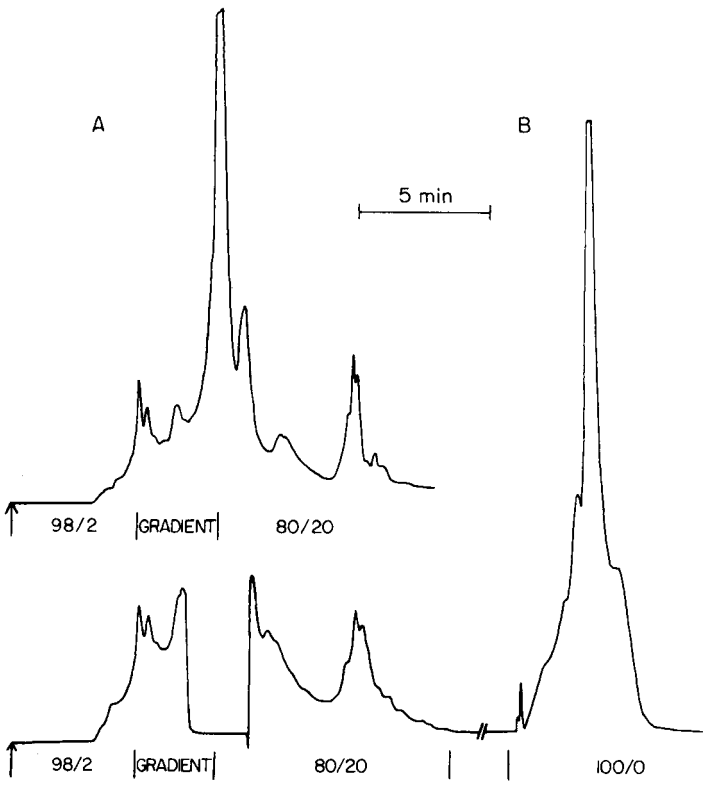

Fig. 5. Single-valve heartcut chromatogram, amino to silica column for a residual fuel sample with hexane/dichloromethane as mobile phase. (A) Single-column elution; (B) heartcut elution.

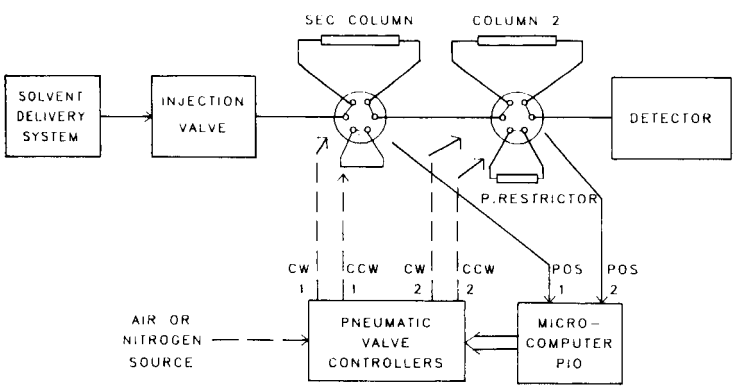

Fig. 6. Valve configurations for executing heartcuts of a size-exclusion column.

The Ultragel size-exclusion column contains a highly cross-linked polystyrene/divinylbenzene (PS/DVB) gel which is extremely sensitive to pressure shocks. In fact, it is necessary to bring this column up to flow in 0.1 ml min^{-1} increments. The stand-alone program capabilities of the solvent-delivery system are not sufficient for this purpose. However, it is a simple task with microcomputer/keypad emulator control. Special arrangements are also necessary to allow column switching with the Ultragel size-exclusion column. The action of switching a column in and out of line by a Type-B valve produces a drastic change in back-pressure. Such a pressure shock can compress the PS/DVB gel. Therefore, a pressure restrictor is necessary in the bypass loop of the second valve to maintain a reasonably constant back-pressure. Furthermore, this pressure sensitivity precludes the execution of sequential heartcuts from the Ultragel column. A sequential heartcut experiment has been reported for a 10-μm microparticulate PS/DVB column [22]. In our experiment, the Ultragel column had to be switched out of line after each cut had been made. After the cut had been developed, the entire system was returned to the original chromatographic conditions. Thus, an injection was required for each heartcut, which resulted in a very lengthy experiment. However, with a totally automated system, this experiment need not monopolize operator time. The addition of a third valve, configured as an autoinjector, would eliminate the need for human intervention.

A second two-valve configuration consists of a Type-A valve followed by a Type-B valve. This configuration is very useful for sample clean-up, where the material of interest is eluted from the first column in the forward direction, and then the remaining part of the sample is back-flushed. A heartcut of either the forward-eluted or the back-flushed materials can be done to achieve further resolution. For instance, a pair of components which are poorly resolved by the first column can be back-flushed onto another column, having a different selectivity, for further separation. A chromatogram obtained in this way is shown in Fig. 7. The sample was a model mixture used to investigate the ring-separating capability of an amino column in the presence of heteroaromatic compounds. As shown in Fig. 7, single-column separation results in the co-elution of the three-ring hydrocarbon compound with the two-ring heteraromatic. When these are back-flushed onto the silica column, acceptable resolution is achieved.

The above experiment would also be possible with a single Type-D valve, because no heartcutting is necessary. In this case, the use of a single valve would be advantageous because it would require less tubing, and so limit the associated band-broadening. An additional valve would be beneficial with either the two-valve or the single-valve setup. In either configuration, the first column is always in-line. This limits the choice of mobile phases and can lengthen separation times because of the need for re-equilibration. A third valve could be used to isolate the back-flush column and would be configured as a Type-B valve with the Type-A (back-flush) valve and column in place of the single column shown in the Type-B diagram.

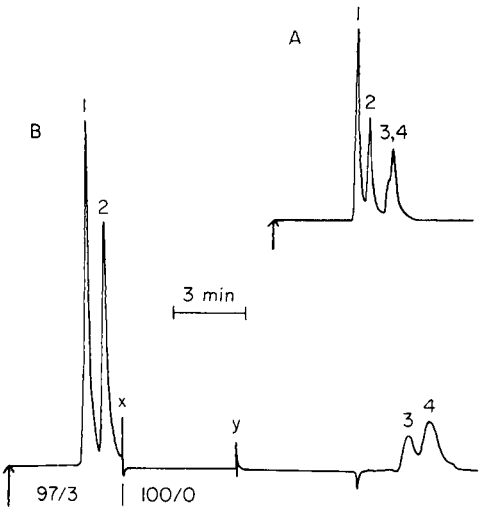

Fig. 7. Multidimensional back-flush chromatogram for a four-component mixture: (1) benzene; (2) naphthalene; (3) anthracene; (4) dibenzothiophene. (A) Single-column elution with 97:3 hexane/dichloromethane; (B) back-flush from amino to silica column with solvent change to pure hexane. X indicates the start of back-flushing and Y the switch to the silica column.

Another two-valve configuration has proved useful, especially for handling samples with constituents having widely varying polarities. It consists of a Type-A valve followed by a Type-C valve, and is called "selectivity programming with back-flush". The two columns on the second valve have two different selectivities by virtue of two different stationary phases. The column that is in the back-flush configuration on the first valve, is actually a precolumn packed with the same stationary phase as that in column 1 on the second valve. The components which are quickly eluted from the precolumn are sent on to column 1 for actual separation. The components which are highly retained on the precolumn are back-flushed onto column 2 of the second valve. Column 2 contains a stationary phase which provides reasonable resolution and separation times for these later components.

A chromatogram obtained with the selectivity-programming technique is shown in Fig. 8. The two separation columns were an amino column, used in a normal mode, and an ODS column, used in a nonaqueous, reverse-phase mode. Thus the most polar constituents were retained on the amino packing of the precolumn, and then sent onto the ODS column, where they were more readily eluted and separated. This approach proved very successful for achieving separations of the heavy end of a residual fuel within a reasonable time. The only restriction is that the mobile phases must be miscible and compatible with both stationary phases because a volume of the first mobile phase will still be present in the connecting tubing when the precolumn is back-flushed onto the second column. A third valve configured to provide a vent could eliminate this problem.

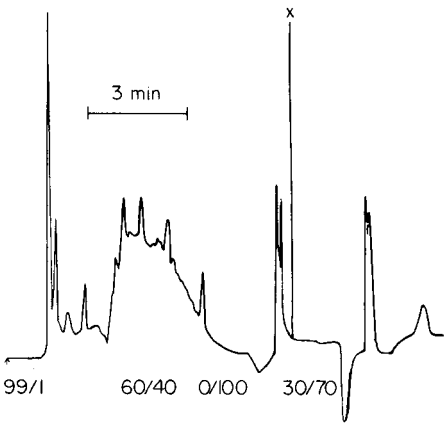

Fig. 8. Chromatogram obtained by selectivity programming with back-flush for a residual fuel sample composed of heteroaromatic components. Chromatography on an amino column starts with 99:1 hexane/tetrahydrofuran as mobile phase, with programming to 60:4 and then pure tetrahydrofuran; at point X, back-flushing is done to the ODS column and solvent is switched to 30:70 acetonitrile/tetrahydrofuran.

Conclusions

Centralized computer-control, intelligent event control, and flexible solvent delivery make this a very powerful multidimensional HPLC instrument. Reconfiguration of the system for a variety of studies is possible by simply replumbing and writing appropriate software. The capabilities can be further expanded by feeding the detector output back to the microcomputer and using its decision-making capabilities to establish a set of improved chromatographic parameters. These can then be implemented via the keypad emulator. With the addition of an auto-inject valve, this configuration would result in a self-optimizing system.

The financial assistance of NASA (Lewis Research Center, Cleveland, OH) is gratefully acknowledged.

REFERENCES

1 J. F. Huber, R. Vanderlinden and E. Ecker, J. Chromatogr., 83 (1973) 267.
2 H. Hulpke and U. Werthmann, Chromatographia, 13 (1980) 395.
3 C. D. Scott, D. D. Chilcote and N. E. Lee, Anal. Chem., 44 (1972) 85.
4 R. E. Majors, Liq. Chromatogr. HPLC Mag., 2 (1984) 1.
5 J. F. K. Huber and R. Vodenik, J. Chromatogr., 122 (1976) 331.
6 M. C. Harvey and S. D. Stearns, Am. Lab., Feb. (1981) 151.
7 J. C. Suatoni, H. R. Barber and B. E. Davis, J. Chromatogr. Sci., 13 (1975) 367.
8 G. Schmidt and W. Slavin, Chromatogr. Newsl., 9(1) (1981) 21.
9 R. L. Miller, Perkin-Elmer App. Note LC213, (1981) 1—18.
10 J. A. Apffel, T. V. Alfredson and R. E. Majors, J. Chromatogr., 206 (1981) 43.
11 F. Erni and R. W. Frei, J. Chromatogr., 149 (1978) 561.
12 F. W. Willmott, I. Mackenzie and R. J. Dolphin, J. Chromatogr., 167 (1978) 31.

13 R. A. Henry, S. H. Byrne and D. R. Hudson, J. Chromatogr. Sci., 12 (1974) 197.
14 C. J. Little, D. J. Tompkins, O. Stahel, R. W. Frei and C. E. Wekhoven-Goewie, J. Chromatogr., 264 (1983) 183.
15 H. P. M. Van Vliet, T. H. C. Boatsman, R. W. Frei and U. A. T. H. Brinkman, J. Chromatogr., 185 (1979) 483.
16 L. R. Snyder, J. W. Dolan and S. J. Vanderwal, J. Chromatogr., 203 (1981) 3.
17 B. Newcome and C. G. Enke, Rev. Sci. Instrum., 55 (1984) 2017.
18 P. M. Wiegand, K. K. Trischan and S. R. Crouch, Anal. Instrum., 14 (1985) 127.
19 P. M. Wiegand and S. R. Crouch, Talanta, 32 (1985) 37.
20 L. Brodie, Starting FORTH, Prentice-Hall, Englewood Cliffs, NJ, 1981.
21 R. J. Dolphin and F. W. Willmott, J. Chromatogr. Sci., 14 (1976) 584.
22 E. L. Johnson, R. Gloor and R. E. Majors, J. Chromatogr., 149 (1978) 571.

Analytica Chimica Acta, 187 (1986) 255—269
Elsevier Science Publishers B.V., Amsterdam — Printed in The Netherlands

DISPERSION IN PHASE SEPARATORS FOR FLOW-INJECTION EXTRACTION SYSTEMS

KENNETH BÄCKSTRÖM*, LARS-GÖRAN DANIELSSON and LAGE NORD
Department of Analytical Chemistry, Royal Institute of Technology, S-100 44 Stockholm (Sweden)

(Received 12th November 1985)

SUMMARY

Cylindrical phase separators with various volumes, incorporating a supported teflon membrane, are evaluated with respect to phase separation efficiency and dispersion, and are compared with grooved separators. At the flow rates normally used in analytical flow-extraction systems, the separation efficiency is better than 99% for a large range of phase-volume ratios (Q_{aq}/Q_{org} = 0.05—30), with some exceptions for the smallest separator, which had a total volume of only 5.6 μl. The dispersion is very low when the injection volumes are those common in f.i.a. (dispersion coefficient 1.0—1.3 for 47 μl) provided that the separation of organic phase is complete. Under these conditions, the volume of the unsegmented cavity is most important for the dispersion in the separator. The cylindrical separators are similar to the grooved type with respect to dispersion. Pulsations in the flows give lower dispersion in the unsegmented parts of the system.

In the design of a mechanized extraction system based on the concepts of flow injection analysis (f.i.a.), one vital component of the manifold is the phase separator. For the flow-injection extraction to be meaningful, the extract must be delivered to the detection system free from the other phase with reasonable recovery and without excessive sample zone broadening. Consequently, considerable efforts have been made in recent years to design efficient phase separators. The principle most often applied is to use a hydrophobic membrane to exclude the aqueous phase, thus forming a stream of organic extract free from undissolved aqueous phase. Various designs for different applications and flow systems have been reported [1—6] and an integrated extraction unit with a membrane separator has been developed and validated [7].

In earlier work with a two-step preconcentration extraction system for atomic spectrometry, it was soon found that a very high recovery of the organic phase from the first extraction was mandatory to achieve good enrichment [8]. This was not possible with the separator having a PTFE membrane supported only by its own polyethylene backing [1]. Therefore, a polyethylene net was placed behind the membrane as a more rigid support and with this modification it was possible to reach a recovery of about 97% [8]. The separator was further developed with standard circular membranes

0003-2670/86/$03.50 © 1986 Elsevier Science Publishers B.V.

and rigid supports and the groove configuration was abandoned for a cylindrical shape of the compartments because this simplified manufacture [9]. This design gave high recovery of the organic phase over a wide range of phase flow ratios.

Although the dispersion properties of phase separators have been considered [1, 6], no study has been made to elucidate the effects of various possible designs. Practical experience with a number of different designs of phase separators has shown that there are two main factors governing the contribution of the phase separator to the total dispersion of a flow-injection extraction system, namely the recovery of the separated phase and the size of the separator. It has been shown that when the recovery of organic phase increases the peak height also increases, i.e., the dispersion decreases [1]. This effect was similar for the grooved separator and the original T-piece separator [10]. Obviously, the recovery is not only an important factor in itself but also influences the dispersion.

If the internal volume of the separator is small, its contribution to the total dispersion will obviously also be small. The separator consists, however, of two compartments, one on the segmented stream side of the membrane and one on the unsegmented side. There is reason to believe that the volumes of these two compartments will affect the dispersion in different ways. It is important to have some knowledge about these contributions to the dispersion because the volume of the separator cannot be reduced indefinitely if recoveries are to be satisfactory. The configuration of the two compartments obviously will also influence the dispersion. Two different types can be distinguished, the grooved type [1] and the cylindrical type [9].

The aim of the work presented here was to examine the influence on dispersion of four important factors to be considered in the design and use of phase separators, i.e., the recovery of organic phase, the volume of the segmented flow compartment, the volume of the unsegmented flow compartment, and the shape of the compartments (i.e., cylindrical or grooved type).

THEORY

The dispersion coefficient, D, was defined by Růžička and Hansen [11] as the quotient between the concentration of the injected sample solution, C_0, and the concentration of the imaginary element of fluid that corresponds to the maximum of the recorded curve, C_{max}: $D = C_0/C_{max}$. The overall dispersion coefficient of a flow-injection system, D_{tot}, equals the product of the dispersion coefficients of the constituent parts [11]: $D_{tot} = \Pi D_i$. Thus for a flow-injection extraction system, D_{tot} could be considered as the product of the dispersion coefficients of the unsegmented and the segmented parts of the system, D_{unseg} and D_{seg}: $D_{tot} = D_{unseg}\, D_{seg}$.

In the present work, in which only the dispersion in the separators was examined, no extractions were used. Samples of coloured organic phase were injected into the organic stream and the absorbance of this phase was moni-

tored after phase separation. Thus the volumes of the segmentor and the extraction coil could be minimized so that the dispersion in these parts became negligible. Consequently, the approximation $D_{sep} \approx D_{seg}$ is reasonable, D_{sep} being the dispersion coefficient of the separator. Thus, $D_{sep} \approx D_{tot}/D_{unseg}$.

EXPERIMENTAL

Reagents and equipment

Copper diethyldithiocarbamate was prepared as described by Wyttenbach and Bajo [12] by precipitation from an aqueous solution and recrystallization. Copper diethyldithiocarbamate solutions were prepared in carbon tetrachloride (8 mg l^{-1}) or in chloroform (200 mg l^{-1} and 20 mg l^{-1}). Protected from light these solutions showed absorbance changes of <2% during 12 h. All reagents were of analytical grade.

The manifolds used are shown in Figs. 1 and 2.

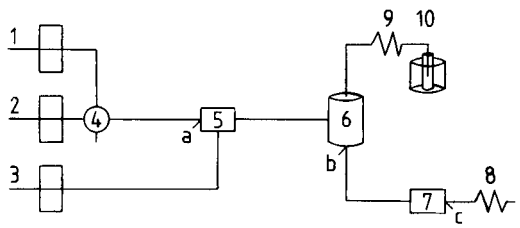

Fig. 1. Flow system: (1) coloured organic solution; (2) pure organic solvent; (3) water; (4) injector, volume 47 μl; (5) segmentor; (6) membrane phase separator; (7) photometric detector, λ = 435 nm, 8-μl flow cell; (8) and (9) restrictors; (10) vessel for monitoring the loss of organic phase. The connecting tubings (teflon) were as follows: (4—5) 8.5 cm, 0.5 mm i.d.; (5—6) 5 cm, 0.7 mm i.d.; (6—7) 19 cm, 0.35 mm i.d. plus stainless steel 9.5 cm, 0.35 i.d.

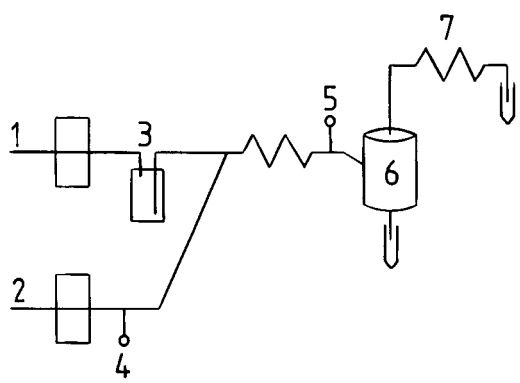

Fig. 2. Flow system: (1) water feed to displacement bottle delivering the coloured organic solution (3); (2) 0.7 M NaCl; (4) pulse damper; (5) pressure sensor; (6) membrane phase separator; (7) restrictor.

TABLE 1

Design parameters for the cylindrical separators

Separator no.	Cavity diameter (mm)	Segmented cavity volume (μl)	Unsegmented cavity volume (μl)
1	11	291	38
2	10	7.8	15.7
3[a]	10	7.8	15.7
4	6	42.3	8.5
5	6	14.1	8.5
6	6	14.1	2.8
7	6	8.5	2.8
8	6	2.8	2.8

[a]Separator 3 was of a "diagonal type" such that the outlet channel for the aqueous phase in the segmented cavity was situated opposite to the inlet channel of the segmented flow instead of at the centre of the cavity.

TABLE 2

Design parameters for the grooved separators[a]

Separator no.	Segmented groove		Unsegmented groove	
	Depth (mm)	Volume (μl)	Depth (mm)	Volume (μl)
I	0.8	63	0.4	32
II	0.4	40	0.2	23

[a]The groove length was 40 mm in each case.

Several phase separators of the cylindrical type [9] with different internal volumes were produced. For comparison, measurements were also made on two separators of the grooved type [1]. The design parameters of the separators are given in Tables 1 and 2. Here, "segmented cavity" means the cavity into which the segmented flow is introduced and "unsegmented cavity" means the cavity in which the organic phase is collected after passing through the membrane.

The membranes used in the cylindrical separators were polyethylene-backed 0.2-μm Fluoropore filters (Millipore), supported by a teflon-coated stainless steel filter support screen (13-mm diameter; Millipore). In the grooved separators, 1.0-μm Fluoropore filters (Millipore) were supported by a polyethylene net (0.17 mm thick, 150 mesh). Because this support has some flexibility, the actual volumes of the cavities will not necessarily be exactly those listed in Table 2. When the dispersion coefficient was evaluated as a function of loss of the organic phase, a more rigid support was used in the grooved separator. This support was of stainless steel (0.06 mm thick) per-

forated with hexagonal and parallelepipedal holes (each 0.2—0.4 mm^2, about 170 per cm^2) and was originally part of a Braun electric razor; this is referred to later as the "Braun support".

The use of a membrane phase separator necessitates the maintenance of a pressure drop across the membrane, in order to force the organic phase through the membrane. This is most easily achieved with the aid of a restrictor on the aqueous outflow from the separator. Further, in order to avoid the formation of gas bubbles, the whole flow system should be put under a slight overpressure [13]. Thus, effective functioning of the separator is based on proper matching of the restrictors on both outflows from the separator (8 and 9 in Fig. 1).

Two peristaltic pumps (FIA-08; Bifok, Sollentuna, Sweden) were used to pump the aqueous and organic phases through the system. The pump controlling the loss of organic phase in some experiments was also an FIA-08. The sample solution was pumped to the injector by an ALITEA-C4 peristaltic pump (Ventur Tekniska, Sweden). Pulse dampers were used in some experiments; they consisted of PTFE tubing filled with air, sealed at one end and connected to the flow system at the other end with the aid of T-joints. The volumes of the tubings were 2.8 ml for damper 1, 3.4 ml for damper 2, and 0.18 ml for damper 3. The sample was introduced to the flow system via the six-port valve injector of an FIA-05 analyzer (Bifok). The detector was a Perkin-Elmer LC-55B spectrophotometric detector equipped with an 8-μl flow cell. The pressure meter was a home-made device utilizing a piezoresistive pressure sensor (KP100 A; Philips) giving an analog output signal (0—4 V). The liquid flow meter was from Phase Separations (England).

Procedures

Evaluation of efficiency of phase separation. The manifold used is shown in Fig. 2. Tygon pump tubings were used for aqueous solutions and a displacement bottle was used for the chloroform solution, as the Acidflex tubes normally used for this solvent produced black particles accumulating on the membrane of the separator. The coloured organic solution used was a solution of copper diethyldithiocarbamate in chloroform. The concentration of the solution was 20 mg l^{-1} for flow ratios $Q_{aq}/Q_{org} \leqslant 1$ and 200 mg l^{-1} for flow ratios $Q_{aq}/Q_{org} > 1$.

Four cylindrical separators with different volumes were examined with flow ratios Q_{aq}/Q_{org} ranging from 0.05 to 30. The total flow rate was about 5 ml min^{-1} for $Q_{aq}/Q_{org} \geqslant 1$ and about 2.5 ml min^{-1} for $Q_{aq}/Q_{org} < 1$. Pulse damper 1 was used. The pressure sensor was that previously used [9]. The measuring procedure was that described earlier [9], i.e., the loss of organic phase was measured during a run of 10—20 min by adding 3 ml of pure chloroform to the collected aqueous phase and measuring the absorbance of the resultant organic solution. Any leakage of aqueous phase through the membrane was detected by measuring the sodium content in the collected organic phase.

Procedure for the evaluation of the dispersion coefficients of the separators at optimal phase separation. The dispersion coefficients of the separators were measured by injecting coloured organic solutions (47 μl) into the organic flow. The manifold used is shown in Fig. 1. Pump tubings were Tygon for water and Solvaflex for organic solutions. The organic phase was carbon tetrachloride and the coloured organic solution was 8 mg l^{-1} copper diethyldithiocarbamate in carbon tetrachloride. First, the dispersion coefficient of the unsegmented part of the system was measured by connecting **a** directly to **b** (Fig. 1). Then the segmentor/separator part of the system was inserted and the procedure was repeated to evaluate the dispersion coefficient of the total system. The dispersion coefficient of the phase separator was calculated from the approximation $D_{sep} \approx D_{tot}/D_{unseg}$.

Procedure for the evaluation of the dispersion coefficients of the separators when organic phase is lost. In order to evaluate the dispersion coefficients of the phase separators as a function of loss of organic phase, a peristaltic pump was connected to the aqueous outflow from the separator replacing the restrictor, **9** (Fig. 1). The loss of organic phase was regulated by the speed of that pump. The organic flow rate into the flow system was determined gravimetrically and the organic flow rate from the separator was measured by the PhaseSep flowmeter. The loss of organic phase was calculated from their difference. The injected sample volumes were 12 μl and 47 μl. Pulse damper 2 was connected to the aqueous outflow and damper 3 to the organic outflow of the pumps. The dispersion coefficients were evaluated as described above.

RESULTS AND DISCUSSION

Efficiency of phase separation

Of the cylindrical separators used here all but the smallest (no. 8) managed to separate more than 99% (in most cases more than 99.8%) of the organic

TABLE 3

Separation efficiency at various phase volume ratios for cylindrical separators

Total flow rate (ml min^{-1})	Phase-volume ratio Q_{aq}/Q_{org}	Loss of organic phase (%)[a]			
		Sep. no. 4 (42.3/8.5 μl)	Sep. no. 5 (14.1/8.5 μl)	Sep. no. 6 (14.1/2.8 μl)	Sep. no. 8 (2.8/2.8 μl)
5	29–33	0.67	0.19	0.49	5.9
5	18—20	0.67	0.35	0.46	1.0
5	9–12	0.16	0.08	0.07	1.0
5	4—6	0.07	0.04	0.05	0.35
5	1.0—1.1	0.02	0.11	0.74	3.7
2.5	0.2—0.3	0.10	0.05	0.08	0.18
2.5	0.09—0.10	0.04	0.03	0.17	0.21
2.5	0.04—0.05	0.22	0.02	0.00	0.02

[a]The pressure drop across the membrane was 0.5—1.1 atm.

phase from the segmented flow at the flows and phase-volume ratios tested (Table 3). The smallest phase separator (no. 8) showed good efficiency for phase-volume ratios $Q_{aq}/Q_{org} < 1$, but at higher phase-volume ratios and a total flow rate of 5 ml min^{-1}, problems occurred for $Q_{aq}/Q_{org} = 1$ and $Q_{aq}/Q_{org} = 30$. However, even under these conditions a separation efficiency of about 95% was achieved.

Tests were made to see if a more open support would give even better separation and/or less bubble formation. However, no differences were revealed when the Millipore support with 16% holes was replaced by the Braun support having 45% holes in the smallest cylindrical separator and the performances were compared at a total flow rate of 7 ml min^{-1} and Q_{aq}/Q_{org} of 13 and 22. Thus, the Millipore supports were used in all subsequent experiments with the cylindrical separators.

The pressure drop across the membrane was $\leqslant 1.1$ atm., thus virtually no sodium was detected in the organic outflow from the separators, i.e., there was no penetration of aqueous phase through the membrane ($<10^{-3}$%). It was noted that if the pressure drop across the membrane briefly exceeded 1.4 atm., the separation efficiency decreased in some cases when work was continued at normal pressure. This is believed to be due to partial water blockage of the membrane pores. After the membrane had been dried at room temperature for 1—2 h, the separation efficiency returned to normal.

Evaluation of the dispersion coefficients of the separators at optimal phase separation

At the start and end of each working day, the absorbance of the coloured organic sample solution, A_0, was measured by pumping the solution directly to the flow cell without contacting water. Then the coloured solution was pumped continuously in channel 2 (Fig. 1) and the absorbance was measured after segmentation and separation. In this way, it was checked that no loss of colour could be attributed to contact with the aqueous phase.

The dispersion coefficient of the unsegmented part of the system, D_{unseg}, was measured by connecting **a** directly to **b** (Fig. 1), then injecting the coloured solution into the organic flow and measuring the absorbance at the peak maximum, A_{max}: $D_{unseg} = A_0/A_{max,\,unseg}$. Then the segmentor/separator part of the system (**a**—**b**) was connected as shown in Fig. 1, the coloured solution was injected, the absorbance at the peak maximum was measured, and the dispersion coefficient of the total system was calculated from $D_{tot} = A_0/A_{max,tot}$.

The dispersion coefficients of the separators were evaluated for three different flow rates of organic phase, each combined with three or four different flow rates of the aqueous phase. The results are summarized in Table 4; each D_{sep} value is the mean of 3—6 determinations. The relative standard deviations for the dispersion coefficients, σ_{rel}, were estimated by the Range method [14] for each separator and are given in Table 4. The day-to-day variation, estimated by the Range method on the results for the unsegmented part of

TABLE 4

Dispersion coefficients of the separators (D_{sep}) for Q_{aq} = 0.2—6.5 ml min^{-1} and Q_{org} = 0.1—1.3 ml min^{-1}

Separator	Cavity volumes seg./unseg. (μl)	D_{sep} for Q_{org} = 0.10—1.3											σ_{rel}[a] (%)	n_{tot}[b] (%)
		Q_{aq} = 0.2			Q_{aq} = 0.9			Q_{aq} = 3.5			Q_{aq} = 6.5			
		0.10	0.54	1.3	0.10	0.54	1.3	0.10	0.54	1.3	0.54	1.3		
1 cyl.	291/38	1.07	1.24	1.30	1.04	1.04	1.15	0.91	1.22	1.16	1.20	1.15	1.0	48
2 cyl.	7.8/15.7	1.01	—	1.02	0.84	—	1.07[c]	—	—	—	—	—	1.3	18
3 cyl.	7.8/15.7	1.03	—	1.07	0.88	—	1.08	—	—	—	—	—	1.6	23
5 cyl.	14.1/8.5	0.97	1.17	—	0.92	1.00	1.05	0.90[c]	1.15	1.07[c]	1.16	—[d]	0.8	33
6 cyl.	14.1/2.8	0.90	1.11	1.25[c]	0.83	0.95	1.00	0.84	1.07[c]	1.04[c]	—	—	1.2	33
7 cyl.	8.5/2.8	0.88	1.09	—	0.83	0.95	0.98	—[d]	1.07[c]	0.98	—	—	0.7	24
8 cyl.	2.8/2.8	0.92	1.09	—	0.80	0.95	0.99	—[d]	—[d]	1.03	—	—	0.8	29
I grooved	63/32	1.00	—	1.17	0.87	—	1.07	0.92	—	1.13	—	1.10	1.1	39
II grooved	40/23	1.24	—	1.31	1.09	—	1.25	1.13	—	1.23	—	1.24	1.5	43

[a] σ_{rel}, the pooled relative standard deviation of the results for D_{sep}, estimated by the Range method. [b] n_{tot}, the total number of measurements of D_{sep}. [c] A small visible loss of organic phase, estimated to be <3%. [d] The losses of organic phase were >3%, thus it was considered inappropriate to evaluate D_{sep}.

the system, was σ_{rel} = 3.4% (n_{tot} = 24). All values for the dispersion coefficients of the separators, D_{sep}, were less than or equal to 1.3. This can be compared with the dispersion coefficient for the unsegmented part of the system, D_{unseg}, which varied slightly with the flow rate around 1.5. Although this part of the system was made as small as was practicable, its dispersion was nevertheless larger than that in the separator. This means that when a sample of 47 μl was injected into the system, the decrease in peak height caused by the phase separator was <30%, which must be considered as a rather low loss of sensitivity.

The dispersion coefficient, D_{sep}, decreased with decreasing volume of the separator, and it is the volume of the unsegmented cavity that is most important for the dispersion. This can be concluded by comparing the results for separators 5, 6, 7 and 8 in Table 4. The latter three all have the same volume of the unsegmented cavity (2.8 μl) but different volumes of the segmented cavity (14.1 μl, 8.5 μl and 2.8 μl, respectively). Separator no. 5 has the same volume of the segmented cavity as separator no. 6 but a larger volume of the unsegmented cavity (8.5 μl). The values of the dispersion coefficients, D_{sep}, for separators 6, 7 and 8 are all very similar, whereas those for separator 5 are systematically higher for all the tested flow ratios. This means that it is possible to increase the cavity volume of the segmented part of the separator with practically no loss of sensitivity by dispersion if this is necessary in order to achieve high separation efficiency at high flow rates.

Surprisingly, the values of the dispersion coefficient for the grooved separator II are higher than those for no. I, although the volume of I is larger. A possible explanation is that the supporting polyethylene net is rather flexible so that the actual volumes of the segmented and unsegmented parts of the separators are unknown; only their total is known. As the segmented and unsegmented parts of the separators contribute differently to the total dispersion, it is rather difficult to predict the result if the actual volumes of these are unknown.

The effect of flow pulsation. In many cases, the dispersion coefficients D_{sep} were found to be <1.0, i.e., the peak height in fact increased when the segmented flow with the segmentor and the separator was included in the system. However, the peak areas were the same, indicating a true change in dispersion. This effect was particularly marked for the smallest separators when a low organic flow was segmented with a higher aqueous flow. The effect could, however, also be seen when the largest separator (no. 1) was used. An example of the effect is given in Fig. 3. It must be emphasized that the flow rates were checked in each experiment and the effect could not be attributed to a decrease in flow rate caused by increased pressure, when the segmentor and the separator were introduced into the system (this pressure increase was $\leq$1 atm. and was mainly due to the restrictors used on the outflows). For an unsegmented system (**a** connected to **b** in Fig. 1), the same effect (i.e., higher peak heights) could be obtained by connecting the segmentor and the separator after the flow cell (at **c** in Fig. 1). The effect was

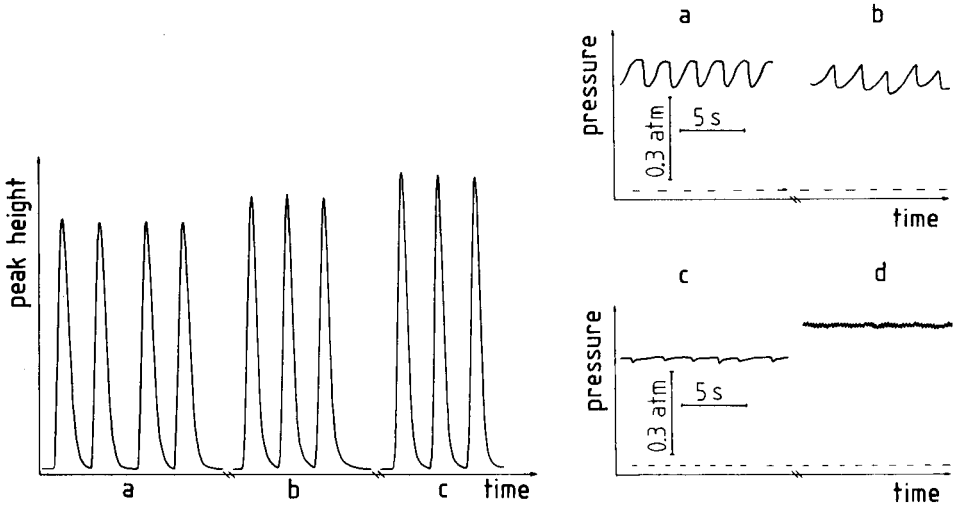

Fig. 3. Detector output signal, for the flow system of Fig. 1. Flow rates: Q_{aq} = 3.5 ml min^{-1}, Q_{org} = 0.1 ml min^{-1}. (a) Unsegmented system, (a connected to b in Fig. 1). (b) Segmented system, phase separator 1 (291-μl segmented cavity 38-μl unsegmented cavity). (c) Segmented system, phase separator 6 (14.1-μl segmented cavity 2.8-μl unsegmented cavity).

Fig. 4. Pressure pulses generated by a peristaltic pump (FIA-08, Bifok) with 2 m of 0.35-mm i.d. teflon tube as restrictor. (a—c) Pump tube, purple/black (Tygon); pump setting 140; flow rate 0.8 ml min^{-1}; mean pressure 0.42 atm. above ambient. (a) Clockwise pumping; (b) counter-clockwise pumping; (c) clockwise pumping with pulse damper 2. (d) Pump tube, orange/white (Tygon); pump setting 999; flow rate 1.1 ml min^{-1}; mean pressure 0.57 atm. above ambient. The ambient pressure is indicated by the dotted lines.

thus shown to be due to pulsations in the flow system. The pressure pulses generated by the peristaltic pumps produce fast fluctuations in the flow velocities, though the mean flow rates remain constant. The introduction of the aqueous phase increases the pulsations in the system and this reduces the dispersion in the unsegmented parts. The value used for D_{unseg} in the calculations of D_{sep} was obtained under less pulsating conditions and is therefore too high, giving measures of the dispersion in the separators that are too low. When pulse damper 2 was connected to the aqueous outflow and damper 3 to the organic outflow from the pumps, this effect disappeared for all the combinations of flow rates tested.

A closer study of the pressure pulses was made by connecting a pressure meter between the peristaltic pump and the restrictor in a one-channel system. Some examples of the recorded signals are given in Fig. 4. An interesting result was the different shape of the pulses depending on the direction in which the pumping was made. The pulses were smaller when a narrower pump tube and a higher pump setting were used to give the same flow rate. The efficiency of the pulse damper is also demonstrated in Fig. 4.

TABLE 5

Dispersion coefficients of the separators evaluated with pulse dampers in the system for Q_{aq} = 0.9 ml min^{-1}
The organic flow rate, Q_{org}, is given in ml min^{-1}.

Separator[a]	D_{sep} for Q_{org} =								σ_{rel}[b] (%)
	0.09	0.15	0.24	0.31	0.48	0.62	0.79	1.4	
1	1.15	1.15	1.18	1.20	1.18	1.23	1.27	1.31	1.3
5	1.11	1.10	1.12	1.09	1.07	1.14	1.15	1.20	0.5
8	1.01	0.99	1.03	1.01	0.99	1.01	1.05	n.d.	0.3

[a]Description and cavity volumes as in Table 4. [b]As in Table 4.

Measurements with pulse dampers in the flow streams. In order to compare the values of the dispersion coefficients D_{sep} given above with results obtained under more pulse-free conditions, experiments were done with pulse damper 2 connected to the aqueous outflow and damper 3 to the organic outflow of the pumps. The results are given in Table 5; each D_{sep} value is the mean of 3—5 determinations. A comparison with Table 4 shows that the dispersion is about 15% higher under these more pulse-free conditions. Still, the dispersion must be considered to be very small. For example, with separator 8, the dispersion coefficients were in the range 0.99—1.05 for Q_{aq} = 0.9 ml min^{-1} and Q_{org} in the range 0.09—0.79 ml min^{-1}; thus, under these flow conditions this separator gives a negligible contribution to the total dis-

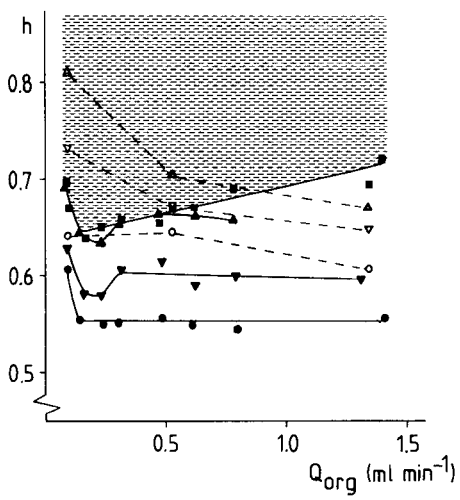

Fig. 5. Peak height h as a function of organic flow rate Q_{org} for Q_{aq} = 0.9 ml min^{-1}. (■) Unsegmented flow system. (---) Systems without pulse dampers: (○) sep. 1 (291 μl/38 μl); (▽) sep. 5 (14.1 μl/8.5 μl); (△) sep. 8 (2.8 μl/2.8 μl). (—) Systems with pulse dampers: (●) sep. 1 (291 μl/38 μl); (▼) sep. 5 (14.1 μl/8.5 μl); (▲) sep. 8 (2.8 μl/2.8 μl). $D_{sep} < 1$ in the shaded area.

persion. Figure 5 shows the dependence of the peak heights on the organic flow rate obtained for the separators 1, 5 and 8 with and without pulse dampers, as well as the peak heights obtained in the unsegmented system. The values of the apparent dispersion coefficients of the separators, D_{sep}, are < 1.0 when the recorded peak heights are higher than those for the unsegmented system.

As the values of the dispersion coefficients given in Table 4 were obtained without pulse dampers in the flow system, they also include the influence from the pressure pulses. Thus they do not give a true picture of the contribution of the separators themselves to the total dispersion. However, the results do show the relative influence of the separators on the dispersion of a normal flow-injection extraction system. Comparison of the values of the dispersion coefficients obtained with different separators and different flow conditions is valid and the results can be used as guidelines for the design of phase separators.

The results can be summarized as follows. The dispersion in the separators is low and decreases with decreasing volume of the separator. The volume of the unsegmented cavity in the separator is the most important parameter affecting the dispersion. Cylindrical separators are similar to grooved separators with respect to dispersion. The overall dispersion is decreased by the pulsating flow generated by peristaltic pumps; the use of pulse dampers results in about 15% higher dispersion.

Determination of the dispersion coefficients of the separators when some organic phase is lost

In some cases, it is difficult to achieve very high efficiency of phase separation. This may be due to high flow rates, mutual solubility of the phases or the presence of surface-active agents. Surfactants render the membrane more hydrophilic so that a high pressure drop across the membrane becomes impossible. It is therefore of interest to study the dispersion as a function of loss of organic phase. The dispersion coefficients of different separators were evaluated as functions of the loss of organic phase in the range 0—40% for injections of 47 μl or 12 μl of sample. The flow rates were 0.4 ml min^{-1} for the organic phase and 1.7 ml min^{-1} for the aqueous phase. The results are given in Fig. 6, except for the largest separator (no. 1), for which the results are listed in Table 6.

As shown above, there is very little difference in dispersion coefficient between phase separators with equal volumes in the unsegmented cavity but with different volumes in the segmented cavity at optimal phase separation. When 47 μl of sample was injected, the D_{sep} values for separators 4 and 5 were 1.05 and 1.02, respectively, and the corresponding D_{sep} values for 12-μl injections were 1.28 and 1.30, respectively. However, as soon as the pressure is too low to obtain complete phase separation, organic phase accumulates in the segmented cavity and the difference between the dispersion coefficients of the separators increases dramatically: for 47 μl of sample the D_{sep} value

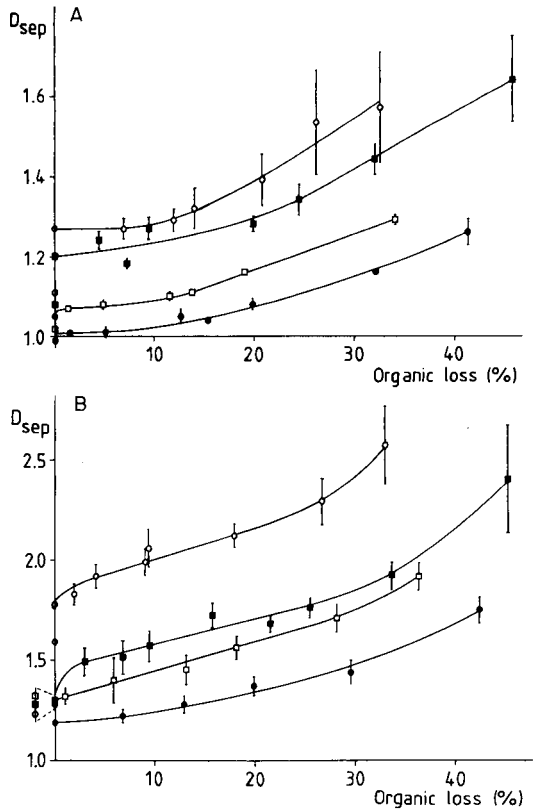

Fig. 6. Dispersion coefficients of the separators, D_{sep}, as a function of loss of organic phase. Injected sample volume: (A) 47 μl; (B) 12 μl. Separator: (○) 4 (42.3 μl/8.5 μl); (■) I (63 μl/32 μl); (□) 5 (14.1 μl/8.5 μl); (●) 8 (2.8 μl/2.8 μl). The results are given as the mean of 10 determinations ±2 σ. The results on the D_{sep} axes, for which the ±2 σ are not given in the figure, are as follows. For A: (○) 1.05 ± 0.015, 1.11 ± 0.027 and 1.27 ± 0.020; (■) 1.08 ± 0.013 and 1.20 ± 0.053; (□) 1.02 ± 0.010; (●) 0.99 ± 0.008. For B: (○) 1.28 ± 0.036, 1.59 ± 0.080 and 1.78 ± 0.160; (■) 1.29 ± 0.021; (□) 1.30 ± 0.018; (●) 1.19 ± 0.017.

TABLE 6

Dispersion coefficients, D_{sep}, of separator no. 1 (291 μl/38 μl) as a function of loss of organic phase. Injected sample volume = 47 μl

Loss of organic phase (%)	D_{sep}	σ_{rel} (%)	n
0.0	1.10	0.2	10
1.7	4.36	12.3	5
4.4	4.74	14.2	4
7.6	4.13	7.9	5
12.4	4.58	13.3	5
21.3	5.32	3.3	5
27.2	5.62	10.3	5

was 1.27 for separator 4 and 1.07 for 5; and for 12 μl of sample the D_{sep} value was 1.78 for separator 4 and 1.32 for 5. Thus, if losses occur, the importance of the segmented cavity volume increases and it will be the total volume of the separator that governs the dispersion. As the loss of organic phase increases further, there will also be an increase in dispersion caused by the decrease in sample amount reaching the flow cell. Under such conditions, there is also an increase in the variation of the dispersion coefficient, especially for separators with large segmented cavity volumes.

Because the volume of the unsegmented cavity is the most important parameter affecting the dispersion in separators under conditions without loss of organic phase, it may be advantageous to use a separator with a larger volume in the segmented cavity at high flow rates to provide high separation efficiency. However, if the pressure drop across the membrane is not high enough, there may be a gradual increase of the volume of organic phase within the segmented cavity leading to a gradual increase in dispersion. During this period, there may be no visible losses of organic phase to suggest that the pressure is too low. This is the reason for different results being obtained at zero loss for separator 4 (Fig. 6).

The grooved separator I was tested for comparison and showed the same behaviour as the cylindrical separators. The most probable reason for the increase in dispersion when losses occur in this case is axial mixing in the unsegmented groove caused by different flow velocities on either side of the membrane. When the pressure drop across the membrane is high, most of the organic phase penetrates the membrane at the start of the groove, and there is little axial mixing in the unsegmented groove. However, when losses occur, the organic segments penetrate the membrane along the whole length of the groove so that axial mixing can be significant if the flow velocities in the grooves are different.

The results can be summarized as follows. If complete phase separation can be achieved by increasing the volume of the segmented cavity of the separator, this is to be preferred. If the working conditions of the separator change from complete phase separation to losses of organic phase, a large increase in dispersion is obtained. It will then be the sum of the volumes of the two cavities in the separator that governs the dispersion coefficient of the separator.

CONCLUSIONS

This study has shown the importance of high efficiency in the phase separation in keeping the dispersion low. The incorporation of a rigid support for the membrane in the cylindrical separators makes it possible to apply the pressure drop across the membrane necessary to obtain essentially complete separation of the phases for a large range of phase-volume ratios and flow rates, even for cavity volumes below 10 μl. Provided that the separators are used under conditions such that this separation is achieved, their contri-

bution to the total dispersion in the system is almost negligible. For an injection volume of 47 μl, a dispersion coefficient below 1.3 is obtained under a variety of flow conditions. With correct choice of separator, segmented flow can be incorporated into f.i.a. practically without adding extra dispersion ($D_{sep} < 1.05$).

With close to total phase separation, the dispersion takes place in the unsegmented part of the separator. Thus relatively large segmented cavities can be used if necessary to facilitate separation at high total flow rates. When losses occur in the separation, the total volume of the separator will determine its dispersion. The dispersion of the separator is only slightly affected by the shape of the cavities. As pointed out earlier [9], these separators meet the requirements of two-step extraction methods. Further, in organic systems with slow kinetics, longer reaction times can be used without excessive dispersion by segmentation with water in a coil of some hydrophilic material (e.g., glass or steel) and subsequent separation before detection [15, 16]. This could be useful in post-column derivatization, where excessive dispersion must be avoided [17].

The kind interest shown by Professor Folke Ingman in this work is gratefully acknowledged. The separators were machined in the workshop of the Department of Physics, where Rune Persson and Lars Danielsson were especially helpful.

REFERENCES

1 L. Nord and B. Karlberg, Anal. Chim. Acta, 118 (1980) 285.
2 J. Kawase, Anal. Chem., 52 (1980) 2124.
3 T. Imasaka, T. Harada and N. Ishibashi, Anal. Chim. Acta, 129 (1981) 195.
4 L. Fossey and F. F. Cantwell, Anal. Chem., 54 (1982) 1693; 55 (1983) 1882.
5 K. Ogata, K. Taguchi and T. Imanari, Anal. Chem., 54 (1982) 2127.
6 J. A. Apffel, U. A. Th. Brinkman and R. W. Frei, Chromatographia, 18 (1984) 5.
7 Y. Sahlestrom and B. Karlberg, Anal. Chim. Acta, 185 (1986) 259.
8 K. Bäckström, L-G. Danielsson and L. Nord, Analyst, 109 (1984) 323.
9 K. Bäckström, L-G. Danielsson and L. Nord, Anal. Chim. Acta, 169 (1985) 43.
10 B. Karlberg and S. Thelander, Anal. Chim. Acta, 98 (1978) 1.
11 J. Růžička and E. H. Hansen, Anal. Chim. Acta, 99 (1978) 37.
12 A. Wyttenbach and S. Bajo, Anal. Chem., 47 (1975) 2.
13 B. Karlberg and S. Thelander, Anal. Chim. Acta, 114 (1980) 129.
14 E. L. Bauer, A Statistical Manual for Chemists, Academic Press, New York, 1960.
15 C. E. Werkhoven-Goewie, U. A. Th. Brinkman and R. W. Frei, Anal. Chim. Acta, 114 (1980) 147.
16 L. Nord and B. Karlberg, Anal. Chim. Acta, 164 (1984) 233.
17 J. F. Lawrence, U. A. Th. Brinkman and R. W. Frei, J. Chromatogr., 171 (1979) 73; 185 (1979) 473.

Analytica Chimica Acta, 187 (1986) 271—277
Elsevier Science Publishers B.V., Amsterdam — Printed in The Netherlands

DETERMINATION OF TRACES OF RARE EARTHS IN HIGH-PURITY THORIUM DIOXIDE BY NEUTRON ACTIVATION ANALYSIS

S. R. KAYASTH, H. B. DESAI and M. SANKAR DAS*
Analytical Chemistry Division, Bhabha Atomic Research Centre, Bombay 400 085 (India)
(Received 31st December 1985)

SUMMARY

The use of thorium dioxide as a nuclear fuel requires the determination of individual rare earth impurities at 0.08—1 mg kg^{-1} levels. Neutron activation is sufficiently sensitive but separation from the matrix is essential. In the proposed method, thorium dioxide (5—20 g) is dissolved in concentrated nitric acid with a little hydrofluoric acid; after evaporation, thorium is complexed with ammonium carbonate and the solution is passed through a small column of Chelex-100 resin which retains the rare earths quantitatively without retaining thorium. The rare earth elements are eluted with dilute nitric acid, concentrated, and irradiated with standards; after irradiation the rare earths are collected on a lanthanum carrier and measured by γ-ray spectrometry. The recoveries of rare earths were checked with tracers and by standard addition to thorium dioxide matrices. The reproducibility for La, Eu and Dy was satisfactory at 0.01, 0.003 and 0.002 mg kg^{-1}, respectively; as was the reproducibility for all rare earths added to thorium dioxide (1—4 μg/5 g). Limits of detection are adequate for certification of nuclear-grade material.

The use of thorium dioxide as a nuclear fuel [1] requires its analysis for rare earth contents below 1 mg kg^{-1}. The neutron activation determination of rare earths at these levels of concentration in the presence of significant amounts of thorium is not possible because of the complex γ-ray spectrum of ^{233}Pa produced from the thorium and the production of light rare earths by fast-neutron fission of thorium. The quantitative removal of thorium is therefore essential. In an early method for this analysis, the bulk of the thorium was removed by extraction with dibutoxytetraglycol (tetraethylene glycol dibutyl ether) [2]. The residual thorium was separated from the rare earths by extraction with 8-quinolinol. Rare earths from the aqueous phase were then collected on lanthanum carrier for spectrographic analysis [3, 4]. The extractant is no longer available, hence other methods of separation were sought. Thorium is quantitatively absorbed from 7 M nitric acid on strong anion exchangers [5]. However, removal of even 1 g of thorium required three passes through 20 g of resin in a 10-cm column, and the resin was attacked because of the high acid concentration.

Thorium is reported to form strong anionic carbonate complexes [6]. Attempts were therefore made to coprecipitate traces of the other rare earths with milligram amounts of lanthanum added to a solution in which thorium

0003-2670/86/$03.50 © 1986 Elsevier Science Publishers B.V.

was kept in solution with excess of ammonium carbonate. The recovery of lanthanum itself, however, was not more than 50%, as assessed by addition of ^{140}La tracer. The use of a cation-exchanger to obtain a more effective separation between the rare earths and thorium from ammonium carbonate medium was then examined. The weak cation-exchangers Zeocarb-226 and Chelex-100 were selected for this purpose because acid elution of the adsorbed rare earths would be easier [7]. When the carbonate complex of thorium with a ^{140}La tracer was passed through a pre-equilibrated 4-ml column of the carboxylate exchanger, Zeocarb-226, thorium was not adsorbed but there was only 40—50% retention of lanthanum. When a similar solution was passed through an 8-ml column of Chelex-100, retention of ^{140}La was quantitative and no thorium was retained. A systematic study of this method was therefore initiated. The results so obtained are described below.

EXPERIMENTAL

Preliminary tests

Adsorption was examined by using ^{140}La, ^{153}Sm, ^{152m}Eu, ^{160}Tb and ^{169}Yb tracers individually from a 5% (w/v) ammonium carbonate solution on an 8-ml column of Chelex-100 exchanger pre-equilibrated with dilute ammonium carbonate solution. When the column was washed with 2—4 M nitric acid, the tracer recoveries were in the range 95—98%.

All the above tracers were added to a solution containing 2 g of thorium nitrate complexed with 6 g of ammonium carbonate in a final volume of 50 ml or 250 ml. The solution was passed through the pre-equilibrated column, which was then washed with 10 ml of ammonium carbonate of the same strength before elution with 2—4 M nitric acid. The recoveries of the tracers were quantitative when the volume of the initial solution was 250 ml.

Further distribution studies were done with ^{152m}Eu as a representative tracer at different molarities of ammonium carbonate. The K_d values were found to decrease with increase in ammonium carbonate concentration. Based on these experiments, the following procedure was developed for the separation of rare earths from thorium.

Procedure

High-purity thorium dioxide (10 g) was dissolved in 100 ml of concentrated nitric acid and a few drops of 2% (w/v) hydrofluoric acid. The solution was evaporated to dryness on a water bath and the residue was taken up in a saturated aqueous solution of 30 g of ammonium carbonate. This solution was diluted to 800 ml and passed through the pre-equilibrated Chelex-100 column (10-mm diameter, 10 cm high) at a flow rate of 100 ml h^{-1}. The column was washed with 25 ml of 0.2 M ammonium carbonate. The rare earths were eluted with 100 ml of 2—4 M nitric acid. The eluted solution was evaporated to 5 ml on a water bath and taken up in 10 ml of water for irradiation in a polystyrene vial along with mixed rare-earths standards in a

similar volume. The irradiation was done at the Apsara reactor for 15 h at a neutron flux of 1×10^{12} cm^{-2} s^{-1}. After irradiation, the total rare earths were precipitated on lanthanum carrier as their oxalates after one fluoride/hydroxide cycle [8] and the rare earths were quantified by γ-ray spectrometry with a multichannel analyzer coupled to a 40-cm^3 Ge(Li) detector.

Thorium was spiked with known amounts of rare earths in the range 1–4 μg and the above procedure was applied to check the recoveries of all the rare earths. All experiments were done at least in duplicate.

RESULTS AND DISCUSSION

Plots of the percentage recovery of europium and the distribution coefficient (K_d) as a function of ammonium carbonate concentration are shown in Fig. 1. It can be seen that the recoveries of europium decreased with increase in concentration of ammonium carbonate and were quantitative at $\leqslant 0.4$ M. The operational carbonate concentration was thus fixed at 0.2 M. The results obtained in the application of the method for the analysis of nuclear-grade thoria are discussed below.

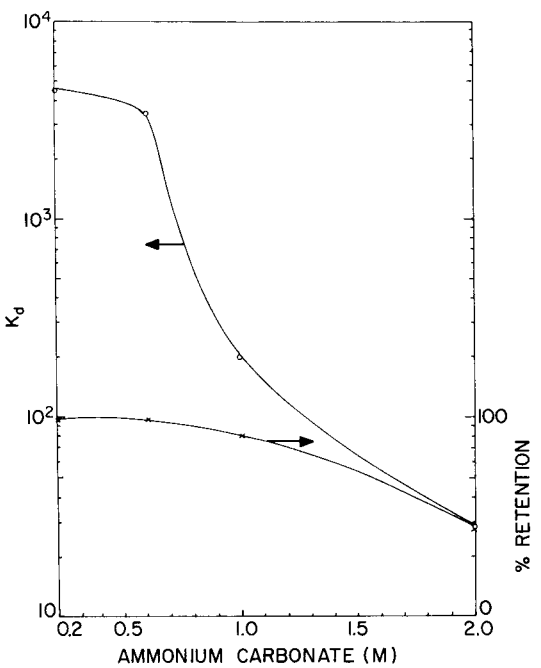

Fig. 1. Values of K_d (○) and percentage retention (×) of europium on Chelex-100 at different concentrations of ammonium carbonate.

Process blank

Because the procedure involves the pre-separation of rare earths before they are quantified, the lower limits of the determination by this method will be decided by the reproducibility of the process blank [9, 10]. The size of the blanks is governed by the intrinsic content of the rare earths in the ammonium carbonate used for complexing the thorium and the purity of the water used for the dilution of the ammonium carbonate before the solution is passed through the chelating resin. While a sample size of 5 g was considered adequate for the final determination of the rare earths by neutron activation, use of a larger sample, as much as 20 g, was envisaged for the final measurements by the simpler emission spectrometric methods which also require quantitative separation of rare earths from thorium. Thus the process blanks for 10—30 g of ammonium carbonate and the appropriate volumes of distilled water required to dilute the solution to 0.2 M in ammonium carbonate were determined. The results are given in Table 1. While the γ-ray spectra were scanned for all the rare earth elements, only the values for the four most sensitive elements are listed in Table 1. The values for other rare earth elements are not included because the photopeak signals were below the limits of detection (see below). At the very low blank levels found, it was not possible to relate them to the concentration values and their uncertainties are listed in the last column of Table 1.

Purification of the ammonium carbonate solution by passing it through an ion-exchange resin was considered but not pursued for the following reasons. Complexation of thorium is effective if the thorium solution is treated with a saturated solution of ammonium carbonate but not with the dilute 0.2 M solution. In fact, if the thorium solution is treated with dilute ammonium carbonate, the precipitated thorium carbonate does not dissolve. Further, as the retention curves indicated, the rare earth elements were not adsorbed quantitatively from carbonate solutions of strength greater than 0.5 M (cf. Fig. 1).

Application to samples of thorium dioxide

The results obtained for the analysis of a thorium dioxide sample are listed in Table 2, which also shows the specifications demanded from these analyses.

TABLE 1

Process blank for rare earths with different amounts of ammonium carbonate and distilled water (shown as 30 g/800 ml, etc.)

Element	Blank found (ng)			Mean ± s.d.
	30 g/800 ml	20 g/600 ml	15 g/400 ml	
La	37	40	40	39 ± 2
Sm	4.7	3	5	4.5 ± 1.5
Eu	2	7	4	4 ± 2.5
Dy	2	3	5	3.3 ± 1.5

TABLE 2

Analysis of thorium dioxide for rare earth elements

Element	Specification[a] (mg kg^{-1})	Element found (μg)[b]		
		Unspiked sample	Spiked sample	
			Added	Recovered
La	—	0.04	—	—
Ce	<1	<0.15	4.0	4.1
Pr	<1	<0.01	4.1	4.4
Nd	—	<0.1	4.0	3.8
Sm	<0.2	0.014	1.0	1.1
Eu	<0.08	0.017	0.2	0.22
Gd	<0.08	<0.01	4.1	4.2
Tb	—	<0.01	1.6	1.6
Dy	<0.2	0.01	0.4	0.4
Ho	—	—	2.1	2.1
Er	<0.2	<0.004	4.2	4.2
Tm	—	0.03	—	—
Yb	<0.2	<0.01	2.1	2.0
Lu	—	<0.001	1.0	0.98

[a]By Indian Rare Earths, Ltd., 1984. [b]For a 5-g sample.

The results shown, for a 5-g sample of thorium dioxide, are similar to the blanks and so are not dependable. In a second set of measurements, 5 g of thorium oxide was spiked with different rare earths at the levels of concentration expected from the specifications. The amounts added and recovered are listed in Table 2; these recoveries are quite satisfactory and the results are considered dependable in view of the significantly higher amounts of the analytes compared to the blank values.

Because the method of separation depends on the quantitative sorption of the analytes rather than the matrix, and because the magnitude of the blanks is not significantly different whether 10 or 30 g of ammonium carbonate is used, it was decided to examine the separation on 20 g of the thorium oxide in order to assess the intrinsic capability of the method for lower concentrations of the rare earth elements than could be assessed on a 5-g sample. These results are presented in Table 3 along with an assessment of the quality of the results. Against each element is shown the gross photopeak activity, the spectral background (with its standard deviation), the net signal-to-background ratio (S/B) and the limits of detection (LOD) and quantitation (LOQ). The uncertainties of measurements expressed as standard deviations were calculated from counting statistics. It can be seen that the S/B ratio ranges from a high value of 30 for lanthanum to as low as 0.08 for gadolinium. In general, La, Pr, Sm, Eu and Dy, which are quantified well above the LOQ, have S/B ratios greater than 0.5 and are measured with acceptable relative standard deviations (<10%). The signals from Ce, Nd, Tm, Yb and Gd are in the range

TABLE 3

Analysis of a 20-g sample of thorium oxide, showing the quality of the results and the limits of determination

Element	*GPPA*[a]	*B*[b]	*S/B*	Element[c] found (ng)	Limits of analysis (ng)[d]	
					LOD	*LOQ*
La	20910	675(26)	30	220(0.7)	1.5	5
Ce	1930	1590(39)	0.21	[280](13)	150	500
Pr	810	425(21)	0.9	80(7)	20	70
Nd	2560	2280(47)	0.12	[310](18)	245	800
Sm	14350	7710(88)	0.86	130(2)	8	25
Eu	8910	750(27)	11	70(1)	1	4
Gd	2590	2390(49)	0.08	[60](25)	70	220
Tb	700	630(25)	0.11	10(38)	17	60
Dy	755	440(21)	0.72	30(9)	10	30
Er	140	100(10)	0.40	[30](29)	36	150
Tm	2730	2250(47)	0.21	[80](11)	37	120
Yb	520	390(20)	0.33	[10](18)	7	25
Lu	1480	1305(36)	0.13	[2](22)	2	6

[a]Gross photopeak activity for a counting period of 4000 s, except for Dy (200 s). [b]Background count with standard deviation in parentheses. [c]Values in square brackets are indicative, being calculated on signals $\geqslant LOD$ but $< LOQ$; relative standard deviations (%) are given in parentheses. [d]$LOD = 2.71 + 4.65(B)^{1/2}$ and $LOQ = 50[1 + (B/12.5)^{1/2}]$ as defined by Currie [11].

of high uncertainty ($LOD <$ signal $\leqslant LOQ$). In such cases, the relative standard deviations are very high (15—30%). The signals from Tb and Er are uncertain (signal $< LOD$).

Conclusions

This method of separation of traces of rare earth elements from thorium can handle large samples (up to 20 g) with less than a few micrograms of thorium finally accompanying the separated rare earths. Thus it should be useful in quantifying rare earth elements not only by neutron activation but by more widely available techniques such as inductively-coupled plasma, or even d.c., emission spectrometry, which also need nearly quantitative elimination of thorium.

The use of neutron activation analysis for the final measurement of rare earth elements allows the analysis of nuclear-grade thorium dioxide to the specification limits. The practical limits of quantitation computed from the spectral background for the observed composition of rare earths after the irradiation, cooling and counting routine for the most feasible rare earths (La, Pr, Sm, Eu and Dy) are better than 70 ng, which when translated to a 20-g sample of thorium dioxide works out to better than 4 $\mu g\ kg^{-1}$. It is possible that the signals for the next five elements (Ce, Nd, Gd, Yb and Tm) which are just above *LOD* could be improved to beyond the *LOQ* by

counting the sample for a longer period, but this seems impractical because the measurements would have to be made for more than 4000 s.

The approach is also applicable for the analysis of uranium, which can be separated by the same process.

REFERENCES

1 J. P. Howe, in H. A. Wilhem (Ed.), The Metal Thorium, American Society of Metals, Cleveland, OH, 1958, Chap. 1.
2 E. K. Hyde, Proceedings of International Conference on Peaceful Uses of Atomic Energy, United Nations Publications, New York, Vol. 7 (1956) 284.
3 T. R. Saranathan and A. P. D'Silva, Atomic Energy Establishment Trombay, Report AEET/Anal 23, Bombay, India, 1963.
4 T. R. Saranathan and K. Kamala, Atomic Energy Establishment Trombay, Report AEET/Anal 24, Bombay, India, 1963.
5 J. Danon, J. Am. Chem. Soc., 78 (1956) 5953.
6 C. J. Rodden, Analytical Chemistry of the Manhattan Project, McGraw-Hill, New York, 1950, p. 182.
7 S. Ganapathy, Ph.D. Thesis, University of Bombay, 1978.
8 ORNL Master Analytical Manual, TID-7015, 1957, Oak Ridge National Laboratory, Oak Ridge, TN, U.S.A.
9 ACS Sub-committee, Recommendations on Guidelines for Data Acquisition and Data Evaluation in Environmental Change, Anal. Chem., 52 (1980) 2242.
10 IUPAC Report on Nomenclature, Symbols, Units and their Usage in Spectrochemical Analysis, Spectrochim. Acta, Part B, 33 (1978) 242.
11 L. A. Currie, Anal. Chem., 40 (1968) 586.

Analytica Chimica Acta, 187 (1986) 279—285
Elsevier Science Publishers B.V., Amsterdam — Printed in The Netherlands

RELATIONSHIP OF TWO-DIMENSIONAL PREDOMINANCE-ZONE DIAGRAMS WITH CONDITIONAL CONSTANTS FOR COMPLEXATION EQUILIBRIA

ALBERTO ROJAS

Facultad de Estudios Superiores-Cuautitlán U.N.A.M., Campo 1 Av. Quetzalcóatl, Cuautitlán-Izcalli, Edo. de México (Mexico)

IGNACIO GONZÁLEZ*

Universidad Autónoma Metropolitana-Iztapalapa, Depto. de Química, P.O. Box 55-534, 09340 México, D.F. (Mexico)

(Received 2nd January 1986)

SUMMARY

A method for the construction of two-dimensional predominance-zone diagrams for non-redox chemical species is proposed. The theory for systems containing the species L, ML and ML_2 and buffer X is developed. The chemical interactions of L, M, ML and ML_2 with X are considered through complexation coefficients dependent only on X, whereas the chemical interactions between the M/L species are treated with conditional constants which depend only on X. The method can be extended to systems which contain the species ML_3, ML_4, ..., ML_n. This permits the construction of two-dimensional predominance-zone diagrams for non-redox chemical species, with interpretation and applications similar to those of Pourbaix diagrams.

Those who work with species in solution need to know not only which species exist in a given system, but also the relative importance of each of them under certain conditions. In many aqueous systems, a cation M which reacts with a ligand L, or other species X (e.g., buffer), may be distributed among various solvated chemical species, such as M, ML, ML_2, ..., ML_n, M(OH), $M(OH)_2$, ..., $M(OH)_n$, MLH, ML(OH), M_2L, M_2LH, $M_2L(OH)$, MX, MLX, etc. (charges are omitted for simplicity).

Such systems have been studied extensively [1—3]. These treatments include concepts such as mass and charge balance [1, 2], identification of representative equilibria [2], principal equilibria which define conditional constants [3] and the use of graphic methods such as distribution diagrams [1], reaction-prediction scales [2], predominance-zone diagrams [1—3] and pM—pX diagrams [1—3]. Approaches have been suggested to handle such problems which may involve up to 15 different species in solution [3—8]. The general approach of Ringbom and Harju [6] involves attacking the overall problem in steps in order to simplify calculations but without losing sight of the larger problem. It is noteworthy that these reports cited do not

0003-2670/86/$03.50 © 1986 Elsevier Science Publishers B.V.

give much importance to predominance-zone diagrams which, despite their limitations, have proven useful as Pourbaix diagrams of potential vs. pH and in other applications [8—12].

The aim of the work reported here was to find a relationship between the conditional constant concept [3] and the predominance-zone diagrams. This can be done by generalizing Charlot's concepts and treatments [2]. Lines in predominance-zone diagrams are interpreted as conditional constants. The concepts and notation to be used are first presented for an ideal case and then applied to some real situations.

THEORY

For the species M and L, the equilibria considered are $M + L \rightleftharpoons ML$, $ML + L \rightleftharpoons ML_2$, $M + 2L \rightleftharpoons ML_2$ and $2ML \rightleftharpoons ML_2 + M$. To illustrate the notation used, the thermodynamic equilibrium constant for the first reaction above is written

$$K_{ML}^{M,L} = [ML]/[M][L]$$

and the constant for the third reaction ($M + 2L \rightleftharpoons ML_2$) is written in terms of analogous constants for the first two reactions as

$$K_{ML_2}^{M,2L} = (K_{ML}^{M,L})(K_{ML_2}^{ML,L})$$

Other reactions and constants are treated analogously. Charlot [2] showed that if $K_{ML,M}^{2ML} < 1$ (or $K_{ML}^{M,L} > K_{ML_2}^{ML,L}$) the predominance-zone diagram is

$$\underset{\log K_{ML_2}^{ML,L}}{ML_2} \quad \underset{\log K_{ML}^{M,L}}{ML} \quad M \longrightarrow \quad pL = -\log [L]$$

whereas if $K_{ML_2,M}^{2ML} \geqslant 1$, the predominance-zone diagram is

$$\underset{1/2 \log K_{ML_2}^{M,2L}}{ML_2} \quad M \longrightarrow \quad pL = -\log [L]$$

If more species (e.g., $ML_3, \ldots, ML_n$) are present, the treatment can be generalized to n successive equilibria.

Systems with M and L buffered in X

For the reactions of L, M, ML and ML_2 with X, the mass balance equations and complexation coefficients [3] are considered as $[L'] = \alpha_{L(X)}[L]$, $[M'] = \alpha_{M(X)}[M]$, $[ML'] = \alpha_{ML(X)}[ML]$ and $[ML_2'] = \alpha_{ML_2(X)}[ML_2]$. To illustrate the notation used, the complexation coefficient of ML with X is written as

$$\alpha_{ML(X)} = 1 + \sum_i K_{MLX_i}^{ML,iX}[X]^i$$

For M' and L', generalized equilibria are defined as $M' + L' \rightleftharpoons ML'$, $ML' + L' \rightleftharpoons ML_2'$, $M' + 2L' \rightleftharpoons ML_2'$ and $2ML' \rightleftharpoons ML_2' + M'$. Likewise, the conditional con-

stants [3] can be written (e.g., for the fourth reaction) as

$$K^{2ML'}_{ML'_2,M'} = [ML'_2][M']/[ML']^2 = K^{2ML}_{ML_2,M}\,\alpha_{ML_2(X)}\alpha_{M(X)}/\alpha^2_{ML(X)}$$

and can also be expressed in terms of analogous conditional constants:

$$K^{2ML'}_{ML'_2,M'} = (K^{ML'_2,L'})/(K^{M',L'}_{ML'})$$

in which L′, M′, ML′ and ML'_2 are called generalized species because at constant pX their concentrations are directly proportional to those of the chemical species of the same kind. Also, there is a direct proportionality between conditional constants of generalized equilibria and the analogous thermodynamic constants of chemical equilibria. Therefore it is possible to generalize Charlot's treatment for M with L systems buffered in X.

For example, at constant pX, if $K^{2ML'}_{ML'_2,M'} < 1$, the predominance-zone diagram for the generalized species is

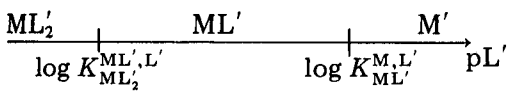

but if $K^{2ML'}_{ML'_2,M'} \geqslant 1$, then

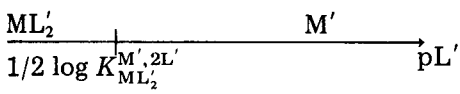

Predominance-zone diagrams using pL′ vs. pX

A two-dimensional predominance-zone diagram (pL′ vs. pX) can summarize the effects that buffering with X or changes in pL′ produce on the system. The distribution of generalized species in this diagram is related to the values of the conditional constants.

Figure 1 shows the different kinds of diagrams that can be obtained. Lines a, b and c represent $\log K^{M',L'}_{ML'}$, $\log K^{ML'_2,L'}_{ML'_2}$ and $1/2 \log K^{M',2L'}_{ML'_2}$, respectively.

The establishment of conditions under which a given generalized species (or even a chemical species alone) may predominate in the system, has practical significance because the physicochemical properties of systems depend on the relative importance of generalized species as well as the stoichiometric relationship of reactions between M′ and L′ on buffering with X. The similarity between these pL′ vs. pX diagrams, and Pourbaix's diagrams is noteworthy; whereas the latter diagrams show the thermodynamic stability zones of a specific oxidation state, the former show the same information for generalized species in a given degree of complexation.

Fundamental difference from Ringbom's treatment

The scope and treatment previously reported by Ringbom and coworkers [3–7] and those presented here are aimed at different problems. While the former is used for the evaluation of stability constants or spectrophotometric titrations, the present treatment is used for the construction of predominance-zone diagrams.

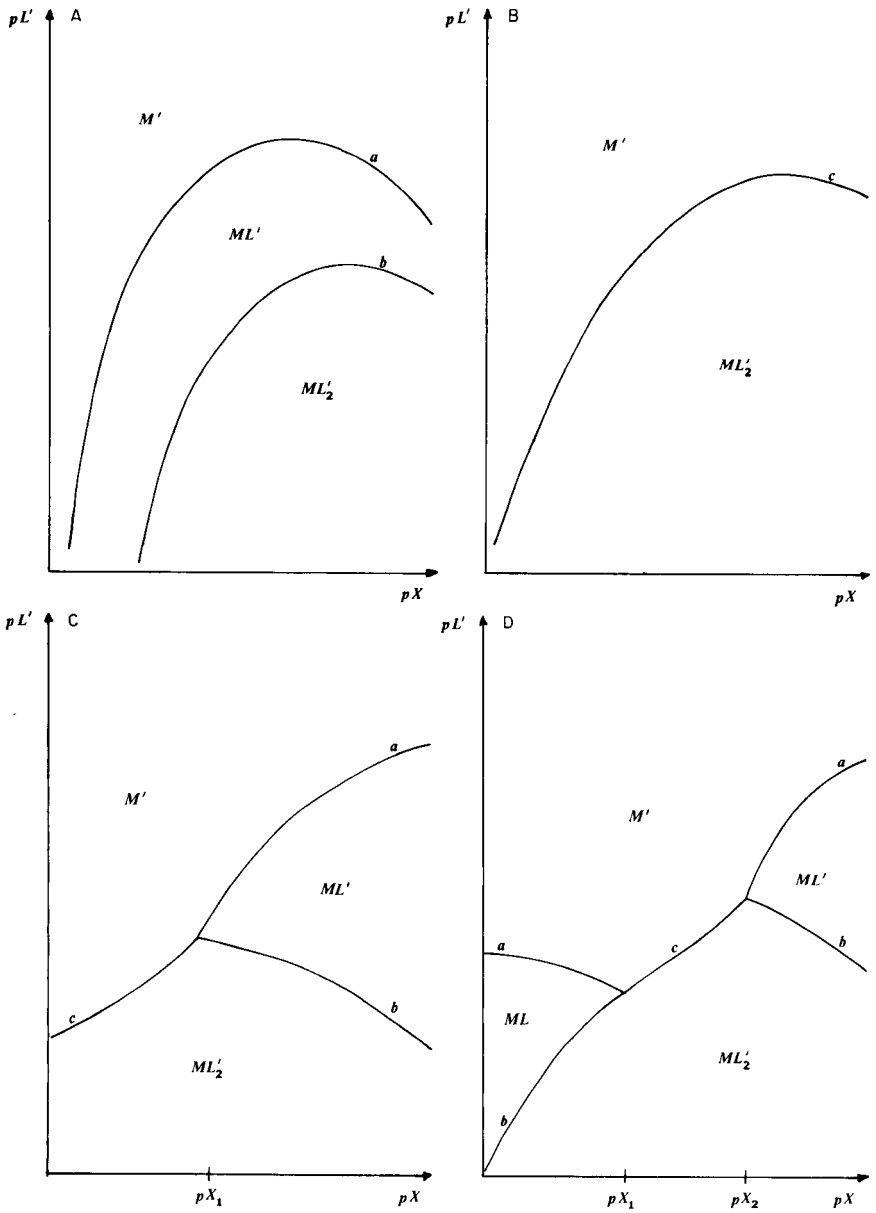

Fig. 1. Diagrams of the predominance-zone of the generalized species M', ML' and ML'_2 as functions of pL' and pX, showing the influence of the value of the equilibrium constant ($K^{2ML'}_{ML'_2,M'}$). (A) $K^{2ML'}_{ML'_2,M'} < 1$ at any pX value; (B) $K^{2ML'}_{ML'_2,M'} \geq 1$ at any pX value; (C) $K^{2ML'}_{ML'_2,M'} \geq 1$ if $pX < pX_1$, and $K^{2ML'}_{ML'_2,M'} < 1$ if $pX > pX_1$; (D) $K^{2ML'}_{ML'_2,M'} \geq 1$ if $pX_1 < pX < pX_2$, and $K^{2ML'}_{ML'_2,M'} < 1$ if $pX > pX_2$ or $pX < pX_1$. Lines a—c are explained in the text.

To illustrate this, a titration of M with L to two end-points in buffered solution is discussed below. Harju and Sara [7] proposed that such a titration be studied before and near the first end-point, in agreement with Ringbom [3], by using the principal equilibrium, $M' + L' \rightleftharpoons ML'$, the conditional constant of which includes $\alpha_M = \alpha_{M(X)}$, $\alpha_{ML} = \alpha_{ML(X)}$ and $\alpha_L = \alpha_{L(X)} + \alpha_{L(ML)} - 1$. Regarding the titration near and after the second end-point, they proposed the principal equilibrium $ML' + L' \rightleftharpoons ML_2'$ with conditional constant including $\alpha_L = \alpha_{L(X)}$, $\alpha_{ML_2} = \alpha_{ML_2(X)}$ and $\alpha_{ML} = \alpha_{ML(X)} + \alpha_{ML(diss)} - 1$. It is noteworthy that the influence of ML_2' on the former equilibrium and of M' on the last equilibrium are considered through $\alpha_{L(ML)}$ and $\alpha_{ML(diss)}$, respectively, otherwise these complexation coefficients depend upon [L] [7], and thereby the conditional constants of the principal equilibria also vary with [L] despite the buffer species, X.

In the treatment proposed here, in agreement with Charlot [2], the generalized equilibrium $2ML' = ML_2' + M'$, accounts for the reciprocal influence of ML_2' on ML' stability and of M' on ML_2' stability without the use of complexation coefficients.

EXAMPLES OF REAL SYSTEMS

Zinc(II) with oxalate (L^{2-}) as a function of pH

Based on the stability constants reported by Ringbom [3], and the generalized equilibria considered at different pH values ($Zn' + L' \rightleftharpoons ZnL'$, $ZnL' + L' \rightleftharpoons ZnL_2'$, $Zn' + 2L' \rightleftharpoons ZnL_2'$ and $2ZnL' \rightleftharpoons ZnL_2' + Zn'$), the complexation coefficients and the conditional constants were calculated as explained above. The predominance-zone diagram pL' vs. pH of the zinc(II) species is shown in Fig. 2.

Figure 2 shows that ZnL' (either ZnL or $ZnHL^+$) can predominate at pH <9.75 because $K^{2ZnL'}_{ZnL_2',Zn'} < 1$. The stoichiometry and completeness of Zn(II) reaction with oxalate at different pH values can also be predicted; at pH 6.0, two successive reactions (1:1) are expected; at pH 10.5, only one

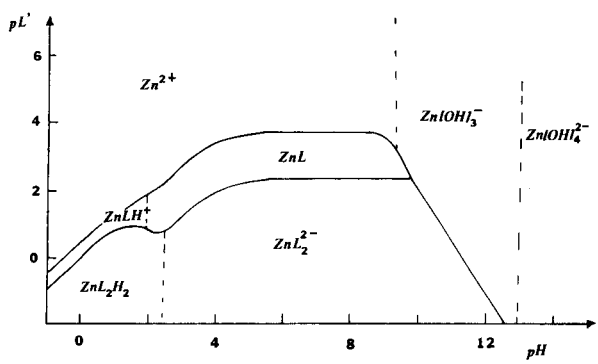

Fig. 2. Predominance-zone diagram of Zn(II)/oxalate (L^{2-}) complexes, as functions of the generalized oxalate activity (L') and pH.

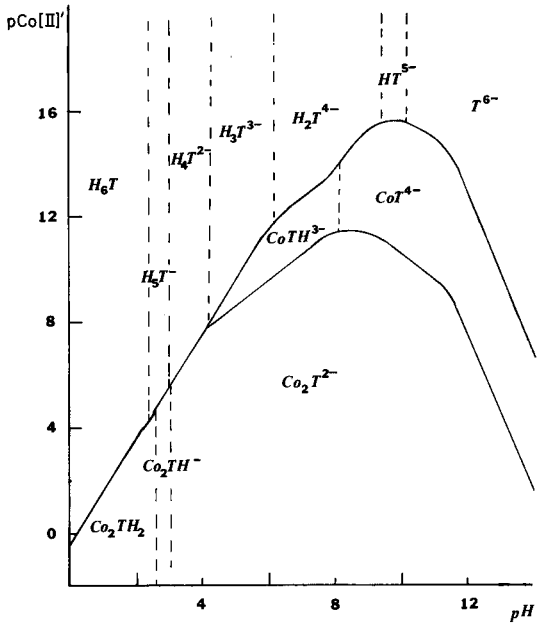

Fig. 3. Predominance-zone diagram of triethylenetetraminehexaacetic acid (H_6T)/Co(II) complexes as functions of generalized Co(II) activity, [Co(II)'] and pH.

incomplete reaction (1:2) is expected. Finally, in a system with [Zn(II)] = 10^{-4} M and [L'] = 10^{-2} M at pH 1.0, Zn^{2+} predominance is observed despite the high generalized oxalate concentration relative to the total zinc(II) concentration.

TTHA with cobalt(II) as a function of pH

Triethylenetetraminehexaacetic acid (TTHA; H_6T) reacts readily with cobalt(II) ions. Based on the stability constants reported by Ringbom and Wänninen [8], and on the generalized equilibria, $T' + Co' \rightleftharpoons CoT'$, $Co' + CoT' \rightleftharpoons Co_2T'$, $T' + 2Co' \rightleftharpoons Co_2T'$ and $2CoT' \rightleftharpoons Co_2T' + T'$, complexation coefficients and conditional constants were calculated as explained above. The predominance-zone diagram pCo' vs. pH of TTHA species given in Fig. 3 shows that the treatment proposed here can be used for predominance-zone diagrams of polybasic systems. Similar conclusions to those obtained in the previous example were obtained for such systems. Finally, the comparison between the predominance-zone diagram shown in Fig. 3 and the plots of $\log K' = f(\mathrm{pH})$ and $\mathrm{pM_{eq}} = g(\mathrm{pH})$ obtained for the same system by Ringbom and Harju [6] illustrate the different approaches of the two treatments.

We thank Dr. J. Ibañez for the English translation.

REFERENCES

1 I. M. Kolthoff, E. B. Sandell, E. J. Meehan and S. Bruckenstein, Quantitative Chemical Analysis, MacMillan, New York, 1969.
2 G. Charlot, Cours de Chimie Analytique Générale, Masson, Paris, 1967.
3 A. Ringbom, Complexation in Analytical Chemistry, Wiley-Interscience, New York, 1963.
4 L. Harju and A. Ringbom, Anal. Chim. Acta, 49 (1970) 205.
5 L. Harju, Anal. Chim. Acta, 50 (1970) 475; 63 (1973) 95.
6 A. Ringbom and L. Harju, Anal. Chim. Acta, 59 (1972) 33, 49.
7 L. Harju and R. Sara, Anal. Chim. Acta, 73 (1974) 129.
8 A. Ringbom and E. Wänninen, in I. M. Kolthoff and P. J. Elving (Eds.), Complexation Reactions, Treatise on Analytical Chemistry, Vol. 2, Part A, Wiley, New York, 1979.
9 M. Pourbaix, Atlas of Electrochemical Equilibria in Aqueous Solutions, Pergamon Press, Oxford, 1966.
10 F. J. C. Rossotti and H. S. Rossotti, The Determination of Stability Constants, McGraw-Hill, New York, 1961.
11 S. Vicente-Pérez, Química de las Disoluciones, Alhambra, Madrid, 1979.
12 J. Kragten, Atlas of Metal Ligand Equilibria in Aqueous Solution, Horwood, Chichester, 1978.

Analytica Chimica Acta, 187 (1986) 287—291
Elsevier Science Publishers B.V., Amsterdam — Printed in The Netherlands

Short Communication

A MICROSENSOR FOR ADENOSINE-5′-TRIPHOSPHATE pH-SENSITIVE FIELD EFFECT TRANSISTORS

MASAO GOTOH

Research Department, NOK Corporation, 4-3-1 Tsujidoshinmachi, Fujisawa 251 (Japan)

EIICHI TAMIYA and ISAO KARUBE*

Research Laboratory of Resources Utilization, Tokyo Institute of Technology, Nagatsuta, Midori-ku, Yokohama 227 (Japan)

YASUO KAGAWA

Department of Biochemistry, Jichi Medical School, Minamikawachi, Tochigi-ken, 329-04 (Japan)

(Received 4th April 1986)

Summary. The sensor for adenosine-5′-triphosphate (ATP) is based on H^+-ATPase immobilized via a polyvinylbutyral resin on a pH-sensitive field effect transistor. A linear relationship was obtained between the initial rate of change of the differential gate output voltage and the logarithm of the ATP concentration over the range 0.2—1.0 mM ATP. The optimum pH was 9.0 at 40°C but pH 7.0 was preferred for routine measurements. Only slight responses were obtained for 1 mM glucose, creatinine or urea. The ATP-sensing system exhibited a response to 1 mM ATP for at least 18 days.

The determination of adenosine-5′-triphosphate (ATP) is important in industrial processes and clinical analysis and is usually based on spectrophotometry [1] or bioluminescence [2, 3]; these methods are rather lengthy because of the multi-step reactions involved. The development of a simple, inexpensive assay is therefore of interest and the miniaturization of enzyme sensors is especially important for clinical analysis. Semiconductor fabrication technology has permitted the development of ion-selective field-effect transistor (ISFET) devices which have been utilized as pH and enzyme-based sensors [4]. The enzyme H^+-ATPase catalyzes the hydrolysis of ATP to ADP and orthophosphate. Several studies on its function in biological membranes have been reported [5—8]. In this communication, the preparation and characteristics of a bioelectrochemical system for ATP determination based on ISFETs and H^+-ATPase, are described.

Experimental

Materials. The H^+-ATPase (E.C. 3.6.1.3 from thermophilic bacterium PS3) was prepared as described by Yoshida et al. [5]. This enzyme is classified as thermophilic F_1 or TF_1. The ATP was purchased from Kyowa Hakko Co.

0003-2670/86/$03.50 © 1986 Elsevier Science Publishers B.V.

and polyvinylbutyral resin from Wako Pure Chemical Industries. The structure of polyvinylbutyral resin is as follows:

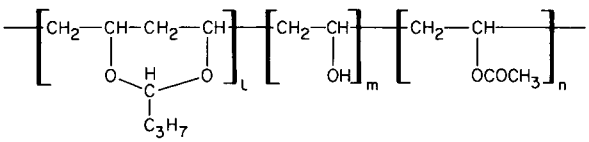

It consists of vinylbutyral, vinyl alcohol and vinyl acetate moieties in the approximate ratio 75:22:3. Dichloromethane and glutaraldehyde were obtained from Kanto Chemical Co., and 1,8-diamino-4-aminomethyloctane was a gift from Asahi Kasei Industries. All other chemicals used were of analytical grade. All solutions were prepared in distilled water.

Construction of the ISFET device. The fabrication procedure for the ISFET was basically the same as for the metal–insulator–semiconductor FET [9]. The gate insulator of the FET is composed of two layers; the lower is thermally grown silicon dioxide and the upper is silicon nitride, which is sensitive to H^+ ions and also has a barrier effect to the penetration of other ions. The thickness of both layers is ca. 0.1 μm. After wire-bonding, the chip was fixed with epoxy resin onto the end of a glass tube.

Formation of the resin membrane over the ISFET. The sensor system consists of two ISFETs; one having a cross-linked polyvinylbutyral resin/H^+-ATPase membrane (ATP-sensitive FET), and the other having only the cross-linked polyvinylbutyral resin membrane (pH-sensitive FET). The membrane was formed over the gate insulator of the two ISFETs as follows: 0.1 g of polyvinylbutyral resin and 1 ml of 1,8-diamino-4-aminomethyloctane were dissolved in 10 ml of dichloromethane; after stirring for ca. 30 min, this polymer solution was added dropwise over the gate insulator of each FET. The FETs were then immersed in 5% (v/v) glutaraldehyde solution at room temperature for 24 h to promote the cross-linking reaction of the amino group of 1,8-diamino-4-aminomethyloctane with glutaraldehyde.

Surface characterization of the membrane. After the polyvinylbutyral resin membrane containing 1,8-diamino-4-aminomethyloctane had been formed over the ISFET, it was dried with a critical-point dryer (Hitachi, HCP–2), gold was sputtered onto it, and its surface structure was observed by scanning electron microscopy (Hitachi, S–415).

Enzyme immobilization and ATP determination. The H^+-ATPase was immobilized on the cross-linked resin membrane covering the gate insulator of the FET by immersing the tip into a 5 mg ml^{-1} H^+-ATPase solution at 4° C for 16–24 h.

The response of the FET to ATP was measured in a differential voltage mode, by measuring the difference in gate output between the ATP-sensitive gate and the pH-sensitive gate. The circuit diagram is shown in Fig. 1. An Ag/AgCl reference electrode was placed directly in the solution with the two FETs. The gate voltage was measured between the Ag/AgCl reference electrode and the source of the enzyme-coated FET and the pH-sensitive FET.

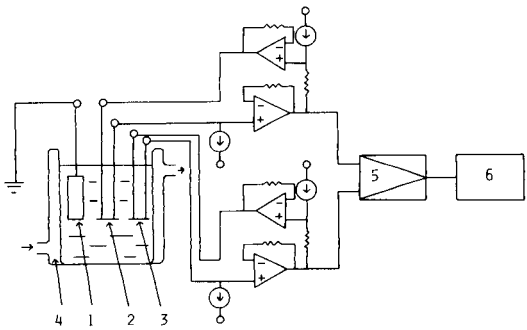

Fig. 1. Circuit diagram of measuring system: (1) Ag/AgCl reference electrode; (2) enzyme-coated FET; (3) pH-sensitive FET; (4) thermostatted cell; (5) differential amplifier; (6) recorder.

Variation in solution pH changes the surface potential on the silicon nitride insulators of the two FETs, giving rise to a proportional change in the gate output voltage. In this case, the voltage between source and drain is held constant at 4.0 V, the current between source and drain also being constant at 500 μA. The differential gate output voltage between the two FETs was displayed on a recorder (TOA Electronics, Model EPR—100A). The total volume of solution in the cell was 3.9 ml, and was composed of 50 mM Tris maleate buffer, 2 mM in magnesium chloride. The ATP samples were also made up in this solution. The cell temperature was controlled at 40 ± 1°C. The two FETs and the Ag/AgCl reference electrode were allowed to remain in this solution for 10—20 min to allow the differential gate output voltage to reach a steady state. A 100 μl aliquot of ATP sample solution was then injected into the cell and the differential gate output voltage change was recorded.

Results and discussion

The cross-linked polyvinylbutyral resin membrane formed on the FET surfaces was observed by scanning electron microscopy. The maximum pore diameter was 0.79 μm and the mean pore diameter 0.25 μm; the observed surface area was 8.1×10^{-7} cm^2. It was therefore concluded that the polyvinylbutyral resin membrane possessed a multipore microfilter structure, with high specific surface area ideally suited for enzyme immobilization. Moreover, this structure is suitable for the diffusion of substrates and products.

The pH dependence of gate output voltage is shown in Fig. 2. It can be seen that pH changes in the solutions were automatically compensated by the differential voltage measurement. The gate output voltage/pH characteristics of the FETs with and without the polyvinylbutyral resin membrane were almost identical. The pH sensitivity was 54—61 mV pH^{-1} at 36—41°C. Both FETs showed a linear relationship between the gate output voltage and pH over the pH range 5—10.

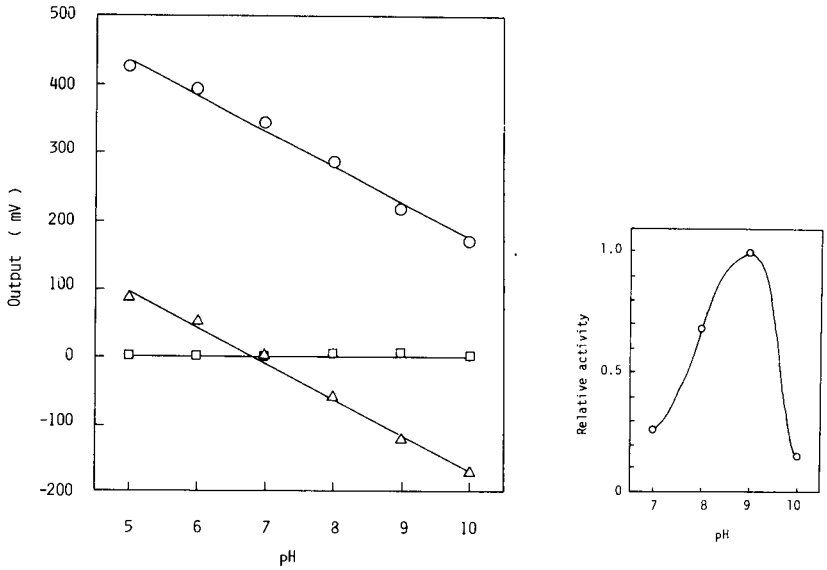

Fig. 2. pH dependence of gate output voltage at 40°C: (○) one FET gate output; (△) other FET gate output; (□) differential gate output.

Fig. 3. Effect of pH on activity of the ATP sensor system at 40° C. The initial rate of change of the differential gate output for 1.0 mM ATP at pH 9.0 is defined as an activity of 1.0.

The temperature was held constant at 40° C because this is the usual temperature for the H^+-ATPase assay [5, 6]. The effect of pH on the activity of the ATP sensor system is shown in Fig. 3. The pH of greatest activity was 9.0. This pH, however, is not generally encountered in biological systems, and pH 7.0 was used in subsequent experiments; the activity was then 27% of that of pH 9.0.

Response to ATP. The response/time curves of the system for different ATP concentrations are shown in Fig. 4. There is a rapid initial increase in the differential output, followed by a gradual decay. A similar response has been reported for a urea-sensitive enzyme-FET [10]. It is considered that the initial rapid increase in the differential output is due to the diffusion of the hydrogen ions generated by the enzyme reaction through the membrane on the enzyme-FET. The gradual drop in the output can be attributed to the following phenomena: a pH change in the vicinity of the immobilized enzyme causes a decrease in enzyme activity and the substrate concentration surrounding the immobilized enzyme gradually decreases because of diffusion limitations in unstirred solution.

The initial rate of change in the differential gate output voltage after injection was plotted against the logarithm of the ATP concentration. A linear relationship was obtained in the range 0.2—1.0 mM ATP at pH 7.0. No

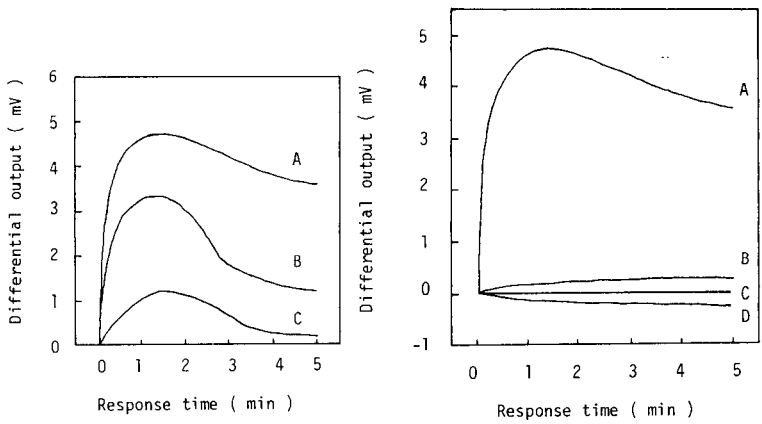

Fig. 4. Responses to ATP: (A) 1.0 mM; (B) 0.6 mM; (C) 0.2 mM. ATP was injected into the buffer solution at pH 7.0, 40° C, at time zero.

Fig. 5. Responses of the ATP-sensing system to various compounds: (A) ATP; (B) glucose; (C) creatinine; (D) urea. Solutions (1 mM) were injected into the buffer pH 7.0, 40° C.

detectable response was observed below 0.2 mM ATP compared to the buffer solution, and above 1.0 mM, the response did not increase appreciably.

Selectivity. The selectivity of the system is indicated in Fig. 5. Only slight responses were obtained for 1 mM glucose, urea or creatinine when the measurements were made in the differential mode. The responses found are attributed to slight unknown differences in the samples affecting the differential voltage between the enzyme-FET and the pH-sensitive FET, and not to lack of H^+-ATPase selectivity.

Between measurements, the coated FETs were stored at 4° C. The ATP-sensor system showed a 90% decreased response to 1 mM ATP after 18 days, probably because of enzyme denaturation during storage and operation.

We thank Mr. J. M. Dicks for helpful discussions.

REFERENCES

1 T. Bucher, Biochim. Biophys. Acta, 1 (1947) 292.
2 M. Deluca, in A. Meister (Ed.), Advances in Enzymology, Wiley, New York, 44 (1976) 37.
3 L. J. Blum, P. R. Coulet and D. C. Gautheron, Biotechnol. Bioeng., 27 (1985) 232.
4 S. Caras and J. Janata, Anal. Chem., 52 (1980) 1935.
5 M. Yoshida, N. Sone, H. Hirata and Y. Kagawa, J. Biol. Chem., 250 (1975) 7910.
6 M. Yoshida, N. Sone, H. Hirata and Y. Kagawa, J. Biol. Chem., 252 (1977) 3480.
7 T. Hamamoto, K. Ohno and Y. Kagawa, J. Biochem., 91 (1982) 1759.
8 Y. Kagawa, J. Biochem., 95 (1984) 295.
9 T. Matsuo and E. Esashi, Sensors and Actuators, 1 (1981) 77.
10 Y. Miyahara, F. Matsu, T. Moriizumi, H. Matsuoka, I. Karube and S. Suzuki, in T. Seiyama, K. Fueki, J. Shiokawa and S. Suzuki (Eds.), Chemical Sensors, Kodansha, Tokyo, Elsevier, Amsterdam, 1983, p. 513.

Analytica Chimica Acta, 187 (1986) 293—299
Elsevier Science Publishers B.V., Amsterdam — Printed in The Netherlands

Short Communication

THERMAL CYCLING FOR PIEZOELECTRIC GAS DETECTOR SYSTEMS

T. E. EDMONDS*

Department of Chemistry, Loughborough University of Technology, Loughborough, Leics. LE11 3TU (Great Britain)

M. J. HEPHER[a] and T. S. WEST

The Macaulay Institute for Soil Research, Craigiebuckler, Aberdeen AB9 2QJ (Great Britain)

(Received 15th March 1986)

Summary. The effect of temperature (0—60°C) on the operation of a piezoelectric gas monitor is discussed. The development and application of small solid-state systems incorporating Peltier devices to allow rapid thermal cycling or isothermal operation of these monitors are evaluated. Thermal performance of the Peltier/gas monitor system is discussed, and frequency response profiles for a model analyte gas/crystal coating system (sulphur dioxide/triethanolamine) are reported.

The development of dynamic real-time piezoelectric monitors is still at an early stage [1—4]. However, the prospects are promising for instant monitoring of gas concentrations at a coated piezoelectrical crystal by following the decrease in frequency. The linear relationship between frequency and mass may be expressed by the Sauerbrey equation which is adequately discussed elsewhere [1—5]. A typical piezoelectric crystal monitor consists of an AT-cut quartz crystal (resonant frequency 9.0 MHz) fitted into a cell (internal volume 2.5 cm^3) and incorporated into an oscillator circuit [2].

Temperature control

Close temperature control is important for monitoring low ppm(V) gas concentrations because of the value of the temperature coefficient (k) of the resonant frequency of a quartz crystal. For an AT-cut piezoelectric crystal, k varies sinusoidally with operating temperature T [5—9]. The dependence of k on T poses some problems in the design of temperature-corrected piezoelectric monitors. The problem can be decreased by operating the crystal at temperatures where k is more or less temperature-independent (i.e., at temperatures on the peak or in the trough of the sinusoidal curve). Two such regions for a 35° 19.5′ AT-cut crystal resonating at 9 MHz appear to occur at

[a]Present address: West of Scotland College of Agriculture, Auchincruive, Ayrshire KA6 5HW, Great Britain.

0003-2670/86/$03.50 © 1986 Elsevier Science Publishers B.V.

20° C and 45° C. In a third region, 0° C, k is ca. 110 Hz K^{-1} [4]. However, the k/T curves vary because of small variations in the angle of cut, so that each crystal may have different temperature regions in which k is constant. The effect of temperature on the fundamental frequency of the quartz crystal used in this work was such that between 15° C and 50° C the crystal frequency varied by only 0.44 Hz K^{-1} while in the 0° C region it varied by 9.33 Hz K^{-1}. Thus operation of the crystal in the region 15–50°C is best for achieving lowest frequency drift with temperature changes.

Other factors may also influence the selected operational temperature such as sorption sensitivity and rate and desorption rate for a particular analyte gas/crystal coating system. The sulphur dioxide/triethanolamine system used here exhibits a Langmuir type adsorption isotherm (i.e., fairly rapid sorption followed by slow desorption). Generally, chemisorption is more favoured kinetically and thermodynamically by low temperatures, while the rate of desorption increases with increasing temperatures. Obviously there is conflict between the optimum temperatures required to achieve rapid sorption and desorption responses to increases and decreases in analyte gas concentration. Recent work [4] indicated that improved sensitivity and lower detection limits are attainable by operating a triethanolamine-coated quartz crystal to monitor sulphur dioxide at 10° C. At 40° C, improved detector recovery time was observed at the expense of sensitivity.

In view of the different temperature requirements of sensitivity, sorption and desorption rates and crystal frequency stability, it was decided to investigate the feasibility of cycling the temperature of a piezoelectric detector between fixed, closely controlled temperatures, in order to optimize conditions for both the sorption and desorption processes. The requirement for operating below ambient temperature, the capacity for rapid thermal cycling and the need for small portable equipment for field operation prompted the investigation of Peltier devices for this purpose.

Experimental

An AT-cut quartz crystal (1 cm^2 × 0.018 cm thick, with gold electrodes over the centre 0.28-cm^2 area on each side) was coated over both sides (whole area) with triethanolamine (Phase Sep. Ltd.). This was mounted in a large stainless steel impinger cell [4] and connected to the gas mixing system and associated electronic equipment (Fig. 1). The latter consisted of the piezoelectric crystal oscillators, and a frequency meter connected via a digital-to-analog converter (DAC) to a chart recorder. The progress curves for the sorption of sulphur dioxide by triethanolamine between 0 and 60° C were recorded by monitoring the decrease in the crystal frequency with time.

Two methods were used for extracting analytical data from the sorption progress curves recorded. In one, the equilibrium shift (ES) in frequency was measured, in the other (IRR) the rate of change in frequency was monitored over the initial linear portion of the progress curve (the extent of this linear portion depends on the gas/coating system under study, but with the SO_2/

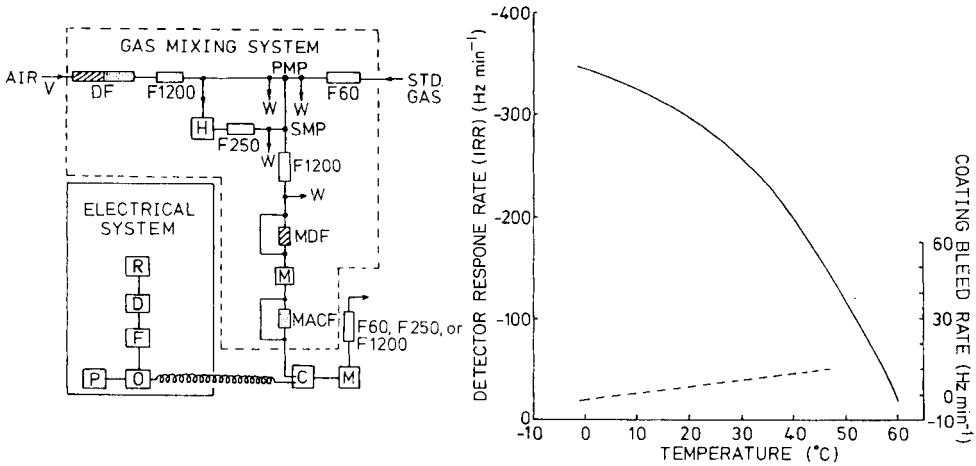

Fig. 1. Piezoelectric gas sorption development system: (DF) drying filter and activated charcoal filter; (MDF) mini-drying filter; (M) green or yellow spot Shaw humidity probes; (MACF) mini-activated charcoal filter; (C) cell in water bath or Peltier device; (H) humidifier; (F1200) flow meter, max. 1200 cm^3 min^{-1}; (F250) flow meter, max. 250 cm^3 min^{-1}; (F60) flow meter, max. 60 cm^3 min^{-1}; (V) pressure regulator; (•) 2- or 3-way taps; (→ W) gas bleed points, to waste, for flow balance; (PMP) primary mixing point for analyte gas dilution; (SMP) secondary mixing point for further analyte gas dilution; (— — — —) oven (room temperature—80°C); (R) recorder; (D) DAC; (F) frequency meter; (O) main OX oscillator; (P) power pack.

Fig. 2. Effects of temperature (—) on initial sorption rate for SO_2/triethanolamine system; (— —) on coating bleed rate (5 ppm(V) SO_2, <800 ppm(V) H_2O, 50 cm^3 min^{-1} gas flow, 79 μg coating over whole area ≡ 22 μg over gold electrodes).

triethanolamine system used here, it was generally less than 60 s). The latter method was assumed to measure the initial rate of sorption during a period in which pseudo-first-order kinetics was followed. In this case, the temperature of the cell was controlled by use of an ice bath and a thermostatted water bath. The sorption reaction was allowed to continue only while pseudo-first-order kinetics was obeyed. Figure 2 shows the effect of temperature on the IRR detector response and coating bleed rate.

Various Peltier cooler and cell geometries were examined. Initially, two water-cooled Peltier devices (De La Rue Frigister Ltd.) were mounted in a sandwich configuration around a small detector cell (Fig. 3a) made from ca. 0.1 mm thick steel with an internal volume of 2.5 cm^3. The entire cell and Peltier/water cooler assembly measured ca. 4 × 4 × 4 cm. At a Peltier current of 3.8 A, heating and cooling rates of 12—13°C min^{-1} from 14—59°C were achieved. It was also noted that during a test at supposedly constant temperature a shift in temperature of several degrees took place within the cell, varying according to the ambient temperature (range 18—27° C), and arising from the gas flow. This effect was decreased but not completely eliminated by attaching a 10 cm × 0.04 cm i.d. stainless steel coil to the gas inlet port, between the Peltier device and the cell.

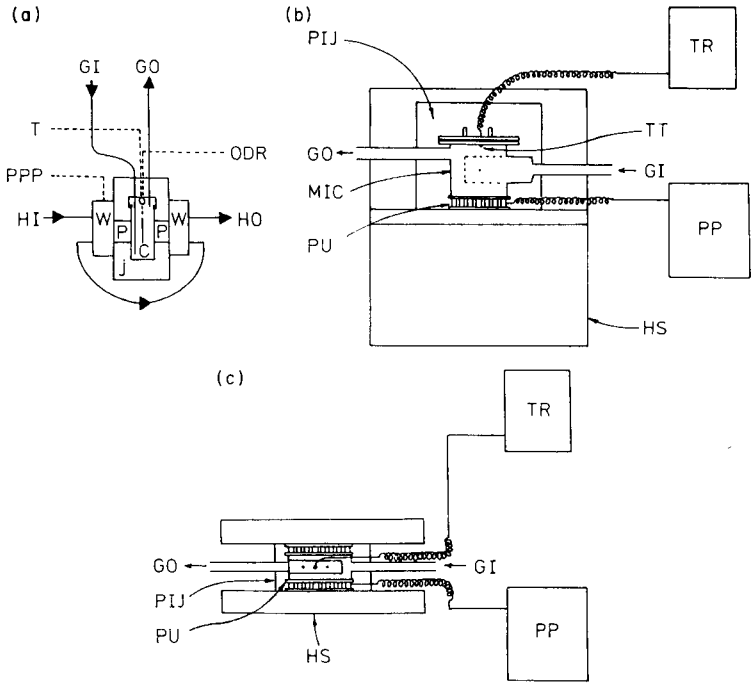

Fig. 3. (a) Water-cooled Peltier units in a sandwich configuration with a wall impinger cell: (C) wall-impinger cell; (J) polystyrene insulation jacket; (P) Peltier units; (W) water jackets; (GI) gas in; (GO) gas out; (T) thermistor line to temperature recorder; (PPP) line to Peltier power pack; (ODR) line to oscillator and data recorder; (HI) cooling water in; (HO) cooling water out. (b) Air-cooled Peltier base unit with a thin-walled prototype mini-impinger cell: (PIJ) polystyrene insulation jacket; (TR) temperature recorder; (TT) Thornton thermistor type FF; (GI) gas in; (GO) gas out; (PP) 3 V d.c. 0—15 A power pack; (MIC) mini-impinger cell; (PU) Peltier unit; (HS) 0.5° C W^{-1} heat sink. (c) Air-cooled Peltier units in a sandwich configuration with a thin-walled prototype mini-impinger cell: (HS) 2.1° C W^{-1} heat sink, otherwise as for (b).

During trials with two larger Peltier devices (type CP.1106-L, Mectron Frigister Ltd.), water cooling of the Peltiers was superseded by the use of heat sinks. Two differently rated heat sinks (0.5 and 2.1° C W^{-1}) were tested with the new Peltier devices using the prototype mini-impinger cell with Peltier assemblies as shown in Fig. 3(b and c). The mini-impinger cells were very similar in construction and size to the small detector cell used previously, except that the gas entrance and exit ports were rearranged to provide a better flow pattern of analyte around the crystal. The sandwich arrangement of Fig. 3(c) incorporating a minicell between two Peltier devices linked in series, each with a 2.1° C W^{-1} heat sink, gave the most rapid temperature change times (e.g., 0° C to 60° C in 1.25 min and 60° C to 0° C in 2.5 min) at a constant 10 A operating current. (Peltier devices can be switched from a cooling to a heating function simply by reversing the current flow.)

Two further improvements were made to the cooler/cell systems to achieve better temperature stability and to obtain sorption/desorption data using a thermal program. A new stainless steel impinger cell with an internal volume of 2 cm^3 was used (Fig. 4), and a temperature control circuit was incorporated between the Peltier cooler and the power supply (Fig. 5). The cell was sandwiched between two Peltier devices and was lagged with 1-cm thick polystyrene. The temperature controller was fitted in-line between the Peltier devices and the Peltier power pack; the thermistor from the temperature controller was incorporated into the piezoelectric crystal ceramic base holder.

Results and discussion

Some of the characteristics of this last system described may be seen in Fig. 6, which shows the temperature stability during the sorption cycle, the temperature changes during the thermal cycling, and the detector response to successive passes of 5 ppm(V) sulphur dioxide, when using the thermal desorption technique. In this experiment, the detector was exposed to pulses of analyte gas of varying duration (2–9 min). Although the overall change in frequency produced by each pulse is different (because the system does not

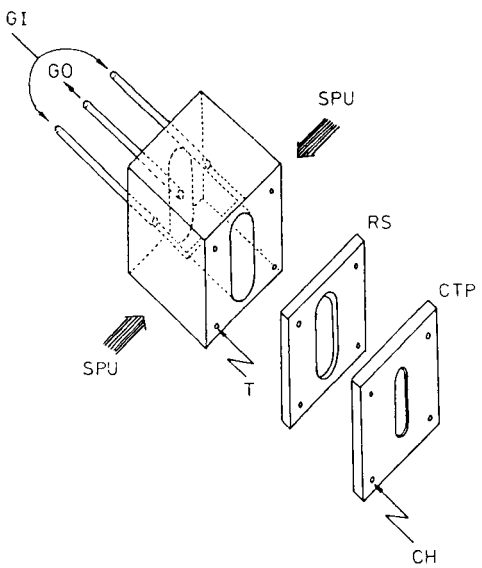

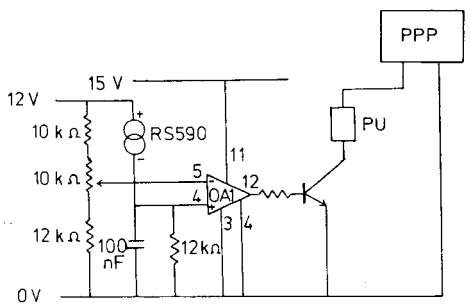

Fig. 4. Stainless steel impinger cell (2-cm^3 volume): (GI) gas in; (GO) gas out; (SPU) side attached to Peltier unit; (RS) 2-mm rubber seal; (CTP) cell top plate and crystal clamp (crystal base fixture recess not shown); (T) 4 × 8 BA screw holes, 5 mm long; (CH) 4 × 8 BA clearance holes.

Fig 5. Temperature-control circuit: (OA1) comparator; (RS590) temperature sensor; (PPP) Peltier power pack; (PU) Peltier unit.

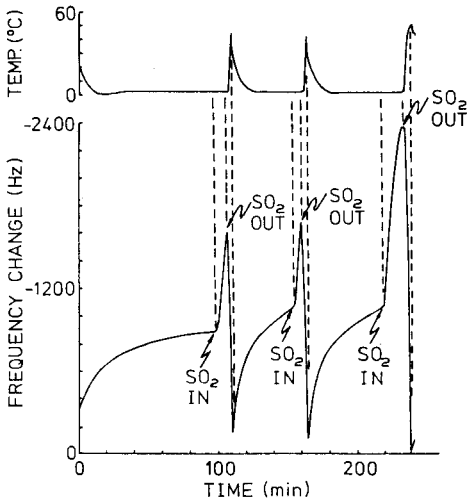

Fig. 6. Thermal cycling of 2.5 ppm(V) SO_2/triethanolamine system with Peltier equipment (preheat oven temperature, 30° C; gas flow rate, 50 cm^3 min^{-1}; coating mass at start, 33 μg; crystal frequency at zero time is 8.9843 MHz).

reach an equilibrium value), IRR measurements of 237, 210 and 233 Hz min^{-1} were obtained for three exposures. The relative standard deviation (6.5%) compares with the 8.8% obtained for a similar experiment run under isothermal (25° C) conditions.

The IRR was chosen to represent detector response for several reasons. Although ES measurements are more sensitive and yield lower detection limits than the IRR, they do not give rapid real-time sulphur dioxide responses with triethanolamine below ambient temperature. Typically, it takes 30 min for the SO_2/triethanolamine system to reach equilibrium at 0° C for 1 ppm(V) sulphur dioxide with a 200 cm^3 min^{-1} carrier gas. Also the reproducibility of ES measurements is subject to variation because of changes in mass, area and composition of the coat on ageing. The subject has been discussed more fully elsewhere [10].

Some advantages of operating the detector below ambient temperature can be deduced from Fig. 2. Improved detector response to analyte with IRR measurements, and greater base-line stability in terms of coating bleed, are obtained compared to measurements at higher temperature. However, coating bleed increases from 0.5 to 4.0 Hz min^{-1} during the course of several exposures to sulphur dioxide and thermal desorption cycles. This may be attributed to accelerated ageing effects (physical and chemical) [4]. The physical component of the ageing effect arises from a decrease in coating viscosity with temperature and the effects of impinger cell design. This combination causes a greater radial migration of coating material during each thermal cycle. The chemical component of the ageing effect may be attributed to hydrolysis and sulphate formation.

Previous work with the sulphur dioxide/triethanolamine system indicates that longer detector dead time (because of slower desorption) occurs with isothermal measurements compared to measurements made during cycling. Desorption of an equilibrium concentration of sulphur dioxide from a triethanolamine-coated crystal previously exposed to 1 ppm(V) sulphur dioxide takes >90 min at 0° C with a 200 cm^3 min^{-1} carrier gas. If the crystal monitor were to be operated only at 0° C, a single measurement of sulphur dioxide could take >2 h. The Peltier heater/cooler system used here could be cycled every 30 min. Clearly, the technique of thermal cycling is an effective approach to improving the characteristics of a piezoelectric detector in which Langmuir adsorption behaviour of the gas coating prevails. There are some solid polymeric coating materials at present under investigation where thermal desorption is essential. The Peltier/gas monitor systems that have been developed should be suitable for this type of material.

REFERENCES

1 J. Hlavay and G. G. Guilbault, Anal. Chem., 49(13) (1977) 1820.
2 T. E. Edmonds and T. S. West, Anal. Chim. Acta, 117 (1980) 147.
3 J. F. Alder and J. J. McCallum, Analyst, 108 (1983) 1169.
4 S. Cooke, Ph.D. Thesis, University of Aberdeen, 1979.
5 G. Sauerbrey, Z. Phys., 155 (1959) 206.
6 C. D. Stockbridge, Vac. Microbalance Tech., 5 (1966) 193.
7 W. P. Mason, Bell. Syst. Tech. J., 13 (1934) 405.
8 F. R. Lack, G. W. Willard and I. E. Fair, Bell. Syst. Tech. J., 13 (1934) 453.
9 A. E. H. Love, Mathematical Theory of Elasticity, 4th edn., Dover Publications, New York, 1944.
10 M. J. Hepher, Ph.D. Thesis, University of Aberdeen, 1984.

Analytica Chimica Acta, 187 (1986) 301—305
Elsevier Science Publishers B.V., Amsterdam — Printed in The Netherlands

Short Communication

THE MICROARC AS AN EMISSION SOURCE FOR ATOMIC SPECTROMETRY

R. B. GREEN* and R. R. WILLIAMS[a]

Chemistry Division, Research Department, Naval Weapons Center, China Lake, CA 93555 (U.S.A.)

(Received 6th March 1986)

Summary. The potential of an atmospheric-pressure microarc as a primary emission source for multi-element determinations is described. Emission from Na, Li, K, In, Cd, Sn, Ba, W, and Cu was observed. Several of these elements were detected in subnanogram quantities. The feasibility of using a microarc as a detector for the gas chromatography of an organotin compound is demonstrated.

The microarc was developed in the late 1970s primarily as an introduction device for very small samples, i.e., 10 μl or less [1]. It consists of a pair of tungsten electrodes operating at atmospheric pressure, usually in flowing argon or helium. The sample is deposited on the cathode, and the solvent is evaporated prior to excitation by a high-voltage, low-current, full- or half-wave rectified, unfiltered power supply. Depending on the operating conditions, analyte can be vaporized into the plasma by sputtering and/or thermal vaporization. More recent work has indicated that the microarc, operating with helium, may be useful as an emission source for quantitative atomic spectrometry [2].

The inductively-coupled plasma (ICP) is currently regarded as the most valuable source for quantitative atomic spectrometry because of its excellent detection limits, relative freedom from interferences, and utility for multi-element determinations. When compared to the ICP, the microarc would offer some advantages, provided that similar limits of detection for a sufficient number of elements were possible. This was the rationale for this preliminary investigation.

The microarc is one of the simplest and least expensive atom sources to construct and operate. It can be miniaturized, is potentially portable, and might be suitable for process monitoring. Very small, discrete samples can be used and the process of solvent evaporation (if necessary) is separated from atomization and excitation. If the sample is introduced by deposition on the microarc cathode, the analyte mixes intimately with the plasma which forms around it. Other studies have indicated that the analyte recondenses on the

[a]Permanent address: Department of Chemistry, Ohio University, Athens, OH 45701.

0003-2670/86/$03.50 © 1986 Elsevier Science Publishers B.V.

electrodes and is vaporized on succeeding current cycles [3]. These factors should contribute to effective excitation. Because the microarc is operated in an alternating-current (a.c.) mode, the analyte concentration is inherently modulated. Because this "sample modulation" is more efficient than source modulation with continuous sample introduction, it may prove useful.

Experimental

Apparatus and chemicals. The microarc used was similar to those previously reported for sample introduction [1] except that a 0.10-mm diameter tungsten wire (Johnson Matthey; 99.98% pure) was used instead of a 0.25-mm wire and there was no resistive heating of the electrodes. Samples were deposited on the cathode with a 10-μl Hamilton syringe.

The power supply was constructed specifically for the microarc and consisted of an 800 V_{p-p} transformer which was full-wave rectified and unfiltered. The operating current of the microarc was 40 mA.

Welder's grade, oil-free helium was used as support gas with a helium flow rate of 100 ml min^{-1}. All chemicals were ACS reagent grade and were used as received.

The optical system was a Spex 1404 double monochromator with a CD2 Compudrive which was controlled by a Hewlett-Packard 9836 microcomputer. The detector was a 1P28 photomultiplier operated at 900 V. A Hewlett-Packard 6940B Multiprogrammer with a 69422A high-speed analog-to-digital converter (ADC) was used to record the emission intensity of the microarc and interface with the HP-9836. All data-acquisition and data-processing software were written in Hewlett-Packard BASIC 2.0 with 2.1 extensions.

In most cases, the modulated emission was digitized and the integrated area was used to quantify signals. For experiments in which sample was introduced into the microarc continuously, a software cross-correlation technique was developed for demodulating the signal after its acquisition (see below).

Procedure. Samples (1 μl) were deposited on the cathode and allowed to evaporate in the flowing helium stream. The microarc discharge was initiated by switching on the power supply set for the maximum current. Just prior to turning on the power supply, the data-acquisition subroutine was manually triggered and data were taken at the maximum rate of the ADC (approximately 60 μs per point) for 2 s. There was no further synchronization between data acquisition and plasma initiation.

The 20,000 points acquired by the ADC were averaged in blocks of 20 to provide 1000 data points which reflected the individual oscillations of the microarc. Usually the emission of the analyte occurred within the acquisition of the first 500 data points and during the first five current oscillations for most elements. A typical result for 1 μl of 10 ng ml^{-1} indium is illustrated in Fig. 1.

Results and discussion

The first concern in evaluating the utility of the microarc as a source for atomic emission spectrometry was to establish the range of elements which can be excited. Aside from the emission of the helium carrier gas and tungsten (400.9 nm) and copper (324.8 nm) sputtered from the cathode, emissions were observed from sodium, lithium, potassium, indium, cadmium, tin and barium (Table 1). Detection limits were not rigorously evaluated; the information in Table 1 provides only an indication of possible sensitivity and should not be interpreted as definitive. Figure 1 A—C gives a clearer idea of sensitivity. Iron (372.0 nm) was the only element examined for which no emission was observed. The reasons for this are not yet understood.

Severe matrix effects were observed when trace quantitation was attempted in the presence of easily-ionized concomitants such as potassium and barium. In all cases, signal intensities were enhanced, some in excess of two orders of magnitude. A typical example is presented in Fig. 1B, C which shows the emissions for cadmium alone and in presence of a 5-fold amount of potassium; the latter signal is clipped because it exceeds the dynamic range of the ADC. The mechanism of this enhancement may lie in the higher current density caused by the presence of the easily-ionized concomitant as well as ionization suppression. The temporal behavior of indium emission was also affected by the presence of 200 $\mu g\ ml^{-1}$ sodium, being delayed approximately 150 ms. This effect was not observed for the remaining elements studied, but it may be a factor in some cases.

The microarc also exhibited unusual memory effects if care was not taken in cleaning the electrodes by introducing hydrogen into the helium stream prior to each sample [3]. Figure 1D shows the emission at the 326.1-nm line of cadmium when 1 μl of distilled water was deposited on the cathode after a 10-ng ml^{-1} cadmium sample without the cleaning step. This emission was observed only after evaporation of distilled, deionized water on the cathode prior to microarc initiation. Apparently, significant amounts of cadmium are dispersed over the surface of the cathode during plasma formation; the water dissolves this residual cadmium and evaporation of the water concentrates it

TABLE 1

Wavelengths monitored and quantities deposited on the cathode for some of the metals detected by microarc emission.

Element	Wavelength (nm)	Quantity deposited (ng)	*S/N*
Na	589.0	0.2	>90
Li	670.7	0.002	25
K[a]	766.5	—	—
In	451.2	0.01	30
Cd	326.1	0.1	30
Sn	303.9	10	60
Ba	553.6	20	>30

[a] K = 500 $\mu g\ ml^{-1}$ as a "concomitant" or "excess".

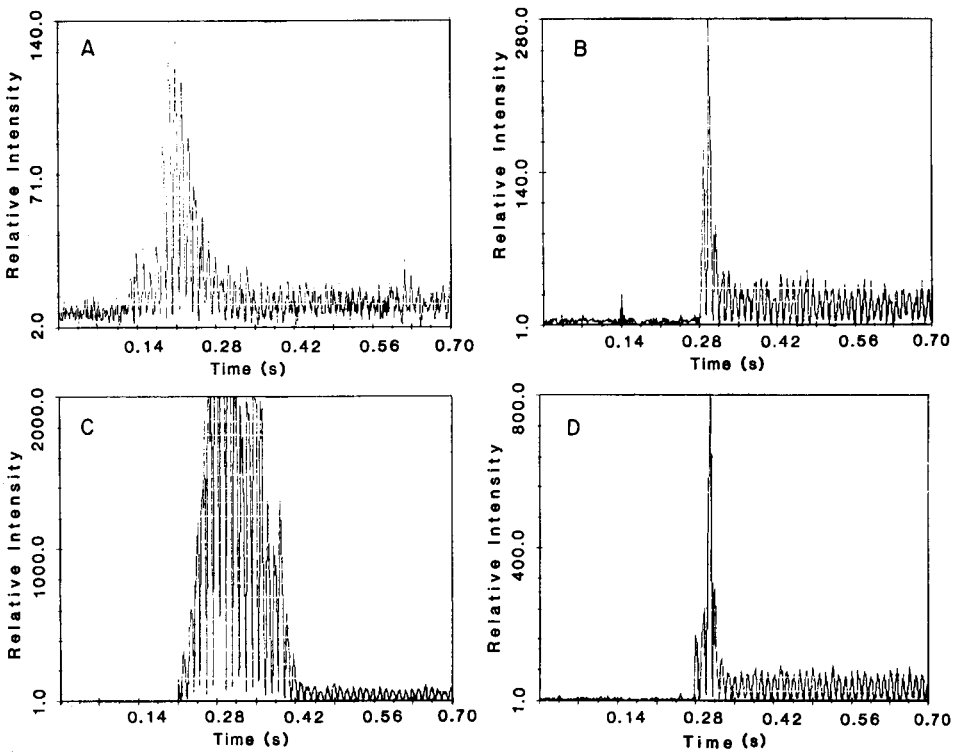

Fig. 1. Temporal emission from different solutions: (A) 1 μl of 10 ng ml^{-1} indium in distilled water; (B) 1 μl of 100 ng ml^{-1} cadmium in distilled water; (C) 1 μl of 100 ng ml^{-1} cadmium and 500 ng ml^{-1} potassium in distilled water; (D) 1 μl of distilled water taken after quantitation of a cadmium sample without subsequent hydrogen cleaning of the cathode.

at the tip of the cathode. This memory effect can easily be eliminated by using the hydrogen cleaning procedure, but it could be useful for dilute solutions if it were controlled.

The possibility of using the microarc as a detector for gas chromatography of organometallic species was investigated with the apparatus outlined in Fig. 2. Using the standard cathode arrangement, the emission of tin from n-dibutyltin dichloride was monitored at 25 and 80°C. This change in temperature increased the signal by a factor of 18. In order to confine the effluent better within the plasma region, the standard cathode was replaced with a 16-gauge hypodermic needle with a fine copper mesh screen wrapped tightly over its tip. Helium was introduced through the needle only, rather than through the central tube as indicated in Fig. 2. When the discharge was initiated, the plasma dispersed over the copper mesh at the needle tip. The helium carrying the analyte flowed through the mesh and was efficiently introduced into the plasma. A signal-to-noise enhancement of about 4 was observed for the n-dibutyltin dichloride with the flow-through cathode.

In applications such as gas chromatography or head-space analysis, the

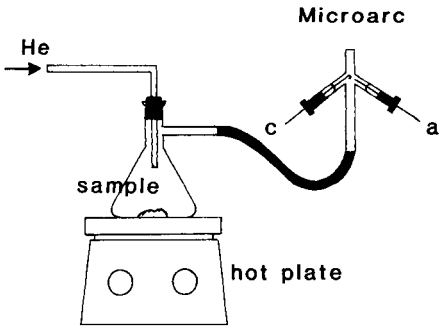

Fig. 2. Apparatus for the introduction of n-dibutyltin dichloride into the microarc; (a) and (c) are the anode and cathode, respectively.

sample would be introduced into the plasma continuously during the elution of a peak. A new data-processing technique was developed for such applications. Basically, a correlation mask containing the emission of helium at 667.8 nm was recorded and stored on disk. In subsequent runs, the mask was retrieved and cross-correlated with the emission observed at the analyte wavelength. The resulting correlogram was filtered using a moving window average. The use of cross-correlation will be examined for situations in which lock-in amplification has traditionally been used.

Because of the large number of variables involved, all aspects of microarc operation, including sample introduction, require automation to improve performance. An optical multichannel detector will be used for better characterization of emissions, so that line and background intensity can be measured simultaneously for many different elements. Photodiode array detection will also permit simultaneous quantitation of ion-to-atom ratios which are important for studies of fundamental processes in the microarc. The time resolution of atomic emission in the microarc will also be explored. In a sample containing both sodium and aluminum, sodium emission precedes aluminum emission [3]; if the emission of the microarc were recorded without dispersion as a function of time, sodium emission would be temporally separated from that of aluminum and both species might be determined directly. Straightforward resolution enhancement techniques such as computation of derivatives could be applied to separate overlapping signals mathematically.

This research was supported by the Independent Research program at the Naval Weapons Center and by Jim Short, Naval Weapons Support Center, Crane, Ind. One of the authors (RRW) was a U.S. Navy-ASEE Summer Faculty Research associate.

REFERENCES

1 J. P. Keilsohn, R. D. Deutsch and G. M. Hieftje, Appl. Spectrosc., 37 (1983) 101.
2 M. E. Churchwell, T. Beeler, J. D. Messman and R. B. Green, Spectrosc. Lett., 18 (1985) 679.
3 R. I. Bystroff, L. R. Layman and G. M. Hieftje, Appl. Spectrosc., 33 (1979) 230.

Analytica Chimica Acta, 187 (1986) 307—311
Elsevier Science Publishers B.V., Amsterdam — Printed in The Netherlands

Short Communication

IMPROVED CESIUM SENSITIVITY IN ELECTROTHERMAL ATOMIC ABSORPTION SPECTROMETRY

JAMES F. CHAPMAN* and LESLIE S. DALE

CSIRO Division of Energy Chemistry, Lucas Heights Research Laboratories, New Illawarra Road, Lucas Heights, NSW 2234 (Australia)

SHARON A. TOPHAM

AAEC Materials Division, Lucas Heights Research Laboratories, New Illawarra Road, Lucas Heights, NSW 2234 (Australia)

(Received 23rd April 1986)

Summary. The sensitivity for cesium determination by electrothermal atomic absorption spectrometry is improved four-fold by the addition of a large excess of potassium nitrate. Zeeman background correction is used to compensate for the large non-specific absorption signal resulting from the potassium. The characteristic concentration and detection limit are 0.44 and 2 $\mu g\ l^{-1}$, respectively, and the coefficient of variation is 2% at the 50 $\mu g\ l^{-1}$ level. The procedure is suitable for the rapid determination of cesium in leach solutions from nuclear waste fixation experiments.

In studies of nuclear waste fixation, radioactive waste is incorporated into inert materials such as Synroc [1, 2]. To assess the stability of these materials, aqueous leach tests were applied initially on materials containing simulated inactive waste. Because cesium is one of the most chemically mobile of the radioactive waste elements, its determination at low concentrations is important in leachability studies of these materials.

In this laboratory, cesium has been determined in leach solutions by flame atomic emission spectrometry with potassium as an ionization suppressor. A 20-fold increase in sensitivity was achieved, leading to a detection limit of 2 $\mu g\ l^{-1}$. Although the procedure was satisfactory for inactive samples, it could not be applied to radioactive samples leached from inert materials containing actinides because of the potential hazard of aspirating a radioactive solution into a conventional burner/nebulizer system. Electrothermal atomic absorption spectrometry offered a better procedure because, with the small volumes used, contamination of equipment would be minimal and the small volume of vapour generated could be contained. However, because the detection limit for cesium for the instrument available was 8 $\mu g\ l^{-1}$, it was insufficient to provide leach rate data comparable with that obtained in the inactive leach tests. To improve the sensitivity, the addition of potassium as an ionization suppressant was considered.

Studies of ionization in electrothermal atomizers have been undertaken by

0003-2670/86/$03.50 © 1986 Elsevier Science Publishers B.V.

numerous workers [3—9]. Some of them observed slight enhancements of the analyte signal in the presence of added buffer [3, 4], whereas others found no enhancement [5—7]. More detailed studies suggested that ionization is negligible owing to the high population of background electrons generated by the graphite [8, 9] and small compared to that obtained in conventional flames owing to the different time- and temperature-dependence of the atom and ion populations [9]. In several of these investigations, the conclusions were drawn from the results of experiments in which either the atom excess of buffer was small, or volatilization losses may have been caused by the use of chloride media.

The present investigations into the use of potassium to improve the sensitivity for cesium show that with a large excess of potassium, the atomic absorption signal for cesium can be increased by a factor of four. In view of this, and because of conclusions reached by previous workers, the enhancement effect of potassium on cesium was studied in more detail.

Experimental

Apparatus and reagents. All measurements were made on a Hitachi Polarized Zeeman atomic absorption spectrometer, model 7000, equipped with a pyrolytic graphite tube cuvette and autosampler. All absorbance measurements were taken in the peak-height mode with Zeeman background correction. They were displayed and recorded on a Hitachi AA data processor. The spectral bandpass was 1.3 nm. Hollow-cathode lamps were operated at their recommended currents.

All chemicals and acids were of analytical-reagent grade. Water from a Millipore Milli-Q purification system was used.

Procedure. To 1.00 ml of sample was added 0.10 ml of potassium nitrate modifier solution (1.000 g of potassium as its nitrate, made up to 100 ml in 1 + 1 nitric acid). Portions (40 μl) were injected into the graphite furnace. The heating program is shown in Table 1. The argon carrier gas flow of 200 ml min^{-1} was decreased during the atomization cycle to 30 ml min^{-1}. The peak-height absorbance at 852.1 nm was measured.

Results and discussion

Potassium addition. Poor sensitivity was obtained from a 50 $\mu g\ l^{-1}$ cesium solution, and there was no increase in cesium absorbance when potassium

TABLE 1

Conditions used for cesium determination by electrothermal atomic absorption spectrometry

Step	Temperature (°C)		Time(s)	Step	Temperature (°C)		Time(s)
	Start	End			Start	End	
1. Dry	80	150	50	4. Atomize	2000	2600	6
2. Dry	150	500	10	5. Clean	3000	3000	3
3. Ash	500	500	10	6. Cool	—	—	30

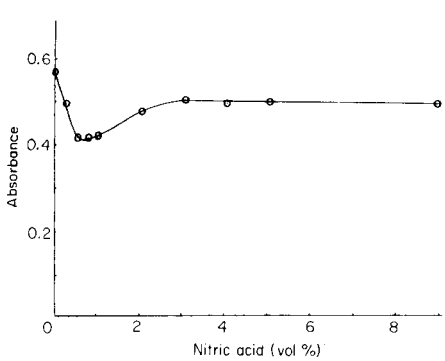

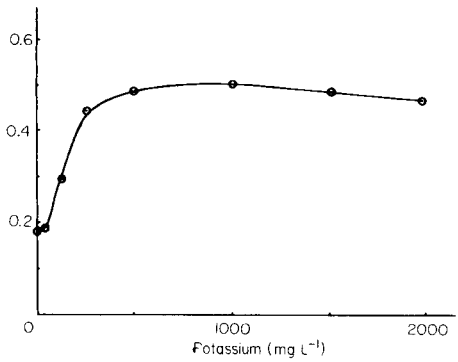

Fig. 1. Effect of nitric acid concentration on cesium absorbance.

Fig. 2. Effect of potassium concentration on cesium absorbance.

chloride was added. However, when potassium nitrate was added, the cesium signal was significantly enhanced. The use of nitrate media to minimize interferences has been recommended by Ottaway and Shaw [10]. The effect of increasing concentrations of nitric acid on a 50 $\mu g\ l^{-1}$ cesium solution was studied; the results are shown in Fig. 1. The reason for the dip in the curve before the plateau region is not clear but it may be due to different volatilization rates of compounds such as $CsNO_3 \cdot HNO_3$ and $CsNO_3 \cdot 2HNO_3$ [11]. Because the plateau region occurs above ca. 3% (v/v) nitric acid, 5% was chosen for subsequent investigations.

The effect of increasing the potassium concentration in the nitric acid was then studied. Figure 2 shows the change in response of 50 $\mu g\ l^{-1}$ cesium in 5% nitric acid with increasing potassium concentration. The plateau region occurs at 1000 mg l^{-1} potassium, an atom ratio (K/Cs) of ca. 68,000. The background absorption signal resulting from the volatilization of the added potassium was very high. However, this was adequately compensated for by Zeeman background correction. This level of potassium addition, which is similar to that used in flame emission spectrometry, was chosen as the optimum. When potassium chloride was used in the presence of nitric acid, the characteristics were similar to those produced with potassium nitrate.

Sturgeon et al. [12] reported that, because the thermionic work function for graphite is 4.6 eV, only those elements with a lower ionization potential (i.p.) would be significantly affected by the presence of an ionization suppressor. These elements are cesium (i.p. = 3.9 eV), rubidium (4.2 eV) and potassium (4.3 eV). The thermionic work functions for other electrothermal atomizer materials are 4.2 eV for tantalum [13] and molybdenum [14] and 4.5 eV for tungsten [15]. Similar ionization behaviour would therefore be expected with devices made from these materials.

Cesium absorbance was also found to be significantly enhanced by addition of rubidium. However, the high level of cesium impurity in the rubidium prevented the determination of cesium at low levels.

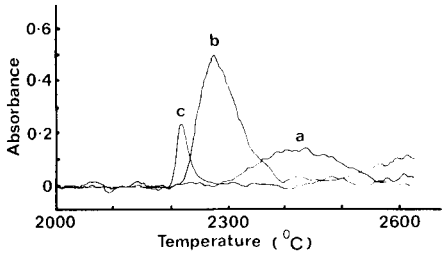

Fig. 3. Absorbance temperature profiles for 50 μg Cs l^{-1} in 5% nitric acid measured at 852.1 nm: (a) alone; (b) in presence of 1000 mg K l^{-1}. Curve (c) is the response for solution (b) measured at 404.4 nm (K lamp).

Atomic absorption/temperature profiles. Figure 3 compares the atomic absorption/temperature profiles for the atomization of cesium in the presence of nitric acid with and without the addition of potassium. Also included is the atomic absorption profile for the potassium. A substantial enhancement of the cesium absorbance can be seen in the presence of potassium. The Saha equation [16] predicts that at 2270°C, the approximate temperature at which the enhanced cesium peak occurs, ca. 90% of the cesium should be ionized. From the heights of peaks (a) and (b), the degree of ionization is estimated by the method of Manning and Capacho-Delgado [17] to be 70—75%.

Some of the confusion about ionization in electrothermal atomizers has arisen because their materials of construction produce a background concentration of electrons which affects the ionization of analyte elements [14]. This is why the degree of ionization of cesium was less than that expected. In flames, the populations of ground-state atoms, excited atoms and ions are in local equilibrium because there is a constant flow of sample into a fixed temperature atomizer. In electrothermal atomizers, these conditions do not prevail and the processes of absorption, emission and ionization reach a maximum in sequence as the temperature rises. This temperature difference explains why the degree of ionization of an analyte element is considerably lower when measured by absorption [8] than by emission [9]. Ionization is known to be greatest after the atom peak has occurred [8]. The observation of the cesium absorption peak at a lower temperature in the presence of potassium may be due to the coincidence of that temperature with the maximum electron density produced by the ionization of potassium.

Analytical method. A calibration graph obtained from 16 points in the range 0—50 μg l^{-1} cesium was linear, with a slope of 0.1025 ± 0.0021 absorbance/μg l^{-1}. The characteristic concentration (sensitivity) derived from the calibration slope was 0.44 μg l^{-1}, and the characteristic mass was 18 pg of cesium.

The reproducibility and detection limit were evaluated for 5 and 50 μg l^{-1} solutions of cesium, respectively. Ten replicate measurements of each solu-

TABLE 2

Comparison of results on leach test solutions by flame atomic emission (a.e.s.) and electrothermal atomic absorption spectrometry

Sample no.	1	2	3	4	5
Cs found ($\mu g\ l^{-1}$)					
A.e.s.	33	17	15	14	<2
This work	37	19	19	12	<2

tion gave relative standard deviations of 20 and 2%, respectively. Each result corresponds to a detection limit of 2 $\mu g\ l^{-1}$ cesium, which is adequate for the screening of leach test solutions. Table 2 compares the results obtained for several samples which had previously been analysed by flame atomic emission spectrometry.

Conclusions

There is substantial evidence to suggest that the improved sensitivity for cesium results from ionization suppression by the large added excess of potassium. This suppression requires a much larger excess of buffer than has been used in most previous investigations of ionization under such conditions. The very high non-specific background absorption signals which then arise can be compensated for by using Zeeman correction. The method has proved suitable for screening leach test solutions for cesium content, particularly when sample volume is a restriction.

REFERENCES

1 A. E. Ringwood, Safe Disposal of High Level Nuclear Reactor Wastes; A New Strategy, Australian National University Press, Canberra, 1978.
2 K. D. Reeve, D. M. Levins, E. J. Ramm, J. L. Woolfrey, W. J. Buykx, R. K. Ryan and J. F. Chapman, At. Energy Aust., 24 (1981) 1.
3 W. G. Schrenk and R. T. Everson, Appl. Spectrosc., 29 (1975) 41.
4 M. S. Epstein, T. C. Rains and T. C. O'Haver, Appl. Spectrosc., 30 (1976) 324.
5 P. Frigieri, R. Trucco, I. Ciaccolini and G. Pampurini, Analyst, 105 (1980) 651.
6 Z. Grobenski, D. Weber, B. Welz and J. Wolff, Analyst, 108 (1983) 925.
7 J. M. Ottaway and F. Shaw, Analyst, 101 (1976) 582.
8 R. E. Sturgeon and C. L. Chakrabarti, Spectrochim. Acta, Part B, 32 (1977) 231.
9 R. E. Sturgeon and S. S. Berman, Anal. Chem., 53 (1981) 632.
10 J. M. Ottaway and F. Shaw, Analyst, 100 (1975) 438.
11 J. C. Bailar and A. F. Trotman-Dickenson (Eds.), Comprehensive Inorganic Chemistry, Pergamon Press, Oxford, 1973, p. 478.
12 R. E. Sturgeon, S. S. Berman and S. Kashyap, Anal. Chem., 52 (1980) 1049.
13 M. D. Friske, Phys. Rev., 61 (1942) 513.
14 R. W. Wright, Phys. Rev., 60 (1941) 465.
15 G. F. Smith, Phys. Rev., 94 (1954) 295.
16 M. N. Saha and N. K. Saha, A Treatise on Modern Physics, Vol. 1, Indian Press, Calcutta, 1934.
17 D. C. Manning and L. Capacho-Delgado, Anal. Chim. Acta, 36 (1966) 312.

Analytica Chimica Acta, 187 (1986) 313—316
Elsevier Science Publishers B.V., Amsterdam — Printed in The Netherlands

Short Communication

DETERMINATION OF PHOSPHORUS DEPTH PROFILES IN SEMICONDUCTOR SILICON BY CHEMICAL ETCHING AND FILAMENT VAPORIZATION INDUCTIVELY-COUPLED PLASMA ATOMIC EMISSION SPECTROMETRY

EIICHI KITAZUME*

Central Research Laboratory, Hitachi Ltd., Kokubunji, Tokyo (Japan)

(Received 8th April 1986)

Summary. Silicon slices are dissolved by anodizing and removal of the silica film by hydrofluoric acid. The phosphorus in the etching solution is determined by the filament vaporization technique and the depth of silicon is measured by determining the silicon content in the etching solution by conventional inductively-coupled plasma atomic emission spectrometry. A lower limit of 10^{18} phosphorus atoms cm^{-3} can be determined at sectioning intervals of 30—50 nm.

Semiconductor characteristics are known to depend on the depth concentration profiles of their dopant elements. Their electro-active impurity concentration has commonly been determined by the differential sheet resistivity method using a four-point probe [1—4] or the Hall effect [4—6]. However, there is no information on electro-inactive impurities, and values are distorted when there are electrically compensating impurities.

Total concentration profiles of impurities have been obtained by combining a sensitive analytical technique, such as activation analysis [4, 7—9], with a suitable chemical sectioning technique. For example, the depth profiles of arsenic and antimony in semiconductor silicon have been determined [10, 11] by non-dispersive atomic fluorescence spectrometry.

Phosphorus is one of the most widely used doping donors. Lanza and coworkers applied an anodic oxidation technique to successive layers of silicon samples and determined the phosphorus [12] and arsenic [13] depth profiles at concentrations as low as 10^{19} atoms cm^{-3} by absorption spectrophotometry and polarography, respectively. Phosphorus can also be determined sensitively by filament vaporization inductively-coupled plasma atomic emission spectrometry (a.e.s.) [14]. This communication extends the application of this technique to the determination of phosphorus depth profiles in semiconductor silicon.

*Present address: College of Humanities and Social Sciences, University of Iwate, Ueda, 020 Japan.

0003-2670/86/$03.50 © 1986 Elsevier Science Publishers B.V.

Experimental

The apparatus for phosphorus determination was as reported previously [14], as was the equipment for silicon anodization [10, 11].

Phosphorus standard solutions were prepared by dissolving potassium dihydrogenphosphate in water. A silicon standard solution was prepared from potassium silicate (Kanto Chemicals Corp). All other chemicals mentioned below were of analytical-reagent grade.

The silicon anodization procedure was similar to that reported previously [10, 11], except that anodization at constant current (50 mA) was done for 10 min to achieve thicker sectioning. The silica film formed was dissolved in 0.5 ml of 0.2 M hydrofluoric acid. A 50-μl aliquot of this solution was diluted to 5 ml for the determination of silicon as described previously [10], in order to estimate the thickness of silicon dissolved. Other etching solutions were transferred to 1-ml teflon beakers and 10 μl of potassium fluoride solution (100 μg ml^{-1} potassium) was added. The solution was evaporated completely by heating at 120—130°C. After cooling, 100 μl of water was added and the residue was dissolved by ultrasonic mixing for 2 min. A 10-μl sample was deposited at the top of the platinum filament from a suitable pipet, and phosphorus was determined under the conditions developed previously [14].

Results and discussion

Phosphorus released from the semiconductor is present in solution as phosphoric acid. As this solution is preconcentrated on the filament by heating to >200°C, it was necessary to test if such treatment could cause any loss

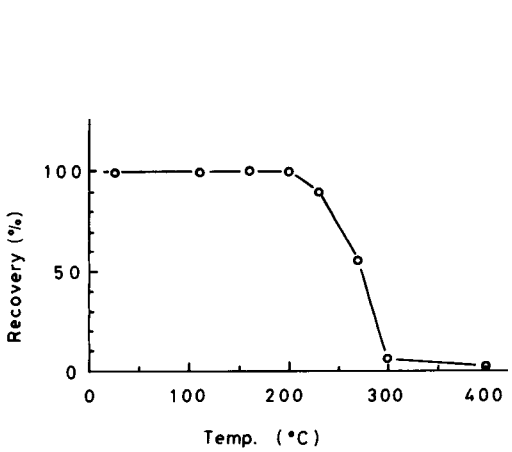

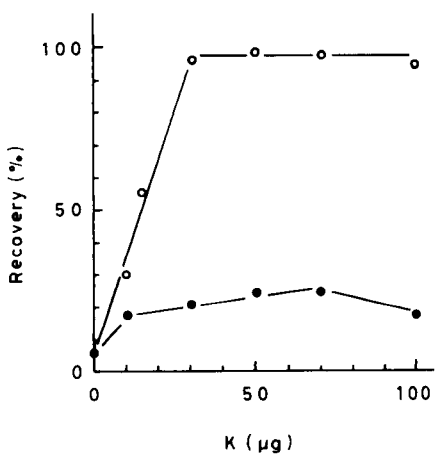

Fig. 1. Recovery of phosphorus when 10 μg of phosphorus as phosphoric acid was heated in a platinum crucible at various temperatures.

Fig. 2. Effect of potassium salts on the recovery of phosphorus when 10 μg of phosphorus as phosphoric acid was heated in a platinum crucible at 300°C: (○) potassium fluoride; (●) potassium chloride.

of phosphorus. This was done by heating very dilute phosphoric acid solutions in a platinum crucible at various temperatures and determining phosphorus by conventional inductively-coupled plasma a.e.s. after dissolving the residue in 5 ml of water. As shown in Fig. 1, the recovery decreased above 200°C. As the emission intensity obtained from potassium dihydrogenphosphate solutions was not affected in this way [14], addition of potassium salts to the phosphoric acid was tried. The results are shown in Fig. 2. When the amount of potassium (as its fluoride) was over three times the amount of phosphorus, the recovery was >95%. Hence potassium fluoride was used as the additive for subsequent analyses, with the added benefit that the fluoride will cause some volatilization of silicon from the test solution prior to phosphorus determination. For the determination of 1 μg ml^{-1} phosphorus, addition of >1 μg ml^{-1} potassium (as its fluoride) gave similar intensities, nearly the same as when potassium dihydrogenphosphate was used as the phosphorus standard. The possible interfering effect of up to 10^3-fold amounts (by weight) of silicon was investigated; none was observed.

The recovery and repeatability of the total procedure were investigated by using test mixtures. The results obtained are shown in Table 1. Relative standard deviations were ca. 4% at such concentrations.

The proposed technique was applied to depth profiling of phosphorus in silicon slices. A typical profile is shown in Fig. 3, which compares well with the profile obtained by a four-point probe resistivity method.

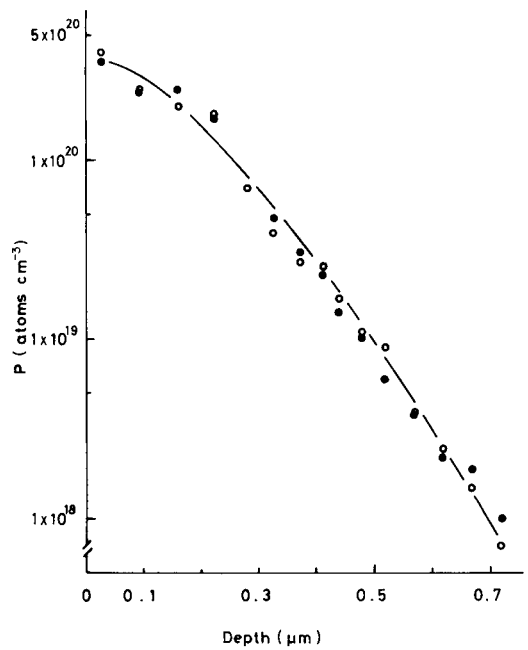

Fig. 3. Depth profile of phosphorus in a silicon slice: (•) present method; (○) four-point probe resistivity method.

TABLE 1

Recovery of phosphorus from synthetic mixtures

SiO_2 present (μg)	P present (μg)	P found (μg)	Recovery (%)
100	0.100	0.092	92
100	0.100	0.096	96
100	0.50	0.52	104
100	0.50	0.48	96
200	0.100	0.095	95
200	0.100	0.095	95
200	0.50	0.47	94
200	0.50	0.49	98

The author is grateful to Dr. Atsushi Mizuike and Dr. Hiroshi Kawaguchi for their helpful suggestions, to Dr. Seiki Harada and Dr. Fumio Nagata for their encouragement, and to Dr. Kanji Tsujii, Mr. Hisao Kojima and Dr. Kazuo Kuga for valuable discussions.

REFERENCES

1 F. M. Smits, Bell Syst. Tech. J., 37 (1958) 711.
2 E. Tannenbaum, Solid-State Electron., 2 (1961) 279.
3 P. J. Severin, Philips Res. Rep., 26 (1971) 279.
4 F. Mousty, P. Ostoja and L. Passari, J. Appl. Phys., 45 (1974) 4576.
5 L. V. van den Pauw, Philips Res. Rep., 13 (1958) 1.
6 N. G. E. Johansson and J. W. Mayer, Solid-State Electron., 13 (1970) 317.
7 R. F. Girardi, F. Girardi, F. Mousty and A. Ostidich, Nucl. Instrum. Methods, 112 (1973) 581.
8 F. Burkhardt, A. Mertens and C. Wagner, Phys. Status Solidi, A22 (1974) K45.
9 K. D. Beyer, J. Electrochem. Soc., 124 (1977) 630.
10 K. Tsujii and E. Kitazume, Anal. Chim. Acta, 125 (1981) 101.
11 K. Tsujii, E. Kitazume and K. Yagi, Anal. Chim. Acta, 128 (1981) 229.
12 P. Lanza and P. L. Buldini, Anal. Chim. Acta, 104 (1979) 139.
13 P. L. Buldini, D. Ferri and P. Lanza, Anal. Chim. Acta, 106 (1979) 137.
14 E. Kitazume, Anal. Chem., 55 (1983) 802.

Analytica Chimica Acta, 187 (1986) 317—323
Elsevier Science Publishers B.V., Amsterdam — Printed in The Netherlands

Short Communication

USE OF ADDITIVES IN PYROLYTIC SEPARATION OF MERCURY FROM INDUSTRIAL SAMPLES FOR COLD-VAPOUR ATOMIC ABSORPTION SPECTROMETRY

B. RÓŻAŃSKA* and M. DOMAŃSKA

Department of Analytical Chemistry, Technical University of Warsaw, 00-664 Warsaw (Poland)

(Received 10th December 1985)

Summary. The role of filter materials and additives in the thermal volatilization of mercury from industrial samples (copper concentrates, lead and zinc oxides and kaolin) is studied. Alumina is shown to be most effective but the calcination temperature and the sodium content of the additive can influence its effectiveness because of changes in surface properties.

Pyrolytic separation of mercury before its determination by atomic absorption spectrometry (a.a.s.) in samples of complex composition containing considerable amounts of heavy metals, organic carbon and sulphur compounds requires the addition of suitable substances to the heated sample. The addition of calcium oxide to soil samples containing sulphide minerals and organic matter has been described [1]. Alumina alone, or together with magnesium oxide or calcium oxide mixed with sodium carbonate, was tested in the analysis of solid fuels [2], and magnesium silicate (Florisil) with calcium oxide was examined for samples containing some organic material (sediments, food) [3]. Magnesium oxide with magnesium nitrate was applied for samples from the lead-zinc industry [4] and a magnesium oxide or Florisil/calcium oxide mixture was used for industrial samples [5]. This communication is a continuation of earlier investigations on the applicability of such additives [5].

Experimental

Reagents. The main reagents used were as described previously [5]. Alumina types b, c and d, were obtained from the Department of Solid-state Technology, and type f from the Department of Heterogeneous Catalysis, Technical University of Warsaw; type e was Al_2O_3 (Pierce Inorganic), type g was γ-Al_2O_3 (Degussa) and type a was Al_2O_3 ("pure"; POCh). Zeolites were obtained from the Institute of Organic Chemistry, Polish Academy of Sciences, Laboratory of Heterogeneous Catalysis (Dr. H. Hoser). The additives were heated for 1 h at 800°C before use in order to remove mercury

0003-2670/86/$03.50 © 1986 Elsevier Science Publishers B.V.

traces, except for the zeolites which were heated for 1 h at only 500°C, to avoid destroying their structure.

Apparatus. A Pye-Unicam SP 90A series 2 atomic absorption spectrometer with a quartz flow cell was used. The home-made device for pyrolytic decomposition of samples and amalgamation of mercury vapour on gold collectors was as described previously [5]. The device consisted of furnace I where samples were heated, furnace II with a set of filters (Ag, SiO_2, Al_2O_3), and furnaces III and IV containing gold collectors. The equipment for mercury determination after trapping in acidified permanganate solution consisted of furnaces I and II followed by a scrubber with a porous frit.

Procedure. The weighed portion of finely ground sample, mixed with the appropriate additives in a 1:1 ratio (w/w), was placed in a quartz boat in furnace I. The air flow was set to 0.1 l min^{-1}. The mercury liberated from the sample heated to 800°C for 15 min (one-step mode) or to 400°C for 5 min followed by 800°C for 6 min (two-step mode) was passed through the scavengers in furnace II (725°C), and trapped on two gold collectors (170°C) sequentially (method A) or in acidic permanganate solution (method B). The above procedures as well as the procedure of determination after acid digestion of samples (method C) were as described in detail previously [5].

A weighed portion (ca. 100 mg) of zinc oxide or lead oxide was dissolved in aqua regia (8 ml or 6 ml, respectively) and mercury was determined as described in method C.

Results and discussion

The effect of additives. The effect of filters and additives on the amount of the mercury recovered (i.e., volatilized) from a sample of copper concentrate and trapped in the oxidizing solution (method B) is shown in Fig. 1. A

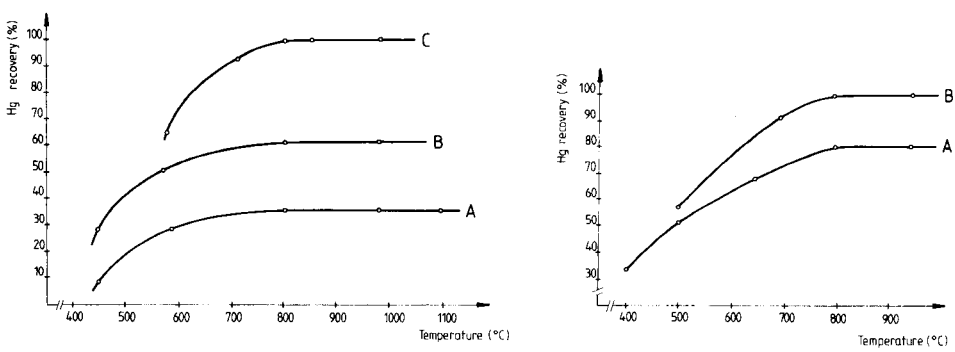

Fig. 1. Influence of heating temperature of a copper concentrate on the mercury recovery by thermal volatilization and absorption in acidic permanganate solution: (A) without additives and filters; (B) with a set of filters (Ag, SiO_2, Al_2O_3); (C) with a set of filters and addition of Florisil/CaO.

Fig. 2. Influence of heating temperature of kaolin KK on the mercury recovery by thermal volatilization and amalgamation on the collectors: (A) without additives; (B) with addition of Florisil/CaO.

similar dependence was observed when mercury liberated from the sample of kaolin was trapped on the two gold collectors before a.a.s. (method A). The amount of mercury recovered in the presence of additives increased, regardless of the kind of trapping. Uchikawa et al. [2] described a decrease in absorbance because of the elimination of the background signal when suitable additives were used. Improved oxidation of the pyrolysis products is probably the main reason for the improved recovery in the above cases. This was confirmed by the poor results of initial experiments on pyrolytic mercury separation from copper concentrates under reducing conditions. The addition of iron or graphite powder and the use of nitrogen as carrier gas, to avoid any oxidation of mercury vapour by copper(II) oxide formed by thermal decomposition of the copper compounds were totally unsuccessful in this respect.

In further experiments, Florisil, which had previously been applied as an additive, was used as a filter; it was placed in furnace II or in furnace I just after the sample boat. Florisil was less efficient when used as a filter (Table 1), even when the filter section was extended, as recommended for solid environmental samples [6]. Similarly, alumina mixed with the sample gave better recoveries than when it was simply used as a covering layer. The role of the additives cannot be explained only as an aid to oxidation or absorption of pyrolytic products.

Influence of some properties of the additives. The various additives were tested and the following mercury recoveries (relative to the accurate result obtained with method C for the copper concentrate [5]) were obtained: CaO 85%; MgO 50—70%; zeolites (two-step sample heating mode) Ca, H, Ce forms of faujasite type 80—86%; mordenite type 90%; aluminosilicate with destroyed structure 80%; alumina 70—100%; Florisil 84%. The com-

TABLE 1

Influence of filters and additives on the recovery of mercury from a copper concentrate (Method B)

[Additive/sample = 1:1 (w/w); Florisil/CaO = 2:1 (w/w); furnace I = 800°C; furnace II = 725°C.]

Additive furnace I	Auxiliary filter furnace I	Filters furnace II	Mercury recovery (%)
CaO	—	Ag/Florisil (1 cm)	76
Florisil/CaO	—	Ag	80
Florisil/CaO	—	Ag, SiO_2, Al_2O_3	100
CaO	Florisil	Ag, SiO_2, Al_2O_3	85
Alumina[a]	—	Ag, SiO_2, Al_2O_3	95
MgO	Al_2O_3[b]	Ag, SiO_2, Al_2O_3	84
CaO	Al_2O_3[b]	Ag, SiO_2, Al_2O_3	91

[a]Alumina "d" (see Table 2), one-step sample heating (800°C, 15 min). [b]As a layer covering the sample.

bination of acidic solids with CaO and MgO in various ratios was not effective except for Florisil/CaO where recoveries were 100% for Florisil/CaO weight ratios of 2—10.

For alumina and magnesia, preparations from various sources differed in effectiveness. The sodium content and, to a lesser degree, the calcination temperature significantly influenced the efficiency of alumina as an additive (Table 2). In order to check on the depressive effect of sodium contained in the alumina, preparation "d" was moistened with sodium hydroxide solution, dried and heated for 5 h at 800°C and used as an additive. The recoveries of mercury were only 84% and 82% for alumina containing 2×10^{-4} and 1×10^{-3} mol Na/g Al_2O_3, respectively.

Silica, alumina and silicates are often used as catalysts or catalyst supports for the thermal decomposition of gas-phase organic compounds (and other types of reactions). These additives also serve in solid-state reactions to facilitate thermal decomposition of inorganic compounds. Their defect structures and surface properties, important for their catalytic activities (in both solid/gas and solid/solid systems), strongly depend on the purity and method of preparation of the materials. The influence of sodium ions on the number and nature of the active centers (changes in alumina surface acidity and basicity) has already been observed [8]. Too much sodium, however, drastically changes the catalyst surface.

Conditions of pyrolysis. The plots of mercury recovery vs. additive/sample weight ratio reached a plateau at ratios ≥ 1 for all tested additives (Fig. 3). A temperature of 800°C was necessary to obtain quantitative recovery from all samples tested with all additives used. Uchikawa et al. [2] applied two-step sample heating; heating at 400°C for several minutes, and then heating at 700°C. This two-step treatment is also advantageous for pyrolysis of copper

TABLE 2

Recovery of mercury from a copper concentrate with addition of alumina samples of various origin

Alumina	Form	Temp. and time of calcination (°C/h)	Specific surface area ($m^2\ g^{-1}$)	Na_2O content (%)	Mercury recovery (%)
a	"Pure"	Unknown	—	—	70
b	α-Al_2O_3 (100%)[a]	1500/3	2	2×10^{-3}	95
c	α-Al_2O_3 (100%)[a]	1300/3	13	2×10^{-3}	98
d	θ-Al_2O_3 (100%)[a]	900/5	190	2×10^{-3}	100
e	γ-Al_2O_3 (99%)	Unknown	78	0.1—0.2	79
f	γ-Al_2O_3 (100%)[b]	800/24	62	<0.1	100
g	γ-Al_2O_3	500/—		<0.1	90

[a]Prepared electrochemically [7]. [b]Prepared as described by Marczewski and Malinowski [8] by precipitation of hydrated oxide from benzene solution of aluminium isopropoxide.

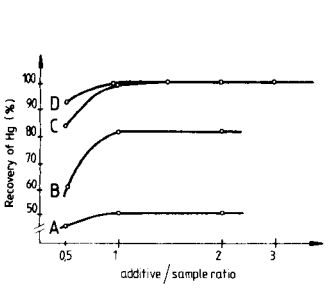

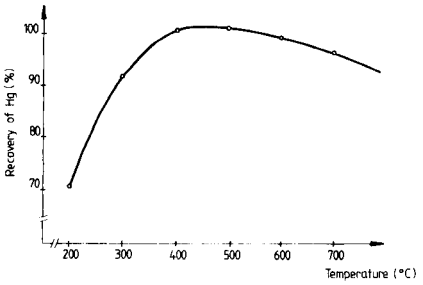

Fig. 3. Dependence of mercury recovery on additive/sample weight ratio (sample of copper concentrate, optimum heating conditions as in Table 3). Additives: (A) MgO; (B) CaO; (C) Florisil/CaO (2:1); (D) Al_2O_3 "d".

Fig. 4. Influence of temperature of first step sample heating treatment on mercury recovery. (First step time, 10 min; second step time, 10 min at 800°C.)

concentrates when alumina is used as additive. Sample heating at a lower temperature probably allows the catalytic surface properties of alumina to act fully.

The choice of optimal temperature (Fig. 4) and time of the two stages allows quantitative liberation of mercury to be achieved. The pyrolysis conditions, additives and the results for mercury determinations are summarized in Table 3. The results are consistent with the results obtained previously [5] with Florisil and with the results obtained after sample dissolution.

TABLE 3

Results for mercury determination in industrial samples under various conditions

Sample	Weight (mg)	Method	Additive	Mode of heating	Mercury content (%)	*n*	R.s.d. (%)
Copper concentr. I[a]	50	B	Al_2O_3	Two-step	5.08×10^{-3}	4	0.03
Copper concentr. II[b]	50	B	Al_2O_3	Two-step	7.10×10^{-3}	4	0.02
Zinc oxide	100	B	Al_2O_3	Two-step	1.06×10^{-3}	4	0.02
		C		—	1.07×10^{-3}	3	0.03
Lead oxide	100	B	MgO	One-step	0.96×10^{-3}	4	0.05
		B	Al_2O_3	One-step	0.98×10^{-3}	4	0.02
		C		—	0.97×10^{-3}	3	0.05
Kaolin KK[c]	100	A	Al_2O_3	One-step	8.75×10^{-6}	4	0.015

[a,b]Independent values: [a]5.12×10^{-3}%; [b]7.15×10^{-3}% [5]. [c]Reported mercury content, 8.8×10^{-6}%.

Application of the selected additives and pyrolytic conditions to other materials. Lead and zinc oxides are readily soluble in aqua regia but determination of mercury after pyrolytic separation was faster because the standard addition method was avoided. The liberation of mercury from zinc oxide without additives and filters, with only a set of filters, with the addition of "e" Al_2O_3, filters and two-step heating, and with "d" Al_2O_3, filters and two-step heating, gave 35%, 70%, 86% and 100% recoveries, respectively. Therefore the conditions selected for the copper concentrate were also optimal for zinc oxide. Results obtained after pyrolysis and after wet digestion agreed well (Table 3). The lead oxide sample completely volatilized during heating at 800°C for 15 min. Additives and samples should form a compound having a higher melting point than the sample. The additives CaO, MgO and Al_2O_3 fulfil that requirement, but only addition of MgO or Al_2O_3 gave accurate results (Table 3). The selected preparations of alumina were also effective for the kaolin sample (two-step heating was not necessary probably because of the small content of organic matter).

Recovery of mercury from samples spiked with mercury. Such experiments were done initially, to find the reason for the inaccuracy of the pyrolytic separation of mercury. Weighed (50 mg) portions of copper concentrate in the boat were spiked with standard mercury solutions ($HgCl_2$ or C_6H_5HgCl), placed in the furnace, and heated at 100°C for 5 min and then at 800°C for 15 min. For μg-amounts of mercury, trapping in an oxidizing solution was used and for ng-amounts, two gold collectors were used. The recovery of added mercury was quantitative even when there was non-quantitative liber-

TABLE 4

Recovery of mercury from samples spiked with mercury standard solutions

Sample	Filters	Additives	Hg found[c] (μg)	Hg added (μg)		Total Hg found (μg)	Recovery of Hg added (%)
				$HgCl_2$	C_6H_5HgCl		
1[a]	—	—	1.76	2	—	3.74	99
1	—	—	1.76	—	1	2.77	101
1	+	—	3.05	2	—	4.97	96
1	+	—	3.05	—	1	4.00	95
1	+	+	5.10	2	—	7.12	101
			(ng)	(ng)	(ng)	(ng)	(%)
2[b]	+	—	6.0	10	—	16.0	100
2	+	—	6.0	—	15	21.0	100
2	+	+	8.7	20	—	28.5	99
2	+	+	8.7	—	15	23.7	100

[a]100 mg of copper concentrate, method B. [b]100 mg of kaolin KK, method A. [c]Mean of 4 results.

ation of mercury contained in the sample (Table 4). The mercury compounds added probably volatilized before the main pyrolytic process started and could not be used to study the thermal evolution of mercury from complex samples or to test accuracy.

This work was supported by the Scientific Programme M.R.I.32.

REFERENCES

1 R. A. Nicholson, Analyst, 102 (1977) 399.
2 H. Uchikawa, R. Furuta and Y. Mihara, Bunseki Kagaku, 31 (1982) 367.
3 T. Baba, S. Ohmiya, M. Hosokawa and T. Ishibashi, Seikatsu Eisei, 27 (1983) 258.
4 Yu. V. Zelyukova and T. O. Didorenko, Ukr. Khim. Zh., 49 (1983) 526.
5 B. Różańska and E. Lachowicz, Anal. Chim. Acta, 175 (1985) 211.
6 R. Dumarey and R. Dams, Mikrochim. Acta, III (1984) 191.
7 E. Boroch, J. Przyłuski and K. Kolbrecka, Przem. Chem., 63 (1984) 315.
8 M. Marczewski and S. Malinowski, Bull. Acad. Polon. Sci. Ser. Sci. Chim., 24 (1976) 1.

Analytica Chimica Acta, 187 (1986) 325—331
Elsevier Science Publishers B.V., Amsterdam — Printed in The Netherlands

Short Communication

EFFECTS OF METAL COMPLEXATION ON THE ACCURACY OF ANODIC STRIPPING VOLTAMMETRY

W. C. GORMAN[a] and R. K. SKOGERBOE*

Department of Chemistry, Colorado State University, Fort Collins, Colorado 80523 (U.S.A.)

P. H. DAVIES

Colorado Division of Wildlife, Fisheries Research, Fort Collins, Colorado 80524 (U.S.A.)

(Received 15th April 1986)

Summary. It is shown that the use of the method of standard additions for electrochemical quantitation, when complexation to form non-electroactive entities can occur, can lead to serious problems with accuracy. It is also shown that the errors can often be compensated through the use of correct calibration models.

Trace metals in natural waters usually exist as the free aquo ions and in various combined chemical forms. Their behaviors are influenced by their chemical forms. Toxicological studies suggest that it is often the free metal ion which is the relevant toxic species [1—7]. Indeed, some reports [6, 7] suggest that toxicity is reduced as the formation constants for specific metal complexes increase. Such observations have led to the evolution of various procedures for quantifying metal-binding ligands and for determining metal-binding or complexation capacities.

The protocol endorsed by Chau et al. [7] and others [8—11], for example, involves the use of measurements by anodic stripping voltammetry (a.s.v.) to estimate the effective concentrations of binding agents capable of converting copper or other metals to non-electroactive forms. In essence, the stripping current is measured under controlled conditions as the copper concentration is incrementally increased and the occurrence of a break in the response curve is used to estimate the copper-complexing capacity of the water (see below). The general operational simplicity and sensitivity of this procedure has encouraged its fairly widespread adoption. Results reported for various waters frequently indicate apparent copper complexation capacities in the 1×10^{-7}—1×10^{-6} mol l^{-1} (6—60 μg l^{-1}) range [7—12].

Indications that natural waters often contain entities capable of converting metal ions to non-electroactive forms, combined with the fact that a.s.v. is often the method of choice, forms the basis of an accuracy problem. The central problem is to decide if electrochemical procedures such as a.s.v. can

[a]Present address: U.S. Borax Research, 412 Crescent Way, Anaheim, CA 92801, U.S.A.

003-2670/86/$03.50 © 1986 Elsevier Science Publishers B.V.

provide accurate results when the samples exhibit significant complexing capacities for the metals of interest. The answer is typically no. The purpose of this communication is to illustrate why the answer is negative and to demonstrate that serious accuracy problems can accrue when complexation occurs.

The formation of a simple metal complex, ML^{n+}, is described by the reaction $M^{n+} + L = ML^{n+}$, with a conditional formation constant defined by $K' = [ML^{n+}]/[M^{n+}][L]$; the brackets indicate the activities of the reactants at the pH in question. As Shuman and Woodward [8, 9] have noted, when K' is large and/or the reversibility of the reaction is slow relative to the time required for the electrochemical measurement so that the dissociation of ML^{n+} is negligible and when the complex formed is not electroactive, the electrochemical signal measured is proportional to the equilibrium concentration of metal ion, $[M^{n+}]$. Thus, for a.s.v. the stripping current is given by $i_a = k\,[M^{n+}]$, where the value of the proportionality constant depends on the conditions used.

If C_L, C_M, [L], and $[ML^{n+}]$ represent the total ligand, total metal, free ligand, and complex concentrations, respectively, mass balance considerations require that $C_L = [L] + [ML^{n+}]$ and $C_M = [M^{n+}] + [ML^{n+}]$. Thus, $[ML^{n+}] = C_M - i_a/k$ and $[L] = C_L - C_M + i_a/k$. When the ligand is in sufficient stoichiometric excess over the metal (e.g., $\geqslant$ 2-fold), the quantity i_a/k is considerably less than C_M, which is smaller than C_L by at least a factor of two, and so can be neglected in the last two equations. The above expression for K' can then be rearranged to show that

$$i_a \approx (k/K')\,[C_M/(C_L - C_M)] \tag{1}$$

Therefore, measurement of i_a with successive additions of known amounts of metal ion in the region of ligand excess should produce a linear plot from which k/K' can be evaluated if C_L is known. The effective value of C_L can be estimated by the procedures described by Chau et al. [7] or by Shuman and Cramer [12]. When continued additions of metal ion drive the complexation reaction into the region of excess of metal ion, the free metal ion concentration is closely approximated by $C_M - C_L$ and the expression $i_a = k\,[M^{n+}]$ becomes

$$i_a = k\,(C_M - C_L) \tag{2}$$

Thus, the titrimetric protocol also allows determination of k from the slope of the plot in this region. Indeed, the above considerations form the basis of the methods used by Chau et al. [7] for estimation of complexation capacity; the break-point in the titrimetric curve used for this estimate should closely approximate the stoichiometric transition from excess of ligand to excess of the metal ion.

Alternatively, Shuman and Cramer [12] have noted that the stripping current vs. added copper data can be fitted to an equation of the form

$$i = (kC_L/2)\left\{[g - 1 - (1/K'C_L)] + [(1 - g + (1/K'C_L))^2 + (4g/K'C_L)]^{1/2}\right\} \tag{3}$$

where $g = C_M/C_L$ and all other terms are as defined above. The fitting of experimental data to an equation of this form by nonlinear least-squares methods allows estimation of C_L, k, and K'. Alternatively, C_L can be estimated from the inflection point of the titration curve and the data can be fit to Eqns. 2 and 3 by linear least squares to estimate k and K'.

When electrochemical techniques such as a.s.v. are used for quantitation of metal ions, the method of standard additions is frequently relied on for calibration. Thus, a measurement is made at the residual metal concentration, C_0, and repeated after the additions of each of two (or more) known concentrations, C_1, $C_2 \cdots C_n$. The relevant equations assumed to be applicable are consequently $i_0 = k' C_0$, $i_1 = k' (C_0 + C_1)$, $i_2 = k' (C_0 + C_2)$, etc. The use of three measurements allows the assumption of linearity to be checked by graphic or by least-squares methods. Thus, the simultaneous solution of these equations is perhaps the simplest means of determining C_0; i.e.,

$$C_0 = i_0 (C_2 - C_1)/(i_2 - i_1) \tag{4}$$

It must be emphasized that the approaches to standard additions embodied in Eqn. 4 assume that the stripping current is directly proportional to C_M. However, it was shown above that this is not the case for the region of ligand excess (Eqn. 1) or the region of metal excess (Eqn. 2) unless $C_M \gg C_L$ for the latter. Consequently, the problem becomes to decide if one is likely to obtain results in the presence of complexation that will be adequately described by Eqn. 4 when, in fact, Eqns. 1 and/or 2 apply. The corollary is to establish what effects this will have on the estimation of C_0. It is simplest to address these problems through the use of illustrative data.

The a.s.v. peak currents given in Table 1 and plotted in Fig. 1 were derived from the paper by Shuman and Cramer [12] for the addition of copper to a solution containing fulvic acid at 60 mg l^{-1}. The peak currents were calculated from Eqn. 3 using the curve parameters given in their Table 1, part A [12], where the effective ligand complexing capacity (C_L) was 2.1×10^{-5} M, the value of K' was 2×10^5 and the slope of the upper portion of the curve (k)

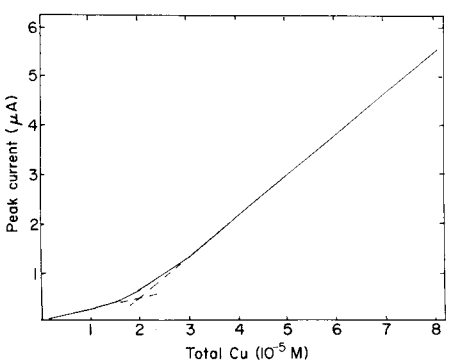

Fig. 1. Effects of complexation on the a.s.v. peak current (data from [12]).

TABLE 1

Evaluation of errors (E%) that could accrue from the use of standard additions when the model is $i = kC_M$

C_M (10^{-5} M)	i[a] (μA)	Results based on standard additions											
		Sequential concns.			Alternate concns.			Every 3rd concn.			Every 4th concn.		
		r[b]	$\hat{C}$[c] (10^{-5} M)	$-E$[d]	r	$\hat{C}$ (10^{-5} M)	$-E$	r	$\hat{C}$ (10^{-5} M)	$-E$	r	$\hat{C}$ (10^{-5} M)	$-E$
0.2	0.037	0.999	0.15	25	0.995	0.11	45	0.992	0.069	65	0.991	0.053	73
0.5	0.103	0.999	0.34	32	0.995	0.24	52	0.969	0.16	68	0.987	0.13	74
0.7	0.154	0.998	0.41	41	0.993	0.26	63	0.993	0.21	70	0.993	0.19	73
1.0	0.244	0.997	0.50	50	0.995	0.35	65	0.994	0.30	70	0.996	0.29	71
1.5	0.433	0.998	0.68	55	0.997	0.55	63	0.997	0.51	66	0.998	0.51	66
2.0	0.677	0.999	0.90	55	0.999	0.81	59	0.999	0.78	61	0.999	0.73	63
3	1.31	0.999	1.6	47	0.999	1.5	50	1.00	1.5	50	0.999	1.5	50
4	2.06	0.999	2.4	40	1.00	2.4	40	1.00	2.5	37	1.00	2.3	43
5	2.88	1.00	3.3	34	1.00	3.3	34	1.00	3.3	34	1.00	3.2	36
6	3.73	1.00	4.2	30	1.00	4.6	23	1.00	4.2	30	—	—	—
7	4.59	1.00	5.5	21	1.00	5.1	27	1.00	5.2	26	—	—	—
8	5.47	1.00	6.8	15	1.00	6.1	24	—	—	—	—	—	—
9	6.28	1.00	7.1	21	1.00	7.0	22	—	—	—	—	—	—
10	7.20	1.00	8.1	20	—	—	—	—	—	—	—	—	—
20	16.1	1.00	17.8	11	—	—	—	—	—	—	—	—	—
50	42.9	1.00	47.9	4.2	—	—	—	—	—	—	—	—	—
100	88.1	1.00	97.9	2.1	—	—	—	—	—	—	—	—	—

[a]Data derived from the report by Shuman and Cramer [12]. [b]r, regression coefficient calculated from linear least-squares fit using the model $i = kC_M$. [c]$\hat{C}$, concentration estimated by solution of simultaneous equations from the standard additions data. [d]$E(\%) = 100\ (C_M - C)/C_M$.

was 9×10^4. It is clear from Fig. 1 that the break in the curve is quite sharp even though K'/k was only 2.2. It is also noted that least-squares fitting of the data to Eqn. 1 for the case where $C_M/C_L \leqslant 0.5$ produces a regression coefficient of 0.9932. A similar treatment for the case where $C_M/C_L \geqslant 2$ provided a regression coefficient of 0.9812. Because the *t*-test indicated that both fits were acceptable at the 95% confidence level, the general validity of the respective models was demonstrated.

To evaluate the magnitudes of errors that could accrue from the use of the quantitation approach by standard additions (Eqn. 4) in the presence of complexation, a minimum of three peak currents from Table 1 was used with linear least-squares techniques to assess the linearity of the peak current response over the concentration range selected. Although the fitted equations were not used to compute C_0, the regression coefficient obtained was inspected to decide if the analyst would be likely to accept the linear model. As shown below, nearly all combinations examined produced regression coefficients greater than 0.99 confirming that most would accept the postulate of linearity. Once this was established for each concentration range explored, the lowest concentration in each range (C_0) was computed from Eqn. 4. The percent error in the estimate ($\hat{C}$) was then computed from $E(\%) = 100\ (C_0 - \hat{C})/C_0$, where C_0 was the actual concentration. The results summarized in Table 1 were obtained for expanding concentration ranges in recognition of the probable variations in the standard concentrations added for the standard additions method.

Inspection of Table 1 demonstrates the following general conclusions. The errors which can accrue in the estimation of the total copper concentration by standard additions all tend to be negative, i.e., the concentrations are underestimated. Those errors tend to be smaller for the smaller C_M/C_L values, increase to maximal values, and decrease thereafter as C_M/C_L exceeds unity. The points at which the error maxima occur clearly depend on the concentration ranges used for the standard additions. It can be shown that the error for values of $C_M/C_L \geqslant$ ca. 10 will be determined by

$$E(\%) = 100\ (C_M - C_L)/C_M \tag{5}$$

Thus, when $C_M/C_L = 20$, the predicted error is -5% and becomes -1% at $C_M/C_L = 100$. Therefore, the central conclusion is that the use of standard additions and the assumption of the usual linear model ($i = mC + b$) is very likely to lead to significant negative errors unless $C_M/C_L \geqslant$ ca. 20 over the entire concentration range explored.

This being so, it becomes necessary to establish if, when complexation is present and $C_M/C_L \leqslant 20$, other models such as Eqns. 1 and 2 can be used with the method of standard additions to obtain acceptably accurate results. Again, the regression approach used above can be applied to obtain a general answer. The results summarized in Table 2 were obtained after inclusion of additional data in the range where $C_M/C_L < 0.5$ to allow more regression evaluations in this range. Inspection of Table 2 indicates that the use of the

TABLE 2

Evaluation of errors that could accrue from the use of standard additions when the model is $i = k\,[C_M/(C_L - C_M)]$

C_M (10^{-5} M)	$C_M/(C_L - C_M)$	i (μA)	Results based on standard additions					
			Sequential concns.			Alternate concns.		
			r	$\hat{C}$ (10^{-5} M)	E (%)	r	$\hat{C}$ (10^{-5} M)	E (%)
0.2	0.105	0.037	0.999	0.23	+15	0.998	0.24	+20
0.3	0.167	0.057	0.999	0.31	+3.3	0.999	0.36	+20
0.4	0.235	0.078	0.998	0.48	+20	0.999	0.50	+25
0.5	0.312	0.103	0.999	0.57	+14	0.994	0.75	+51
0.6	0.400	0.126	0.999	0.75	+25	0.998	0.79	+27
0.7	0.500	0.154	0.993	1.1	+57	—	—	—
0.8	0.615	0.180	0.989	0.87	+8.7	—	—	—
0.9	0.750	0.200	—	—	—	—	—	—
1.0	0.910	0.241	—	—	—	—	—	—

TABLE 3

Evaluation of errors that could accrue from the use of standard additions when the model is $i = k\,(C_M - C_L)$

C_M (10^{-5} M)	$C_M - C_L$ (10^{-5} M)	i (μA)	Results based on standard additions					
			Sequential concns.			Alternate concns.		
			r	$\hat{C}$ (10^{-5} M)	E (%)	r	$\hat{C}$ (10^{-5} M)	E (%)
5	2.9	2.88	1.00	5.4	+8.0	1.00	5.5	+10
6	3.9	3.73	1.00	6.3	+5.0	1.00	6.4	+6.7
7	4.9	4.59	1.00	7.8	+11	1.00	7.2	+2.8
8	5.9	5.47	0.999	8.0	0	1.00	8.2	+2.5
9	6.9	6.28	1.00	9.2	+2.2	1.00	9.1	+1.1
10	7.9	7.20	1.00	10	0	—	—	—
20	17.9	16.1	1.00	20	0	—	—	—
50	47.9	42.9	—	—	—	—	—	—
100	97.9	88.1	—	—	—	—	—	—

model, $i = k\,[C_M/C_L - C_M]$, with standard additions provides results which tend to exhibit positive errors. The errors are, however, consistently less than those observed for the treatment summarized in Table 1. Similar results summarized in Table 3 for the model, $i = k\,(C_M - C_L)$, for $C_M/C_L > 2$, indicate that the results obtained are accurate within general ranges of experimental error.

The above evaluations show that serious errors can accrue from the use of standard additions for the determination of total dissolved metal concentrations by electrochemical techniques when the complexes formed are not electroactive. Alleviation of these errors can be achieved, at least partly, by recognition of the existence of complexation, measurement of the effective ligand complexation capacity, and use of the appropriate linear model with the standard additions approach. Even then, accurate estimates of the metal concentrations will apparently be difficult when the ligand is in stoichiometric excess over the metal. It is true that these conclusions might be identified by many as self-evident on an a priori basis. It appears equally true, however, that many are using electrochemical techniques with the standard additions method to determine dissolved metal concentrations in aqueous samples having significant concentrations of complexing ligands. It is to this latter audience that the present report is addressed. In view of the growing body of evidence that numerous aqueous samples contain ligands that form complexes that are not electroactive [7—12], it is important that the potential problems be understood.

This work was supported in part by Federal Aid in Wildlife Restoration (Dingell-Johnson F-33-R).

REFERENCES

1 E. D. Goldberg, in J. P. Riley and G. Skirrow (Eds.), Chemical Oceanography, Academic Press, New York, 1965, p. 163.
2 A. Siegel, in Organic Compounds in Aquatic Environments, M. Dekker, New York, 1971, p. 265.
3 W. Stumm and H. Bilinski, in S. H. Jenkins (Ed.), Advances in Water Pollution Research, Proc. 6th Int. Conf., Jerusalem, 1972, p. 39.
4 W. Stumm and P. A. Brauner, in J. P. Riley and G. Skirrow (Eds.), Chemical Oceanography, 2nd edn., Academic Press, New York, 1974, p. 264.
5 M. A. Rashed and J. D. Leonard, Chem. Geol., 11 (1973) 89.
6 P. Stoker and T. C. Hutchinson, Workshop on Toxicity to Biota of Metal Forms in Natural Water, Int. Joint Commission, Duluth, MN, 1975, pp. 159—164.
7 Y. K. Chau, R. Gacther and K. Lum-Shue-Chang, J. Fish Res. Board Can., 31 (1974) 1515.
8 M. S. Shuman and G. P. Woodward Jr., Anal. Chem., 45 (1973) 2032.
9 M. S. Shuman and G. P. Woodward Jr., Environ. Sci. Technol., 11 (1977) 890.
10 K. W. Hanck and J. W. Dillard, Anal. Chem., 49 (1977) 404.
11 T. A. O'Shea and K. H. Mancy, Anal. Chem., 48 (1976) 1603.
12 M. S. Shuman and J. L. Cramer, Environ. Sci. Technol., 13 (1979) 543.

Analytica Chimica Acta, 187 (1986) 333—338
Elsevier Science Publishers B.V., Amsterdam — Printed in The Netherlands

Short Communication

ELECTROCATALYTIC OXIDATION OF ASCORBIC ACID AND VOLTAMMETRIC DETERMINATION WITH A FERROCENE-MODIFIED PLATINUM ELECTRODE

MARIANNE PETERSSON

Department of Analytical Chemistry, University of Umeå, S-901 87 Umeå (Sweden)

(Received 10th April 1986)

Summary. Ferrocene attached to the surface of a platinum electrode catalyses the electrochemical oxidation of ascorbic acid in acidic buffer solutions. The overpotential for ascorbic acid oxidation is decreased by 150 mV at pH 2.2 compared with reaction at bare platinum; and an increase in anodic current and decrease in cathodic current for the redox reaction of ferrocene occurs on addition of ascorbic acid to the solution. The ferrocene-modified electrode is useful for the voltammetric determination of ascorbic acid in natural fruit juices. The advantages result from the electrocatalytic effect and from the prevention of adsorption of inhibitory substances from solution.

Much of the earlier work on chemically modified electrodes has been concerned with preparations and characterization of electrode surfaces where the attached species are, in general, electrochemically active molecules [1, 2]. Very few applications of these systems have been reported. Some advantages are to be expected when such modified electrodes are used as sensors in electroanalytical applications. In particular, the species which is bound to the electrode surface may mediate in the transfer of charge between the electrode and a dissolved substrate leading to increased current response and shifts in the potential at which reaction takes place. It is reasonable to expect that improvements in selectivity can be obtained in this way by judicious choice of the surface-bound mediator.

Ascorbic acid often has to be quantified in complicated matrices where the exploitation of chemically modified electrodes might be advantageous. In samples with low pH, for instance, it is almost impossible to determine this substance electrochemically with conventional electrode materials because of fouling by oxidation products. It has been demonstrated [3] that ascorbic acid can be oxidized electrocatalytically in homogeneous solution by electrogenerated hexacyanoferrate(III). In addition, chemically modified electrodes with active surfaces comprising monolayers of benzidine, polymerized vinylferrocene, alkylamine/siloxane polymers containing hexacyanoferrate(III), and polyvinylpyridine films containing hexachloroiridate(IV) have been used to oxidise ascorbic acid in acidic solution [4—7].

0003-2670/86/$03.50 © 1986 Elsevier Science Publishers B.V.

The purpose of this communication is to report the results of voltammetric determinations of ascorbic acid in aqueous buffer solutions and in fresh fruit juices at pH 2.2 and 3.6 with a platinum electrode coated with a monolayer of covalently bound ferrocene. Potentiometric measurements of ascorbic acid with this electrode have already been reported [8]. Voltammetric methods are especially suitable for in vivo analyses and for detection in liquid chromatographic and flow-injection techniques.

Experimental

Electrode preparation. The preparation of the electrodes was described in detail earlier [9, 10].

Solutions. The voltammetric characterization of the electrodes was done in acetone or acetonitrile (spectroscopic grade, Merck Uvasol) with lithium perchlorate (0.1 mol dm^{-3}) as supporting electrolyte. L-Ascorbic acid (Merck p.a.) was dissolved in aqueous glycine buffer (0.1 mol dm^{-3}) at pH 2.2 or 3.6. As additional electrolyte, potassium chloride (0.1 mol dm^{-3}) was added to the above buffer solution.

Fresh juice was obtained by squeezing fruit between two glass beakers to avoid contamination by metal ions which could interfere in the determinations. The juices were then diluted with the above-mentioned buffer solution (5 ml of juice to a final volume of 100 ml) to give an ascorbic acid concentration of approximately 10^{-4} mol dm^{-3}. Solutions were deaerated with nitrogen, saturated with moisture to avoid concentration changes during the measurements, which were made at 20.0 ± 0.5° C.

Instrumentation. For voltammetric measurements, a conventional 3-electrode configuration was connected to a potentiostat (constructed in this laboratory) and a Moseley 7030AM X-Y recorder. Calomel electrodes with sodium chloride (1 mol dm^{-3}) or saturated potassium chloride were used as references in organic and aqueous solutions, respectively. Potentials were measured from the recorded voltammograms with a precision of ±2 mV.

Results and discussion

The voltammetric response of the ferrocene-modified electrode in pure buffer solution at pH 2.2 is shown in Fig. 1 (curve A). The difference in potential between the current peaks corresponding to the ferrocene/ferricinium redox reaction is somewhat larger than that normally observed in non-aqueous solvents and may reflect slower electron-transfer kinetics [9, 10]. Curves B and C in Fig. 1 show the effect of adding ascorbic acid to the solution. The maximum current occurs at 0.405 V vs. SCE. The increase in the anodic peak current accompanied by the decrease in the cathodic peak current is indicative of reaction between the surface-bound ferricinium species and the dissolved ascorbic acid at the potential corresponding to generation of the oxidized form of the mediator. The response at a bare platinum electrode under the same conditions is shown in curve D. This behaviour is compatible with an electrocatalytic mechanism which can be

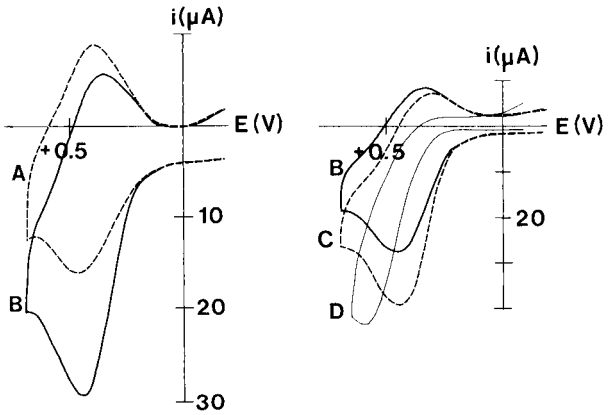

Fig. 1. Cyclic voltammograms recorded at 50 mV s^{-1}: (A) a ferrocene-modified electrode in aqueous glycine buffer (pH 2.2)/KCl (0.1 mol dm^{-3}); (B) after addition of ascorbic acid to give a concentration of 1.5×10^{-4} mol dm^{-3}; (C) after further addition of ascorbic acid to give a concentration of 3×10^{-4} mol dm^{-3}; (D) the bare electrode response to 4×10^{-4} mol dm^{-3} ascorbic acid.

written, analogously to the mode suggested by Winograd et al. [3] for the catalytic action of hexacyanoferrate(III), as

$$\text{-CpFeCp} \rightleftharpoons \text{-CpFe}^{+}\text{Cp} + e$$

$$2\text{-CpFe}^{+}\text{Cp} + AH_2 \rightarrow 2\text{-CpFeCp} + A + 2\,H^{+}$$

A decrease in the scan rate from 50 mV s^{-1} to 10 mV s^{-1} sharpened the anodic peak with the modified electrode but broadened the peak with the bare platinum electrode, compared with curves C and D in Fig. 1. The maximum current with the bare electrode occurred at a potential some 150 mV more positive of that obtained in the presence of the mediating ferrocene layer. This reduction of 140—150 mV in the overpotential for ascorbic acid oxidation was also observed for different concentrations and potential scan rates and clearly demonstrates that the ferrocene layer functions electrocatalytically.

Electrocatalytic oxidation of ascorbic acid by ferricinium species was reported by Dautartas and Evans [5], who used a chemically modified electrode prepared by plasma polymerization of vinylferrocene on a pyrolytic graphite surface; the relationship between the anodic peak current and the concentration of ascorbic acid in solution was not linear. In contrast, the peak currents observed for oxidation of ascorbic acid at the modified platinum electrode studied here, where the surface coverage of ferrocene was much lower ($5—10 \times 10^{-10}$ mol cm^{-2} [9, 10]), were linearly dependent on the substrate concentration and on the square root of the applied potential scan rate (Figs. 2 and 3). Figure 3 indicates that the current is diffusion-controlled; effects of slow charge-transfer kinetics are not apparent. Thus the

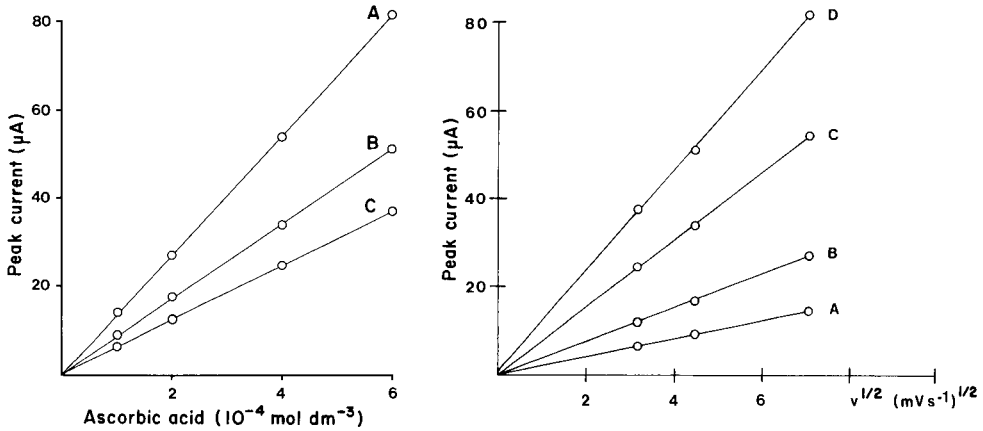

Fig. 2. Dependence of peak current on concentration of ascorbic acid at pH 2.2 with different scan rates: (A) 50 mV s^{-1}; (B) 20 mV s^{-1}; (C) 10 mV s^{-1}.

Fig. 3. Dependence of peak current on the square root of the scan rate at pH 2.2 for different ascorbic acid concentrations: (A) 1.0×10^{-4}; (B) 2.0×10^{-4}; (C) 4.0×10^{-4}; (D) 6.0×10^{-4} mol dm^{-3}.

ferrocene-modified electrode can readily be applied for the determination of ascorbic acid.

Determination of ascorbic acid in fresh fruit juice. Curve A in Fig. 4 shows a typical voltammogram recorded for the oxidation of ascorbic acid (ca. 2×10^{-4} mol dm^{-3}) in fresh orange juice diluted with glycine buffer (pH 2.2). A well shaped current peak, which is easily evaluated, is seen at the potential corresponding to ferrocene oxidation. A minor reduction wave appears on the reversed scan which probably results from remaining ferricinium species. The voltammogram was reproducible but the current/potential curve for ascorbic acid oxidation was slightly broader in the natural matrix compared with the pure buffer solution. Figure 4, curve B, illustrates attempts to determine ascorbic acid under the same conditions as for curve A at a bare platinum electrode. No discernible current peak is observed. The oxidation of ascorbic acid in the natural matrix at bare platinum may be masked by adsorption. This comparison clearly demonstrates the advantage of the ferrocene-modified platinum electrode.

To investigate the reproducibility and accuracy of determinations with the ferrocene-modified electrode, three such electrodes were used to determine ascorbic acid in fresh grapefruit juice. The standard addition technique was adopted because the peaks were slightly broader in the fruit juices than in the standard solutions used for calibration. Peak currents were evaluated from an approximate base-line and corrected for a small contribution from the oxidation of ferrocene. The concentration of ascorbic acid in grapefruit juice was found to be 38.2 mg/100 ml (standard deviation 1.7%, $n = 9 = 3 \times 3$) which agreed well with a value of 40.0 mg/100 ml obtained titrimetrically with

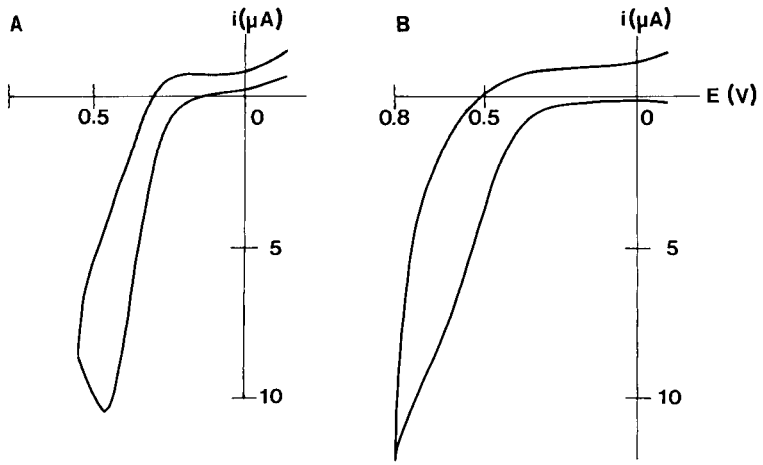

Fig. 4. Cyclic voltammograms showing the oxidation of ascorbic acid at a concentration of 2×10^{-4} mol dm^{-3} in fresh orange juice at pH = 2.2 (glycine buffer). Scan rate = 10 mV/s. Ferrocene-modified electrode (curve A), bare platinum electrode (curve B).

TABLE 1

Summary of voltammetric determinations of L-ascorbic acid in fresh orange juice with ferrocene-modified platinum electrodes

[Medium: aqueous glycine buffer (pH 3.6)/KCl (0.1 mol dm^{-3}). Scan rate: 10 mV s^{-1}. Surface coverage of ferrocene = 7×10^{-10} mol cm^{-2}.]

Electrode	Concentration of ascorbic acid (mg dl^{-1})	E_p (V)
Pt (5)	62.7	0.397
	63.2	0.399
	61.5	0.405
Pt (8)	62.9	0.368
	62.9	0.383
	63.3	0.390
Pt (13)	63.4	0.370
	62.9	0.388
Mean values:	62.9 ± 0.60	0.388 ± 0.013

2,6-dichlorophenolindophenol and visual end-point detection. Similar determinations were done at pH 3.6 with three ferrocene-modified electrodes (Table 1). An average ascorbic acid concentration of 62.9 mg/100 ml of fresh orange juice was obtained (s.d. 0.95%). Corresponding titrimetric measurements gave 63.4 mg/100 ml of juice.

These results demonstrate that the chemically-modified ferrocene-platinum electrode can be used with advantage for the determination of ascorbic acid in natural samples.

The author thanks Dr. Michael Sharp for valuable discussions and the Swedish Natural Science Research Council for financial support.

REFERENCES

1 R. W. Murray, Acc. Chem. Res., 13 (1980) 135.
2 K. D. Snell and A. G. Keenan, Chem. Soc. Rev., 8 (1979) 259.
3 N. Winograd, H. N. Blount and T. Kuwana, J. Phys. Chem., 73 (1969) 3456.
4 J. F. Evans, T. Kuwana, M. T. Henne and G. P. Royer, J. Electroanal. Chem., 80 (1977) 406.
5 M. F. Dautartas and J. F. Evans, J. Electroanal. Chem., 109 (1980) 301.
6 K.-N. Kuo and R. W. Murray, J. Electroanal. Chem., 131 (1982) 37.
7 J. Facci and R. W. Murray, Anal. Chem., 54 (1982) 772.
8 M. Petersson, Anal. Chim. Acta, 147 (1983) 359.
9 M. Sharp, M. Petersson and K. Edström, J. Electroanal. Chem., 109 (1980) 271.
10 M. Sharp and M. Petersson, J. Electroanal. Chem., 122 (1981) 409.

Analytica Chimica Acta, 187 (1986) 339—342
Elsevier Science Publishers B.V., Amsterdam — Printed in The Netherlands

Short Communication

AN AUTOMATED FLOW-INJECTION EXTRACTION METHOD FOR DETERMINATION OF BITTERING COMPOUNDS IN BEER

YLVA SAHLESTRÖM

Department of Analytical Chemistry, Royal Institute of Technology, S-100 44 Stockholm (Sweden)

SIGRID TWENGSTRÖM and BO KARLBERG*

Bifok AB, Box 124, S-191 22 Sollentuna (Sweden)

(Received 11th April 1986)

Summary. The manual standard liquid—liquid extraction method for determining bitterness in beer is adapted for a flow-injection extraction system. With the flow-injection method, the separate solvent blank extraction required in the batch procedure is unnecessary. The injected sample volume is 100 μl, the sampling frequency is about 60 h^{-1} and the consumption of iso-octane is only about 1 ml/sample.

The bittering compounds in beer consist mainly of iso-α-acids, which have been identified as three pairs of diastereoisomeric compounds, namely isohumulone, isocohumulone and isoadhumulone. These are converted from the α-acids in hops during the wort boiling process. The complete structure of all bitter-tasting compounds is not yet fully understood [1]. This has been the main reason for the difficulties in finding relevant analytical methods. Consequently, a variety of methods is applied: α-acids can be measured conductometrically or gravimetrically as their corresponding lead salts, and polarimetric assay has been suggested, but this measurement does not include racemic α-acids [1]. All these methods are very sensitive to interfering compounds. Liquid chromatography has long been regarded as an attractive way of solving the selectivity problems and much research has been devoted to the development of a fast and reliable routine method primarily for iso-α-acids [2—4]. However, there remain unsolved problems involving selection of an internal standard, a relevant reference compound, resolution speed and column packing material. A modification of a method developed by Moltke and Meilgaard [5] in 1955 is now widely used for routine purposes.

Degassed beer is extracted after acidification with iso-octane in a 1:2 (v/v) ratio. After centrifugation, the absorbance of the organic phase is measured at 275 nm against pure iso-octane. This absorbance value is used to define an empirical entity called a Bittering Unit: $BU = 50 \times$ absorbance. The *BU* was introduced by the EBC Analysis Committee [6] in order to avoid arbitrary assumptions about the chemical structure and nature of the bittering

0003-2670/86/$03.50 © 1986 Elsevier Science Publishers B.V.

compounds in beer. This communication presents an automation of this extraction method based on a flow-injection extraction unit described recently [7].

Experimental

Reagents and solvents. All reagents and solvents were of analytical grade. Distilled water was used throughout. Iso-octane (Merck) was used as the extraction solvent and distilled water was poured through before use. The carrier was 0.1 M hydrochloric acid. Iso-octanol was added to the beer samples as an anti-foaming agent.

Beer samples. All beer samples were supplied from Pripps AB (Sweden); they included a variety of dark and light beers as well as worts and unfiltered green beer.

Apparatus. A FIAstar 5020 unit (Tecator, Sweden) was used together with the extraction manifold described earlier [7]. The flow scheme is shown in Fig. 1. The organic solvent (iso-octane) was introduced via a displacement bottle. A Pye-Unicam SP6-550 u.v. spectrophotometer with a flow cell (8-μl internal volume, 10-mm light path) was used as detector (275 nm). A recorder was coupled to the spectrophotometer and all peak values were automatically recorded and displayed on the FIAstar unit. The injection volume was 100 μl. The separating membrane was of PTFE (1.0-μm pore size) and the separated organic phase was rejoined with the aqueous stream to a common waste outlet (see Fig. 1). All measurements were made at room temperature.

Procedure. Pump 1 in the FIAstar unit was reserved for expelling the organic solvent from the displacement bottle and pump 2 for propelling aqueous carrier into the extraction unit. On starting up the system, pump 1 was activated first and pump 2 was started when the system had been filled with organic solvent. On closing down, the reversed procedure was applied. The beer samples were degassed in an ultrasonic bath for a couple of minutes in order to eliminate gas bubbles. When necessary, water droplets or other impurities in the flow cell were rinsed out with ethanol introduced via a special gauge in the extraction unit [7].

Manual batch extractions were done simultaneously with the flow-injection extractions in order to compare the two methods. Thus, 10 ml of degassed beer was pipetted into a flask, followed by addition of 1 ml of 3 M

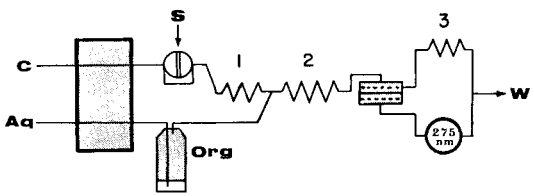

Fig. 1. Flow-injection manifold for the extraction of bittering compounds in beer. C, 0.1 M HCl at 1.0 ml min^{-1}; org, iso-octane at 0.5 ml min^{-1}. Coil lengths: (1) 50 cm; (2) 200 cm; (3) 50 cm.

hydrochloric acid and 20 ml of iso-octane. The flask was shaken vigorously for 10 min on a wrist action shaker. Worts, green beers and beer samples from fermentation tanks were then centrifuged. The extract was transferred to a 10-mm quartz cell and measured against water-equilibrated iso-octane at 275 nm.

Calculations. In order to compare the two methods, all values were individually related to one sample (Pripps Blå III). This product was intermittently used as an in-house standard at Pripps to calibrate the method.

Results and discussion

The results of the comparative evaluation of the automatic and manual methods are presented in Table 1. Samples from 22 products were tested: the first seven were sampled from the manufacturing process and the rest

TABLE 1

Comparison between batch and flow-injection extraction (f.i.e.) methods for the determination of bitterness in a variety of beer and malt samples

Sample		F.i.e.		Batch		Batch/ f.i.e.
No.	Type	A_{sample}	A_{sample}/A_{22}	A_{sample}	A_{sample}/A_{22}	
1	Unfiltered bulk product	0.351	0.98	0.500	1.02	1.04
2	As 1	0.359	1.0	0.509	1.03	1.03
3	Incompletely fermented malt	0.386	1.08	0.585	1.19	1.10
4	As 3	0.401	1.12	0.562	1.14	1.02
5	As 3	0.626	1.74	0.903	1.84	1.06
6	As 3	0.389	1.08	0.540	1.10	1.02
7	As 3	0.107	0.30	0.152	0.31	1.03
8	Light[a]	0.260	0.72	0.371	0.75	1.04
9	Dark[a]	0.227	0.63	0.320	0.65	1.03
10	Light[a]	0.234	0.65	0.334	0.68	1.05
11	Light[a]	0.250	0.70	0.351	0.71	1.01
12	Dark[b]	0.246	0.69	0.342	0.70	1.01
13	Light[b]	0.215	0.60	0.308	0.63	1.05
14	Light[b]	0.496	1.38	0.640	1.30	0.94
15	Light[b]	0.307	0.86	0.417	0.85	0.99
16	Dark[b]	0.357	0.99	0.516	1.05	1.06
17	Light[c]	0.409	1.14	0.525	1.07	0.94
18	Dark[c]	0.366	1.02	0.504	1.02	1.0
19	Light[c]	0.321	0.89	0.449	0.91	1.02
20	Light[c]	0.260	0.72	0.361	0.73	1.01
21	Light[c]	0.349	0.97	0.475	0.97	1.0
22	Light[c] (standard)	0.359	1.0	0.492	1.0	1.0

[a]1.7% ethanol. [b]2.7% ethanol. [c]4.1% ethanol.

from marketed beer products. Sample 22 was used as a standard (Pripps Blå III).

The correlation equation was calculated as $y = 1.011\ x + 0.007$, where y respresents the f.i.e. values and x the batch values. The repeatability was 1.7% when one sample was injected 25 times. For each flow-injection set-up, a specific BU/f.i.e. factor could be estimated by running parallel determinations by the two methods:

$$\text{BU/f.i.e. factor} = A_{\text{sample}}\ (\text{batch}) \times 50/A_{\text{sample}}\ (\text{f.i.e.})$$

The average BU/f.i.e. factor was 70 for the results presented in Table 1 with an r.s.d. of 3.3%. By using different sample volumes the factor value could be varied within certain limits. The phase-volume ratio also influenced the BU/f.i.e. factor, thus offering a second possibility for its variation. In a separate experiment, the two methods were compared for identical phase-volume ratios. The flow-injection values were about 30% lower than corresponding batch values when the injected volume was 100 μl. This is in excellent agreement with earlier findings for caffeine [7].

In conclusion, the flow-injection method offers the following advantages: (a) blanking is automatic as the solvent background absorbance is automatically taken as the baseline; (b) less than 200 μl of sample is used per analysis; (c) the sample throughput is large, at about 60 h^{-1}; (d) consumption of organic solvent is low, at about 1 ml per determination; (e) reproducible sample handling is ensured with respect to time and volume; and (f) washing-up is minimal.

The authors are indebted to Dr. Claes-Göran Johansson and Prof. Folke Ingman for valuable discussions.

REFERENCES

1 J. S. Hough, D. E. Briggs, R. Stevens and T. W. Young, Malting and Brewing Science, 2nd edn., London, 1982.
2 M. Verzele, C. Dewaele and M. van Kerrebroeck, J. Chromatogr., 244 (1982) 321.
3 E. J. Knudson and K. J. Siebert, J. Am. Soc. Brew. Chem., 41, 2 (1983) 51.
4 M. Verzele and M. de Potter, J. Chromatogr., 166 (1978) 320.
5 A. B. Moltke and M. Meilgaard, Brygmesteren, 12 (1955) 65.
6 Analytica-EBC, 3rd edn., 1975.
7 Y. Sahleström and B. Karlberg, Anal. Chim. Acta, 179 (1986) 315.

Analytica Chimica Acta, 187 (1986) 343—346
Elsevier Science Publishers B.V., Amsterdam — Printed in The Netherlands

Short Communication

KINETIC TREATMENT OF UNSEGMENTED FLOW SYSTEMS
Part 4. Equations for a System with Gradient Chamber Corrected to Account for Detectors with Finite Sensitivities

PAUL JAGER and HARRY L. PARDUE
Department of Chemistry, Purdue University, West Lafayette, IN 47907 (U.S.A.)
(Received 28th April 1986)

Summary. Corrected equations are presented for a flow-injection sample-processing system that includes a gradient chamber. In earlier treatments, the initial and final points of a time-interval measurement were defined to correspond to a detection system with infinite sensitivity. The more exact equations now presented account for the effects of using practical detectors with finite sensitivities. Data are presented to show that the revised equations correctly predict the curvature observed in calibration plots at low analyte concentrations.

An early paper described an approach to flow-injection sample-processing that included a gradient chamber [1]. Subsequent reports from this laboratory have presented a kinetic model, with a mathematical treatment and experimental evaluation of that approach [2—4]. The purpose of this communication is to correct an error in these earlier treatments [2—4].

In the approach discussed [1], a sample containing the analyte of interest is intercalated into a flowing stream that carries it into the gradient chamber where analyte concentration initially increases rapidly but then decreases continuously as a result of solution flow into and out of the chamber. Analyte concentration is quantified from a time interval, Δt_{ep}, required for a signal to rise above and return to preset levels. In the earlier treatments [2—4], it was assumed that the preselected signal levels corresponded to analyte concentrations that were negligibly small relative to the bulk concentrations to be quantified. In practice, it is not always possible to achieve this ideal condition at the lowest analyte concentrations of interest, and to the extent that this assumption is invalid, so are equations based on it. This communication presents corrected equations and experimental data to illustrate the significance of the changes.

Experimental

The quantitation of triiodide was used as a model system to evaluate the equations. Triiodide concentration was monitored amperometrically and thiosulfate was used as a reactant in the flow stream in some experiments. Experimental details have been presented [4] and are not repeated here.

0003-2670/86/$03.50 © 1986 Elsevier Science Publishers B.V.

Model and mathematical treatment

The kinetic model has been presented in detail, and only those features that relate directly to this discussion are presented here.

The processes in the gradient chamber and the origin of errors in earlier treatments are discussed with the aid of Fig. 1. The ordinates in Fig. 1 represent the ratio of the instantaneous analyte concentration in the gradient chamber, C_{ag}, to the maximum concentration, C_{ag}^{max}, and the ratio of the instantaneous reactant concentration in the gradient chamber, C_{bg}, to the initial concentration of reactant in the gradient chamber, C_{bg}^{0}. This figure represents the situation in which the gradient chamber contains reactant (thiosulfate) concentration initially at the same concentration as the flow stream.

As sample containing analyte (triiodide) begins to enter the chamber at t_0, it begins to react with reactant in the chamber, decreasing its concentration. At t_1, all reactant is cleared from the chamber and analyte concentration begins to increase toward the maximum at t_2 when all of the sample aliquot has entered the chamber. Between t_2 and t_3, analyte concentration decreases continuously as a result of mass flow from the chamber, dilution by reagent flowing into the chamber, and reaction with reactant in the flow stream if, as in this case, the flow stream contains reactant.

In earlier treatments, it was assumed that the time interval, Δt_{ep}, was determined between the points, t_1 and t_3, at which analyte concentration just exceeds and returns to zero. In practice, the time interval is actually determined between times, t_a and t_b, at which the analyte concentration rises above and below finite values. Clearly, the equations developed earlier [2—4], with the time interval defined as $\Delta t_{ep} = t_3 - t_1$, will predict values of Δt_{ep} that are larger than experimental values, and the discrepancy should be larger for lower analyte concentrations.

To generate corrected equations, Δt_{ep} is now defined as

$$\Delta t_{ep} = t_b - t_a \qquad (1)$$

and the analyte concentration at t_a and t_b is defined as the "end-point" con-

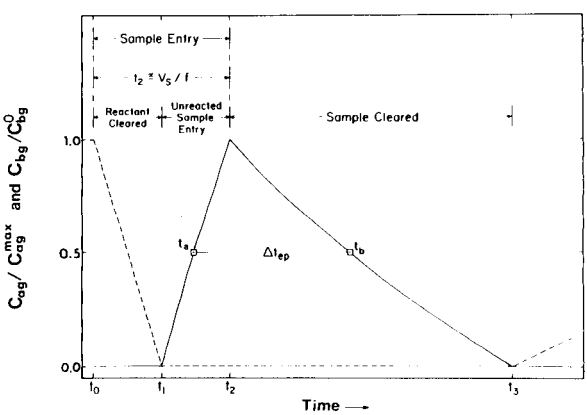

Fig. 1. Time-dependent concentrations of analyte and reactant: (—) analyte; (---) reactant.

centration, C_{ag}^{ep}. After substituting $t = t_a$, $C_{ag} = C_{ag}^{ep}$, and the equation for t_1 (Eqn. 1c in [3] with z in the denominator [4]; the position of the reaction ratio, z, is inverted in all equations in [3] as explained earlier [4]) into the equation for C_{ag} (Eqn. 2b in [3]), and rearranging, it is shown that

$$t_a = (V_g/f) \ln [(C_{as}^0 + C_{bg}^0/z)/(C_{as}^0 - C_{ag}^{ep})] \quad (2)$$

in which V_g is the volume of the gradient chamber, f is the reagent flow rate, C_{as}^0 is the concentration of analyte in the undiluted sample, and C_{bg}^0 is the initial concentration of reactant in the gradient chamber. Similarly, after substituting $C_{ag} = C_{ag}^{ep}$ at $t = t_b$, $t_b = \Delta t_{ep} + t_a$, $t_2 = V_s/f$ and t_a, as in Eqn. 2, into the equation for C_{ag} when $t \geqslant t_2$ (Eqn. 3b in [3]), and rearranging, it is shown that

$$\Delta t_{ep} = (V_g/f) \ln \{[C_{as}^0 - C_{ag}^{ep}][(C_{as}^0 + C_b^0/z)(\exp(V_s/V_g))(C_{as}^0 + C_{bg}^0/z)]/[(C_{as}^0 + C_{bg}^0/z)(C_{ag}^{ep} + C_b^0/z)]\} \quad (3)$$

in which V_s is the volume of sample and other symbols are as defined above.

The main difference between Eqn. 3 above and the analogous equation presented earlier (Eqn. 9e in [3]) is the bracketed terms including C_{ag}^{ep} in Eqn. 3. If it is assumed that the analyte concentration at the end-point is negligibly small relative to the sample concentration, $C_{ag}^{ep} \ll C_{as}^0$, then Eqn. 3 above reduces to the form presented earlier [3]. Thus, the equations developed earlier are special cases of this more exact equation and are valid only when the sensitivity of the detection system is sufficiently high that negligibly small amounts of analyte are needed to detect the "end-points" in the process.

Equation 3 can be manipulated and simplified to conform to the different situations discussed earlier. In the interest of brevity, the results are not presented here but are reported in detail elsewhere [5].

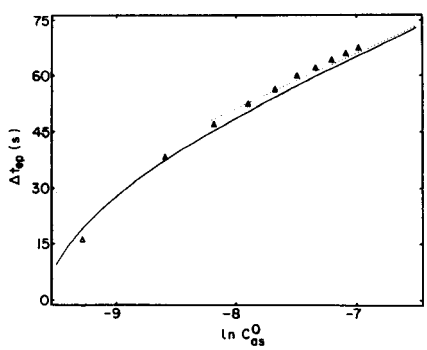

Fig. 2. Calibration plot of Δt_{ep} vs. ln C_{as}^0 for the situation in which $C_{ag}^{ep} \approx C_{as}^0$ and $C_b^0 = C_{bg}^0 > 0$. (△) Experimental results; (—) computed from Eqn. 3; (...) computed from Eqn. 9e in [3]. V_s = 1.395 ml, V_g = 0.4840 ml, f = 0.03250 ml s^{-1}, C_{ag}^{ep} = 0.05452 mM I_3^-, $C_b^0 = C_{bg}^0$ = 0.2577 mM $S_2O_3^{2-}$.

Results and discussion

Data presented earlier [4] were re-interpreted with these more exact equations. Although there were subtle improvements, in most instances C_{ag}^{ep} was sufficiently small relative to C_{as}^{0} that corrections were small. Therefore, to evaluate the new equations under more appropriate conditions, solutions of triiodide with concentrations between 0.1 and 1.0 mM were processed with a preselected detection level of C_{ag}^{ep} = 0.05 mM. Results for the situation in which $C_{b}^{0} = C_{bg}^{0} > 0$ are summarized in Fig. 2. Whereas the equations developed earlier predicted a linear relationship (dotted line), Eqn. 3 correctly predicts the curvature that is observed experimentally. Although the fit between theory and experiment is not exact, it is much better than for any equations presented previously. Similar results were obtained for the situation in which $C_{b}^{0} = C_{bg}^{0} = 0$.

This work was supported in part by Grant No. CHE8319014 from the National Science Foundation.

REFERENCES

1 J. Růžička, E. H. Hansen and H. Mosbaek, Anal. Chim. Acta, 92 (1977) 235.
2 H. L. Pardue and B. Fields, Anal. Chim. Acta, 124 (1981) 39.
3 H. L. Pardue and B. Fields, Anal. Chim. Acta, 124 (1981) 65.
4 H. L. Pardue and P. Jager, Anal. Chim. Acta, 179 (1986) 169.
5 P. Jager, Kinetic Treatment of Unsegmented Flow Systems with Gradient Chamber, M.S. Thesis, Purdue University, IN, U.S.A., 1986.

Analytica Chimica Acta, 187 (1986) 347—351
Elsevier Science Publishers B.V., Amsterdam — Printed in The Netherlands

Short Communication

EVALUATION OF THE CALIBRATION MATRIX CONDITION NUMBER AS A CRITERION FOR OPTIMAL DERIVATIVE-SPECTROPHOTOMETRIC MULTICOMPONENT QUANTITATION

L. L. JUHL and J. H. KALIVAS*
Department of Chemistry, Idaho State University, Pocatello, ID 83209 (U.S.A.)
(Received 14th April 1986)

Summary. A criterion is described that will help predict the optimal derivative order to be used for a given quantitative procedure. The procedure is tested with a two-component sample of acid-base indicators at pH 4 and pH 6. The method predicted that the second derivative should be used at pH 4 while the first derivative is optimal at pH 6.

Derivative spectrometry [1—3] is often used to obtain increased selectivity [4, 5]. Increased selectivity can offer improved accuracy, whether it be qualitative or quantitative [4, 6, 7]. Most applications of derivative spectrometry have used only one sensor (i.e., wavelength). Recently, Pardue and co-workers [4, 8, 9] have evaluated multiwavelength derivative spectrometry for quantifying multicomponent samples.

In multicomponent derivative spectrometry, the question arises as to what is the optimal derivative order for acceptable accuracy and precision. The most favorable order varies from component to component in a sample. A compromise order needs to be selected such that good selectivity, sensitivity, precision, and accuracy can be obtained for all components. The most common derivative orders used are first and second. To date, however, the choice of derivative order has been empirical.

Error propagation is an important consideration in establishing the optimal derivative order for a chemical identification or quantitation. When spectral interferences and matrix effects are present in a multicomponent procedure, theory states that measurement errors can be amplified to produce larger uncertainties for the estimated analyte concentrations [10]. This error amplification can be represented by the condition number of the calibration matrix. When the condition number of the matrix is large, the matrix is said to be ill-conditioned [10—12]. Thus, the condition number of a calibration matrix provides useful information about the potential error in estimating the analyte concentrations; the larger the condition number, the larger the error. Similarly, a large condition number represents a high degree of non-orthogonality in the spectra. The upper limit of the relative error for the estimated concentrations depends on the condition number of the calibration

0003-2670/86/$03.50 © 1986 Elsevier Science Publishers B.V.

matrix and the relative errors in the data. Particularly, the upper bound for the relative error in the estimated concentrations ($||\delta \vec{c}||/||\vec{c}||$) can be obtained by multiplying the condition number of the calibration matrix, cond(**K**), by the sum of the relative errors arising from absorbance ($||\delta \vec{r}||/||\vec{r}||$) and calibration ($||\delta \mathbf{K}||/||\mathbf{K}||$) [10—12]. The $||\ ||$ signs mean the Euclidian norm of a vector or matrix, $\vec{c}$ represents the vector of concentrations of n components, $\vec{r}$ is the vector of sample responses measured at p sensors, and **K** is the p x n calibration matrix of linear response constants. The error propagation is expressed by

$$||\delta \vec{c}||/||\vec{c}|| \leqslant \text{cond}(\mathbf{K})\ (||\delta \vec{r}||/||\vec{r}|| + ||\mathbf{K}||/||\mathbf{K}||) \qquad (1)$$

The condition number of the calibration matrix, cond(**K**), is calculated from $\text{cond}(\mathbf{K}) = ||\mathbf{K}||\ ||\mathbf{K}^{-1}||$ for a square **K** matrix ($p = n$). If the **K** matrix is rectangular ($p > n$, more sensors than analytes), its condition number is given by $\text{cond}(\mathbf{K}) = [\text{cond}(\mathbf{K}^T\mathbf{K})]^{1/2}$.

It has been shown that a minimum in the condition number of the calibration matrix represents an optimization of the selectivity and accuracy for a given multicomponent quantitation scheme [13]. This study was limited to finding the optimal set of sensors for a particular multicomponent system. Separate investigations provided similar results [14, 15]. Additionally, it was found that the condition number of the calibration matrix could be used to establish the optimal complexing agent for spectrophotometric multicomponent quantitation of trace metals [14]. The condition number of the calibration matrix has also been used as a criterion to find the optimal pH and solvent for a two-component mixture [16].

Because differentiation of the spectra can alter the selectivity, the calibration matrix is also influenced. Correspondingly, differentiation can increase or decrease cond(**K**). A logical conclusion is that the derivative order should be varied until the minimum in cond(**K**) is reached. If this is done, one should have simultaneously optimized the multicomponent procedure for maximum selectivity and sensitivity as well as for maximum accuracy. Specifically, cond(**K**) will reduce the error propagation, as shown in Eqn 1. The purpose of this study was to investigate the effectiveness of this method of selecting derivative orders for multicomponent quantitation.

Experimental

The spectra used were obtained in a previous study and recorded at 1-nm intervals over the spectral range 350—650 nm. Derivatives were calculated with stored spectra by using a two-point slope procedure developed by the manufacturer of the spectrophotometer. All derivative values were transferred to the Idaho State University HP-1000 computer for subsequent data processing. Concentrations were estimated from derivatives sampled at 6-nm intervals over the measured spectral range, allowing for the advantage of the overdetermination of the chemical system [8, 13]. Standard deviations were

estimated for analyte concentrations by a Monte Carlo method [16]. Normal random noise with a zero mean and a relative standard deviation of 1% was used to generate 50 response data sets. These were then used to estimate concentrations and standard deviations by a standard regression procedure. The relative concentration errors were calculated from the true sample concentrations and the estimated concentrations.

Results and discussion

To test the use of cond(**K**) as a predictor for optimal derivative order, separate data sets were processed for a two-component sample of acid-base indicators at two pH values. The components used were chlorophenol red (CR) and phenol red (PR). In earlier work [16], a pH of 6 was found to be optimal while a pH of 4 was unacceptable. Zero-order spectra of CR and PR at pH 6 and pH 4 are shown in Fig. 1. The data obtained at pH 4 were processed to evaluate the effectiveness of derivatives in improving the selectivity for poorly resolved spectra. The zero-, first- and second-order derivatives of the two-component mixture at pH 4 are illustrated in Fig. 2A. In proceeding from zero order to second order, there is a slight increase in selectivity and simultaneously an increase in the noise, as expected [2, 3]. The results at pH 4 are listed in Table 1. The condition number of the calibration matrix drops substantially from the zero order to the first-order derivative. This is reflected in the total relative errors as well as in the individual relative errors. However, the precision appears to be degraded for the first order compared to the zero order. This is attributed to the increase in noise with higher orders of derivative. The second order shows a further decrease in cond(**K**) but an increase in the relative errors. In addition, there is a considerable deterioration in the precision. Apparently, the noise is too great with the second-order derivative to obtain acceptable results even though the cond(**K**) decreases. Indeed, Fig. 2A shows a large amount of noise with the second-order spectrum. It appears that cond(**K**) is insensitive to noise in predicting the best order to use. The noise level was too great at higher orders for the higher orders to be useful.

Figure 2B shows the zero-, first-, second-, and third-order spectra for the

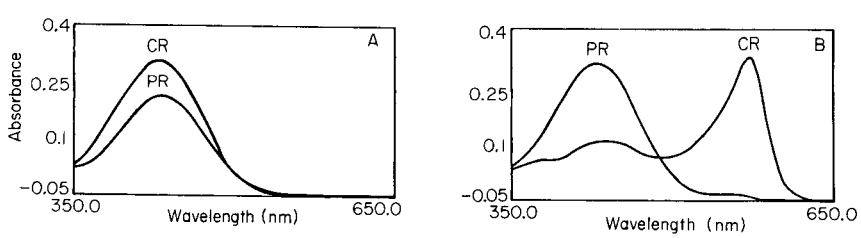

Fig. 1. Absorbance spectra of chlorophenol red (CR) and phenol red (PR): (A) at pH 4; (B) at pH 6.

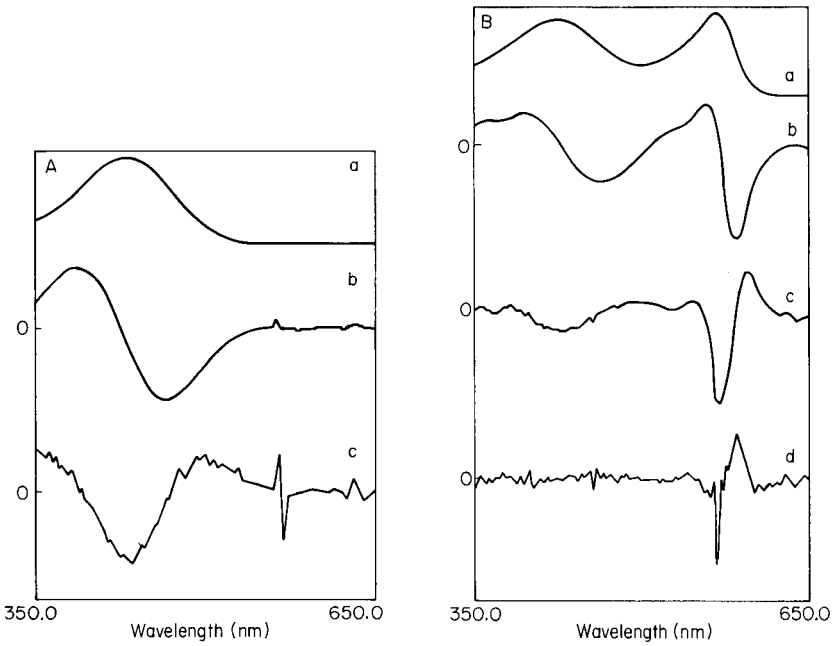

Fig. 2. Spectra of a mixture of chlorophenol red and phenol red: (A) at pH 4; (B) at pH 6. (a) Zero order; (b) first-order derivative; (c) second-order derivative; (d) third-order derivative.

TABLE 1

Results obtained with zero-, first- and second-order derivatives at pH 4 and at pH 6

Derivative order	Cond(K)	Component[a]	Calculated concentration (10^{-5} M)	$\|\|\delta\hat{c}\|\|/\|\|\hat{c}\|\|$ (%)	Relative error (%)	RSD (%)
At pH 4						
0	26.0	CR	0.75	53	61	3.2
		PR	3.34		46	0.77
1	15.3	CR	1.41	26	27	2.9
		PR	2.88		26	1.4
2	9.83	CR	0.61	52	68	12
		PR	3.16		38	2.8
At pH 6						
0	1.91	CR	1.80	6.5	7.5	0.34
		PR	2.10		6.3	0.21
1	1.86	CR	2.04	4.6	5.0	0.41
		PR	2.38		4.3	0.64
2	4.61	CR	2.01	15	3.5	0.85
		PR	1.83		18	1.9
3	3.52	CR	2.28	29	18	0.58
		PR	1.49		33	7.2

[a]Chlorophenol red (CR) at 1.939×10^{-5} M; phenol red (PR) at 2.238×10^{-5} M.

mixture at pH 6. Again, the noise level increases with increasing order. Also, the sensitivity of the broad PR absorption band is very low at shorter wavelengths. This is reflected in the cond(**K**) listed for pH 6 in Table 1. With the first order, there is a decrease in cond(**K**) with respect to the zero order. Cond(**K**) for the second order increases markedly, indicating less selectivity. The decrease in cond(**K**) with the third order is probably artificial and stems from peak-height ratios approaching unity [14]. A t test at the 95% confidence level showed that the calculated molarities for CR and PR based on the zero- and first-order derivatives were significantly different from each other. Therefore, best accuracy is obtained with the first order as predicted by cond(**K**). With the second order a decrease in relative error is observed for CR but the overall relative error is found to be larger. The total relative error predicted by Eqn. 1 will increase with an increase in cond(**K**) but the individual relative errors do not necessarily increase. The total relative errors listed in Table 1 are those calculated from the true and estimated concentrations and should not be confused with the predicted propagated relative error. This could be obtained by calculating $||\delta \vec{r}||$ and $||\delta \mathbf{K}||$ and using Eqn. 1. It should also be noted that Eqn. 1 only represents an upper bound to the relative error; the relative error is often less than that predicted [17, 18].

This communication is intended only to suggest the potential applicability of condition numbers and much work remains to be done to verify and utilize this potential.

This project was supported by funding from the Idaho State University Chemistry Department.

REFERENCES

1 T. C. O'Haver, Anal. Chem., 51 (1979) 91A.
2 T. C. O'Haver, Anal. Chem., 53 (1981) 1876.
3 G. Talsky, L. Mayring and H. Kreuzer, Angew. Chem. Int. Ed. Engl., 17 (1978) 785.
4 Y. R. Tahboub and H. L. Pardue, Anal. Chem., 57 (1985) 38.
5 M. R. Whitbeck, Appl. Spectrosc., 35 (1981) 93.
6 L. Meal, Anal. Chem., 55 (1983) 2448.
7 A. H. Lawrence and J. D. MacNeil, Anal. Chem., 54 (1982) 2385.
8 D. T. Rossi and H. L. Pardue, Anal. Chim. Acta, 175 (1985) 153.
9 W. E. Weiser and H. L. Pardue, Clin. Chem., 29 (1983) 1673.
10 C. Jochum, P. Jochum and B. R. Kowalski, Anal. Chem., 53 (1981) 85.
11 G. W. Stewart, Introduction to Matrix Computations, Academic Press, New York, 1973.
12 P. Jochum and E. L. Schrott, Anal. Chim. Acta, 157 (1984) 211.
13 J. H. Kalivas, Anal. Chem., 55 (1983) 565.
14 M. Otto and W. Wegscheider, Anal. Chem., 57 (1985) 63.
15 S. Ebel, E. Glaser, S. Abdulla, U. Steffens and V. Walter, Fresenius Z. Anal. Chem., 313 (1982) 24.
16 J. H. Kalivas, Anal. Chem., 58 (1986) 989.
17 R. W. Gerlach and B. R. Kowalski, Anal. Chim. Acta, 134 (1982) 119.
18 B. Høyer and L. Kryger, Anal. Chim. Acta, 167 (1985) 11.

Analytica Chimica Acta, 187 (1986) 353—356
Elsevier Science Publishers B.V., Amsterdam — Printed in The Netherlands

Short Communication

HIGH-PERFORMANCE LIQUID CHROMATOGRAPHIC DETECTOR BASED ON NEAR-INFRARED SEMICONDUCTOR LASER FLUORIMETRY

KOUJI SAUDA, TOTARO IMASAKA and NOBUHIKO ISHIBASHI*
Faculty of Engineering, Kyushu University, Hakozaki, Fukuoka 812 (Japan)
(Received 15th April 1986)

Summary. Three polymethine dyes, which fluoresce at 780—820 nm, are separated by reversed-phase chromatography and detected fluorimetrically with a semiconductor laser for excitation. The detection limit for anhydro-3,3,3′,3′-tetramethyl-1,1′-bis(4-sulfomethyl)-4,5,4′,5′-dibenzoindotricarbocyanine hydroxide (sodium salt) is 0.3 pg, which is almost three orders of magnitude better than the value obtained by conventional fluorimetry.

Laser fluorimetry has recently been used for sensitive detection in high-performance liquid chromatography (h.p.l.c.) [1—4]. However, the lasers are expensive and can be difficult to operate, so that they have not been used in practical instrumentation. A semiconductor laser has the advantage of being much smaller and cheaper, and is a practical light source for fluorimetry [5, 6]. As little as 10 fg of a polymethine dye can be detected by injecting the sample directly into a stream [7]. Recently, several polymethine dyes, which fluoresce in the near-infrared region (780—820 nm), have been used as materials for data recording in optical disk systems. For system evaluation, the chemical composition and chemical properties of these compounds must be investigated at ultratrace levels. In this communication, a h.p.l.c. system with a detector based on semiconductor laser fluorimetry is described and its use in ultratrace determination of polymethine dyes is demonstrated. The performance of the proposed detector is compared with that of other instruments.

Experimental

Apparatus. A block diagram of the apparatus is shown in Fig. 1. The light source of the semiconductor laser (Hitachi, HL7801, 780 nm, 3 mW; Sharp, LT024MD, 780 nm, 15 mW) is modulated to square waves at 100 Hz by a pulse generator (Hewlett-Packard, 8013B). Fluorescence from the sample is collected by a lens (focal length, 31 mm) and passes through an interference filter (Ditric 15-20785, transmission 830 nm, $\Delta\lambda$ = 13 nm) and a color filter (Toshiba V-R63, 630-nm cut-off). Fluorescence is focused by a lens (focal length, 60 mm) to a monochromator (Jasco, CT-10) equipped with a

0003-2670/86/$03.50 © 1986 Elsevier Science Publishers B.V.

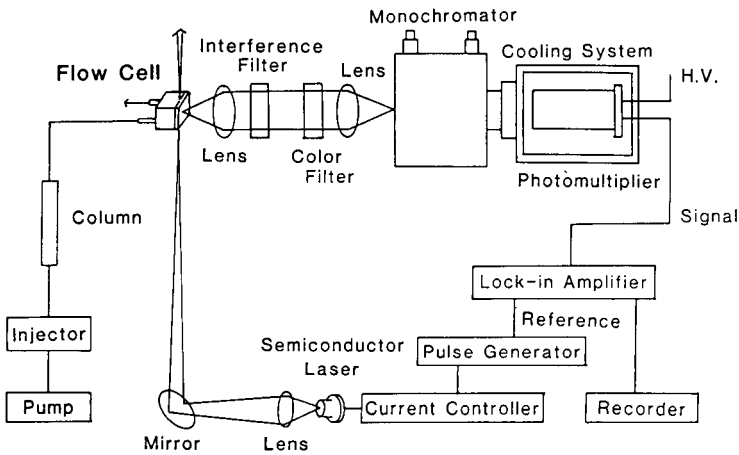

Fig. 1. Block diagram of the apparatus.

photomultiplier (Hamamatsu, R943-02, 160-930 nm) with a red-sensitive photocathode. A photomultiplier cooling system (Hamamatsu, C659-A) is used to reduce the temperature to —20° C. The output signal is fed to a lock-in amplifier (NF Circuit Design Block, LI-570) combined with a chart recorder (Rikadenki, R-50).

The sample (100 μl) is injected into the reversed-phase h.p.l.c. column (Toyo Soda, TSK gel ODS-120T) from a loop injector. The flow rate is 1 ml min^{-1}. The specially designed flow cell is entirely of quartz (path length 1 cm; total volume 18 μl). The eluted sample was also detected with a commercial fluorimetric detector (Kyowa, KLF-3080) and a spectrophotometric detector (Kyowa, KLC-2290).

Reagents. The dyes used were 3,3′-dimethyl-2,2′-(4,5,4′,5′-dibenzo)thiatricarbocyanine iodide (NK427), 3,3,3′,3′-tetramethyl-1,1′-dimethyl-4,5,4′5′-dibenzoindotricarbocyanine perchlorate (NK2014), and anhydro-3,3,3′,3′-tetramethyl-1,1′-bis(4-sulfomethyl)-4,5,4′-5′-dibenzoindotricarbocyanine hydroxide sodium salt (NK2611), all from Nippon Kanko-Shikiso Kenkyusho. Organic solvents were from Wako Pure Chemical Company. The eluent was a mixture of water and methanol (1:9), containing 15 mM choline chloride [(2-hydroxyethyl) trimethylammonium chloride]. The polymethine dyes were dissolved in methanol to give concentrations of 5×10^{-8} M.

Results and discussion

The polymethine dyes fluoresce and have absorption maxima at around 780 nm, which coincides with the emission wavelength of the semiconductor laser [6]. The emission maxima of the polymethine dyes in methanol are located at around 810 nm. The relative fluorescence intensities were 1.0, 0.4, and 0.1 for NK2611, NK2014, and NK427, respectively.

A chromatogram obtained for the mixture of the polymethine dyes with the semiconductor laser fluorimetric detector is shown in Fig. 2. The detection

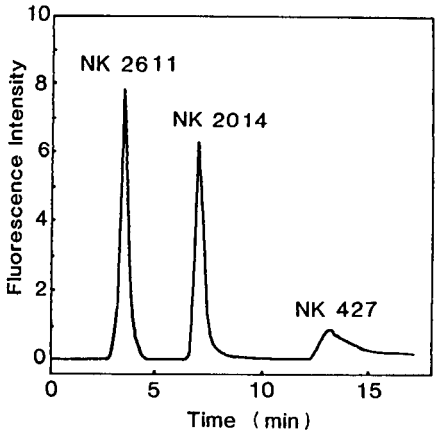

Fig. 2. Chromatogram for an equimolar mixture of the three polymethine dyes with semiconductor laser fluorimetry for detection. For details, see text.

wavelength was adjusted to 830 nm, because it gave a better signal-to-noise ratio. The fluorescence intensity for NK427 was found to decrease gradually on repeating the measurements, probably because of the poor chemical stability of this compound.

The detection limits for NK2611 in methanol obtained with various spectrometric detectors are compared in Table 1. The photomultiplier (Hamamatsu, R931) in a commercial fluorimeter was replaced by a photomultiplier with a red-sensitive photocathode (Hamamatsu, R928). The detection limit obtained with a semiconductor laser fluorimeter equipped with a room-temperature photomultiplier (1.9 pg) was two orders of magnitude better than the value obtained with a conventional fluorimeter and very much better than the value obtained with a spectrophotometric detector, as expected. The detection limit in fluorimetry depended on the dark current noise from the photomultiplier, and could be improved by increasing the output power.

TABLE 1

Detection limits for NK-2611

Method	Detection limit (pg)
Semiconductor laser fluorimetry[a]	0.3
Semiconductor laser fluorimetry[b]	1.9
Conventional fluorimetry	190
Conventional spectrophotometry[c]	810

[a]Photomultiplier cooled to −20° C. [b]Photomultiplier operated at room temperature. [c]At 740 nm, the longest wavelength available with the spectrophotometer used.

A semiconductor laser with a power exceeding 500 mW is now commercially available. The use of such a laser is very attractive for ultratrace detection of suitable analytes. Visible semiconductor lasers can be operated to 579 nm in the pulsed mode and 671 nm in the continuous-wave mode. Such lasers will extend the present approach to many other applications.

We thank Hideo Watanabe, Yukitada Kurihara, and Toshinori Hayashi of Toyo Soda for their helpful suggestions and for providing the h.p.l.c. system. We also thank Shigeo Yasui of Nippon Kanko-Shikiso Kenkyusho for helpful suggestions about polymethine dyes. This research was supported by a Grant-in-Aid for Scientific Research from the Ministry of Education of Japan.

REFERENCES

1 R. N. Zare and G. J. Diebold, Science, 196 (1979) 1439.
2 R. N. Zare, Science, 226 (1984) 298.
3 E. S. Yeung and M. J. Sepaniak, Anal. Chem., 52 (1980) 1465A.
4 R. B. Green, Anal. Chem., 55 (1983) 20A.
5 T. Imasaka, A. Yoshitake, A. Hirata, Y. Kawabata and N. Ishibashi, Anal. Chem., 57 (1985) 947.
6 T. Imasaka, A. Yoshitake and N. Ishibashi, Anal. Chem., 56 (1984) 1077.
7 Y. Kawabata, T. Imasaka and N. Ishibashi, Talanta, 33 (1986) 281.

ANALYTICA CHIMICA ACTA, VOL. 187 (1986)

AUTHOR INDEX

ACA announcements

ANNOUNCEMENTS OF MEETINGS

INTERNATIONAL SYMPOSIUM ON ANALYSIS OF NEUROTRANSMITTERS, STOCKHOLM, SWEDEN, APRIL 7—10, 1987

Analysis for neurotransmitters is an essential part of research activities in physiology, pharmacology and drug development. New potential neurotransmitters are frequently discovered, but knowledge about the roles and functions of these compounds is still scanty. One important limiting factor has been the availability of sensitive and accurate analytical methods for their assays and identifications. The main aim of this symposium is to review the present state of the art regarding analytical scientific knowledge about neurotransmitters. In addition, the physiological and pharmacological implications of analytical data will be discussed. A strong emphasis will be put on quality control and validation aspects on the methodologies used; from sampling, sample handling, sample work-up and measurements, to calculations of results.

Internationally recognized specialists will review major topics such as the physiological and pharmacological backgrounds for the analyses of peptides, catecholamines, serotonin, acetylcholine, GABA, trace amines and purines (neuromodulators); physiological aspects on sample treatment, perfusion techniques and in vivo voltammetry; methodological and statistical aspects on method validation; the most important analytical techniques – radioenzymatic, radioreceptor assays, immunology, immunohistochemistry, GC/MS and liquid chromatography with different detection techniques, including electrochemistry and mass spectrometry. A discussion session on sampling and sample handling as well as poster sessions are also included.

The Symposium will be held at the SAS Arlandia Hotel, 40 km north of Stockholm. It is organized by the Swedish Academy of Pharmaceutical Sciences and sponsored by Uppsala University Neuroscience Research Centre. For further information please contact: Symposium on Analysis of Neurotransmitters, The Swedish Academy of Pharmaceutical Sciences, P.O. Box 1136, S-11181 Stockholm, Sweden.

ARCH '87, AUTOMATED REASONING IN CHEMISTRY, BUDAPEST, HUNGARY, MAY 27–29, 1987

The Committee for Analytical Chemistry of the Hungarian Academy of Sciences, the Computer Working Group of the Hungarian Chemical Society and the Institute of Isotopes are organizing ARCH '87, at which recent trends and problems in the application of contemporary mathematical techniques in chemistry, especially analytical chemistry, will be discussed. The conference is now announced and papers are called for.

Main topics will be: automated structure elucidation, expert systems, handling of chemical structures, molecular modelling, simulation, and synthesis planning. Contributed papers for oral presentations and posters are invited.

For further information, contact: ARCH '87 Conference, Mrs. O. Enyedy, Secretary, Institute of Isotopes of the Hungarian Academy of Sciences, P.O. Box 77, H-1525 Budapest, Hungary.

INTERNATIONAL SYMPOSIUM ON TITRATION TECHNIQUES, LUND, SWEDEN, JUNE 12–15, 1987

An international symposium on titration techniques will be arranged by the Analytical Division of the Swedish Chemical Society at Lund on June, 12–15, 1987. The symposium will deal with various aspects of titrations as presented in plenary lectures by invited speakers. Submitted papers and posters will also be presented. An exhibition of modern titration equipment will be arranged and it will be supplemented with technical presentations by the exhibiting instrument manufacturers.

The programme will cover the following aspects of titration techniques: acid–base titrations, complexometric titrations, non-aqueous and two-phase titrations, continuous titrations in flow systems, coulometric titrations, thermometric titrations, numerical evaluation methods, modern titration equipment, and application of titration in *e.g.* the pharmaceutical, pulp and paper, metallurgical and petrochemical industries. Some fifteen international and national experts have been invited to give overviews over these fields.

Those interested in contributing to the symposium are invited to send a preliminary abstract of the paper (maximum 200 words) to the Analytical Division, The Swedish Chemical Society, Wallingatan 26 A, S-111 24 Stockholm, Sweden, not later than December 1, 1986.

The symposium will be held at the Chemical Center at the University of Lund in the south of Sweden. The official language will be English. No translation facilities will be available.

All correspondence concerning the symposium should be addressed to: "Symposium on Titration Techniques", c/o The Swedish Chemical Society, Wallingatan 26 A, S-111 24 Stockholm, Sweden.

INTERNATIONAL SYMPOSIUM ON APPLIED MASS SPECTROMETRY IN THE HEALTH SCIENCES, BARCELONA, SPAIN, SEPTEMBER 28–30, 1987

An International Symposium on Applied Mass Spectrometry in the Health Sciences will be held in Barcelona, September 28–30, 1987. The symposium is organized in conjunction with the International Symposium on Pharmaceutical and Biomedical Analysis to be held from September 23–25, 1987 also in the Barcelona Congress Centre and which will cover complementary analytical approaches.

The scientific programme will consist of invited plenary lectures, invited and submitted research lectures, group discussions and poster presentations covering the whole field of applied mass spectrometry including: instrumentation and novel techniques; methods of ionization and fragmentation mechanisms (SIMS, FD, PD, FAB); GC–MS, LC–MS and MS–MS coupling; applications in: biomedicine, environmental and food chemistry, toxicology, pharmacology, data processing.

The official language of the meeting will be English.

For further information, contact: Dr. Emilio Gelpí, Symposium Secretariat, International Symposium on Applied Mass Spectrometry in the Health Sciences, Palau De Congressos, Avgda. Reina M.ª Cristina, s/n, 08004 Barcelona, Spain. Tel.: (325) 3000-223 99 40, telex: 53.117 FOIMB-E.

SCIENTIFIC SOFTWARE

SOFTWARE AVAILABLE FROM AUTHORS

A new section of this journal has started, which will give authors of computer programs the opportunity to announce software that they are willing to share with their colleagues. The aims of the section have been outlined in an Editorial (*Anal. Chim. Acta*, 173 (1985) 1). The programs offered will be listed in this section of the journal, as information becomes available.

Further details and forms for entry are available from Professor J.T. Clerck, Universität Bern, Pharmazeutisches Institut, Baltzerstrasse 5, CH-3102 Bern, Switzerland.

CALENDAR OF FORTHCOMING MEETINGS

Jan. 26–29, 1987
Incline Village, NV, U.S.A.

Laser Applications to Chemical Analysis
Contact: Optical Society of Ameria, Laser Applications Meeting, 1816 Jefferson Place, N.W., Washington, DC 20036, U.S.A.

Feb. 4–6, 1987
Nice, France

Formula, 1st International Forum on Formulation Physical Chemistry and Applications
Contact: Scientific Committee of Formula, Société Française de Chimie, Département Congrès, 250 rue Saint-Jacques, 75005 Paris, France.

March 9–13, 1987
Atlantic City, NJ, U.S.A.

38th Pittsburgh Conference and Exposition on Analytical Chemistry and Applied Spectroscopy
Contact: Mrs. Alma Johnson, Program Secretary, 12 Federal Drive, Suite 322, Pittsburgh, PA 15235, U.S.A. (Further details published in Vol. 184.)

April 3–9, 1987
Beijing, China

ChinaChem '87, International Exhibition on Chemical and Petrochemical Industries
Contact: Adsale Exhibition Services, 21/F Tung Wai Commercial Building, 109–111 Gloucester Road, Hong Kong. Tel.: (5) 8920511, telex: 63109 ADSAP HX, Fax: (5) 731709.

April 6–9, 1987
Cardiff, U.K.

International Symposium on Electroanalysis in Biomedical, Environmental and Industrial Sciences
Contact: Short Courses Section, UWIST, P.O. Box 68, Cardiff CF1 3XA, Wales, U.K. Tel.: (0222) 42588, ext. 2213. (Further details published in Vol. 178, No. 2.)

April 7–10, 1987
Stockholm, Sweden

International Symposium on Analysis of Neurotransmitters
Contact: The Swedish Academy of Pharmaceutical Sciences, P.O. Box 1136, S-111 81 Stockholm, Sweden.

April 27–May 1, 1987
Sydney, Australia

9th Australian Symposium on Analytical Chemistry
Contact: The Secretary 9AC, Mr. John Eames, P.O. Box 137, North Ryde, N.S.W. 2133, Australia. Tel.: (02) 887-8688. (Further details published in Vol. 178, No. 2.)

May 11–14, 1987
Ghent, Belgium

2nd International Symposium on Quantitative Luminescence Spectrometry in Biomedical Sciences
Contact: Dr. W. Bayens, State University of Ghent, Laboratory of Pharmaceutical Chemistry and Drug Quality Control, Harelbekestraat 72, B-9000 Ghent, Belgium. (Further details published in Vol. 178, No. 2.)

May 13–15, 1987
Amsterdam, The Netherlands

Scientific Computing and Automation (Europe)
Contact: K. Foley, Scientific Computing and Automation, P.O. Box 330, 1000 AH Amsterdam, The Netherlands. Tel.: (020) 5862 828. (Further details published in Vol. 184.)

May 17–22, 1987 Tokyo, Japan	**CHEMRAWN VI, World Conference on Advanced Materials Needed for Innovations – Energy, Transportation and Communications** Contact: Mr. H. Hamada, Executive Director, The Chemical Society of Japan, 1-5 Kanda-Suragadi, Chiyoda-ku, Tokyo, Japan.
May 24–27, 1987 Columbia, SC, U.S.A.	**1st International Symposium on the Interface between Analytical Chemistry and Microbiology** Contact: 1st International Symposium on the Interface between Analytical Chemistry and Microbiology, P.O. Box 7126, Columbia, SC 29202, U.S.A. (Further details published in Vol. 184.)
May 27–29, 1987 Budapest, Hungary	**ARCH '87, Automated Reasoning in Chemistry** Contact: ARCH '87 Conference, Mrs. O. Enyedy, Secretary, Institute of Isotopes of the Hungarian Academy of Sciences, P.O. Box 77, H-1525 Budapest Hungary.
June 12–15, 1987 Lund, Sweden	**International Symposium on Titration Techniques** Contact: "Symposium on Titration Techniques", c/o The Swedish Chemical Society, Wallingatan 26 A, S-111 24 Stockholm, Sweden.
June 17–19, 1987 Fort Collins, CO, U.S.A.	**Conference on Chemically Modified Surfaces** Contact: W. Collins, Mail Stop C41C00, Dow Corning Corporation, Midland, MI 48686-0994, U.S.A.
June 21–26, 1987 Toronto, Canada	**XXV Colloquium Spectroscopium Internationale** Contact: Mr. L. Forget, Executive Secretary CSI XXV, National Research Council of Canada, Ottawa, K1A 0R6 Canada. Tel.: (613) 993-9009, telex: 053-3145. (Further details published in Vol. 172.)
June 28–July 4, 1987 Amsterdam, The Netherlands	**HPLC '87, 11th International Symposium on Column Liquid Chromatography** Contact: Organisatie Bureau Amsterdam bv, Europaplein, 1078 GZ Amsterdam, The Netherlands. Tel.: (31) 20-440807, telex: 13499 raico nl. (Further details published in Vol. 181.)
July 13–18, 1987 Sofia, Bulgaria	**31st IUPAC Congress** Contact: Dr. R. Vlahov, Institute of Organic Chemistry, Bulgarian Academy of Sciences, 1113 Sofia, Bulgaria. Telex: 22729 ECHBAN BG. (Further details published in Vol. 181.)
Aug. 24–28, 1987 Vienna, Austria	**6th International Conference on Fourier Transform Spectroscopy** Contact: Interconvention, P.O. Box 80, A-1107 Vienna, Austria. Tel.: (222) 57 63 05, 57 62 88, telex: 11 12 10.
Aug. 25–30, 1987 Beijing, China	**8th International Conference on Computers in Chemical Research and Education** Contact: Cheng Qian, 345 Lingling Road, 200032 Shanghai, China. Telex: 33354 SIOC CN.
Aug. 30–Sept. 4, 1987 Amsterdam, The Netherlands	**EUCMOS XVIII, 18th European Congress on Molecular Spectroscopy** Contact: EUCMOS XVIII, c/o Municipal Congress Bureau, P.O. Box 2289, 1000 CG Amsterdam, The Netherlands. Tel.: (3120) 552 3459, telex: 16460 anal. chem.

Sept. 7–11, 1987 Paris, France	**Euroanalysis VI, European Conference on all Aspects of Analytical Sciences** Contact: G.A.M.S., 88 Boulevard Malesherbes, 75008 Paris, France. (Further details published in Vol. 181.)
Sept. 23–25, 1987 Barcelona, Spain	**International Symposium on Pharmaceutical and Biomedical Analysis** Contact: Dr. Emilio Gelpi, Symposium Secretariat, International Symposium on Pharmaceutical and Biomedical Analysis, Palau de Congressos, Avgda. Reina Mª. Cristina s/n, 08004 Barcelona, Spain. Tel.: (325) 30 00-223 99 40, telex: 53.117 foimb-e.
Sept. 28–30, 1987 Barcelona, Spain	**International Symposium on Applied Mass Spectrometry in the Health Sciences** Contact: Dr. Emilio Gelpi, Symposium Secretariat, International Symposium on Applied Mass Spectrometry in the Health Sciences, Palau de Congressos, Dept. de Convencions, Avgda. Reina Mª. Cristina s/n, 08004 Barcelona, Spain. Tel.: (325) 30 00-223 99 40, telex: 53.117 foimb-e.
Sept. 28–Oct. 1, 1987 Gaithersburgh, MD, U.S.A.	**Accuracy in Trace Analysis – Accomplishments, Goals, Challenges** Contact: Harry Hertz, A309 Chemistry Building, National Bureau of Standards, Gaithersburg, MD 20899, U.S.A. Tel.: (301) 921 2851. (Further details published in Vol. 181.)
Sept. 28–Oct. 2, 1987 Amsterdam, The Netherlands	**2nd Amsterdam HPLC Summercourse** Contact: Dr. J.C. Kraak, Laboratory for Analytical Chemistry, University of Amsterdam, Nieuwe Achtergracht 166, 1018 WV Amsterdam, The Netherlands.
Oct. 19–23, 1987 Fellbach, F.R.G.	**ECASIA '87, European Conference on Applications of Surface and Interface Analysis** Contact: U. Nagorny, Max-Planck-Institut für Metallforschung, Institut für Werkstoffwissenschaften, Seestrasse 92, D-7000 Stuttgart 1, F.R.G.
April 18–21, 1988 Las Vegas, NV, U.S.A.	**Flow Analysis IV, An International Conference on Flow Analysis** Contact: Dr. Gilbert E. Pacey, Department of Chemistry, Miami University, Oxford, OH 45056, U.S.A. (Further details published in Vol. 181.)
May 18–20, 1988 Amsterdam, The Netherlands	**CAC–88, 4th International Conference on Chemometrics in Analytical Chemistry** Contact: CAC–88, Laboratory for Analytical Chemistry, University of Amsterdam, Nieuwe Achtergracht 166, 1018 WV Amsterdam, The Netherlands. Tel.: (020)-5223541 (Dr. Smit).
June 19–24, 1988 Washington, DC, U.S.A.	**HPLC '88, 12th International Symposium on Column Liquid Chromatography** Contact: Symposium Manager, Barr Enterprises, P.O. Box 279, Walkersville, MD 21793, U.S.A. Tel.: (301) 898 3772.
Aug. 28–Sept. 1, 1989 Wiesbaden, F.R.G.	**11th International Symposium on Microchemical Techniques** Contact: Gesellschaft Deutscher Chemiker, Abt. Tagungen, P.O. Box 900440, D-6000 Frankfurt/Main 90, F.R.G. Tel.: (069) 79 17-366/360, telex: 4170497 gdch d.

(*Continued from inside back cover*)

ontinued from outside back cover)

(Continued on p. 360)

CONTENTS

(Abstracted, Indexed in: Anal. Abstr.; Biol. Abstr.; Chem. Abstr.; Curr. Contents Phys. Chem. Earth Sci.; Life Sci.; Index Med.; Mass Spectrom. Bull.; Sci. Citation Index; Excerpta Med.)

(Continued on inside back